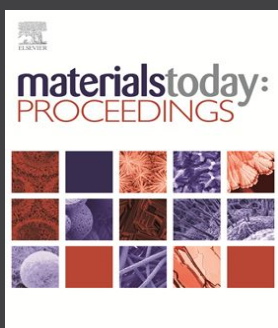




Padmabhushan
Dr. Karmaveer Bhaurao Patil



Rayat Shikshan Sanstha's

**Annasaheb Awate Arts, Commerce and
Hutatma Babu Genu Science College, Manchar**

Tal. Ambegaon , Dist. Pune , Maharashtra, India -410 503

Affiliated to

Savitribai Phule Pune University, Pune

Website: aacmanchar.edu.in

Organizes

Hybrid (Online/Onsite mode) International Conference on

**“ Integrative Nanotechnology Perspectives for
Multidisciplinary Applications 2022 (INPMA-2022)”**

held on

January 16-18, 2022

About the Parent Institution

Rayat Shikshan Sanstha was established by the great social reformer Padmabhushan Dr. Karmaveer Bhaurao Patil in 1919 with the motto- Education for masses is principle instrument and the tool for eradication of all-pervasive social evils and desirable effective social change. The vision of the institute- "Education through self-help is a significant and chief drive of social change to achieve different tasks of nation building by establishing social equality and social justice". At present the institution is working with the network of 772 branches spreading over 15 Districts of Maharashtra & 1 District of Karnataka including colleges, ITI's, High Schools, Primary Schools, Pre-primary Schools, Hostels, Ashramshalas & others. The Sanstha operates through 8 administrative offices and has a strong workforce to cater the educational needs of 4.6 lakhs students.

Organizing Institute

Annasaheb Awate Arts, Commerce and Hutatma Babu Genu Science College, Manchar was established in 1966 & is run by the Rayat Shikshan Sanstha, Satara. The college is one of the leading colleges in Savitribai Phule Pune University, Pune that provides a quality education in Arts, Commerce and Science faculty. College offers 17 UG courses and 9 PG courses including Marathi, English, Economics, Commerce, Analytical Chemistry, Organic Chemistry, Botany and Physics. College is also having recognized research centre for Botany, Chemistry and Economics along with these our college has professional courses like Biotechnology, B.Voc. and BBA(CA). College is accredited by NAAC for the 3rd cycle in "A" grade with CGPA 3.09.

Nearby Destinations

- **'Bhimashankar'**, one of the twelve Jotirlingas, situated 60 km away from Manchar. It is famous for Giant Squirrel and evergreen rich flora.
- **'Shivneri Fort'**- Birth place of Chattrapati Shivaji Maharaj is 35 km away from Manchar. On the way of Junnar, **Ozar** (23 km) and **Lenyadri** (35 km) are among the Ashtavinayaka temples.
- **GMRT, Khodad**, world famous radio telescope is 20 km away from our college.
- **Buddhist caves** in Western Ghat region(27 km).
- **Western Ghat region** (60km) is declared as heritage by UNESCO.

Themes of the Conference :

- Nanotechnology: An Elixir to Life
- Nanomaterials in Sensors
- Nanomaterials in Diagnostics and Therapy
- Nanobiosciences
- Novel Applications of Nanotechnology
- Nanotechnology in Catalysis
- Nanomaterial Synthesis and Characterization

Registration Details :

Registration Fee:

Student participants for oral/poster presentation: Rs. 500/-
Faculty & Research Scholars for oral/poster presentation: Rs. 1000/-
Foreign delegates: \$ 50/-
Accepted Full length paper: Rs. 3000/-
Registration Fee is waived off for only virtual attendance.
For Registration : <https://forms.gle/pKu2x2EAVjT8aKEz6>

Bank Details

Registration fee can be deposited through NEFT/ RTGS/ IPS to

Principal, Annasaheb Awate College, Manchar, Tal.- Ambegaon, Dist.- Pune (M.S.), India

Account No.: **60357495658**

Bank Name: **Bank of Maharashtra**

IFSC code: **MAHB0000112**

For query regarding registration and submission of abstract, please contact:

Mr. S. S. Gaikwad: +91 9970469708

Dr. N.B. Admuthe : +91 9423909080



Volume 73

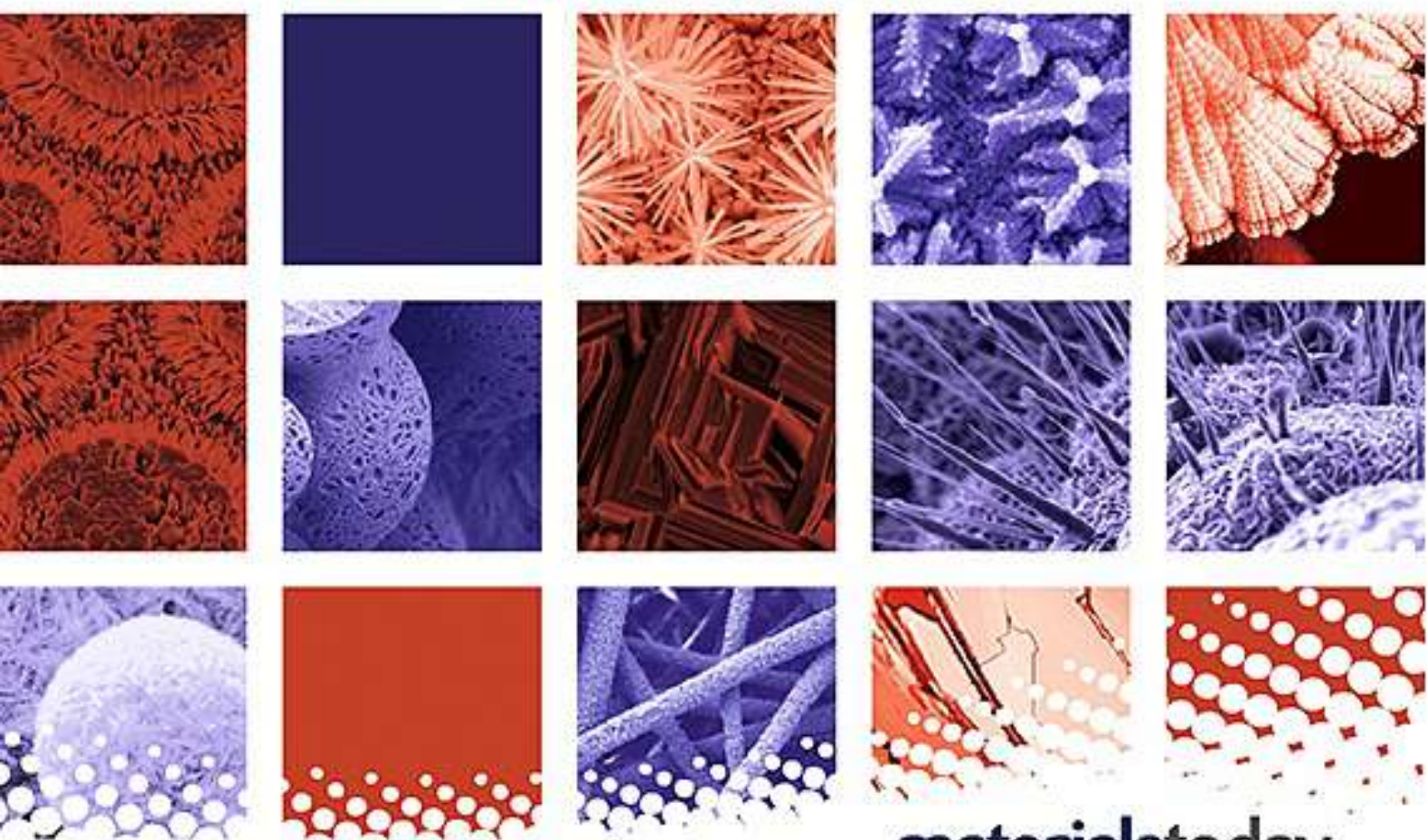
Part 3

Pages 383-538

ISSN 2214-7853

materialstoday: PROCEEDINGS

Integrative Nanotechnology Perspectives for
Multidisciplinary Applications 2022



materialstoday
Connecting the materials community



Special Issue - Materials Today Proceedings
“Integrative Nanotechnology Perspectives for Multidisciplinary Applications 2022 (INPMA-2022)”

Index

Sr. No	Title of papers	Name of Authors	Volume	Page No.
1.	Synergistic effect of copper, silver nanoparticles and hydrogen peroxide on <i>Xanthomonas axonopodis</i> pv. <i>punicae</i>	Kavyashri B. Joshi, A. M. Bhosale, M. N. Kharde	73	383-389
2.	Acoustic, volumetric and viscometric study relative to inter-molecular interaction in aqueous $KIO_3 + 1\% KH_2PO_4$	Meenakshi Rathi	73	390-395
3.	Synthesis, characterization, and biological evaluation of N- substituted indolyl chalcones as anticancer, anti-inflammatory and antioxidant agents	Hemant V. Chavan, Shriram D. Ganpure, Nikita N. Mali c, Pravin S. Bhale,	73	396-402
4.	Embelin isolated from <i>Embelia ribes</i> derived silver nanoparticles and its application in breast cancer nanomedicine.	Rutika R. Jagtap, Aniket Garud , Bhagyashri Warude, Shubhangi S. Puranik	73	403-411
5.	A systematic review on antifungal and insecticidal applications of biosynthesized metal nanoparticles	Bapusaheb H. Shinde, Shaukatali N. Inamdar, Sagar A. Nalawade, Sushilkumar B. Chaudhari	73	412-417
6.	Investigation of structural and optical properties of graphene derivatives as a route for optical sensing	Anil B. Patil, Umesh J. Tupe, Dharma K. Halwar, Vikas V. Deshmane, Arun V. Patil	73	418-426
7.	A review on biosynthesis and applications of various nanoparticles using extracts of medicinal plant <i>Tribulus terrestris</i>	Sagar A. Nalawade, Bapusaheb Shinde, Sushilkumar Chaudhari, Manisha S. Badhe, Vikas K. Kadam, Manohar G. Chaskar, Shirish S. Pingale	73	427-430
8.	Phytofabricated Br-AgNP synthesis using <i>Brassica oleracea</i> var. <i>italica</i> and their anti-carcinogenic applications	Shubhangi Puranik, Imran Patel	73	431-437
9.	Antioxidant activity and antimicrobial evaluation of iron nanoparticles prepared by the plant mediated biosynthesis involving root extract of <i>Picrorhiza kurroa</i>	Hema Koli, B. B. Bahule, Khursheed Ahmed, Basavani Patil	73	438-443
10.	Photoluminescence of Si nanostructured films by Pulsed Laser Deposition	Tushar Salve, Amar Katkar, Ashok Kanade, Gotan Jain	73	444-447
11.	Simple Co-precipitation synthesis and characterization of magnetic spinel $NiFe_2O_4$ nanoparticles	Subiya Kazi, Shaukatali Inamdar, Yuvraj sarnikar, Dhanraj Kamble, Radhakrishnan Tigote	73	448-454

12.	Stabilization of dairy industry sludge with leaf litter using as composting and its effect on Spinacia oleracea plant growth	Chougale Sanjivani Tanaji, Sarkale Prajkta Shahaji, Jadhav Aasawari Suhas	73	455-463
13.	Variation in band gap of antimony doped ZnO nanostructures with doping concentration	Leena.M. Mahajan	73	464-467
14.	Removal of nitrate from aqueous solution by using orange peel and wheat straw	Sarkale Prajkta Shahaji, Chougale Sanjivani Tanaji, Jadhav Aasawari Suhas	73	468-473
15.	IoT based dielectric constant measurement system for solid or semi-liquid materials using Arduino WeMos D1R1	Somnath A. Wankhede, Vijay S. Kale, A. D. Shaligram, Arun Patil, Dharma K Halwa	73	474-480
16.	Synthesis of Benzimidazole and Benzothiazole Derivatives using Reusable Waste Stem of Trigonella Foenum-graecum Assisted Zinc Sulphide Nanoparticles: A Green and Efficient Solid Acid Catalyst	Arun K. Valvi, Hemangi J. Gavit, Shubhada S. Nayak, Vitthal S. Shivankar, Gurumeet C. Wadhawa	73	481-486
17.	Synthesis and biological screening of novel series of 2-(4-hydroxy-3-methoxy-5-nitro-phenyl)-[1,3,4]oxadiazole by conventional and non conventional techniques	Ranjana Jadhav, Sunayna Pawar, Chandrakant Khilare, Arun Nikumbh	73	487-493
18.	Applications of plant-based nanomedicines for wound healing – An emerging paradigm for effective therapy	Priya Lokare, E. Keshamma, Anil Kumar, Yasser Ali Abdullah Alsowadi, Mohammad Mobarak Hossain, Laxmi Kirana Pallathadka	73	494-501
19.	Study of solvation and pollution approach of atrazine and chlorothalonil pesticides in binary liquid mixtures	Kalyan R. Langore, Arun B. Nikumbh	73	502-507
20.	Silica supported phosphotungstic acid catalyzed one pot efficient synthesis of pyrazolopyranopyrimidine derivatives	S. Abirami, G. Viruthagiri, K. Ashokkumar	73	508-514
21.	Formulation of healthy cookies incorporated with orange peel powder and Moringa oleifera leaf powder	Nikita Vilas Teke, Karuna Wasudeo Patil, Hemangi Jayram Gavit	73	515-521
22.	Isolation of biofilm formers from aquaculture and study, the effect of antibiofilm activity of chitosan mediated silver nanoparticle	G. Ganga	73	522-529
23.	Development of value-added cookies supplemented with giloy and tulsi powder	Disha Sunil Gawade, Karuna Wasudeo Patil, Gavit Hemangi Jayram	73	530-534
24.	Structural, morphological, and anti-bacterial activities of pure SnO ₂ nanoparticles prepared by chemical precipitation method	S. Abirami, G. Viruthagiri, K. Ashokkumar	73	535-538



Synergistic effect of copper, silver nanoparticles and hydrogen peroxide on *Xanthomonas axonopodis* pv. *punicae*

Kavyashri B. Joshi^{a,*}, A.M. Bhosale^b, M.N. Kharde^a

^a Department of Botany, P.V.P. College, Pravaranagar, Loni Kd 413713, India

^b Department of Biotechnology, P.V.P. College, Pravaranagar, Loni Kd 413713, India

ARTICLE INFO

Article history:

Available online 21 September 2022

Keywords:

Xanthomonas axonopodis
Pomegranate
Bacterial blight
Copper nanoparticles
Silver nanoparticles
Hydrogen peroxide
Antibacterial activity

ABSTRACT

Bacterial blight disease of pomegranate caused by *Xanthomonas axonopodis* pv. *punicae* decrease crop productivity. *X. axonopodis* was isolated from infected fruits, stem and leaves collected from Pravara area on NAS medium. Pure culture was obtained by regular subculture and maintained on NAS medium. *Trichoderma harizanium* fungal biomass was generated for nanoparticle synthesis on liquid PDA medium. The aqueous cell free culture filtrate (CFCF) obtained by filtration. Nanoparticles were synthesized using 50 ml of aqueous CFCF in flasks by stirring appropriate amount of, CuSO_4 (1–2 mM) solution in dark at 45 °C. Silver nanoparticles were synthesized using *Trichoderma viride*. SEM analysis proved silver nanoparticle size in the range 5–10 nm. Spread plate and colony count techniques proved significant antibacterial activity of silver nanoparticles against *Xanthomonas axonopodis*.

Copyright © 2022. Elsevier Ltd. All rights reserved.

Selection and peer-review under responsibility of the scientific committee of the Integrative Nanotechnology Perspective for Multidisciplinary Applications - 2022.

1. Introduction

Pomegranate (*Punicagranatum* L.) is an economically important fruit crop because of its immense nutraceutical value. It is used in pharmaceutical, dye and leather industries. This crop is adaptable to diverse climate, soil and water condition and high tolerance to drought [1]. It has potentials to develop wastelands available in the arid and semi-arid regions of India. This is an ideal crop for diversification. Moreover, it can make higher contribution to GDP with small area [13]. The pomegranate originated in Iran/Turkey; it grown over the whole Mediterranean region of Asia, Africa and Europe; later it migrated to Far East along silk route here It has been cultivated since the pre-Christian era [10]. Recently pomegranate cultivation is harmed by bacterial blight caused by *X. axonopodis* pv. *punicae* loss crop yield up to 60–80 %. This disease could not be effectively controlled by antibiotics, chemicals [1]. Bacterial blight of pomegranate was first reported in India from Delhi in 1952 and later from Bangalore (Karnataka) in 1959 [29]. The disease had no importance until 1991, but it appeared in epidemic form at IIHR lead to 60–80 per cent yield losses [5]. Further, severe outbreak of disease was noticed in Karnataka caused heavy losses

in yield and quality of fruits. Attack of bacterial blight disease also reported in Western Maharashtra. Particularly in Solapur district it was occurred throughout the year [16]. Fig. 1. Table 1. Table 2..

Now a days nanotechnology is an emerging field which has many novel applications as a nanomaterials widely used in nanomedicine and biotechnology [6,41]. The nanoparticles have applications in optoelectronics, nanodevices and information storage technology because of their unique electrical, optical, catalytic and magnetic properties differ from bulk materials [35]. Recently, many chemical and physical methods are used for synthesis of inorganic nanoparticles but these methods are toxic, costly and non-eco-friendly. On the other hand biological methods are non-toxic and eco-friendly [3]. So there is need to develop biosynthesis strategies which are easy to scale up, simple, cost-effective and environment friendly..

To survive in toxic metal environment conditions microbes are involved in mechanisms to transform toxic metal forms to their corresponding non-toxic forms such as metal sulfide/oxides [34]. Bacteria, yeasts, fungi, algae and plants could be used for the synthesis of nanoparticles among these bacteria are significant as these are easy to culture and produce extracellular nanoparticle [32,33,42]. They require mild experimental conditions like pH, temperature and have easy downstream processing and short generation time for nanoparticle synthesis [39].

* Corresponding author.

E-mail address: kavyashreejoshi@gmail.com (K.B. Joshi).



Fig. 1. (a) Sample collection; (b) Isolation.

Table 1
Antibacterial activity of silver nanoparticles against *Xanthomonasaxonopodis*.

Sr. No.	Sterile Broth (ml)	Ag Nanoparticle solution (ml)	O.D. at 600 nm at 0 min	O.D. at 600 nm after 24 h	Number of colonies
1	2	1	0.063	0.018	79
2	2	2	0.028	0.087	29
3	2	3	0.021	0.075	00
4	2	4	0.062	0.062	00
5	2	5	0.054	0.053	00
SD	±949.84				
SE	±424.78				

Table 2
Antibacterial activity of copper nanoparticles against *Xanthomonasaxonopodis*.

Sr. No.	Concentration of CuSO4 (ppm)	Sterile Broth (ml)	Culture (µl)	Number of colonies observed
1	5	5	200	0
2	10	5	200	0
3	15	5	200	0
4	20	5	200	0
5	25	5	200	0
6	Control	5	200	37

Copper nanoparticles has gained attention because of its unique properties and applications [9,12,14], such as, lubricants [50], thermal transfer nanofluids [35], nanocomposite coatings [23] electronic materials [29], catalysts [31]. Copper nanoparticles (CuNPs) has applications in antibiotic treatment which have been shown significant antibacterial property to *Escherichia coli* and *Bacillus subtilis* [46].

Nanoparticles bound to the cell wall results in death of pathogen. Copper based fungicides produce highly reactive hydroxyl radicals to damage lipids, proteins, DNA and other biomolecules. Therefore CuNPs play an important role in disease prevention and management of variety of crop diseases [46].

Among several nanomaterials, silver nanoparticles (AgNPs) are widely used in the field of nanotechnology [41]. Nanosilver is one of the nanomaterials with the highest degree of commercialization [41] and silver has physiochemical properties such as conductivity, chemical stability, and catalytic and antibacterial activities [7,54]. Because of their unique properties and high surface area to volume ratio, AgNPs are widely used as antibacterial agents in the health industry, food storage [11], textile coating

[59] and a number of environmental [7,54,2] antiangiogenic [20] and as anticancer agents [55].

Metal nanoparticles are widely used because of their unique properties and applications in catalysis, photonics, optoelectronics, biological tagging, agriculture and pharmaceuticals. Their performance depends critically on their size, shape, reducing agents and composition. Biologically synthesized AgNPs have biocompatibility, stability, high solubility, and high yield without aggregation. Therefore, the synthesis of nanomaterials using biological methods is a simple, nontoxic and more environmentally friendly than chemical methods, which are expensive and hazardous to living organisms [20,21,55]. Many natural resources are available for the environment friendly synthesis of nanoparticles, such as plants, plant products, bacteria, fungi, algae, yeast, and viruses [20,21,55]. Interestingly, biological molecules can serve as both reducing and capping agents for nanoparticle synthesis. Capping agents are essential for preventing nanoparticle aggregation and increasing solubility of the nanosystem, and they can also be used as a site for bioconjugation of the nanoparticle with important molecules [48,53]. Stabilization of nanoparticles can be achieved

by adding capping agents, which bind to the nanoparticle surface via covalent bonds or chemical interactions [59]. Thus, biologically prepared nanomaterials are extremely valuable because nanoparticles can be coated with a lipid or protein layer that confers physiological solubility and stability which is critical.

Considering importance of nanotechnology in plant disease management the present investigation is planned to study the role of copper, silver and hydrogen peroxide against *Xanthomonas axonopodis* bacterial blight of pomegranate.

2. . Materials and methods

2.1. Isolation and purification of the pathogen

The infected parts of the pomegranate showing bacterial blight diseases symptoms were collected in sterile plastic bags from different locality pomegranate orchard in Pravara area. Infected portions along with small portions of healthy tissue were cut into 5 mm bits. These bits were further surface sterilized with 0.1 per cent HgCl_2 for 1 min and washed thoroughly with sterile distilled water three times. The surface sterilize bits were then crushed in 2 to 3 ml sterile distilled water and allowed to diffuse for 5 to 10 min at room temperature. A loop full leachate was streaked on Nutrient Agar medium (NA) / Yeast Dextrose Calcium Carbonate Agar medium (YDCA) plates aseptically and incubated at 30 ± 1 °C temperature for 48 h. The colonies grown within 72 h were picked and again streaked on fresh Nutrient Agar plates. The discrete colonies were sub cultured on nutrient agar slants for further studies [40].

The isolated bacterial colonies were further picked up with the sterilized inoculation loop and streaked on the surface of sterilized NA medium petri plates [46]. The inoculated plates were incubated at 30 °C for 72 h. Observations were noted for the developed well-separated typical, bright yellow, mucoid colonies. These pure colonies were further streaked onto the NA medium slants and incubated at 30 °C for 72 h. The pure cultures slants were stored in the refrigerator at 5 °C, as a stock culture for further studies. In long-term storage, the culture preserved in 70 per cent glycerol and kept at -4 °C.

2.2. Identification of the pathogen

The bacterial blight pathogen *X. axonopodis* was identified on the basis of morphological, biochemical characteristics of the pathogen.

2.3. Morphological characterization

The morphological characteristics of the pathogen like, cell shape, gram reaction, pigmentation, growth characters were observed to identify pathogen [4,22,47].

2.4. Biochemical characterization

The bacterial isolates from the different locality were tested to various biochemical tests viz citrate test, starch hydrolysis, lysine utilization, urease production, phenylalanine deamination, nitrate reduction, H_2S production, and carbohydrates utilization with the standard protocols of Hi media KB 002 Hi Assorted TM biochemical test kit. The KOH solubility test, indole production test were done [47].

2.5. Synthesis of Silver Nanoparticles

Silver nitrate was used as a precursor for the synthesis of silver nanoparticles. 5 ml of 1 mM AgNO_3 (99.99 %) aqueous solution was added with 100 ml of *Trichoderma* in 250 ml conical flask at room temperature. The flask was put into shaker (150 rpm) at 30 °C and reaction was carried out for a period of 72 h [43–45].

2.6. Characterization of Nanoparticles:

After addition of Ag⁺ ions plant extract mixture will turn into brownish colour with in four hours [36–38].

2.7. UV-visible spectroscopy analysis

The colour change in reaction mixture was recorded through visual observation. The bioreduction of silver ions in aqueous solution was monitored by periodic sampling of aliquots (1 ml) and subsequently measuring UV-vis spectra of the solution. UV-vis spectra of these aliquots were monitored as a function of time of reaction on UV-vis spectrophotometer operated at a resolution of 1 nm.

2.8. Synthesis and characterization of copper nanoparticles

2.8.1. Trichoderma biomass production

Trichoderma harzianum procured from the agricultural biotechnology college Loni further it was grown on PDA plates to develop fresh culture. To develop biomass for synthesis of nanoparticle young mycelia were inoculated in 500 ml PDA liquid medium and incubated in an orbital shaker at 24 ± 2 °C at speed 150 rpm^{-1} for 72 hr in dark. 10 g of mycelium biomass was harvested with a plastic sieve, washed with sterile double distilled water to remove medium components traces. The 10g biomass was inoculated in 150 ml sterile double distilled water in 500 ml flask and incubated for 48 h at 22 °C in orbital shaker. After incubation, the fungal biomass was filtered through Whatman filter paper to collect cell free culture filtrate (CFCF) [10].

2.8.2. Synthesis of copper nanoparticles

CuSO_4 was added in 50 ml CFCF to make a final concentration 1–2 mM and incubated in orbital shaker at 100 rpm in dark at 45 °C. Synthesis of copper nanoparticles indicated change in colour of solution [51,52]. The CFCF without copper sulphate and 1–2 mM of metal salt in deionized water, were kept as controls for comparison. The nanoparticles were separated by centrifugation, at 8000 rpm^{-1} for 10 min, washed twice with double distilled water and lyophilized. Lyophilized NPs were stored in polypropylene tubes in dark at room temperature [17].

2.9. Antibacterial activity of silver and copper nanoparticles against *X. Axonopodis*

Antibacterial activity was tested on *X. axonopodis* by spread plate method. The reaction mixture was prepared by taking 2 ml broth, 1 ml silver nanoparticles to 5 ml, 200 l *X. axonopodis* culture. Sterilized NAS medium plates were prepared and 200 l l reaction mixture was spread on sterile medium plates. Plates were incubated for 24 h.

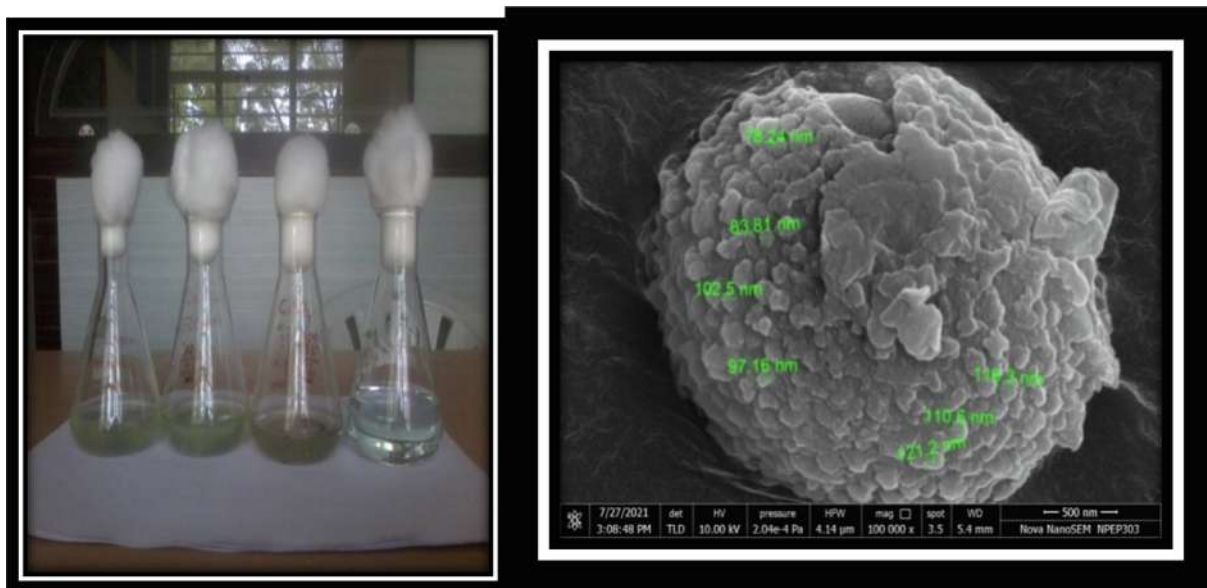


Fig. 2. (a) Biosynthesis of CuNP; (b) SEM ForCuNP.

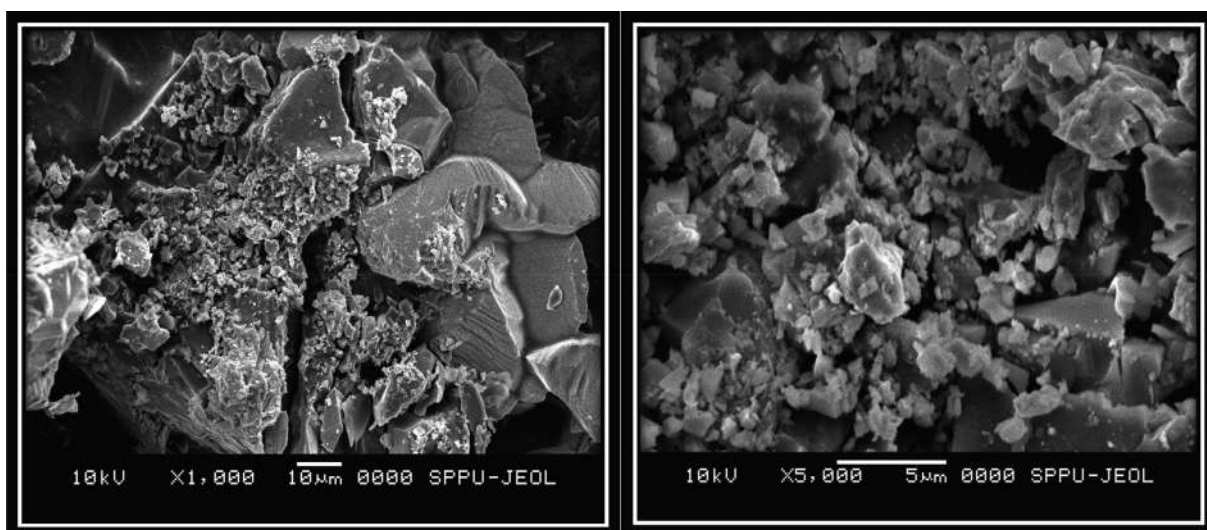


Fig. 3. Scanning Electron Microscopy of AgNP.

3. Results and discussion

3.1. Isolation and characterization of pathogen

The morphological and biochemical characteristics tests were used to identify pathogen. Morphologically all the isolated strains showed light to pale yellow colour, profuse slimy smooth growth. Further characterization through a biochemical tests proved Gram negative reaction, positive to citrate utilization, starch hydrolysis, KOH solubility and lysine utilization etc., inconformity with past findings [29,40,5].

3.2. Synthesis of copper nanoparticle

Colour of copper metal salts in CFCF solution was changed from blue to dark green. This change in colour (Plate 1) indicated synthesis of copper nanoparticles. The UV-vis absorption spectrum of CuNPs CFU solution showed distinct absorption peak in the region

of 550–650 nm also confirmed synthesis of CuNPs in agreement with past report [42].

3.3. Characterization of copper nanoparticle

Scanning electron microscopy (SEM) of CuNP showed that particle size within range of 1–100 nm. The SEM showed number of aggregates. The morphology of the nanoparticles was highly variable.

3.4. Synthesis of silver nanoparticle

Study with attempt synthesized AgNPs with controlled particle size, using *Trichoderma virida* extracts as reducing and stabilizing agents with optimized conditions [19,59]. The change in color of the reaction mixture from colorless to brown confirms biosynthesis of AgNPs with reports Lekshmi, *et al.*, (2012). The UV-vis spectra recorded from the reaction vessel at different times of reaction

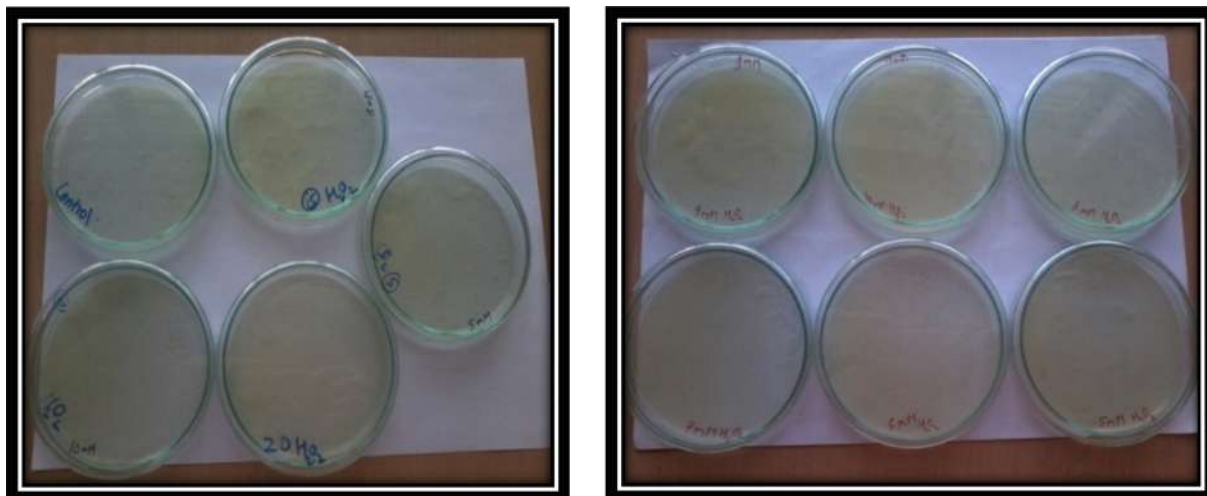


Fig. 4. Synergistic Effect of AgNP; Cu NP and Hydrogen Peroxide.

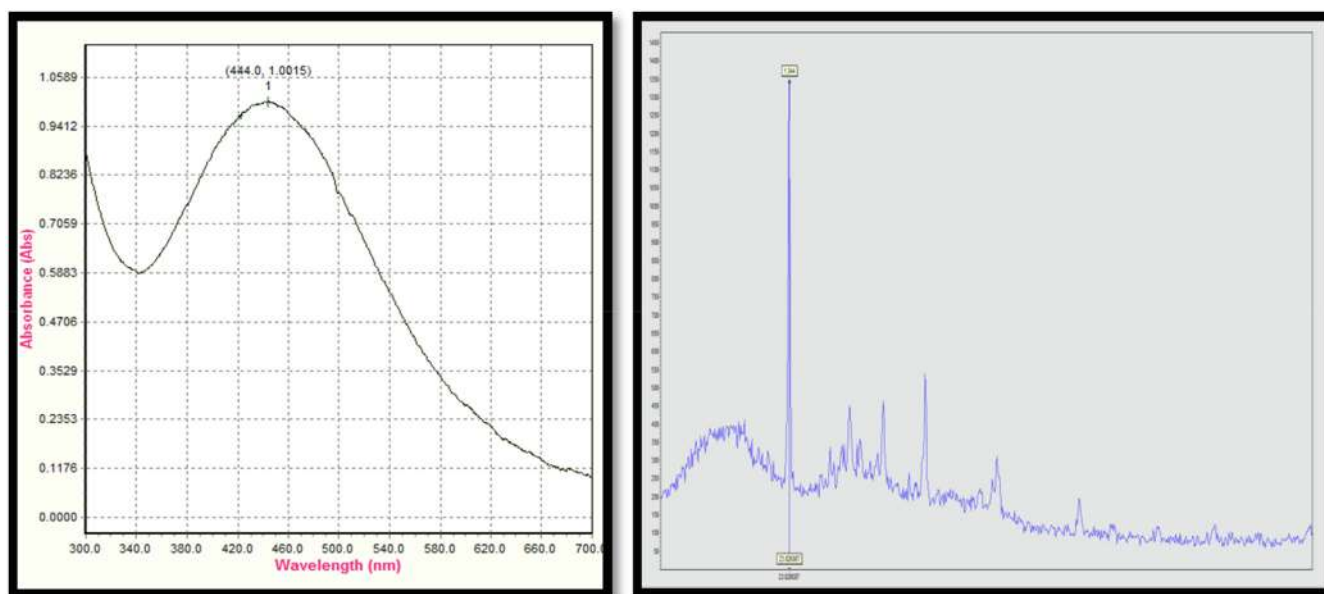


Fig. 5. (a) UV-spectroscopy characterization of AgNP; (b) XRD pattern of biogenic synthesized silver nanoparticles.

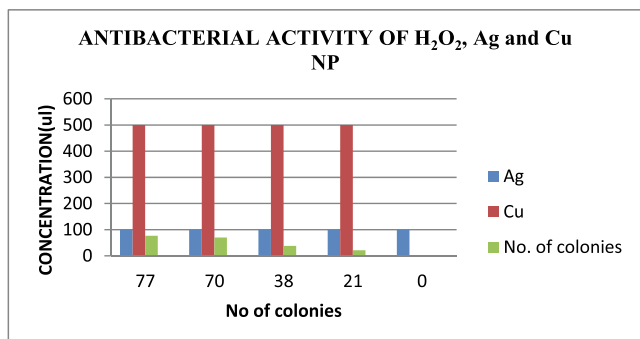


Fig. 6. Antibacterial Activity of H₂O₂, Ag and Cu NP.

(2.0786) and 397 nm (2.2080) for AgNPs synthesised and colour change; colourless to brown. UV-visible spectroscopy of silver nanoparticles characterized by UV visible spectrometer at resolution 300 to 600 nm. proved strong surface plasmon resonance centered at 422 nm clearly indicates an increased in intensity with time and stability proved synthesis of silver nanoparticles. (Fig. 2). The metal particles stability in solution was up to two years. Absorption peak of silver nanoparticles at 414–420 nm [18] at 414–420 nm with increased intensity up to 72 hr. [26] at 420 nm [15] at 440 nm [49] and at 380,400–420 nm [15]. SEM micrograph recorded from the silver nanoparticles showed tetrahedral shape, size in the range the 5–10 nm. The SEM shows complex nanoparticles as well as number of aggregates. The morphology of the nanoparticles was highly variable and was not single. Past reports also reported variable size of AgNPs 5–40 nm [18,26], 5–50 nm and 28 nm [8]. Fig. 3. Fig. 4. Fig. 5. Fig. 6..

Result summarized in table 1 support that AgNP solution at 3 l M proved inhibitory for *Xanthomonas axonopodis*, however table

were plotted [53]. The UV-Spectroscopic analysis showed peak at 399 nm (2.012) and at 394 nm (2.022) [24,25,27,28,30] also observed strong but broad, surface plasmon peak at 399 nm

Table 3
Synergistic Antibacterial activity of H₂O₂, Ag nanoparticles and Cu nanoparticles against *Xanthomonas axonopodis*.

Sr. No	Conc. of H ₂ O ₂ (mM)	Conc. of Ag NP (μM)	Conc. of Cu NP (ppm)	Incubation (min)	Number of colonies
1	1	1	1	10	77
2	2	1	2	10	70
3	3	1	3	10	38
4	4	1	4	10	21
5	5	1	5	10	0
6	Control	0	0	10	Luxuriant growth
SD	±764.56				
SE	±341.925				

2 proved that 5 ppm CuNP concentration is significantly inhibitory for *X. axonopodis*.

Results summarized in table for antibacterial activity of CuNP showed that no colonies were recorded even at 5 ppm concentration. For silver nanoparticles, results showed that 1 μM concentration showed zero colony growth 56–58,60,61.

From the result summarized in Table 3, it was found that as the concentration of H₂O₂ increases in combination with Ag, Cu nanoparticles, 1 μM and 5 ppm respectively at 5 min decrease in number of colonies. This confirmed that 5 mM concentration of H₂O₂ in combination with Ag and Cu nanoparticles will be effective at specific time period of incubation. Therefore, to standardize specific time period of incubation, time period was increased to 10 min. (Table 3). Result summarized in table 3 proved that 5 Mm concentration of H₂O₂ in combination with 1 μM Ag NP and 5 ppm Cu NP was significantly effective at 10 min incubation.

4. Conclusion

Foliar spray and drenching of silver nanoparticles at 1 μM concentration, copper nanoparticles at 5 ppm concentration and hydrogen peroxide at 5 mM concentration in combination significantly effective to control bacterial blight of pomegranate.

CRedit authorship contribution statement

Kavyashri B. Joshi: Conceptualization, Methodology, Software, Validation, Formal analysis, Investigation, Data curation, Writing – original draft, Visualization, Funding acquisition. A.M. Bhosale: Conceptualization, Validation, Formal analysis, Investigation, Resources, Data curation, Writing – original draft, Writing – review & editing, Visualization, Supervision, Project administration, Funding acquisition. M.N. Kharde: Conceptualization, Validation, Resources, Writing – original draft, Writing – review & editing, Visualization, Supervision, Project administration, Funding acquisition.

Declaration of Competing Interest

The authors declare that they have no known competing financial interests or personal relationships that could have appeared to influence the work reported in this paper.

Acknowledgement

Authors would like to thank Principal, Dr.Dighe ,P.V.P. College, Pravaranagar and Department of Biotechnology , P.V.P. College , Pravaranagar Loni for providing necessary facilities during the experiment and Central Instrumentation facility, Savitribai Phule University of Pune for providing facilities.

Declaration of Conflict of Interest.

The authors declare that they have no known conflict of interest or personal relationships that could have appeared to influence the work reported in this paper.

References

- [1] C.V. Ambadkar, A.S. Dhawan, V.A. Shinde, Integrated management of bacterial blight disease (oily spot) of pomegranate caused by *Xanthomonas axonopodis* pv.punica, *Int. J. Plant Sci.* 10 (1) (2015) 19–23.
- [2] K.J.P. Anthony, M. Murugan, S. Gurunathan, Biosynthesis of silver nanoparticles from the culture supernatant of *Bacillus marisflavi* and their potential antibacterial activity, *J IndEngChem* 20 (4) (2014) 1505–1510.
- [3] K.C. Anyaogu, A.V. Fedorov, D.C. Neckers, Synthesis, characterization, and antifouling potential of functionalized copper nanoparticles, *Langmuir* 24 (8) (2008) 4340–4346.
- [4] J.F. Bradbury, Isolation and preliminary study of bacteria from plants, *Review of PlantPathology.* 49 (1970) 213218.
- [5] R. Chand, R. Kishun, Studies on bacterial blight (*Xanthomonas campestris* sp. *Punicae*) of pomegranate, *Indian Phytopath* 44 (1991) 370–371.
- [6] P.S. Chandran, M. Chaudhary, R. Pasricha, A. Ahmad, M. Sastry, Synthesis of gold nanotriangles and silver nanoparticles using Aloe vera plant extract, *Biotechnol. Prog.* 22 (2006) 577–583.
- [7] X. Chen, H.J. Schluesener, Nanosilver: a nanoparticle in medical application, *Toxicol. Lett.* 176 (1) (2008) 1–12.
- [8] K. Chitra, Annadurai, Bioengineered silver nanobowles using Trichodemaviride and its antibacterial activity against gram-positive and gram-negative bacteria, *J. Nanostruct. Chem.* 3 (9) (2013).
- [9] N. Cioffi, L. Torsi, N. Ditaranto, G. Tantillo, L. Ghibelli, L. Sabbatini, T. Blev-Zacheo, M. D-Alessio, P.G. Zamboni, E. Traversa, Copper nanoparticle / polymer composites with antifungal and bacteriostatic properties, *Chem. Mater* 17 (2005) 5255–5262.
- [10] C.V. Fabiana, A. Torres Nicolini, V.A. Alvarez, Mycosynthetized Ag, CuO and ZnO nanoparticles from a promising Trichodemaharizianum strain and their antifungal potential against important phytopathogens, *Scientific Report* 10 (2020) 20499.
- [11] M. Cushen, J. Kerry, M. Morris, M. Cruz-Romero, E. Cummins, Evaluation and simulation of silver and copper nanoparticle migration from polyethylene nanocomposites to food and an associated exposure assessment, *J. Agric. Food Chem.* 62 (6) (2014) 1403–1411.
- [12] R. De Lima, A.B. Seabra, N. Durán, Silver nanoparticles: a brief review of cytotoxicity and genotoxicity of chemically and biogenically synthesized nanoparticles, *J. Appl. Toxicol.* 32 (11) (2012) 867–879.
- [13] D. Condolle, A. Origine of cultivated plants, Halfner publishers, New York; 1967, 648 pp.
- [14] Demonstration of model pomegranate practices for effective management of bacterial blight disease, *Project report ICAR*, Jan 2014–March 2017.
- [15] D. Prameela, S. Kulanthival, D. Kamil, J. Borah, N. Prabhakaran, N. Srinivasa, Biosynthesis of silver nanoparticle from Trichoderma species, *IJEB* 51 (2013) 543–547.
- [16] D.G. Dhandar, P. Nallathambi, R.D. Rawat, D.M. Sawant, Bacterial leaf and fruit spot-A new threat to pomegranate orchards in Maharashtra, *J. Mycol. Plant Pathol.* 34 (2004) 971.
- [17] J.A. Eastman, S.U.S. Choi, S. Li, W. Yu, L.J. Thompson, Anomalously increased effective thermal conductivities of ethylene glycol-based nanofluids containing copper nanoparticles, *Appl. Phys. Lett.* 78 (2001) 718–720.
- [18] M. Fayaz, C. Tiwary, P. Kalaichelvan, R. Venkatesan, Blue and orange light emission from biogenic synthesized silver nanoparticles using *Trichodemaviride*, *Colloids and Surface B: Biointerfaces* 75 (Elsevier) (2010) 175–178.
- [19] R. Foldbjerg, D.A. Dang, H. Autrup, Cytotoxicity and genotoxicity of silver nanoparticles in the human lung cancer cell line, A549, *Arch Toxicol* 85 (7) (2011) 743–750.
- [20] S. Gurunathan, K.J. Lee, K. Kalishwaralal, S. Sheikpranbabu, R. Vaidyanathan, S. H. Eom, Antiangiogenic properties of silver nanoparticles, *Biomaterials*, 30 (31) (2009) 6341–6350.
- [21] S. Gurunathan, J. Raman, S.N. AbdMalek, P.A. John, S. Vikineswary, Green synthesis of silver nanoparticles using *Ganoderma neo-japonicum* Imazeki: a

- potential cytotoxic agent against breast cancer cells, *Int. J. Nanomed.* 8 (2013) 4399–4413.
- [22] M.K. Hingorani, Mehta, Bacterial leaf spot of pomegranate, *Indian Phytopath.* 5 (1952) 55–56.
- [23] M.K. Hingorani, N.J. Singh, *Xanthomonas* sp. Nov. on *Punicagranatum* L. *Xanthomonas* sp. Nov. on *Punicagranatum* L., *Indian J. Agric. Sci.* 29 (1959) 45–48.
- [24] J. Huang, Q. Li, D. Sun, Y. Lu, Y. Su, X. Yang, H. Wang, Y. Wang, W. Shao, N. He, J. Hong, C. Chen, Biosynthesis of silver and gold nanoparticles by novel sundried *Cinnamomum camphora* leaf, *Nanotechnology* 18 (2007) 105104–105114.
- [25] J. Kasthuri, K. Kathiravan, N. Rajendiran, Phyllanthin-assisted biosynthesis of silver and gold nanoparticles: a novel biological approach, *J. Nanopart. Res.* 11 (2009) 1075–1085.
- [26] V. Khabat, G. Mansoori, S. Karimi, Biosynthesis of silver nanoparticle by Fungus *Trichoderma Reesei*, *Insci. J.* 1 (1) (2011) 65–79.
- [27] M. Kowshik, S. Ashtaputre, S. Kharrazi, W. Vogel, J. Urban, S.K. Kulkarni, K.M. Paknikar, Extracellular synthesis of silver nanoparticles by a silver-tolerant yeast strain MKY3, *Nanotech* 14 (2003) 95–100.
- [28] C. Krishnaraj, E.G. Jagan, S. Rajasekar, P. Selvakumar, P.T. Kalaichelvan, N. Mohan, Synthesis of silver nanoparticles using *Acalypha indica* leaf extracts and its antibacterial activity against water borne pathogens, *Colloids Surf. B: Biointerfaces* 76 (2010,) 50–56.
- [29] F.E. Kruijs, H. Fissan, A. Peled, Synthesis of nanoparticle in the gas phase for electronic, optical and magnetic applications a review, *J. Aerosol. Sci.* 29 (1998) 511–535.
- [30] N.C.J. Lekshmi, S. Packia, S. BenarcinSumi, S.J. Viveka, J. Raja Brindha, Antibacterial activity of nanoparticles from *Allium* sp., *J. Microbiol. Biotech. Res.* 2 (1) (2012) 115–119.
- [31] M.E. Lyn, DanYang Ying, Drying model for calcium alginate beads, *Ind. Eng. Chem* 49 (2010) 19861990.
- [32] P. Mukherjee, A. Ahmad, D. Mandal, et al., Fungus-mediated synthesis of silver nanoparticles and their immobilization in the mycelial matrix: a novel biological approach to nanoparticle synthesis, *Nano Lett* 1 (10) (2001) 515–519.
- [33] K.B. Narayanan, N. Sakthivel, Coriander leaf mediated biosynthesis of gold nanoparticles, *Mater. Lett.* 68 (2008) 4588–4590.
- [34] A.G. Nasibulin, P.P. Ahonen, O. Richard, E.I. Kauppinen, I.S. Altman, Copper and copper oxide nanoparticle formation by chemical vapor nucleation from copper (II) acetylacetonate, *J. Nanopart. Res.* 3 (2001) 383–398.
- [35] D.H. Neis, Heavy-metal resistance, *Appl. Microbiol. Biotechnol.* 51 (1999) 730–750.
- [36] R.Y. Parikh, S. Singh, L.V. Prasad, M.S. Patole, M. Sastry, Y.S. Souche, Extracellular synthesis of crystalline silver nanoparticles and molecular evidence of silver resistance from *Morganella* sp. towards understanding biochemical synthesis mechanism, *Chem. BioChem* (2008) 1415–1422.
- [37] D. Philip, Green synthesis of gold and silver nanoparticle using *Hibiscus rosasinensis*, *Phys. E* 42 (2010) 1417–1424.
- [38] D. Philip, Honey mediated green synthesis of silver nanoparticles, *Spectrochim. Acta Part A* 75 (2010) 1078–1081.
- [39] A.A. Ponce, K.J. Klabunde, Chemical and catalytic activity of copper nanoparticles prepared via metal vapour synthesis, *J. Mol. Catal. A* 225 (2005) 1–6.
- [40] K.S. Raghuvanshi, B.A. Hujare, V.P. Chimote, S.G. Borkar, Characterization of *Xanthomonas axonopodisp. punicae* isolates from western Maharashtra and their sensitivity to chemical treatments, *Bio scan.* 8 (3) (2013) 845–850.
- [41] B. Reidy, A. Haase, A. Luch, K.A. Dawson, I. Lynch, Mechanisms of silver nanoparticle release, transformation and toxicity: a critical review of current knowledge and recommendations for future studies and applications, *Materials* 6 (6) (2013) 2295–2350.
- [42] Shantkriti, P. Rani, Biological synthesis of Copper nanoparticles using *Pseudomonas fluorescens*, *Int. J. Curr. Microbiol. Appl. Sci.* 3 (9) (2014) 374–383.
- [43] M. Sastry, A. Ahmad, M.I. Khan, R. Kumar, Biosynthesis of metal nanoparticles using fungi and actinomycetes, *Curr. Sci.* 85 (2003) 162170.
- [44] M. Sathishkumar, K. Sneha, Y.S. Yun, Immobilization of silver nanoparticles synthesized using *Curcuma longatuber* powder and extract on cotton cloth for bactericidal activity, *Bioresour. Technol.* 101 (2010) 7958–7965.
- [45] M. Sathishkumar, K. Sneha, W.S. Won, C.W. Cho, S. Kim, Y.S. Yun, Cynamonzeilanicum bark extract and powder mediated green synthesis of nanocrystalline silver particles and its bactericidal activity, *Colloids Surf. B: Biointerfaces* 73 (2009) 332–338.
- [46] N.W. Schaad, S.R.E. *Xanthomonas*, Laboratory Guide for Identification of Plant Pathogenic Bacteria, *Am. Phyto Pathol. Soc.* (1988) 81–94.
- [47] N.W. Schaad, Laboratory Guide for Identification of Plant Pathogenic Bacteria, Second Ed., Lucknow, International Book Distributing Co, 1992, p. 165.
- [48] A.B. Seabra, N. Durán, Nitric oxide-releasing vehicles for biomedical applications, *J. Mater. Chem.* 9 (2010) 1624–1637.
- [49] S.S. Shankar, A. Rai, A. Ahmad, M. Sastry, Controlling the optical properties of lemongrass extract synthesized gold nanotriangles and potential application in infrared-absorbing optical coatings, *Chem. Mater.* 17 (2005) 566–572.
- [50] L. Shaobin, H. Ming, H. Tingying, W. Ran, J. Rongrong, W. Jun, W. Liang, K. Jing, C. Yuan, Lateral Dimension-Dependent Antibacterial Activity of Graphene Oxide Sheets, *ACS Nano* 28 (12364) (2012) 12372.
- [51] N.C. Sharma, S.V. Sahi, S. Nath, J.G. Parsons, J.L. GardeaTorresdey, T. Pal, Synthesis of plantmediated gold nanoparticles and catalytic role of biomatrix embedded nanomaterials, *Environ. Sci. Technol.* 41 (2007) 5137–5142.
- [52] G. Shelar, A. Chavan, Myco-synthesis of silver nanoparticle from *Trichoderma harzianum* and its impact on germination status of oil seed, *Biolife* 3 (1) (2015) 109–113.
- [53] S. Singh, P. Patel, S. Jaiswal, A.A. Prabhune, C.V. Ramana, B.L.V. Prasad, A direct method for the preparation of glycolipid-metal nanoparticle conjugates: sophorolipids as reducing and capping agents for the synthesis of water redispersible silver nanoparticles and their antibacterial activity, *New J. Chem.* 33 (3) (2009) 646–652.
- [54] I. Sondi, B. Salopek-Sondi, Silver nanoparticles as antimicrobial agent: a case study on *E. coli* as a model for Gram-negative bacteria, *J. Colloid Interface Sci.* 275 (1) (2004) 177–182.
- [55] M.I. Sriram, S.B. Kanth, K. Kalishwaralal, S. Gurunathan, Antitumor activity of silver nanoparticles in Dalton's lymphoma ascites tumor model, *Int. J. Nanomed.* 5 (2010) 753–762.
- [56] S. Tarasov, A. Kolubaev, S. Belyaev, M. Lerner, F. Tepper, Study of friction reduction by nanocopper additives to motor oil, *Wear* 252 (2002) 63–69.
- [57] K.N. Thakkar, S.S. Mhatre, R.Y. Parikh, Biological synthesis of metallic nanoparticles, *Nanomedicine* 6 (2) (2010) 257–262.
- [58] A. Vilchis-Nestor, V. Sanchez-Mendieta, M. Camacho-Lopez, R. Gomez-Espinosa, M. Camacho-Lopez, J. Arenas-Alatorre, Solventless synthesis and optical properties of Au and Ag nanoparticles using *Camellia sinensis* extract, *Mater. Lett.* 62 (2008) 3103.
- [59] T. Walsler, E. Demou, D.J. Lang, S. Hellweg, Prospective environmental life cycle assessment of nanosilver T-shirts, *Environ. Sci. Technol.* 45 (10) (2010) 4570–4578.
- [60] X. Liu, W.P. Cai, H.J. Bi, Optical absorption of copper nanoparticles dispersed within pores of monolithic mesoporous silica, *J. Mater. Res.* 17 (5) (2002) 1125–1128.
- [61] Y. Xuan, Q. Li, Heat transfer enhancement of nanofluids, *Int. J. Heat. Fluid. Flow.* 21 (2000) 58–64.



Acoustic, volumetric and viscometric study relative to inter-molecular interaction in aqueous $\text{KIO}_3 + 1\% \text{KH}_2\text{PO}_4$

Meenakshi Rathi

Department of Chemistry, RNC Arts, JDB Commerce, NSC Science College, Nasik Road, Nasik 422101, Maharashtra, India

ARTICLE INFO

Article history:

Available online 24 September 2022

Keywords:

KIO_3
Jones-Dole constants
B-coefficient
Adiabatic compressibility
Masson's Constant

ABSTRACT

This research paper comprises of the effect of temperature and concentration on the acoustic volumetric and viscometric properties viz. ultrasonic velocity, density and viscosity of aqueous KIO_3 solutions in 1% KH_2PO_4 . The research findings is quite useful to expound the various inter molecular interactions like ion-ion, ion-solvent, and solvent-solvent between the chosen solute-solvent system. Based on the data obtained, various derived acoustical parameters viz. acoustic impedance (Z), adiabatic compressibility (β), intermolecular free length (Lf), free volume (Vf), Rao's constant (R), Wada's constant (W), density dependent apparent molar volumes (ϕ_v) viscosity dependent viscosity B-coefficients for KIO_3 solutions in aqueous 1% KH_2PO_4 and pure water system have been determined at 298.15 to 313.15 K. Additionally Masson's constants, Jones-Dole constants are supported to study various molecular interactions. Copyright © 2022. Elsevier Ltd. All rights reserved.

Selection and peer-review under responsibility of the scientific committee of the Integrative Nanotechnology Perspective for Multidisciplinary Applications - 2022.

1. Introduction

KIO_3 is a colourless crystalline solid that is widely used as an oxidising agent while Potassium dihydrogen phosphate, KDP (KH_2PO_4) is the inorganic compound. Both are used in many different applications such as a food ingredient, fertiliser, and fungicide. [3 25]. Potassium iodate is occasionally used as a flouring agent in baking, [21], also used as a source for dietary iodine. It is also found in certain formula milk that is marketed to babies. [7] KDP can be found in energy drinks, coffee creamers, cheddar cheese, and low-sodium foods..It supplies potassium and phosphorus nutrients. Incorporating the current research into multiple applications like the solutes for medical, food, and agricultural science encourages us to carry on the current investigation.

In food, medicine, and pesticide industries, molecular and ionic interactions of oxidising agents in presence of aqueous salts plays a vital role. The ion-water interactions in understanding the effects of oxidising agents, particularly their temperature dependence [17 30,19]. The information gained from ultrasonic propagation parameters in liquid mixtures and solutions, such as ultrasonic velocity and its variation with concentration of one of the compo-

nents, aids in better understanding of how molecular interactions in a mixture affect each other and provides a way to test theories dealing with liquid structure. The transport and acoustic data will be very useful to understand solvolysis behaviour and ion-molecular interaction [6] of KIO_3 in used solvent systems.

2. Experimental

2.1. Materials

All chemicals were taken from Sigma Aldrich, Germany, with more than 99% purity and was further desiccated over anhydrous CaCl_2 before use. Tripally distilled water with a specific conductance of $< 10^{-6} \text{ S.cm}^{-1}$ was used for the preparation of solutions at room temperature in a molality range (0.03–0.21) mol.kg^{-1} . The precision of balance used was $\pm 1 \times 10^{-5} \text{ g}$. (See Table 2 Table 3. Table 4. Table 5.).

2.1.1. Measurements of density

Densities of aqueous solutions were determined using a 15 cm^3 double arm pycnometer housed in a transparent glass walled water bath. The pycnometer was calibrated using triple distilled water. The densities of KIO_3 solutions in aqueous 1% KH_2PO_4 , and pure water were measured by bi-capillary pycnometer at dif-

Abbreviations: KDP, Potassium Dihydrogen Phosphate.
E-mail address: meenakship2@gmail.com

Table 1

Molality (m), density (ρ), viscosity(η),ultrasonic velocity (u), acoustic impedance (Z), adiabatic compressibility (β), intermolecular free length (Lf), free volume (Vf), Rao's constant (R), Wada's constant (W), partial molar volume (VΦ) and Relaxation time for the solution of KIO₃ in KH₂PO₄ at 298.15 K and atmospheric pressure.

m, mol kg ⁻¹	ρ kg/m ³	η × 10 ⁻³ Ns m ⁻²	u, m s ⁻¹	Z × 10 ⁻⁵ , kg m ⁻² s ⁻¹	β × 10 ⁻¹⁰ , m ² N ⁻¹	Lf × 10 ⁻¹¹ , m	Vf × 10 ⁶ m ³ mol ⁻¹	R	W × 10 ⁻¹³ m ^{5/7} /N ^{1/7}	VΦ × 10 ⁻⁶ , m ³ mol ⁻¹	Relaxation Time
0.03	1005.18	0.9289	1501.3	15.091	4.437	4.332	1390.756	0.00181	1.2759	3.163	5.4990
0.06	1006.66	0.9349	1512.8	15.229	4.362	4.296	1561.904	0.00195	1.3772	2.979	5.4378
0.09	1008.51	0.9417	1527.7	15.407	4.271	4.251	1677.296	0.00204	1.4422	2.820	5.3628
0.12	1010.73	0.9497	1539.6	15.561	4.197	4.214	1752.351	0.00211	1.4864	2.670	5.3141
0.15	1013.33	0.9592	1548.4	15.690	4.139	4.184	1797.759	0.00215	1.5176	2.535	5.2934
0.18	1016.49	0.9699	1559.7	15.854	4.067	4.148	1830.806	0.00218	1.541	2.425	5.2597
0.21	1018.45	0.9743	1571.3	16.003	3.996	4.111	1873.288	0.00221	1.5612	2.292	5.1907

Table 2

Molality (m), density (ρ), viscosity(η),ultrasonic velocity (u), acoustic impedance (Z), adiabatic compressibility (β), intermolecular free length (Lf), free volume (Vf), Rao's constant (R), Wada's constant (W), partial molar volume (VΦ) and Relaxation time for the solution of KIO₃ in KH₂PO₄ at 303.15 K and atmospheric pressure.

m, mol kg ⁻¹	ρ kg/m ³	η × 10 ⁻³ Ns m ⁻²	u, m s ⁻¹	Z × 10 ⁻⁵ , kg m ⁻² s ⁻¹	β × 10 ⁻¹⁰ , m ² N ⁻¹	Lf × 10 ⁻¹¹ , m	Vf × 10 ⁶ m ³ mol ⁻¹	R	W × 10 ⁻¹³ m ^{5/7} /N ^{1/7}	VΦ × 10 ⁻⁶ , m ³ mol ⁻¹	Relaxation Time
0.03	1003.91	0.8461	1520.8	15.267	4.307	4.307	1610.849	0.00182	1.283	2.880	4.859
0.06	1005.31	0.8516	1534.8	15.429	4.223	4.265	1811.086	0.00196	1.386	2.759	4.795
0.09	1007.11	0.8586	1547.5	15.585	4.146	4.226	1937.609	0.00206	1.450	2.629	4.747
0.12	1009.25	0.8669	1558.6	15.730	4.079	4.192	2018.936	0.00212	1.495	2.532	4.715
0.15	1011.76	0.8767	1571.4	15.899	4.003	4.152	2074.958	0.00216	1.527	2.446	4.679
0.18	1014.76	0.8879	1589.8	16.133	3.899	4.098	2121.895	0.00220	1.553	2.380	4.616
0.21	1016.25	0.8924	1596.3	16.222	3.862	4.079	2158.602	0.00223	1.572	2.320	4.595

Table 3

Molality (m), density (ρ), viscosity(η),ultrasonic velocity (u), acoustic impedance (Z), adiabatic compressibility (β), intermolecular free length (Lf), free volume (Vf), Rao's constant (R), Wada's constant (W), partial molar volume (VΦ) and Relaxation time for the solution of KIO₃ in KH₂PO₄ at 308.15 K and atmospheric pressure.

m, mol kg ⁻¹	ρ kg/m ³	η × 10 ⁻³ Ns m ⁻²	u, m s ⁻¹	Z × 10 ⁻⁵ , kg m ⁻² s ⁻¹	β × 10 ⁻¹⁰ , m ² N ⁻¹	Lf × 10 ⁻¹¹ , m	Vf × 10 ⁶ m ³ mol ⁻¹	R	W × 10 ⁻¹³ m ^{5/7} /N ^{1/7}	VΦ × 10 ⁻⁶ , m ³ mol ⁻¹	Relaxation Time
0.03	1002.64	0.7672	1534.6	15.387	4.235	4.30	1865.751	0.00183	1.288	2.642	4.332
0.06	1004.01	0.7742	1555.3	15.615	4.118	4.250	2102.814	0.00197	1.392	2.547	4.250
0.09	1005.72	0.7824	1568.9	15.779	4.040	4.209	2243.369	0.00207	1.458	2.479	4.214
0.12	1007.75	0.7924	1581.6	15.939	3.967	4.171	2329.952	0.00213	1.503	2.413	4.191
0.15	1010.18	0.8042	1596.5	16.128	3.884	4.127	2386.204	0.00218	1.536	2.359	4.164
0.18	1012.93	0.8177	1610.8	16.316	3.805	4.085	2415.863	0.00222	1.561	2.298	4.148
0.21	1014.25	0.8224	1625.8	16.490	3.730	4.045	2474.348	0.00225	1.583	2.250	4.090

Table 4

Molality (m), density (ρ), viscosity(η),ultrasonic velocity (u), acoustic impedance (Z), adiabatic compressibility (β), intermolecular free length (Lf), free volume (Vf), Rao's constant (R), Wada's constant (W), partial molar volume (VΦ) and Relaxation time for the solution of KIO₃ in KH₂PO₄ at 313.15 K and atmospheric pressure.

m, mol kg ⁻¹	ρ kg/m ³	η × 10 ⁻³ Ns m ⁻²	u, m s ⁻¹	Z × 10 ⁻⁵ , kg m ⁻² s ⁻¹	β × 10 ⁻¹⁰ , m ² N ⁻¹	Lf × 10 ⁻¹¹ , m	Vf × 10 ⁶ m ³ mol ⁻¹	R	W × 10 ⁻¹³ m ^{5/7} /N ^{1/7}	VΦ × 10 ⁻⁶ , m ³ mol ⁻¹	Relaxation Time
0.03	1000.99	0.6834	1558.1	15.596	4.115	4.289	2238.271	0.00184	1.295	2.442	3.750
0.06	1002.38	0.6902	1574.4	15.781	4.025	4.242	2508.292	0.00199	1.399	2.347	3.704
0.09	1004.07	0.7011	1591.9	15.984	3.930	4.191	2664.792	0.00208	1.466	2.267	3.674
0.12	1006.15	0.7128	1610.6	16.205	3.831	4.139	2766.668	0.00215	1.513	2.193	3.641
0.15	1008.55	0.7263	1623.5	16.374	3.762	4.101	2810.691	0.00220	1.546	2.113	3.643
0.18	1011.01	0.7419	1642.4	16.605	3.667	4.049	2837.329	0.00223	1.573	2.056	3.627
0.21	1014.65	0.7624	1665.6	16.900	3.553	3.985	2833.837	0.00226	1.594	2.000	3.611

Table 5

. Masson (ϕ_v⁰, S_v), Moulik(M,K) Jone-Dole (A,B,) Roots(R,S) parameters of of KIO₃ in 1% KH₂PO₄ at different temperatures.

Temperature K	Masson Constant		Jone-Dole's Parameters		Moulik Parameters		Roots Parameter		'β' values
	ϕ _v ⁰	S _v	A (dm ^{3/2} .mol ^{-1/2})	B/ (dm ³ .mol ⁻¹)	K	M	R	S	β
298.15 K	213.4	-12.8	0.28	0.54	71.27	1.08	0.74	-2.36	1.5
303.15 K	213.7	-12.64	0.3	0.47	80.91	1.07	0.73	-2.31	1.7
308.15 K	214.1	-13.12	0.28	1.14	108.8	1.08	0.73	-2.21	2.27
313.15 K	214.9	-12.20	0.29	1.16	142.7	1.07	0.59	-2.36	2.96

ferent temperatures. The density was determined with an accuracy of $\pm 1.28 \times 10^{-4} \text{ g.cm}^{-3}$ using an average of triple measurements. The thermostat temperature is maintained at the desired level using a demerstat with a 0.1 K precision.

2.1.2. Measurement of viscosity

The viscosities of all seven concentration of KIO_3 solutions in aqueous 1 % KH_2PO_4 , were determined using an Ubbelohde viscometer at 298.15, 303.15, 308.15, and 313.15 K. At least three times, measurements were taken to ensure the reproducibility of the results. Viscosity measurements were performed with an overall precision of $\pm 2.5 \times 10^{-4} \text{ mPa.s}$. The flow time is reliably measured at 0.01 s intervals. Before injecting each sample, the equipment was cleaned with distilled water and acetone and thoroughly dried.

2.1.3. Measurement of ultrasonic velocity

The Ultrasonic Interferometer (Model No. F-81, Mittal Enterprises, New Delhi, India) was used at a frequency of 2 MHz to measure the sound velocity in the aqueous systems and aqueous 1 % KH_2PO_4 , systems of KIO_3 . In each case, the measurement was repeated three times, and the accuracy of the sound velocity measurement was found to be within 0.5 m/s.[29]In the end, it all averages out.

2.2. Data evaluation

The data on density and ultrasonic velocity were used to calculate acoustical parameters[30]viz., acoustic impedance (Z), adiabatic compressibility (β), intermolecular free length (Lf), free volume (Vf), Rao's constant (R), Wada's constant (W), and partial molar volume (Vm) by the following equations:[18].

$$1. \text{ Adiabatic compressibility } (\beta) = \frac{1}{u^2 \rho} \text{ Kg}^{-1} \text{ms}^2.$$

u = velocity; ρ = Density of liquid.

$$2. \text{ Specific Acoustic impedance } (Z) = U \times \rho \text{ Kg}^{-1} \text{ms}^{-3}.$$

$$3. \text{ Relative association } (RA) = \left[\frac{\rho}{\rho_0} \right] \left[\frac{U_0}{U} \right]^{1/3}.$$

Where ρ and ρ_0 are the densities of solution and solvent respectively. U and U_0 are the ultrasonic velocities of solution and solvent respectively.

$$4. \text{ Molar compressibility } (W) = \frac{(M, \beta)}{\rho}$$

Where ρ = density, M = Molecular weight, β = adiabatic compressibility.

$$5. \text{ Rao's constant } (R) = \frac{M}{\rho} [U]^{1/2}.$$

Where, M = Molecular Weight, ρ = density.

$$6. \text{ Free volume } (Vf) = [M_{\text{eff}} \cdot U \cdot K \eta]^{1/2} \text{ m}^3,$$

Where M eff = effective molecular weight,

K-temperature independent constant $K = 4.28 \times 10^9$ for all liquid) [21].

$$7. \text{ Intermolecular Free Length } (Lf) = KT \times \sqrt{\beta}.$$

Where, Jacobson's Constant, $KT = (93.875 + 0.375 \times T)$.

The apparent molar volumes \varnothing_V , were obtained from the density results using the following equation [9;48].

$$v = \frac{1000(\rho_0 - \rho)}{C\rho_0} + \frac{M_2}{\rho}$$

Where M_2 , C, ρ and ρ_0 are the molar mass of the KIO_3 , concentration (mol kg^{-1}) and the densities of the solution and the solvent, respectively.

The apparent molar volumes (\varnothing_V) were plotted against the square root of concentration ($C^{1/2}$) in accordance with the Masson's equation [24;41].

$$v = v^0 + S_V \cdot C^{1/2}$$

Where v is the limiting apparent molar volume \varnothing_V^0 and S_V a semi-empirical parameter which depends on the nature of solute, solvent as well as temperature. When v are plotted against molality, the intercept on Y axis and slope gives the values of the apparent molar.

volume, v^0 and S_V respectively.

The viscosity results were plotted in accordance with Jones-Dole equation [11;32].

$$\eta_r - 1 / C^{1/2} = A + BC^{1/2}.$$

Where $\eta_r = (\eta/\eta_0)$ and η , η_0 are viscosities of the solution and solvent respectively, C is the molar concentration.

The B-coefficients were obtained from the linear plots using the least-square fitting method. [14] The A- coefficient reflects solute-solute interaction[5]and the B-coefficient reflect the solute-solvent interactions. Since in general, $A/B \ll 1$, the Jones -Dole equation reduces[30]to,

$$\eta_r = l + \beta \cdot C$$

The relative viscosity data of these solutions have also been fitted in Moulik equation [32],

$$\eta_r^2 = M + K C^2.$$

The density data of these solutions have also been fitted in Root's equation[8],

$$(d - d_0)/C = R - SC^{1/2}$$

Where R and S are constants.

3. Results and discussion

Density (ρ), viscosity(η),ultrasonic velocity (u), acoustic impedance (Z), adiabatic compressibility (β), intermolecular free length (Lf), free volume (Vf), Rao's constant (R), Wada's constant (W), partial molar volume ($V\Phi$) and Relaxation time for the solution of KIO_3 in 1 % KH_2PO_4 solvent systems and different temperatures are reported (See Table-1,2,3 and 4.) Fig. 1, Fig. 2 and Fig. 3 show that the values of densities and viscosities and ultrasonic velocities of KIO_3 solutions under investigation increases with increase in concentration. Similar observations were also made previously [2,12] other solutions. At higher temperatures, the solution shows higher values of the ultrasonic velocity [13].

The positive values of \varnothing_V decrease with concentration in 1 % KH_2PO_4 , and pure water solvent systems. The relative viscosities are found to increase with concentrations.

The apparent molar volumes at infinite dilution ($\varnothing_V^0 = V_2^0$) and slopes S_V , calculated using Masson equation (2) are given in Table-5. The \varnothing_V^0 values of KIO_3 under investigation in 1 % KH_2PO_4 , and in pure water solvent systems are large and positive suggests presence of strong solute-solvent interactions promotes structure making effect. [15] It is clear that the values of \varnothing_V ($\text{m}^3 \cdot \text{mol}^{-1}$) are positive and more or less similar in water and in salt solutions at different temperatures. The slope S_V is negative for KIO_3 solution in 1 % KH_2PO_4 , and in pure water. Since S_V is measure of solute-solute interactions [23]These results indicate that there is presence of strong solute-solute interactions. S_V values do not change systematically with change in temperature, and hence it suggests that the solute-solute interactions are insensitive to change in temperature. [1]. The acoustic impedance is the product of density and ultrasonic velocity (Z).and dependent on both concentration and temperature. Z increases gradually with increase in concentration and temperature. This reveals the structure making action via strong hydrogen bonding. [4] Adiabatic compressibility (β) varies inversely the molality of the solution, at all four studied temperature.(See Fig. 4) [27].This indicates the close packing of the molecules [26]. Values of intermolecular free length (Lf) is the indicator of the interactions between the solute and solvent due

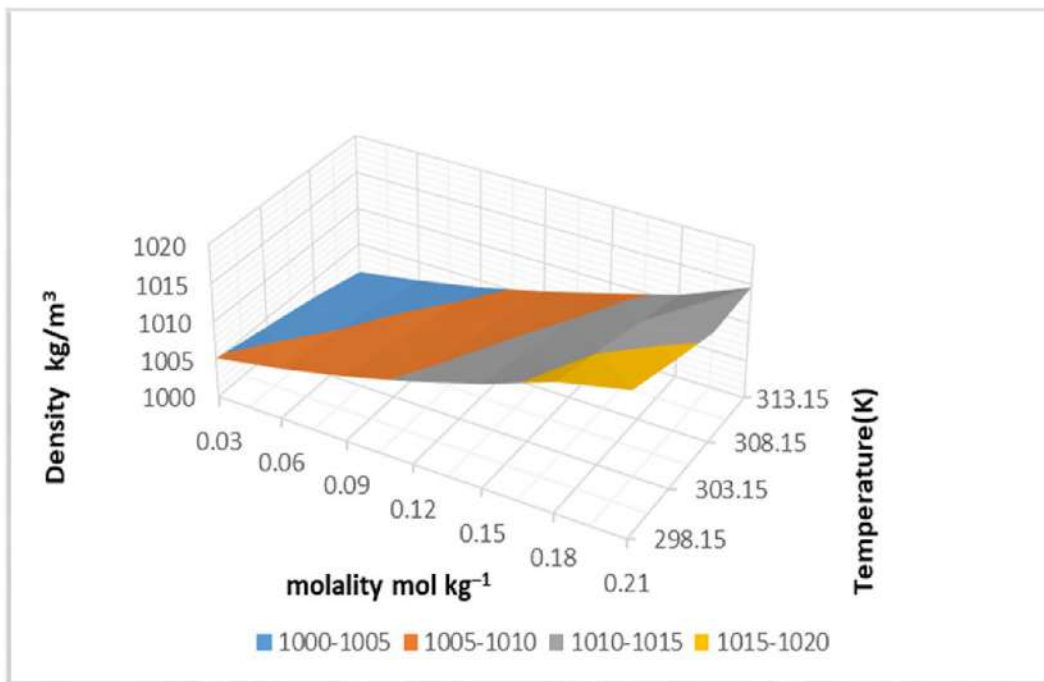


Fig. 1. 3-D plot of Density vs molality (*m*) of KIO₃ in KH₂PO₄ at temperature 298.15 K,303.15 K,308.15 K and 313.15 K.

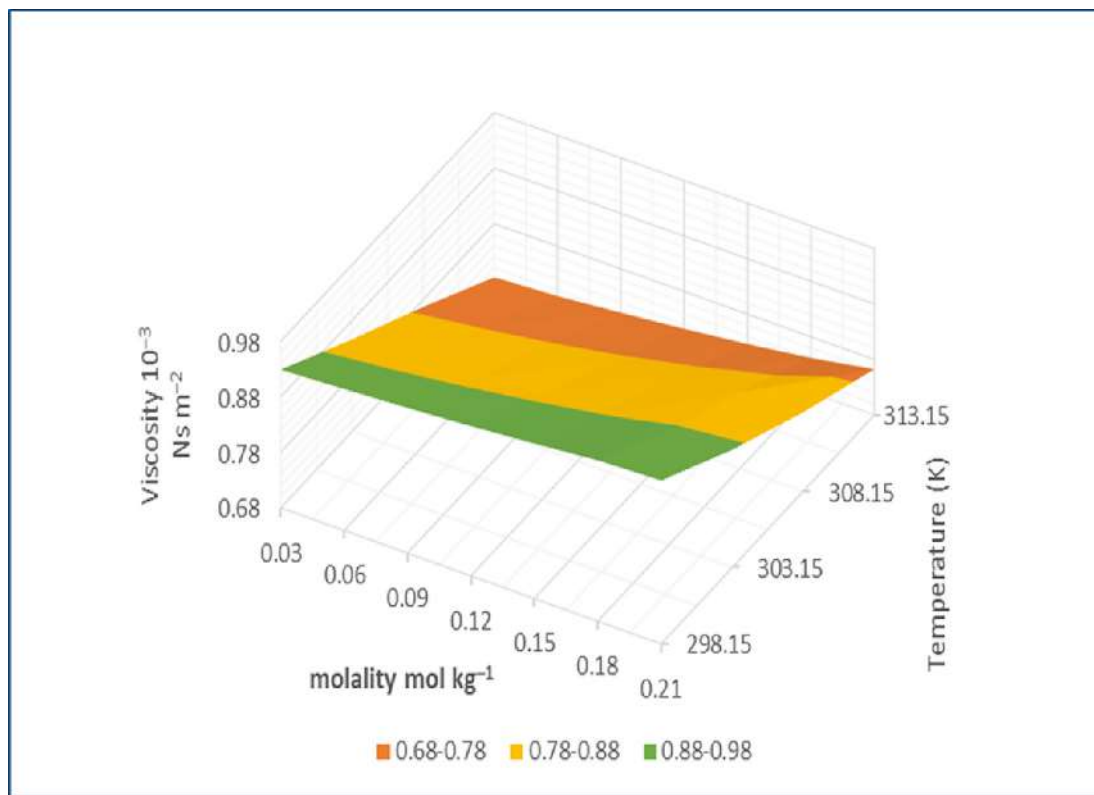


Fig. 2. 3-D plot of Viscosity vs molality (*m*) KIO₃ in KH₂PO₄ at temperature 298.15 K,303.15 K,308.15 K and 313.15 K.

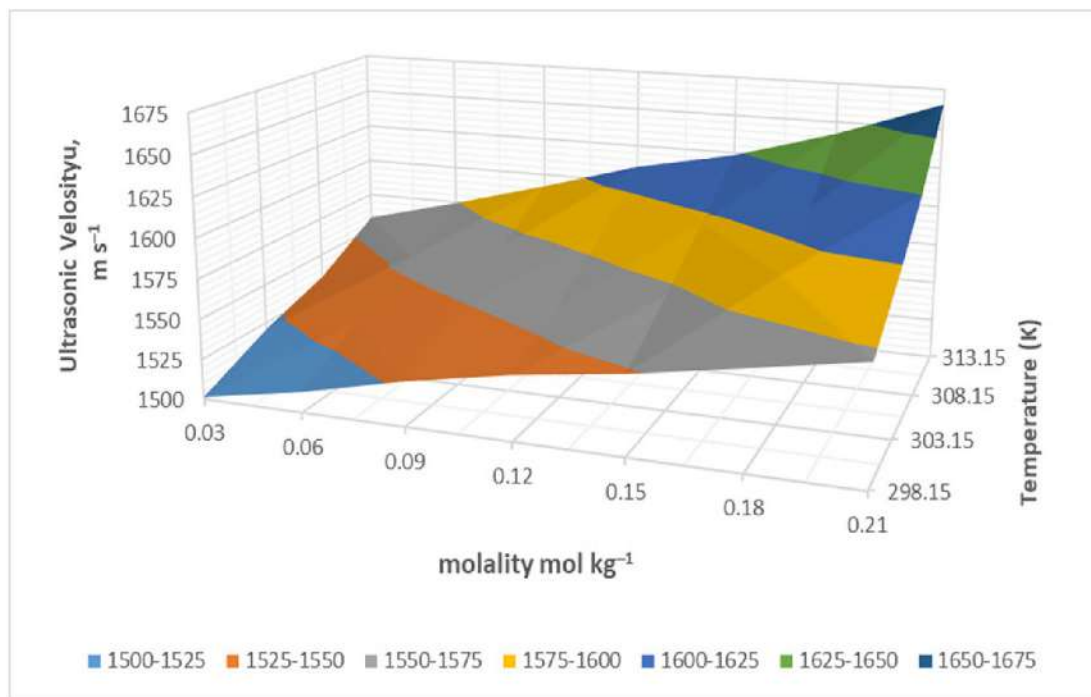


Fig. 3. 3-D plot of Ultrasonic Velocity vs molality (m) KIO_3 in KH_2PO_4 at temperature 298.15 K, 303.15 K, 308.15 K and 313.15 K.

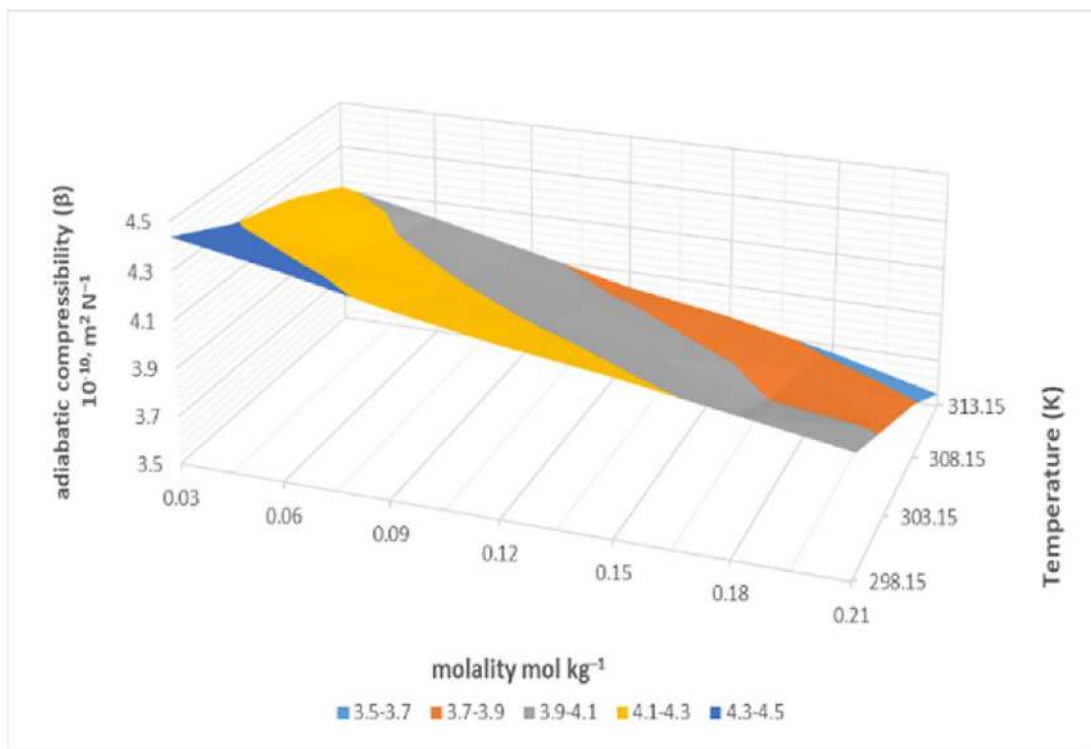


Fig. 4. 3-D plot of adiabatic compressibility (β) vs molality (m).

to association between the molecules through ionic interactions. With the increase in the concentration, the decrease in the L_f values reflects the strong solute- solvent interactions. The increases in the value of V_f with increase in the concentration may be due to the dispersive forces of the component molecules. The increase in the Rao's constant and Wada's constant values confirms that solute and solvents are associated in solution due to dipole-dipole interaction.[25].

4. Conclusions

The physicochemical properties of KIO_3 solutions in water and 1 % KHD solutions at various temperatures are presented in this report in a systematic manner.

The density and viscosity parameters drop as the temperature increases. The reason would be that an internal molecular force decreases and thermal energy increases. In these systems, it has

been observed that there are strong solute–solvent interactions. Positive v_{ϕ} values indicate the presence of ion–solvent interactions. For KIO_3 , the Moulik, Roots, and Jones-Dole reduced equations are validated.

The higher densities of KIO_3 in 1 % KH_2PO_4 are due to the salts' relative solvation, corresponding relative volumes of system, and molar mass. Densities may increase with concentration due to the strengthening of solute–solvent interactions. [10]. By using values of acoustical parameters of the solute over the entire concentration range, it is interpreted that there is molecular interactions between solute and solvent.

Declaration of Competing Interest

The authors declare that they have no known competing financial interests or personal relationships that could have appeared to influence the work reported in this paper.

Acknowledgement

I would like to sincerely acknowledge the guidance and help provided by Dr. Arun B. Nikumbh for compilation of this research report.

References

- P. Banipal, S. Arti, T. Banipal, Densities and viscosities of polyhydroxy solutes in aqueous tetraethylammonium bromide solutions at different temperatures, *J. Chem. Eng. Data* 61 (5) (2016) 1756–1776, <https://doi.org/10.1021/acs.jced.5b00940>.
- R.C. Bhujbal, Densitometric and viscometric study of sodium salicylate in pure water at different temperatures, *Curr. Pharma Res.* 9 (2) (2019) 2824–2830, <https://doi.org/10.33786/JCPR.2019.V09I02.015>.
- D. Meng, P. Xu, Q. Dong, S. Wang, Z. Wang, Comparison of foliar and root application of potassium dihydrogen phosphate in regulating cadmium translocation and accumulation in Tall Fescue (*Festuca arundinacea*), *Water Air Soil Pollut.* 228 (3) (2017), <https://doi.org/10.1007/s11270-017-3304-x>.
- D. Dhingra, S. Pandey, Effect of lithium chloride on the density and dynamic viscosity of choline chloride/urea deep eutectic solvent in the temperature range (303.15–358.15) K, *J. Chem. Thermodyn.* 130 (2019) 166–172, <https://doi.org/10.1016/j.jct.2018.10.003>.
- H. Falkenhagen, M. Dole, Viscosity of electrolyte solutions and its significance to the Debye theory, *Zeitschrift Für Physik* 30 (1929) 611–616.
- P. Ganjare, Prediction of molecular interactions in liquids from density, *Vidyabharati Int. Interdiscip. Res. J.* (2020) 479–499.
- T. Gebreegziabher, B.J. Stoecker, Comparison of two sources of iodine delivery on breast milk iodine and maternal and infant urinary iodine concentrations in southern Ethiopia: a randomized trial, *Food Sci. Nutr.* 5 (4) (2017) 921–928, <https://doi.org/10.1002/fsn3.477>.
- K. Harsh, A. Katal, P.K. Sharma, Temperature-dependent thermodynamic properties of amino acids in aqueous imidazolium-based ionic liquid, *J. Chem. Eng. Data* 65 (4) (2020) 1473–1487, <https://doi.org/10.1021/acs.jced.9b00902>.
- L. Hnedkovsky, L. Rasanen, P. Koukkari, G. Hefter, Densities and apparent molar volumes of aqueous solutions of zinc sulfate at temperatures from 293 to 373 K and 0.1 MPa pressure, *J. Chem. Eng. Data* 66 (1) (2020) 38–44, <https://doi.org/10.1021/acs.jced>.
- Y. Iwadate, T. Ohkubo, Densities and refractive indices of molten alkali iodides: estimation of electronic polarizability of an iodide ion, *J. Chem. Eng. Data* 65 (11) (2020) 5240–5248, <https://doi.org/10.1021/acs.jced.0c00411>.
- G. Jones, M. Dole, The viscosity of aqueous solutions of strong electrolytes with special reference to barium chloride, *J. Am. Chem. Soc.* 51 (10) (1929) 2950–2964.
- J. Khan, M. Farooqui, S. Quadri, Verification of the molar refraction as an additive and constitutive property of binary liquid mixtures of water-ethanol and benzene-ethanol, *Rasayan J. Chem.* 4 (2011) 944–946.
- S.J. Kharat, Ultrasonic velocity and density studies of solutions of maleic acid and tartaric acid in water at $T = (298.15 \text{ and } 308.15) \text{ K}$, *Int. J. Thermophys.* 31 (2010) 585–594, <https://doi.org/10.1007/s10765-010-0736-6>.
- S. Lomesh, V. Nathan, M. Bala, P. Thakur, Volumetric and acoustic methods for investigating molecular interactions of antibiotic drug doxycycline hyclate in water and in aqueous solution of sodium chloride and potassium chloride at different temperatures (293.15–313.15) K, *J. Mol. Liq.* 284 (2019) 241–251, <https://doi.org/10.1016/j.molliq.2019.04.006>.
- X. Lu, S. Xie, J. Zhang, Q. Lei, W. Fang, Density, viscosity and electrical conductivity of alcohol solutions of 2, 2-diethyl-1, 1, 3, 3-tetramethylguanidinium bis (trifluoromethylsulfonyl) imide, *J. Chem. Thermodyn.* 151 (2020) 106241, <https://doi.org/10.1016/j.jct.2020.106241>.
- L.-N. Luo, C.-L. Li, F. Wu, S.-P. Li, S.-Q. Han, M.-F. Li, Desuckering effect of KH_2PO_4 mixed with paclitaxel and its influence on banana (*Musa paradisiaca* AA) mother plant growth, *Sci. Hortic.* 240 (2018) 484–491, <https://doi.org/10.1016/j.scienta.2018.06.033>.
- Y. Marcus, *Ions in Solution and their Solvation*, John Wiley & Sons, 2015.
- N.P. Mohabansi, Study of excess parameters and partial molar volume for the molecular interactions of an aqueous 2-(tert-butylamino)-1-(3-chlorophenyl) Propan-1-one and NaCl solution at different temperatures, *J. Scient. Res.* 64 (2) (2020) 352–358, <https://doi.org/10.37398/JSR.2020.640248>.
- A. Nikumbh, M. Rath, Study of molar refraction and polarisability constant of aqueous solutions of KCl and KBRO_3 at different temperatures, *Int. J. Technical Res. Appl* 2 (6) (2014) 116–122, <https://doi.org/10.21474/IJAR01/3872>.
- A. Nikumbh, M. Rath, Densities, viscosities and apparent molar volumes of KClO_3 in water and some aqueous electrolyte solutions at different temperatures, *SSRG Int. J. Appl. Chem. (SSRG-IJAC)* 3 (3) (2016) 1–6, <https://doi.org/10.14445/23939133/IJAC-V3I5P102>.
- T.S. Nori, Characteristic IR-acoustical analysis and surface tension variations in organic liquid mixtures at different temperatures, *Mater. Today: Proc.* 18 (2019) 2060–2064.
- J.D. Pandey, K. Misra, A. Shukla, V. Mushran, R.D. Rai, Apparent molal volume, apparent molal compressibility, verification of Jones-Dole equation and thermodynamic studies of aqueous urea and its derivative, *Thermochim. Acta* 117 (1987) 245–259, [https://doi.org/10.1016/0040-6031\(87\)88119-4](https://doi.org/10.1016/0040-6031(87)88119-4).
- M. Rath, A. Nikumbh, Interactions of KIO_3 in aqueous 0.1%, *J. Emerg. Technol. Innovative Res.* 6 (1) (2019) 167–175.
- P.G. Raundal, A.A. Sheikh, S.S. Kasim, Study the temperature effect on apparent molar volumes and viscosity (Jones Dole Coefficient) of magnesium sulphate, aluminium ammonium sulphate and potassium aluminium sulphate in binary mixture of aqueous DMF and aqueous DMSO, *J. Adv. Scient. Res.* 12 (01) (2021) 99–105.
- S.S. Reddy, The study of solute–solvent interactions in 1-ethyl-3-methylimidazolium ethylsulfate+ 2-ethoxyethanol from density, speed of sound and refractive index measurements, *J. Mol. Liq.* 218 (2016) 83–89, <https://doi.org/10.1007/s10973-015-5205-9>.
- S.M. Reena Roy, Acoustic data on molecular interactions in mixtures of nitromethane and nitroethane in acetone at 303–318 K, *Russ. J. Phys. Chem. A* 92 (13) (2018) 2606–2611, <https://doi.org/10.1134/S0036024418130253>.
- R.R. Naik, S.V. Bawankar, S.D. Kukade, Acoustical studies of molecular interaction in the solution of propranolol hydrochloride drug at different temperatures and concentrations, *Russ. J. Phys. Chem. A* 89 (11) (2015) 2149–2154, <https://doi.org/10.1134/S003602441511014X>.
- M. Roy, V.K. Dakua, B. Sinha, Partial molar volumes, viscosity B-coefficients, and adiabatic compressibilities of sodium molybdate in aqueous 1,3-dioxolane mixtures from 303.15 to 323.15 K, *Int. J. Thermophys.* 28 (2007) 1275–1284, <https://doi.org/10.1007/s10765-007-0220-0>.
- R.P. Saxena, Introduction of ultrasonic interferometer and experimental techniques for determination of ultrasonic velocity, density, viscosity and various thermodynamic parameters, *Int. J. Appl. Res.* 1 (9) (2015) 562–569.
- M. Shakeel, K. Mahmood, Use of Masson's and Jones-Dole equations to study different types of interactions of three pharmacologically important drugs in ethanol, *J. Chin. Chem. Soc.* 67 (9) (2020) 1552–1562, <https://doi.org/10.1002/jccs.202000128>.
- J.J. Spitzer, P.P. Singh, I.V. Olofsson, L.G. Hepler, Apparent molar heat capacities and volumes of aqueous electrolytes at 25°C: $\text{Cd}(\text{ClO}_4)_2$, $\text{Ca}(\text{ClO}_4)_2$, $\text{Co}(\text{ClO}_4)_2$, $\text{Mn}(\text{ClO}_4)_2$, $\text{Ni}(\text{ClO}_4)_2$, and $\text{Zn}(\text{ClO}_4)_2$, *J. Sol. Chem.* 7 (8) (1978) 623–630, <https://doi.org/10.1007/BF00646039>.
- P. Tank, R. Sharma, A. Sharma, Viscometric Studies of Cu (II) surfactants derived from mustard oil in benzene at 303.15 K, *Tenside, Surfactants, Deterg.* 56 (2) (2019) 158–163, <https://doi.org/10.3139/113.110601>.



Synthesis, characterization and biological evaluation of N- substituted indolyl chalcones as anticancer, anti-inflammatory and antioxidant agents

Hemant V. Chavan^a, Shriram D. Ganapure^b, Nikita N. Mali^c, Pravin S. Bhale^{d,*}

^a Department of Chemistry, A.S.P. College, Devrukh, Dist-Ratnagiri-415804, Maharashtra, India

^b Department of Chemistry, Annasaheb Awate Arts, Commerce and Hutatma Babu Genu Science College, Manchar, Tal. Ambegaon, Dist. Pune-410 503, Maharashtra, India

^c Department of Chemistry, Dr. Babasaheb Ambedkar Marathwada University(Aurangabad), Sub-Campus, Osmanabad-413501, Maharashtra, India

^d Department of Chemistry, Yeshwantrao Chavan Mahavidyalaya, Tuljapur, Dist-Osmanabad-413601, Maharashtra, India

ARTICLE INFO

Article history:

Available online 27 September 2022

Keywords:

Indole
Chalcones
Anti-cancer
Anti-inflammatory
Antioxidant activity

ABSTRACT

A series of N- substituted indolyl chalcones were synthesized and evaluated for their anticancer, anti-inflammatory and antioxidant activity. Adequate confirmation of the synthesized compounds was achieved using modern analytical techniques like FT-IR, HRMS, ¹H NMR and ¹³C NMR spectroscopic techniques. Eighteen compounds were tested against MCF7 breast cancer cell line and monkey normal Vero cell line and calculated GI₅₀ values from averages of 3 experiments. Compound **3a** and **3m** exhibited potent activity (GI₅₀ = <0.1 and 16.3 μM respectively) against the MCF7 (estrogen receptor-positive) cell line which was almost as good as that of standard drug adriamycin (GI₅₀ = <0.1 μM). Synthesized compounds were also evaluated for their antioxidant and anti-inflammatory activity. Most of the N- substituted indolyl chalcones displayed excellent antioxidant and anti-inflammatory activity.

© 2022 Elsevier Ltd. All rights reserved.

Selection and peer-review under responsibility of the scientific committee of the Integrative Nanotechnology Perspective for Multidisciplinary Applications - 2022.

1. Introduction

Cancer is a disease of international anxiety that is a major reason of worldwide human deaths. [1]. According to the World Health Organization (WHO) report, 9.6 million deceases happened globally in 2018 due to this deadly disease (WHO, 12 Sep 2018; Bray *et al.*, 2018). Any type of tissue or cell in the body is at a threat of abnormal proliferation and that is the cause for the diversity in cancer. Moreover, the causes of cancer are hurriedly growing, while treatment strategies have concurrently been increased and customized into advanced means of combating this terrible disease. Treatment strategies for various types of cancers include radiation therapy, surgeries, chemotherapy, hormonal therapy, immunotherapy, bone marrow transplantation, targeted therapy, cryoablation, radiofrequency ablation, and so on[2]. While chemotherapy is an invasive treatment, many anticancer agents in the market suffer from various serious and sometimes

intolerable toxic limitations. So, the development of novel antitumor agents is a crucial need of time [3,4].

Chalcones are essential pharmacophores of many natural products such as curcumin, flavokawain, millepachine, and xanthohumol [5]. Indolyl chalcones have received notable attention because of their wide ranges of biological activities, such as antioxidant, antibacterial, anti-fungal, anticancer [6–9], and antidiabetic activities [10]. El-Sawy *et al.* reported N-methylsulphonyl and N-benzenesulphonyl-3-indolyl heterocycles as anticancer and antimicrobial agents[11]. Kumar *et al.* also reported α-cyano bis(indolyl)chalcones as novel anticancer agents[12]. Recently, our research group reported α-cyano substituted bis-indolyl chalcone[13], extended conjugated indolyl chalcones[14], E)-3-(benzo [d]thiazol-2-ylamino)-2-(1-methyl-1H-indole-3-carbonyl)-3(methylthio)acrylonitrile derivatives[15], 1,3,4,5-tetrasubstituted pyrazole derivatives[16], indole-pyrazole based α-cyano substituted chalcones[17] and indolyl bis-chalcone [18] as potent anti-breast cancer agents. Our constant efforts to discover potent anticancer agents [19–21], herein we have synthesized a series of N- substituted indolyl chalcone and *in vitro* evaluated for their anti-breast cancer, anti-oxidant and anti-inflammatory activity.

* Corresponding author.

E-mail address: bhale.ps@gmail.com (P.S. Bhale).

2. Materials and methods

All the chemicals used for the synthesis of N- substituted indolyl chalcone were of synthetic grade and obtained from commercial sources. The development of the reactions was checked by thin-layer chromatography (TLC) using TLC plates (silica gel 60 F254, aluminum back, Merck). Visualization of the TLC plate was achieved with UV light. Melting points of N- substituted indolyl chalcone were determined by the open-end capillary method and are uncorrected. All the ^1H NMR spectra were recorded in CDCl_3 and chemical shifts in ppm were reported on instrument Bruker AV-400 MHz, for ^1H NMR and 75 MHz for ^{13}C NMR relative to TMS as an internal standard. The IR spectra were recorded on Shimadzu FT-IR spectrophotometer by using 1 % potassium bromide discs. Anticancer activities were carried out under the supervision of Dr. Jyoti Kode, Scientific Officer, Tata Memorial Centre, Advanced Centre for Treatment Research and Education in Cancer (ACTREC), Kharghar, Navi Mumbai-410210.

2.1. General procedure for the preparation of N- substituted indole-3-carbaldehyde (2a-e)

To a mixture of indole-3-carbaldehyde **1** (1 mmol) in tetrahydrofuran (THF) was added sodium hydride (3 mmol) under N_2 atmosphere at 0°C , and the mixture was vigorously stirred at 0°C for 30 min. To this suspension, substituted benzyl chloride (1 mmol) was carefully added dropwise for 10 min at 0°C , and the reaction mixture was allowed to stir at 0°C for 1 h. Upon completion of the reaction, monitored by TLC, the reaction mixture was poured into ice water. The solid obtained was filtered, washed with water and recrystallized from ethanol.

2.2. General procedure for the preparation of N- substituted indolyl chalcones (3a-r)

To a mixture of 3',4',5'-Trimethoxyacetophenone (1 mmol) in ethanol (15 ml) was added 10 % sodium hydroxide and stirred for 5 min. Then, added N- substituted indole-3-carbaldehyde **2a-e** (1 mmol) and this mixture was stirred at room temperature for 6–8 h. After completion of the reaction (monitored by TLC), desired product N- substituted indolyl chalcone **3a-r** was precipitated out as solid in the round bottom flask. Obtained solid was filtered, washed with cold ethanol and oven-dried. It was column purified by column chromatography using silica gel mesh size, 100–200 and elution with 10 % ethyl acetate in hexane.

2.3. Spectral data of representative compounds

(E)-3-(1H-indol-3-yl)-1-(3,4,5-trimethoxyphenyl)prop-2-en-1-one (3a): Yellow solid; 89 %; 240–242 $^\circ\text{C}$; IR (KBr cm^{-1}): 3228 (NH), 2986 (C–H), 1625 (C=O), 1580 (C=C); ^1H NMR (CDCl_3 , 400 MHz): δ = 11.23 (broad s, 1H, NH), 8.00 (d, J = 12.4 Hz, 1H), 7.74 (s, 1H), 7.60 (d, J = 6.9 Hz, 1H), 7.51 (d, J = 12.4 Hz, 1H), 7.19–7.14 (m, 2H), 6.88–6.76 (m, 3H), 3.76 (s, 9H, OCH_3); HRMS: 338.2120 (M + H).

(E)-3-(1-(4-chlorobenzyl)-1H-indol-3-yl)-1-(3,4,5-trimethoxyphenyl)prop-2-en-1-one (3b): Yellow solid; 92 %; 220–222 $^\circ\text{C}$; IR (KBr cm^{-1}): 2980 (C–H), 1672 (C=O), 1618 (C=C); ^1H NMR (CDCl_3 , 400 MHz): δ = 8.56 (s, 1H), 8.32 (d, J = 6.8 Hz, 1H), 8.11 (d, J = 12.0 Hz, 1H), 7.62 (d, J = 12.0 Hz, 1H), 7.39–7.23 (m, 3H), 7.17–6.93 (m, 4H), 6.34 (s, 2H), 5.42 (s, 2H), 3.56 (s, 9H, OCH_3); ^{13}C NMR (CDCl_3 , 75 MHz): δ = 186.2, 154.3, 145.4, 144.0, 136.1, 135.2, 135.0, 132.1, 128.9, 128.4, 128.1, 127.6, 127.1, 121.0, 119.6, 118.3, 112.7, 109.4, 99.4, 60.6, 56.3, 50.5; HRMS: 462.1221 (M + H).

(E)-4-((3-(3-oxo-3-(3,4,5-trimethoxyphenyl)prop-1-enyl)-1H-indol-1-yl)methyl)benzotrile (3d): Yellow solid; 77 %; 286–288 $^\circ\text{C}$; IR (KBr cm^{-1}): 2980 (C–H), 2222 (CN), 1656 (C=O), 1612 (C=C); ^1H NMR (CDCl_3 , 400 MHz): δ = 9.02 (s, 1H), 8.69 (d, J = 6.4 Hz, 1H), 8.10 (d, J = 12.00 Hz, 1H), 7.68–7.51 (m, 3H), 7.36–7.19 (m, 3H), 7.14 (d, J = 7.0 Hz, 2H), 6.44 (s, 2H), 5.23 (s, 2H), 3.61 (s, 9H, OCH_3); HRMS: 453.1924 (M + H).

(E)-3-(1-(2,4-dichlorobenzyl)-1H-indol-3-yl)-1-(3,4,5-trimethoxyphenyl)prop-2-en-1-one (3e): Yellow solid; 92 %; 266–268 $^\circ\text{C}$; IR (KBr cm^{-1}): 2969 (C–H), 1698 (C=O), 1620 (C=C); ^1H NMR (CDCl_3 , 400 MHz): δ = 8.91 (s, 1H), 8.49 (d, J = 6.4 Hz, 1H), 7.97 (d, J = 12.4 Hz, 1H), 7.48 (s, 1H), 7.41 (d, J = 12.4 Hz, 1H), 7.27 (d, J = 6.8 Hz, 1H), 7.09 (d, J = 7.4 Hz, 1H), 7.00–6.92 (m, 3H), 6.38 (s, 2H), 5.30 (s, 2H), 3.76 (s, 9H, OCH_3); HRMS: 496.0918 (M + H).

(E)-3-(5-bromo-1H-indol-3-yl)-1-(3,4,5-trimethoxyphenyl)prop-2-en-1-one (3g): Yellow solid; 94 %; 258–260 $^\circ\text{C}$; IR (KBr cm^{-1}): 3306 (NH), 2958 (C–H), 1667 (C=O), 1621 (C=C); ^1H NMR (CDCl_3 , 400 MHz): δ = 11.09 (broad s, 1H, NH), 7.98 (d, J = 12.4 Hz, 1H), 7.55 (s, 1H), 7.35 (d, J = 12.4 Hz, 1H), 7.20–7.04 (m, 3H), 6.29 (s, 2H), 3.72 (s, 9H, OCH_3); HRMS: 416.1013 (M + H).

(E)-3-(5-bromo-1-(4-fluorobenzyl)-1H-indol-3-yl)-1-(3,4,5-trimethoxyphenyl)prop-2-en-1-one (3i): Faint yellow solid; 94 %; 228–230 $^\circ\text{C}$; IR (KBr cm^{-1}): 2974 (C–H), 1698 (C=O), 1623 (C=C); ^1H NMR (CDCl_3 , 400 MHz): δ = 7.94 (d, J = 12.4 Hz, 1H), 7.80 (s, 1H), 7.59–7.41 (m, 4H), 7.29–7.12 (m, 4H), 6.31 (s, 2H), 5.23 (s, 2H), 3.66 (s, 9H, OCH_3); HRMS: 524.0911 (M + H).

(E)-4-((5-bromo-3-(3-oxo-3-(3,4,5-trimethoxyphenyl)prop-1-enyl)-1H-indol-1-yl)methyl)benzotrile (3j): Yellow solid; 90 %; 232–234 $^\circ\text{C}$; IR (KBr cm^{-1}): 2970 (C–H), 2220 (CN), 1685 (C=O), 1604 (C=C); ^1H NMR (CDCl_3 , 400 MHz): δ = 8.54 (s, 1H), 8.01 (d, J = 12.4 Hz, 1H), 7.63 (d, J = 12.4 Hz, 1H), 7.44–7.27 (m, 5H), 7.14 (s, 1H), 6.99 (d, J = 3.4 Hz, 1H), 6.40 (s, 2H), 5.21 (s, 2H), 3.77 (s, 9H, OCH_3); ^{13}C NMR (CDCl_3 , 75 MHz): δ = 188.5, 153.0, 145.5, 145.1, 141.6, 135.7, 135.1, 132.2, 129.6, 128.8, 128.5, 127.4, 124.8, 121.2, 118.9, 113.0, 112.5, 110.4, 108.7, 99.3, 60.5, 56.1, 50.7; HRMS: 531.1923 (M + H).

(E)-3-(5-bromo-1-(2,4-difluorobenzyl)-1H-indol-3-yl)-1-(3,4,5-trimethoxyphenyl)prop-2-en-1-one (3l): Yellow solid; 88 %; 244–246 $^\circ\text{C}$; IR (KBr cm^{-1}): 2964 (C–H), 1690 (C=O), 1609 (C=C); ^1H NMR (CDCl_3 , 400 MHz): δ = 8.67 (s, 1H), 8.02 (d, J = 12.0 Hz, 1H), 7.53 (d, J = 12.0 Hz, 1H), 7.34 (d, J = 6.4 Hz, 1H), 7.21–7.10 (m, 3H), 7.01–6.92 (m, 4H), 5.35 (s, 2H), 3.70 (s, 9H, OCH_3); HRMS: 542.1781 (M + H).

(E)-3-(5-methoxy-1H-indol-3-yl)-1-(3,4,5-trimethoxyphenyl)prop-2-en-1-one (3m): Yellow solid; 94 %; 262–264 $^\circ\text{C}$; IR (KBr cm^{-1}): 3289 (NH), 2968 (C–H), 1688 (C=O), 1630 (C=C); ^1H NMR (CDCl_3 , 400 MHz): δ = 11.76 (broad s, 1H, NH), 8.00 (d, J = 12.0 Hz, 1H), 7.60 (s, 1H), 7.34 (d, J = 12.0 Hz, 1H), 7.28–7.09 (m, 2H), 6.56–6.40 (m, 3H), 3.78 (s, 12H, OCH_3); HRMS: 368.2201 (M + H).

(E)-3-(1-(4-chlorobenzyl)-5-methoxy-1H-indol-3-yl)-1-(3,4,5-trimethoxyphenyl)prop-2-en-1-one (3n): Yellow solid; 89 %; 270–272 $^\circ\text{C}$; IR (KBr cm^{-1}): 2970 (C–H), 1694 (C=O), 1621 (C=C); ^1H NMR (CDCl_3 , 400 MHz): δ = 9.02 (s, 1H), 7.91 (d, J = 12.4 Hz, 1H), 7.62–7.54 (m, 2H), 7.32 (d, J = 8.0 Hz, 2H), 7.12–7.02 (m, 3H), 6.78–6.55 (m, 3H), 5.34 (s, 2H), 3.80 (s, 12H, OCH_3); HRMS: 492.2109 (M + H).

(E)-4-((5-methoxy-3-(3-oxo-3-(3,4,5-trimethoxyphenyl)prop-1-enyl)-1H-indol-1-yl)methyl)benzotrile (3p): Yellow solid; 82 %; 244–246 $^\circ\text{C}$; IR (KBr cm^{-1}): 2973 (C–H), 2225 (CN), 1693 (C=O), 1621 (C=C); ^1H NMR (CDCl_3 , 400 MHz): δ = 8.56 (s, 1H), 7.90 (d, J = 12.0 Hz, 1H), 7.59–7.48 (m, 2H), 7.40 (d, J = 8.0 Hz, 2H), 7.26 (d, J = 8.0 Hz, 2H), 7.08 (s, 1H), 6.71–6.49 (m, 3H), 5.22 (s, 2H), 3.82 (s, 12H, OCH_3); HRMS: 483.1920 (M + H).

(E)-3-(1-(2,4-difluorobenzyl)-5-methoxy-1H-indol-3-yl)-1-(3,4,5-trimethoxyphenyl)prop-2-en-1-one (3r): Yellow solid; 94 %; 278–280 °C; IR (KBr cm⁻¹): 2961 (C–H), 1690 (C=O), 1604 (C=C); ¹H NMR (CDCl₃, 400 MHz): δ = 8.40 (s, 1H), 8.09 (d, J = 12.0 Hz, 1H), 7.78–7.67 (m, 2H), 7.21 (s, 1H), 6.98–6.73 (m, 3H), 6.60–6.46 (m, 3H), 5.24 (s, 2H), 3.80 (s, 12H, OCH₃); ¹³C NMR (CDCl₃, 75 MHz): δ = 187.4, 163.0, 158.5, 154.2, 153.9, 145.3, 145.0, 135.1, 132.6, 128.7, 128.4, 127.5, 127.1, 120.5, 112.8, 112.2, 111.0, 109.3, 104.6, 104.2, 99.4, 60.3, 56.4, 55.7, 48.5; HRMS: 494.2123 (M + H).

Procedure of the SRB-assay: Tumor cells (human breast cancer cell line MCF-7, Source: NCI, USA and NCCS, Pune) were grown in tissue culture flasks in a growth medium (RPMI-1640 with 2 mM glutamine, pH 7.4, 10 % fetal calf serum, 100 µg/mL streptomycin, and 100 units/mL penicillin) at 37 °C under the atmosphere of 5 % CO₂ and 95 % relative humidity employing a CO₂ incubator. The cells at subconfluent stage were harvested from the flask by treatment with trypsin (0.05 % trypsin in PBS containing 0.02 % EDTA) and placed in a growth medium. The cells with >97 % viability (trypan blue exclusion) were used for cytotoxicity studies. An aliquot of 100 µL (5 × 10³ cells/well) of cells was transferred to a well of 96-well tissue culture plate. As mentioned above, the cells were allowed to grow for one day at 37 °C in a CO₂ incubator. The test materials at different concentrations were then added to the wells and cells were further allowed to grow for another 48 h. Suitable blanks and positive controls were also included. Each test was performed in triplicate. The cell growth was stopped by gently layering 50 µL of 50 % trichloroacetic acid. The plates were incubated at 4 °C for an hour to fix the cells attached to the bottom of the wells. Liquids of all the wells were gently pipette out and discarded. The plates were washed five times with doubly distilled water to remove TCA, growth medium, etc and were air-dried. 100 µL of SRB solution (0.4 % in 1 % acetic acid) was added to each well and the plates were incubated at ambient temperature for half an hour. The unbound SRB was quickly removed by washing the wells five times with 1 % acetic acid. Plates were air-dried, tris-buffer (100 µL of 0.01 M, pH 10.4) was added to all the wells and plates were gently stirred for 5 min on a mechanical stirrer. The optical density was measured on an ELISA reader at 540 nm. The cell growth in the absence of any test material was considered 100 % and in turn growth inhibition was calculated. GI₅₀ values were determined by regression analysis.

In vitro anti-inflammatory activity by protein denaturation method: The reaction mixture (10 ml) consisted of 0.4 ml of egg albumin (from fresh hen's egg), 5.6 ml of phosphate-buffered saline (PBS, pH 6.4) and 4 ml of synthetic derivative (1 mM). A similar volume of double-distilled water served as control. Then the mixtures were incubated at (37 °C ± 2) in an incubator for 15 min and then heated at 70 °C for 5 min. After cooling, their absorbance was measured at 660 nm by using a vehicle as blank. Diclofenac sodium (1 mM) was used as a reference drug and treated similarly for the determination of absorbance. The percentage inhibition of protein denaturation was calculated by using the following formula, % inhibition = 100 × (Vt / Vc – 1), Where, Vt = absorbance of a test sample, Vc = absorbance of control.

DPPH radical scavenging activity: In this method, 0.1 mM DPPH solution was prepared in methanol by adding 39.4 mg of DPPH in 1000 ml of methanol, and to 0.5 ml of this solution, 1.5 ml of test compounds of the dissolved in DMSO were added at various concentrations of all (1, 10, 100, 500 and 1000 µg/mL). The mixtures were shaken vigorously and allowed to stand at room temperature for 30 min. Then the absorbance was measured at 517 nm using a UV–vis spectrophotometer (Shimadzu, spectrophotometer). Vitamin-C was used as a standard compound. Reduction in absorbance by test compounds indicates radical scavenging

activity. The scavenging activity by the DPPH radical was determined by.

$$\text{DPPH scavenging effect (\% inhibition)} = \{(A_0 - A_1) / A_0\} \times 100\}$$

Where, A₀ is the absorbance of the control reaction, A₁ is the absorbance test compound and vitamin C.

NO radical scavenging activity: The various concentrations of test compounds (as 1, 10, 100, 500, and 1000 µg/ml) were prepared in ethanol. To 0.5 ml of 10 mM sodium nitroprusside in phosphate-buffered saline, to this, 1 ml of various concentrations of test compounds were mixed, and to this equal volume of freshly prepared Griess reagent was added, the solution was then incubated at 25 °C for 3 h. From this, 100 µL of the reaction mixture was transferred to a 96-well plate, and the absorbance was read at 546 nm using a microplate reader (Biotek, Italy). Ascorbic acid was used as standard control.

The percentage of nitrite radical scavenging activity of test compounds was calculated by.

$$\text{Nitric oxide scavenging activity} = \frac{\text{Absorbance of control} - \text{Absorbance of test compounds}}{\text{Absorbance of control}} \times 100$$

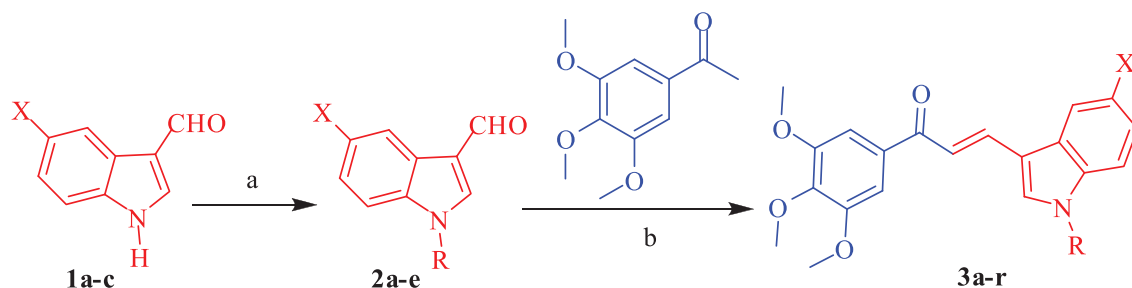
Superoxide radical (SOR) scavenging assay: The reaction mixture consisting of 1 ml of nitro blue tetrazolium (NBT) solution (156 mM NBT in phosphate buffer, pH 7.4), 1 ml NADH solution (468 mM NADH in phosphate buffer, pH 7.4), and 1 ml of synthetic compound (1 mM) solution was mixed. The reaction was started by adding 1 ml of phenazine methosulfate (PMS) solution (60 mM PMS in phosphate buffer, pH 7.4) to the mixture. The reaction mixture was incubated at 25 °C for 5 min and the absorbance was measured at 560 nm against the blank sample and compared with standards and the percentage of inhibition was calculated using the same formula as above. Decreased absorbance of the reaction mixture indicated increased SOR scavenging activity.

Hydrogen peroxide scavenging (H₂O₂) assay: A solution of H₂O₂ (40 mM) is prepared in phosphate buffer (50 mM, pH 7.4). The concentration of H₂O₂ was determined by measuring absorption at 230 nm using a spectrophotometer. Synthetic compound (1 mM) in DMSO was added to H₂O₂ and absorbance was measured at 230 nm after 10 min against a blank solution containing phosphate buffer without H₂O₂. The percentage inhibition of H₂O₂ was calculated by formula, % inhibition (H₂O₂) = (A₀ – A₁) / A₀ × 100, Where A₀ is the absorbance of control and A₁ is the absorbance of test sample.

3. Results and discussion

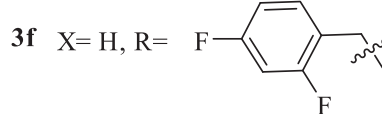
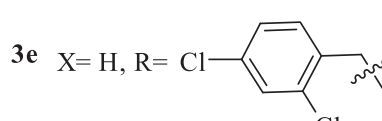
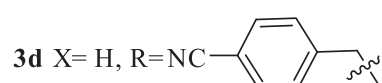
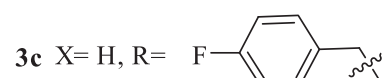
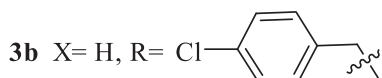
3.1. Chemistry

In the current study, syntheses of N- substituted indolyl chalcones (**3a-r**) were accomplished by the Claisen-Schmidt condensation reaction of 3',4',5'-Trimethoxyacetophenone with N-substituted indole-3-carbaldehydes **2a-e** in the presence of 10 % NaOH in ethanol (Scheme 1). The starting compound, namely N-substituted indole-3-carbaldehydes **2a-e** were synthesized in good yield from the reaction of substituted indole-3-carbaldehydes **1a-c** with substituted benzyl chloride in presence of sodium hydride using the method described in the literature with minor modifications[22]. The obtained crude products were purified by column chromatography using silica gel mesh size, 100–200 and elution with 10 % ethyl acetate in hexane. The structures of synthesized compounds were analyzed by IR, ¹H NMR, ¹³C NMR and HRMS spectroscopic techniques.

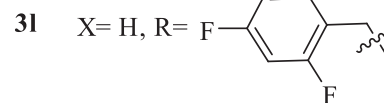
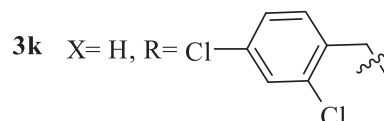
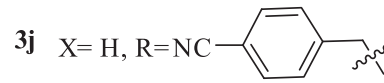
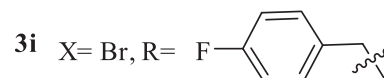
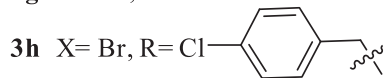


Where,

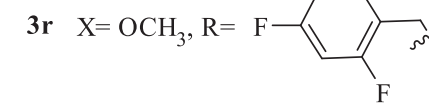
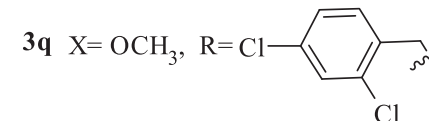
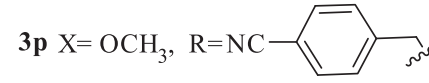
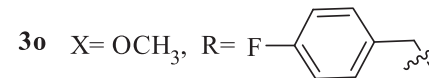
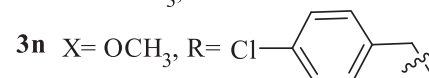
3a X= H, R= H



3g X= Br, R= H



3m X= OCH₃, R= H



Scheme 1. Synthesis of N- Substituted Indolyl Chalcones. Reagents and conditions: a) Sodium hydride, substituted benzyl chloride, THF; b) NaOH (10%), Ethanol, 6–8 hr, RT.

3.2. Biological evaluation

3.2.1. *In vitro* anticancer activity

All the synthesized N- substituted indolyl chalcones (**3a-r**) were evaluated for their *in vitro* anticancer activity against human breast cancer cell line MCF-7 (estrogen receptor-positive) and monkey normal Vero cell line by sulforhodamine B (SRB) assay method [23]. It is noteworthy that most of the compounds with the concentration of the drug that produced 50 % inhibition of cell growth (GI_{50}). Three parameters such as GI_{50} , TGI and LC_{50} were determined during the screening process and the results summarized in Table 1.

Compound **3a** and **3m** exhibited potent activity (GI_{50} = <0.1 and 16.3 μ M respectively) against the human breast cancer MCF7 (estrogen receptor-positive) cell line which was almost as good as that of standard drug adriamycin (GI_{50} = <0.1 μ M). On the other hand, all other N- substituted indolyl chalcones showed moderate to weak cytotoxicity (GI_{50} = 41.5 – 68.2 μ M) against the MCF-7 cell line. A comparison of the TGI and LC_{50} concentrations of the compounds with adriamycin were also done. All the N- substituted indolyl chalcones **3a-r** were inactive (TGI and LC_{50} > 100 μ M) like adriamycin against the MCF-7 cell line.

Many reported drugs in literature influence normal cell growth, which is a major disadvantage in the development of anticancer drug progress. Therefore, we have ensured the selectivity of some active compounds by *in vitro* screening against the normal Vero Monkey cell line. This cellular level normal screening outcomes

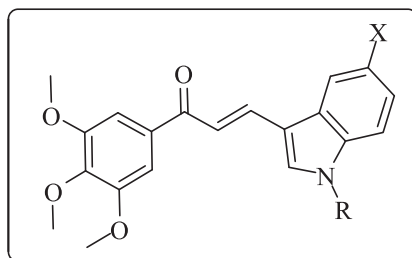
help to reveal the safety profile of active compounds. This cytotoxicity study revealed that the GI_{50} values for **3a**, **3b**, **3c**, **3g**, **3i**, **3m** and **3o** are 54.8, 68.1, 97.0, 76.3, 88.6, 44.0 and 78.2 μ M respectively (Table 1). These N- substituted indolyl chalcones showed moderate selectivity against cancer cell lines over normal cell line.

Structure-activity relationship (SAR) study revealed that the free N–H of indole is essential for activity. Compounds **3a** and **3m** have free N–H of indole exhibited potent activity (GI_{50} = <0.1 and 16.3 μ M respectively) against MCF-7 cell line. After comparing GI_{50} values of **3a**, **3m** (GI_{50} = <0.1 and 16.3 μ M respectively) and remaining N- substituted indolyl chalcones (GI_{50} = 41.5 – 68.2 μ M), it is clear that free NH of indole is essential for activity. It is noteworthy that, presence of electron donating group at 5-position of indole ring exhibited potent activity. Here indole acquiring methoxy group at 5-position of indole ring exhibited potent activity (GI_{50} = 16.3 μ M) against MCF-7 cell line.

3.2.2. *In vitro* anti-inflammatory activity

Inhibition of albumin denaturation.

Denaturation of proteins is a well documented cause of inflammation. In the current study, the *in vitro* anti-inflammatory effect of N- substituted indolyl chalcones was evaluated against denaturation of egg albumin and obtained results are summarized in Table 2. Compounds **3k** and **3p** showed significant inhibition (88.21 and 89.92 % respectively) compared to the Diclofenac sodium, a standard anti-inflammation drug (90.21 %) at 1 mM concentration. All the other compounds were showed weak to moder-

Table 1*In vitro* anticancer screening of N- substituted indolyl chalcones (**3a-r**) against human breast cancer cell line MCF-7^a and monkey normal Vero cell line.

Compound	MCF-7			Vero		
	LC ₅₀ ^b	TGI ^c	GI ₅₀ ^d	LC ₅₀	TGI	GI ₅₀
3a	>100	> 100	< 0.1	> 100	> 100	54.8
3b	> 100	> 100	44.7	> 100	> 100	68.1
3c	> 100	> 100	48.2	> 100	> 100	97.0
3d	> 100	> 100	48.9	> 100	97.3	> 100
3e	> 100	> 100	47.0	> 100	88.9	> 100
3f	> 100	> 100	55.3	> 100	83.1	> 100
3 g	> 100	> 100	41.5	> 100	79.5	76.3
3 h	> 100	> 100	51.7	> 100	72.2	> 100
3i	> 100	> 100	46.6	> 100	69.3	88.6
3j	> 100	> 100	56.6	> 100	> 100	> 100
3 k	> 100	> 100	53.7	> 100	> 100	> 100
3 l	> 100	> 100	56.2	> 100	> 100	> 100
3 m	> 100	> 100	16.3	> 100	> 100	44.0
3n	> 100	> 100	49.1	> 100	90.0	> 100
3o	> 100	> 100	65.2	> 100	> 100	78.2
3p	> 100	> 100	68.2	> 100	> 100	> 100
3q	> 100	> 100	56.0	> 100	> 100	> 100
3r	> 100	> 100	55.1	> 100	> 100	> 100
Adriamycin	> 100	29.6	< 0.1	> 100	10.0	0.03

^a Concentrations in μM .^b Concentration of drug resulting in a 50 % reduction in the measured protein at the end of the drug treatment as compared to that at the beginning) calculated from $[(Ti - Tz)/Tz] \times 100 = -50$.^c Drug concentration resulting in total growth inhibition (TGI) will calculated from $Ti = Tz$.^d Growth inhibition of 50 % (GI_{50}) calculated from $[(Ti - Tz)/(C - Tz)] \times 100 = 50$.**Table 2***In vitro* anti-inflammatory and anti-oxidant activity of N- substituted indolyl chalcones (**3a-r**).

Comp. No.	Anti-inflammatory activity		Anti-oxidant activity			
			% inhibition (1 mM)			
	% inhibition (1 mM)		DPPH	NO	SOR	H ₂ O ₂
3a	84.30	46.42	41.71	58.54	28.22	
3b	57.80	41.53	32.82	65.10	39.31	
3c	71.20	25.71	37.14	37.56	48.00	
3d	39.30	42.57	24.28	37.45	33.01	
3e	41.29	38.35	21.42	66.64	42.57	
3f	61.17	25.10	41.53	72.52	42.35	
3 g	37.44	28.56	27.14	45.67	35.00	
3 h	49.74	33.29	42.78	55.72	35.32	
3i	71.98	42.57	41.42	70.34	47.19	
3j	69.59	24.54	11.53	74.67	32.39	
3 k	88.21	43.13	25.71	54.66	22.37	
3 l	78.36	26.66	43.57	43.41	45.06	
3 m	75.20	10.24	43.07	64.55	33.80	
3n	61.00	22.14	21.08	63.44	20.24	
3o	82.20	42.76	41.92	44.12	32.34	
3p	89.92	46.44	42.23	39.29	43.27	
3q	81.76	47.19	40.01	74.74	33.29	
3r	77.92	36.64	41.50	64.28	34.66	
AA	-	44.18	42.63	74.07	47.17	
DS	90.21	-	-	-	-	

Standard: AA = Ascorbic acid; DS: Diclofenac sodium; data represent mean of three replicates.

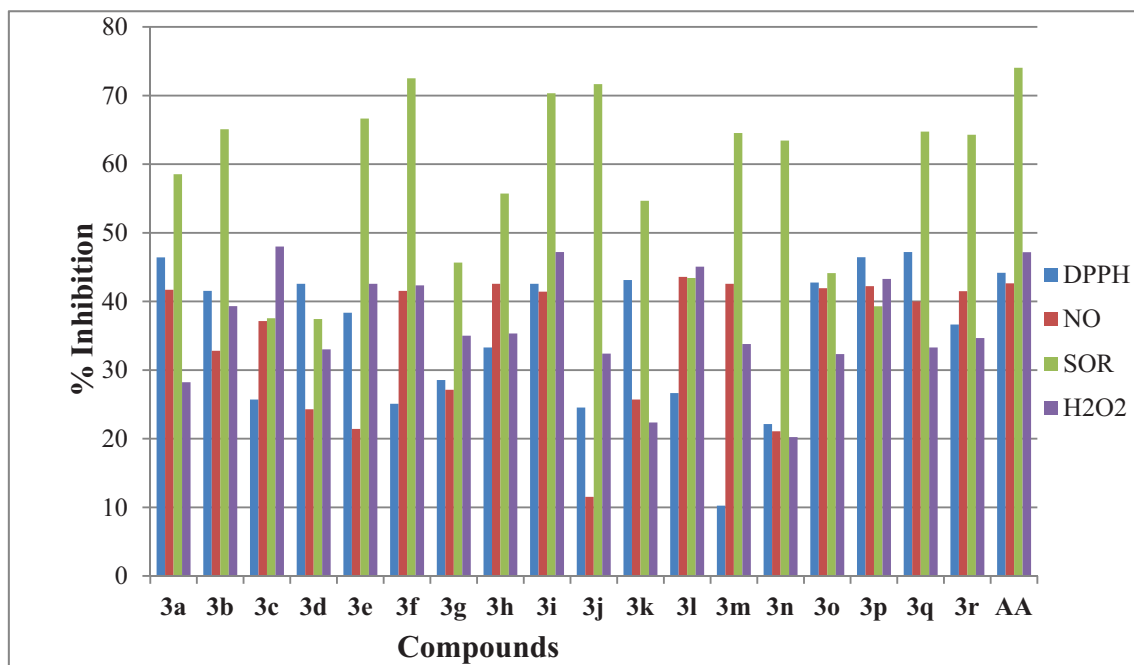


Fig. 1. Antioxidant activity profile of synthesized compounds (3a-r).

ate inhibition (37.44–84.30 %) as compared to the Diclofenac sodium.

3.2.3. *In vitro* antioxidant activity

The series of N- substituted indolyl chalcones **3a-r** were evaluated for their direct scavenging activity against various reactive oxygen and nitrogen species such as 2,2-diphenyl-2-picrylhydrazyl (DPPH), nitric oxide (NO) and superoxide (SOR), hydrogen peroxide (H₂O₂). Free radical scavenging activity was calculated in terms of percent inhibition by using a known procedure in literature and results are presented in Table 2. All the synthesized N- substituted indolyl chalcones **3a-r** have shown good to excellent scavenging activity against DPPH and NO radicals (Fig. 1). The compounds **3a**, **3p** and **3q** showed excellent DPPH free radical scavenging activity (46.42, 46.44 and 47.19 % respectively) as compared to standard ascorbic acid (AA) (44.18 %). The remaining N- substituted indolyl chalcones showed moderate to weak DPPH free radical scavenging activity (10.24–43.13 %). Compounds **3h**, **3l** and **3m** showed excellent NO free radical scavenging activity (42.78, 43.57 and 43.07 % respectively) as compared to standard ascorbic acid (42.63 %). All other compounds N- substituted indolyl chalcones showed moderate NO free radical scavenging activity (11.53 – 42.23 %). Compound **3j** and **3q** exhibited excellent activity (74.67 and 74.74 % respectively) against SOR radical as compared to standard ascorbic acid (74.07 %). All other compounds were moderate SOR scavengers (37.45–72.52 %). Compound **3c** and **3i** showed excellent H₂O₂ radical scavenging activity (48.0 and 47.19 % respectively), whereas all other compounds showed weak to moderate activity (20.24–45.06 %).

4. Conclusion

We synthesized a series of N- substituted indolyl chalcones and *in vitro* evaluated them for their cytotoxic potential against human breast cancer cell line MCF-7 (estrogen receptor-positive) and monkey normal Vero cell line. Most of the N- substituted indolyl chalcones under investigation demonstrated significant antitumor activities. Among them, compound **3a** and **3m** showed potent

activity against breast carcinoma as good as adriamycin. In general, substitution at 5-position of indole ring by electron-donating group and free N–H of indole exhibited potent cytotoxic activity. These results further support its safety margin by studying the activity on normal Vero monkey cell line. *In vitro* anti-inflammatory and antioxidant potential of synthesized compounds were also evaluated. All the compounds were found to possess marked anti-inflammatory potential by effectively inhibiting the heat-induced albumin denaturation. Some N- substituted indolyl chalcones exhibited excellent DPPH, NO, SOR and H₂O₂ radical scavenging activity. The current study has thus given impetus for the design and development of more potent chalcone derivatives as anticancer leads.

CRedit authorship contribution statement

Hemant V. Chavan: Methodology. **Shriram D. Ganapure:** Writing – original draft. **Nikita N. Mali:** Software, Validation. **Pravin S. Bhale:** Writing – original draft, Writing – review & editing, Supervision.

Declaration of Competing Interest

The authors declare that they have no known competing financial interests or personal relationships that could have appeared to influence the work reported in this paper.

Acknowledgment

Authors express deep thanks to Tata Memorial Centre, Advanced Centre for Treatment Research and Education in Cancer (ACTREC), Kharghar, Navi Mumbai-410210 for conducting the *in vitro* anticancer screening and Biocyte Institute of Research and Development, Sangli, India for *in vitro* anti-oxidant and anti-inflammatory activity determinations.

References

- [1] M.H. El-Wakil, H.M. Ashour, M.N. Saudi, A.M. Hassan, I.M. Labouta, Target identification, lead optimization and antitumor evaluation of some new 1,2,4-triazines as c-Met kinase inhibitors, *Bioorg. Chem.* 73 (2017) 154–169.
- [2] U. Bughani, S. Li, H. Joshi, Recent patents reveal microtubules as persistent promising target for novel drug development for cancers, *Recent Pat. Anti-Infect. Drug Discovery* 4 (3) (2009) 164–182.
- [3] E. Espinosa, P. Zamora, J. Feliu, M. González Barón, Classification of anticancer drugs—a new system based on therapeutic targets, *Cancer Treat. Rev.* 29 (6) (2003) 515–523.
- [4] B. Mansoori, A. Mohammadi, S. Davudian, S. Shirjang, B. Baradaran, The different mechanisms of cancer drug resistance: a brief review, *Adv. Pharma. Bull.* 7 (3) (2017) 339–348.
- [5] B. Zhang, D. Duan, C. Ge, J. Yao, Y. Liu, X. Li, J. Fang, Synthesis of xanthohumol analogues and discovery of potent thioredoxin reductase inhibitor as potential anticancer agent, *J. Med. Chem.* 58 (4) (2015) 1795–1805.
- [6] J. Chen, C.-M. Li, J. Wang, S. Ahn, Z. Wang, Y. Lu, J. Dalton, D. Miller, W. Li, Synthesis and antiproliferative activity of novel 2-aryl-4-benzoyl-imidazole derivatives targeting tubulin polymerization, *Bioorg. Med. Chem.* 19 (16) (2011) 4782–4795.
- [7] S. Ducki, D. Rennison, M. Woo, A. Kendall, J. Chabert, A. McGown, N. Lawrence, Combretastatin-like chalcones as inhibitors of microtubule polymerization. part 1: synthesis and biological evaluation of antivasular activity, *Bioorg. Med. Chem.* 17 (22) (2009) 7698–7710.
- [8] M. Edwards, D. Stemerick, P. Sunkara, Chalcones: a new class of antimetabolic agents, *J. Med. Chem.* 33 (7) (1990) 1948–1954.
- [9] D. Kumar, N. Kumar, K. Akamatsu, E. Kusaka, H. Harada, T. Ito, Synthesis and biological evaluation of indolyl chalcones as antitumor agents, *Bioorg. Med. Chem. Lett.* 20 (13) (2010) 3916–3919.
- [10] W. Seo, J. Kim, J. Kang, H. Ryu, M. Curtis-Long, H. Lee, M. Yang, K. Park, Sulfonamide chalcone as a new class of α -glucosidase inhibitors, *Bioorg. Med. Chem. Lett.* 15 (24) (2005) 5514–5516.
- [11] E.R. El-Sawy, A.H. Mandour, S.M. El-Hallouty, K.H. Shaker, H.M. Abo-Salem, Synthesis, antimicrobial and anticancer activities of some new N-methylsulphonyl and N-benzenesulphonyl-3-indolyl heterocycles: 1st cancer update, *Arabian J. Chem.* 6 (1) (2013) 67–78.
- [12] D. Kumar, N. Maruthi Kumar, M.P. Tantak, M. Ogura, E. Kusaka, T. Ito, Synthesis and identification of α -cyano bis(indolyl)chalcones as novel anticancer agents, *Bioorg. Med. Chem. Lett.* 24 (22) (2014) 5170–5174.
- [13] P.S. Bhale, H.V. Chavan, S.B. Dongare, S.N. Shringare, Y.B. Mule, P.B. Choudhari, B.P. Bandgar, Synthesis, characterization and evaluation of 1,3-Bisindolyl-2-Propen-1- one derivatives as potent anti-breast cancer agents, *Curr. Bioact. Compd.* 14 (3) (2018) 299–308.
- [14] P.S. Bhale, H.V. Chavan, S.B. Dongare, S.N. Shringare, Y.B. Mule, S.S. Nagane, B.P. Bandgar, Synthesis of extended conjugated indolyl chalcones as potent anti-breast cancer, anti-inflammatory and antioxidant agents, *Bioorg. Med. Chem. Lett.* 27 (7) (2017) 1502–1507.
- [15] P.S. Bhale, H.V. Chavan, S.B. Dongare, S.T. Sankpal, B.P. Bandgar, α -Aroylketene Dithioacetal mediated synthesis of (E)-3-(benzo[d]thiazol-2-ylamino)-2-(1-methyl-1H-indole-3-carbonyl)-3-(methylthio)acrylonitrile derivatives and their biological evaluation, *Anti-Cancer Agents Med. Chem.* 18 (5) (2018) 757–764.
- [16] Bhale, P., Bandgar, B., Dongare, S., Shringare, S., Sirsat, D. and Chavan, H. (2019). "Ketene dithioacetal mediated synthesis of 1, 3, 4, 5-tetrasubstituted pyrazole derivatives and their biological evaluation," *Phosphorus, Sulfur, and Silicon and the Related Elements*, 194, 843–849
- [17] P. Bhale, S. Shringare, A. Khade, H. Chavan, Synthesis, characterization and biological evaluation of Indole-Pyrazole Amalgamated α -Cyano substituted Chalcones, *Anti-Cancer Agents Med. Chem.* 21 (16) (2021) 2216–2223.
- [18] P. Bhale, H. Chavan, R. Endait, A. Kadam, R. Bopalkar, M. Gaikwad, Synthesis and biological evaluation of bis-chalcone as anti-breast cancer and anti-oxidant agents, *Croatica Chem. Acta* 94 (1) (2021) 35–41.
- [19] S. Dongare, B. Bandgar, P. Bhale, S. Shringare, H. Chavan, Design, synthesis, and spectroscopic study of 7-Azaindolyl Hydrazones with anti-breast cancer activity, *Croatica Chem. Acta* 92 (1) (2019) 1–9.
- [20] S.N. Shringare, H.V. Chavan, P.S. Bhale, S.B. Dongare, Y.B. Mule, S.B. Patil, B.P. Bandgar, Synthesis and pharmacological evaluation of combretastatin-A4 analogs of pyrazoline and pyridine derivatives as anticancer, anti-inflammatory and antioxidant agents, *Med. Chem. Res.* 27 (4) (2018) 1226–1237.
- [21] S. Shringare, H. Chavan, P. Bhale, S. Dongare, Y. Mule, N. Kolekar, B. Bandgar, Synthesis and pharmacological evaluation of pyrazoline and pyrimidine analogs of combretastatin-A4 as anticancer, anti-inflammatory and antioxidant agents, *Croatica Chem. Acta* 91 (2018) 357–366.
- [22] J. Muchowski, D. Solas, Protecting groups for the pyrrole and indole nitrogen atom. The [2-(trimethylsilyl)ethoxy]methyl moiety. lithiation of 1-[[2-(trimethylsilyl)ethoxy]methyl]pyrrole, *J. Org. Chem.* 49 (1) (1984) 203–205.
- [23] P. Skehan, R. Storeng, D. Scudiero, A. Monks, J. McMahon, D. Vistica, J.T. Warren, H. Bokesch, S. Kenney, M.R. Boyd, New colorimetric cytotoxicity assay for anticancer-drug screening, *J. Natl Cancer Inst.* 82 (13) (1990) 1107–1112.



Embelin isolated from *Embelia ribes* derived silver nanoparticles and its application in breast cancer nanomedicine

Rutika R. Jagtap^{a,*}, Aniket Garud^b, Bhagyashri Warude^b, Shubhangi S. Puranik^a

^a Post Graduate Research Centre, Department of Zoology, Modern College of Arts, Science and Commerce, Shivajinagar, Pune, Maharashtra, India

^b Rasiklal M. Dhariwal Institute of Pharmaceutical Education and Research, Chinchwad, Pune, Maharashtra, India

ARTICLE INFO

Article history:

Available online 23 September 2022

Keywords:

Embelia ribes
Embelin
AgNPs
Cytotoxicity
Apoptosis
Molecular docking

ABSTRACT

Breast cancer is one of the most predominant cancers in female claiming millions of lives every year. Our current research work proposes that the synthesis of silver nanoparticles using phytochemical constituent Embelin from *Embelia ribes* fruits provides significant result as a potent anticancer agent along with its probable mechanism of action depicted by molecular docking. UV–Visible spectroscopy was used to characterise Embelin–AgNPs, and the maximum absorbance was recorded at 374.5 nm. Particle size determination indicated monodispersity of nanoparticles; particle size recorded as 25–30 nm and zeta potential analysis well explained the stability of the nanoparticles. *In vitro* cytotoxicity study was done by MTT assay on MCF-7 cell line. Embelin–AgNPs induced apoptosis in MCF-7 cells as measured by the Annexin-V PI apoptosis assay. To predict the binding mode of ligand and receptor and probable mechanism of action in-silico study was done against ER alpha and HER2 receptors of breast cancer cells by molecular docking and it has revealed Embelin could act as potential modulator against ER positive and HER2 positive breast cancers.

© 2022 Elsevier Ltd. All rights reserved.

Selection and peer-review under responsibility of the scientific committee of the Integrative Nanotechnology Perspective for Multidisciplinary Applications - 2022.

1. Introduction

Cancer defines to a large and lethal, heterogeneous group of diseases with an underlying pathology identified by uncontrolled cellular growth. As cancer cells evades the growth suppressor signals, they turn out to be proliferative and invasive, eventually shows metastasis.[1] Breast cancer is still one of the leading causes of death among women worldwide and it is a type of tissue cancer which mainly involves inner layer of milk glands or lobules and ducts.[2] As per the statistics, breast cancer has accounted for 11.7 percent of all cancer cases in 2020, with approximately 685,000 fatalities. The World Health Organization lists a number of other risk factors, including heavy drinking and smoking, a family history of breast cancer, radiation exposure, reproductive history, early menopause, obesity and lack of physical activity, frequent miscarriages, and hormonal therapy used after menopause. Despite significant progress in understanding disease biology and various treatment aids including surgery, radiation therapy, chemotherapy and targeted therapy, effective breast can-

cer care has yet to be attained.[3] Number of side-effects, non-specificity, a high cost involved in treatment, re-occurrence and metastasis of cancer makes conventional therapies unsuitable.[4] Thus, there is an intent need to discover unique, target-oriented, safe, and low-cost therapeutic drug.

The development of nanotechnology, which provides remarkable solutions to cope with life-threatening disorders, has boosted advancement in the field of medical science. Nanotechnology is a multidisciplinary field comprising of biology, chemistry, and physics attributing to number of unique properties such as high surface area to volume ratio.[5] Metal nanoparticles (particle size smaller than 100 nm) have a wide range of applications due to a variety of unique characteristics. Different chemical and physical methods such as chemical reduction of metals, photochemical reduction, and electrochemical processes are widely used for synthesis of nanoparticles.[6] However, these production techniques are labour-intensive, costly and potentially harmful to the environment and living organisms. The alternate, eco-friendly and cost-effective approach which have gained importance in past few years is 'Green synthesis' method of nanoparticles synthesis. In green synthesis, biological systems including plants and microorganisms act as reducing and capping agents to transform metal ions into

* Corresponding author.

E-mail address: rutika.jagtap@gmail.com (R.R. Jagtap).

metal nanoparticles.[7] and this techniques doesn't even require any sophisticated instruments and chemicals. Plants being a big repository of large number of phytoconstituents provide reducing, stabilizing, and capping agent for synthesis of nanoparticles.

Medicinal plants have been used to treat diseases since ancient times, and medicinal plants form the indispensable backbone of traditional healthcare systems all over the world. Medicinal plants and medication development have remained a major source of hope for treating a variety of human degenerative disorders, such as cancer.[8] The number of medicinal plants has been screened for their wide spectrum property against cancer. Eventually this search has led for the isolation of important anticancer drugs such as paclitaxel, Vincristine, Vinblastine, Vinorelbine and camptothecin.[9] The major research goal in the field of medicinal plants is of comprehensive and integrative manner to better address nature of medicinal plants in cancer therapy.

Embelia ribes, a traditional medicinal plant belongs to *Myrsinaceae* family and widely used in ayurvedic preparations; commonly known for Krmighna meaning antihelmentic property. It possesses potential anti-inflammatory, antioxidant, cytotoxic, anti-bacterial, anti-fungal and wound healing activity.[10] Embelin (2,5-dihydroxy-3-undecyl-1,4-benzoquinone) is one of the potent quinine derivative phytoconstituent of *Embelia ribes* (specially in fruits) and widely studied as it possesses various therapeutic applications such as anthelmintic, anti-tumour[11], anti-inflammatory and anti-diabetic anti-bacterial anticancer and anticonvulsant.[12] *In vivo* studies in rodents have shown that Embelin has anti-cancer effects in pancreas[13] colon[14] and liver cancers.[15].

In vitro cytotoxicity studies are intended to measure the ability of drug or cytotoxic compounds to cause cell death. Nanoparticles being used as an extensive tool for drug delivery can be used to study its cytotoxic effect. The colorimetric assay using tetrazolium dyes such as MTT can be utilized to assess cell metabolic activity. Reduction of MTT dye depends on cellular metabolic activity; if a drug induces cytotoxicity the viability of cells is reduced and thus can be extrapolate. [16,17] Apoptosis is programmed cell death and intensively regulated process which can be induced by intracellular as well as extracellular signals. Apoptosis can be distinguished from necrosis depending on morphological and biochemical factors. In a well coordinated cellular mechanism, phosphatidylserine (PS) is located in inner leaflet of cellular membrane but during apoptosis it can be translocated to outer leaflet. Annexin V, a 35–36 kDa Ca²⁺-dependent phospholipid-binding protein with a high affinity for PS, is a human anticoagulant.[18] By attaching to PS exposed on the outside leaflet, annexin V tagged with a fluorophore or biotin can identify apoptotic cells. The FITC annexin V/Dead Cell Apoptosis Kit for flow cytometry uses FITC annexin V and PI to deliver a quick and easy apoptosis assay.

Computational biology and bioinformatics have the potential to accelerate drug discovery and repurposing process. This involves prediction and scoring of binding free energy in between target and desired molecule by molecular docking. *In silico* approaches have paved the way for the solution of many biological problems, leading to the discovery of novel inhibitors against a variety of diseases. One way to predict the activity of drug is *in silico* study. In triple positive breast cancer, estrogen receptor (ER), progesterone receptors(PR) and human epidermal growth factor receptor 2 (HER2) are overexpressed. [19] As hormone receptor positive breast cancer accounts for over 75 %, hormonal therapy is helping in reducing the risk of breast cancer recurrence.[20] Estrogen and human epidermal growth factor receptor are involved in normal breast cell growth, proliferation and development. Upon binding with ligand, these receptor dimerizes and regulate expression of another genes involved in growth and proliferation of breast cells, eventually leading to breast cancer.[21,22] These receptors holds

molecular targets for cancer treatment and thus *in silico* study provide a wide spectrum to study binding of molecule and its action.

The most intensively investigated nanoparticles are silver metal nanoparticles, which have extraordinary broad-spectrum activity. The development of efficient and reliable experimental techniques for the synthesis of silver nanoparticles is required due to their numerous applications that benefit humans. In nanoscience, AgNP research has made huge achievements especially as antimicrobial, antibacterial, antioxidants, antifungal, anti-inflammatory, anti-cancer, anti-angiogenic.[23] Plant extract metabolites oxidise and coat freshly formed particles, acting as reducing agents for silver ions. These metabolites lose their electron and become oxidised by ordinary cellular operations in the presence of oxygen, such as in silver nitrate (AgNO₃), acting as reducing agents.[24,25] Embelin being a active phytoconstituent able to reduce silver metal ions. In light of the foregoing, we were compelled to perform the current study in order to provide accountability of silver nanoparticle synthesis by Embelin, its characterization and anti-cancer potential against MCF-7 breast cancer cells. For studying the role in inducing apoptosis, a study was carried out by annexin PI FITC assay. In addition to understand the possible mechanism of embelin in breast cancer treatment, *in silico* study by molecular docking was carried out against estrogen receptor(ER α) and human epidermal growth factor receptor 2 (HER2).

2. Materials and method

2.1. Preparation of plant extract and isolation of embelin

Embelia ribes fruits were harvested from Maharashtra's Koyna region and shed dried. The dried fruit of *Embelia ribes* was coarsely pulverised and extracted continuously in chloroform using the hot percolation method with the Soxhlet equipment. The extract was separated on silica column to isolate embelin from the mixture, which was eluted by benzene.[26] Orange coloured crystalline embelin was isolated and further used to synthesize silver nanoparticles.

2.2. Synthesis of silver nanoparticles

A stock solution of 0.5 % was prepared. 1 mM solution of AgNO₃ was prepared using deionised water as solvent. 0.5 % of embelin solution was added to vigorously stirred silver nitrate solution (100 ml). Stirring was continued for 30 min to obtain colloids. [27] Upon the addition of embelin to the solution of AgNO₃, the colour of AgNO₃ solution changed from colourless to yellow in 30 min. Further the colour intensified and changed to light brown after 24 h of incubation at room temperature.

2.3. Characterization of embelin derived silver nanoparticles

Different factors modulate the characteristics and there are several characterization technique available to study the characters and properties of nanoparticles.

2.3.1. UV-Visible spectroscopy

The change in colour is due to the size and shape of silver nanoparticles (AgNPs) generated during the reduction process. UV-vis spectra was recorded in the range of 200 to 800 nm after 30 min (Shimadzu) of addition of embelin solution with vigorous stirring. [27].

2.3.2. Particle size and zeta potential analysis

Particle size analysis and stability of the prepared silver nanoparticles were examined using Nanophox-SympaTec (Ger-

many). The analysis volume in Nanophox is 50 μ l to 4 ml and the size range of scattering is 0.5 nm to 10,000 nm. The liquid sample was diluted 10 times with double distilled water before centrifugation and transferred to a cuvette for DLS analysis. (Delsa Nano C by Beckmen Counter Inc). The zeta potential of the generated NPs was assessed in the presence of water as dispersion. [23,27].

2.4. Cell viability by MTT assay

2.4.1. Cell line and cell culture

Human breast cancer cell line MCF-7 was procured from NCCS, Pune. The cells were maintained in Dulbecco's Modified Eagle Medium (DMEM) supplemented with 10 % foetal bovine serum (Gibco1X) and antibiotic Antimycotic (Gibco). Cell line was incubated at 37 °C in a humidified atmosphere of 5 % CO₂.

The viability of cells was measured using the 3-(4, 5-Dimethylthiazol-2-yl)-2, 5-Diphenyltetrazolium Bromide (MTT) assay. Adhered cells were trypsinized to detach from surface and seeded in 96-well plates. Cells were allowed to adhere for 24 h and were subsequently incubated with the relevant drug concentrations for 48 h in triplicate. 0.5 mg/mL MTT was added to each well and covered with aluminium foil. Plates were incubated at 37 °C for 4 h. After the incubation, culture medium was removed and DMSO was added in each well to dissolve the blue-purple formazan crystals. The absorbance in blank, control and treated wells were measured in a microplate reader at 570 nm. [16,17].

2.5. Annexin PI apoptosis assay

Embelin AgNPs mediated apoptotic induction was determined by FITC Annexin V/Dead Cell Apoptosis Kit with FITC annexin V and PI (Invitrogen) as per manufacture's instruction. [28] Briefly, cells were induced for apoptosis and washed by phosphate-buffered saline (PBS). Then cells were stained by FITC Annexin V and PI, and incubated for 15 min at room temperature as per the instructions in manufacture's kit. After the incubation the stained cells were analyzed by flow cytometry. [18] Untreated and positive control (cells treated with doxorubicin 6 μ g/mL) were also analyzed by flow cytometer.

2.6. Anti-breast cancer activity prediction by molecular docking

2.6.1. Preparation of Embelin for docking-

The basic structure of standard anticancer drug Raloxifene and HER2 inhibitor TAK-285 was retrieved from PubChem database (<https://pubchem.ncbi.nlm.nih.gov>). Structure of Embelin was drawn using ChemDraw Ultra 12.0 software and converted to SDF file. Open Babel tool was used for optimizing designed embelin with force fields MMFF94 and GHEMICAL.[29] Embelin's energy was minimized by conjugate gradient and steepest descent optimization algorithms. Finally, all ligand option was used to convert the minimised files to PDBQT format in order to generate their atomic coordinates, which are used as input in PyRx software. (<http://PyRx.sourceforge.net/>).

2.6.2. Protein preparation

The 3D structure of ER α bound with selective estrogen receptor modulator i.e. Raloxifene (PDB ID: 1ERR) [30] and HER2 in complex with TAK-285 (inhibitor) (PDB ID: 3RCD) [31] were selected from Protein Data Bank (PDB) (<https://www.rcsb.org/>) as the preferred docking target protein and was analysed for its active site by discovery studio visualizer (<http://accelrys.com>) Preparation of the proteins was carried out with the Biovia Discovery Studio Visualizer (DSV) 2017 (Prepare protein protocol). Protein preparation entailed adding hydrogen atoms, defining bond orders, deleting unwanted water molecules and salts, and optimising the hydrogen

bond network. Polar hydrogen were added to optimize the hydrogen-bonding network. The proteins were minimised in terms of energy and active sites were predicted with the selection of maximized GRID parameters using DSV. Finally the prepared structure of protein was saved in the PDB file format for docking.

2.6.3. Identification of cavity and active amino acid residues-

The crystal structure of the homodimer Estrogen receptor 1ERR, represents a human estrogen receptor-ligand-binding domain in complex with Raloxifene, and HER2 receptor 3RCD represents a human epidermal growth factor receptor- ligand- binding domain in complex with TAK-285 provided a suitable guiding template for studying the binding interactions of designed ligands. Both designed ligands and proteins were imported in AutoDockVina Wizard and both macro molecules converted into PDBQT format. The three dimensional grid boxes were generated. [32,33].

2.6.4. Docking procedure

Molecular docking of embelin, 1ERR and 3RCD were subjected to docking using AutodockVina Wizard of PyRx virtual screening 0.8 version software to find the reasonable binding geometry and discover the protein ligand connections.[34,35] Docking predicted non-bonded, non-covalent interactions between a receptor or active site region of a protein and a drug or chemical molecule forming an intermolecular complex. The final docking result includes affinity prediction (scoring) for the molecules investigated; resulting in a relative rank ordering of the docked compounds in terms of affinity, reported as kcal/mol. [36] A greater negative binding energy indicates a greater binding affinity. DSV was used to analyse binding interactions on complexes with higher docked scores.

3. Result and discussion

3.1. Preparation of plant extract and isolation of embelin

Hot percolation method was utilized to extract the phytochemicals from *E. ribes* berries/fruits. The solvent used was chloroform, as embelin could solubilised in it and was extracted. The purification of embelin was done through silica column and orange coloured embelin was eluted with benzene, and allowed to recrystallized.

3.2. Synthesis of silver nanoparticles

The colourless solution of AgNO₃ turned yellow and colloids developed after embelin was added to AgNO₃. The colour intensified to orange and changed to light brown after 24 h of incubation at room temperature. The reduction of silver nitrate to elemental silver (Ag + to Ag₀) was caused by the interaction of AgNO₃ with embelin.(See Fig. 1).

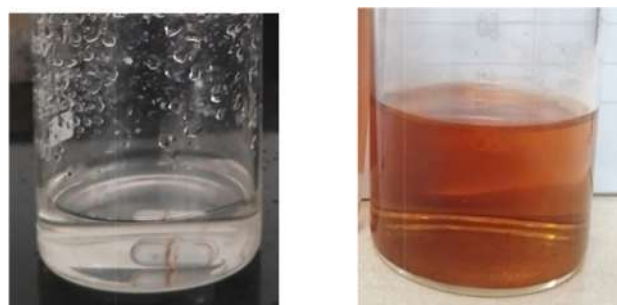


Fig. 1. Colourless solution turned into light brown colour after 24 h.

3.3. Characterization of embelin derived silver nanoparticles

1. UV–vis spectroscopy

The UV/Vis spectrum of AgNPs synthesized in the range of 200 to 700 nm gave the maximum absorption peak at 374.5 nm. The peak's appearance was typical of AgNP surface plasmon resonance (SPR), and the free electrons produced the SPR absorption band, which was caused by AgNP collective oscillation in resonance with the light wave. Few other reports also stated that the UV/Vis absorption peaks for biogenic AgNPs were obtained at 378 nm and 384 nm. Silver nanoparticles were analysed by UV visible spectroscopy (Shimadzu). The result of UV spectroscopy is shown in the absorption spectrum of silver nanoparticles maximum absorbance was found 374.5 nm. (Fig. 2).

3.4. Particle size and zeta potential analysis

For the determination of the surface charge and stability of the formulation, zeta potential analysis is carried out. By measuring the velocity of the nano-sized particles, this also assesses the colloidal stability of AgNPs. Distinct peak between 25 and 30 nm clearly indicates formation of AgNPs with uniformity. Higher peak value indicates monodispersity of nanoparticles. Zeta potential of -5.42 mV was recorded which indicates good stability of silver nanoparticles. (Fig. 3a Fig. 4a). (See Fig 3b).

3.5. Cell viability by MTT assay

Cytotoxic potential of Embelin AgNPs against the human breast cancer cell line MCF-7 was assessed by using MTT assay which is widely used in cytotoxicity and cell viability assays. For the cytotoxicity study, MCF-7 breast cancer cells were incubated with different concentrations of Embelin AgNPs (0.5, 1, 2.5, 5, 7.5 and 10 $\mu\text{g/ml}$). After 24 h of incubation, viability of cells was determined by the MTT assay. It was observed that Embelin AgNPs induced cell cytotoxicity in a concentration dependent manner. IC 50 value was measured to be 5.16 $\mu\text{g/ml}$. Embelin AgNPs could exhibit cytotoxicity at low doses (Fig. 4b).

3.6. Annexin PI apoptosis assay

The human breast cancer MCF-7 cells were treated by Embelin AgNPs IC50 value in triplicate and exhibited cytotoxic activity. After induction of apoptosis, cells were stained with FITC-labeled

Annexin V and Propidium Iodide (PI) dyes. The cell suspension was analyzed by flow cytometry. The Annexin V assay revealed that Embelin AgNPs induced early and late stage of apoptosis in MCF-7 cells. (Fig. 5) The Annexin V-FITC graphs in Fig. 5 a depict the distribution of MCF-7 cells in four quadrants (Q1, Q2, Q3, Q4) and represent one of three independent experiments undertaken. In comparison to untreated cells, all treated cells had a lower percentage of viable cells. There was very little cell dispersion in Q1, Q2, and Q4 in untreated cells, indicating a very low amount of necrotic, late, and early apoptotic cells, respectively. Distribution of cells in these quadrants increased after treatment with Embelin AgNPs. In the Embelin AgNPs-treated cells, 18.9 % of cells were in the early stages of apoptosis (Q4), whereas 7.4 % were in the late stages of apoptosis (Q2) according to a triplicate study. (Fig. 5a) Q1 represented necrotic cells, which showed just a small increase in cell dispersion. In the untreated cells, only 1.6 % necrotic cells were observed along with 0.5 % late apoptotic cells (Fig. 5b) while in Embelin AgNPs treated cells it was found to be 11.3 %. In the positive control, cells were treated with Doxorubicin, a known anti-cancer drug at a concentration of 6 $\mu\text{g/ml}$ and showed higher apoptotic induction. Doxorubicin has shown 10.4 % of cells in early apoptosis while 37.4 % cells in late apoptosis, but it has also shown 31.6 % necrotic cells. (Fig. 5c) Embelin being a phytoconstituent and thus Embelin AgNPs has shown less necrotic cells after treatment. Fig. 6. Fig. 7.

Apoptotic cell death is a tightly controlled process marked by distinct morphological changes in the cellular membrane structure. Apoptosis is characterised by cell shrinkage, plasma membrane blebbing, cell separation, phosphatidylserine translocation, nuclear condensation, and finally DNA fragmentation. The current apoptotic study implies Embelin AgNPs induced apoptosis in MCF-7 cells. Apoptosis can be induced by various underlying mechanisms. A molecular mechanism study can determine exact signalling pathway and apoptotic mechanism.

3.7. Anti-breast cancer activity prediction by molecular docking

Molecular docking is a way of predicting activity of a drug and thus accelerates drug discovery process. *In silico* molecular docking approaches have provided novel inhibitors against variety of diseases by predicting an interaction between target and desired molecule. Molecules that bind tightly to the receptor inhibit its function, or modulate it and can thus be used as a drug. [37] In current study, a possible mechanism of embelin against hormone pos-

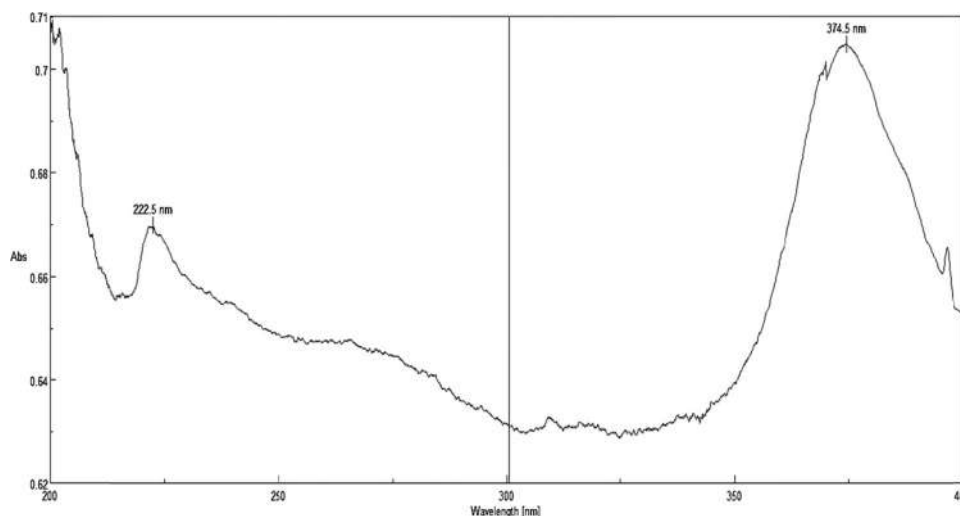


Fig. 2. UV-vis Spectroscopy Analysis.

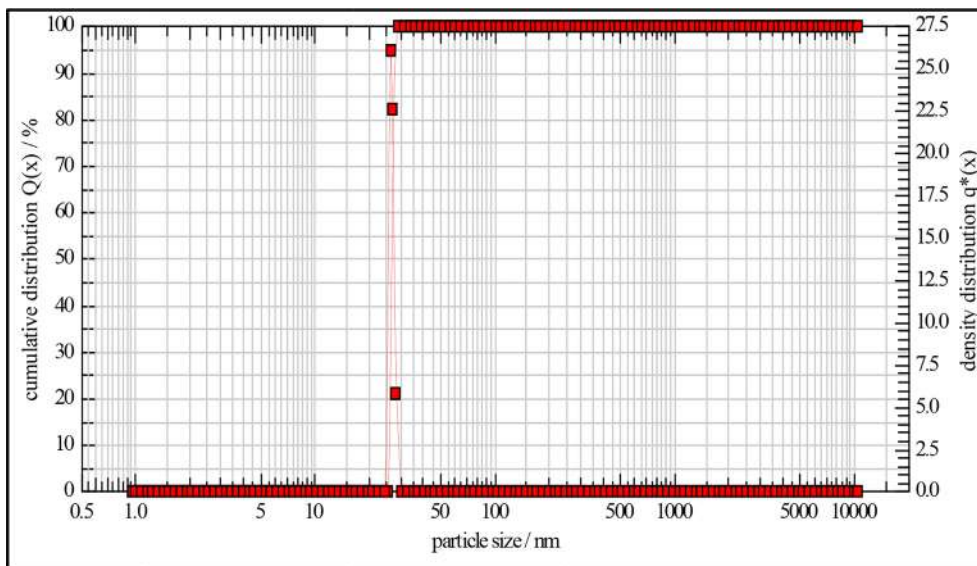


Fig. 3a. NANOPHOX (NX0088), Cross correlation for Particle Size Analysis.

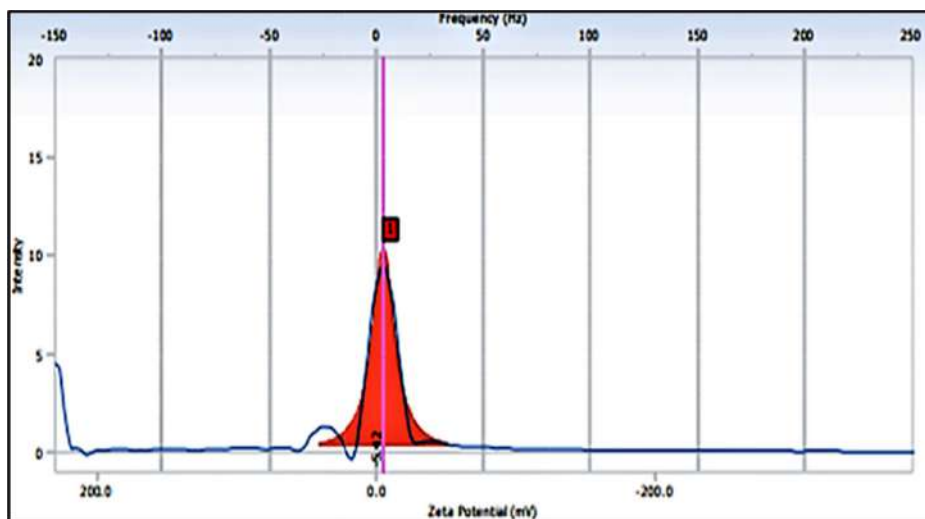


Fig. 3b. Zeta Potential of Embelin AgNPs.

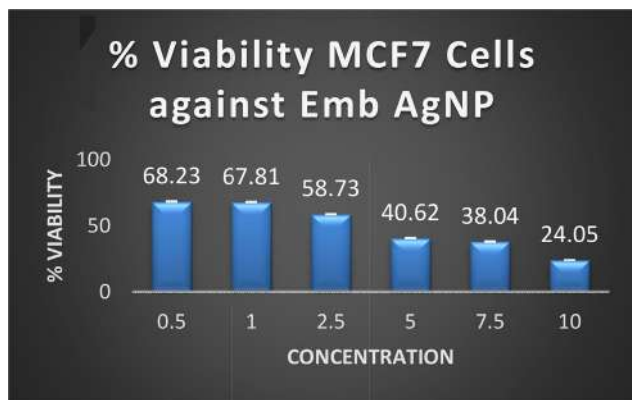


Fig. 4a. % Cell Viability by MTT assay.

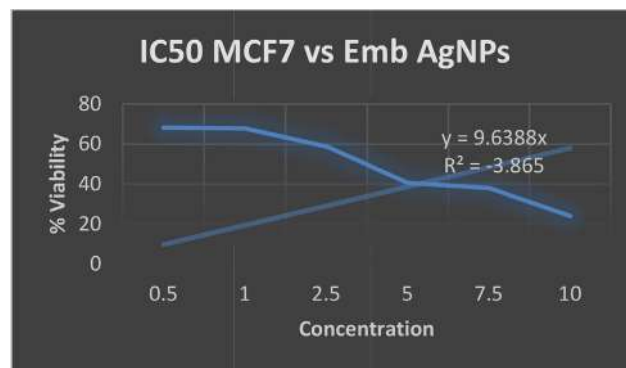


Fig. 4b. IC50 Value.

itive receptors was investigated. From Protein Data Bank, structure of 1ERR and 3RCD was selected for ER α and HER2 receptors respec-

tively and were prepared for docking by Biovia Discovery Studio Visualizer (DSV) 2017. For the identification of cavity and active amino acid residue three dimensional grid boxes were generated

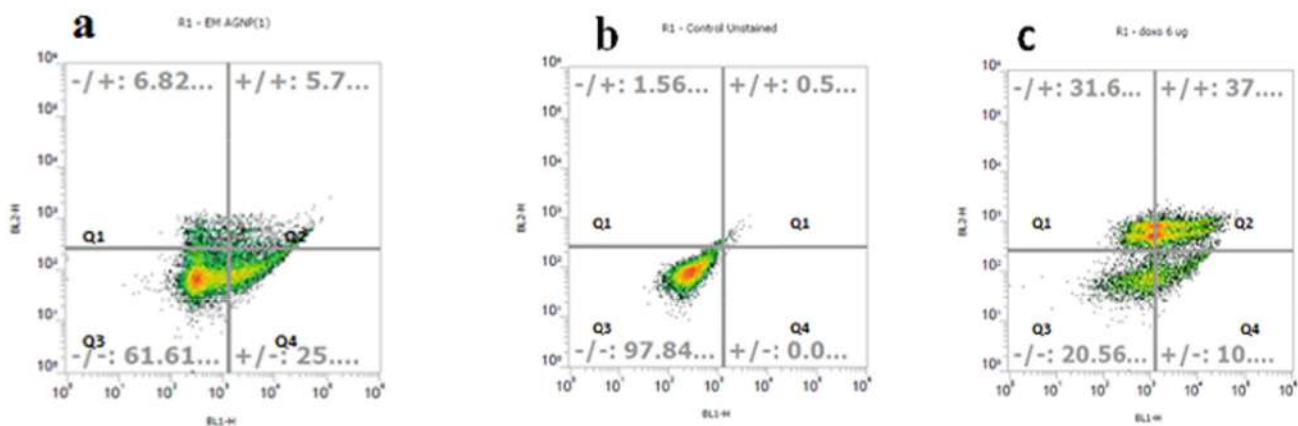


Fig. 5. Shows apoptosis occurred in a) Embelin AgNPs treated cells b) Untreated cells c) Doxorubicin standard anticancer drug treated cells at concentration of 6 µg/mL.

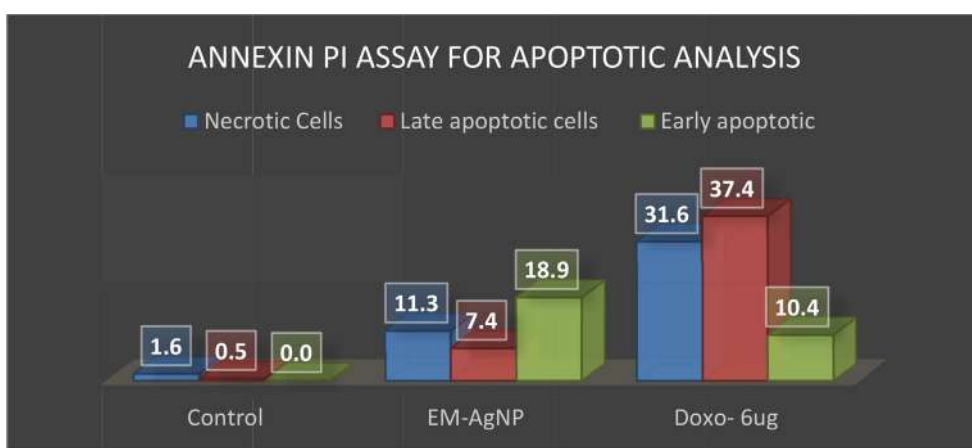


Fig. 6. Graphical representation of Annexin PI assay.

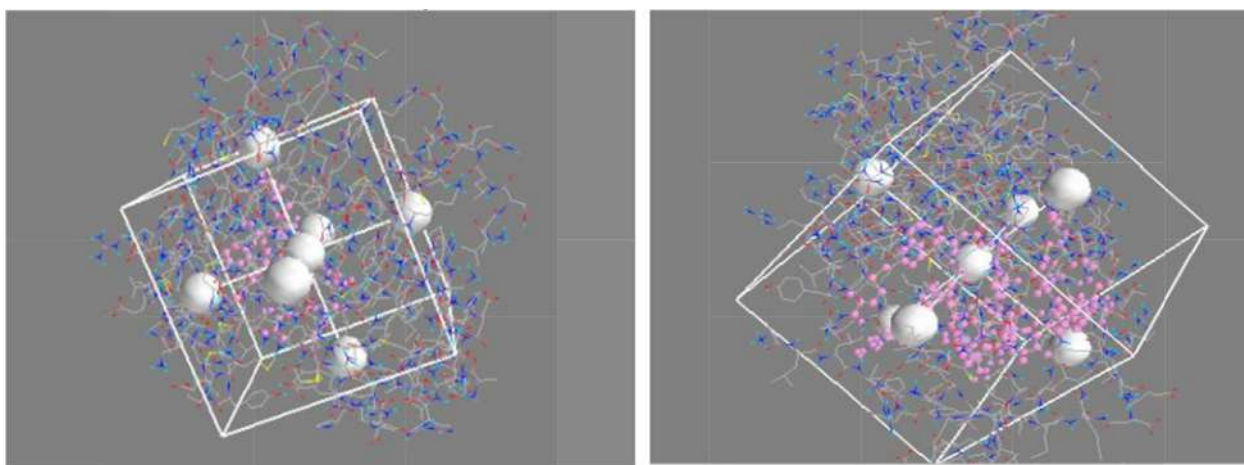


Fig. 7. a and b Grid generation for protein 1ERR and 3RCD with Embelin.

with dimensions (size_x = 61.63; size_y = 42.96; size_z = 68.70) and (size: x = 29.20; y = 32.53; z = 25.25) for ERα and HER2 respectively. Using the *Toggle Selection Sphere* option, the active amino acid residues were chosen to define the cavity. [32,33].

Embelin, a major phytochemical constituent of *Embelia ribes*, was docked with 1ERR and 3RCD PDB in the targeted cavity. Embelin showed binding energies with ERα and HER2 as -7 kcal/mol

and -7.2 kcal/mol respectively compared with standard drug Raloxifene and TAK-85 using AutoDock Vina. Embelin interactions with active amino acid residues are shown in Table 1. Docking poses of standard drug and embelin with 1ERR and 3RCD PDB in 3D- and 2D-poses along with the number of hydrogen bonds involved in the interaction are shown in Fig 8b. Fig 9a. Fig 9b. Fig 10a. Fig 10b. Fig 11a. Fig 11b..

Table 1
Embelin interactions with active amino acid residues.

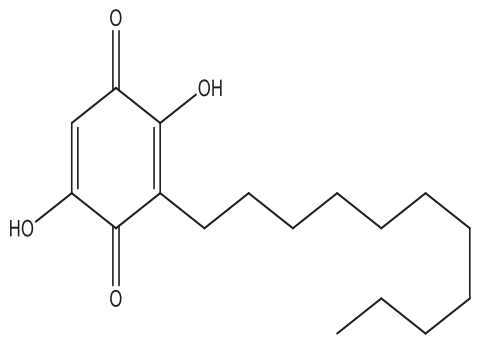
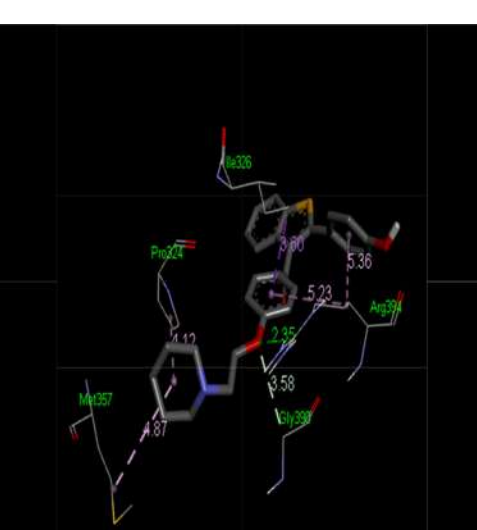
Sr. No.	Structure of the compound	Protein	G- Score	Name of the interaction with active amino acid residue and distance in Å
1.	Embelin 	1ERR	-7 kcal/mol	1. Conventional H bonds Ala 350 (2.16) Arg 394 (3.09) Phe404 (2.82) 2. Alkyl bonds Met421 (4.27) Ile 424 (4.37) Leu 387 (4.41) 3. π -alkyl Leu384 (4.83) Leu391 (5.33) Leu525 (4.39) 4. π - π Stage Phe 404 (5.10)
2.		3RCD	-7.2 kcal/mol	1. Conventional H-bonds Ser783 (2.26) Leu785 (2.45) 2. π -alkyl Met774 (5.39) 3. Alkyl Lys753 (4.71) Leu796 (5.43) Val734 (5.26)



Fig. 8a. 3D pose of 1ERR with Raloxifene.

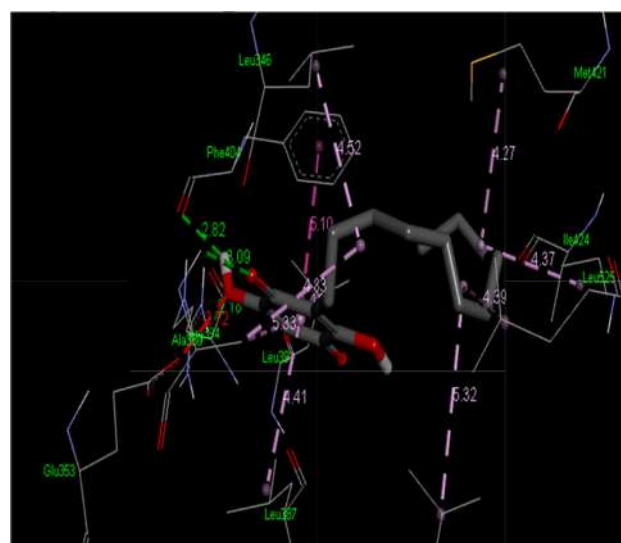


Fig. 9a. 3D pose of 1ERR with Embelin.

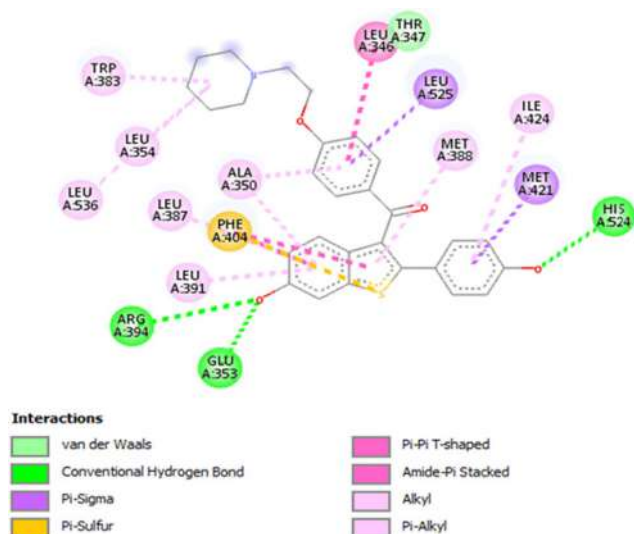


Fig. 8b. 2D pose of 1ERR with Raloxifene.

The shown images focus on the interactions of functional groups on ligands with active amino acid residues in the targeted cavity. Embelin established a network of molecular interactions (H-bonds, Van der Waals [VdW], alkyl, π -alkyl, and π -sigma bonds) with the active-site residues of ER α when analyzed with standard Raloxifenin 2D pose as shown in Fig. 8a. It established various binding interactions including conventional H-bonds (Arg 394, Glu 353, His 524), π -alkyl (Leu354, Trp 383, Leu 536, Leu 391), alkyl (Ile 424, Met 388), π - π Stage (Leu346), π - sulphur (Phe 404) and VdW (Thr 347). Likewise embelin established bonding interactions H-bonds (Ala350, Arg 394, Phe404) alkyl (Met421, Ile 424, Leu 387), π -alkyl (Leu384, Leu391, Leu525) π - π stack (Phe 404) with active site residues of ER α which is shown in Fig 9a. and Fig 9b..

The Fig 10a. and Fig 10a. shows interactions of functional group on ligand TAK- 285 with active amino acid residue in the targeted cavity of 3RCD. It established molecular interactions including conventional H-bonds (Ser783, Asn 850), C—H bonds (Gln799) halogen bond (Arg 784) π -alkyl (Leu 796, Lys 753, Ala 751, Val734), π - π

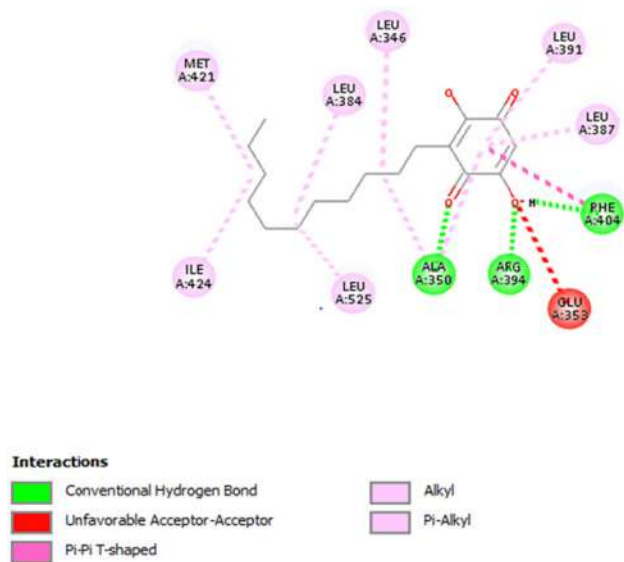


Fig. 9b. 2D pose of IERR with Embelin.

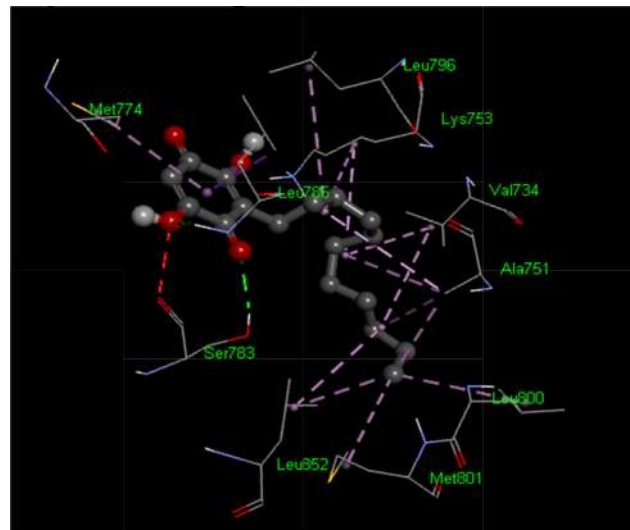


Fig. 11a. 3D pose of 3RCD with Embelin.

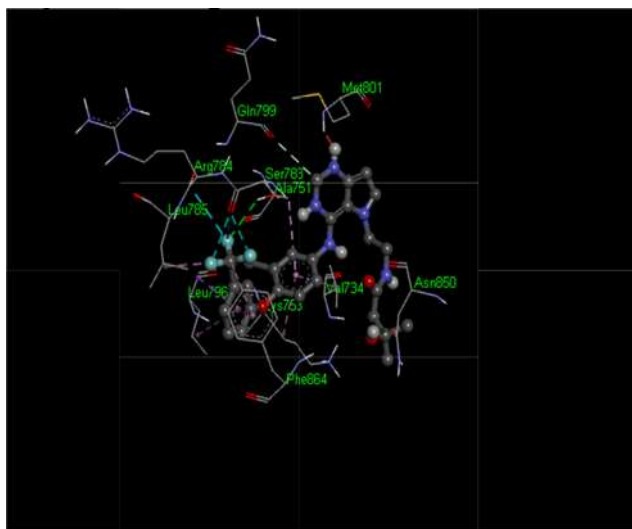


Fig. 10a. 3D pose of 3RCD with TAK-85.

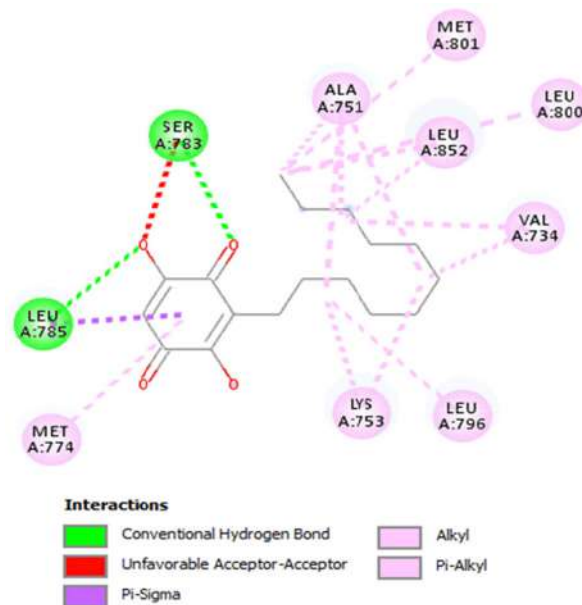


Fig. 11b. 2D pose of 3RCD with Embelin.

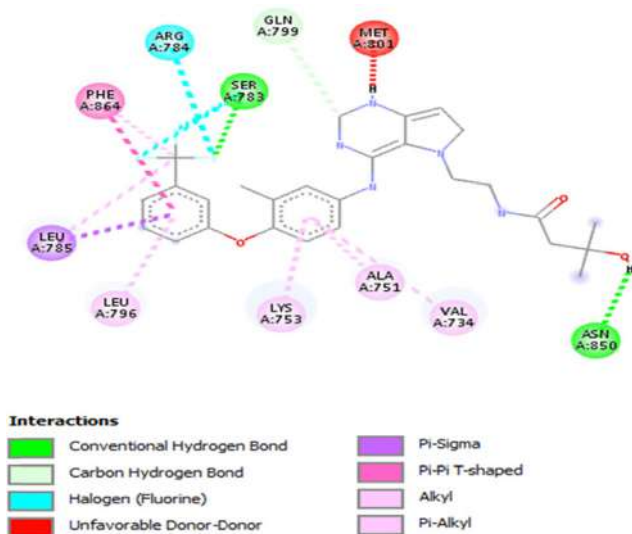


Fig. 10b. 2D pose of 3RCD with TAK-85.

stack (Phe 864). Fig 11a.A and Fig 11b. represents the 3D and 2D poses of Embelin with 3RCD. It established binding interactions involving conventional H-bonds (Ser783, Leu785), π -alkyl (Met774), alkyl (Lys753, Leu796, Val734).

The current study is an effort to identify anti-breast cancer activity of embelin that may be considered for drug development to treat breast cancer in conjugation with AgNPs. The binding energy of the ligand and its receptor quantifies the efficiency of the ligand–protein complex. Taken together, we therefore suggest that the embelin could act as potential inhibitors against ER positive and HER2 positive breast cancers.

4. Conclusion

The present study comprises the therapeutic prospective of Embelin of *Embelia ribes* derived AgNPs in the treatment of breast cancer. In this study, we reported a simple method of AgNPs

synthesis from Embelin and were characterized for size and stability. Nanoparticles used as drug carriers are of high stability, high carrier capacity, feasibility of incorporation of both hydrophilic and hydrophobic substances, feasibility of variable routes of administration. The Embelin AgNPs exhibited significant anticancer activity against MCF7 breast cancer cells. Apoptosis is a regulated and organized programmed cell death mechanism which could be studied with Annexin PI assay; which has shown a significant induction of apoptosis in MCF7 cells. FITC-labeled Annexin V shows high affinity towards phosphatidylserine PS exposed to outer leaflet of plasma membrane during apoptosis. The presence of PS in the outer leaflet initiates the signalling process of apoptosis resulting in cell death which can be quantified by flow cytometer. Embelin is a potent molecule and to understand it thoroughly more studies need to be conducted. Amalgamation of silver with Embelin in molecular nano level can do wonders and can be a potential drug.

Declaration of Competing Interest

The authors declare the following financial interests/personal relationships which may be considered as potential competing interests: Rutika R. Jagtap reports equipment, drugs, or supplies and statistical analysis were provided by Modern College of ASC, Shivajinagar, Pune 05.

References

- Hanahan D and Weinberg RA, Hallmarks of Cancer: The Next Generation, Cell 144, March 4, 2011, 646-674.
- J. Sario, Breast cancer in the young patient, Am. Surg. 76 (12) (2010) 1397–1400.
- Chakraborty S., Rahman T., The difficulties in cancer treatment, e-cancermedicallscience. 6:ed, (2012)16.
- I. Karmous, A. Pandey, K. Ben, K.B. Haj, A. Chaoui, Efficiency of the green synthesized nanoparticles as new tools in cancer therapy: insights on plant-based bioengineered nanoparticles, biophysical properties, and anticancer roles, Bio. Tra. Ele. Res. 196 (2020) 330–342.
- S.J. Amina, B. Guo, A review on the synthesis and functionalization of gold nanoparticles as a drug delivery vehicle, Int. J. Nanomed. 15 (2020) 9823–9857.
- Burdus, el, A.C.; Gherasim, O.; Grumezescu, A.M.; Mogoantă, L.; Ficai, A.; Andronescu, E. Biomedical Applications of Silver Nanoparticles: An Up-to-Date Overview. Nanomaterials 2018, 8, 681
- I. Ijaz, E. Gilani, A. Nazir, A. Bukhari, Detail review on chemical, physical and green synthesis, classification, characterizations and applications of nanoparticles, Green Chem. Lett. Rev. 13 (3) (2020) 223–245.
- Pešić, M. Development of natural product drugs in a sustainable manner. Brief for United Nations Global Sustainable Development: Report 2015
- M. Greenwell, P.K.S.M. Rahman, Medicinal plants: their use in anticancer treatment, Int. J. Pharm. Sci. Res. 6 (2015) 4103–4112.
- M. Bist, S.B. Prasad, *Embelia ribes* : a medicinal plant, J. Chem. Pharma. Res. 8 (4) (2016) 1229–1233.
- M. Chitra, E. Sukumar, V. Suja, C.S. Devi, Antitumor, anti-inflammatory and analgesic property of embelin, a plant product, Chemotherapy 40 (1994) 109–113, <https://doi.org/10.1159/000239181>.
- S. Mahendran, B.S. Thippeswamy, V.P. Veerapur, S. Badami, Anticonvulsant activity of embelin isolated from *Embelia ribes*, Phytomedicine 18 (2011) 186–188.
- M. Peng, B. Huang, Q. Zhang, S. Fu, D. Wang, X. Cheng, X. Wu, Z. Xue, L. Zhang, D. Zhang, et al., Embelin inhibits pancreatic cancer progression by directly inducing cancer cell apoptosis and indirectly restricting IL-6 associated inflammatory and immune suppressive cells, Cancer Lett. 354 (2014) 407–416.
- Y. Dai, H. Jiao, G. Teng, W. Wang, R. Zhang, Y. Wang, L. Hebbard, J. George, L. Qiao, Embelin reduces colitis-associated tumorigenesis through limiting IL-6/STAT3 signaling, Mol. Cancer Ther. 13 (2014) 1206–1216.
- M. Sreepriya, G. Bali, Chemopreventive effects of embelin and curcumin against N-nitrosodiethylamine/phenobarbital-induced hepatocarcinogenesis in Wistar rats, Fitoterapia 76 (2005) 549–555.
- Gaikwad D., Puranik S., In-Vitro Cytotoxicity Assay of Curry Leaves Silver Nanoparticles Against Thp-1 Cell Line, International Journal of Scientific Research in Science and Technology IJSRST, Volume 7, Issue 1, 45-52.
- Argade P. and Puranik S., Effect of Organically Grown Curcuma longa (Turmeric) on Leukemic and MCF-7 Cell Lines, International Journal of Current Microbiology and Applied Science (2015) Special Issue-2: 182-186.
- T. Atsumi, Y. Murakami, K. Shibuya, K. Tonosaki, S. Fujisawa, Induction of cytotoxicity and apoptosis and inhibition of cyclooxygenase-2 gene expression, by Curcumin and its analog, -Diisoegenol, Anticancer Res. 25 (2005) 4029–4036.
- Y. Feng, M. Spezia, S. Huang, C. Yuan, Z. Zeng, L. Zhang, X. Ji, W. Liu, B. Huang, W. Luo, B. Liu, Y. Lei, S. Du, A. Vuppapalapati, H.H. Luu, R.C. Haydon, T.C. He, G. Ren, Breast cancer development and progression: Risk factors, cancer stem cells, signaling pathways, genomics, and molecular pathogenesis, Genes & Diseases 5 (2) (2018) 77–106.
- N. Harbeck, M. Gnant, Breast cancer, Lancet 389 (2017) 1134–1150.
- H. Tan, Y. Zhong, Z. Pan, Autocrine regulation of cell proliferation by estrogen receptor-alpha in estrogen receptor-alpha-positive breast cancer cell lines, BMC Cancer 9 (2009) 31.
- J. Baselga, S. Swain, Novel anticancer targets: revisiting ERBB2 and discovering ERBB3, Nat. Rev. Cancer 9 (2009) 463–475.
- N. Jain, P. Jain, D. Rajput, U.K. Patil, Green synthesized plant-based silver nanoparticles: therapeutic prospective for anticancer and antiviral activity, Micro Nano Syst. Lett. 9 (2021) 5.
- S.S. Sanjay, Safe nano is green nano, Green Synth. Characterizat. Applicat. Nanopart. 14 (2019) 27–36.
- S. Ghosh, Green synthesis of nanoparticles and fungal infection, Green Synth. Characterizat. Applicat. Nanopart. 7 (2019) 75–86.
- S.N.N. Othman, M. Sekar, In-vitro antioxidant and cytotoxic Activities of silver nanoparticles of embelin isolated from *Embelia ribes*, Res. J. Pharm. Tech. 12 (9) (September 2019).
- M. Leema, G. Sreekumar, A. Sivan, Z.S. Pillai, Synthesis of silver nanoparticles from a bioactive precursor, Mater. Today: Proc. 18 (2019) 4724–4728.
- <https://www.thermofisher.com/in/en/home/references/protocols/cell-and-tissue-analysis/flow-cytometry-protocol/apoptosis/alexa-fluor-488-annexin-v-dead-cell-apoptosis-kit.html>.
- Dundas J, Ouyang Z, Tseng J, Binkowski A, Turpaz Y, Liang J. CASTp: computed atlas of surface topography of proteins with structural and topographical mapping of functionally annotated residues. Nucleic Acids Res. 2006;34(Web Server issue):W116–W118.
- Andrzej, M.; Brzozowski, k.; Ashley, C.W.; Pike, k.; Zbigniew, D.; Roderick, E.; Hubbard, T. B.; Owe, E.; Lars, O.; Geoffrey, L.G.; Jan-A, k. G.; Mats, C. Molecular basis of agonism and antagonism in the oestrogen receptor.NATURE.,1997,VOL 389, 753-757.
- Z. Yousuf, K. Iman, N. Iftikhar, M.S. Mirza, Structure-based virtual screening and molecular docking for the identification of potential multi-targeted inhibitors against breast cancer, Breast Cancer - Targets Ther. 9 (2017) 447–459.
- S. Dallakyan, A.J. Olson, Small-molecule library screening by docking with PyRx, Methods Mol. Biol. 1263 (1263) (2015) 243–250.
- O. Trott, A.J. Olson, AutoDock Vina: improving the speed and accuracy of docking with a new scoring function, efficient optimization, and multithreading, J. Comput. Chem. 31 (2) (2010) 455–461.
- M. Sivashanmugam, C. Raghunath, U. Vetrivel, Virtual screening studies reveal linarin as a potential natural inhibitor targeting CDK4 in retinoblastoma, J. Pharmacol. Pharmacother. 4 (4) (2013 Oct) 256–264.
- R. Xiong, J. Zhao, L. Gutgesell, Y. Wang, S. Lee, B. Karumudi, H. Zhao, Y. Lu, D. Tonetti, G. Thatcher, Novel selective estrogen receptor down regulators (SERDs) developed against treatment-resistant breast cancer, J. Med. Chem. 23 (2017) 1325–1342.
- S. Huang, S.Z. Grinter, X. Zou, Scoring functions and their evaluation methods for protein–ligand docking: recent advances and future directions, Phys. Chem. Chem. Phys. 12 (40) (2010) 12899, <https://doi.org/10.1039/c0cp00151a>.
- L. Ferreira, R. Dos Santos, G. Oliva, A. Andricopulo, Molecular docking and structure-based drug design strategies, Molecules 20 (7) (2015) 13384–13421, <https://doi.org/10.3390/molecules200713384>.



A systematic review on antifungal and insecticidal applications of biosynthesized metal nanoparticles

Bapusaheb H. Shinde^a, Shaukatali N. Inamdar^b, Sagar A. Nalawade^b, Sushilkumar B. Chaudhari^{a,*}

^a Department of Zoology, Institute of Science, Mumbai 400 032, India

^b Department of Chemistry, Dattatray Govindrao Walse Patil College, Pargaon Tarfe Awsari, Pune 412 406, India

ARTICLE INFO

Article history:

Available online 11 October 2022

Keywords:

Silver
Copper
Nanoparticles
Antibacterial
Antifungal
Insecticidal activity

ABSTRACT

Biosynthesized Metal nanoparticles are reported showing various activities viz. antibacterial, antifungal and insecticidal activity. There are various reports on the applicability of silver nanoparticles to control the human and animal diseases published recently. Silver nanoparticles especially are reported showing Antifungal activity against *Candida albicans*, Antibacterial activity against *Pseudomonas aeruginosa*, *E. coli*, and phytopathogenic fungi like *Bipolaris sorokiniana* and *Magnaporthe grisea*. Various metal nanoparticles were reported recently showing antifungal activity against pathogenic fungi like *Phoma glomerata*, *Phoma herbarium*, *Fusarium semitectum*, *Trichoderma* and *Candida albicans*. Insecticidal applications were also reported for the biosynthesized copper nanoparticles. This review aims for systematic appraisal of selected reports published during last few years (2014–2022) on biosynthesized metal nanoparticles demonstrating bioactivities viz. antifungal, antibacterial, insecticidal activities.

© 2022 Elsevier Ltd. All rights reserved.

Selection and peer-review under responsibility of the scientific committee of the Integrative Nanotechnology Perspective for Multidisciplinary Applications - 2022.

1. Introduction

Nanotechnology is a modern science which emerges from the various disciplines like physical, chemical, biological and engineering sciences. The development of the nanotechnology using these various nanoparticles is on high demand especially in the biomedical field. Nanoscience and nanotechnology have the potential to transform the food and agriculture industry, by providing novel tools to treat phytopathogenic diseases, and by also the enhancement of plant's nutrients absorption. Metal nanoparticles (NPs) signify a potential alternative way to prevent fungal proliferation in foodstuffs as they can effectively act as antifungal agents. Various nanomaterials reported to show the antifungal properties, the main are Ag, Au, Cu, ZnO, and NiO. The nanoparticles act as good candidates as antifungal agents in crops due to their unique physical and chemical properties, which often differ significantly from their bulk properties, The size of NPs directly alters the opto-electronic, catalytic, and even electric properties of the materials that can enhance the applicability of the NPs viz. antifungal, antibacterial, insecticidal etc. (Refer Fig. 1).

Recently biosynthetic methods employing either microorganisms or plant extracts have emerged as a simple and viable alternative to chemical and physical methods. Instead of using those eco-toxic chemical and physical methods, an eco-friendly "green synthesis" method for the synthesis of noble metal nanoparticles have identified. Fungi, actinomycetes and plant extracts are reported to be used for the synthesis of silver and gold nanoparticles. Shivshankar et al. reported synthesis of gold nanoparticles using lemon grass leaf extract.[1] Neem (*Azadiracta indica*) leaf extract was used to synthesize biometallic Au and Au-Ag core shell nanoparticles by Shiv Shankar et al.[2,3] Gold nanoparticles were also synthesized by Anukamwar et al. using Tamarind leaf extract.[4] Shivshankar et al. also reported synthesized silver nanoparticles using Geranium leaf extract.[5] Synthesis of gold and silver nanoparticles using Aloe vera (*L. Brum. f.*) plant extract was done by Chandra et al.[6] Synthesis of silver nanoparticles was also made successful by using Papaya fruit extract.[7].

There are some reports regarding the synthesis of metal nanoparticles using microorganisms. In the literature, synthesis of silver nanoparticles using fungus *Verticillium* sp. and extracellular biosynthesis of biometallic Au-Ag Alloy nanoparticles were reported using *Fusarium oxysporum* by use of fungi and actinomycetes for biosynthesis of metal nanoparticles.[8].

* Corresponding author.

E-mail address: sushil@iscm.ac.in (S.B. Chaudhari).

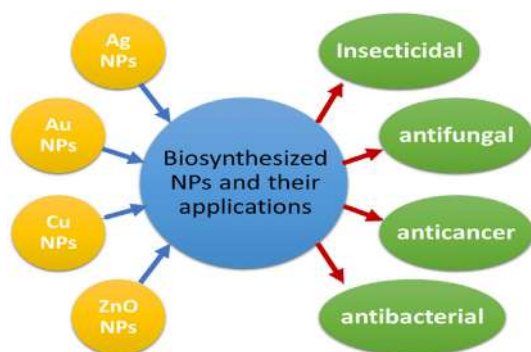


Fig. 1. Illustrative representation of bioactivities of various biosynthesized NPs.

This review aims to give brief of recent (2014–2022) approaches for the biosynthesis of metal nanoparticles viz. Silver and gold, copper oxide, zinc oxide and other NPs. The synthesized nanoparticles were reportedly tested against the animal and human infecting fungi species viz. *microsporium canis*, *trichophyton mentagrophytes*, *Phoma glomerata*, *Phoma herbarium*, *Fusarium semitectum* and many more.

2. Biosynthesis of nanoparticles

The details of the recent reports were formulated in terms of the table, giving details as nanoparticles formed, source used for the synthesis, bioactivity it showed and the targeted species as shown in the Table 1.

2.1. Synthesis using extracts of plant materials

Synthesis of silver nanoparticles

Nadia Hussein Mohamed *et al.* synthesized 12–32 nm sized Ag NPs using serum latex of *Calotropis procera* at 80 °C and were evaluated them against bacteria, dermatophytes and phytopathogenic fungi comparing with the activity of untreated latex. [12] Rihab Dridi *et al.* recently reported the Ag NPs biosynthesis with the help of *Anagallis monelli* extract. The Ag NPs obtained were 22 nm sized with face-centered cubic structure (fcc). [13] The product showed high antibacterial activity against both gram-positive and gram-negative bacteria. [13].

Manal A. Al-Mosa *et al.* used cheese weed mallow (*Malva parviflora* L.) for the synthesis of spherical 50 nm sized Ag NPs. [19] Sabah Ansar *et al.* utilized the leaf extract of Coriander sativum (CS) containing structural polymers, phenolic compounds and glycosidic bioactive macromolecules for the synthesis of Ag NPs. [21].

Afnan A. Alobathani *et al.* reported the synthesis of silver nanoparticles using *Saussurea costus* root aqueous extract. [24] Giovanni Benelli *et al.* utilized aqueous leaf extract of *Zornia diphylla* as reducing as well as capping agent for the synthesis of silver nanoparticles (Ag NP). [25].

Ravichandran Ramanibai *et al.* reported the synthesis of silver nanoparticles using isoamyl acetate isolated from *Annona squamosa* to test against mosquito larvae. [26].

Sumitra Chanda *et al.* synthesized silver nanoparticles with the help of flower broth of *Tagetes erecta* as reductant as a simple green way. The flower broth reduced silver ions and resulted in green synthesis of 10 to 90 nm spherical, hexagonal and irregular shaped Ag NPs. [27] Narayanasamy Mathivanan *et al.* synthesized Ag NPs with potent larvicidal activity against *Aedes aegypti*. [30] Venkatesan Thivaharan *et al.* reported the silver nanoparticles synthesized using *Calliandra haematocephala* leaf extract. [32] Said I. Behiry *et al.* demonstrated the green synthesis of spherical shaped

10 to 30 nm sized Ag NPs using *Acalypha wilkesiana* aqueous leaf extract. [35] Turki M. Dawoud *et al.* evaluated the effect of myco-synthesized silver nanoparticles using *Nigrospora oryzae* for the controlling plant diseases. [17].

Synthesis of copper nanoparticles

Rohini Trivedi *et al.* reported an environmentally friendly green synthesis of Cu NPs using the leaf extract of *Celastrus paniculatus*. The obtained copper nanoparticles were spherical in shape with 2–10 nm size, the average size was 5 nm obtained using the SEM and TEM techniques. [11].

Synthesis of gold nanoparticles

Gurumallesh Prabu *et al.* synthesized Au NPs by green method using extract of *Acorus calamus* rhizome as reducing agent. [29].

Synthesis of zinc oxide nanoparticles

Pragati Jamdagni *et al.* demonstrated the synthesis of ZnO NPs utilizing the aqueous flower extract of *Nyctanthes arbor-tristis*. [10] Flower extract acted as the biological reducing agent for the preparation of ZnO NPs from zinc acetate dihydrate. These nanoparticles were tested for their antifungal potential against the five phytopathogens. [10] Abdolhossien Miri *et al.* synthesized ZnO NPs having hexagonal shaped sheet like structures formed with sizes of 40–80 nm. The zinc oxide nanoparticles were obtained by green synthesis using $Zn(SO_4) \cdot 7H_2O$ and aqueous extract of *Prosopis farcta*. [15] Nikte M. Gómez-Ortíz *et al.* reported the synthesis of antifungal ZnO NPs by using the Avocado (*Persea americana*) and papaya (*Carica papaya*) fruits. [40].

Mohammed N. Al-anbr *et al.* reported synthesis of ZnO NPs using the hot water extract of *Sargassum wightii* (Sw). [28] Giovanni Benelli *et al.* reported the green synthesis of ZnO NPs using the *Ulva lactuca* extract, which showed high toxicity against *Aedes aegypti* larvae. Histopathological effects caused by ZnO nanoparticles penetration in the insect's body were also reported in the study. [31].

Synthesis of other oxide nanoparticles

M. Jayachandran *et al.* synthesized 12 nm sized NiO NPs by green method utilizing the phytoconstituents present in the neem leaf. [3] Henam Sylvia Devi *et al.* utilized the *Urtica dioica* leaf extract for the synthesis of CuO and Al_2O_3 NPs using biosynthetic approach. [18].

Nikte M. Gómez-Ortíz *et al.* also reported the synthesis of anti-fungal MgO NPs by using the Avocado (*Persea americana*) and papaya (*Carica papaya*) fruits. [40].

2.2. Synthesis using bacterial materials

Merlin P. Thangaraj *et al.* reported the synthesis of *Bacillus thuringiensis* coated zinc oxide nanoparticles (Bt-ZnO NPs). [22] Rajan Maheswaran *et al.* reported the synthesis of silver nanoparticles using isolated entomopathogenic actinobacteria *Actinokineospira fastidiosa*. These biosynthesized Ag NPs were tested as ovicidal, larvicidal, oviposition deterrent and enzyme activity against *Aedes aegypti*, *Anopheles stephensi* and *Culex quinquefasciatus*. [36].

2.3. Synthetic route using various fungi

Sardell *et al.* utilized the *Penicillium citrinum* to synthesize Ag NPs. [9] Utilization of plant pathogenic fungi in the Ag NPs biosyn-

Table 1

An overview of the recently reported (during 2014–2022) metal and metal oxide nanoparticles biosynthesized for various biological applications.

Nanoparticles	Source for Synthesis	Bioactivity	Targeted for treatment of	Year	reference
Ag NPs	<i>Penicillium citrinum</i>	Antifungal	<i>Aspergillus flavus</i>	2017	Sardella et al.[9]
ZnO NPs	flower extract of <i>Nyctanthes arbor-tristis</i> .	Antifungal	<i>Alternaria alternata</i> , <i>Aspergillus niger</i> , <i>Botrytis cinerea</i> , <i>Fusarium oxysporum</i> and <i>Penicillium expansum</i>	2018	Pragati Jamdagni et al.[10]
Cu NPs	leaf extract of <i>C.paniculatus</i> .	Antifungal activity	<i>F.oxysporum</i> .	2020	Rohini Trivedi et al.[11]
Ag NPs	latex of <i>Calotropis procera</i>	antibacterial antifungal	<i>Escherichia coli</i> , <i>Pseudomonas aeruginosa</i> and <i>Serratia sp. Trichophyton rubrum</i> , <i>Candida albicans</i> and <i>Aspergillus terreus</i> .	2014	Nadia Hussein Mohamed et al. [12]
Ag NPs	<i>Anagallis monelli</i> extract.	antibacterial	species <i>Escherichia coli</i> , <i>Serratia marcescens</i> , and <i>Klebsiella pneumoniae</i> . <i>Staphylococcus aureus</i> and <i>Micrococcus luteus</i> <i>Candida albicans</i>	2022	Rihab Dridi et al. [13]
Ag NPs	yeast	yeast antifungal activity	<i>Cryptococcus laurentii</i> and <i>Rhodotorula glutinis</i> .	2016	Jorge G. Fernández et al. [14]
ZnO-NPs	<i>Prosopis farcta</i> extract	antifungal	against <i>Candida albicans</i>	2019	Abdolhossein Miri et al.[15]
Ag NPs	Purchased Ag NPs solution	antifungal	<i>Trichosporon asahii</i> .	2016	Zhi-Kuan Xia et al.[16]
Ag NPs	<i>Nigrospora oryzae</i>	antifungal	<i>Fusarium spp</i>	2021	Turki M. Dawoud et al.[17]
CuO and Al ₂ O ₃ NPs	<i>Urtica dioica</i> leaf extract	antifungal activity	<i>Mucor piriformis</i>	2021	Henam Sylvia Devi et al.[18]
Ag NPs	<i>Leaf Malva parviflora</i>	antifungal	<i>Helminthosporium rostratum</i> , <i>Fusarium solani</i> , <i>Fusarium oxysporum</i> , and <i>Alternaria alternata</i> .	2021	Manal A. Al-Mosa et al.[19]
Ag NPs	<i>Penicillium verrucosum</i>	antifungal	<i>Fusarium chlamydosporum</i> and <i>Aspergillus flavus</i>	2021	Bandar M. A. Almunqedhi et al. [20]
Ag NPs	<i>Coriander sativum</i>	anticancer	MCF-7 cell line	2021	SabahAnsar et al. [21]
ZnO NPs	<i>Bacillus thuringiensis</i>	biopesticidal	pulse beetle, <i>Callosobruchus maculatus</i>	2017	Merlin P. Thangaraj et al. [22]
Gold	<i>Mentha</i> and <i>Pelargonium</i> Extracts	medical applications	PBS media as human blood	2015	D. Ekinci et al.[23]
NiO NPs	Neem leaves	antibacterial	<i>Staphylococcus aureus</i> <i>Escherichia coli</i>	2016	M. Jayachandran et al.[3]
Ag NPs	<i>Saussurea costus</i> root aqueous extract	catalytic	catalytic degradation efficacy of safranin dye	2021	Afnan A. Alobathani et al. [24]
Ag NPs	<i>Zornia diphylla</i> leaves	larvicidal	against malaria and arbovirus vectors <i>Anopheles subpictus</i> , the dengue vector <i>Aedes albopictus</i> and the Japanese encephalitis vector <i>Culex tritaeniorhynchus</i> .	2016	Giovanni Benelli et al.[25]
Ag NPs	<i>Annona squamosa</i> leaves	larvicidal	<i>Aedes aegypti</i> and <i>Culex quinquefasciatus</i>	2016	Ravichandran Ramanibai et al. [26]
Ag NPs	from marigold flower	antimicrobial	<i>Staphylococcus aureus</i> and <i>Bacillus cereus</i>), Gram negative (<i>Escherichia coli</i> and <i>Pseudomonas aeruginosa</i>) <i>Candida glabrata</i> , <i>Candida albicans</i> , <i>Cryptococcae neoformans</i> . <i>. subtilis</i> , <i>S. aureus</i>) and Gram-negative (<i>S. sonnei</i> , <i>P. aeruginosa</i>) <i>Aedes aegypti</i> 3	2015	Sumitra Chanda et al.[27]
ZnO NPs	<i>Sargassum wightii</i>	antibacterial and insecticidal	<i>Staphylococcus aureus</i> and <i>Bacillus cereus</i>)	2018	Mohammed N. Al-anbr et al.[28]
Au NPs	herbal <i>Acorus calamus</i> rhizome extract	antibacterial	<i>Staphylococcus aureus</i> and <i>Bacillus cereus</i>)	2019	Gurumallesh Prabu et al.[29]
Ag NPs	<i>Annona reticulata</i>	larvicidal and antimicrobial	<i>Aedes aegypti</i> . <i>Bacillus cereus</i> , <i>Staphylococcus aureus</i> , <i>Pseudomonas aeruginosa</i> , <i>Escherichia coli</i> and <i>Candida albicans</i> respectively.	2019	Narayanasamy Mathivanan et al. [30]
ZnO	<i>Ulva lactuca</i> seaweed extract	insecticidal bactericidal	<i>Aedes aegypti</i> (<i>Bacillus licheniformis</i> and <i>Bacillus pumilis</i>) and Gram negative (<i>Escherichia coli</i> and <i>Proteus vulgaris</i>)	2018	Giovanni Benelli et al.[31]
Ag NPs	<i>Calliandra haematocephala</i> leaf extract	bactericidal	<i>Escherichia coli</i> – pathogenic bacteria	2017	Venkatesan Thivaharan et al. [32]
Cu NPs	actinomycete <i>Streptomyces capillspiralis</i>	antimicrobial	applications against infectious microorganisms, biocontrol of phytopathogenic fungi and health nasty insects	2018	Abdullah M. Abdo et al.[33]
Ag NPs	green algae (<i>Spirogyra hyalina</i>)	antibacterial, antifungal, insecticidal,	<i>Pseudomonas aeruginosa</i> , <i>Fusarium solani</i>	2022	Syed Ali Raza Shah et al.[34]
Ag NPs	<i>Acalypha wilkesiana</i> extract	nematicidal activity	<i>Tribolium castaneum</i> (a common grain pest). root-knot nematode	2021	Said I. Behiry et al.[35]
Ag NPs	<i>Actinokineospora fastidiosa</i>	Insecticidal; ovicidal, larvicidal,	<i>Aedes aegypti</i> , <i>Anopheles stephensi</i> and <i>Culex quinquefasciatus</i> .	2021	Rajan Maheswaran et al [36]
Ag/AgCl-NPs	from <i>Zizyphus mauritiana</i> fruit extract	antibacterial, antifungal	(<i>Bacillus subtilis</i> , <i>Shigella boydii</i> , and <i>Escherichia coli</i>) and two fungi (<i>Aspergillus niger</i> and <i>Trichoderma spp.</i>)	2020	Mohammad Taufiq Alam et al. [37]

Table 1 (continued)

Nanoparticles	Source for Synthesis	Bioactivity	Targeted for treatment of	Year	reference
Ag NPs	curcumin	antibacterial	<i>Staphylococcus aureus</i> , <i>Pseudomonas aeruginosa</i> , and <i>Candida auris</i> .	2020	Iza Radecka et al [38]
Ag NPs	hydroxyapatite	Antifungal	<i>Candida Species</i>	2019	Diogo P. Volanti et al.[39]
MgO and ZnO NPs	Avocado (<i>Persea americana</i>) and papaya (<i>Carica papaya</i>)	Antifungal	<i>Colletotrichum gloeosporioides</i>	2018	Nikte M. Gómez-Ortiz et al.[40]
ZnO NPs	Plant Parts of <i>Bixa orellana</i>	Antibacterial and antifungal	<i>Staphylococcus aureus</i> and <i>Bacillus subtilis</i> <i>Penicillium</i> sp., <i>Aspergillus flavus</i> , <i>Fusarium oxysporum</i> , and <i>Rhizoctonia solani</i>)	2022	Balaprasad Ankanwar et al. [41]

thesis as well as the use of bio-Ag NPs to control fungal plant diseases were successfully achieved.

Jorge G. Fernández *et al.* reported biosynthesis of silver nanoparticles, using the yeast. [14] Bandar M. A. Almunqedhi *et al.* also reported the biosynthesis of 10–12 nm sized Ag NPs, using the fungus *Penicillium verrucosum*. [20] In this method, the silver nanoparticles were synthesized by reacting silver nitrate (AgNO₃) with the cell free filtrates of the fungal culture.

3. Applications of the biosynthesized nanoparticles

3.1. Fungicidal applications

Jorge G. Fernández *et al.* reported the antifungal activity of the biosynthesis of Ag NPs against the *Cryptococcus laurentii* and *Rhodotorula glutinis*. [14] Henam Sylvia Devi *et al* reported the antifungal activity of prepared CuO NPs against the fungus *Aspergillus niger* and *Mucor piriformis*. [18] The NPs exhibited significant antimycotic activity against the examined fungal pathogens along with synergistic effects of small size and free radical scavenging potential of the synthesized CuO NPs in enhancing the antifungal activity.

Manal A. Al-Mosa *et al.* reported maximum reduction in mycelial growth by biosynthesized Ag NPs against *H. rostratum* (88.6 %). [19] Whereas, the leaf extract of *M. parviflora* was found most effective against *F. solani* (65.3 %). Further the silver nanoparticles and leaf extract of *M. parviflora* could be explored for the development of the new types of fungicide.

Bandar M. A. Almunqedhi *et al.* demonstrated the antifungal activity of biosynthesized Ag NPs, 150 ppm of the Ag NPs reported suppressing the growth of *F. chlamyosporum* and *A. flavus* by about 50 %.[20].

3.2. Antibacterial applications

High antibacterial activities were reported by Dridi *et al* against both the gram-positive and gram-negative bacteria. The bacteria species studied were *Staphylococcus aureus*, *Micrococcus luteus*, *Escherichia coli*, *Serratia marcescens*, and *Klebsiella pneumoniae*. [13] Sardell *et al.* narrated the applications of metal nanoparticles and current trends in relation to food packaging, air filter coating and water disinfection, packaging material. [9].

Sumitra Chanda *et al.* utilized Ag NPs for the evaluation of various commercial antibiotics against Gram positive (*Staphylococcus aureus* and *Bacillus cereus*), Gram negative (*Escherichia coli* and *Pseudomonas aeruginosa*) bacteria and fungi (*Candida glabrata*, *Candida albicans*, *Cryptococcae neoformans*). [27].

Mohammed N. Al-anbr *et al.* used ZnO NPs which showed high antibiofilm activity against Gram-positive (*B. subtilis*, *S. aureus*) and Gram-negative (*S. sonnei*, *P. aeruginosa*) microbial pathogens. The report demonstrated that ZnO nanoparticles can be used as the bacteriostatic and immunostimulant agents through

immersion and dietary administration enhancing immunity of green tiger shrimp. [28] Gurumallesh Prabu *et al.* reported antibacterial activity of AuNPs coated cotton fabrics tested against Gram positive (*Staphylococcus aureus*) and Gram negative (*Escherichia coli*) bacterial strains. It showed that gold nanoparticles coated cotton fabric exhibited higher antibacterial activity than other test samples against *E. coli*. [29].

Narayanasamy Mathivanan *et al.* reported silver nanoparticle as a potent antimicrobial activity against *Bacillus cereus*, *Staphylococcus aureus*, *Pseudomonas aeruginosa*, *Escherichia coli* and *Candida albicans* respectively. [30].

Giovanni Benelli *et al.* reported excellent bactericidal activity by the ZnO NPs on Gram positive (*Bacillus licheniformis* and *Bacillus pumilis*) and Gram negative (*Escherichia coli* and *Proteus vulgaris*) bacteria. [31].

3.3. Insecticidal uses

Merlin P. Thangaraj *et al.* studied the action of *Bacillus thuringiensis* coated zinc oxide nanoparticles (Bt-ZnO NPs) on the pulse beetle, *Callosobruchus maculatus*. The Bt-ZnO NPs were highly effective in the control of *C. maculatus* and caused 100 % mortality at 25 µg/mL. the effect was due to decrease in the mid-gut α-amylase, cysteine protease, α-glucosidase and glutathione S-transferase (GST) activity in *C. maculatus*. [22].

Giovanni Benelli *et al.* checked acute toxicity of *Z. diphylla* leaf extract and biosynthesized AgNP against larvae of the malaria vector *Anopheles subpictus*, the dengue vector *Aedes albopictus* and the Japanese encephalitis vector *Culex tritaeniorhynchus*. Both the *Z. diphylla* leaf extract and Ag NP showed dose dependent larvicidal effect against all tested mosquito species. Compared to the leaf aqueous extract, biosynthesized Ag NP showed higher toxicity against *An. subpictus*, *Ae. albopictus*, and *Cx. tritaeniorhynchus* with LC₅₀ values of 12.53, 13.42 and 14.61 µg/ml, respectively. [25].

Mohammed N. Al-anbr *et al.* reported that ZnO NPs enhanced immune parameters of the green tiger shrimp, *Penaeus semisulcatus*. The ZnO NPs nanoparticles showed high antibiofilm activity on Gram-positive and negative bacteria. They were reported to be toxic to larvae of *Aedes aegypti* mosquitoes, which vector Zika virus. [28].

Syed Ali Raza Shah *et al.* reported that silver nanoparticles synthesized using green algae *Spirogyra hyalina* as a capping and reducing agent, showed 30 % mortality against *Tribolium castaneum* (a common grain pest). The maximum antibacterial and antifungal activity was reported for *Pseudomonas aeruginosa* (18 ± 1.2 mm) and *Fusarium solani* (14.3 ± 0.6 mm), respectively. [34] Rajan Maheswaran *et al.* reported the synthesis of Ag-NPs using a novel stain *Actinokineospora fastidiosa* can tested it to control various mosquito species and its pharmacological applications. The highest ovicidal, larvicidal, oviposition deterrent and

enzyme activity were noted against *Aedes aegypti*, *Anopheles stephensi* and *Culex quinquefasciatus*. [36].

3.4. Anticancer and other applications

Sabah Ansar *et al.* synthesized Ag NPs using extract of *Coriander sativum* and utilized the synthesized NPs for the anticancer studies. The in vitro anticancer effect was confirmed at different concentrations on the MCF-7 cell line with decrease in cell viability which was proportionately related to the concentration of CS-AgNPs illustrating the toxic nature of synthesized silver nanoparticles on cancerous cells. [21].

D. Ekinci *et al.* utilized the *Mentha* and *Pelargonium* plant extracts for the synthesis of gold nanoparticles. For medical applications gold nanoparticles performance was observed in PBS media which resembles the human blood. [23].

Abdullah M. Abdo *et al.* biosynthesized Cu NPs, which showed various biomedical applications against infectious microorganisms, biocontrol of phytopathogenic fungi and health nasty insects that represented the hopeful uses of copper nanoparticles as a unique approach to manage these health threatening problems. [33].

Said I. Behiry *et al.* biosynthesized silver nanoparticles (Ag NPs) using *Acalypha wilkesiana* aqueous leaf extract. The nematocidal activity of biosynthesized Ag NPs were evaluated in vitro against root-knot nematode (*Meloidogyne incognita*). [35].

4. Conclusions

Silver nanoparticles have well-evolved as antimicrobial, antifungal as well as insecticidal agents and a nano-drug carrier with enormous potential for the success in the field of medicine which can bring a new era of agrochemicals. The CuO and ZnO NPs prepared utilizing green synthesis were reported to show higher antifungal and insecticidal activities respectively. Its advantageous to utilize these biosynthesized nanoparticles as insecticides as there is a low risk of developing resistance by the insects in long term usages of these materials. Further exploration of novel applications of the combined effect of biosynthesized composite nanoparticles to produce the effective and newer outcomes is yet open to new researchers in the field of nanoscience and nanotechnology. Thus, a systematic appraisal of selected reports published on biosynthesized metal nanoparticles demonstrating bioactivities viz. antifungal, antibacterial, insecticidal activity during the past few years (during 2014–2022) were described in the current review.

CRedit authorship contribution statement

Bapusaheb H. Shinde: Conceptualization, Writing – original draft. **Shaukatali N. Inamdar:** . **Sagar A. Nalawade:** . **Sushilkumar B. Chaudhari:** Project administration, Supervision.

Declaration of Competing Interest

The authors declare that they have no known competing financial interests or personal relationships that could have appeared to influence the work reported in this paper.

Acknowledgements

The authors would like to thank Dattatray Govindrao Walse Patil College, Pargaon Tarfe Awsari, Pune for their constant support.

References

- [1] S.S. Shankar, A. Rai, A. Ahmad, M. Sastry, Controlling the optical properties of lemongrass extract synthesized gold nanotriangles and potential application in infrared-absorbing optical coatings, *Chem. Mater.* 17 (3) (2005) 566–572.
- [2] S.S. Shankar, A. Rai, A. Ahmad, M. Sastry, Rapid synthesis of Au, Ag, and bimetallic Au core–Ag shell nanoparticles using Neem (*Azadirachta indica*) leaf broth, *J. Colloid Interface Sci.* 275 (2) (2004) 496–502.
- [3] V. Helan, J.J. Prince, N.A. Al-Dhabi, M.V. Arasu, A. Ayeshamariam, G. Madhumitha, S.M. Roopan, M. Jayachandran, Neem leaves mediated preparation of NiO nanoparticles and its magnetization, coercivity and antibacterial analysis, *Results Phys.* 6 (2016) 712–718.
- [4] B. Ankamwar, M. Chaudhary, M. Sastry, Gold nanotriangles biologically synthesized using tamarind leaf extract and potential application in vapor sensing, *Synth. React. Inorg., Met.-Org., Nano-Met. Chem.* 35 (1) (2005) 19–26.
- [5] S.S. Shankar, A. Ahmad, M. Sastry, Geranium Leaf Assisted Biosynthesis of Silver Nanoparticles, *Biotechnol. Prog.* 19 (6) (2003) 1627–1631.
- [6] S.P. Chandran, M. Chaudhary, R. Pasricha, A. Ahmad, M. Sastry, Synthesis of gold nanotriangles and silver nanoparticles using aloe vera plant extract, *Biotechnol. Prog.* 22 (2) (2006) 577–583.
- [7] D. Jain, H. Daima, S. Kachhwala, S. Kothari, Synthesis of plant-mediated silver nanoparticles using papaya fruit extract and evaluation of their anti microbial activities, *Digest J. Nanomater. Biostruct.* 4 (2009) 557–563.
- [8] R. Sanghi, P. Verma, Biomimetic synthesis and characterisation of protein capped silver nanoparticles, *Bioresour. Technol.* 100 (1) (2009) 501–504.
- [9] D. Sardella, R. Gatt, V.P. Valdramidis, Metal nanoparticles for controlling fungal proliferation: quantitative analysis and applications, *Curr. Opin. Food Sci.* 30 (2019) 49–59.
- [10] P. Jamdagni, P. Khatri, J.S. Rana, Green synthesis of zinc oxide nanoparticles using flower extract of *Nyctanthes arbor-tristis* and their antifungal activity, *J. King Saud Univ. – Sci.* 30 (2) (2018) 168–175.
- [11] S.C. Mali, A. Dhaka, C.K. Githala, R. Trivedi, Green synthesis of copper nanoparticles using *Celastrus paniculatus* Willd. leaf extract and their photocatalytic and antifungal properties, *Biotechnol. Rep.* 27 (2020) e00518.
- [12] N.H. Mohamed, M.A. Ismail, W.M. Abdel-Mageed, A.A. Mohamed Shoreit, Antimicrobial activity of latex silver nanoparticles using *Calotropis procera*, *Asian Pacific J. Trop. Biomed.* 4 (11) (2014) 876–883.
- [13] R. Dridi, B. Essghaier, H. Hannachi, G.B. Khedher, C. Chaffei, M.F. Zid, Biosynthesized silver nanoparticles using *Anagallis monelli*: evaluation of antioxidant activity, antibacterial and antifungal effects, *J. Mol. Struct.* 1251 (2022) 132076.
- [14] J.G. Fernández, M.A. Fernández-Baldo, E. Berni, G. Camí, N. Durán, J. Raba, M.I. Sanz, Production of silver nanoparticles using yeasts and evaluation of their antifungal activity against phytopathogenic fungi, *Process Biochem.* 51 (9) (2016) 1306–1313.
- [15] A. Miri, N. Mahdinejad, O. Ebrahimi, M. Khatami, M. Sarani, Zinc oxide nanoparticles: biosynthesis, characterization, antifungal and cytotoxic activity, *Mater. Sci. Eng., C* 104 (2019) 109981.
- [16] Z.-K. Xia, Q.-H. Ma, S.-Y. Li, D.-Q. Zhang, L. Cong, Y.-L. Tian, R.-Y. Yang, The antifungal effect of silver nanoparticles on *Trichosporon asahii*, *J. Microbiol. Immunol. Infect.* 49 (2) (2016) 182–188.
- [17] T.M. Dawoud, M.A. Yassin, A.R.M. El-Samawaty, A.M. Elgorban, Silver nanoparticles synthesized by *Nigrospora oryzae* showed antifungal activity, *Saudi J. Biol. Sci.* 28 (3) (2021) 1847–1852.
- [18] H.S. Devi, M.A. Boda, S. Rubab, S. Parveen, A.H. Wani, M.A. Shah, Chapter Thirteen - Biosynthesis and antifungal activities of CuO and Al₂O₃ nanoparticles, in: S.K. Verma, A.K. Das (Eds.), *Comprehensive Analytical Chemistry*, Elsevier, 2021, pp. 533–546.
- [19] F. Al-Otibi, K. Pervveen, N.A. Al-Saif, R.I. Alharbi, N.A. Bokhari, G. Albasher, R.M. Al-Otaibi, M.A. Al-Mosa, Biosynthesis of silver nanoparticles using *Malva parviflora* and their antifungal activity, *Saudi J. Biol. Sci.* 28 (4) (2021) 2229–2235.
- [20] M.A. Yassin, A.M. Elgorban, A.-E.-R.-M.-A. El-Samawaty, B.M.A. Almunqedhi, Biosynthesis of silver nanoparticles using *Penicillium verrucosum* and analysis of their antifungal activity, *Saudi J. Biol. Sci.* 28 (4) (2021) 2123–2127.
- [21] R. Alsubki, H. Tabassum, M. Abudawood, A.A. Rabaan, S.F. Alsobaie, S. Ansar, Green synthesis, characterization, enhanced functionality and biological evaluation of silver nanoparticles based on *Coriander sativum*, *Saudi J. Biol. Sci.* 28 (4) (2021) 2102–2108.
- [22] B. Malaikozhundan, B. Vaseeharan, S. Vijayakumar, M.P. Thangaraj, *Bacillus thuringiensis* coated zinc oxide nanoparticle and its biopesticidal effects on the pulse beetle, *Callosobruchus maculatus*, *J. Photochem. Photobiol. B: Biol.* 174 (2017) 306–314.
- [23] A. Jafarizad, K. Safaee, S. Gharibian, Y. Omid, D. Ekinci, Biosynthesis and in vitro study of gold nanoparticles using mentha and pelargonium extracts, *Procedia Mater. Sci.* 11 (2015) 224–230.
- [24] A.R.M. Abd El-Aziz, A. Gurusamy, M.R. Althoman, S.M. Shehata, S.M. Hisham, A. A. Alobathani, Silver nanoparticles biosynthesis using *Saussurea costus* root aqueous extract and catalytic degradation efficacy of safranin dye, *Saudi J. Biol. Sci.* 28 (1) (2021) 1093–1099.
- [25] M. Govindarajan, M. Rajeswary, U. Muthukumar, S.L. Hoti, H.F. Khater, G. Benelli, Single-step biosynthesis and characterization of silver nanoparticles using *Zornia diphylla* leaves: a potent eco-friendly tool against malaria and arbovirus vectors, *J. Photochem. Photobiol. B: Biol.* 161 (2016) 482–489.
- [26] K. Velayutham, R. Ramanibai, Larvicidal activity of synthesized silver nanoparticles using isoamyl acetate identified in *Annona squamosa* leaves

- against *Aedes aegypti* and *Culex quinquefasciatus*, *J. Basic Appl. Zool.* 74 (2016) 16–22.
- [27] H. Padalia, P. Moteriya, S. Chanda, Green synthesis of silver nanoparticles from marigold flower and its synergistic antimicrobial potential, *Arabian J. Chem.* 8 (5) (2015) 732–741.
- [28] R. Ishwarya, B. Vaseeharan, S. Subbaiah, A.K. Nazar, M. Govindarajan, N.S. Alharbi, S. Kadaikunnan, J.M. Khaled, M.N. Al-anbr, Sargassum wightii-synthesized ZnO nanoparticles – from antibacterial and insecticidal activity to immunostimulatory effects on the green tiger shrimp *Penaeus semisulcatus*, *J. Photochem. Photobiol. B: Biol.* 183 (2018) 318–330.
- [29] R.M. Ganesan, H. Gurumallesh Prabu, Synthesis of gold nanoparticles using herbal *Acorus calamus* rhizome extract and coating on cotton fabric for antibacterial and UV blocking applications, *Arabian J. Chem.* 12 (8) (2019) 2166–2174.
- [30] E. Parthiban, N. Manivannan, R. Ramanibai, N. Mathivanan, Green synthesis of silver-nanoparticles from *Annona reticulata* leaves aqueous extract and its mosquito larvicidal and anti-microbial activity on human pathogens, *Biotechnol. Rep.* 21 (2019) e00297.
- [31] R. Ishwarya, B. Vaseeharan, S. Kalyani, B. Banumathi, M. Govindarajan, N.S. Alharbi, S. Kadaikunnan, M.N. Al-anbr, J.M. Khaled, G. Benelli, Facile green synthesis of zinc oxide nanoparticles using *Ulva lactuca* seaweed extract and evaluation of their photocatalytic, antibiofilm and insecticidal activity, *J. Photochem. Photobiol. B: Biol.* 178 (2018) 249–258.
- [32] S. Raja, V. Ramesh, V. Thivaharan, Green biosynthesis of silver nanoparticles using *Calliandra haematocephala* leaf extract, their antibacterial activity and hydrogen peroxide sensing capability, *Arabian J. Chem.* 10 (2) (2017) 253–261.
- [33] S.E.L.D. Hassan, S.S. Salem, A. Fouda, M.A. Awad, M.S. El-Gamal, A.M. Abdo, New approach for antimicrobial activity and bio-control of various pathogens by biosynthesized copper nanoparticles using endophytic actinomycetes, *J. Radiat. Res. Appl. Sci.* 11 (3) (2018) 262–270.
- [34] N.S. Abdullah, T. Al-Radadi, S. Hussain, S. Faisal, Ali Raza Shah, Novel biosynthesis, characterization and bio-catalytic potential of green algae (*Spirogyra hyalina*) mediated silver nanomaterials, *Saudi J. Biol. Sci.* 29 (1) (2022) 411–419.
- [35] A.A. Heflish, A.E. Hanfy, M.J. Ansari, E.S. Dessoky, A.O. Attia, M.M. Elshaer, M.K. Gaber, A. Kordy, A.S. Doma, A. Abdelkhalik, S.I. Behiry, Green biosynthesized silver nanoparticles using *Acalypha wilkesiana* extract control root-knot nematode, *J. King Saud Univ. – Sci.* 33 (6) (2021) 101516.
- [36] K. Raguvaran, M. Kalpana, T. Manimegalai, R. Maheswaran, Insecticidal, non-target organism activity of synthesized silver nanoparticles using *Actinokineospora fastidiosa*, *Biocatal. Agric. Biotechnol.* 38 (2021) 102197.
- [37] S.R. Kabir, A.K.M. Asaduzzaman, R. Amin, A.S.M.T. Haque, R. Ghose, M.M. Rahman, J. Islam, M.B. Amin, I. Hasan, T. Debnath, B.-S. Chun, X. Zhao, M.K. Rahman Khan, M.T. Alam, Zizyphus mauritiana fruit extract-mediated synthesized silver/silver chloride nanoparticles retain antimicrobial activity and induce apoptosis in MCF-7 cells through the Fas pathway, *ACS Omega* 5 (32) (2020) 20599–20608.
- [38] A. Gupta, S.M. Briffa, S. Swingler, H. Gibson, V. Kannappan, G. Adamus, M. Kowalczyk, C. Martin, I. Radecka, Synthesis of silver nanoparticles using curcumin-cyclodextrins loaded into bacterial cellulose-based hydrogels for wound dressing applications, *Biomacromolecules* 21 (5) (2020) 1802–1811.
- [39] B. Gottardo, T.H. Lemes, G. Byzynski, M.H. Paziani, M.R. von-Zeska-Kress, M.T. G. de Almeida, D.P. Volanti, One-Pot Synthesis and Antifungal Activity of Nontoxic Silver-Loaded Hydroxyapatite Nanocomposites against *Candida* Species, *ACS Applied Nano Materials* 2(4) (2019) 2112–2120.
- [40] S.C. De la Rosa-García, P. Martínez-Torres, S. Gómez-Cornelio, M.A. Corral-Aguado, P. Quintana, N.M. Gómez-Ortiz, Antifungal activity of ZnO and MgO nanomaterials and their mixtures against *Colletotrichum gloeosporioides* strains from tropical fruit, *J. Nanomater.* 2018 (2018) 3498527.
- [41] S. Gharpure, R. Yadwade, B. Ankamwar, Non-antimicrobial and non-anticancer properties of ZnO nanoparticles biosynthesized using different plant parts of *Bixa orellana*, *ACS Omega* 7 (2) (2022) 1914–1933.



Investigation of structural and optical properties of graphene derivatives as a route for optical sensing

Anil B. Patil ^{a,*}, Umesh J. Tupe ^b, Dharma K. Halwar ^c, Vikas V. Deshmane ^d, Arun V. Patil ^e

^a Department of Electronic Science and Research Center, L.V.H College, Nashik, Dist.-Nashik (M.S.), India

^b Department of Electronics, Panchavati College of Management & Computer Science, Nashik (M.S.), India

^c Department of Electronic Science, MSG College, Malegaon Camp Dist., Nashik (M.S.), India

^d Department of Physics, SICES Degree College, Ambarnath, Dist. Thane, India

^e Arts, Science and Commerce College, Manmad Dist., Nashik (M.S.), India

ARTICLE INFO

Article history:

Available online 17 October 2022

Keywords:

Reduced Graphene Oxide (rGO)

FTIR

UV Spectra

XRD

SEM

ABSTRACT

In the present research work, thick films of graphene oxide (GO) and reduced graphene oxide (rGO) were fabricated on glass substrate by using standard screen-printing technique. Silver paste was used to make contacts of thick films. Fabricated thick films of GO and rGO were characterized by scanning electron microscopy (SEM), elemental data analysis (EDS), and X-ray diffraction (XRD) to make sure the morphological, elemental and structural characteristics of the thick films. Optical characteristics of the fabricated thick films were carried out by UV Spectra, Raman spectroscopy and Fourier Transform Infrared Spectroscopy (FTIR). In addition, the optical studies were performed by homemade system to investigate the effect incident light intensity with different colour (Blue, Yellow, and Green) filters on GO and rGO sensing. XRD and EDS confirms the materials were GO and rGO. The findings revealed that reduced graphene oxide has a high light absorption capacity to consider as an optical sensor.

Copyright © 2022. Elsevier Ltd. All rights reserved.

Selection and peer-review under responsibility of the scientific committee of the Integrative Nanotechnology Perspective for Multidisciplinary Applications - 2022.

1. Introduction

Graphene is now widely emerged as a potential material for a wide range of applications, including transparent electronics products, which are the subject of much research. Because of their distinct physiochemical properties, graphene oxide (GO) and reduced graphene oxide (rGO) nanomaterials have attracted a lot of research attention. It can be used in a number of biological fields due to its 2D allotropic structure [1]. The distribution of graphene layers in the polymer matrix and the interfacial bonding between the graphene layers and polymer matrix determine the physical and chemical properties of graphene-based polymer nanocomposite. However, since graphene is incompatible with organic polymers, it does not form homogeneous composites. Graphene oxide (GO) sheets, on the other hand, are compatible with organic polymers since they are highly oxygenated graphene [2]. As a result, GO is commonly used in polymer nanocomposites as a nanofiller. Graphene oxide is electrically insulating and therefore cannot be used

to make conductive nanocomposites. However, graphene produced by thermal or chemical reduction of GO (i.e., the removal of oxygen) can produce large quantities of rGO platelets with low sheet resistance, making rGO behave as a semiconductor with electrical conductivity of ~ 1000 S/m. This makes it suitable for antistatic coatings and semi-transparent electric circuits, among other applications [3]. rGO is intended to be used in energy storage supercapacitors, Li-ion battery electrodes, and solar cell transparent electrodes [4,5].

Modification of the electronic structure to form islands of pristine graphene, or graphene quantum dots, within the GO sheet affects the tuning of electronic and optical properties. The energy gap reduces as the number of O atoms removed or the dot diameter grows, allowing for tuning across the UV, visible, and IR light spectrums. In contrast to completely oxidised graphene has insulating properties. rGO has both insulating and conducting properties depending on the percentage of oxygen remaining on the graphene layer. Nanometric sp^2 graphitic islands separated by oxidised graphene regions are commonly used to define the structure of rGO [6,7]. First principles and statistical calculations have

* Corresponding author.

E-mail address: anilbpatil1@gmail.com (A.B. Patil).

demonstrated the propensity of oxygen to agglomerate into heavily oxidised domains surrounded by pristine graphene regions [8].

Based on residual oxygen group coverage and defects within the carbon sheets, the optical properties of rGO vary depending on the various reduction methods [8,9]. However, understanding optical properties is important for industrial process control and relating theoretical predictions to experimental findings [10]. The properties of rGO are similar to those of graphene and graphene oxide, with the reduction process having a significant impact on these properties. Super capacitors, transparent conductors, sensors, storage cells, and actuators are all examples of nano-electronics applications that include electrical conductivity [11]. Optical properties of material are important for evaluating experiments involving electronic and biomedical processes. Photothermal therapy (PTT) refers to efforts to treat various medical conditions, including cancer, by using electromagnetic radiation (most commonly in infrared wavelengths). This method is a variation on photodynamic therapy, in which a photosensitizer is activated by a specific band of light. A few other studies have also reported the use of PTT in conjunction with chemotherapy based on carbon dots nanoplateforms for the delivery of DOX in the treatment of cancer cells. Most of the requirements for PTT appear to be met by carbon dots [12,13].

In general, screen printing is one of the most promising methods for preparing cost-effective large-area deposition techniques for devices on a wide range of substrates, regardless of shape or thermal stability. The current study focuses on the fabrication of GO and rGO thick films on glass substrates using a less costly standard screen-printing technique, as well as the investigation of the structural and optical properties of rGO thick films in the visible and near infrared regions and its route to consider itself as an optical sensor.

2. Experimental

2.1. Fabrication of graphene oxide (GO) and reduced graphene oxide (rGO) thick films by standard screen-printing technique

Commercially available AR grade (99.99 % purity) GO powder was used in this study. Some portion of GO powder was used for heat treatment at 200 °C for 1 h in inert atmosphere. After confirming an elemental presence using energy dispersive X-ray spectroscopy, thermally treated powder was used as rGO. On a clean glass substrate, the GO and rGO films were fabricated. To prepare thick films, all glass substrates were thoroughly washed with double distilled water and acetone, then put under an IR lamp for 30 min to eliminate impurities. Initially, silver ink was used to grow electrodes on a glass substrate. Pure thick films of GO/rGO were prepared using 70 % inorganic and 30 % organic material composition. Inorganic materials included available GO/rGO nano powder and organic materials included ethyl cellulose as a local binder and Diethylene glycol mono-butyl ether (digol) ($C_8H_{18}O_3$) as vehicle for paste formation. In a mortar and pestle, the GO/rGO nano powder and ethyl cellulose were combined and crushed for an hour, and then digol was added drop by drop to create a thixotropic paste. This paste was spread uniformly on glass substrate using a screen-printing setup. The prepared thick films were kept under IR irradiation for 45 min to eliminate local binder or impurity residue, and then fabricated films were used for further work.

2.2. Characterization of fabricated thick films

2.2.1. Structural characterization

The surface morphology, elemental analysis, and structural properties of the films were studied using scanning electron micro-

scopy (SEM), Energy-dispersive X-ray spectroscopy (EDAX), and X-ray diffraction (XRD) respectively. To characterize the surface morphology of the films, a scanning electron microscopy model JOEL 6300 LA GERMANY was used. The elemental analysis was performed using an EDS energy dispersive X-ray spectrometer (JOEL-2300, Germany).

The model Rigaku diffractometer (DMAX-500), X-ray diffractometer with $CuK\alpha$ radiation and wavelength = 0.1540598 nm, was used to record XRD patterns of fabricated rGO thick films. The films were scanned for the range from 10° to 80°. The obtained values of 2θ are compared to JCPDS data files. The Origin 9.5 software was used to compute the full width of half maxima (FWHM). Debye Scherrer's formula, Eq. (3.1), was used to calculate the crystallite size (D).

$$D = \frac{K\lambda}{\beta \cos\theta} \quad (3.1)$$

where

- K = Scherrer constant (0.9),
- β = Full width of half maxima (FWHM),
- λ = wavelength of X source (1.540598 Å°).

2.2.2. Optical characterization

The optical properties of GO and rGO films were studied by FTIR, Raman Spectroscopy and UV-vis Spectra. Bonding characteristics of the thick films were analysed by using Shimadzu IR Affinity-1 Fourier transformed infrared spectrometer (FTIR). The FTIR was recorded from 400 to 4000 cm^{-1} with a resolution of 2 cm^{-1} . Raman spectroscopy is a widely known method for characterising carbon products because conjugated and double carbon-carbon bonds produce high Raman intensities. Raman spectroscopy of fabricated thick films was obtained by using SENTERRA-Bruker, Germany with a laser source (Nd: YAG) at a wavelength of 532 nm. The films were also characterized by a double beam UV-Visible spectrophotometer (Model- JASCO, V-730).

The Absorption coefficient (α) as a function of photon energy was investigated using Eq. (3.2),

$$\alpha = \frac{2.303 * A\%}{\text{Thickness}(t)} \quad (3.2)$$

where

- α = Absorption coefficient.
- A% = Absorption (%).
- Thickness of the film (t) = 4.894 μm.

The optical band gap (E_{op}) was determined using following Eq. (3.3),

$$E_{op} = \frac{h\nu}{\lambda} = \frac{1241}{\lambda} \text{ eV} \quad (3.3)$$

where

- E_{op} = Optical band gap in eV.
- h = Planks Constant.
- ν = Speed of light.
- λ = Wavelength (cm).

3. Experimental results

3.1. Structural characterization

3.1.1. Scanning electron microscopy

Fig. 1 shows the SEM images of the commercially available AR grade GO powder at different scale with magnification at (a)

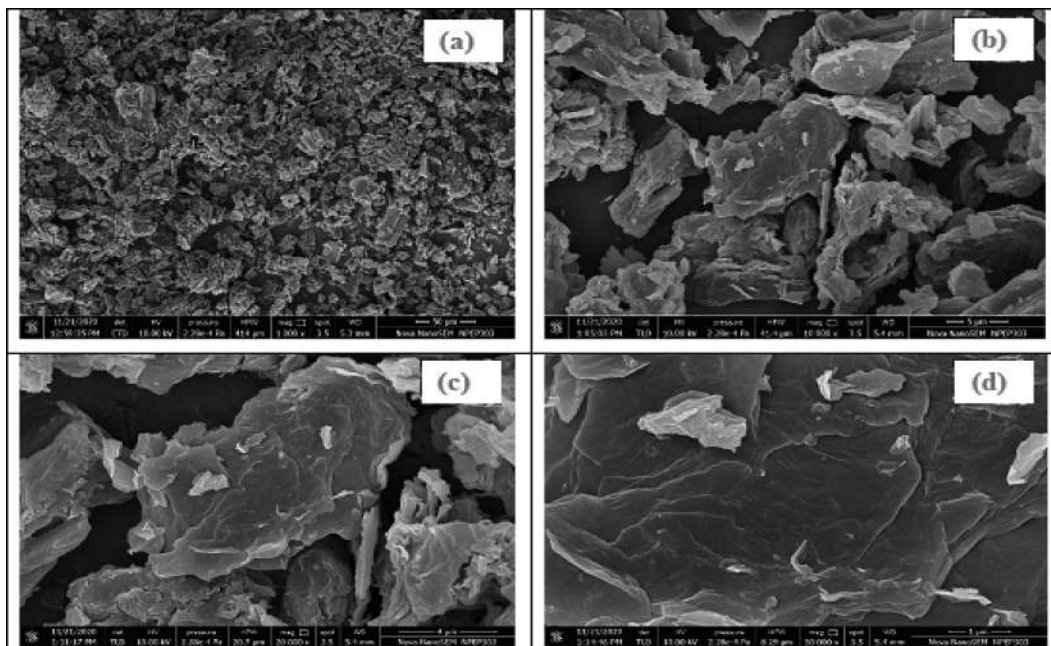


Fig. 1. SEM micrograph of commercially available AR grade GO Powder with magnification at (a) 1000 (b) 10,000 (c) 20,000 and (d) 50,000.

1000 (b) 10,000 (c) 20,000 and (d) 50,000, while Fig. 2 shows the SEM micrograph at different scale for GO thick films with magnification at (a) 1000 (b) 10,000 and rGO thick films with magnification at (c) 1000 and (d) 10,000. It has been found that the structure of GO is little bit folded and wrinkled. Also, there may be existence of some crumple. It might be due to graphite exfoliation to become graphene oxide and may results in deformation due to exfoliation and restacking. From SEM image of rGO, more folded and wrinkled structure has been observed. It can be due to losses of

oxygen functional groups. When the reduction is greater, the form becomes more folded and wrinkled [14,15].

3.1.2. Energy-dispersive X-ray spectroscopy

Fig. 3 shows elemental data analysis of GO and rGO thick films using Energy-dispersive X-ray spectroscopy (EDAX). It clearly reveals that after heat treatment, GO gets converted into rGO material. There is reduction in oxygen observed from the data of rGO as compared to GO. The elemental data analysis reveals the presence of only C and O in both GO and rGO thick film.

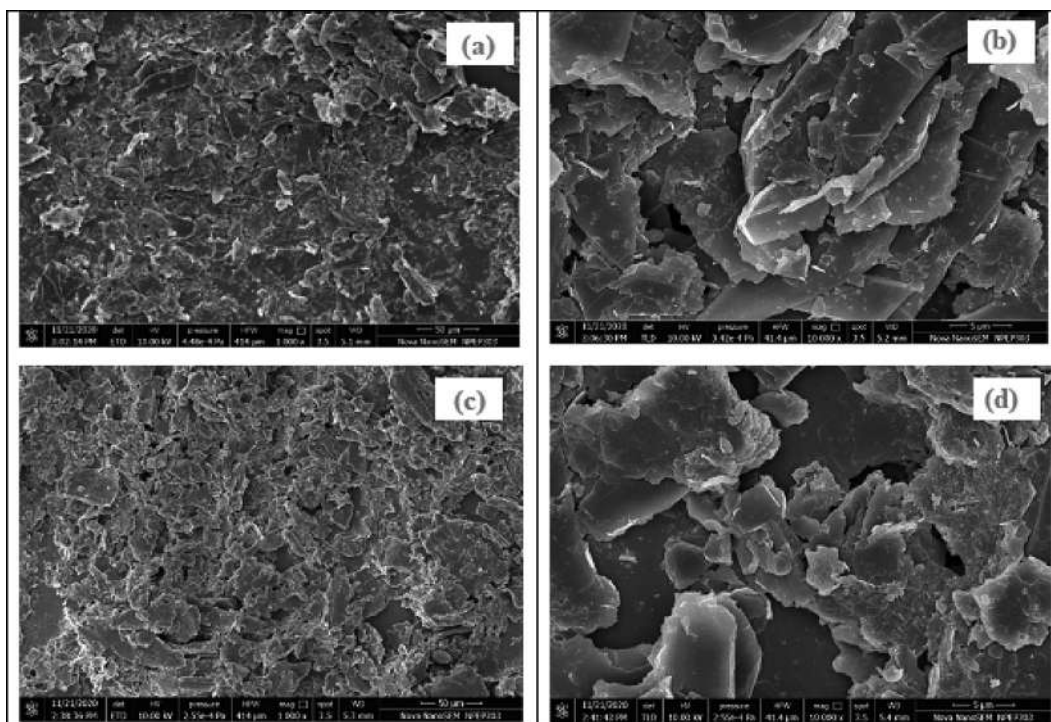


Fig. 2. SEM micrograph of GO thick films with magnification at (a) 1000 (b) 10,000 and rGO with magnification at (c) 1000 and (d) 10,000 thick films.

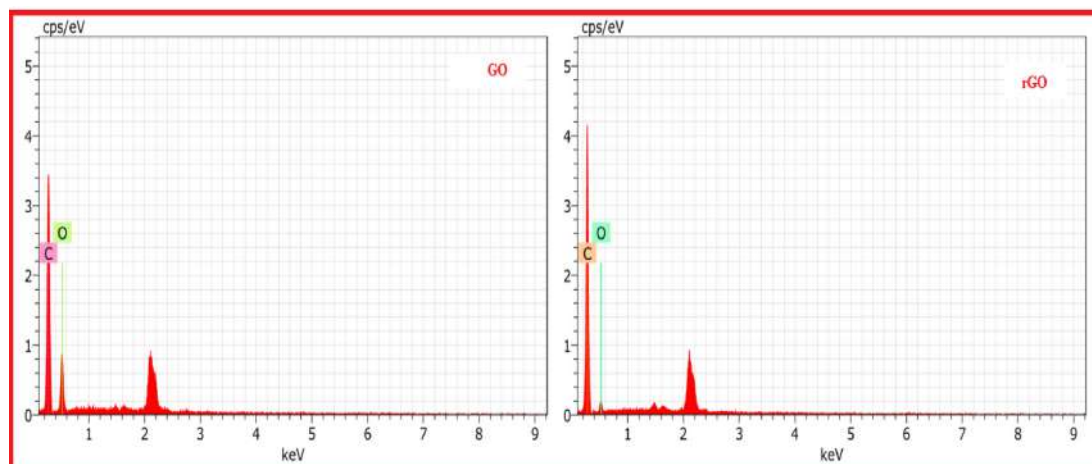


Fig. 3. EDAX spectra of GO and rGO films.

The peak observed at energies 2.1 KeV position might be due to the impurities induced during the synthesis of the material. Chemicals such as H_2SO_4 if used in synthesis process results in impurities like Sulphur (S) and Phosphorous (P) which remain even after the complete synthesis and observed that the atomic percentage of these impurities is negligible. Hence it does not affect the overall outcomes of the current study.

3.1.3. X-ray diffraction

Fig. 4 shows the XRD pattern of GO and rGO films. As shown in figure, the prominent peak for GO was observed at $2\theta = 11.03^\circ$ and for rGO at $2\theta = 26.48^\circ$. As compared to JCPDS card No.74-1229 for graphite, the prominent peak should be at 26.4° . So, there is shift in peak for rGO was observed. It may be due to removal of oxygen containing functional groups during the heat treatment. For GO, the prominent peak was observed at lower diffraction angle. It may be due to exfoliated GO where oxygen functional and epoxy group are introduced between the layer of GO. By using Bragg's equation, the interplaner distance for GO was calculated as

0.80 nm and for rGO, it was calculated as 0.35 nm. It means inter-planar distance for GO is greater than rGO. It may be due that, the water molecules and various oxygen containing functional groups present in GO as identified by FTIR. It indicates the hydration and exfoliation of GO [16–18].

The hkl planes of rGO corresponding with JCPDS Card No. 75-2078. The preferred orientation was observed at 2θ (26.80) along the direction (002) plane. It reveals presence of crystalline cubic phase. It is observed that this prominent peak shows swing in its position with corresponding JCPDS. The shifting of peak may be due to variation in the stoichiometric chemical composition of the material. This concurrence can be attributed to the non-uniform annealing process employed during the reduction of GO (See Table 3.1).

Table 3.2 shows summary of structural parameters of fabricated GO and rGO electrodes. The crystallite size was calculated from XRD pattern by using Eq. (3.1) i.e. Debye Scherrer formula and was found to be 32.34 nm for GO and 20.57 nm for rGO. From SEM, the average particle size of GO and rGO SPEs was found about

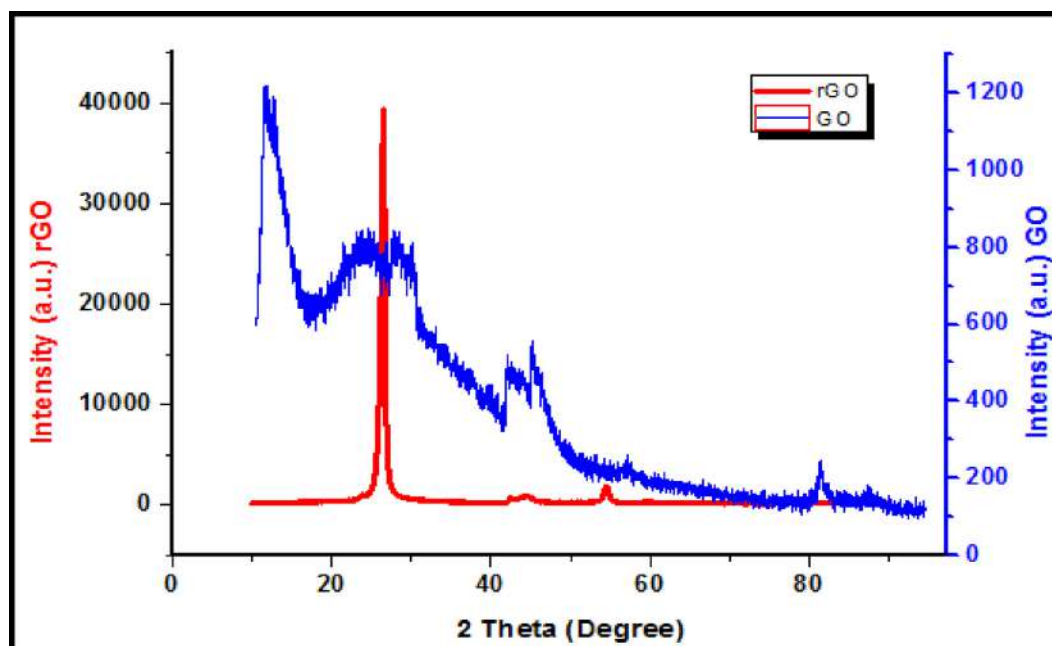


Fig. 4. XRD pattern of GO and rGO films.

Table 3.1

Structural parameters of fabricated GO and rGO thick films.

Thick films	(hkl)	2 θ theta	d spacing	FWHM	Count	I/I ₀
GO	(001)	11.03	8.01508	0.25791	1221	100
rGO	(002)	26.80	3.32387	0.41388	38,458	100

Table 3.2

Summary of structural parameters:

Thick Films	Crystallite (grain) size, D (XRD)	Average particle size, d (SEM)	Specific surface area (SEM)	Atomic % (EDAX)	
				C	O
GO	32.34 nm	315 nm	1.018 m ² /g	72.67	27.33
rGO	20.57 nm	232 nm	1.354 m ² /g	88.40	11.60

315 and 232 nm respectively. EDAX shows 72.67 and 27.33 as the atomic % of carbon and oxygen respectively in the GO and 88.40 and 11.60 as the atomic % of carbon and oxygen respectively in the rGO.

3.2. Optical characterization

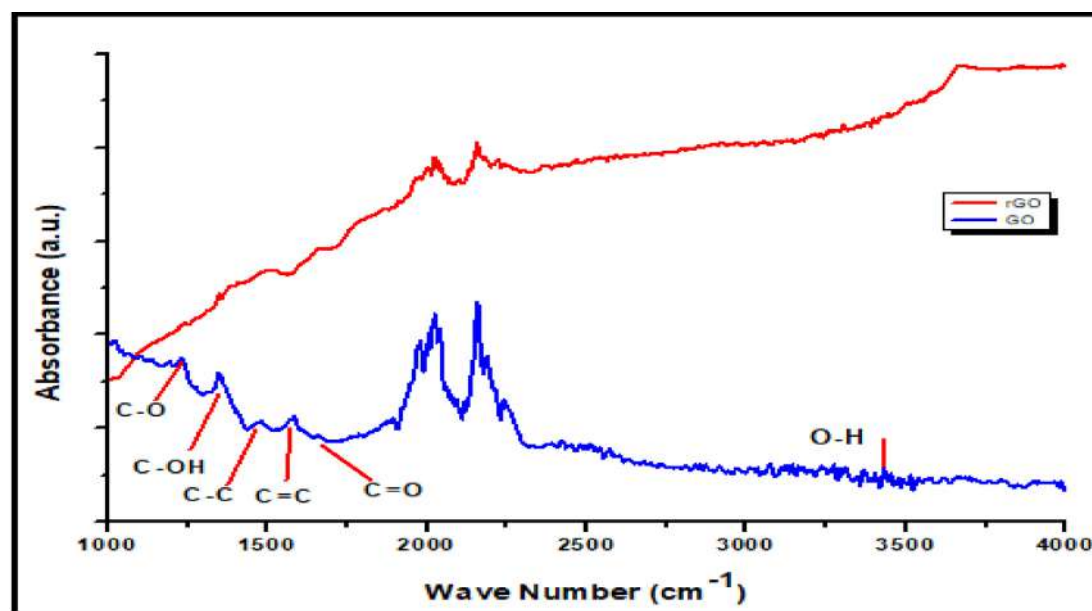
3.2.1. Fourier transform infrared spectrometry

Fig. 5 shows the spectra obtained by FTIR of GO and rGO samples. The wide band vibrations observed between 3000 and 3600 cm⁻¹ are characteristic of the stretching vibration mode of O–H bond, reveals the presence of hydroxyl groups or the remaining adsorbed water molecules in graphene oxide [16,19]. In the spectrum, the typical peaks indicating the oxygen-containing groups are visible as 1755.22 cm⁻¹ for C=O (carbonyl/carboxyl), 1230.58 cm⁻¹ for carboxylic C–O stretched, and the peak at 1346.31 cm⁻¹ arises from C–OH group. The peaks corresponding to the stretching vibration of aromatic C–C stretched in-ring group is visible at 1481.33 cm⁻¹. The peak at 1658.78 cm⁻¹ corresponding to the in-plane vibrations of aromatic C=C stretched. The stretching and bending vibrations of the graphene sheets validates for the success of oxidation of graphitic domains. The presence of the carboxylic and carbonyl functional group shows the successful oxidation of graphite.

The FTIR spectra of rGO after heat treatment shows decrease in intensities of the bands that correspond to C–OH hydroxyl and C=O groups, while the peaks relating to epoxy and alkoxy C–O groups have disappeared. In this FTIR spectra, low-temperature reduction processes confirm significantly de-oxidation [18,20–23] which result in decreasing the intensities by decomposition of carbonyl and carboxyl functional group in reduced graphene oxide compared than graphene oxide. This leads to less oxygen functional groups, with some residual species of oxygen-containing groups remain in the material in the rGO.

3.2.2. Raman spectroscopy

Raman characterization is a widely used technique for obtaining material structural details. D (disorder) and G (gap) are two distinct peaks in the Raman spectra of GO and rGO. Fig. 6 shows the Raman spectra of GO and rGO thick film. Raman spectra show two distinct bands between 1200 and 1700 cm⁻¹. The graphitic character and degree of disorder was measured using the G- and D-peak intensities, respectively. In spectra, G bands to pure graphite which is due carbon atoms vibration with SP² hybridization. D peak is called as peak of defects. It is caused due to vibration of carbon atoms with SP³ hybridization. From figure, D and G peaks of GO were at 1356.285 cm⁻¹ and 1578.453 cm⁻¹ respectively. For rGO, D and G peaks were observed at 1357.95 cm⁻¹ and

**Fig. 5.** FT-IR Spectra of GO and rGO films.

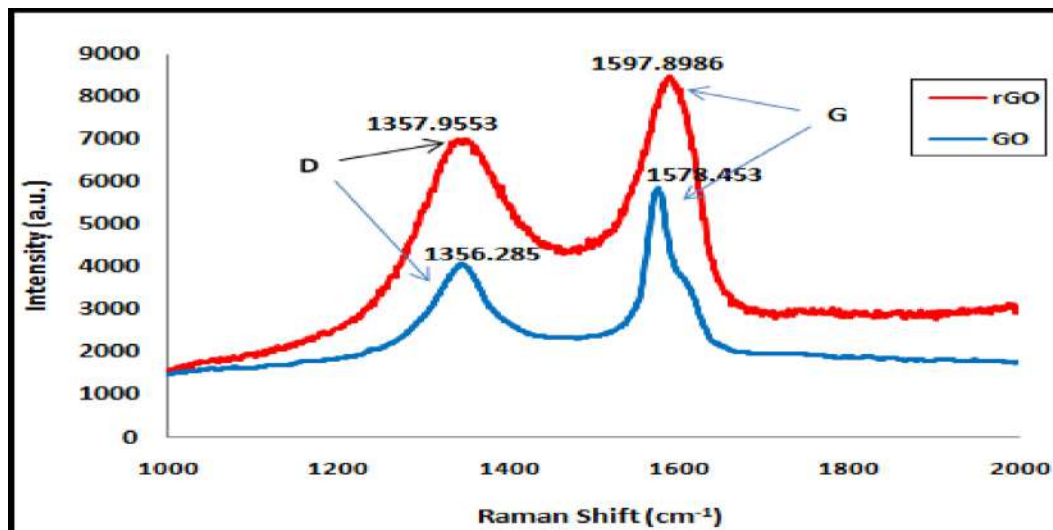


Fig. 6. Raman spectra of Go and rGO films.

1597.89 cm^{-1} respectively. In GO, these peaks are slightly shifted. This may be due to formation of defects and destruction in SP^2 bonds. It means the structural defect induces by hydroxyl and epoxide groups on the carbon basal plane [11,24]. After oxidation, the disappearance of the 2D band at 2726 cm^{-1} indicates that all graphite layers have been oxidised. The D and G bands (about 1578 cm^{-1}) are almost identical to the graphene oxide characteristic peaks. As a result, graphene oxide generated from graphite and oxidised expandable graphite are the same material.

3.2.3. UV Spectroscopy

Fig. 7 shows the UV-vis absorption spectrum of GO and rGO samples. According to the absorbance spectra, the main spectrum of graphene oxide has a strong absorption peak at 237 nm, attributed to $\pi\text{-}\pi^*$ transition of the C–C conjugated aromatic domains and weak absorption (shoulder) at 351 nm due to $n\text{-}\pi^*$ transition of C=O bond. [25].

The absorption peak observed at 237 nm of GO (blue line) has been shifted to 267 nm and weak absorption (shoulder) at 410 nm for rGO (red line), suggesting that the aromatic structure

might be refurbished. Absorption peaks and overall features of these spectra are analogous to those of GO and rGO reported in the literature [26–28]. Most significantly, as expected for graphene, considering different reduction times, the rGO spectra are featureless in the visible band. Thus, UV-vis spectra of GO and rGO samples gives indication of the presence of a sufficient number of oxygen functionalities, such as carboxyl, carbonyl, hydroxyl and epoxide on graphene oxide.

3.2.4. Energy band gap calculations

Band gap can be defined as energy difference between valence band (highest occupied molecular orbital, HOMO) and conduction band (lowest occupied molecular orbital, LUMO) [29]. Energy gap (E_g) shows a significant meaning of semiconductor which determines their applications. The optical band gap (E_g) associated with the graphene materials was estimated from the Fig. 8, and can be determined by extrapolating the linear trend observed in the spectral dependence of the curve to the x-axis [30].

When GO is reduced for 1hr at $200 \text{ }^\circ\text{C}$, the band gap decreased from 1.49 eV to 1.24 eV. The decreasing value of band gap in rGO is

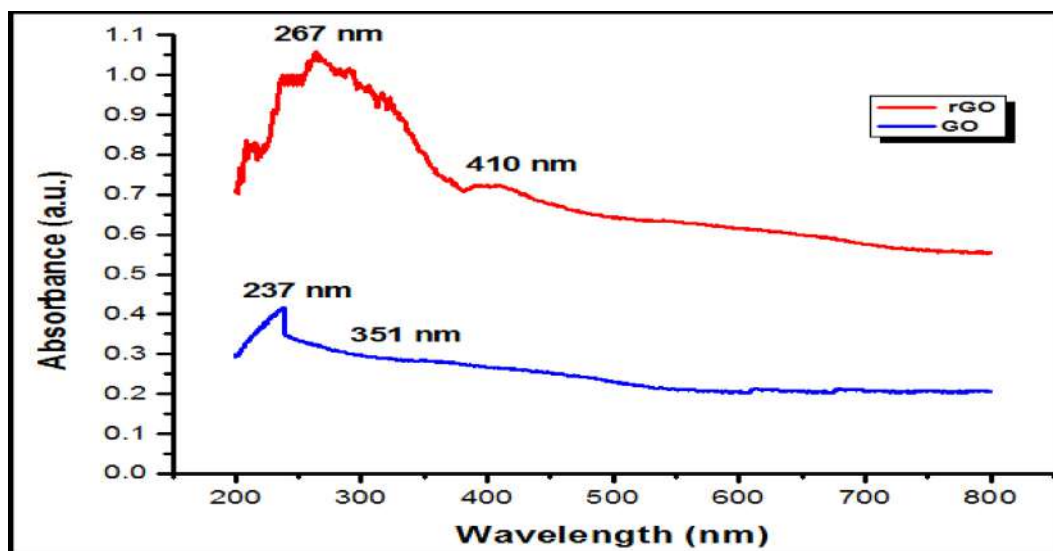


Fig. 7. UV-vis absorption spectra GO and rGO films.

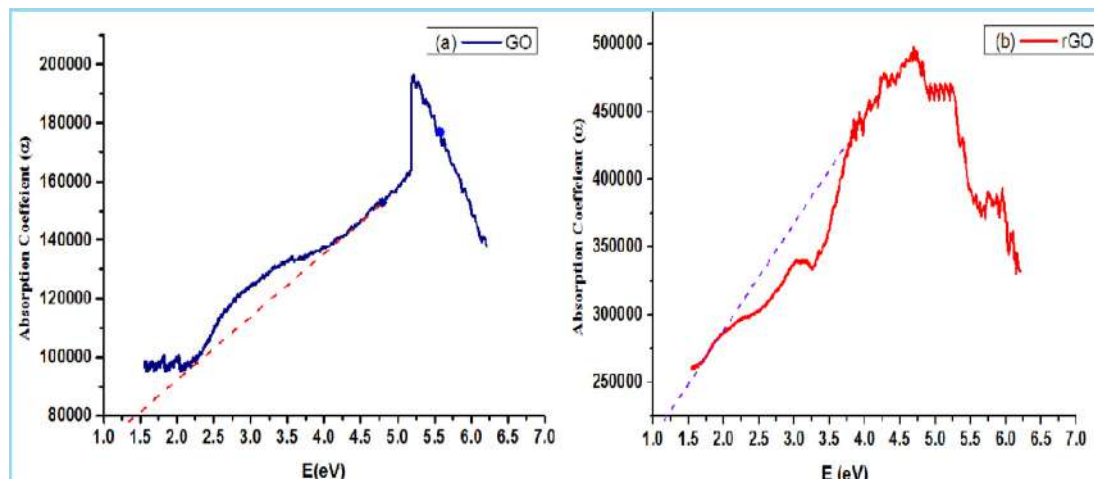


Fig. 8. Optical band gap of GO and rGO films.

due to the removal of some functional groups on the surface of the material [31,32] and also consequent conversion of sp^3 carbon to sp^2 [33]. The band gap value concludes that the reduction of rGO can also be applied in certain applications as the range of band gap value (<5.0 eV) suitable for optical sensing.

3.2.5. Homemade system to study optical properties

Light dependent conductance variation of only rGO thick films were studied as an optical sensor in this study due to its lower band gap. The sensing response of the thick films to different wavelengths were studied by using colour filters (Green, Blue, Yellow) and homemade system. The actual image and schematic diagram of homemade setup is shown in Fig. 9 for optical characterization.

This system consists of a light source, distance variation facility, colour filter holder, and thick film sample holder, the fixed power source of +30 V. In this system, change in current was measured concerning light intensity by varying the distance of the sample from a light source. The distance was varied from 12 cm to

40 cm as per the dimensions of Instrument. Variation in current for change in intensity was measured using a Lux meter.

Fig. 10 shows that the distance versus current response of rGO thick films at different wavelengths 580, 535, and 467 nm by using yellow, green and blue colour filters respectively. The maximum output current obtained to blue filter ($\lambda = 467$ nm) and minimum output current for yellow filter ($\lambda = 580$ nm). It has been also observed that wavelength decreases output current increases. Also, as a distance of light source increases from the film, the current decreases for each wavelength.

3.2.6. Photo sensing mechanisms of rGO under illumination and bias

The transformation of GO to rGO built rGO flakes. The flakes are stacking of graphene like layers and for layer. For layer-based photo detectors, commonly-three types of photocurrent generation mechanisms are proposed that are photovoltaic effect, photoconductive effect, and photo thermoelectric effect. The results show that the photoconductive effect is the dominating factor for the generation of photocurrent in the rGO based photo detector. The general operational principle of a photodetector in a solid state

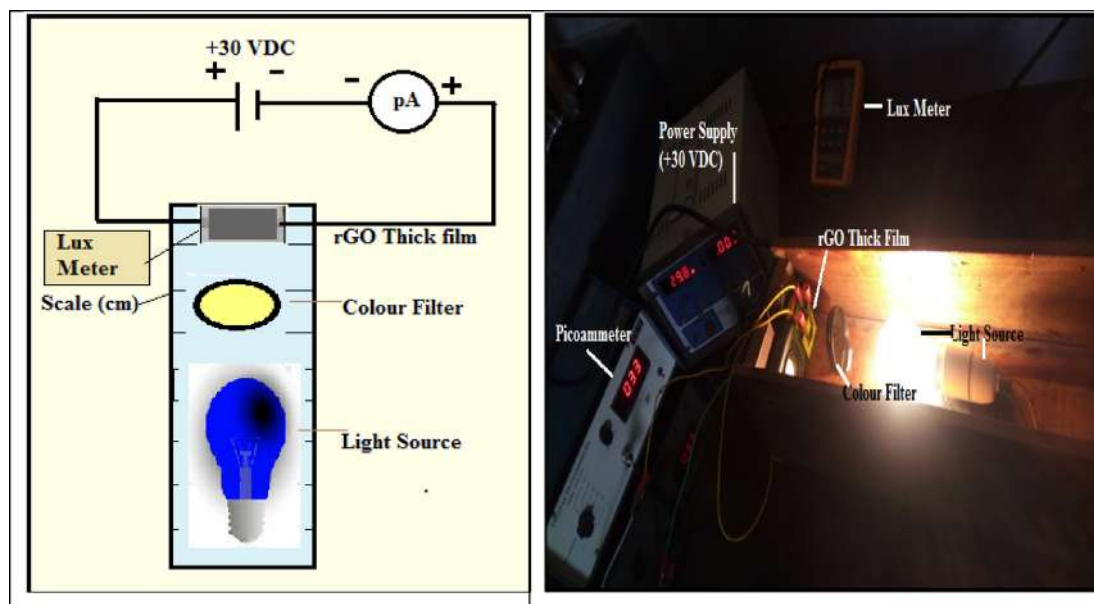


Fig. 9. Actual image and schematic diagram of homemade setup.

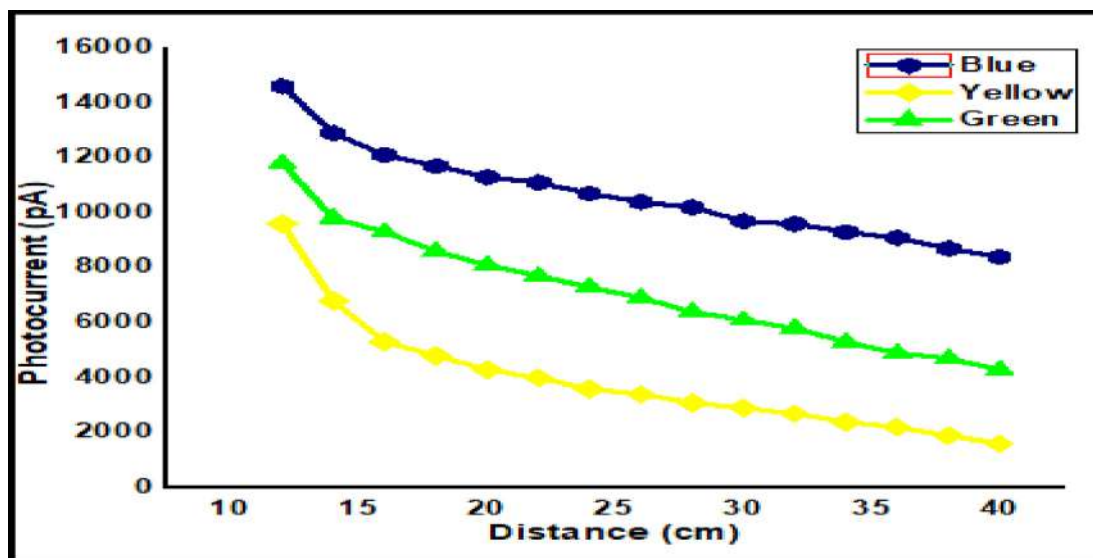


Fig. 10. Photocurrent for different wavelengths.

consists of: (a) generating carriers through the absorption of photons incident in the semiconductive layer; (b) transporting and propagating of these carriers; and (c) driving out these carriers into an external circuit to circulate until electrons and holes recombine together [34]. Where photogenerated transporters drift within channel space, they may only be trapped or defeated in the band-gap and the rGO/electrode interfaces, and then trapped through photons. The confined carriers prefer to return to their respective bands rather than recombining under light illumination. It may be the incident photons have much higher activation energy than the trap barrier potential, and the photon flux is sufficient to minimise the effective recombination rate of carriers. The electrons are often exchanged between bands and trap or defect states under illumination at different wavelengths by using colour filters, any change in the number of electrons in the conduction band or in defect states must include changes in the quantity of electrons on the defect states due to excitation to the conduction band, and changes in the number of conduction band electrons due to photogeneration [34,35].

3.2.7. Photoresponsivity of fabricated rGO thick films

The maximum photoresponsivity recorded at 467 nm indicates that the transition is interband and originates from the rGO field, where sp³ carbon bonding dominates. From Fig. 11, observed that

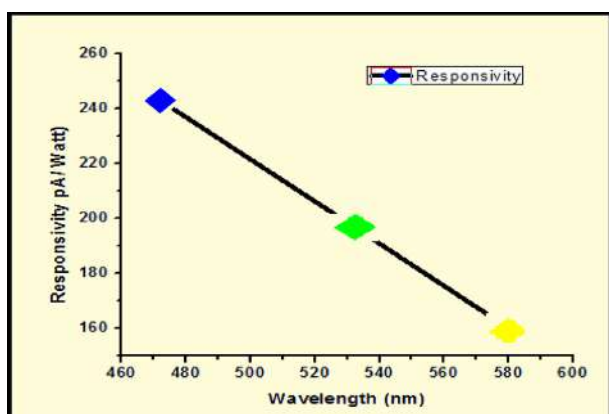


Fig. 11. Photoresponsivity rGO thick film illuminated under various wavelengths.

wavelength increases, photoresponsivity decreases. The response time is calculated using the dark current's amplitude ranging from 10 % to 90 %, and the recovery time is calculated using the dark current's amplitude ranging from 90 % to 10 %. At room temperature, response and recovery times for 467 nm illumination were found to be 1.4 and 1.6 s respectively [35,36]. In comparison to the green and yellow bands, the maximum photoresponsivity for rGO films was recorded for the blue colour (at 467 nm) wavelength. Reduced graphene oxide has a high light absorption capacity, allowing it to be used as an optical sensor as well as in biomedical applications.

4. Conclusion

The GO and rGO thick films were successfully fabricated by using standard screen-printing technique. XRD and EDS confirmed that thermally treated material was rGO. SEM showed folded and wrinkled structure of rGO. FTIR represents the stretching vibrations due to O–H groups. After heat treatment, there is significant decrease of C–OH hydroxyl and C=O groups. Raman spectra revealed that there is shift of D and G peaks after heat treatment. Ratio of relative intensities of D to G peaks increases for rGO. From UV spectra, the absorption peak observed at 237 nm of GO has been shifted to 267 nm for rGO, suggesting that the aromatic structure might be restore. When GO is reduced for 1hr at 200 °C, the band gap decreased to from 1.49 eV to 1.24 eV.

The maximum photoresponsivity for rGO films was recorded for blue colour (at 467 nm) wavelength as compared to green and yellow bands. The findings revealed that rGO- based films can be employed as an effective and potential photo-absorbing agent for photo-thermal therapy (PTT) in biomedical application, due to high photothermal sensitivity, nontoxicity and low price.

CRediT authorship contribution statement

Anil B. Patil: Writing – original draft, Data curation, Writing – original draft, Visualization, Writing – review & editing. Umesh J. Tupe: . Dharma K. Halwar: . Vikas V. Deshmane: . Arun V. Patil:

Declaration of Competing Interest

The authors declare that they have no known competing financial interests or personal relationships that could have appeared to influence the work reported in this paper.

Acknowledgment

The authors thank to Principal, L. V. H. College and Research Centre in Electronic Science, Panchavati, Nashik, India, for providing laboratory facilities. The authors also acknowledge and pay sincere thanks to Head, Department of Physics, S. P. Pune University, Pune, and Head, Department of Chemistry, B. R. Gholap College, Pune for providing the laboratory facilities for SEM, EDAX, XRD, FTIR, UV-VIS and Raman Spectroscopy characterization for present research work.

References

- [1] G. Wang, Y. Zhang, Y. Congya, L. Beiyun, Y. Yanhan, L. Huangjingwei, C. Ajuan, L. Danmin, Y. Hui, Two dimensional materials-based photodetectors, *Infrared Phys. Technol.* 88 (2018) 149–173.
- [2] B. Alemour, M.H. Yaacob, H.N. Lim, R.H. Mohd, Review of Electrical Properties of Graphene Conductive Composites, *Int. J. Nanoelectron. Mater.* 11 (4) (2018) 371–398.
- [3] J.R. Potts, D.R. Dreyer, C.W. Bielawski, R.S. Ruoff, Graphene-based polymer nanocomposites, *Polymer* 52 (1) (2011) 5–25.
- [4] K.S. Novoselov, V.I. Falko, L. Colombo, P.R. Gellert, M.G. Schwab, K. Kim, A roadmap for graphene, *Nature* 490 (7419) (2012) 192–200.
- [5] L. Weijie, P. Soukiassian, J. Boeckl, Graphene: Fundamentals and functionalities, *MRS Bull.* 37 (12) (2012) 1119–1124.
- [6] C. Gómez-Navarro, Electronic transport properties of individual chemically reduced graphene oxide sheets, *Nano Lett.* 7 (11) (2007) 3499–3503.
- [7] S. Zhou, B. Angelo, Origin of the chemical and kinetic stability of graphene oxide, *Sci. Rep.* 3 (1) (2013) 1–7.
- [8] M. Lundie, Š. Željko, T. Stanko, Electronic and optical properties of reduced graphene oxide, *J. Mater. Chem. C* 3 (29) (2015) 7632–7641.
- [9] S. Schöche, N. Honga, M. Khorasanineja, A. Ambrosio, O. Emanuele, M. Pasqualino, C. Federico, Optical properties of graphene oxide and reduced graphene oxide determined by spectroscopic ellipsometry, *Appl. Surf. Sci.* 421 (2017) 778–782.
- [10] I. Jung, M. Vaupel, M. Pelton, P. Richard, D. Dikin, A. Sasha, J. Stankovich, R.S. Ruoff, Characterization of thermally reduced graphene oxide by imaging ellipsometry, *J. Phys. Chem. C* 112 (23) (2008) 8499–8506.
- [11] Y. Shen, P. Zhou, Q.Q. Sun, L. Wan, J. Li, L.Y. Chen, D.W. Zhang, X.B. Wang, Optical investigation of reduced graphene oxide by spectroscopic ellipsometry and the band-gap tuning, *Appl. Phys. Lett.* 99 (14) (2011).
- [12] J.F.Y. Fong, Y.H. Ng, M.N. Sing, Carbon dots as a new class of light emitters for biomedical diagnostics and therapeutic applications, in: *Fullerenes, Graphenes and Nanotubes*, William Andrew Publishing, 2018, pp. 227–295.
- [13] D. Jaque, Nanoparticles for photothermal therapies, *Nanoscale* 6 (16) (2014) 9494–9530.
- [14] L.K. Hyung, S.-J.B. Hwang, L. Jae-Ung, C. Hyeonsik, K. Oh-Sun, S. Kwanwoo, H.N. Hwi, Large scale production of highly conductive reduced graphene oxide sheets by a solvent-free low temperature reduction, *Carbon* 69 (2014) 327–335.
- [15] E. Jaafar, M. Kashif, S.K. Sahari, Z. Ngaini, Study on morphological, optical and electrical properties of graphene oxide (GO) and reduced graphene oxide (rGO), in: *Materials Science Forum*, Trans Tech Publications Ltd., Zürich, Switzerland, vol. 917, 2018, p. 112–116.
- [16] L. Shahriary, A.A. Athawale, Graphene oxide synthesized by using modified hummers approach, *Int. J. Renew. Energy Environ. Eng.* 2 (1) (2014) 58–63.
- [17] S.P. Abid, S.S. Islam, P. Mishra, S. Ahmad, Reduced graphene oxide (rGO) based wideband optical sensor and the role of Temperature, Defect States and Quantum Efficiency, *Sci. Rep.* 8 (1) (2018) 1–13.
- [18] S. Rao, J. Upadhyay, K. Polychronopoulou, R. Umer, R. Das, Reduced Graphene Oxide: Effect of Reduction on Electrical Conductivity, *J. Compos. Sci.* 2 (2018) 25, <https://doi.org/10.3390/jcs2020025>.
- [19] T. Zhang, D. Zhang, Aqueous colloids of graphene oxide nanosheets by exfoliation of graphite oxide without ultrasonication, *Bull. Mater. Sci.* 34 (1) (2011) 25–28.
- [20] Z. Lin, Y. Yao, Z. Li, Y. Liu, Z. Li, C.P. Wong, Solvent-Assisted Thermal Reduction of Graphite Oxide, *J. Phys. Chem. C* 114 (2010) 14819–14825.
- [21] M.J. Deka, U. Baruah, D. Chowdhury, Insight into Electrical Conductivity of Graphene and Functionalized Graphene: Role of Lateral Dimension of Graphene Sheet, *Mater. Chem. Phys.* 163 (2015) 236–244.
- [22] V.G. Sreeja, G. Vinita, R. Reshmi, E.I. Anila, M.K. Jayaraj, Effect of reduction time on third order optical nonlinearity of reduced graphene oxide, *Opt. Mater. (Amst)* 66 (2017) 460–468.
- [23] A. Shalaby, D. Nihtianova, P. Markov, A.D. Staneva, R.S. Jordanova, Y.B. Dimitriev, Structural analysis of reduced graphene oxide by transmission electron microscopy, *Bulg. Chem. Commun.* 47 (1) (2015) 291–295.
- [24] Schmiedova Veronika, Pospisil Jan, Kovalenko Alexander, Ashcheulov Petr, Fekete Ladislav, Cubon Tomas, Kotrusz Peter, Zmeskal Oldrich, and Weiter Martin, Physical Properties Investigation of Reduced Graphene Oxide Thin Films Prepared by Material Inkjet Printing *Hindawi Journal of Nanomaterials* Volume 2017, Article ID 3501903, 8, <https://doi.org/10.1155/2017/3501903>.
- [25] Tene Talia, Usca Gabriela Tubon, Guevara Marco, Molina Raul, Veltri Francesco, Melvin Arias, S. Caputi Lorenzo, Gomez Cristian Vacacela, Toward Large-Scale Production of Oxidized Graphene, *Nanomaterials* 10 (2020) 279, <https://doi.org/10.3390/nano10020279>.
- [26] D.C. Marcano, D.V. Kosynkin, J.M. Berlin, A. Sinitskii, Z. Sun, A. Slesarev, J.M. Tour, Improved synthesis of graphene oxide, *ACS Nano* 4 (2010) 4806–4814.
- [27] J. Chen, B. Yao, C. Li, G. Shi, An improved Hummers method for eco-friendly synthesis of graphene oxide, *Carbon* 64 (2013) 225–229.
- [28] G. Eda, J. Ball, C. Mattevi, M. Acik, L. Artiglia, G. Granozzi, M. Chhowalla, Partially oxidized graphene as a precursor to graphene, *J. Mater. Chem.* 21 (2011) 11217–11223.
- [29] H.A. Van Mullekom, J.A. Vekemans, E.E. Havinga, E.W. Meijer, Developments in the Chemistry and Band Gap Engineering of Donor Acceptor Substituted Conjugated Polymers, *Mater. Sci. Eng.* (2001) 1–40.
- [30] S. Umrao, S. Abraham, F. Theil, S. Pandey, V. Ciobotă, P.K. Shukla, C.J. Rupp, S. Chakraborty, R. Ahuja, J. Popp, B. Dietzek, A. Srivastava, A possible mechanism for the emergence of an additional band gap due to a Ti–O–C bond in the TiO₂–graphene hybrid system for enhanced photodegradation of methylene blue under visible light, *RSC Adv.* 4 (2014) 59890–59901.
- [31] A. Mathkar, D. Tozier, P. Cox, P. Ong, C. Galande, K. Balakrishnan, A. Leela, M. Reddy, P.M. Ajayan, Controlled, Stepwise Reduction and Band Gap Manipulation of Graphene Oxide, *J. Phys. Chem. Lett.* 3 (8) (2012) 986–991.
- [32] A.N. Fatihah, T.A. Madzlan, Effect of Reduction Time on Optical Properties of Reduced Graphene Oxide, *Jurnal Teknologi (Sci. Eng.)* 79 (1–2) (2017) 25–28.
- [33] H.F. Liang, C.T.G. Smith, C.A. Mills, S.R.P. Silva, The Band Structure of Graphene Oxide Examined Using Photoluminescence Spectroscopy, *Electron. Suppl. Mater. (ESI) J. Mater. Chem. C* (2012) 1–3.
- [34] S.M. Sze, M.K. Lee, *Semiconductor Devices: Physics and Technology*, John Wiley & Sons, 2012, pp. 323.
- [35] S.P. Abid, S.S. Islam, P. Gulati, M. Talib, P. Mishra, M. Khanuja, Development of highly sensitive optical sensor from carbon nanotube-alumina nanocomposite free-standing films: CNTs loading dependence sensor performance Analysis, *Sens. Actuators, A* 269 (2018) 62–69.
- [36] F. Rana, Electron-hole generation and recombination rates for Coulomb scattering in graphene, *Phys. Rev. B* 76 (15) (2007) 155431.



A review on biosynthesis and applications of various nanoparticles using extracts of medicinal plant *Tribulus terrestris*

Sagar A. Nalawade^{a,c}, Bapusaheb Shinde^b, Sushilkumar Chaudhari^b, Manisha S. Badhe^c, Vikas K. Kadam^d, Manohar G. Chaskar^e, Shirish S. Pingale^{a,f,*}

^a Department of Chemistry, Baburaoji Gholap College Sangavi, Pune, India

^b Department of Zoology, Institute of Science, Mumbai, India

^c Department of Chemistry, Dattatray Govindrao Walse Patil College, Pargaon, Pune, India

^d Department of Chemistry, Shri Shiv Chhatrapati College, Junnar, Pune, India

^e Department of Chemistry, Ramkrushna More ACS College, Akurdi, Pune, India

^f Hutatma Rajguru College, Rajgurunagar, Pune, India

ARTICLE INFO

Article history:

Available online 18 October 2022

Keywords:

Tribulus Terrestris

Silver

Gold

Nanoparticles

Antibacterial

Antifungal

ABSTRACT

The plant *Tribulus Terrestris* commonly known as *Gokhru* or *Sarata* is used in household medicine as a tonic, Aphrodisiac, Palliative, Astringent, Gastric, anti-infective medicine. The literature when surfaced shows use of leaf, stem, shoots, roots, fruit and whole plant extract of the medicinal plant *Tribulus Terrestris* for various nanoparticles synthesis viz. Silver, gold, nickel, nickel oxide. The synthesised nanoparticles were reported to show various bioactivities viz. antibacterial, antifungal activities. The photocatalytic and cytotoxicity effects of the synthesized nanoparticles were also reported in the recent literatures. This review aims to give a comprehensive overview of various researchers' efforts towards the biosynthesis of various nanoparticles using the extracts of this medicinal plant *Tribulus Terrestris* during 2012–2021.

© 2022 Elsevier Ltd. All rights reserved.

Selection and peer-review under responsibility of the scientific committee of the Integrative Nanotechnology Perspective for Multidisciplinary Applications - 2022.

1. Introduction

Nanotechnology is a vital subject of modern research concerned with the synthesis, processing, and control of molecular structures ranging in size from 1 to 100 nm.[1] Due to their completely new or improved properties based on size, distribution, and shape, nanoparticles are gaining popularity on a variety of fronts[2]. It is rapidly gaining traction in a wide range of fields, including human services, cosmetics, biomedical, nutrition and feed, health, mechanics, optics, concoction businesses, hardware, space ventures, vitality science, catalysis, light producers, single electron transistors, nonlinear optical devices, and numerous others[1]. Major advancements in these expanding advancements have opened linked wildernesses and uncommon fundamentals. The production of nano scale materials are examined or used for its intriguing physiochemical characteristics, as well as optoelectronic capabilities.[3,4] Metallic nanoparticles are the most promising

because they have remarkable antibacterial characteristics due to their large surface to volume ratio, which is critical for analysts because of the growing microbial resistance to metal particles, anti-infection medications, and the development of safe strains. [4].(See Fig. 1. Table 1.).

Plant-mediated nanoparticle biosynthesis is widely regarded as a broadly accepted approach for the quick creation of metallic nanoparticles, resulting in a reduction in production of dangerous compounds to public health[5]. Plants, microorganisms have been employed as a “bio-factory” in the manufacture of metallic nanoparticles since they are inexpensive and require little care. [6] To counteract metal toxicity and preserve homeostasis, plants have a variety of cellular structures and physiological mechanisms in place. Scientists have now resorted phytoremediation since they feature dynamic ways to detoxify metals.[7] Immobilization, exclusion, chelation, and segregation of metal ions, as well as the production of more general stress response mechanisms, are among the methods used in detoxification.[8] Plants have long been known to have the ability to endure hazardous metal concentrations that are harmful. Essential nutrients including copper,

* Corresponding author.

E-mail address: drshirishpingale@gmail.com (S.S. Pingale).



Fig. 1. Distribution of various activities for the tribulus terrestris plant extracts mediated NPs.

iron, zinc, and selenium, as well as non-essential elements like cadmium, mercury, lead, aluminium, and arsenic were shown to have a high propensity to collect significant quantities of metals.[9] A wide range of metabolites with redox potentials have been identified in plants or plant-derived materials, and they have played a key role as a reducing agent in the biogenic production of nanoparticles. As compared to the microbial creation of nanoparticles, very stable nanoparticles are created at a faster pace by plants or plant extracts[10]. As a result of the benefits of plant-mediated metal nanoparticle synthesis, researchers are looking into the bio-reduction process of metal ions by plants, as well as the probable mechanism of metal nanoparticle formation in and by plants.[11] Biosynthesis of metal nanoparticles, particularly silver and gold nanoparticles, utilising plant extracts has become a hot topic in bio-nanotechnology research. [12].

Tribulus terrestris has been utilised as a health tonic in traditional medicine since Vedic times.[13] In medicine, a formulation containing *Tribulus terrestris* extract is often used to reduce blood pressure and cholesterol.[13] In humans, rats, and mice, the *Tribulus terrestris* extract lowers blood cholesterol levels. Plants are found all throughout the planet. Manly in low-moisture climates like as China, India, the southern United States, Spain, Bulgaria, Bangladesh, and Pakistan.[14].

This plant's fruits and seeds are employed in oriented medicines because they are aphrodisiac, diuretic, anthelmintic, Urolithiatic, and analgesic. It's a plant extract that's used to treat cough and kid-

ney problems.[15] This plant has been shown to have haemolytic, antibacterial, diuretic, anti-acetylcholine anti-hypertension, anticancer, spermatogenesis, and cardiovascular system activities. [16] Many ayurvedic medications, including *gokshuradi dash-moolarishtha*, *guggulu*, *churna*, *rasayana*, and *jatyaditaila*, included *Tribulus terrestris* as an ingredient.[17] It is utilised as a health tonic, palliative, aphrodisiac, antihypertensive, astringent, lithon- triptic, stomachic, diuretic, and urinary anti-infectives in tradi- tional medicine.[18].

The goal of this research is to learn more about metal nanopar- ticles made from *Tribulus terrestris* and their potential use in many fields. The alkaloids, flavonoids, and phenolic chemicals found in *Tribulus terrestris* are abundant. *Tribulus terrestris* was utilised to make metal nanoparticles that were well diffused and tiny in size. The antibacterial characteristics, anticancer activity, catalytic activity, cytotoxic qualities, and gas sensing capabilities of *Tribulus terrestris* biosynthesized metal nanoparticles have a wide variety of applications.

2. Bio-applications of nanoparticles synthesized using *Tribulus terrestris* extract

2.1. Antibacterial applications

Nanoparticles have been produced for a number of uses as a sig- nificant feature of nanotechnology, particularly in the field of Nano-medicines[19]. Nanoparticles have unique features that set them apart from their bulk counterparts.[20] Because of their abil- ity to avoid microbial resistance while meeting the present demand for new antibiotics, nanoparticles are increasingly being used in microbial applications[21–23]. The incidence of illnesses and outbreaks caused by multidrug-resistant (MDR) bacteria has risen, posing a hazard to public health.[24] Nitric oxide-releasing nanoparticles, chitosan nanoparticles, and metallic nanoparticles are among the nanoparticles utilised to overcome microbial resistance[25]. The therapeutic potentials of gold nanoparticles and sil- ver nanoparticles among metallic nanoparticles have been thoroughly studied elsewhere.[26] Ag nanoparticles have potent antibacterial, antiviral, and antifungal properties.[27] Metallic nanoparticles are often produced using classic chemical and

Table 1

The details of biosynthesized nanoparticles using *Tribulus terrestris* plant extract and their antibacterial applications.

Nanoparticles synthesized	Extract	Shape	Nanoparticle Size	Activity against bacteria	Ref.
Silver nanoparticles	aqueous extract of fruit powder	Spherical	16 nm to 28 nm	<i>Streptococcus pyogenes</i> , <i>Pseudomonas aeruginosa</i> , <i>Escherichia coli</i> , <i>Bacillus subtilis</i> and <i>Staphylococcus aureus</i>	V.Gopinath et al.[33]
Silver nanoparticles	aqueous extract of leaf powder	Spherical	18 nm to 47 nm	<i>Staphylococcus aureus</i> , <i>Escherichia coli</i> , <i>Pseudomonas aeruginosa</i> , <i>Streptococcus pyogenes</i> , <i>Proteus vulgaris</i> and <i>Bacillus subtilis</i>	V Gopinath et al.[34]
Silver nanoparticles	aqueous extract of leaf powder		15 nm average	<i>Staphylococcus aureus</i> , <i>Bacillus cereus</i> , <i>Escherichia coli</i> <i>Klebsiella pneumonia</i> , <i>Bacillus subtilis</i> , and <i>Salmonella typhimurium</i>	Djahaniani Hoorieh et.ai. [35]
Silver nanoparticles	aqueous extract of shoot powder	Spherical	25 nm average	<i>Staphylococcus aureus</i> , <i>Escherichia coli</i> , <i>Bacillus subtilis</i> and <i>Pseudomonas aeruginosa</i>	Majid Darroudi et.al. [36]
Gold nanoparticles	aqueous extract of fruit powder	triangular, spherical, hexagonal and truncated shapes	7 nm and 55 nm	<i>H. pylori</i> strains	V.Gopinath et al.[37]
Gold nanoparticles	aqueous extract of dried plant powder	–	6 nm to 25 nm	<i>Staphylococcus aureus</i> (<i>S. aureus</i>) and <i>Escherichia coli</i> (<i>E. coli</i>)	Farzad Molani et.al.[38]
nickel Oxide nanoparticles	aqueous extract of dried plant powder	Spherical	60 nm to 90 nm	<i>E. Coli</i> and <i>S. aureus</i>	Zia Ul Haq Khan et.al.[39]
copper nanoparticles/graphene oxide-chitosan	aqueous extract of leaf powder	–	2.4 nm to 257.6 nm	<i>E. coli</i>	Subramanian Mughesh et.al. [40]

physical processes.[28] However, contemporary environmental concerns have prompted investigations into eco-friendly and green synthesis of metallic nanoparticles based on a variety of biological organisms.[29].

Yemeni *T. terrestris* ethanolic extracts had no appreciable antibacterial action against any of the reference microorganisms.[30] However, ethanolic extracts of all components (fruits, stems, leaves, and roots) of Turkish *T. terrestris* shown antibacterial action against all reference microorganisms.[31] Furthermore, ethanolic extracts of Indian *T. terrestris* fruit and leaf were potent against *Escherichia coli* and *Staphylococcus aureus*.[32] The antibacterial properties of *Tribulus terrestris* biosynthesized nanoparticles are discussed in details below.

2.2. Catalytic uses

Ag nanoparticles biosynthesized using aqueous extract of *T. terrestris* has been reported for reduction of Methylene blue dye. The λ max value of pure methylene blue dye is steadily decreased from 664 nm. and the wavelength shifted to a higher wavelength after 30 min of adding the Ag nanoparticles extract of *T. terrestris* to the dye. At the end of a 30-minute time period, a system including dye, Ag nanoparticles, and the extract have revealed a substantial drop in methylene blue absorbance and an increase in Ag nanoparticles' SPR peak. This has indicated that the biosynthesized colloidal Ag nanoparticles actually functioned as a "green catalyst." [40].

Biogenic gold nanoparticles have been used as catalyst for the reduction of p-nitro aniline. Size dependent catalytic activity has been studied with help of the UV-Vis spectroscopic method. The rate of conversion of p-nitroaniline to p-phenylenediamine with NaBH_4 has boosted by aqueous gold nanoparticles, when gold nanoparticles of size 7 nm (GNP7) were combined with p-nitroaniline in the presence of NaBH_4 medium, the absorbance at 380 nm moved to 220 nm and a new peak at 305 nm formed after an incubation time of 0–56 min. while gold nanoparticles of size 55 nm (GNP55) have an incubation time of 0–72 min. for same conversion. The reduction process was completed in 56 min when GNP7 was employed as a catalyst, and in 72 min when GNP55 was utilised.[37].

It has been reported that the oxidation of organic sulphides to sulphoxides was bring out using 30 % H_2O_2 over gold-*Tribulus* nano-composite. 30 % H_2O_2 over gold-*Tribulus* nanocomposite has acted as a safe and green oxidant. An array of aliphatic and aromatic sulphides was oxidized over gold-*Tribulus* catalyst. All reactions were highly chemo selective and none were over-oxidized to sulphones. An increase in the amount of H_2O_2 did not improve the yield. Gold nanoparticles have shown high catalytic activity and good selectivity for the oxidation of sulphides to sulphoxides using H_2O_2 as an oxidant.[41].

2.3. Anticancer applications

The cytotoxicity of the biosynthesized Ag nanoparticles has been tested with a murine neuroblastoma cell line. The findings of the MTT (3-(4,5-dimethylthiazole-2-yl)-2, 5-diphenyltetrazolium bromide) dye assay experiment revealed a dose-dependent decrease in the viability percentage of Neuro2A cells after 24 h. The potential benefits of colloidal silver nanoparticles in cancer therapy have been reported by this research.[36].

Tribulus terrestris aqueous extract and green synthesised gold nanoparticles has been used to kill acute leukaemia cancer cell (THP-1 cells). Changes in the viability and morphology of cells treated with the *Tribulus terrestris* aqueous extract and green synthesised gold nanoparticles has been studied under inverted light microscopy. It is reported that gold nanoparticles had a good

antioxidant and cytotoxicity impact on acute leukaemia cancer cell lines. The gold nanoparticles can be employed as an alternatively constructed chemotherapeutic medication for the treatment of leukaemia.[41].

2.4. Other applications

A biological approach employing *T. terrestris* leaf extract was used to effectively generate Ag-coated ZnO nanoparticles, which were demonstrated to have improved ethanol-sensing characteristics at room temperature. It opened new possibilities of using these materials as efficient electron mediators in the manufacture of a variety of chemical sensors by simply manufacturing them.[42].

The concentrations that cause a 50 % inhibition have been reported in terms of IC_{50} values. Lower IC_{50} values are indicative of high DPPH radical scavenging activity as well as higher reducing powers. In the reducing assay, the presence of reducing agents (antioxidants) in plant samples causes the $\text{Fe}^{3+} / \text{Fe}^{2+}$ reduction reaction. The capacity of extract samples to reduce at various concentrations are reported. In the reducing power assay, PS may be considered an efficient antioxidant, and it can also be used as a reducing agent in the preparation of Ag nanoparticles.[35].

3. Conclusions

The literature is full of reports about the plant *Tribulus Terrestris* extract utilized for the synthesis of various nanoparticles viz. Ag, Au, Ni and NiO. We have arranged the reports from the past few years based on their various applications viz. antibacterial, catalytic, gas sensing, anticancer and as antioxidants. Thus, this review is formulated with aims to give a comprehensive overview of various researchers' efforts towards the biosynthesis and bio-applications of various nanoparticles using the extracts of this medicinal plant *Tribulus Terrestris*. Though there are few reports demonstrating the various antifungal, microbial and other applications, there are enough rooms to discover the novel applications are yet to be discovered.

CRedit authorship contribution statement

Sagar A. Nalawade: Conceptualization, Writing – original draft. **Bapusaheb Shinde:** . **Sushilkumar Chaudhari:** . **Manisha S. Badhe:** . **Vikas K. Kadam:** Writing – review & editing. **Manohar G. Chaskar:** Formal analysis, Data curation. **Shirish S. Pingale:** Project administration, Supervision.

Data availability

No data was used for the research described in the article.

Declaration of Competing Interest

The authors declare that they have no known competing financial interests or personal relationships that could have appeared to influence the work reported in this paper.

Acknowledgements

SAN would like to thank Dattatray Govindrao Walse Patil College, Pargaon Tarf Awsari, Pune for their constant support.

References

- [1] I. Khan, K. Saeed, I. Khan, Nanoparticles: Properties, applications and toxicities, *Arabian J. Chem.* 12 (7) (2019) 908–931.

- [2] J. Jeevanandam, A. Barhoum, Y.S. Chan, A. Dufresne, M.K. Danquah, Review on nanoparticles and nanostructured materials: history, sources, toxicity and regulations, *Beilstein J. Nanotechnol.* 9 (2018) 1050–1074.
- [3] H. Korbekandi, S. Irvani, S. Abbasi, Optimization of biological synthesis of silver nanoparticles using *Lactobacillus casei* subsp. *casei*, *J. Chem. Technol. Biotechnol.* (2012), <https://doi.org/10.1002/jctb.3702>.
- [4] M.M.H. Khalil, E.H. Ismail, K.Z. El-Baghdady, D. Mohamed, Green synthesis of silver nanoparticles using olive leaf extract and its antibacterial activity, *Arabian J. Chem.* 7 (6) (2014) 1131–1139.
- [5] J. Singh, T. Dutta, K.-H. Kim, M. Rawat, P. Samddar, P. Kumar, 'Green' synthesis of metals and their oxide nanoparticles: applications for environmental remediation, *Journal of nanobiotechnology* 16(1) (2018) 84–84.
- [6] N.N. Rupiasih, A. Aher, S. Gosavi, P.B. Vidyasagar, Green synthesis of silver nanoparticles using latex extract of *Thevetia peruviana*: a novel approach towards poisonous plant utilization, *J. Phys. Conf. Ser.* 423 (2013).
- [7] Y. Abboud, T. Saffaj, A. Chagraoui, A. El Bouari, K. Brouzi, O. Tanane, B. Ihssane, Biosynthesis, characterization and antimicrobial activity of copper oxide nanoparticles (CONPs) produced using brown alga extract (*Bifurcaria bifurcata*), *Appl. Nanosci.* 4 (5) (2014) 571–576.
- [8] F. Sánchez, Mentiras, corrupción y confianza. Apuntes de una relación, *Encuentros Multidiscip.* 13 (2011).
- [9] K. Sahayaraj, R. Sathiyamoorthy, J. Rathi, Silver nanoparticles biosynthesis using marine algae *Padina pavonica* (Linn.) and its microbial activity, *Digest J. Nanomater. Biostruct.* 7 (2012) 1557–1567.
- [10] R.K. Das, V.L. Pachapur, L. Lonappan, M. Naghdi, R. Pulicharla, S. Maiti, M. Cledon, L.M.A. Dalila, S.J. Sarma, S.K. Brar, Biological synthesis of metallic nanoparticles: plants, animals and microbial aspects, *Nanotechnol. Environ. Eng.* 2 (1) (2017) 18.
- [11] N. Ahmad, Green synthesis of silver nanoparticles using extracts of *Ananas comosus*, *Green Sustain. Chem.* 02 (2012) 141–147.
- [12] S. Irvani, Green synthesis of metal nanoparticles using plants, *Green Chem.* 13 (2011) 2638–2650.
- [13] L. Hechtman, 185 - Infertility, Male, in: J.E. Pizzorno, M.T. Murray (Eds.), *Textbook of Natural Medicine* (Fifth Edition), Churchill Livingstone, St. Louis (MO), 2020, pp. 1453–1472.e7.
- [14] W. Zhu, Y. Du, H. Meng, Y. Dong, L. Li, A review of traditional pharmacological uses, phytochemistry, and pharmacological activities of *Tribulus terrestris*, *Chem. Cent. J.* 11 (1) (2017) 60.
- [15] M. Akram, M. Asif, A. Naveed, P. Shah, M. Uzair, G. Shaheen, T. Shamim, D.S. Ali Shah, K. Ahmad, *Tribulus terrestris* Linn.: a review article, *J. Med. Plants Res.* 5 (2011) 3601–3605.
- [16] M. Jameel, J. Ansari, A. Abuzer, J. Ahamad, M. Ali, E. Tamboli, Pharmacological scientific evidence for the promise of *Tribulus terrestris*, *Int. Res. J. Pharm.* 3 (2012) 403–406.
- [17] C.P. Khare, *Indian medicinal plants: an illustrated dictionary*, Springer Science & Business Media, 2008.
- [18] S.Y. Kang, H.W. Jung, J.H. Nam, W.K. Kim, J.-S. Kang, Y.-H. Kim, C.-W. Cho, C.W. Cho, Y.-K. Park, H.S. Bae, Effects of the Fruit Extract of *Tribulus terrestris* on Skin Inflammation in Mice with Oxazolone-Induced Atopic Dermatitis through Regulation of Calcium Channels, Orai-1 and TRPV3, and Mast Cell Activation, *Evidence-based complementary and alternative medicine : eCAM* 2017 (2017) 8312946–8312946.
- [19] J.K. Patra, G. Das, L.F. Fraceto, E.V.R. Campos, M.d.P. Rodriguez-Torres, L.S. Acosta-Torres, L.A. Diaz-Torres, R. Grillo, M.K. Swamy, S. Sharma, S. Habtemariam, H.-S. Shin, Nano based drug delivery systems: recent developments and future prospects, *Journal of Nanobiotechnology* 16(1) (2018) 71.
- [20] J. Jeevanandam, A. Barhoum, Y.S.S. Chan, A. Dufresne, M. Danquah, Review on nanoparticles and nanostructured materials: history, sources, toxicity, and regulations, *Beilstein J. Nanotechnol.* 9 (2018) 1050–1074.
- [21] L. Wang, C. Hu, L. Shao, The antimicrobial activity of nanoparticles: present situation and prospects for the future, *Int. J. Nanomed.* 12 (2017) 1227–1249.
- [22] N.-Y. Lee, W.-C. Ko, P.-R. Hsueh, Nanoparticles in the Treatment of Infections Caused by Multidrug-Resistant Organisms, *Frontiers in pharmacology* 10 (2019) 1153–1153.
- [23] B. Mubeen, A.N. Ansar, R. Rasool, I. Ullah, S.S. Imam, S. Alshehri, M.M. Ghoneim, S.I. Alzarea, M.S. Nadeem, I. Kazmi, Nanotechnology as a Novel Approach in Combating Microbes Providing an Alternative to Antibiotics, *Antibiotics* 10 (12) (2021).
- [24] D. van Duin, D.L. Paterson, Multidrug-resistant bacteria in the community: trends and lessons learned, *Infect. Dis. Clin. North Am.* 30 (2) (2016) 377–390.
- [25] P.V. Baptista, M.P. McCusker, A. Carvalho, D.A. Ferreira, N.M. Mohan, M. Martins, A.R. Fernandes, Nano-strategies to fight multidrug resistant bacteria—“a battle of the titans”, *Front. Microbiol.* 9 (2018).
- [26] A. Bhat, K. Huan, T. Cooks, H. Boukari, Q. Lu, Probing interactions between AuNPs/AgNPs and giant unilamellar vesicles (GUVs) using hyperspectral dark-field microscopy, *Int. J. Mol. Sci.* 19 (4) (2018) 1014.
- [27] A. Gibała, P. Żeliszewska, T. Gosiewski, A. Krawczyk, D. Duraczyńska, J. Szaleniec, M. Szaleniec, M. Oćwieja, Antibacterial and antifungal properties of silver nanoparticles—effect of a surface-stabilizing agent, *Biomolecules* 11 (10) (2021) 1481.
- [28] A.M.E. Shafey, Green synthesis of metal and metal oxide nanoparticles from plant leaf extracts and their applications: a review, *Green Process. Synth.* 9 (1) (2020) 304–339.
- [29] V. Soni, P. Raizada, P. Singh, H.N. Cuong, R. S. A. Saini, R.V. Saini, Q.V. Le, A.K. Nadda, T.-T. Le, V.-H. Nguyen, Sustainable and green trends in using plant extracts for the synthesis of biogenic metal nanoparticles toward environmental and pharmaceutical advances: A review, *Environmental Research* 202 (2021) 111622.
- [30] S. Chhatre, T. Nesari, G. Somani, D. Kanchan, S. Sathaye, Phytopharmacological overview of *Tribulus terrestris*, *Pharmacogn. Rev.* 8 (15) (2014) 45–51.
- [31] F.A. Al-Bayati, H.F. Al-Mola, Antibacterial and antifungal activities of different parts of *Tribulus terrestris* L. growing in Iraq, *J. Zhejiang Univ. Sci. B* 9 (2) (2008) 154–159.
- [32] M.P. Mishra, S. Rath, S.S. Swain, G. Ghosh, D. Das, R.N. Padhy, In vitro antibacterial activity of crude extracts of 9 selected medicinal plants against UTI causing MDR bacteria, *J. King Saud Univ. – Sci.* 29 (1) (2017) 84–95.
- [33] V. Gopinath, D. MubarakAli, S. Priyadarshini, N.M. Priyadarshini, N. Thajuddin, P. Velusamy, Biosynthesis of silver nanoparticles from *Tribulus terrestris* and its antimicrobial activity: a novel biological approach, *Colloids Surf. B: Biointerfaces* 96 (2012) 69–74.
- [34] V. Gopinath, S. Priyadarshini, N. Meera Priyadarshini, K. Pandian, P. Velusamy, Biogenic synthesis of antibacterial silver chloride nanoparticles using leaf extracts of *Cissus quadrangularis* Linn, *Mater. Lett.* 91 (2013) 224–227.
- [35] D. Hoorieh, Facile synthesis of silver nanoparticles using *Tribulus longipetalus* extract and their antioxidant and antibacterial activities, *International journal of food properties v. 20*(no. 4) (2017) pp. 922–930–2017 v.20 no.4.
- [36] A. Hamidi, M.E. Taghavizadeh Yazdi, M.S. Amiri, H.A. Hosseini, M. Darroudi, Biological synthesis of silver nanoparticles in *Tribulus terrestris* L. extract and evaluation of their photocatalyst, antibacterial, and cytotoxicity effects, *Res. Chem. Intermed.* 45 (5) (2019) 2915–2925.
- [37] V. Gopinath, S. Priyadarshini, D. MubarakAli, M.F. Loke, N. Thajuddin, N.S. Alharbi, T. Yadavalli, M. Alagiri, J. Vadivelu, Anti-*Helicobacter pylori*, cytotoxicity and catalytic activity of biosynthesized gold nanoparticles: multifaceted application, *Arabian J. Chem.* 12 (1) (2019) 33–40.
- [38] F. Molani, F. Veisi, S. Mohammadiazar, A nano-bio-eco interaction to synthesis of gold nanoparticles using *Tribulus Terrestris* extract and its antibacterial activity, *Adv. J. Chem.-Sect. A* 4 (3) (2021) 197–205.
- [39] Z.U.H. Khan, A. Khan, N.S. Shah, I.U. Din, M.A. Salam, J. Iqbal, N. Muhammad, M. Imran, M. Ali, M. Sayed, M.A. Gohar, Photocatalytic and biomedical investigation of green synthesized NiONPs: Toxicities and degradation pathways of Congo red dye, *Surf. Interfaces* 23 (2021).
- [40] S. Mughesh, R. Arun, K. Arunkumar, M. Murugan, Synthesis of biogenic copper nanoparticles embedded in graphene oxide-Chitosan composite and its antibacterial and cytotoxic activities, *J. Nanosci. Nanotechnol.* 19 (5) (2019) 2625–2632.
- [41] P. Zhao, A. El-kott, A.E. Ahmed, A. Khames, M.A. Zein, Green synthesis of gold nanoparticles (Au NPs) using *Tribulus terrestris* extract: investigation of its catalytic activity in the oxidation of sulfides to sulfoxides and study of its anti-acute leukemia activity, *Inorg. Chem. Commun.* 131 (2021).
- [42] Z.-Y. Zhao, M.-H. Wang, T.-T. Liu, *Tribulus terrestris* leaf extract assisted green synthesis and gas sensing properties of Ag-coated ZnO nanoparticles, *Mater. Lett.* 158 (2015) 274–277.



Phytofabricated Br-AgNP synthesis using *Brassica oleracea var. italica* and their anti-carcinogenic applications

Shubhangi Puranik, Imran Patel *

Post Graduate Research Centre in Zoology, Modern College of Arts, Science and Commerce, Shivajinagar, Pune, India

ARTICLE INFO

Article history:
Available online 17 October 2022

Keywords:
AgNPs
Broccoli
Anticarcinogenic
Apoptosis

ABSTRACT

Nanobiotechnology involves extraction of reducing agents from biological sources and their application for synthesis of nanoparticles. This study is based on identification and purification of natural reducing agents in medicinal plants like *Brassica oleracea var. italica* to analyse their anti-cancerous potential against HeLa and THP-1. Biogenic reduction of silver nanoparticles was performed using these plant extracts by single step bottom up approaches. Colorless to red coloured solution and a peak at 417 nm in UV-vis spectroscopy confirmed the synthesis of AgNPs. Scanning Electron Microscopy confirmed the spherical nature of AgNPs whereas XRD confirmed the crystalline nature. PSA, SEM and Zeta potential analyzer confirmed the AgNPs with range of size between 14.53 and 38.15 nm with higher stability. AgNPs were treated with HeLa and THP-1 cell line. The % inhibition from AgNPs on HeLa cell line was found to be highest at 80 μ l concentration (26.3 %) and lowest at 10 μ l concentration (19.49 %) whereas on THP-1 cell line was found to be highest at 80 μ l concentration (22.96 %) and lowest at 10 μ l concentration (2.26 %).

Copyright © 2022. Elsevier Ltd. All rights reserved.

Selection and peer-review under responsibility of the scientific committee of the Integrative Nanotechnology Perspective for Multidisciplinary Applications - 2022.

1. Introduction

Nanotechnology mainly deals with the fabrication of nanoparticles having various shapes and size and to manage their chemical and physical parameters for further use in human benefits [1]. Nanoparticles are fine entities having size ranging from 0.1 to 100 nm. Nanoparticles are prepared using physical and chemical methods [2]. However, physical methods give a low yield, and chemical methods are toxic to the environment due to usage of toxic chemical- reducing agents, such as citrate, borohydride [3,4]. It is also difficult to prepare NPs with well-defined size by these methods. Biological methods/Green synthesis, involve synthesis of NPs by means of enzymatic reduction, by plant extracts with better control over the shape and size of the NPs [5–8]. Besides these, biological methods have several additional merits, such as low toxicity, cost-effectiveness, biocompatibility, stability and significant dispersity and do not flocculate [8,9]. Nanobiotechnology (green synthesis) represents an economic alternative for chemical and physical methods of nanoparticles formation. Gold

nanoparticles (AuNPs) and silver nanoparticles (AgNPs) have been used as medicinal agent since a long time [6,7]. AuNPs & AgNPs are excellent labels for biosensors. They provide non-toxic routes to drug and gene delivery application. They have anti cancerous, antioxidant & antibacterial activity. Nanoparticles of noble metals such as silver have antibacterial and anti-cancerous activities [10,11]. These have low toxicity levels and are used in various drug delivery systems. The chemical composition of plant extract greatly influences on the size and shape of the nanoparticles, which in turn effects on the therapeutic and catalytic properties of nanoparticles [12,13]. Hence there is necessity to screen more plant extract for the green synthesis of AgNPs of desired size and shape. For this study *Brassica oleracea var. italica* was selected since it contains 3, 3' Diindolylmethane which has antiviral, antibacterial and anti-cancer activity. Indole-3- carbinol- boosts DNA repair in cells and blocks the growth of cancer cells. Glucoraphanin, and Sulforaphane shows anti-cancerous activity [14–16]. (See Fig. 1. Fig. 2. Fig. 3. Fig. 4. Fig. 5. Fig. 6. Graph 1).

Cancer cases have been on the rise in recent years leading to increased morbidity and mortality; accounting for approximately 63 % deaths in developing countries in 2008 [17]. All forms of cancer are incurable and current drugs have many side effects prompt-

* Corresponding author at: Post Graduate Research Centre in Zoology, Modern College of Arts, Science and Commerce, Shivajinagar, Pune, India.

E-mail address: imranpatelq@gmail.com (I. Patel).



Fig. 1. Colour Change during AgNP synthesis after 24 hr.

ing the urgent need to search for the next generation therapy. Nanoparticles received much attention recently due to their used in cancer therapy. In that different metal oxide nanoparticles induce cytotoxicity in cancer cells but not in normal cells. [18]. Cancer is a group of diseases involving abnormal cell growth with the potential to invade or spread to other parts of the body. Leukemia cancer is one type blood cancer characterized by an abnormal increase of immature white blood cell called blast [19,20].

Cervical cancer is the most common cause of cancer death among woman in developing countries and second most common cancer in woman worldwide. It is caused by a change in the epithelial cells, which lines the wall of the cervix, and the most common risk factor for these type of cancer is the human papillomavirus. [20,21]. THP-1 is a human monocytic cell line derived from an acute monocytic leukemia. HeLa is the 1st human cervical cancer cell line [21,22].

The main objectives of this study includes synthesis of Silver nanoparticles (AgNPs) from *Brassica oleracea* var. *italica* and check the anti-cancerous activities of crude extract and silver nanoparticles on THP-1 and HeLa cell lines by MTT assay.

2. Experimental section

2.1. Reagents

RPMI-1640 medium, fetal bovine serum (FBS), trypsin/ EDTA, penicillin–streptomycin were purchased from Gibco. Analytical

grade silver nitrate (AgNO_3), trypan blue, phosphate buffered saline (PBS), NaCl , Na_2EDTA , Tris, DMSO, ethidium bromide, 2,7-dichlorofluorescein diacetate, Propidium iodide were obtained from Sigma Aldrich (St. Louis, MO, USA). HeLa and THP-1 cell lines were obtained from NCCS, Pune.

2.2. Sample collection and preparation of extract

Healthy plant samples were collected. 25 g of plant material i.e. Broccoli fruit was washed with distilled water to remove dust particles and it was cut into small pieces. 100 ml of distilled water was added to it and boiled for 10–15 min in water bath at 100°C . Suspension was filtered using Whatman No. 1 Filter paper. At the end, the filtered extract was collected in the storage amber bottle. The extract was preserved inside a refrigerator for further use.

2.3. Silver nanoparticles synthesis

2 ml of broccoli leaves extract was added to 25 ml of AgNO_3 solution and they were kept for incubation at 37°C for 24 hrs. Colour change was observed which primitively concluded the formation of silver nanoparticles. The AgNPs were centrifuged at $12000g$ for 25 min and the residual was dried in hot air oven at 150°C overnight to obtain powder. This powder was collected and stored in clean vials for further use [5,7,23].

2.4. Characterization

This is an important aspect in nanoparticles research to achieve better interpretation of results with primitive understanding. The colour changes were recorded along with periodic sampling and scanning using UV–vis spectrophotometry (Systronics type 108-double beam) ranging from 200 to 680 nm for a maximum time period upto 120 min [2,24]. Particle size analysis (Nanophox NX0088, Sympatec GmbH) and zeta potential measurement (Delsa Tm Nano, Beckman Coulter) were carried to analyse the size and stability of AgNPs. An FTIR spectrum (Bruker) of the AgNPs was measured in the transmittable mode at the range 4000 to 500 cm^{-1} in KBr pellets. FESEM analysis i.e. field emission scanning electron microscopy was performed using Nova Nano SEM 450. XRD measurements of AgNPs was performed using XRD Bruker D8 Diffractometer operating at a voltage 40 KV and current of

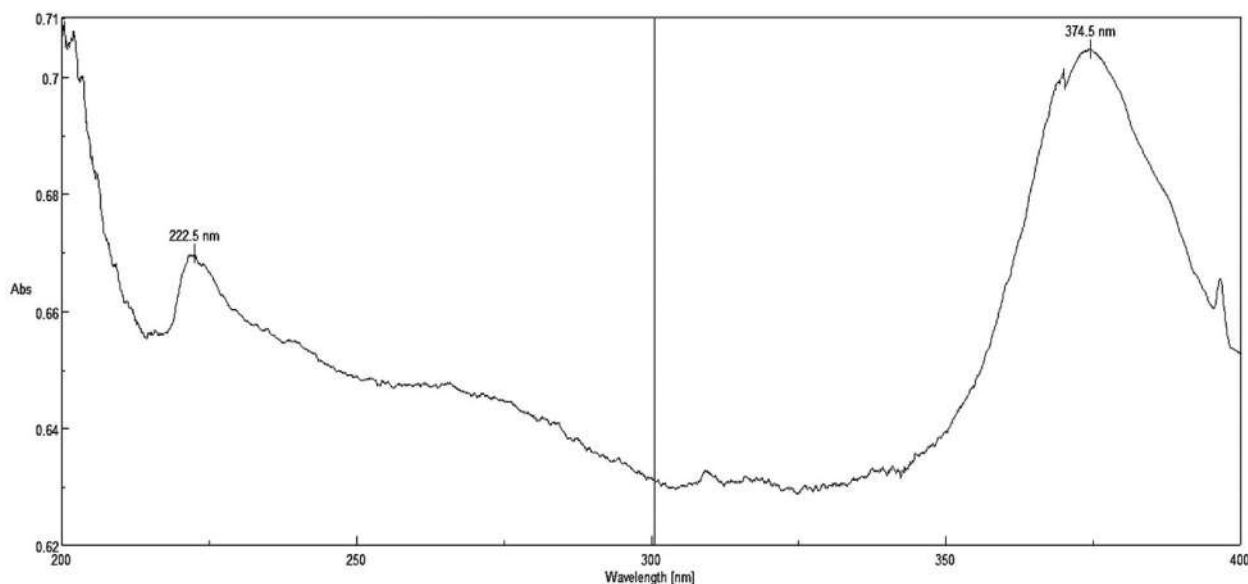


Fig. 2. UV–vis Spectra of AgNps.

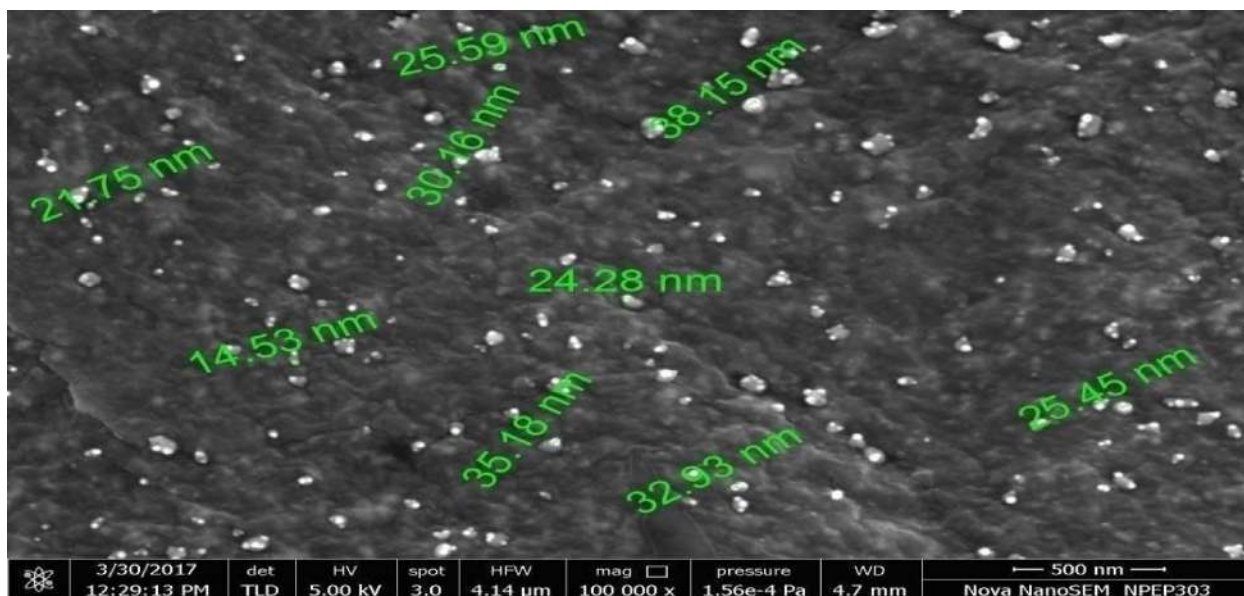


Fig. 3. FESEM image of AgNPs.

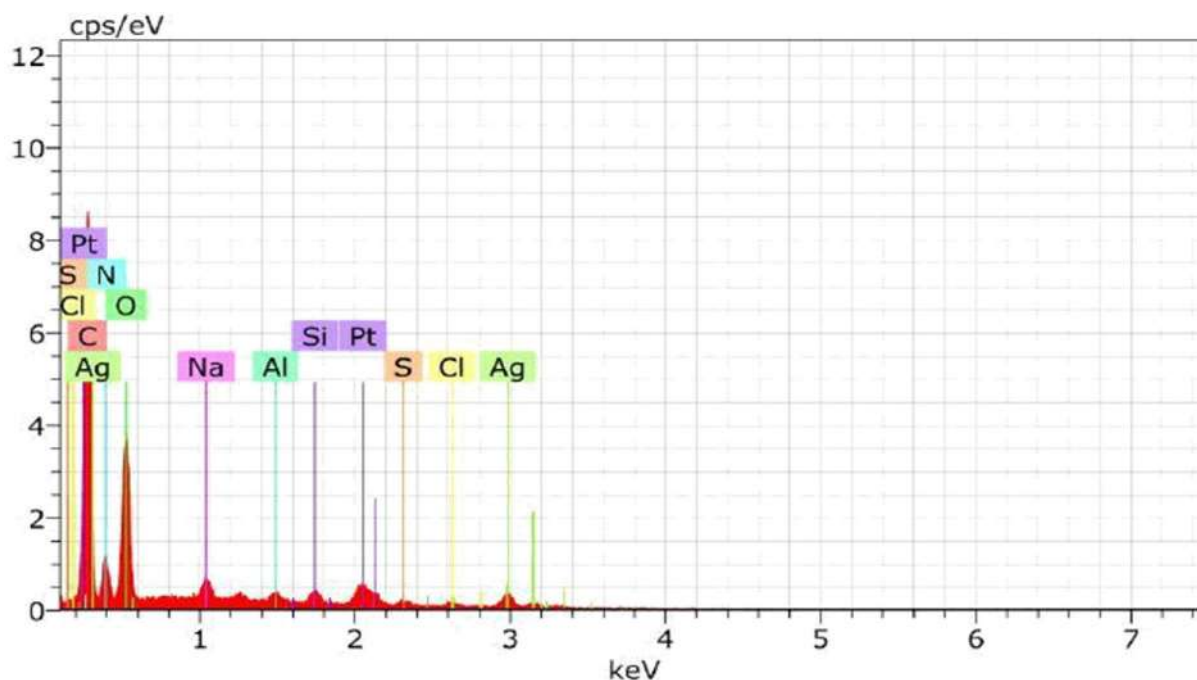


Fig. 4. EDS spectra of AgNPs.

20 mA with Cu-K radiation was performed to confirm the size and morphology of the AgNPs [22].

2.5. Anticarcinogenic activity of AgNPs by MTT assay

Hela and THP-1 cell lines were purchased from the NCCS cell bank, Pune, India and grown in RPMI-1640 medium containing 10 % foetal bovine serum (FBS), 2 mM L-glutamine, 100 IU ml⁻¹ penicillin and streptomycin. The cultured cells maintained at 37 °C with 5 % CO₂ in a humidified CO₂ incubator. The cells were subcultured to assess their growth and viability [22]. Before the treatment of AgNPs, cells were washed with PBS, and fresh medium was added to complete evaporation of growth signals released

by growing cells. Assessment of anticancer activity on cancer cells needs at least 90 % of the cells to be alive. This was analysed using Dye exclusion test, and a haemocytometer used to determine the number of viable cells [25].

Blank were set up using only media without cells in the micro titer plate. Control (Untreated cells) was set up and the two types of cells were seeded. 100 μl media was added in each well and the plates were incubated in CO₂ incubator at 37 °C for 24 hrs. 100 μl solution of Plant extracts and silver nanoparticle solution were added in wells independently in two micro titer well plates. Plates were incubated for 37 °C for 48 hrs. 10 μl MTT was added in each well. Plates were covered and incubated in CO₂ incubator at 37 °C for 4 hrs. 100 μl DMSO and 25 μl glycine buffer was added to wells.

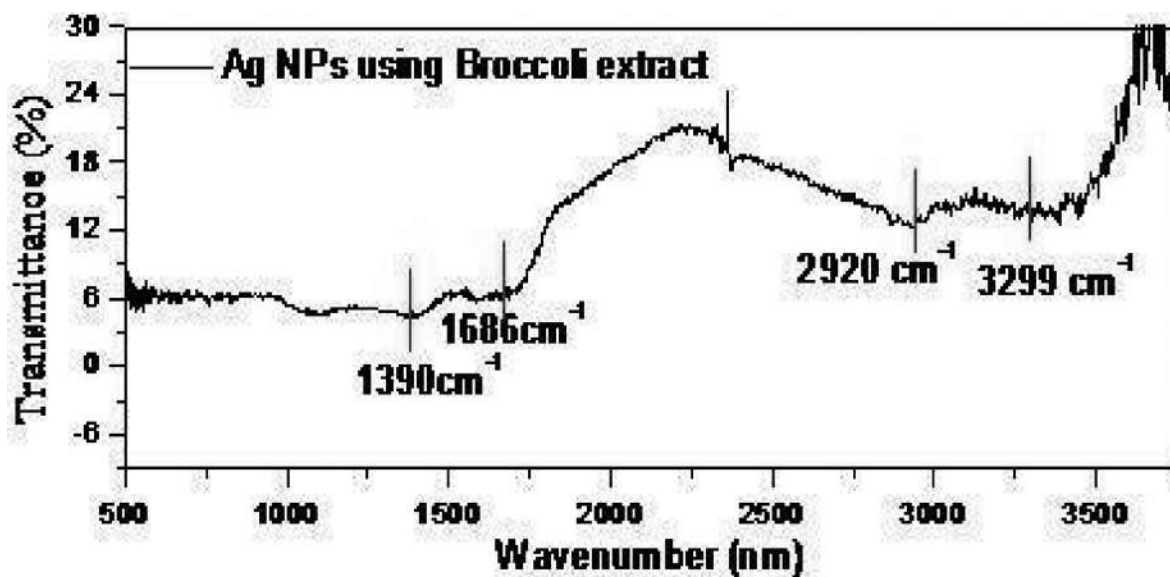


Fig. 5. FTIR spectra of AgNPs.

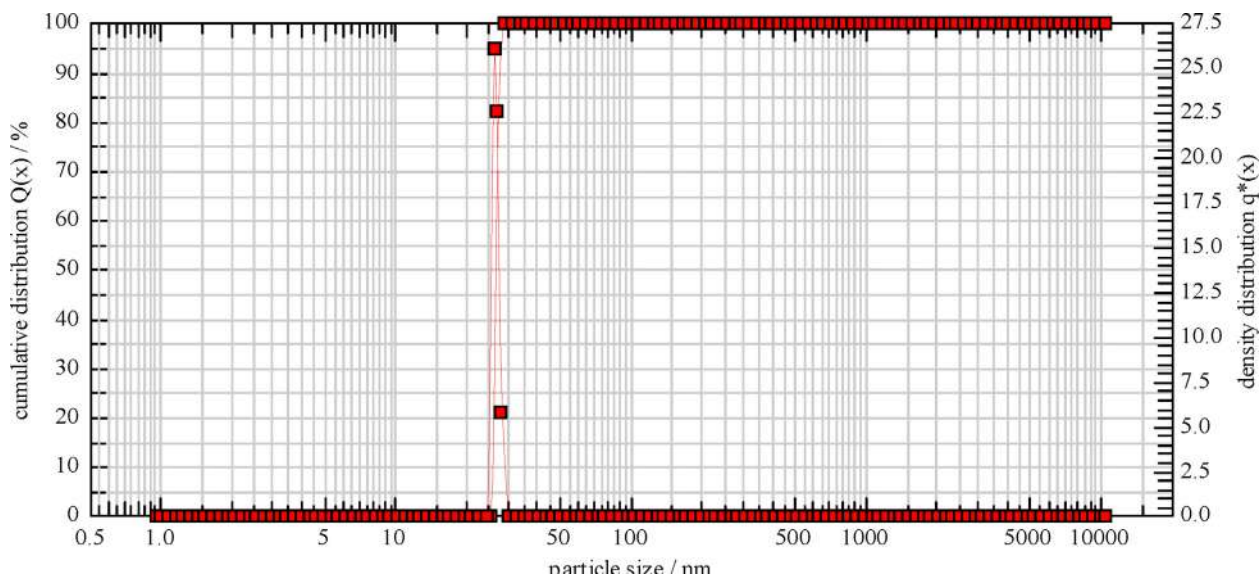


Fig. 6. Particle Size Analysis.

Supernatant were taken out of the wells into another micro titer plates. Readings were taken out on micro titer plate reader at 570 nm. Results were tabulated and % viability (survival) was calculated. The experiments were carried out in triplicates in two plates [26].

2.6. Statistical analysis

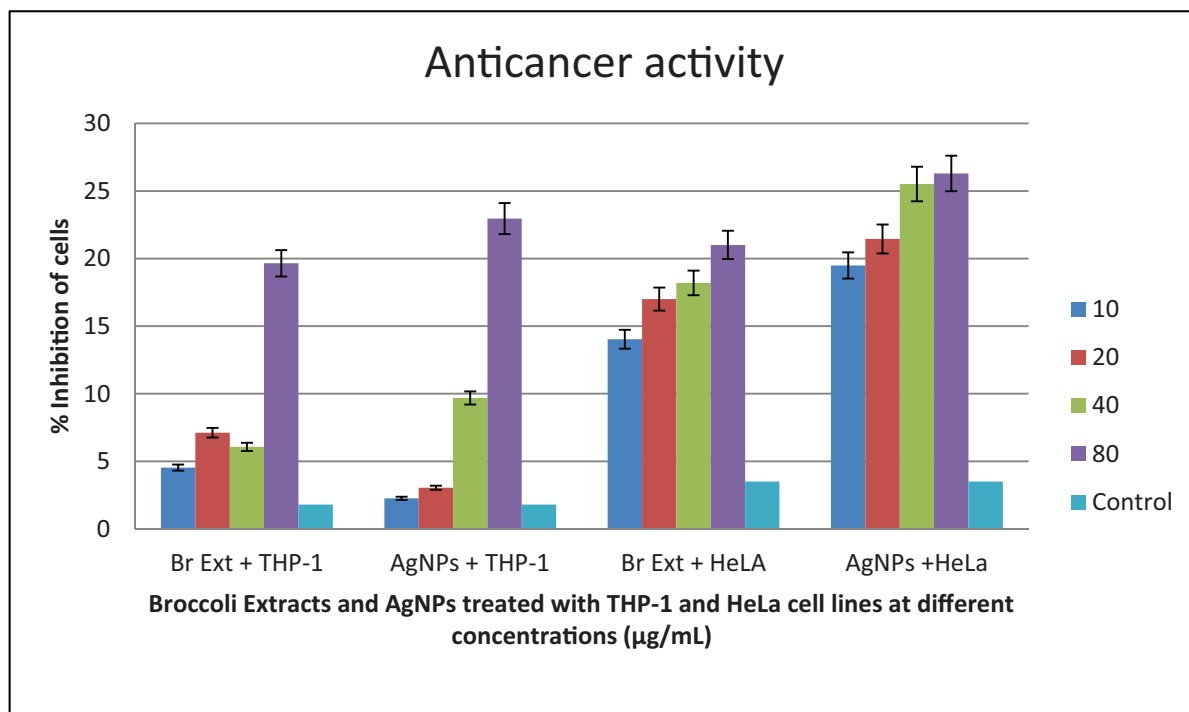
All experiments were repeated in triplicates and all data were expressed through the mean \pm standard error of the mean. SPSS version 21.0 statistical software (SPSS Inc., Chicago, IL, USA) used for all analyses. The one-way ANOVA (University Park, USA) used for comparing the means of control and treated groups, and differ-

ences were considered as statistically significant if the P value was ≤ 0.05 .

3. Results and discussion

3.1. Colour change and UV-vis spectroscopy

When silver ions are exposed to reducing agents from plant extracts, they get converted to Ag^0 atom which club together to form spherical nanoparticles. Colour change was observed from colourless to light yellow in 30 min and reddish brown after 24 hr indicated the formation of AgNPs [8,9,24]. Similar observations were reported by Kuppaswamy *et.al*. In addition, UV-vis spectrophotometry showed the SPR peaks at 374.5 nm for AgNPs which



Graph 1. Percentage inhibition of THP-1 and HeLa cell treated with Broccoli extracts and Br-AgNPs.

confirmed their synthesis. A characteristic peak between 370 and 420 nm reveals the spherical nature of silver nanoparticles.

3.2. Scanning electron microscopy and EDS spectra

FE-SEM analysis confers the shape, size and morphology of particles. It was concluded that the spherical shape of AgNPs was observed having size in the range of 14.53 nm to 38.15 nm. EDS spectra confirms the presence of silver nanoparticles with minor contamination of O, Na, Si, N and Al. This conclusively creates an observation that the AgNPs were formed with low polydispersity and maximised uniformity.

3.3. FTIR spectrum and XRD analysis

FTIR result showed that the absorption bands at 1368 cm^{-1} and 1689 cm^{-1} , which showed the signatures of Dimethyl and quinone or conjugated Ketone functional groups. FTIR result showed that the absorption bands at 3299 cm^{-1} , 2920 cm^{-1} , 1686 cm^{-1} , 1390 cm^{-1} and 1085 cm^{-1} showed skeletal vibration C—C stretching, Methylene C—H asymmetric stretching, presence of *gem*-Dimethyl or iso- (doublet) functional group and Aromatic C—H in-plane bending was observed respectively. The presence of these functional groups on the surface of AgNPs act as stabilizing agents and disallow the formation of aggregates in the AgNPs solution. It is observed that these functional groups have been acting as reducing agents and surface stabilizing agents as well.

Small amount of dry nanoparticles was used for XRD analysis. The XRD analysis of synthesized AgNPs from leaf extract showed diffraction peaks at 2θ angle values of 38.2° , 44.4° , 66.2° and 77.2° correspond to crystal plane of (111), (200), (220) and (311) of gold nanoparticles. The peak 2θ angle values of 38.13° , 44.50° , 46.28° and 77.36° correspond to crystal plane of (111), (200), (220), and (311) of silver nanoparticles. This confirmed that the AgNPs showed crystalline nature with high peaks indicating the active silver composition.

3.4. Anticarcinogenic activity by MTT assay

In this study the toxic effect or anticarcinogenic effect of AgNPs and Broccoli was tested against two cancer cell lines mainly THP-1 and HeLa cell lines. MTT assay observes a dose-dependent exposure to nanoparticles and extracts. The AgNPs showed significant activity against both the cell lines. It can be observed that Broccoli extract synthesized AgNPs were more effective on HeLa cell lines as compared to THP-1. Significant increase in the inhibition is observed in a dose dependent manner from 2.26 to 22.96 % inhibition for THP-1 cell line and 19.49 to 26.3 % inhibition for HeLa cell lines. The drug percentage was 100 % more effective than the others. Presence of reducing compounds in the extracts also showed anti proliferative activity which can also be observed for both the cell lines. The extracts were found to be more effective on HeLa while the Nanoparticles were more effective on THP-1. This study proved to be an effective and Ecofriendly method to produce AgNPs that showed anticancerous activity on HeLa and THP-1 cell line. This data showed a toxic impact of synthesized nanoparticles against cancer cells.

4. Discussion

It has been reported that the extracts of broccoli leaves show the presence of numerous biological active reducing compounds such as flavonoids, alkaloids, terpenes, saponins, etc. as reported [15,16]. In this study, synthesis of silver nanoparticles was carried out with the help of broccoli leaves extract which contain antioxidants that play a major role in converting silver ions to silver metal nanoparticles. SPR peak and FE-SEM images confirms the spherical nature of silver nanoparticles. The characteristic of SPR is largely affected by the shape and size of the nanoparticles and dielectric constant of the surrounding medium [27]. Absorption bands are readily affected due to various sizes, shapes and morphology of AgNPs. Specifically, it was observed that AgNPs showed

negative zeta potential which resulted in disaggregation and increased the stability of them [28].

The surface chemistry of these particles is largely explained by FTIR. This technique helps to identify the functional group present in the extracts. In this present study, absorption bands at 3299 cm^{-1} , 2920 cm^{-1} , 1686 cm^{-1} , 1390 cm^{-1} and 1085 cm^{-1} showed skeletal vibration C—C stretching, Methylene C—H asymmetric stretching, presence of *gem*-Dimethyl or iso- (doublet) functional group and Aromatic C—H in-plane bending was observed respectively [29]. The presence of these functional groups on the surface of AgNPs act as stabilizing agents and disallow the formation of aggregates in the AgNPs solution. These antioxidants played a major role in stabilizing the surface as well as increase the cytotoxicity of AgNPs. As mentioned before the most important phytochemical constituents responsible for the reduction and capping of silver nanoparticles as revealed by FTIR and phytochemical studies are alkaloids, flavonoids, tannins, terpenes and quinones as reported by Kuppusamy et al. [30].

The present study reveals the current knowledge about the biosynthesis of silver nanoparticles from broccoli extracts and their potential anticarcinogenic activities. MTT assay was used to analyses the inhibitory potential of AgNPs. Studies by Ullah et al. reveal that AgNPs show induced cell death in cancer cells due to increased oxidative stress leading to apoptosis of these cells [31]. In the present study, it was found that AgNPs synthesized from Broccoli extracts showed a dose dependent anti-cancer activity against cervical cancer and leukemia cancer even at a very low concentration. Wang et al. has suggested that the anticancer activity of nanoparticles is attributed to the enhancement of intracellular ROS generation due to oxidative stress leading to mitochondrial apoptosis [32]. AgNPs and Broccoli extract showed intensifying anticancer activity against HeLa and THP-1 cell lines. Surprisingly it was also seen that the extracts showed higher inhibitory effect at higher concentration. It is suggested that broccoli could be used as a potent anticancer preventive medicine if brought in everyday diet.

5. Conclusion

This study suggests an eco-friendly method to obtain AgNP using broccoli extract which possesses potent anticancer activity against THP-1 and HeLa cell lines. Our findings suggest that AgNPs selectively increased toxicity in cancer cells with a dose-dependent increase. The role of AgNPs in cell toxicity is not fully understood; we suggest that future work is needed to unveil the role of potential anticarcinogenic reducing present in the extract and enhancing the ability of AgNPs.

CRedit authorship contribution statement

Shubhangi Puranik: Conceptualization, Methodology, Visualization, Supervision, Investigation. **Imran Patel:** Data curation, Writing – original draft, Software, Validation, Writing – review & editing.

Data availability

The data that has been used is confidential.

Declaration of Competing Interest

The authors declare that they have no known competing financial interests or personal relationships that could have appeared to influence the work reported in this paper.

Acknowledgements:

The authors are grateful to Savitribai Phule Pune University, Pune for financial assistance for this project under BCUD.

References

- [1] S.R. Prasad, S.B. Teli, J. Ghosh, N.R. Prasad, V.S. Shaikh, G.M. Nazeruddin, A.G. Al-Sehemi, I. Patel, Y.I. Shaikh, A review on bio-inspired synthesis of silver nanoparticles: their antimicrobial efficacy and toxicity, *Eng. Sci.* (2021).
- [2] J.I. Hussain, S. Kumar, A.A. Hashmi, Z. Khan, Silver nanoparticles: preparation, characterization, and kinetics, *Adv. Mater. Lett.* 2 (3) (2011) 188–194.
- [3] N. Rajput, Methods of preparation of nanoparticles-a review, *Int. J. Adv. Eng. Technol.* 7 (6) (2015) 1806.
- [4] Jingyue, Z. H. A. O., & Bernd, F. (2015). Synthesis of gold nanoparticles via chemical reduction methods. *Proceedings of the Nanocon, Brno, Czech Republic*, 14–16.
- [5] Ahmed, S., Saifullah, Ahmad, M., Swami, B. L., & Ikram, S. (2016). Green synthesis of silver nanoparticles using *Azadirachta indica* aqueous leaf extract. *Journal of radiation research and applied sciences*, 9(1), 1–7
- [6] B.S. Bhau, S. Ghosh, S. Puri, B. Borah, D.K. Sarmah, R. Khan, Green synthesis of gold nanoparticles from the leaf extract of *Nepenthes khasiana* and antimicrobial assay, *Adv. Mater. Lett.* 6 (1) (2015) 55–58.
- [7] C. Singh, V. Sharma, P.K. Naik, V. Khandelwal, H. Singh, A green biogenic approach for synthesis of gold and silver nanoparticles using *Zingiber officinale*, *Digest J. Nanomater. Biostruct.* 6 (2) (2011) 535–542.
- [8] G.H. Priyaa, K.B. Satyan, Biological synthesis of silver nanoparticles using ginger (*Zingiber officinale*) extract, *J. Environ. Nanotechnol.* 3 (4) (2014) 32–40.
- [9] Koyale, R., Pingale, S., Patel, I., & Puranik, S. Plant based synthesis of silver nanoparticles using *Musa paradisiaca* and evaluation of its antimicrobial potential.
- [10] C. Uboldi, D. Bonacchi, G. Lorenzi, M.I. Hermanns, C. Pohl, G. Baldi, R.E. Unger, C.J. Kirkpatrick, Gold nanoparticles induce cytotoxicity in the alveolar type-II cell lines A549 and NCIH441, *Part. Fibre Toxicol.* 6 (2009) 18, <https://doi.org/10.1186/1743-8977-6-18>.
- [11] A.A. Ezhilarasi, J.J. Vijaya, K. Kaviyarasu, M. Maaza, A. Ayeshamariam, L.J. Kennedy, Green synthesis of NiO nanoparticles using *Moringa oleifera* extract and their biomedical applications: cytotoxicity effect of nanoparticles against HT-29 cancer cells, *J. Photochem. Photobiol. B: Biol.* 164 (2016) 352–360.
- [12] S. Eustis, M.A. El-Sayed, Why gold nanoparticles are more precious than pretty gold: noble metal surface plasmon resonance and its enhancement of the radiative and nonradiative properties of nanocrystals of different shapes, *Chem. Soc. Rev.* 35 (3) (2006) 209–217.
- [13] Biswal, S.K., Nayak, A.K., Parida, U.K., & Nayak, P.L. (2012). APPLICATIONS OF NANOTECHNOLOGY IN AGRICULTURE AND FOOD SCIENCES.
- [14] J.R. Devi, E.B. Thangam, Mechanisms of anticancer activity of sulforaphane from *Brassica oleracea* in HEP-2 human epithelial carcinoma cell line, *Asian Pacific J. Cancer Prevent.* 13 (5) (2012) 2095–2100.
- [15] I. Ravikummar, Therapeutic potential of *Brassica oleracea* (Broccoli) - a review, *Int. J. Drug Develop. Res.* 7 (2015).
- [16] M.Z. Saavedra-Leos, C. Leyva-Porras, A. Toxqui-Terán, V. Espinosa-Solis, Physicochemical properties and antioxidant activity of spray-dry Broccoli (*Brassica oleracea* var *Italica*) stalk and floret juice powders, *Molecules* 26 (7) (2021) 1973.
- [17] J. Ferlay, H.R. Shin, F. Bray, D. Forman, C. Mathers, D.M. Parkin, Estimates of worldwide burden of cancer in 2008: GLOBOCAN 2008, *Int. J. Cancer* 127 (12) (2010) 2893–2917.
- [18] Y. Bendale, V. Bendale, S. Paul, Evaluation of cytotoxic activity of platinum nanoparticles against normal and cancer cells and its anticancer potential through induction of apoptosis, *Integr. Med. Res.* 6 (2) (2017) 141–148.
- [19] A. Schildberger, E. Rossmanith, T. Eichhorn, K. Strassl, V. Weber, Monocytes, peripheral blood mononuclear cells, and THP-1 cells exhibit different cytokine expression patterns following stimulation with Lipopolysaccharide, *Mediat. Inflamm.* 2013 (2013) 1–10.
- [20] M. Schnoor, I. Buers, A. Sietmann, M.F. Brodde, O. Hofnagel, H. Robenek, S. Lorkowski, Efficient non-viral transfection of THP-1 cells, *J. Immunol. Methods* 344 (2) (2009) 109–115.
- [21] S. Shukla, A.C. Bharti, S. Mahata, S. Hussain, R. Kumar, S. Hedau, B.C. Das, Infection of human papillomaviruses in cancers of different human organ sites, *Indian J. Med. Res.* 130 (2009) 222–223.
- [22] B.P. Lucey, W.A. Nelson-Rees, G.M. Hutchins, Henrietta Lacks, HeLa cells, and cell culture contamination, *Arch. Pathol. Lab. Med.* 133 (9) (2009) 1463–1467.
- [23] Gannimani, R., Perumal, A., Krishna, S. B., Sershen, M., Mishra, A., & Govender, P. (2014). Synthesis and antibacterial activity of silver and gold nanoparticles produced using aqueous seed extract of *Protorus longifolia* as a reducing agent.
- [24] S. Irvani, H. Korbekandi, S.V. Mirmohammadi, B. Zolfaghari, Synthesis of silver nanoparticles: chemical, physical and biological methods, *Res. Pharm. Sci.* 9 (6) (2014) 385.
- [25] S. Patel, N. Gheewala, A. Suthar, A. Shah, In-vitro cytotoxicity activity of *Solanum nigrum* extract against Hela cell line and Vero cell line, *Int. J. Pharm. Pharm. Sci.* 1 (1) (2009) 38–46.
- [26] J.A. Plumb, Cell sensitivity assays: the MTT assay, in: *Cancer Cell Culture*, Humana Press, 2004, pp. 165–169.

- [27] M.A. Mahmoud, M. Chamanzar, A. Adibi, M.A. El-Sayed, Effect of the dielectric constant of the surrounding medium and the substrate on the surface plasmon resonance spectrum and sensitivity factors of highly symmetric systems: silver nanocubes, *J. Am. Chem. Soc.* 134 (14) (2012) 6434–6442.
- [28] A.M.E. Badawy, T.P. Luxton, R.G. Silva, K.G. Scheckel, M.T. Suidan, T.M. Tolaymat, Impact of environmental conditions (pH, ionic strength, and electrolyte type) on the surface charge and aggregation of silver nanoparticles suspensions, *Environ. Sci. Technol.* 44 (4) (2010) 1260–1266.
- [29] Branduardi, P., Doglia, S. M., Porro, D., Mereghetti, P., Posteri, R., & Ami, D. (2014). Fourier transform infrared spectroscopy as a method to study lipid accumulation in oleaginous yeasts.
- [30] P. Kuppusamy, S.J. Ichwan, N.R. Parine, M.M. Yusoff, G.P. Maniam, N. Govindan, Intracellular biosynthesis of Au and Ag nanoparticles using ethanolic extract of *Brassica oleracea* L. and studies on their physicochemical and biological properties, *J. Environ. Sci.* 29 (2015) 151–157.
- [31] I. Ullah, A.T. Khalil, M. Ali, J. Iqbal, W. Ali, S. Alarifi, Z.K. Shinwari, M. Saxena, Green-synthesized silver nanoparticles induced apoptotic cell death in MCF-7 breast cancer cells by generating reactive oxygen species and activating caspase 3 and 9 enzyme activities, *Oxid. Med. Cell. Longevity* 2020 (2020) 1–14.
- [32] J. Wang, J.Z. Li, A.X. Lu, K.F. Zhang, B.J. Li, Anticancer effect of solidoside on A549 lung cancer cells through inhibition of oxidative stress and phospho-p38 expression, *Oncol. Lett.* 7 (4) (2014) 1159–1164.



Antioxidant activity and antimicrobial evaluation of iron nanoparticles prepared by the plant mediated biosynthesis involving root extract of *Picrorhiza kurroa*

Hema Koli ^{a,*}, B.B. Bahule ^a, Khursheed Ahmed ^a, Basavani Patil ^b

^a Department of Chemistry, Abeda Inamdar College, Affiliated to Savitribai Phule Pune University, Pune 411001, India

^b Department of Chemistry, Nowrosjee Wadia College, Affiliated to Savitribai Phule Pune University, Pune 411001, India

ARTICLE INFO

Article history:

Available online 17 October 2022

Keywords:

Picrorhiza kurroa
Green synthesis
DPPH
Antioxidant activity
Iron nanoparticles

ABSTRACT

Green protocol of synthesizing nanoparticles has emerged as an optional way to overcome the limitation of the conventional physical and chemical methods. In the present paper, we wish to report a green synthesis of iron nanoparticles employing the aqueous root extract of *Picrorhiza kurroa* plant as an effective reducing and stabilizing agent. The green nanoparticles thus prepared are characterised using UV–Visible, FTIR, XRD and FESEM techniques. The average particle size of biosynthesised iron nanoparticles was found to be 26 nm. The antioxidant activity of these nanoparticles was determined by 2, 2-diphenyl-1-picrylhydrazyl (DPPH) free radical method. It was found to have IC₅₀ value comparable with that of standard ascorbic acid. The in-vitro antibacterial activity of biosynthesised iron nanoparticles was evaluated using an agar disc-diffusion method against Gram positive and Gram negative bacteria and has displayed their potential efficacy.

Copyright © 2022. Elsevier Ltd. All rights reserved.

Selection and peer-review under responsibility of the scientific committee of the Integrative Nanotechnology Perspective for Multidisciplinary Applications - 2022.

1. Introduction

Nanotechnology is a rapidly growing innovative technology for manipulation, creation and application of nanomaterials [1]. It has the conjunction of new ideas and knowledge from various fields like chemistry, physics, biotechnology, material sciences, engineering, and medicine. This branch has become significant in all spheres of life such as pharmaceutical [2], agriculture, electronics [3], catalysis [4], energy, fuel cells [5], electrochemical products, optics [6]. Metallic nanoparticles are of great interest due to their excellent physical and chemical properties, such as high surface-to-volume ratio and heat transfer (thermal conductivity) which make the particles very reactive or catalytic [4]. Although numerous physical and chemical methods have been employed to produce metal nanoparticles, their pharmaceutical and medical applications face limitations due to the use of toxic chemicals in their production. The incorporation of green chemistry into nanotechnology has developed a multifunctional, environmental

approach that allows nanoparticles synthesis in aqueous conditions [7].

The “green chemistry” approach helps us to control the reaction process, high production rate, resource efficiency low energy requirements and ecofriendly nature [8] providing a single-step technique for the nanobiosynthesis process as it does not require any specific isolation and maintenance procedures [9]. In recent years, the convergence of metallic nanoparticles and biological techniques has given rise to a new field of nanomedicine. An eco-friendly plant mediated synthesis of nanoparticles has become a hotspot in the field of nanoparticles synthesis which excludes harmful chemicals, high temperature, energy and pressure [10]. Use of herbal plants is advantageous, as their medicinal properties are added to the nanoparticles during the synthesis, offering numerous benefits of compatibility for pharmaceutical and biomedical applications [11].

In the present study, we are reporting a novel green approach for the synthesis of iron nanoparticles using the aqueous root extract of medicinal plant *Picrorhiza kurroa*. The bioactive components present in the root extract replace the toxic reducing agents that are involved in the chemical synthesis of iron nanoparticles. *Picrorhiza kurroa* is a small perennial herb, commonly known as

* Corresponding author.

E-mail address: hema.koli79@gmail.com (H. Koli).

Kutki, belonging to the family Scrophulariaceae. It is found in the alpine Himalayas from Kashmir to Sikkim. Traditionally rhizomes of *Picrorhiza kurroa* are used to cure various diseases like diarrhea, fever, jaundice, eye infection, skin problems, asthma, arthritis, cancer, diabetes, gastrointestinal problems. anti-microbial, anti-oxidant, anti-bacterial, anti-mutagenic, cardio-protective, hepato-protective, anti-malarial, anti-diabetic, anti-inflammatory, anti-cancer, anti-ulcer and nephro-protective activities are various pharmacological activities of *Picrorhiza kurroa* [12]. The main chemical constituents found in *Picrorhiza kurroa* include iridoid glycosides, cucurbitacins (triterpenoids), sterols, glycosides and phenolic compounds. These can act as a natural source for reducing and capping agent in stable nanoparticles synthesis reaction that eliminates multistep synthesis practice problems and costs of chemical reagents [13].

The bioactive phytochemicals present in the root extract of *Picrorhiza kurroa* may be accountable for significant antioxidant and antimicrobial activities of green synthesized nanoparticles. Antioxidants may have a great benefit in improving the quality of life by either preventing or postponing the onset of degenerative diseases [14]. The present study was attempted to find out the antioxidant activity along with IC_{50} values of metal nanoparticles, synthesised ecofriendly by using *Picrorhiza kurroa* root extract as a reducing agent against the 2, 2-diphenyl-1-picrylhydrazyl (DPPH) free radical. Further nanoparticles were screened for their antibacterial activity against Gram positive and Gram negative bacterial strains.

2. Materials and methods

2.1. Materials

Ferric nitrate, Ascorbic acid, and DPPH were of analytical grade with 99 % purity and used as it is without further purification. Aqueous extract was prepared by using powdered dried roots of *Picrorhiza kurroa* plant.. All the solutions were freshly prepared using deionised water. All glasswares used in the process, were washed with double distilled water and acetone and dried before use.

2.2. Preparation of extract from roots of *Picrorhiza kurroa*

The extract was prepared by taking 3 gm of powdered dried roots of *Picrorhiza kurroa* in a 250 mL Erlenmeyer flask with 100 mL of deionised water. The mixture was heated at 70 °C at 1500 rpm for 45 min. by using magnetic heating stirrer. The extract thus obtained was filtered through Whatman paper no.41 and the resulting filtrate (extract) was used for the synthesis of iron nanoparticles.

2.3. Preparation of ferric nitrate solutions

Aqueous solution of 10,000 ppm of $Fe(NO_3)_3 \cdot 9H_2O$ is prepared by dissolving 1 gm of Ferric nitrate in 100 mL deionised water.

2.4. Green synthesis of iron nanoparticles

The biosynthesis of iron nanoparticles was carried out by adding slowly 3 mL aqueous extract from roots of *Picrorhiza kurroa* to 50 mL solution of aq. ferric nitrate along with constant stirring at 80 °C. Within 15 min. the light brown colour of the reaction mixture turned to wine red colour and after 10 min. the solution became dark. No any change in colour of the reaction mixture was observed after 24 hrs. (Fig. 1a, 1b, 1c).

2.5. Isolation of synthesised iron nanoparticles

The aqueous solution containing the signatory colour of iron nanoparticles was transferred in a petri dish by pouring and left in an oven for drying at 250 °C for 24 hrs. Decomposition of organic matters and evaporation of moisture and impurities resulted in completely dried powder of iron nanoparticles.

2.6. Characterisation of biosynthesised iron nanoparticles

The green synthesised iron nanoparticles were subjected to various characterisation techniques which helped us to study their specific properties such as optical, structural, morphological, particle size, crystallinity, functional groups studies etc. These techniques were helpful to verify the utility of our synthesis method and to get the nanoparticles with these desired properties. In addition, organic and inorganic ligands present in the root extracts and also on the surface of synthesised nanoparticles may affect other properties and possible applications of the nanoparticles [15]. The nanoparticles are thoroughly investigated using different characterisation techniques like UV–Visible, FTIR, Powder XRD and FESEM.

UV–Visible spectroscopy can be used as a simple and reliable method for monitoring the stability of nanoparticle solutions. UV visible spectroscopy analysis was carried out by a computer controlled UV–vis double beam spectrophotometer (JASCO –2202) at the wavelength range between 200 and 800 nm possessing a scanning speed of 330 nm/min and at a resolution of 1 nm. Fourier Transform Infrared (FTIR) spectroscopy measurements were carried out for both the root extract and phytosynthesised iron nanoparticles to identify the possible bioactive molecules responsible for the reduction of the ferric ions and the capping of the iron nanoparticles. FTIR spectra were investigated using Fourier transform infrared (FTIR) spectrometer at a spectrum wavelength in the range of 4000 to 500 cm^{-1} with a resolution of 4 cm^{-1} . Crystalline structure, nature of the phase, lattice parameters of biosynthesised nanoparticles were determined by powder X-ray diffractometer (XRD) using $CuK\alpha$ radiation ($\lambda = 1.5406 \text{ \AA}$) Low angle diffractograms were recorded in the 2θ range 20° – 80°. Field Emission Scanning Electron Microscopy (FESEM) is an advanced technique used to characterize the surface morphologies and size distribution of biosynthesised nanoparticles through different microstructure images. This method is based on electron microscopy.

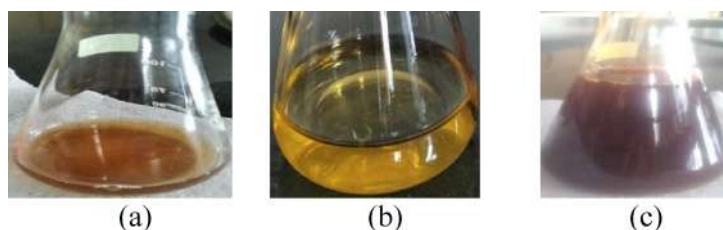


Fig. 1. (a) aq. solution of extract from roots of *Picrorhiza kurroa* (b) aq. solution of ferric nitrate (c) solution containing iron nanoparticles.

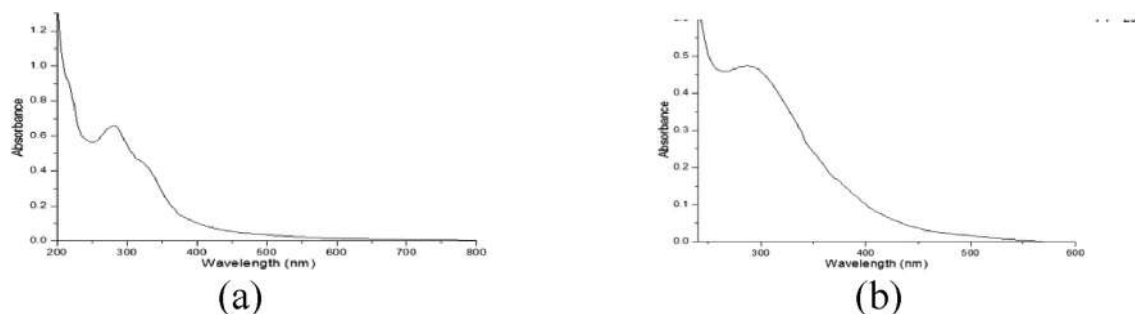


Fig. 2. UV-vis absorption spectrum of (a) *Picrorhiza kurroa* root extracts (b) iron nanoparticles.

2.6.1. UV-vis spectral analysis

Bioreduction of metal ions to metal nanoparticles on exposure to aqueous root extract of *Picrorhiza kurroa* was monitored using UV-visible double beam spectroscopy. Amount of 0.2 mL of the suspension was diluted in 2 mL of deionised water and absorbance was measured at room temperature. The results obtained from UV-Visible spectroscopic analysis of root extract and the reaction mixture containing iron nanoparticles are presented in (Fig. 2a, 2b).

The UV-visible absorbance spectra recorded for currently employed root extract and as synthesised iron nanoparticles exhibited λ_{\max} of 280 and 300 respectively, conforming eco-friendly synthesis of stable metal nanoparticles.

2.6.2. FT-IR analysis

FT-IR analysis of root extract of *Picrorhiza kurroa* as well as green synthesised iron nanoparticles are as shown in Fig. 3a, 3b.

FTIR graphs represent the functional groups of phytochemicals appearing in the root extract as well as on the surface of bio-reduced nanoparticles. The strong band at 3303.49 cm^{-1} correlated

to alcoholic or phenolic $-\text{OH}$ stretching vibration and the medium-intensity peak at 1595.99 cm^{-1} assigning conjugated carbonyl ($\text{C}=\text{O}$) stretching vibration or aromatic ring $\text{C}=\text{C}$ stretching vibrations are present in the IR spectrum of root extract but both of these peaks are disappeared from IR spectrum of synthesised nanoparticles. Also the IR frequency of root extract at 1393.68 cm^{-1} denoting $\text{C}-\text{O}$ stretch due to aldehydes or phenols was shifted to a small peak at 1390.28 cm^{-1} in the iron spectrum. The IR band at 1017.63 cm^{-1} , which is characteristic of glycoside or ether ($\text{C}-\text{O}-\text{C}$) groups in root extract, is absent in iron nanoparticles. In addition, absorption peaks located at 2072.85 belongs to $\text{C}\equiv\text{C}$ stretch due to alkynes and 699.73 cm^{-1} related to $=\text{C}-\text{H}$ bending vibration of substituted benzene are concerned with green synthesised iron nanoparticles. Stretching vibrational frequency due to metal-oxide bond appeared at 515.70 and 532.62 cm^{-1} in the spectra of root extract and iron nanoparticles respectively.

2.6.3. X-ray diffraction analysis

Ecofriendly synthesised iron nanoparticles when subjected to XRD analysis, showed the diffraction peaks at 2θ values of 23.84 ,

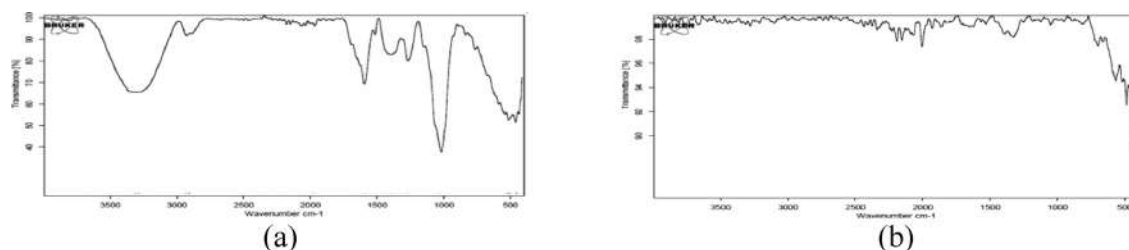


Fig. 3. FT-IR spectrum of (a) *Picrorhiza kurroa* root extract (b) iron nanoparticles.

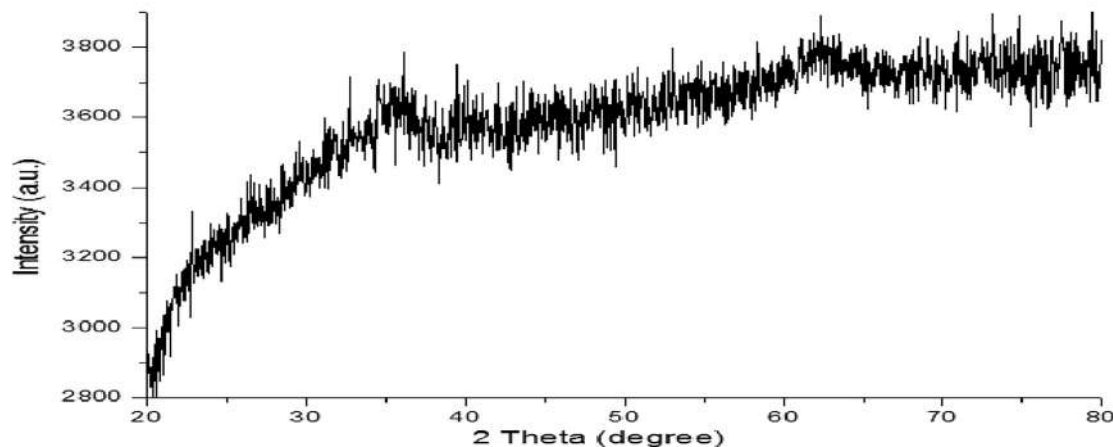


Fig. 4. X-ray diffraction pattern for iron nanoparticles.

32.72, 36.12, 39.52, 54.04, 58.01, 62.36 and 72.92° corresponding to Miller indices (1 1 0), (1 2 1), (1 1 0), (2 2 2), (1 3 2), (3 3 2), (1 3 0) and (3 4 3) respectively (Fig. 4) The characteristic peaks in the XRD spectrum indicate the crystalline nature of as synthesised nanoparticles.

2.6.4. FESEM

The typical FESEM images at different magnification levels suggested further clear picture of surface morphology with variable size of biosynthesised iron nanoparticles (Fig. 5).

2.7. Determination of antioxidant activity by DPPH method

The antioxidant property of biosynthesised nanoparticles was analyzed by 2, 2-diphenyl-1-picrylhydrazyl (DPPH) free radical method. The free radical scavenging activity of green synthesised iron nanoparticles and that of standard ascorbic acid were determined using the stable radical DPPH. 3 mL of each of different concentrations (100, 200, 300, 400 and 500 µg/mL) of iron nanoparticles were mixed with 2 mL freshly prepared DPPH solution. In the same way different aliquots of the ascorbic acid solutions corresponding to 100–500 µg/mL were used for calibration. Then all the solutions were incubated at room temperature in the dark for 30 min. The absorbance was recorded at 517 nm using UV-Visible spectrophotometer. The free radical scavenging activity which is expressed as the percentage of inhibition was determined by using following formula,

$$\text{Scavenging effect(\%)} = [(Ac - As)/Ac] \times 100$$

Where, *Ac* is the absorbance of the control and *As* is the absorbance of the sample or standard. The result of different concentrations of biosynthesised iron nanoparticles on DPPH radical scavenging activity is shown in Table no.1. An antioxidant activity of root extract mediated iron nanoparticles against DPPH radical were assessed and compared with standard ascorbic acid.

2.8. Antimicrobial evaluation

The in vitro antibacterial activity of as synthesised iron nanoparticles was evaluated using an agar disc-diffusion method against a Gram positive bacteria like *Bacillus cereus* and a Gram negative pathogenic bacteria like *Escherichia coli*. Microbial strains were obtained from the Culture Collection Centre, Pune. Prior to an antibacterial activity test, the bacterial strains were cultured in nutrient broth for 24 h to obtain logarithmic growth phase of the test bacteria. The actively growing bacterial cultures were spread into the Muller Hinton Agar (MHA). The extract was prepared at

1 mg/mL. The Whatman filter paper disks were punched at 6 mm diameter and impregnated with the dissolved extract and then placed to the MHA surface. The plates were incubated at 37 °C for 24 h. The antimicrobial activity was evaluated in terms of zone of inhibition, measured, and recorded in millimeters using a ruler.

3. Result and discussion

An environmental friendly method is adopted here for the biosynthesis of iron nanoparticles using *Picrorhiza kurroa* root extract. Addition of *Picrorhiza kurroa* root extract to aq. ferric nitrate solution caused a change in colour of the reaction mixture from light brown to dark wine red colour, indicates the completion of reaction with formation of stable iron nanoparticles (Fig. 1). The advantage of using biomolecules present in the root extract is that they not only act as a reducing agent but also as a stabilizing agent. The synthesis of iron nanoparticles was confirmed by UV-Visible spectrophotometer. The root extract mediated iron nanoparticles displayed the absorption peak within UV-vis range of wavelength of 300 nm, validating the completion of reaction for synthesis of stable nanoparticles (Fig. 2).

The variations in the spectral positions of FTIR bands in root extract and phytosynthesised iron nanoparticles indicated presumably, hydroxyl, ether, aromatic and carbonyl groups of some active metabolites are present in the *Picrorhiza kurroa* root extract that might be involved in the reduction of the metal ions and also responsible for capping and efficient stabilization of the bioreduced nanoparticles (Fig. 3).

The synthesis of iron nanoparticles is further revealed by X-ray diffraction analysis. The resulting diffraction patterns are compared with the standard patterns to get the final information, which clearly indicated the presence of iron oxide nanoparticles with hexagonal Rhomb-Centered geometry. XRD pattern includes some unassigned peaks which may be of fewer bio compounds (Fig. 4).

FESEM images at different magnification levels revealed that the green synthesised iron oxide nanoparticles were aggregated as irregular rhombic spherical shapes (Fig. 5) The average particle size of as synthesised nanoparticles was found to be 26 nm.

The presence of a variety of phytochemicals in *Picrorhiza kurroa* roots allows their extracts to contain antioxidant properties. These phytochemicals may be enhancing the antioxidant activity of metal nanoparticles [15]. The antioxidant activity of root extract mediated nanoparticles determined by using DPPH free radical are recognized to be due to the hydrogen or electron donating abil-

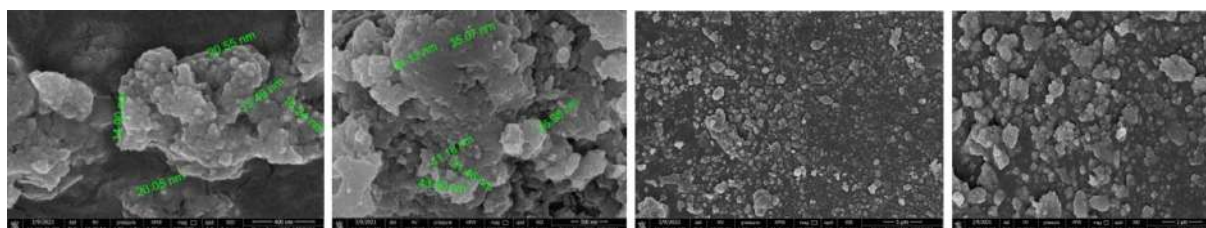


Fig. 5. FESEM images of iron nanoparticles at different magnification levels.

Table 1

Profile of DPPH radical scavenging activity with IC₅₀ values.

Sample	% Inhibition at concentrations					IC ₅₀ µg/mL
	100 µg/mL	200 µg/mL	300 µg/mL	400 µg/mL	500 µg/mL	
Iron Nanoparticles	19.33	23.19	45.61	49.37	51.22	209
Ascorbic acid	22.89	27.01	49.77	67.48	70.82	231

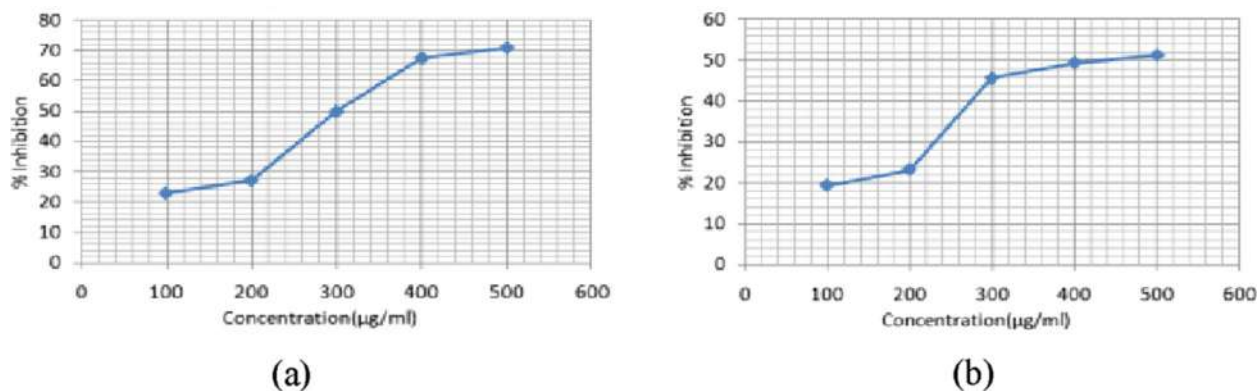


Fig. 6. Graphical representation of antioxidant activity shown by (a) standard Ascorbic acid (b) iron nanoparticles.

ities of nanoparticles. The free radical scavenging activity of green synthesised nanoparticles tends to increase with an increase in their concentration (Fig.6). Notably, antioxidant activity of synthesised iron nanoparticles was found to be 51.22 % at 500 µg/mL with a remarkable IC_{50} value of 209 µg/mL. However, the standard Ascorbic acid demonstrated 70.82 % inhibition in the same concentration with the IC_{50} value of 231 µg/mL. The results confirmed that as synthesised iron nanoparticles have good antioxidant activity, which may discover a new way to ripening traditional medicine and treat many incurable diseases.

The antibacterial properties of ecofriendly synthesised iron nanoparticles were evaluated against Gram positive and Gram negative bacterial strains using agar disc-diffusion method. Of the bacterial strains tested, iron nanoparticles strongly inhibited the growth of Gram negative pathogenic bacteria - *Escherichia coli* with the effective zone of inhibition of 10 mm at a concentration of 500 µg. On the other hand, iron nanoparticles showed a low inhibitory effect on the growth of Gram positive bacteria - *Bacillus cereus* with the zone of inhibition of 5 mm. Accordingly, this result showed that the biosynthesised iron nanoparticles are more active against pathogenic Gram negative bacteria than Gram positive bacterial strains tested which is possibly due to the difference in the structure of cell walls of bacteria. It has been established by researchers that the lower the size of nanoparticles, the higher its stability and biocompatibility. For example, Lee *et al.* reported that the inactivation of *Escherichia coli* by iron nanoparticles could be because of the penetration of the small particles (sizes ranging from 10 – 80 nm) into *E. coli* membranes. Nano scale iron could then react with intracellular oxygen, leading to oxidative stress and eventually causing disruption of the cell membrane. Thus the bactericidal effect of phytosynthesised iron nanoparticles has been attributed to their small size and high surface to volume ratio, allows them to interact closely with microbial membranes, which in turn will have significant impact on biomedical applications [16].

4. Conclusion

An ecofriendly method adopted here for the formulation of iron nanoparticles employing root extract is proved to be one of the most stable, economical, energy efficient and cost effective processes. Nano scaled iron nanoparticles coated with bioactive phytochemicals have shown their potential efficacy as an antioxidant and antibacterial agent. This offers numerous benefits of compatibility for their pharmaceutical and biomedical applications. This green approach also provides healthier work places and communities, protecting human health and environment. This method leads to lesser waste and safer products. Hence, use of medicinal plant

extract for the synthesis of metal nanoparticles can have an immense impact in coming decades.

CRediT authorship contribution statement

S. Koli Hema: Methodology, Writing – original draft, Investigation. **B.B. Bahule:** Supervision, Conceptualization. **Khurshed Ahmed:** . **K. Patil Basavani:** Project administration.

Data availability

No data was used for the research described in the article.

Declaration of Competing Interest

The authors declare that they have no known competing financial interests or personal relationships that could have appeared to influence the work reported in this paper.

Acknowledgements

The authors are thankful to the Principal of Nowrosjee Wadia College and Abeda Inamdar College for providing the necessary infrastructural support. We owe a sincere thanks to the Savitribai Phule Pune University for the assistance in recording the various spectra. We are thankful to the Head, Department of Chemistry, Abeda Inamdar College for the help and support given in the execution of this experimental work.

References

- [1] Priya G. Deshmukh, S.S. katariya *Int. J. of Advancements in Research & Technology*, Vol. 2 (3) march 2013.
- [2] Pawel Szymanski, magdalena markowicz Nano vol. 6 (6), 509-539, 2011.
- [3] Electric Power Systems Research, vol 143, 2017, 573-584 J.E. Contreras, E A. Rodriguez, J. Taha- Tijerina.
- [4] Nanoparticles for Catalysis, Nanomaterials (Basel) 2016 Jul 6 (7), 123 Sergio Navalón and H. Garcia.
- [5] Processes, 2021, 9, 1221 Domenico Frattini, Gopalu karunakaran, Eun-Bum Cho and Yongchai kwon.
- [6] *Oriental J. of Chemistry* vol. 31 (special issue) 7 Nov 2015 Sara mohammadi Bilankohi.
- [7] S. Iravani, H. Korbekandi, S.V. Mirmohammadi, B. Zolfaghari, *Synthesis of silver nanoparticles: chemical, physical and biological methods*, *Res. Pharm. Sci.* 9 (2014) 385–406.
- [8] *Open Access Journal of Chemistry* Vol 2 (1), 2018 pp 1-8 Eluchie Nene pear.
- [9] P. Singh, Y.J. Kim, D. Zhang, D.C. Yang, *Biological synthesis of nanoparticles from plants and microorganisms*, *Trends Biotechnol.* 34 (2016) 588–599.
- [10] Anna Pratima Nikalje *medicinal Chemistry* 5(2), 5081-5089, 2015.
- [11] *Scientific Reports* 20 Nov. 2017, 15867, 2017 Siddhant Jain & Mohan Singh Mehata.
- [12] S.K. Jain, D.R. Fillips, *Medicinal Plants of India*, Algonac Publications, MI, 1991, p. 558.

- [13] N. Kumar, T. Kumar, S.K. Sharma, Phytopharmacological review on Genus *Picrorhiza*, *Int. J. Universal Pharm. Bio. Sci.* 2 (4) (2013) 334–347.
- [14] P.P. Shrinivas, T.K.A. Subhash, antibacterial and cytotoxic potential of silver nanoparticles synthesized using terpenes rich extract of *Lantana camara* L. leaves, *Biochem. Biophys. Rep.* 10 (2017) 76–81.
- [15] T. Yamaguchi, H. Takamura, T. Matoba, J. Terao, *Biosci. Biotechnol. Biochem.* 62 (1998) 1201–1204.
- [16] *Frontiers in microbiology* 2017, 8, 1014 Ram Prasad, Atanu Bhattacharya and Quang D. Nguyen



Photoluminescence of Si nanostructured films by Pulsed Laser Deposition

Tushar Salve^{a,*}, Amar Katkar^b, Ashok Kanade^c, Gotan Jain^a

^aSNJB's KKHA Arts, SMGL Commerce and SPHJ Science College, Chandwad, MS 423 101, India

^bDr. B. N. Purandare Arts and Smt. S.G. Gupta Commerce College, Valvan, Lonavla 410 403, India

^cP.V.P. College, Pravaranagar 413 713, India

ARTICLE INFO

Article history:

Available online 11 October 2022

Keywords:

PLD
Si quantum dots
Photoluminescence

ABSTRACT

Nanostructured-Si films with inert (Ar) and reactive (O₂) atmosphere have been synthesized using laser ablation technique. The size distribution of Si nanoparticles found to depend on background gas pressure, observed by shift in photoluminescence components of energy. As deposited samples are mainly constituted by amorphous or highly defective nanoparticles. The annealing was performed at 400 °C and 1000 °C which induced growth of less defective Si-nanocrystals. The increment in PL intensity is evidence of coalescence. The results are interpreted in terms of size distribution (in the range of 2–5 nm), crystallinity and surface oxidation of the Si nanostructures.

© 2022 Elsevier Ltd. All rights reserved.

Selection and peer-review under responsibility of the scientific committee of the Integrative Nanotechnology Perspective for Multidisciplinary Applications - 2022.

1. Introduction

The band-gap engineering using nanostructures for the third-generation solar cells is promising field to increase the efficiency and Si is always being well focused due to its unique properties like quantum confinement and photonic band-gap crystals. The luminescence in visible region from porous silicon at room temperature attracted great attention in investigation of light emission properties of different kinds of silicon based nanostructures [1–3] however; the mechanism of visible PL is not fully understood. Porous silicon, nanocrystalline silicon in SiO_x matrix and several other types of nanostructured silicon have been synthesized using different techniques such as Plasma Chemical Vapour Deposition (P-CVD) [4], Hot Wire Chemical Vapour Deposition (HW-CVD) [5], RF co-sputtering deposition [6] and by Chemical routes [7] to produce Si QDs or nanocrystals.

Pulsed Laser Deposition (PLD) is a novel method for fabricating nanocrystalline, nanoparticles and nanostructured materials with very high purity [8–9]. In the PLD process, atoms ablated by a high energy pulsed laser beam collide with each other and with background gas species such as inert gas to produce clusters and nanoparticles in the gas phase. The thin films or nanostructured

films can be formed by direct deposition of the atoms, clusters and nanoparticles. Here, the nanoparticles act as 'building blocks' of the nanostructure. The size, shape, crystallinity and distribution of the nanoparticles are key parameters for controlling the properties of the films [8]. The morphology of the films produced by PLD under different gases and their tendency towards spontaneous oxidation when samples exposed to ambient air is described by our group [10]. The correlation between morphology of the films and PL energy bands is an important contribution for control of luminescence properties of Si-nanostructured films produced by PLD. There is an extensive work which describes the possibilities offered by PLD for synthesis of Si-nanostructures using inert and reactive gases [11–13]. In this article, we discuss the PL properties depending on morphology of the films produced in Ar and O₂ background gases for wide range of pressure; 0.05–60 Pa of Ar and 1–60 Pa of oxygen. We observed photoluminescence from samples annealed (relatively low temperature) at 400 °C and tried to reveal modification in new components for further annealing at 1000 °C. The pressure plays a key role to form the films with different morphology and annealing happens to aggregate the deposited species into nanoparticles embedded in amorphous matrix.

* Corresponding author.

E-mail address: salve.tsacs@snjb.org (T. Salve).

2. Materials and methods

Si nanostructured films were obtained by irradiating the Si target with second harmonic (532 nm) and fourth harmonic (266 nm) of the Nd:YAG laser. The substrate holder was positioned parallel to the target and substrate to target distance was kept constant, $d_{TS} = 7$ cm. Ar and O₂ gases have been used to study the impact of inert and reactive species on stoichiometry of the composed films. Quartz and single-crystal Si substrates have been used for deposition of different sample conditions. The structural characterization of the films has been performed by micro-Raman spectroscopy with Renishaw InVia spectrometer excited with 514.5 nm of an Ar⁺ laser and same has been employed as excitation source for Photoluminescence study. Morphology and thickness have been acquired with Zeiss Supra 40 field emission (SEM) Scanning Electron Microscopy.

3. Results and discussion

3.1. Morphology study

The morphology of the films in Fig. 1 studied with SEM shows compact to nanoporous structure by increasing the background pressure of oxygen. Morphology of the films prepared in Argon background also found similar to those prepared under oxygen background.

Increasing the background gas pressure; the collisions between ablated particles and gas molecules increases which leads to decrease the kinetic energy of the particles and the film becomes porous and vice-versa. The film deposited at 1 Pa of oxygen is very compact as shown in Fig. 1 (a) compared to that deposited at 60 Pa of oxygen as shown in Fig. 1 (c) which is more porous. It is worth noting that there is no significant change in morphology after annealing the samples.

3.2. Photoluminescence study

i) Si-nanostructures deposited under Ar background

As deposited samples under both Argon and oxygen ambient doesn't show photoluminescence except the samples deposited at very low pressure of 1 Pa. This gives a low intensity PL band at low energy < 1.5 eV for Ar and 1.8 eV for O₂. Fig. 2 (b) shows the PL spectra from Ar samples annealed at 400 °C for 4 hrs.

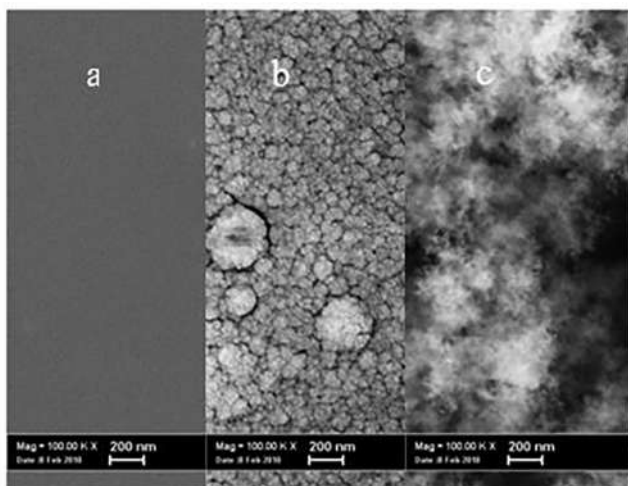


Fig. 1. The SEM Images showing different morphology of the samples prepared under different pressures of oxygen: a) 1 Pa, b) 20 Pa and c) 60 Pa.

Gaussian fitting for all PL spectra with more than two components have been used as indicated in Fig. (a). The blueshift in PL energy bands with increasing pressure shown in Fig. (b) suggest growth and formation of nanocrystals. The films are compact formed under low pressure and porous after increasing the pressure. The compact films formed under lower pressure range from 0.05 to 1 Pa form big nanoclusters after annealing at 400 °C. Here, annealing happens to aggregate the material in to big nanoparticles because of higher density of the material. As we increase the pressure towards 60 Pa, the films become porous and density of material is minimal which after annealing forms smaller nanoparticles. The shift in PL energy band is correlated to quantum confinement.

The films deposited under 0.05 Pa–60 Pa range and their respective PL energy components are presented in Fig. 3. These PL components can be individuated into two different families; one family of components in the range of 1.45–1.75 eV which comes from compact films and another one, in the range of 1.8–2.1 eV which comes from porous films. From Fig. 3 it is clear that we lose the low energy components for porous films and high energy components for compact films which provide important information about morphology dependent PL properties which is function of background gas pressure and can be controlled easily to get appropriate PL components.

The films also have been annealed at 1000 °C to study any modifications in the synthesized nanostructures. Fig. 4 shows the difference in PL intensity for as-deposited, 400 °C and 1000 °C annealed sample prepared under 30 Pa of Argon. For further annealing at 1000 °C the luminescence intensity increases tremendously and shifts the high volume density components towards lower energy.

ii) Si-nanostructures deposited under O₂ background

Fig. 5 shows the PL spectra of samples deposited under oxygen background pressure and annealed at 400 °C. The best Gaussian fit for samples prepared under oxygen gives less PL components than samples prepared in Argon background. The content of oxygen found similar in both samples prepared in Ar and O₂ atmosphere analyzed by EDS. Also, the trend of blueshift in PL energy components after increasing the background pressure found similar for both the gases.

The shape of PL spectra for samples prepared under O₂ background as shown in Fig. 5 are more symmetric than for samples prepared under Ar background, refer Fig. 2. It may possible that the samples prepared in Ar background are defective/amorphous than those prepared in oxygen. As, in presence of oxygen, the high energy radicals of oxygen passivate the defects present in Si nanostructures in-situ. Although, the detail mechanism of interaction between background gas and ablated species has not yet been understood. The interaction of H₂ as a reactive gas with Si in PLD is also described by M. Inada et. al. [14] says that, there are less chemical reactions and morphology is also similar for He and H₂ at higher pressure. In this case we realized that, the mechanism of nanoparticle formation in reactive gases is similar to that of the inert gases. In case of low pressure, 1 Pa, deposited films, the Si clusters get deposited on substrate with very compact morphology, without forming nanoparticles. Decreasing pressure, the collisions of ablated clusters with gas particles is minimized and do not form nanoparticles.

Patrone et al. discusses three possible reasons of luminescence from oxidized films after exposure to air for long period at room temperature. First, oxygen induces passivation by the saturation of dangling bonds which reduces the number of non-radiative recombination centres and, as a result, increases the luminescence intensity. The second effect is the decrease of the cluster silicon

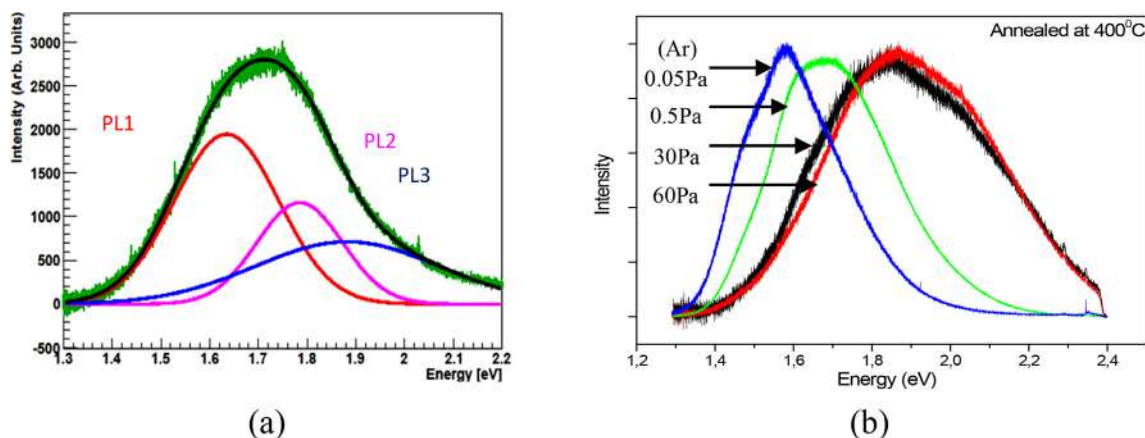


Fig. 2. Gaussian fitted different PL components for a compact sample obtained at 30 Pa (a) and the blueshift in PL energy after increasing the Ar background pressure from 0 to 60 Pa (annealed in vacuum at 400 °C for 4hrs) (b).

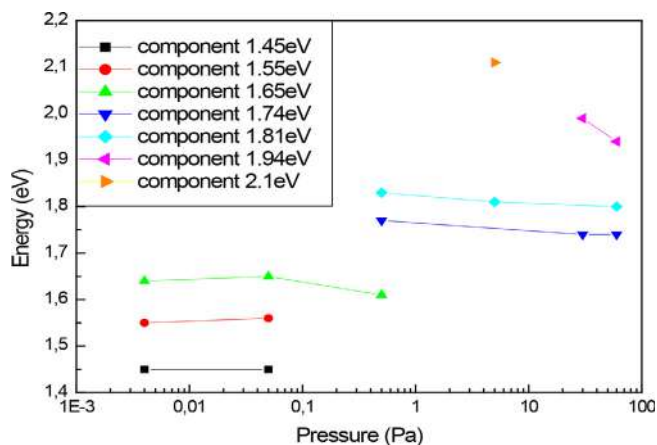


Fig. 3. Different PL components present for films deposited under Ar gas background; blueshift in the components towards higher pressure (annealed at 400 °C).

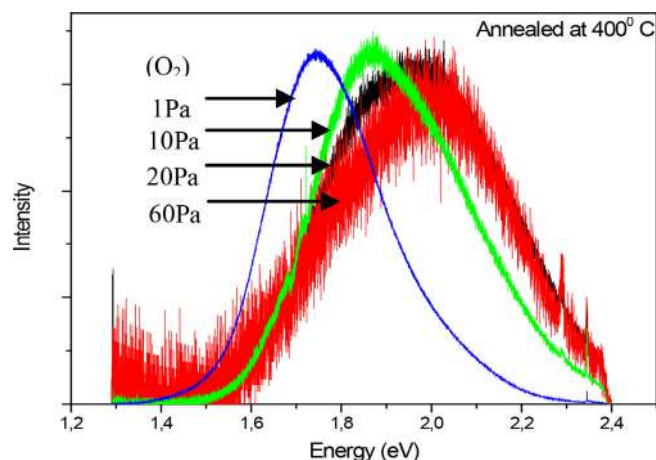


Fig. 5. The blueshift in PL energy after increasing the O₂ background pressure from 1 to 60 Pa (annealed in vacuum at 400 °C for 4hrs).

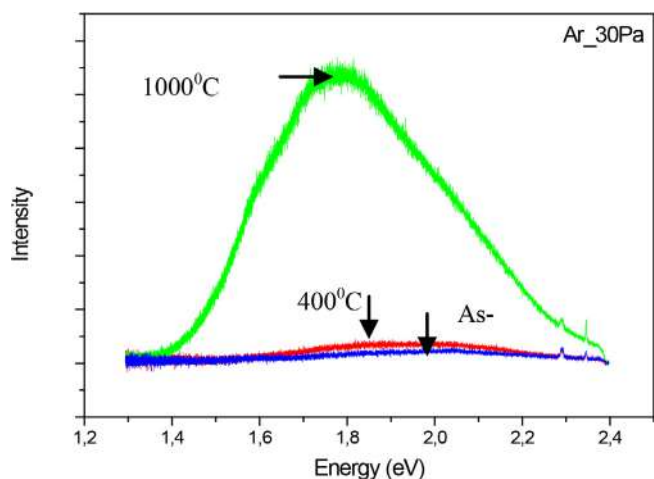


Fig. 4. The effect of different annealing temperatures (sample prepared in Ar background pressure 30 Pa).

core which should lead to blue-shift of the luminescence band. The third effect is the increase of the amount of silicon oxide in the sample which leads luminescence from defects in the oxide layer or at Si-SiO_x interface or to an increase in its intensity if it already

exist [15]. The PL from present samples supports these reasons; annealing at 400 °C in vacuum gives luminescence because of passivation of dangling bonds or because of reducing the non-radiative recombination centres and further increasing the annealing temperature at 1000 °C increases the intensity of photoluminescence and shifts the high volume density components from higher energy towards lower energy because of coalescence or may be because of losing the oxygen on single nanocrystals. Annealing temperature dependent PL intensity is shown in Fig. 4 for Ar (30 Pa) background deposited sample and the redshift in high volume density components is indicated in Fig. 6 for O₂ samples.

4. Conclusion

We have successfully deposited Si nanostructures by PLD where PL properties strongly depend on background gas pressure. The reactive (O₂) and Inert (Ar) gases leads to produce similar energy components, having similar morphology. The 400 °C annealing exhibited wide PL bands from 1.45 to 2.0 eV, further annealing at 1000 °C modified the cluster size of high volume density energy components to redshift. Using Pulsed Laser Deposition technique it is possible to control nanocrystals size and density by varying pressure followed by annealing, which opens the way to further

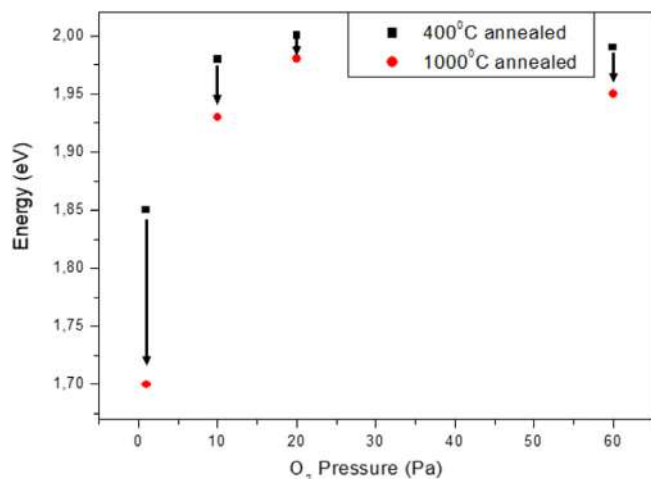


Fig. 6. The high volume density components, shifts from higher energy to lower energy after annealing from 400 °C to 1000 °C for samples prepared in O₂ background pressure.

investigation with aim of developing high efficiency silicon-based third generation solar cells.

Declaration of Competing Interest

The authors declare the following financial interests/personal relationships which may be considered as potential competing interests: [Dr. Tushar Salve reports financial support was provided by Erasmus Mundus. Dr. Tushar Salve reports a relationship with Shree Neminath Jain Brhmacharyashram that includes: employment.]

Acknowledgment

The author would like to acknowledge Andrea LiBassi, David Dellasega, Valeria Russo and Paola Bruno for useful discussion. This work was carried with support of Erasmus-Mundus lot-15.

References

- [1] L.T. Canham, Silicon quantum wire array fabrication by electrochemical and chemical dissolution of wafers, *Appl. Phys. Lett.* 57 (1990) p-1046.
- [2] L. Pavesi, L.D. Negro, C. Mazzoleni, G. Franzo, F. Priolo, Optical Gain in Silicon Nanocrystals, *Nature* (2000) 408–440.
- [3] T. Toyama, Y. Kotani, H. Okamoto, H. Kida, Light emission from nanocrystalline Si thin-film light emitting diodes due to tunneling carrier injection, *Appl. Phys. Lett.* 72 (12) (1998) 1489–1491.
- [4] G. Conibeer, M. Green, E.-C. Cho, D. König, Y.-H. Cho, T. Fangsuwannarak, G. Scardera, E. Pink, Y. Huang, T. Puzzer, S. Huang, D. Song, C. Flynn, S. Park, X. Hao, D. Mansfield, Silicon quantum dot nanostructures for tandem photovoltaic cells, *Thin Solid Films* 516 (20) (2008) 6748–6756.
- [5] A.K. Panchal, C.S. Solanki, Fabrication of silicon quantum dots in SiNx multilayer using hot-wire CVD, *J. Cryst. Growth* 311 (9) (2009) 2659–2663.
- [6] X. Liu, J. Zhang, Z. Yan, S. Ma, Y. Wang, Photoluminescence from SiC Nanocrystals Embedded in SiO₂, *Mat.phy.Mech.* 4 (2001) 80–85.
- [7] A. Tanaka, R. Saito, T. Kamikake, M. Imamura, H. Yasuda, Electronic structures and optical properties of butyl-passivated Si nanoparticles, *Solid State Comm.* 140 (7–8) (2006) 400–403.
- [8] T. Seto, T. Orii, M. Hirasawa, N. Aya, Fabrication of silicon nanostructured films by deposition of size-selected nanoparticles generated by pulsed laser ablation, *Thin Solid Films* 437 (1–2) (2003) 230–234.
- [9] A. Lorusso, V. Nassisi, G. Congedo, N. Lovergine, L. Velardi, P. Prete, Pulsed plasma ion source to create Si nanocrystals in SiO₂ substrates, *Appl. Sur. Sci.* 255 (10) (2009) 5401–5404.
- [10] F.D. Fonzo, A. Bailini, V. Russo, A. Baserga, D. Cattaneo, M. Beghi, P. Ossi, C. Casari, B.A. Li, C. Bottani, Synthesis and characterization of tungsten and tungsten oxide nanostructured films, *Catal. Today* 116 (2006) 69–73.
- [11] W. Marine, L. Patrone, B. Luk'yanchuk, M. Sentis, Strategy of nanocluster and nanostructure synthesis by conventional pulsed laser ablation, *Appl. Surf. Sci.* 154–155 (2000) 345–352.
- [12] A.V. Kabashin, J.P. Sylvestre, S. Patskovsky, M. Meunier, Photoacoustic Fourier transform infrared spectroscopy of nanoporous SiO_x/Si thin films with varying porosities, *J. Appl. Phys.* 91 (5) (2002) 3248.
- [13] D. Riabinina, C. Durand, F. Rosei, M. Chaker, Luminescent silicon nanostructures synthesized by laser ablation, *Phys. Stat. Sol. (a)* 204 (6) (2007) 1623–1638.
- [14] M. Inada, H. Nakagawa, I. Umezu, A. Sugimura, Effects of hydrogen on Si nanoparticles formed by pulsed laser ablation, *Appl. Sur. Sci.* 197–198 (2002) 666–669.
- [15] L. Patrone, D. Nelson, V.I. Safarov, M. Sentis, W. Marine, S. Giorgio, Photoluminescence of silicon nanoclusters with reduced size dispersion produced by laser ablation, *J. Appl. Phys.* 87 (8) (2000) 3829–3837.



Simple Co-precipitation synthesis and characterization of magnetic spinel NiFe₂O₄ nanoparticles

Subiya Kazi^a, Shaukatali Inamdar^b, Yuvraj sarnikar^c, Dhanraj Kamble^d, Radhakrishnan Tigote^{a,*}

^a Department of Chemistry, Dr. Babasaheb Ambedkar Marathwada University, Sub campus Osmanabad, Maharashtra 413 501, India

^b Department of Pharmaceutical Chemistry, College of Health Sciences, University of KwaZulu-Natal (Westville), Durban 4000, South Africa

^c Department of Chemistry, Dayanand Science College Latur, Maharashtra 413 531, India

^d Department of Chemistry, S.B.E.S. College of Science, Aurangabad, India

ARTICLE INFO

Article history:

Available online 14 October 2022

Keywords:

Ni-ferrite Nanoparticles
Band Gap
Size and Shape
Magnetic Properties
Co-precipitation method

ABSTRACT

Nickel ferrite nanoparticles were synthesized using Iron (III) nitrate and nickel nitrate as the starting materials along with the hydrazine hydrate via co-precipitation process and the final product obtained calcined at 700 °C. The structural and optical properties of the synthesised product were determined using various characterization techniques viz. UV-visible spectrometry, X-ray diffractometer (XRD), transmission electron microscopy (TEM), Field Emission Scanning Electron Microscopy (FE-SEM) and vibrating sample magnetometer (VSM). The NiFe₂O₄ nanoparticles showed absorption at ~ 356 nm corresponds to band gap of 4.1 eV. The elemental analysis was carried out using X-ray Fluorescence (XRF) and Energy Dispersive Spectroscopy (EDS). The synthesized NiFe₂O₄ were 10–15 nm in size, and exhibited high saturation magnetization value of 72.66 emu/g.

Copyright © 2022. Elsevier Ltd. All rights reserved.

Selection and peer-review under responsibility of the scientific committee of the Integrative Nanotechnology Perspective for Multidisciplinary Applications - 2022.

1. Introduction

In recent years, magnetic particle synthesis has received a lot of attention due to its prospective applications in high-density magnetic recording and magnetic fluids [1,2]. In terms of applications in high-density magnetic recording media and magnetic fluids, the production of nanosized magnetic particles is being thoroughly researched [3]. Ferrites with good dielectric properties are used in a wide range of applications, from microwaves to radio waves. Because of its high electrical resistivity and low magnetic coercivity [4], Ni²⁺ ferrite is a technologically relevant material for uses in the megahertz frequency range. Nickel ferrite has been extensively investigated due to its unique inverse spinel structure, electrical and magnetic properties, and a wide range of uses in electronic devices and microwave adsorbents. In NiFe₂O₄, Fe³⁺ ions can easily shift between the octahedral (Oh) and tetrahedral (Td) sites, with Fe³⁺ occupying the Td site and Fe³⁺ and Ni²⁺ occupying the Oh site. The stable structural configuration allows it to endure the Fe³⁺ to

Fe²⁺ reaction in a reducing environment. Because of its redox characteristics (LPG), NiFe₂O₄ can be used as a gas sensor material to detect reducing gases, such as liquefied petroleum gas, as a result [5–7].

In overview, several chemical processes, such as precipitation, sonochemical procedure, polymeric precursor approaches, mechanical alloying, pulsed wire discharge, shock wave, reverse micelles, hydrothermal and ultrasonically aided hydrothermal processes, have tremendous disadvantages over physical approaches, including lower costs, room-temperature reactions, and the ability to produce huge quantities, have all been used to make NiFe₂O₄ nanocrystalline [8]. Various shaped NiFe₂O₄ nanoparticles, such as fibre, sheet, ribbon, and rod, have been synthesised using organic gel-thermal decomposition, electrospinning combined with sol-gel technology [9–10], porous anodic aluminium oxide (AAO) templates, mechano-chemical method, and microemulsion method, among other methods, reverse phase micelles [10], hydrothermal micelles [11], and co-precipitation method [12] and also [13].

In the observation of magnetic materials, nanocrystalline spinel ferrites with the formula MFe₂O₄ (M = Ni, Zn, Mn, Co, Mg, etc.) execute high-density magnetic storage media, MRI contrast agents, colour imaging, ferro-fluids, high frequency devices, magnetic

* Corresponding author.

E-mail addresses: kazisubiya123@gmail.com (S. Kazi), saliinamdar@gmail.com (S. Inamdar), sarnikaryp@gmail.com (Y. sarnikar), dhanrajkamble1109@gmail.com (D. Kamble), rmtigote.chemobad@bamu.ac.in (R. Tigote).

refrigerators, catalysts, and microwave devices, etc. investigation. The state of the properties of these magnetic nanoparticles are mostly determined by their size and method of production. Their most prevalent feature is their super-paramagnetic behaviour, which is characterised by a decrease in saturation magnetization as compared to the bulk material [14–18]. Researchers are particularly interested in nickel ferrite (NiFe_2O_4) because of its significant magneto-crystalline anisotropy, high saturation magnetization [19–20], and distinctive magnetic structure [21]. Gas and biosensors [22], sensors, magnetic fluids [23], catalysts, magnetic storage systems, photo magnetic materials [24], site-specific drug delivery [25–26], magnetic resonance imaging, and microwave devices are some of the important applications of NiFe_2O_4 nano material [27–28]. Nickel ferrite (NiFe_2O_4) exhibits ferromagnetic characteristics that are closer to dipole relaxation than ferromagnetic resonance and the magnetic moments of anti-parallel spins between Ni^{2+} ions at octahedral sites and Fe^{3+} ions at tetrahedral sites give nickel ferrite (NiFe_2O_4) its ferromagnetic characteristics [29–32].

A group of soft ferrite materials characterised by high magnetic permeability and research dealing with their other physical properties, such as optical and magnetic properties, is part of the continuation of Nickel Ferrite. These materials are commonly used in various applications, viz. computer memory chips for microwave devices, magnetic recording media, radio frequency, coil processing, transformer cores, rod antennas, and many telecommunications and electronic engineering branches [33–35].

In this work, we have synthesised nickel ferrite using hydrazine hydrate to afford their new fluorescence properties using a modified co-precipitation method. It is recognised as an environmen-

tally friendly procedure and the characterization done using powder X-ray diffraction, scanning electron microscopy (SEM), transmission electron microscopy (TEM), elemental analysis using EDS, XRF, and the determination of NiFe_2O_4 nanoparticles' magnetic behaviour are all covered in this paper.

2. Materials and methods

2.1. Materials

Chemicals with high purity were purchased from Himedia and used without further purification. Distilled water was used for all the experiments. Iron nitrate ($\text{Fe}(\text{NO}_3)_3 \cdot 9\text{H}_2\text{O}$), nickel nitrate ($\text{Ni}(\text{NO}_3)_2 \cdot 6\text{H}_2\text{O}$), and hydrazine hydrate ($\text{NH}_2 \cdot \text{NH}_2 \cdot \text{H}_2\text{O}$) are the starting materials.

2.2. Synthesis of NiFe_2O_4 nanomaterials

A NiFe_2O_4 nanomaterial sample was prepared via a co-precipitation synthesis route by using a modified method of Suresh Sagadevan [39]. In a typical synthesis, 40 mL (2 M) solutions of iron nitrate ($\text{Fe}(\text{NO}_3)_3 \cdot 9\text{H}_2\text{O}$) and 40 mL (1 M) solutions of nickel nitrate ($\text{Ni}(\text{NO}_3)_2 \cdot 6\text{H}_2\text{O}$) were prepared and vigorously mixed under magnetic stirring for 1 h at 40 °C. Then a solution of 1 M hydrazine hydrate was added drop by drop into the reaction mixture to maintain pH = 8 and a blackish brown colored crude NiFe_2O_4 precipitate was formed. Finally, the NiFe_2O_4 nanoparticles were separated by the filtration method and dried at room temperature for 24 hrs. The acquired crude material was calcinated at 700 °C for 4 h to afford a fine powder by the grinding method.

3. Result and discussion

The structural properties of NiFe_2O_4 nanoparticles were defined by the XRD method using the $\text{Cu K}\alpha$ (0.154 nm) radiation X-ray diffractometer to produce diffraction patterns at the scanning angle between 20 ° to 80 ° degrees for powder crystalline samples. The optical study was performed using Ellico's Double Beam Spectrophotometer. The nanocrystalline microstructure and particle size were calculated from Transmission Electron Microscopy (TEM) images obtained at an accelerating voltage of 200 kV using an electron microscope. The Field Emission Scanning Electron Microscopy (FE – SEM) and Energy Dispersive X – Ray Spectroscopy by using Carl Zeiss Model Supra 55 Germany and Bruker XFlash6130 Germany, respectively. In order to eliminate any impu-

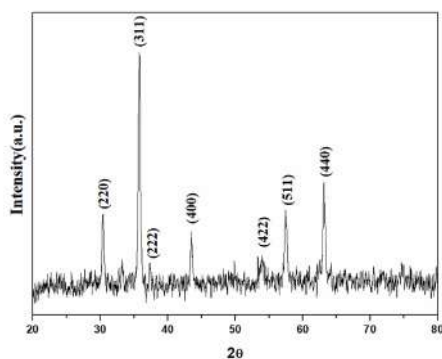


Fig. 1. XRD Spectrum of NiFe_2O_4 Nanoparticles.

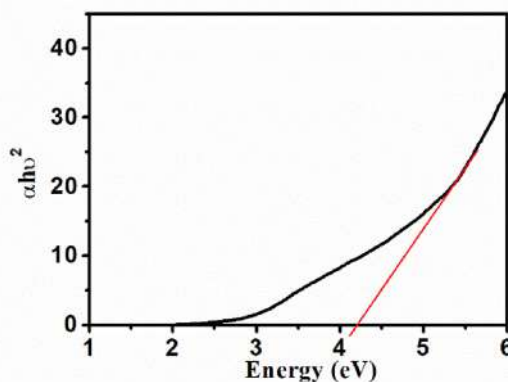
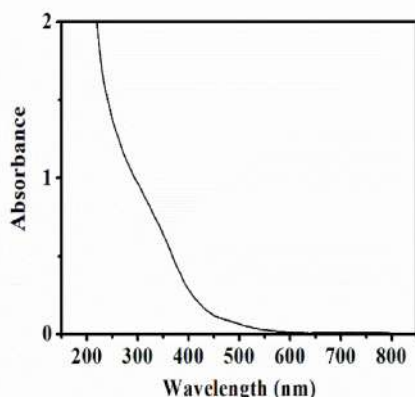


Fig. 2. a) UV-Visible spectrum of NiFe_2O_4 Nanomaterial; b) TAUC plot for optical band gap of NiFe_2O_4 Nanomaterial.

urities, present in the samples, the TGA analysis was performed in the 30–900 °C temperature range.

3.1. X- ray diffraction studies

In the powder XRD analysis, the peaks are found with planes (hkl) 220, 311, 222, 400, 321, 422, 511, and 440, which exhibits a

BCC structure with spinel structure as shown in Fig. 1. This diffraction pattern shows that there are no extra peaks along the sample peak, confirming that the sample contains no impurity. Using the Debye-Scherrer formula for this data, we calculate the average particle size as 29 nm and the interplanar distance (d), lattice constant (a), volume (V) and X-ray density (d_x) are 1.31, 2.63, 18.32, and 1.83×10^{-24} respectively. The hopping lengths of octahedral sites

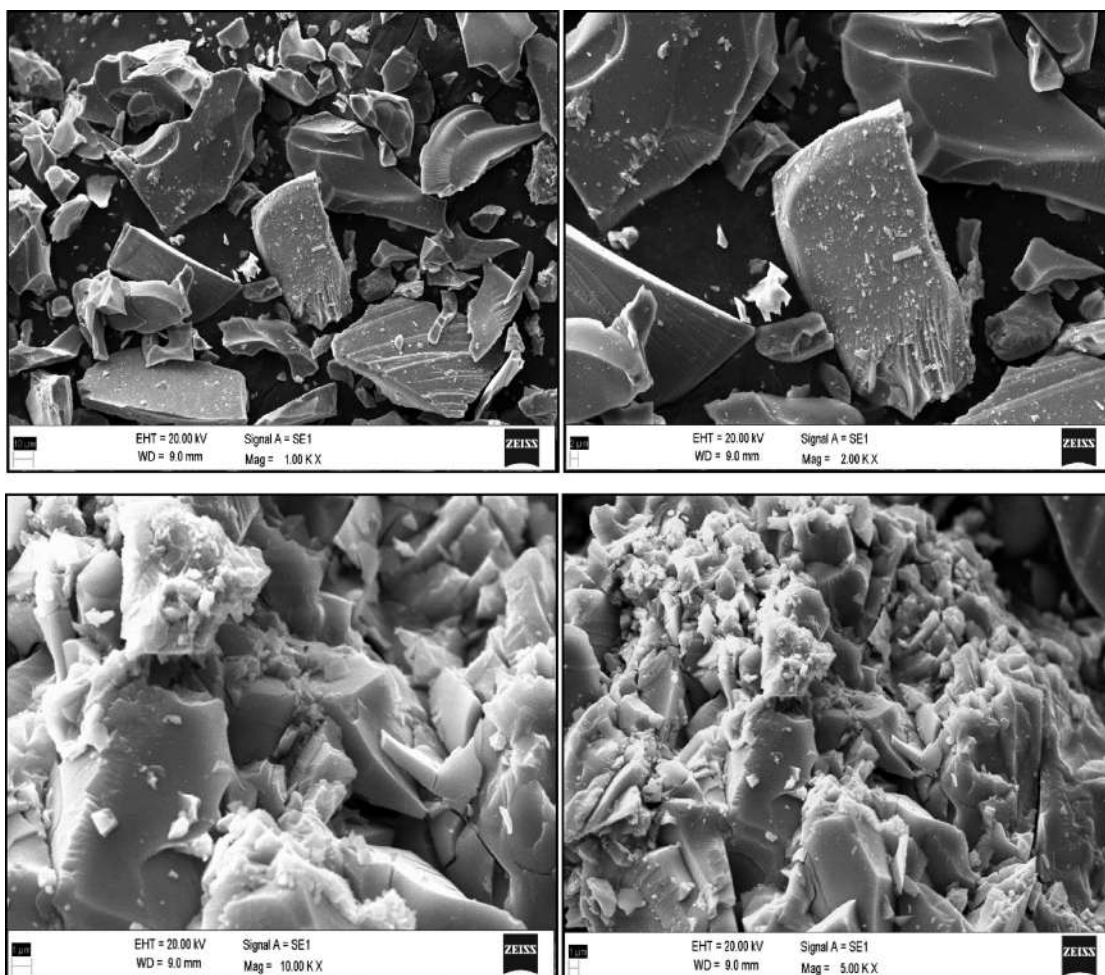


Fig. 3. FE-SEM of NiFe₂O₄ Nanomaterial.

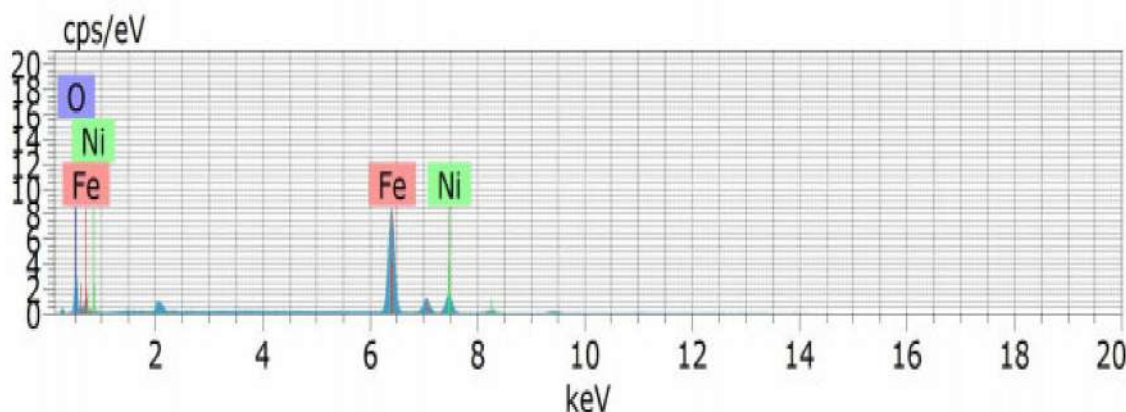


Fig. 4. EDS spectrum of NiFe₂O₄ Nanomaterial.

and tetrahedral sites are 1.139 and 0.930, respectively, correlate with Y. Kinemuchi [5].

3.2. Optical studies

Given the low solubility of transitional elements in organic solvents and water, the sample should be left in an acid solution for

Table 1
Atomic and Elemental composition of NiFe₂O₄ Nanomaterial.

Element	Atomic %	Weight %
Ni	25.04	32.18
Fe	47.64	58.26
O	27.28	9.55

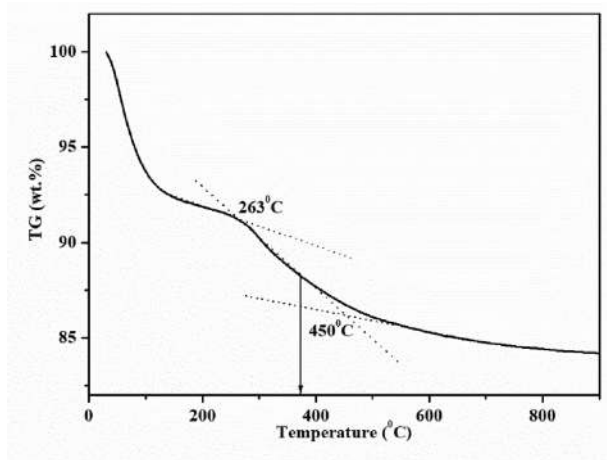


Fig. 5. TGA plot for NiFe₂O₄ Nanomaterial.

the study of the UV–Visible spectrum. The molecule undergoes an electrical transformation in the region of the electromagnetic spectrum. The maximum wavelength absorption charge transition band (~356 nm) is shown in Fig. 2a. The direct band gap was calculated by using the direct TAUC method [36]. The TAUC plot of $(\alpha h\nu)^2$ vs photoenergy ($h\nu$), where $h\nu$ is the photon energy, α is the absorption coefficient, which can be obtained from the scattering and reflectance spectra, gives the transition energy of 4.1 eV as shown in Fig. 2b [37].

3.3. Scanning electron microscopy and elemental analysis

The morphology study of nanoparticles using SEM shows that the synthesised nanoparticles are quasispheroidal and that their size is less than 100 nm, which suggests that the nano-dimensional catalysts are synthesized. This result also supports the knowledge obtained from XRD. As shown in Fig. 3, the results obtained from the above measurements of the prepared ferrite nanoparticles by the co-precipitation method are 29 nm. It was observed that the morphology of the ferrite nanoparticles by SEM data was confirmed by XRD and demonstrated a uniform size distribution.

The morphology of the majority of nanoparticles is quasi-spherical in the SEM picture. Another SEM image determination is related to the particle size, i.e., the nano dimension exhibits the formed particles (less than 100 nm) as analogous to that reported by K. Egizbek [26]. The Ni Ferrite Nanoparticles EDS spectrum is shown in Fig. 4. The atomic and elemental compositions are tabulated in Table 1.

3.4. Thermal analysis

A TGA measurement was used to determine the mass fraction of NiFe₂O₄ shown in Fig. 5. The TGA analysis was used to remove impurities from the sample, from 30 °C to 200 °C. The initial loss is due to the initial breakdown of the complex and evaporation

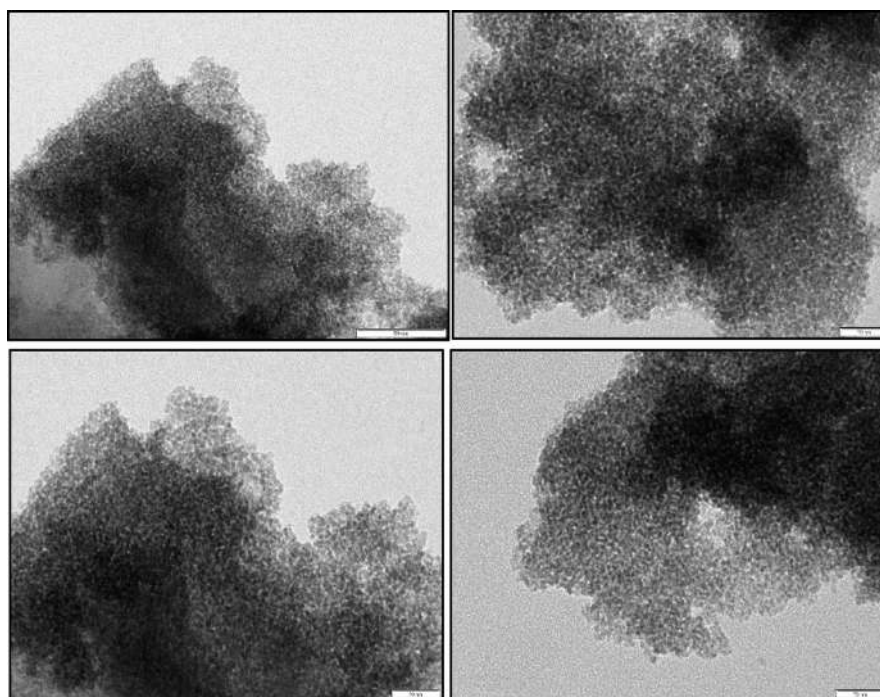


Fig. 6. TEM images of NiFe₂O₄ nanoparticles (scale bar is 50 nm for all images).

of the absorbed water. The second loss is due to further decomposition of inorganic salts and traces of hydrazine hydrate [38]. Then, above 450 °C stable oxides at 900 °C. The first stage of weight loss is 5.5 % due to the breakdown of the complex and evaporation of the absorbed water. The second weight loss is 2.3 % as a result of the decomposition of organic matter and the decomposition of inorganic salts and traces of hydrazine hydrate [39]. No weight loss is found beyond 450 °C, indicating the formation of NiFe₂O₄ nanoparticles. 263 °C is the initial decomposition temperature and 450 °C is the final decomposition temperature. The average of both decomposing materials shows the thermal stability of the material.

3.5. Transmission electron microscopy

Fig. 6 shows the TEM image of NiFe₂O₄ nanomaterial showing an aggregated particle-type structure. The particle size distribution ranges from 10 to 15 nm for NiFe₂O₄ nanomaterial. These nanoparticles are synthesised by a simple co-precipitation technique similar to that of Suresh Sagadevan [39].

3.6. Magnetic studies

The NiFe₂O₄ nanomaterial was synthesised by using the simple co-precipitation method. The magnetic property of the synthesised

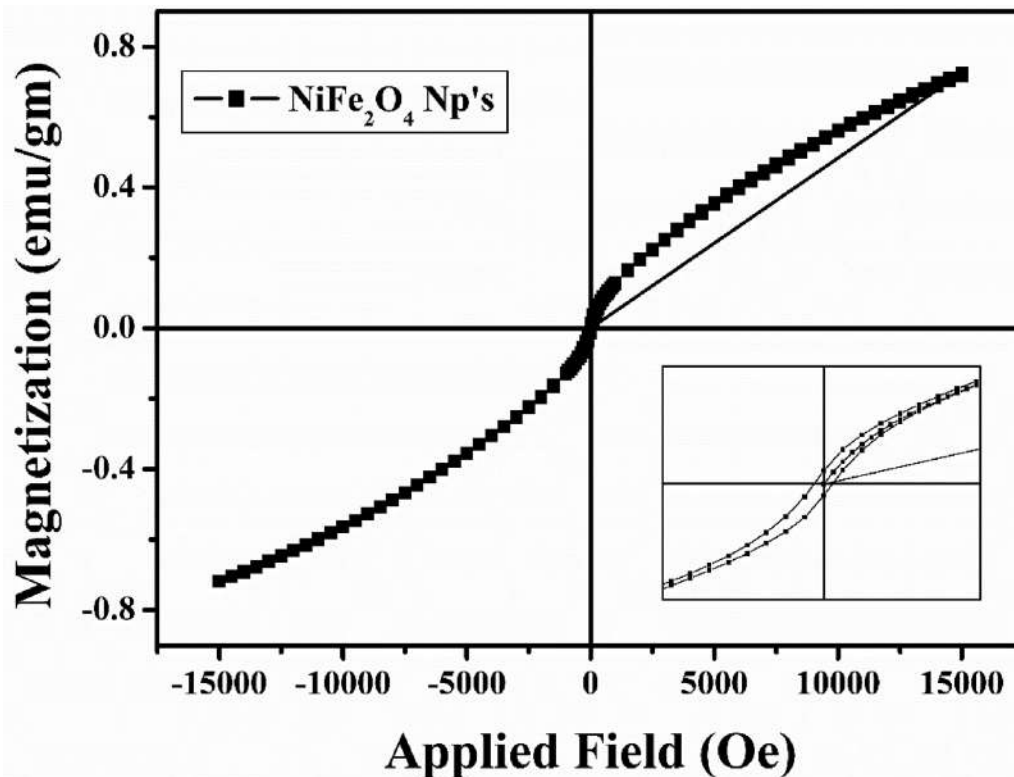


Fig. 7. Magnetic Hysteresis loop of NiFe₂O₄ nanomaterial.

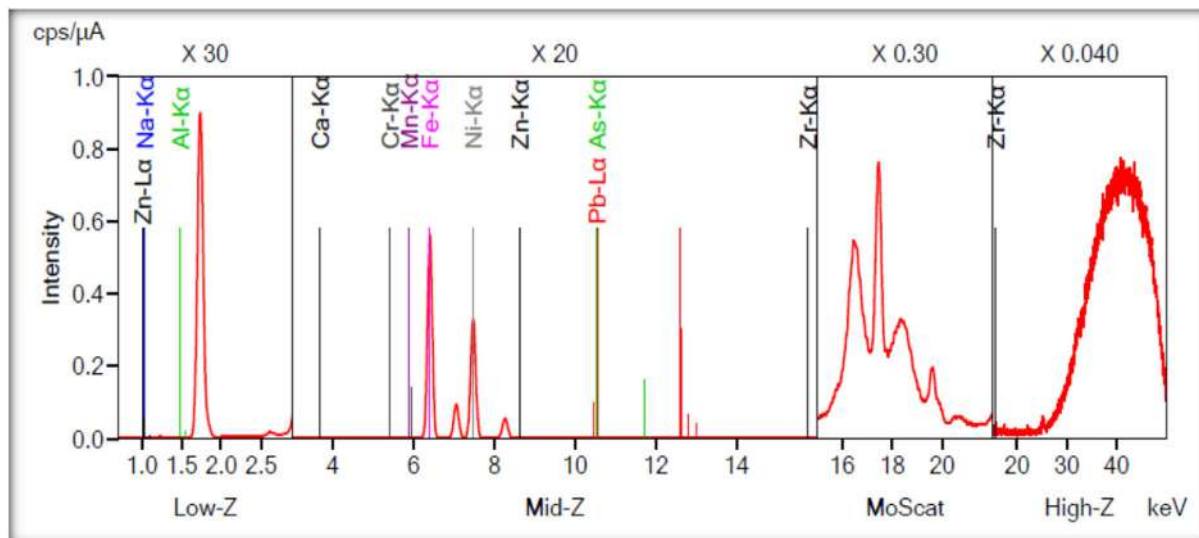


Fig. 8. XRF plot of NiFe₂O₄ nanomaterial.

Table 2
XRF Data of NiFe₂O₄ Nanomaterial.

Materials	Elemental Composition		Total
	NiO	Fe ₂ O ₃	
NiFe ₂ O ₄	26.62	73.38	100 %

spinel ferrite nanoparticles was measured by a Vibrating Sample Magnetometer (VSM). Fig. 7 shows the magnetic hysteresis curve of the NiFe₂O₄ sample. The product was observed to exhibit ferromagnetic behaviour. The saturation magnetization (M_s), the coercivity (H_c), remanence magnetization (M_r), Bohr Magnetization (μB) and anisotropy constant (K₁) are 72.66, 2.627, 2.348, 3.049, and 95.43 (erg/cm³), respectively, and have been determined from the M–H loop. The sample is mainly due to the substitution of the part of Ni²⁺ in octahedral sites by Fe³⁺ with a higher magnetic moment. The saturation magnetization of the sample is higher due to the spin counting effect of the smaller crystalline size. It is reported that [39] the magnetic properties of the material have been believed to be dependent on the particle size, shape, and magnetization direction.

3.7. X-ray Fluorescence

The surface composition of NiFe₂O₄ was also studied by the X-ray Fluorescence technique where the emission spectra are recorded as shown in the following Fig. 8. The total elemental composition was analysed by using this technique. The elemental composition as shown in Table 2.

4. Conclusion

The nickel-doped spinel ferrite nanocrystals were synthesized using an environmentally friendly process of co-precipitation. The synthesized spinel ferrite NiFe₂O₄ nanocrystals were calcinated at temperature of 700 °C. The formation of the NiFe₂O₄ nanocrystals were verified by XRD, UV–Visible Spectrum, EDS, XRF, TGA, FE-SEM, TEM, and VSM studies. Nickel ferrite displayed super-paramagnetic behaviour and increased saturation magnetization. It showed the cubic spinel structure with particle size of 10–15 nm, confirmed by the XRD and TEM techniques. Elemental analysis of the NiFe₂O₄ nanoparticles were done using the EDS and XRF studies. Optical study showed maximum absorption at ~ 356 nm with 4.1 eV band gap value. The quasispheroidal structure was obtained by FE-SEM images. Synthesized material showed high thermal stability, about 85 % even on heating over 800 °C temperature.

CRedit authorship contribution statement

Subiya Kazi: Investigation, Writing – original draft. **Radhakrishnan Tigote:** Supervision.

Declaration of Competing Interest

The authors declare that they have no known competing financial interests or personal relationships that could have appeared to influence the work reported in this paper.

Acknowledgements

We wish to thank the Department of Chemistry, Dr. Babasaheb Ambedkar Marathwada University Sub-Campus, Osmanabad for providing facilities to carry out this research work and the UGC,

New Delhi for providing financial assistance under the Maulana Azad National Fellowship to Miss. Subiya K. Kazi. (F1-17.1/2014-15/MANF-2014-15-MUS-MAH-47640/(SA-III/Website)).

References

- [1] S.H. Chen, S.C. Chang, I.N. Lin, J. Magn. Magn. Mater. 209 (2000) 193–196, [https://doi.org/10.1016/S0304-8853\(99\)00685-X](https://doi.org/10.1016/S0304-8853(99)00685-X).
- [2] Y. Shi, J. Ding, X. Liu, J. Wang, *Journal of Magnetism and Magnetic Materials* **1999**, 205, 249–254. [https://doi.org/10.1016/S0304-8853\(99\)00504-1](https://doi.org/10.1016/S0304-8853(99)00504-1).
- [3] C. Bradley, *Regulated Rivers: Research & Management* **2001**, 17, 295–295. <https://doi.org/10.1002/rrr.637>.
- [4] Y. Kinemuchi, K. Ishizaka, H. Suematsu, W. Jiang, K. Yatsui, *Thin Solid Films* **2002**, 407, 109–113. <https://doi.org/10.1016/j.matpr.2019.07.298>.
- [5] S.S. Jadhav, S.E. Shirsath, B.G. Toksha, S.M. Patange, D.R. Shengule, K.M. Jadhav, *Phys. B* **405** (2010) 2610–2614, <https://doi.org/10.1016/j.physb.2010.03.008>.
- [6] S. Feng, W. Yang, Z. Wang, *Mater. Sci. Eng.: B* **176** (2011) 1509–1512, <https://doi.org/10.1007/s12274-020-2626-y>.
- [7] G.D. Price, S.L. Price, J.K. Burdett, *Phys. Chem. Miner.* **8** (1982) 69–76, <https://doi.org/10.1007/bf00309016>.
- [8] M. Singh, S.P. Sud, *Mater. Sci. Eng.: B* **83** (2001) 180–184, [https://doi.org/10.1016/S0921-5107\(01\)00514-1](https://doi.org/10.1016/S0921-5107(01)00514-1).
- [9] P. Sivakumar, R. Ramesh, A. Ramanand, S. Ponnusamy, C. Muthamizhchelvan, *Mater. Lett.* **65** (2011) 483–485, <https://doi.org/10.1016/j.matlet.2010.10.056>.
- [10] D. Zhang, X. Zhang, X. Ni, J. Song, H. Zheng, *Chem. Phys. Lett.* **426** (2006) 120–123, <https://doi.org/10.1016/j.cplett.2006.05.100>.
- [11] C. Liu, B. Zou, A. Rondinone, Z. Zhang, *J. Phys. Chem. B* **104** (2000) 1141–1145, <https://doi.org/10.1016/HJSE19030000154>.
- [12] P. Sivakumar, R. Ramesh, A. Ramanand, S. Ponnusamy, C. Muthamizhchelvan, *Appl. Surf. Sci.* **258** (2012) 6648–6652, <https://doi.org/10.1016/j.apsusc.2012.03.099>.
- [13] P. Sivakumar, R. Ramesh, A. Ramanand, S. Ponnusamy, C. Muthamizhchelvan, *Mater. Lett.* **66** (2012) 314–317, <https://doi.org/10.1016/j.matlet.2011.09.005>.
- [14] X. Qi, J. Zhou, Z. Yue, Z. Gui, L. Li, *Mater. Sci. Eng.: B* **99** (2003) 278–281, [https://doi.org/10.1016/S0921-5107\(02\)00524-X](https://doi.org/10.1016/S0921-5107(02)00524-X).
- [15] H.M. Widatallah, I.A. Al-Omari, A.M. Gismelseed, O.A. Yassin, A.D. Al-Rawas, M. E. Elzain, A.A. Yousif, O.A. Osman, *Hyperfine Interact.* **169** (2006) 1325–1329, <https://doi.org/10.1007/s10751-008-9773-y>.
- [16] V.A. Fedorov, V.A. Ganshin, Y.N. Korkishko, *Phys. Status Solidi (a)* **139** (1993) 9–65, <https://doi.org/10.1002/pssa.2211390102>.
- [17] P.J. van der Zaag, M. Kolenbrander, M.T. Rekveldt, *J. Appl. Phys.* **83** (1998) 6870–6872, <https://doi.org/10.1063/1.367562>.
- [18] K. Takada, Y. Yamamoto, A. Makino, T. Yamaguchi, I. Sasada, *J. Appl. Phys.* **83** (1998) 6861–6863, <https://doi.org/10.1063/1.367765>.
- [19] R.V. Penney, *J. Phys. Chem. Solids* **25** (1964) 335–345, [https://doi.org/10.1016/0022-3697\(64\)90112-X](https://doi.org/10.1016/0022-3697(64)90112-X).
- [20] P. Sivakumar, R. Ramesh, A. Ramanand, S. Ponnusamy, C. Muthamizhchelvan, *J. Alloy. Compd.* **563** (2013) 6–11, <https://doi.org/10.1016/j.jallcom.2013.02.077>.
- [21] D. Yang, M.J. Campolongo, T.N. Nhi Tran, R.C.H. Ruiz, J.S. Kahn, D. Luo, *WIREs Nanomed. Nanobiotechnol.* **2** (2010) 648–669, <https://doi.org/10.1116/jnn.2010.1722>.
- [22] B. Zeynizadeh, I. Mohammadzadeh, Z. Shokri, S. Ali Hosseini, *J. Colloid Interface Sci.* **500** (2017) 285–293, <https://doi.org/10.1080/17518253.2019.1711202>.
- [23] W.E. Pottker, R. Ono, M.A. Cobos, A. Hernando, J.F.D.F. Araujo, A.C.O. Bruno, S.A. Lourenço, E. Longo, F.A. La Porta, *Ceram. Int.* **44** (2018) 17290–17297, <https://doi.org/10.1021/acsomega.1c04079>.
- [24] C. Thirupathy, S. Cathrin Lims, S. John Sundaram, A.H. Mahmoud, K. Kaviyarasu, *J. King Saud Univ. – Sci.* **32** (2020) 1612–1618, <https://www.researchgate.net/deref/https%3A%2F%2Fdoi.org%2F10.1016%2Fj.ceramint.2021.07.274>.
- [25] K. Egizbek, A. L. Kozlovskiy, K. Ludzik, M. V. Zdorovets, I. V. Korolkov, B. Marciniak, J. M. D. Chudoba, A. Nazarova, R. Kontek, *Ceramics International* **2020**, 46, 16548–16555. <https://doi.org/10.3390/molecules26020457>
- [26] T. Abbas, Y. Khan, M. Ahmad, S. Anwar, *Solid State Commun.* **82** (1992) 701–703, [https://doi.org/10.1016/0038-1098\(92\)90064-G](https://doi.org/10.1016/0038-1098(92)90064-G).
- [27] E. C. Snelling, Butterworths, London; Boston, **1988**. <http://books.google.com/books?id=yRNTAAAMAAJ>.
- [28] Z. V.T. V. Tsakaloudi, E. Papazoglou, *Journal of Electroceramics* **2003**, 11, 107–117. <https://doi.org/10.1023/B:JECR.0000011216.01346.03>
- [29] M. Schaefer, G. Dietzmann, H. Wirth, *J. Magn. Magn. Mater.* **101** (1991) 95–96, [https://doi.org/10.1016/0304-8853\(91\)90689-8](https://doi.org/10.1016/0304-8853(91)90689-8).
- [30] J.A.T. Taylor, S.T. Reczek, A. Rosen, *American Ceramic Society, Westerville, OH (United States), United States*, 1995.
- [31] M. Rozman, M. Drogenik, *J. Am. Ceram. Soc.* **81** (1998) 1757–1764, <https://doi.org/10.1111/j.1151-2916.1998.tb02545.x>.
- [32] R. Arulmurugan, G. Vaidyanathan, S. Sendhilnathan, B. Jayadevan, *J. Magn. Magn. Mater.* **298** (2006) 83–94, <https://doi.org/10.1016/j.jmmm.2005.03.002>.
- [33] S.R. Ahmed, S.B. Ogale, G.C. Papaefthymiou, R. Ramesh, P. Kofinas, *Appl. Phys. Lett.* **80** (2002) 1616–1618, <https://doi.org/10.1063/1.5040890>.
- [34] D.L. Huber, Small 1 (2005) 482–501, <https://doi.org/10.1002/smll.200500006>.
- [35] S.T. Hosseini, S. Khademolhosseini, *J. Mater. Sci.: Mater. Electron.* **27** (2016), <https://doi.org/10.1007/s10854-016-4514-5>.

- [36] M.H. Habibi, F. Fakhri, J. Mater. Sci.: Mater. Electron. 28 (2017) 13455–13463, <https://doi.org/10.1007/s10854-017-7184-z>.
- [37] A. Al-Hunaiti, A. Ghazzy, N. Sweidan, Q. Mohaidat, I. Bsoul, S. Mahmood, T. Hussein, Nanomaterials (2021) 11, <https://doi.org/10.3390/nano11041010>.
- [38] P. Sivagurunathan, S.R. Gibin, J. Mater. Sci.: Mater. Electron. 27 (2016) 2601–2607, <https://doi.org/10.1007/s10854-015-4065-1>.
- [39] S. Sagadevan, Chowdhury, Zaira Zaman and Rafique, Rahman F, *Materials Research [online]* **2018**, 21, 533. <http://dx.doi.org/10.1016/j.rinp.2018.12.058>



Stabilization of dairy industry sludge with leaf litter using as composting and its effect on *Spinacia oleracea* plant growth

Chougale Sanjivani Tanaji, Sarkale Prajkta Shahaji, Jadhav Aasawari Suhas*

Department of Environmental Science, Shivaji University, Kolhapur, India

ARTICLE INFO

Article history:

Available online 29 October 2022

Keywords:

Dairy sludge
Leaf litter
Combination
Composting
Plantation

ABSTRACT

A dairy industry is the large scale food production industries playing an important role in causing environmental pollution. Solid waste is a serious threat to environmental hazards through its liquid and solid waste generation. Hence, it is needed to handle such waste by enhancing new cleaner technologies by recycling the waste and generate safe environment using organic fertilizer to soil. Dairy industry waste is dumped in landfill which has disadvantage of being expensive occupying more open area resulting in alteration of ground water and soil profile quality. The wastewater generated by dairy industry is categorized as raw waste. The activated sludge is treated during analysis of various parameters under the consideration. Thus, the objective of the present study is to analyze physico-chemical and phyto-chemical parameters of combination and *Spinacia oleracea* plant after treating with the Dairy waste and mix leaf litter waste. Current research study, reveals that various concentration of dairy waste and leaf litter combination can turn into good quality compost for ecofriendly crop cultivation. In the present study, Dairy waste + Leaf waste 25 % (T₃) and Dairy waste + Leaf waste 75 % (T₅) combination was good compost and it is a viable organic waste management. It has a potential to enhance proper waste management system, while promoting cultivation of vegetable for food precautions. The application of this organic amendment could promote and improve agro-ecosystem and also helpful for minimization of dairy waste.

© 2022 Elsevier Ltd. All rights reserved.

Selection and peer-review under responsibility of the scientific committee of the Integrative Nanotechnology Perspective for Multidisciplinary Applications - 2022.

1. Introduction

Dairy is a business established for the harvesting of animal milk mostly from Cows, Buffalo, goats, sheep, camels, horses for human consumption. The dairy wastewater is released into the environment and it is hazardous to the surrounding. The dairy plant in the government, cooperatives and private sector produces similar type of the dairy product like milk, butter, ghee, skimmed milk powder and whole milk powder [23]. The study was undertaken

in different areas shows that mixing sludge's to agricultural soil can improve soil structure, root penetration and nutrient levels mainly Nitrogen and Phosphorous [40,24]. However, some urban sewage sludge can have negative effect and shows consequences of their relatively high content in heavy metals, salts, organic toxins and pathogen [35]. Treatment of solid dairy waste and converting it into good compost is important and often many methods are used in the treatment of dairy mud such as anaerobic digestion, composting, soil distribution, wetlands built up and reinforcement of lime. Several laws have been enacted to ensure safe disposal of solid waste ([4]).

The rising cost of organic fertilizer has directed farmers' attention to natural resources that increase soil fertility and improve chemical soil properties. These include access to nutrients and absorption, soil texture, water retention capacity, cation exchange rate, electrical conductivity, pH, bacterial population and soil moisture [1,32]. Dry leaf fallen from trees every day, produces large amount of solid waste. The traditional methods for leaf litter dis-

Abbreviations: pH, Potential of Hydrogen; Ec, Electric Conductivity; WHC, Water Holding Capacity; MC, Moisture Content; OC, Organic Carbon; OM, Organic Matter; NPK, Nitrogen, Phosphorous, Potassium; C:N, Ratio of Carbon to Nitrogen; T1, T2, T3, T4, T5, Treatment; C1, C2, C3, C4, Concentration; mg/g, Milligrams per gram; μ S/cm, Microsiemens per centimeter; %, Percentage; S.D, Standard Deviation; ANOVA, Analysis of Variance; cm, Centimete; mg/lit, Milligrams per litter; Mn, Manganese; Zn, Zinc; Fe, Iron; Cr, Chromium.

* Corresponding author.

E-mail address: asj_env@unishivaji.ac.in (J. Aasawari Suhas).

<https://doi.org/10.1016/j.matpr.2022.09.600>

2214-7853/© 2022 Elsevier Ltd. All rights reserved.

Selection and peer-review under responsibility of the scientific committee of the Integrative Nanotechnology Perspective for Multidisciplinary Applications - 2022.

posal are burning and land filling. Burning process emits several toxic compounds, causing air pollution. Land filling treatment involves huge amount of leaf litter waste which increases transportation cost and more landfill space. Both methods have several disadvantages. Naturally leaf can be degraded by microbial activity into an organic fertilizer, which is safely used for soil amendment [20]. The primary objective of the study is to create an ideal environment for the microorganisms for composting of leaf litter and dairy waste combination. Bacteria break down plant tissue, further fungi and protozoan soon join the bacteria. Centipedes, millipedes, beetles, and earthworms also participate by tearing and chewing the materials into smaller pieces making them more suitable for the microbes [10]. So aim of the present study was to determine the physico-chemical parameters of waste and enrich its quality with compost.

2. Study area

The dairy sludge was collected from Kolhapur Zillah Sahakari Dudh Utpadk Sangh Ltd. situated at Shirgaon, Kolhapur. Fig. 1 Gokul- Shirgaon industrial area which is an industrial park in Kolhapur (16°38' 36.5" N and 74° 17' 12.4" E). It is well known for its popular brand of 'Gokul' which is established on 16th March 1963 during the year 2019–2020, the average milk procurement is 10.64 Lakh liters per day. The ratio of buffalo milk to cow milk procurement is 57:43 % respectively. Their products include milk, shrikhand, ghee, butter, skimmed milk powder and desi butter.

Huge quantity of leaf litter fall in the campus area gathered through normal road sweeping and burn collectively to reduce the amount of litter. The raw material i.e. plant litter required for the study purpose is collected from Shivaji university campus which is a huge area of 853 ha it is free of cost and easily available in campus. The campus trees are of dry deciduous type of plantation. Large amount of fallen leaves produces a pressure on daily solid waste management. In the present study, an attempt is made

by making combination of wastes like leaf litter and dairy sludge with addition of microbial culture which can produce valuable compost.

3. Material and methodology

The sludge was collected from the tertiary treatment unit from Kolhapur Zillah Sahakari Dudh Utpadak Sangh Ltd., Kolhapur. The physico-chemical analysis of sludge was done in Department of Environmental Science, Shivaji University, Kolhapur.

3.1. Physico-chemical characterization of leaf litter and dairy sludge

The Table. 1 shows Physico-chemical characteristics were analyzed for dairy sludge and leaf litter by which elements such as macro and micronutrients are chemically extracted and analyzed. A 45 day's composting trail was performed at laboratory conditions. The dairy sludge is used as a byproduct after treating the wastewater from dairy industry by the activated sludge method. The wastewater from dairy industry contains discarded milk and cleaning agents Sodium Hydroxide (NaOH) and Nitric acid (HNO₃). The dairy industry sludge, have low heavy metal content, and therefore the risk of large quantities of these pollutant coming through the food chain is considerably reduced. Sometimes, this type of sludge has been directly applied to the soil shows this practice to be safe alternatives for its disposal [19]. The collected dairy sludge from Gokul dairy and leaf litter collected from Shivaji University, Campus were analyzed separately before composting.

3.2. Concentration details

To check the best suitable concentration of dairy sludge and leaf litter for composting purpose, five different combinations were made. The five concentrations are given below in the table. 2. The physicochemical parameters were analysed for 15 days,

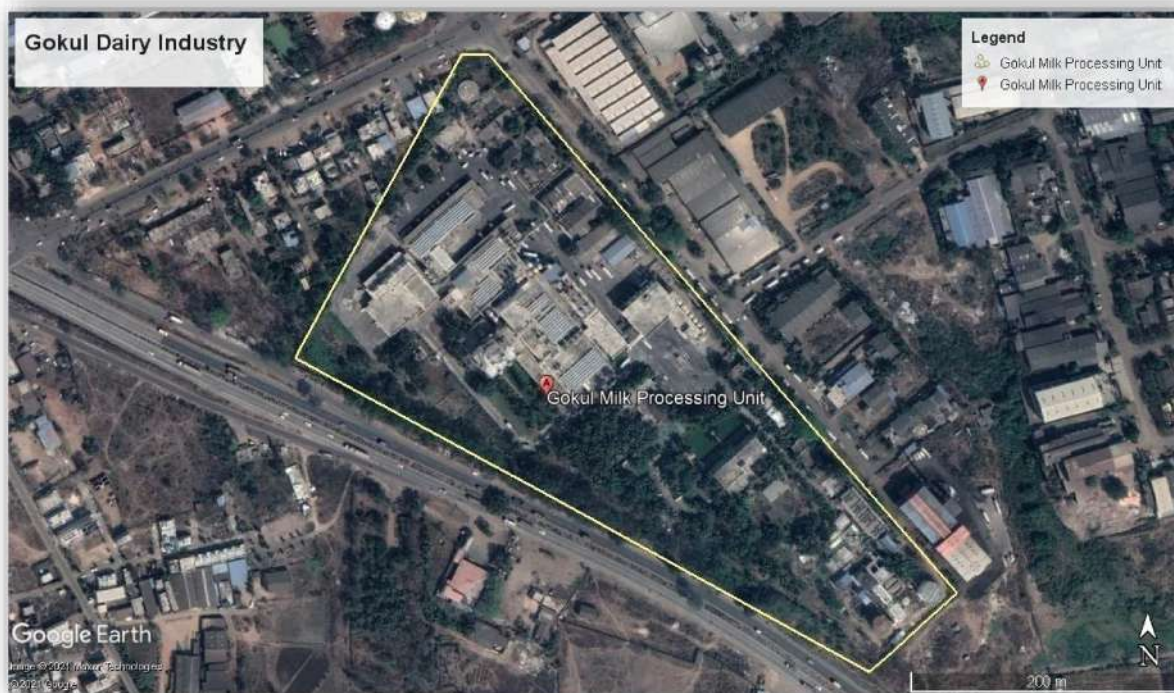


Fig. 1. Satellite view of Gokul Dairy (Image source: Google Earth).

Table 1
Physico-chemical analysis methods for leaf litter and dairy sludge.

Sr. No	Parameters	Method	References
1.	Potential of Hydrogen (pH)	pH meter	[30]
2.	Electric Conductivity (EC)	Conductivity meter	[30]
3.	Water Holding Capacity (WHC)	Gravimetric method	[30]
4.	Moisture Content (MC)	Gravimetric method	[30]
5.	Organic Carbon (OC)	Rapid dichromate oxidation technique method	[2]
6.	Organic Matter (OM)	Rapid dichromate oxidation technique method	[5]
7.	Nitrogen (N)	Kjeldahl method	[26]
8.	Phosphorous (P)	Absorption Spectrophotometer	[33]
9.	Potassium (K)	Standard method	[9]

Table 2
Feedstock and Combination Ratios.

Sr. No.	Treatments	Feedstock and Combination	Ratio v/v
1.	T ₁	Dairy waste	1:0
2.	T ₂	Leaf waste	1:0
3.	T ₃	Dairy waste + Leaf waste (25 %)	1:3
4.	T ₄	Dairy waste + Leaf waste (50 %)	1:1
5.	T ₅	Dairy waste + Leaf waste (75 %)	3:1

30 days, and 45 days. Set was allowed to decompose for 45 days and proper moisture conditions were maintained by sprinkling water. As composting completed, known vegetables were planted in a pot to see the effect of compost.

3.3. Statistical analysis

The mean and standard deviation of the three replicates from each combination were reported for all parameters measured. One-Way analysis of variance (ANOVA) statistical analysis was performed to compare variations in compost properties at different treatment.

4. Results

4.1. Application of dairy sludge and leaf litter as compost on *Spinacia oleracea* plant

The seedling of *Spinacia oleracea* plant was growing in pot experiment during the rabbi season at laboratory condition. The Tables. 5 and 6 shows that application of different combination and concentration of dairy sludge and leaf litter with the help of soil.

5. Discussion

The physico-chemical characteristics of the five different combination of compost were studied. Table. 3 recorded characters like pH, Ec, water holding capacity, moisture content, organic carbon, organic matter, Nitrogen, Phosphorous, Potassium, C:N ratio which plays important role in the plant growth and maintain favorable soil condition.

a) Change in pH:

The mature compost is a dark brown coloured component with earthy smell. The pH was recorded for sample throughout the experiment for T₁, T₂, T₃, T₄, and T₅ combinations was in between 7.12 and 7.81. There was a general decline in pH at the end of com-

posting period. T₁, T₂, T₃, however recorded significantly lower pH than T₃ and T₅ in the composting process. It was seen that as compared to control groups, the treated groups showed an increase in mean values of all parameters. Since the beginning of the process, the pH tends to move towards acidic. This may be due to the incomplete oxidation and formation of organic acids from composting mixtures. [15] and [22]. The microorganism are reported to produce organic acids and hence the pH value of the compost decreases slowly at the initial stage [28].

b) Change in Electrical conductivity (Ec):

Electrical conductivity is essential character which determines the concentration of salts present in experiment. The experimentation showed Electrical conductivity (EC) decreased from 3.52 to 4.66 $\mu\text{S}/\text{cm}$, 4.24–5.54 $\mu\text{S}/\text{cm}$, 4.3–5.43 $\mu\text{S}/\text{cm}$, 3.64–4.88 $\mu\text{S}/\text{cm}$, 4.12–5.68 $\mu\text{S}/\text{cm}$, for T₁, T₂, T₃, and T₄ respectively in the composting period. EC indicates that the mineralization rate and availability of total soluble salts in compost, which is negative effect or inversely proportional to each other plant growth. The increases in EC is reason of the production of extra ammonia, nitrate and nitrite [37,44,43;41].

c) Effect on Water Holding Capacity (WHC):

The water holding capacity is the amount of water that is given by soil holds for crop use. WHC is indicating that soil quality and productivity [31]. The water-holding capacity (WHC) is an important characteristic in composting. The trial reports showed increase WHC for five combinations after 15 days period of composting increases after 15 days. The minimum value of 40.7 was recorded in T₂ and the maximum value of 56.18 was recorded in T₃. After 45 days of composting, the T₃ recorded highest is 67.44 while T₂ recorded the lowest is 45.8, respectively. It increases the percentage of organic matter the water holding capacity will increase.

d) Effect on Moisture Content (MC):

Moisture content was recorded for the combinations which were significantly minimum for T₁ (45.2 %) and the maximum value observed for T₅ (58.98 %) combination. The moisture content is important during composting as the dissolved nutrients required for the physiological and metabolic activities of microorganisms [29]. The microbial communities of compost through their changes on temperature, moisture and aeration of the pile [11], which is due to nutrient content and available form of carbon. For example, adding jaggery increased the number of microorganisms and thus enhanced the enzymatic degradation of cellulose during composting of green wastes [13].

e) Change in Organic carbon (OC) and Organic Matter (OM):

The organic carbon (OC) and organic matter percentage is increased or decreased significantly with change in treatment of the combinations. After 15 days of composting, the organic content of compost was in between a minimum of 16.65 % in T₂ (Leaf waste) and a maximum mean of 20.65 % observed in the T₃ (25%). In T₅ (75%) combination, OC is 20.54 %, respectively, over the period. After 30 days of composting, T₃ (25%) combination showed highest OC i.e. 20.92 %, while T₁ (Dairy waste) observed the lowest OC i.e. 16.39 %. The T₄ and T₅ observed organic carbon content of 19.34 % and 20.45 % respectively. At 45 days of composting, the highest values which are between T₅ (75%) is 19.61 % OC and the lowest values which is between the T₁ (Dairy waste) is 15.36 % respectively (Table. 3) similar results were observed by [42]. The dry mat-

Table 3 Physical-chemical properties with Mean ± SD of five different combinations of Dairy waste and Leaf litter waste:

Concentration Parameters	T ₁ Dairy Sludge Control (100%)			T ₂ Leaf Litter Control (100%)			T ₃ Dairy Sludge + Leaf Litter (25%)			T ₄ Dairy Sludge + Leaf Litter (50%)			T ₅ Dairy Sludge + Leaf Litter (75%)		
	15 Days	30 Days	45 Days	15 Days	30 Days	45 Days	15 Days	30 Days	45 Days	15 Days	30 Days	45 Days	15 Days	30 Days	45 Days
pH	7.51 ± 0.15	7.22 ± 0.12	7.38 ± 0.12	7.4 ± 0.17	7.42 ± 0.14	7.34 ± 0.13	7.32 ± 0.13	7.54 ± 0.14	7.81 ± 0.21	7.21 ± 0.09	7.33 ± 0.24	7.51 ± 0.31	7.12 ± 0.16	7.72 ± 0.20	7.81 ± 0.24
Ec (µS/cm)	4.66 ± 0.22	3.61 ± 0.15	3.52 ± 0.44	4.32 ± 0.11	4.24 ± 0.06	5.54 ± 0.52	5.43 ± 0.60	4.95 ± 0.25	4.3 ± 0.14	4.86 ± 0.64	4.88 ± 0.71	3.64 ± 0.28	5.68 ± 0.75	4.75 ± 0.25	4.12 ± 0.20
Water Holding Capacity (WHC) %	45.4 ± 0.17	46.0 ± 0.16	48.61 ± 0.09	40.7 ± 0.32	42.53 ± 0.11	45.8 ± 0.03	56.18 ± 0.40	52.03 ± 0.06	67.44 ± 0.15	55.51 ± 0.19	52.75 ± 0.36	59.48 ± 1.16	54.11 ± 0.58	54.86 ± 0.87	58.13 ± 0.25
Moisture Content (MC) %	45.2 ± 0.04	46.0 ± 0.54	46.52 ± 0.21	48.4 ± 0.05	49.25 ± 0.03	47.45 ± 0.06	50.02 ± 0.03	54.63 ± 0.10	54.88 ± 0.03	49.61 ± 0.02	54.03 ± 0.03	53.54 ± 0.02	52.14 ± 0.01	56.13 ± 0.02	54.98 ± 0.03
Organic Carbon (OC) %	18.47 ± 0.15	16.39 ± 0.16	15.36 ± 0.11	16.65 ± 0.09	18.46 ± 0.10	17.87 ± 0.57	20.65 ± 0.10	20.92 ± 0.08	19.8 ± 0.49	19.34 ± 0.09	19.49 ± 0.06	18.27 ± 0.06	20.54 ± 0.08	20.45 ± 0.08	19.61 ± 0.54
Organic Matter (OM) %	31.56 ± 0.10	27.56 ± 0.34	28.43 ± 0.13	28.59 ± 0.13	31.29 ± 0.32	31.4 ± 0.39	35.67 ± 0.07	35.51 ± 0.56	31.51 ± 0.34	33.31 ± 0.09	33.36 ± 0.29	34.20 ± 0.85	35.01 ± 0.59	36.28 ± 0.54	34.64 ± 0.27
Nitrogen (N) %	1.06 ± 0.06	1.24 ± 0.061	1.35 ± 0.08	1.36 ± 0.06	1.12 ± 0.11	1.36 ± 0.06	3.41 ± 0.065	2.63 ± 0.08	3.46 ± 0.09	3.45 ± 0.05	2.54 ± 0.08	3.63 ± 0.05	3.84 ± 0.11	3.48 ± 0.13	3.52 ± 0.06
Phosphorous (P) %	1.14 ± 0.04	1.02 ± 0.08	1.33 ± 0.09	0.74 ± 0.09	1.08 ± 0.07	1.32 ± 0.06	1.27 ± 0.04	1.11 ± 0.06	1.74 ± 0.25	0.93 ± 0.18	1.22 ± 0.05	1.64 ± 0.05	1.57 ± 0.06	1.45 ± 0.05	1.78 ± 0.16
Potassium (K) %	0.47 ± 0.05	0.34 ± 0.04	0.51 ± 0.05	0.72 ± 0.04	0.89 ± 0.05	0.71 ± 0.07	0.84 ± 0.06	0.56 ± 0.05	0.86 ± 0.07	0.76 ± 0.07	0.96 ± 0.10	0.81 ± 0.05	0.56 ± 0.08	0.43 ± 0.07	0.72 ± 0.07
C:N ratio	17.31 ± 0.05	13.07 ± 0.07	14.41 ± 0.058	12.25 ± 0.05	16.4 ± 0.03	14.01 ± 0.05	6.07 ± 0.02	7.98 ± 0.05	6.18 ± 0.03	5.15 ± 0.03	7.7 ± 0.08	5.58 ± 0.08	5.33 ± 0.05	6.05 ± 0.03	6.33 ± 0.05

*The value represent mean of triplet and ± SD.

ter lost in the form of carbon dioxide due to microbial activities and moisture evaporation similarly could account for the decline in organic matter over the composting period. This confirms to the results reported by [38]. The total organic carbon increases in some concentration because of lignocellulose materials are present in leaf litter. The organic carbon was decreased at all concentrations as the decomposition progressed. Organic matter (OM) depends on the organic carbon. It was observed for the compost combinations that there is increasing OM in T5 combination after 15 days of treatment. The OM was observed is 36.28 % – 27.56 % in T₁ (Dairy waste).

f) Change in Nitrogen Content (N):

The Total Nitrogen was increased at the end of the composting period. The nitrogen increase indicates the increased compost age [3]. The total nitrogen level in T₁, (15day) combination range is 1.06 % and T₂ (30 days) 1.12 at the end of the study were higher than those of T₅, 15-day's 3.84 and T₄, 15 days 3.75 likely as a result of minimal gaseous exchange within T₁ and T₂. The increased nitrogen was due to the nitrification process, where by biological ammonia degradation oxidized to nitrite (NO₂) and Nitrate (NO₃) [21]. The increased nitrogen is attributed to the concentration effect as a result of substantial degradation of organic compound, and contribution of nitrogen fixing bacteria [36] and [18].

g) Change in Phosphorous (P):

The Total Phosphorous content is increased during composting period. Significantly lower range of total phosphorous is observed for T₂ (15 days) and the highest for T₅ (45 days) of compost. A similar result was observed by (Tibu., 2019). The phosphorous concentration, therefore increased as organic matter decreased over the composting period. The increased phosphorous during composting period, is possibly caused by concentration effect arising from higher rate of carbon loss that occurs when organic matter is degraded.

h) Change in Potassium (K):

The potassium content was increased in the combination. A similar result was observed in [25]. The lower range of potassium was found for T₂ (15 days) of compost is 0.74 % and T₄ (15 days) 0.93 % compost. Then the highest value of potassium was found for T₅ (15 days) compost 3.84 %. In the last 45 days of composting period, this might be due to the loss of potassium salts through excessive leaching [7]. Sometime the Potassium value is not constantly increased due to the interruption of microorganism in the composting. The excessive leaching might have been due to excess moisture content emanating from waste beyond the absorption capacity of bulking agents.

i) C:N ratio:

The C:N ratio of T₃ (6.07), T₄ (5.15) and T₅ (5.33) during the composting period is a similar combination, progressively decreased at the end of the composting process. The reduced C:N ratio at the end of the composting period is observed in this study is (Al Bataina *et al.*, 2016) is stated as C:N ratio decreased with increases in compost age. The application of organic material with a high C: N ratio reduces plant available N owing to an enhanced assimilation of microbial N the high import of organic matter with compost [8].

One-Way ANOVA test: analysis of parameter variables measured in the different treatments of compost. As shown in Table. 4, the null hypothesis states that the mean value of five different

Table 4
One-Way ANOVA test: analysis of parameter variables measured in different treatment of compost.

Parameters	Sum of Squares (SS)	Degree of freedom (df)	Mean square (MS)	F- values	P-value	F critical values	Decision
pH	0.2611	2	0.13055	3.067112	0.057929	3.238096	Reject (H ₁)
Ec	0.304633	2	0.152317	0.573805	0.568062	3.238096	Reject (H ₁)
WHC	337.7258	2	168.8629	3.827813	0.030348	3.238096	Accept (H ₀)
MC	72.37156	2	36.18578	3.247992	0.049578	3.238096	Accept (H ₀)
OC	15.62341	2	7.811707	3.486573	0.040451	3.238096	Accept (H ₀)
OM	42.01873	2	21.00936	4.545309	0.016811	3.238096	Accept (H ₀)
N	2.370033	2	1.185017	1.053556	0.358409	3.238096	Reject (H ₁)
P	0.876633	2	0.438317	10.38692	0.000242	3.238096	Accept (H ₀)
K	0.048229	2	0.024114	0.755964	0.476314	3.238096	Reject (H ₁)
C:N	14.8611	2	7.43055	0.407027	0.668421	3.238096	Reject (H ₁)

P-value 0.05 (>0.05) = statistically insignificant, p-value 0.05 (<0.05) = statistically significant.
H₀ = the null hypothesis is a statement. There exists no relation between two variables.
H₁ = Alternative hypothesis a statement, there exists some relationship between two measured phenomenon.

Table 5
Height (cm) *Spinacia oleracea* plant after using compost.

Concentration Day	C ₁	C ₂	C ₃	C ₄
15 Day	8.5	15.7	11.1	13.1
30 Day	14.7	18.2	15.1	16.4
45 Day	21.8	31.5	27.2	27.8
60 Day	27.1	42.5	33.5	35.2
Mean ± S.D.	18.02 ± 8.13	26.97 ± 12.45	21.72 ± 10.41	23.12 ± 10.22

Table 6
Number of Average leaves *Spinacia oleracea* plant after using compost.

Concentration Day	C ₁	C ₂	C ₃	C ₄
15 Day	6	13	8	10
30 Day	11	15	12	13
45 Day	15	20	16	19
60 Day	20	27	23	24
Mean ± S.D.	13 ± 5.94	18.75 ± 6.23	14.75 ± 6.39	16.5 ± 6.24

concentrations of these parameters pH, Ec, N, K, and C: N over different time spans is equal. Because the p-value is >0.05 (>0.05), we accept the null hypothesis and conclude that five different concentrations of these parameters pH, Ec, N, K, and C: N in different time spans have the same mean. As a result, this figure is statistically insignificant. Also other parameters shows null hypothesis in Table. 4 states that the mean value of five different concentrations of these parameters, WHC, MC, OC, OM, and P, over different time spans is equal. We reject the null hypothesis because the p-value is <0.05 (<0.05), and we conclude that the means of five different concentrations of these parameters over different time span have different mean. As a result, this figure is statistically significant.

5.1. Study of micronutrients

The Fig. 7 shows initial compost was observed with micronutrients such as Cr, Zn, Mn, Fe the Cr 1.12 ± 0.26 mg/kg, Zn 1.29 ± 0.18 mg/kg, Mn 1.44 ± 0.26 mg/kg, Fe 1.09 ± 0.37 mg/kg. Final compost were recorded for Cr, Zn, Mn, Fe shows amount in Mean ± S.D. The Fig. 8 shows that the Cr 1.29 ± 0.26 mg/kg, Zn 1.54 ± 0.44 mg/kg, Mn 1.78 ± 0.47 mg/kg, Fe 1.23 ± 0.46 mg/kg respectively. The heavy metal in soil are bound by the organic compounds and are not available for plant uptake if these complexes are in soluble, but they are slowly released through microbial degradation. [16]. Composting is reducing the mobility of heavy metals and thus their transport to the environment in contrast to the manure. The utilization of composted manure was important and worthwhile in adulterated soils for alleviating heavy metals contamination [17].

5.2. Effects of various treatments on phyto-chemical parameters of *Spinacia oleracea* plant

After analysis of physico- chemical characters of processed dairy sludge compost and leaf litter compost, it is used in a pot with soil for an experiment to analyze its efficiency on *Spinacia oleracea*. Spinach is a leafy green plant native to central and western Asia. It’s order Caryophyllales, family Amaranthaceae, Sub family Chenopodioideae. The leaves are commonly edible as a vegetable. The compost was applied with the six different combinations like Soil Control 100 % (C₁), Dairy Sludge + Leaf Litter 25 % (C₂), Dairy Sludge + Leaf Litter 50 % (C₃), Dairy Sludge + Leaf Litter 75 % (C₄). The physic-chemical and phytochemical parameters of soil and spinach plant respectively were analyzed after interval. The effect of enriched composted dairy sludge and leaf litter combination on physico-chemical character of soil was observed.

5.3. Effect of enriched compost on growth of *Spinacia oleracea*

After analysis of physico-chemical characters, the effect was observed on growth of *Spinacia oleracea* plant after interval. The growth was observed in terms of number of leaves and height of the plant. The effect of compost on a number of leaves of the *Spinacia oleracea* plant was observed. The Fig. 3 shows that C₂ (25%) was with high no. of leaves. The effect of compost on average number of leaves of spinach 15th days, 30th days, 45thday, and 60thday observation of plant leaves compared with other concentrations. The C₂

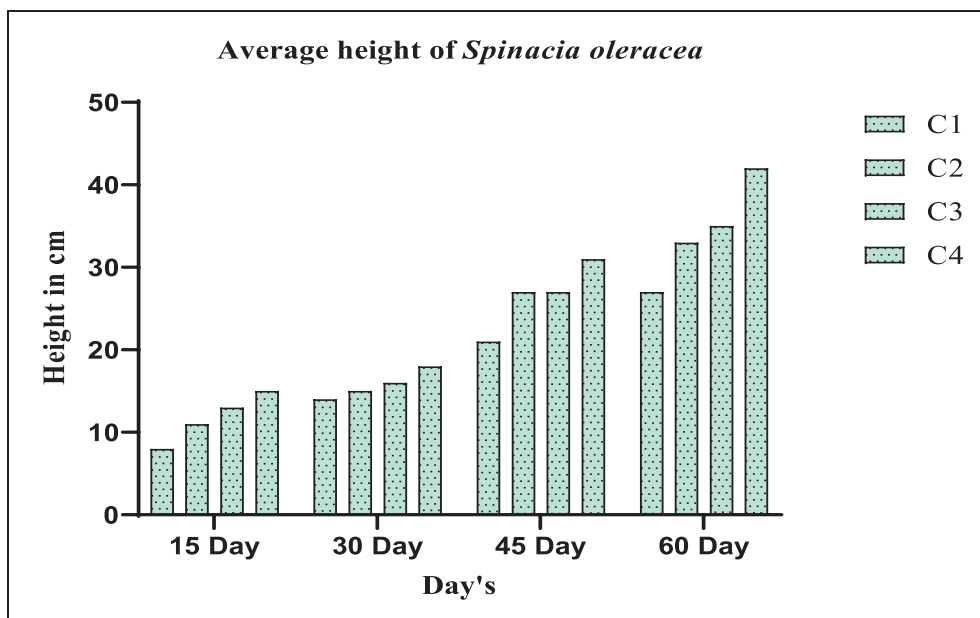


Fig. 2. Height (cm) Spinacia oleracea after using the compost.

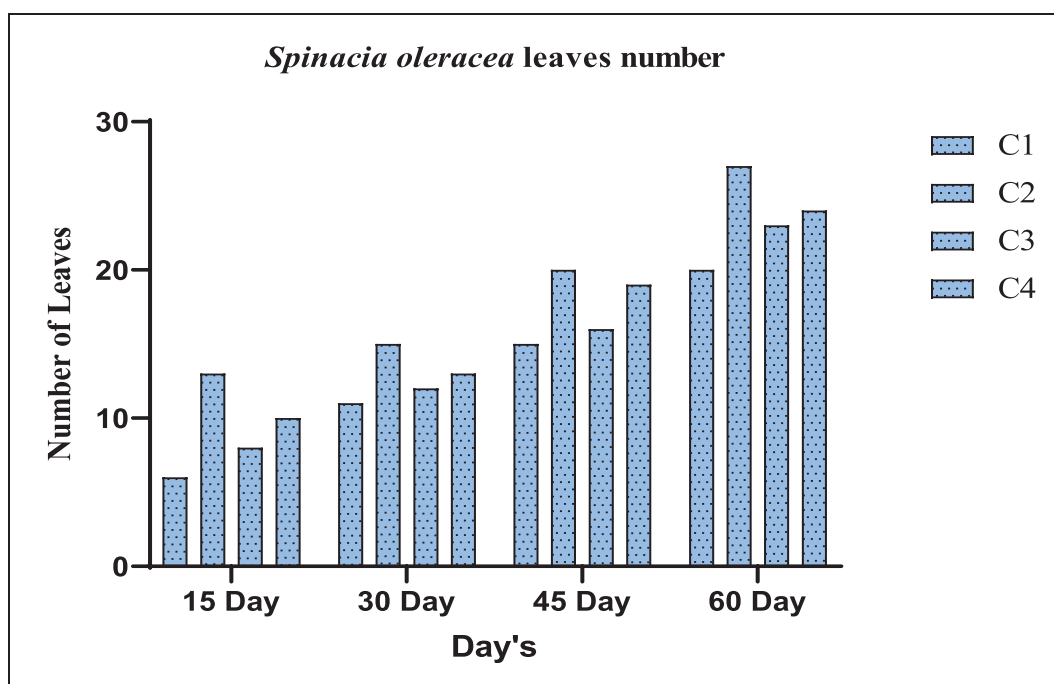


Fig. 3. Effect of compost on average number of leaves of Spinacia oleracea.

(25%) average number of leaves 18.75, whereas C₄ (75%) shows 16.5 average number of leaves. The soil combined with composting shows an increase in the number of leaves than the soil treated without composting, i.e. Control. It was observed Fig. 2 that the plant treated with C₂ (25%) combination shows maximum height i.e. 26.97 cm than other combinations. The combination shows the 18.02 cm C₁ (100%), 21.72 cm C₃ (50%), 23.12 cm C₄ (75%). Overall, the plants with combination i.e. C₂ (25%) showed more height and number of leaves.

The Fig.4 shows effect of compost on chlorophyll content of spinach plant showed the plants grow in higher concentration of chlorophyll content as compared to soil i.e. control. C₂ (25%) combi-

nation shows 1.12 ± 0.03 mg g⁻¹ and for C₄ (75%) it was 1.03 ± 0.05 mg g⁻¹, whereas other combination such as C₁, C₃ shows 0.78 ± 0.03 mg g⁻¹, and 0.97 ± 0.03 mg g⁻¹ of Chlorophyll content respectively. The higher chlorophyll content is the sign of physiological active healthy plants and those which are deprived in their nutritional condition showed poor growth and chlorosis. Chlorosis can be caused by a nutrient deficiency of iron or by magnesium or nitrogen consequently, processed pressmud is rich in nitrogen which is helpful to increase in the chlorophyll pigment level after application [45].

effect of compost on polyphenol content of spinach plant was observed where Fig. 5 shows the C₁ is less polyphenol content and

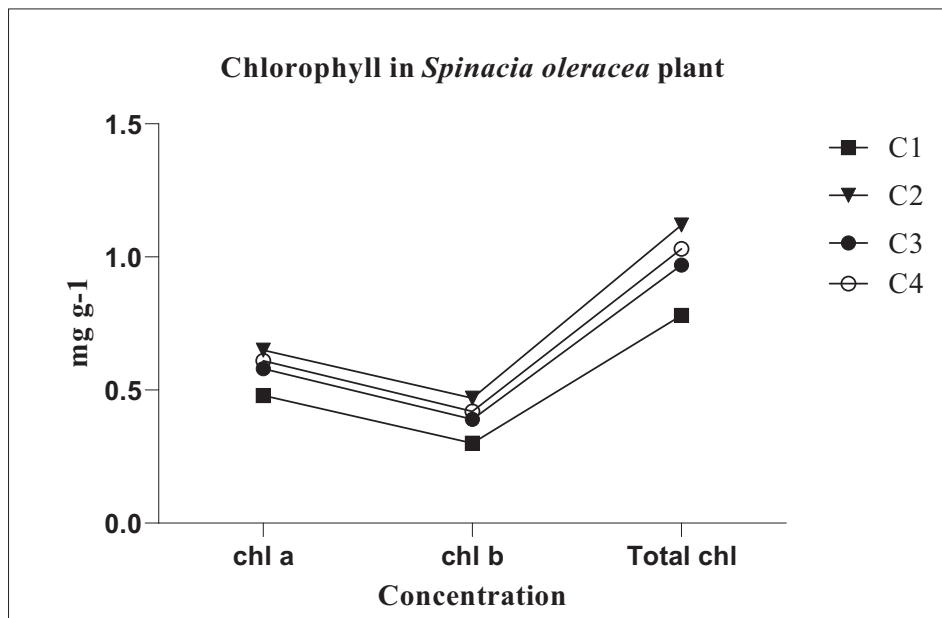


Fig. 4. Effect of compost on chlorophyll content of Spinacia oleracea.

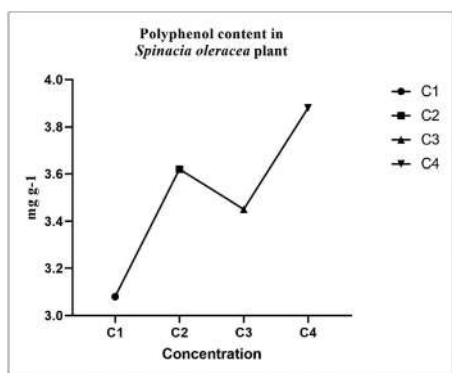


Fig. 5. Effect of compost on Polyphenol content of Spinacia oleracea.

it was 3.08 ± 0.02 mg g⁻¹ while C₃ shows 3.45 ± 0.01 mg g⁻¹ of polyphenol content whereas C₂, C₄ shows maximum polyphenol content, it was 3.62 ± 0.03 mg g⁻¹, and 3.88 ± 0.04 mg g⁻¹ respectively. Hence, the plants rich in antioxidant have established the greater attention and have been studied comprehensively, since they can reduce the risks for cardiovascular disease or several types of cancers [27]. Flavonoid content was found more in plants in C₂ and C₃ combination whereas in other combinations it was similar to that of plain soil. The Fig. 6 shows the flavonoid content of plant grown in C₂ recorded as 0.84 ± 0.03 mg g⁻¹, while flavonoid content of spinach plant grown in other combination, such as C₁, C₃, C₄ were recorded as 0.78 ± 0.03 , 0.81 ± 0.02 , 0.47 ± 0.02 mg g⁻¹ respectively. Flavonoids are the most important plant pigments for flower coloration. In higher plants, they are involved in UV filtration, symbiotic nitrogen fixation and floral pigmentation. They may act as a chemical messenger or physiological regulators [14].

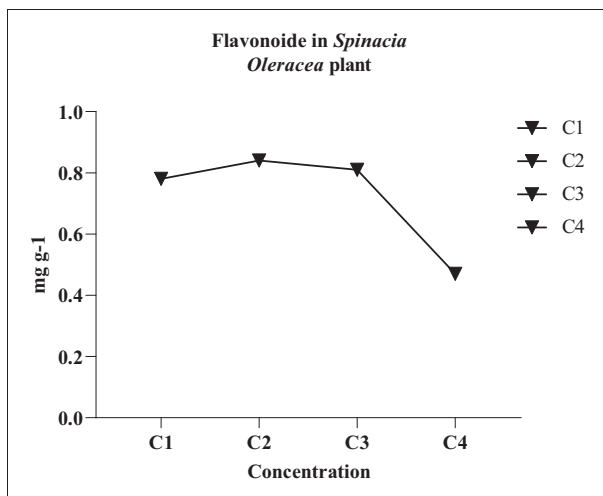


Fig. 6. Effect of compost on Flavonoid content of Spinacia oleracea.

5.4. Effects of compost improved with humus and growth of spinach plant

The spinach plant treated with different combination of Dairy and leaf litter waste showed variation in their height, number of leaves. The plants treated with combination of compost i.e. C₂ observed that maximum height 26.97 ± 12.45 cm and number of leaves 18.75 ± 6.23 per plant. Similarly C₄ combination also showed increase in height, number of leaves followed by C₃ and C₂ combination respectively. The plants improved quantitative and qualitative characteristics of plants and regulated the major and a minor nutrient to favorable concentration [34] it helps to enhance the growth and yield of plant. The influence of compost on the mineralized nitrogen content in soil depends, beyond the quality of available nitrogen, also on the microbiological activity of the compost. [12]. The utilization of organic fertilizer as source of plant nutrients has several benefits. The addition of organic matter is improving the ability to retain water, so the ability to provide ground water for plant growth increases. The addition of organic matter is improving soil infiltration as the result of rising soil macro pores and declining its micro pores [6]

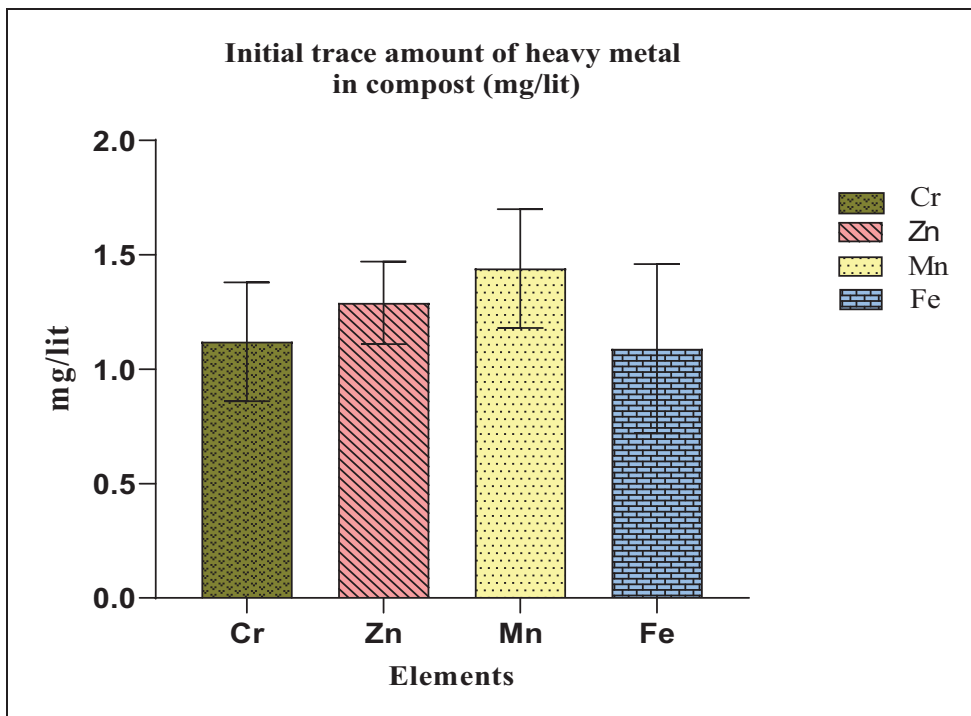


Fig. 7. Heavy metals of initial composting readings (mg/lit.).

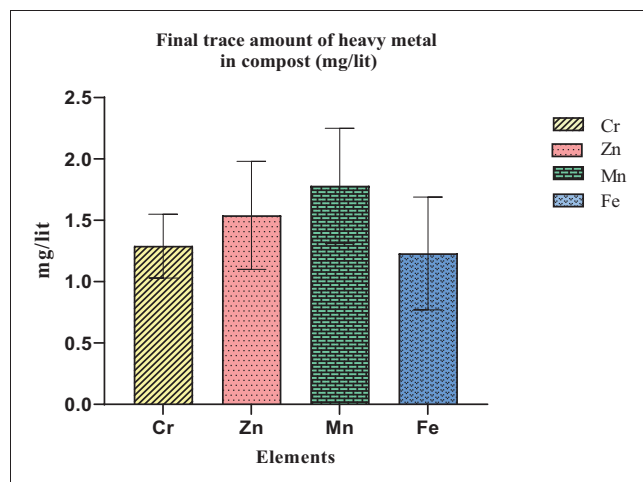


Fig. 8. Heavy metals of final composting readings (mg/lit.).

6. Conclusion

The outcome of the present study revealed that using combinations of agro industrial waste and litter helps to reduce the waste generated from Dairy industry, and leaf litter of Shivaji University Campus. The physicochemical and phyto-chemical characters showed good result in (Dairy Sludge + Leaf litter) 25 % and 75% compost combination as compare to other combination. This study indicate that both 25 % and 75 % can be promising good organic manure and to improve soil quality and for plant growth. The present study is concluded dairy sludge suitable growth medium and production cost of biofertilizers is reduced by reused the dairy sludge as substrate.

CRediT authorship contribution statement

Chougale Sanjivani Tanaji: Conceptualization, Methodology, Software, Writing – original draft. **Sarkale Prajka Shahaji:** Writing – review & editing. **Jadhav Aasawari Suhas:** Visualization, Investigation, Supervision, Validation.

Data availability

Data will be made available on request.

Declaration of Competing Interest

The authors declare that they have no known competing financial interests or personal relationships that could have appeared to influence the work reported in this paper.

Acknowledgements

We sincerely acknowledge the Department of Science & Technology, Government of IndiaPURSE Phase-II for providing financial assistance. We also convey our sincere thanks to Department of Environmental Science, Shivaji University, Kolhapur, for providing all research facilities to carry out this work.

References:

- [1] T.M. Agbede, S.O. Ojeniyi, A.J. Adeyemo, Effect of poultry manure on soil physical and chemical properties, growth and grain yield of sorghum in southwest, Nigeria, *Am. Eur. J. Sustain. Agric.* 2 (2008) 72–77.
- [2] L.E. Allison, Organic carbon in methods of soil analysis, part II. Ed., *Agronomy* 9 (1965) 1367–1378.
- [3] B.B. Al-Bataina, T.M. Young, E. Ranieri, Effects of compost age on the release of nutrients, *ISWCR* 4 (230–236) (2016), <https://doi.org/10.1016/j.iswcr.2016.07.003>.
- [4] S. Anusha, P. Paul, Stabilization of sludge from AAVIN dairy processing plant (Chennai) using vermicomposting, *J. Chem. Pharma. Res.* 7 (3) (2015) 846–851.
- [5] D. Astm, Test method for moisture, ash and organic matter of peat and organic soil, *Ann. Book ASTM Standards* 04 (1974) 1–4.

- [6] S.W. Atmojo, Role of Organic Matter and Soil Fertility Efforts Against Their Management, Inauguration Speech of Professor in Sciences Soil Fertility. UniversitasSebelasMaret, Surakarta, 2003.
- [7] C. Sreemoyee, P. Priti, Assessment of physico-chemical parameters of dairy Waste water and isolation and characterization of Bacterial strains in terms of cod reduction, *Int. J. Sci., Environ. Technol.* 2 (3) (2013) 395–400.
- [8] C. Crecchio, M. Curci, M.D.R. Pizzigallo, P. Ricciuti, P. Ruggiero, Effects of municipal solid waste compost amendments on soil enzyme activities and bacterial genetic diversity, *Soil Biol. Biochem.* 36 (10) (2004) 1595–1605.
- [9] Dean and John A., 1961, Flame photometry. M C Graw Hill Newyork, *SpectrochimicaActa.* 17, 127–127.
- [10] M. Divakar, M. Prasanthrajan, Composting of tree leaf litter using fruit based effective microorganism, *J. Pharmacogn. Phytochem.* 8 (4) (2019) 2663–2667.
- [11] Fuchs J.G (2009) Interactions between beneficial and harmful microorganisms: from the composting process to compost application. In: *Microbes at work: from wastes to resources.* pp 213–229.
- [12] Fuchs Jacques G., Berner Alfred., Mayer Jochen., Ena Smidt., Konrad Schleiss., (2008)., Influence of compost and digestates on plant growth and health: potentials and limits., *International congress, CH-Solothurn.*, pp 101-110.
- [13] J. Gabhane, S.P. William, R. Bidyadhar, P. Bhilawe, D. Anand, A.N. Vaidya, S.R. Wate, Additives aided composting of green waste: effects on organic matter degradation, compost maturity, and quality of the finished compost, *Bioresour. Technol.* 114 (2012) 382–388.
- [14] F. Galeotti, E. Barile, P. Curir, M. Dolci, V. Lanzotti, Flavonoids from carnation (*Dianthus caryophyllus*) and their antifungal activity, *PhytochemLett* 1 (2008) 44–48.
- [15] S. Goyal, S.K. Dhull, K.K. Kapoor, Chemical and biological changes during composting of different organic waste and assessment of compost maturity, *Bioresour. Technol.* 96 (14) (2005) 1584–1591.
- [16] T.X. Guan, H.B. He, X.D. Zhang, Z. Bai, Cu fractions, mobility and bioavailability in soil–wheat system after Cu-enriched livestock manure applications, *Chemosphere* 82 (2) (2011) 215–222.
- [17] S. Gul, A. Naz, A. Khan, S. Nisa, M. Irshad, Phytoavailability and leachability of heavy metals from contaminated soil treated with composted livestock manure, *Soil Sediment Contam.* 25 (2) (2016) 181–194.
- [18] G.F. Huang, J.W.C. Wong, Q.T. Wu, B.B. Nagar, Effect of C/N on composting of pig manure with sawdust, *Waste Manag. (Oxford)* 24 (2004) 805–813.
- [19] IDF (International Dairy Federation), 2000. Disposal and utilization of dairy sludge. *Bulletin of the International Dairy Federation* 356, 3–34.
- [20] N. Inyim, A study on dry leaf composting in reused small- size bottle, *J. Adv. Agric. Technol.* 6 (1) (2019) 38–42.
- [21] Juliastuti S. R., Rian Setya Budi , and Taufiqurrsyidi (2014), Pretreatment of Sludge Milk Waste as Source Of Composting using Microbes, *IPTEK, Journal of Proceeding Series*, Vol. 1, 306-310.
- [22] T. Karak, P. Bhattacharyya, R.K. Paul, T. Das, S.K. Saha, Evaluation of composts from agriculture wastes with pond sediment as bulking agent to improve compost quality, *Clean –Soil Air Water* 41 (7) (2013) 711–723.
- [23] K.G. Karmakar, G.D. Banerjee, Opportunities and challenges in the Indian dairy industry, *Tech. Digest* 9 (2006) 24–27.
- [24] R. Khaleel, K.R. Reddy, M.R. Overcash, Changes in soil physical properties due to organic waste application: a review, *J. Environ. Qual.* 10 (1981) 133–141.
- [25] K. Elsayed, Some physical and chemical properties of compost, *Int. J. Waste Recour.* 5 (1) (2015) 1–5.
- [26] J. Kjeldahl, A new method for the determination of nitrogen in organic matter, *J. Anal. Chem.* 22 (1883) 366–382.
- [27] D. Kromhout, A. Menotti, B. Bloemberg, C. Aravanis, H. Blackburn, R. Buzina, A. S. Dontas, F. Fidanza, S. Giaipali, A. Jansen, M. Karvonen, M. Katan, A. Nissinen, S. Nedeljkovic, J. Pekkanen, M. Pekkarinen, S. Punsar, L. Rasanen, B. Simic, H. Toshima, Dietary saturated and trans fatty acids and cholesterol and 25-year mortality from coronary heartdisease: the Seven Countries study, *Prev. Med.* 24 (3) (1995) 308–315.
- [28] G.X. Li, F.S. Zhang, *Solid wastes composting and organic Fertilizer Production*, Chemical Engineering Press, Beijing, 2000.
- [29] Liang C., R.W. Mc. Clendon. 2003. The influence of temperature and moisture content regimes on the aerobic microbial activity of biosolids composting blend. Vol.86. 2.Pp.131-137.
- [30] Maithi S. K., 2003. *Handbook of Methods in Environmental studies.* Air, Noise, Soil and Overburden analysis, ABD Publishers, Jaipur. ISBN 81-85771-58-8. 1-250.
- [31] A.S. Mangrich, M.C. Cardoso, M.E. Doumer, L.P.C. Romão, M. Vidal, A. Rigol, E.H. Novotny, Improving the water holding capacity of soils of northeast brazil by biochar augmentation, *Am. Chem. Soc.* (2015) 340–354.
- [32] D. Muhammad, R.A. Khattak, Growth and nutrient concentration of maize in pressmud treated saline-sodic soils, *Soil Environ.* 28 (2009) 145–155.
- [33] S.R. Olsen, C.V. Cole, F.S. Watanabe, L.A. Dean, Estimation of available phosphorus in soil by extraction with sodium bicarbonate, *USDA Circular* 939 (1954) 1–19.
- [34] T. Paul, S.K. Halder, A. Das, S. Bera, C. Maity, A. Mandal, P.S. Das, P.K. Das Mohapatra, B.R. Pati, K.C. Mondal, Exploitation of chicken feather waste as a plant growth promoting agent using keratinase producing novel isolate *Paenibacilluswoosongensis* TKB2, *BiocatalAgricBiotechnol.* 2 (2013) 50–57.
- [35] D. Purves, Trace elements contamination of the environment, Elsevier, Amsterdam, 1985, p. 273.
- [36] D. Said-Pullicino, F.G. Erriquens, G. Gigliotti, Changes in the chemical characteristics of water-extractable organic matter during composting and their influence on compost stability and maturity, *Bioresour. Technol.* 98 (2007) 1822–1831.
- [37] M.A. Sanchez-Monedero, A. Roig, C. Paredes, M.P. Bernal, Nitrogen transformation during waste composting by the Rutgers system and its effects on pH, EC and maturity of the composting mixtures, *Bioresour. Technol.* 78 (2001) 301–308.
- [38] A. Sangodoyin, A. Amori, Aerobic composting of cassava peels using cow dung, sewage sludge and poultry manure as supplements, *EIJST* 2 (2013) 22–34.
- [40] L.E. Sommers, Chemical composition of sewage sludge and analysis of their potential use as fertilizer, *J. Environ. Qual.* 6 (1977) 225–229.
- [41] S. Leena, S.G.T. Vincent, Bio- composting of Latex ETP sludge and effect of latex compost on cowpea, *J. Global Biosci.* 6 (8) (2017) 5177–5188.
- [42] T. Carl, T. Annang, N. Solomon, D. Tawiah, Effect of the composting process on physicochemical properties and concentration of heavy metals in market waste with additive materials in the Ga west municipality, Ghana, *Int. J. Recycl. Org. Waste Agric.* 8 (2019) 393–403, <https://doi.org/10.1007/s40093-019-0266-6>.
- [43] Q. Wang, R. Li, H. Caia, M.K. Awasthi, Z. Zhang, J.J. Wang, A. Ali, M. Amanullah, Improving pig manure composting efficiency employing Ca- Bentonite, *Ecol. Eng.* 87 (2016) 157–161.
- [44] J.-C. Wong, S.O. Fung, A. Selvam, Coal fly ash and lime addition enhances the rate and efficiency of decomposition of food waste during composting, *Bioresour. Technol.* 100 (13) (2009) 3324–3331.
- [45] P.J. Zarco-Tejada, J.R. Miller, A. Morales, A. Berjón, J. Agüera, Hyperspectral indices and model simulation for chlorophyll estimation in open-canopy tree crops, *Remote Sens. Environ.* 90 (4) (2004) 463–476.



Variation in band gap of antimony doped ZnO nanostructures with doping concentration

Leena.M. Mahajan

Department of Electronics, K V N Naik Arts, Commerce and Science College, Nashik, India

ARTICLE INFO

Article history:

Available online 14 October 2022

Keywords:

ZnO nanostructures
Sol-gel spin coating
XRD
FESEM

ABSTRACT

ZnO nanostructures were doped with antimony and characterized for structural and optical properties. ZnSbO thin films were fabricated by sol-gel spin coating technology. Structural properties of ZnSbO thin films were investigated by X-ray analysis and FESEM. For determination of transmittance and band gap, UV spectrophotometer characterization was done. XRD reveals single crystal wurtzite structure of ZnSbO thin films. Also results decrease in grain size with doping concentration of antimony in zinc oxide thin films. FESEM and EDAX shows the incorporation of antimony in ZnO. UV spectrophotometer shows increase in transmittance and band gap with doping concentration of antimony in zinc oxide. These results can explore in optoelectronics field.

Copyright © 2022. Elsevier Ltd. All rights reserved.

Selection and peer-review under responsibility of the scientific committee of the Integrative Nanotechnology Perspective for Multidisciplinary Applications - 2022.

1. Introduction

In this work, sol-gel spin coating fabricated Sb doped ZnO nanostructures were analyzed. It is a good alternative to tin doped Indium oxide due to the low cost and absence of any toxicity [1–5]. ZnO represents an optical transparent conducting material [6] due to wide band gap. Crystal defects, controlled by the deposition procedures, strongly affect optical properties [7]. Bi and Sb doping is convenient to modify conduction properties [8,9]. Small quantity of additional dopant increases the nonlinear optical and electrical Properties. [10,11].

The fabrication of stable and reproducible p-type ZnO nanostructures thin films are still not well understood. Group V elements N [12], P [13], As [14], Bi [15] and Sb [16,17] are well known to be the most suitable dopants for p-type ZnO. Among various doping element, Bismuth and Antimony has attracted much attention as a dopant of ZnO [18,19]. Many workers recently used dopants like iron, nickel, and even silver to enhance the physical properties in many ways. The effect of doping in these works clearly suggests that the metal levels are gathered around conduction band to form a new set of continuum which decreases the optical band gap energy of ZnO [20,21]. The decrease in band due to formation of new energy fermi levels can be effectively achieved by transition metals however, it is now reported that the metalloids from p-block can be a suitable dopant and much more efficient than conventional transition metals [22,23].

The dopants do not directly substitute for the oxygen elements in ZnO, the vacancies near extended defects, such as stacking faults and dislocations in ZnO structures are expected to be important to accommodating the large dopants in ZnO films. Bi and Sb have been suggested as promising dopant that may produce more stable p-type conductivity and higher hole concentrations.

In this work, we elaborate the fabrication of Sb doped ZnO thin films using sol-gel spin coating method. Characterizations of deposited films for structural, optical and electrical properties were analyzed.

2. Methodology

ZnO and Sb doped ZnO thinfilms were deposited on glass substrates using sol-gel spin coating technique. Zinc acetate dihydrate ($\text{Zn}(\text{CH}_3\text{COO})_2 \cdot 2\text{H}_2\text{O}$), 2methoxy ethanol ($\text{CH}_3\text{O}(\text{CH}_2)\text{OH}$), antimony acetate, were used as a starting precursor. The mixture of the solution was vigorously stirred on hot magnetic plate at 60°C for 1 h. This prepared solution was used for spin coating after the aging of the solution for 24 h. The samples were coated repeatedly for ten times to get desired thickness. For ten times coating, thickness obtained in the range of 140 to 150 nm. Preheating treatment is given to samples after each coating and cooled down at room temperature. The deposited samples were post annealed at 350°C temperature in open air for one hour. Annealed samples were characterized for structural and optical properties.

3. Results and discussion

3.1. XRD analysis

Fig. 1 shows the XRD patterns of Zn_{1-x}Sb_xO thin films with x = 0.005, 0.01, 0.015. All the peaks in the XRD patterns are indexed to hexagonal structure. A strong (002) peak of ZnO can indicate the films have a preferred orientation along the c-axis normal to the glass substrate. As the amount of doped antimony increased, the intensity and angle of (002) diffraction peak are also decreased and increased respectively. The XRD results suggest that the addition of Sb atoms leads to an inhibition of the crystal growth along the c-axis. Grain size, FWHM calculated from the XRD patterns are presented in Table 1.

The grain sizes were estimated by applying the Scherer's equation to the full width half maximum (FWHM) of the (002) reflection of ZnO. Calculated grain sizes are 16.14 nm, 14.09 nm and 12.595 nm for 0.5 %, 1 % and 1.5 % of Sb concentration respectively. Which is less than grain size of pure zinc oxide thin film.

3.2. SEM and EDAX analysis

Figs. 2 and 3 shows FESEM images and EDAX mapping images of 1 % ZnSbO thin films. Field emission scanning electron microscopy

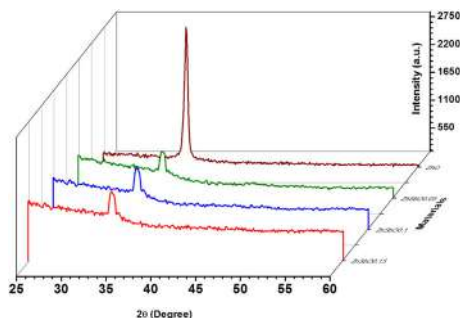


Fig. 1. XRD pattern of ZnO, 0.5%, 1% and 1.5% ZnSbO thin films.

Table 1
Crystallographic data of ZnSbO thin films.

Antimony concentration	2θ (°)	Intensity	FWHM (°)	Grain size (nm)
0(ZnO)	34.55	2953	0.25	33.3
0.5	34.34	1015	0.515	16.14
1	34.21	1106	0.59	14.097
1.5	34.2	1058	0.66	12.595

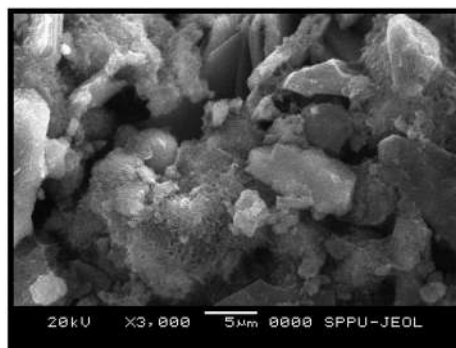


Fig. 2. FESEM image of 1% doped ZnSbO thin films.

exhibits uniform granular structure of the deposited samples. The image was revealed that the product has high density. Images of the thin films were taken at the scale of 5 µm with magnification of 3,000. No voids and cracks were observed on the films. Dispersive X-ray Analysis (EDAX) was performed to find out the concentration of deposited elements. Fig. 3 shows the strong peaks of Zn, O and weak peak of Sb. Moreover, the concentration of Sb in ZnO were obtained 0.87 % for 1 % ZnSbO thin films.

3.3. UV-Visible spectroscopy

Fig. 4 shows the optical transmission spectra of Sb doped ZnO thin films with Sb content of 0.5 %, 1 %, 1.5 % and pure ZnO. The films present high transmittance in the visible region and are highly absorbing in the UV range. The transmittance of the films was observed more than 80 % in the visible which informs about the presence of low defects density and good quality of the films [24]. For all films we can see a sharp decrease, at about 390 nm, relate to the band gap absorption. The average optical transmittance of doped ZnO films as a function of doping concentration was shown in inset of Fig. 4. In order to calculate the optical band gap energy (E_g) of the thin films, we used the formula $(\alpha h\nu)^2 = A(h\nu - E_g)$ At this juncture, α is absorption coefficient, A is constant; $h\nu$ is photon energy and E_g is band gap.

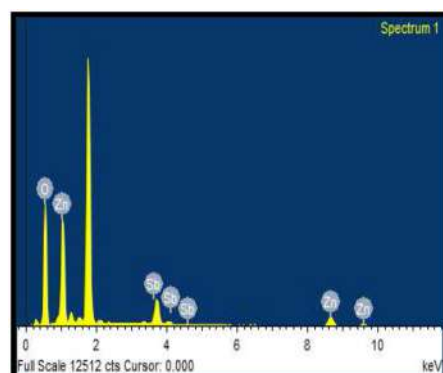


Fig. 3. EDAX of 1% doped ZnSbO thin films.

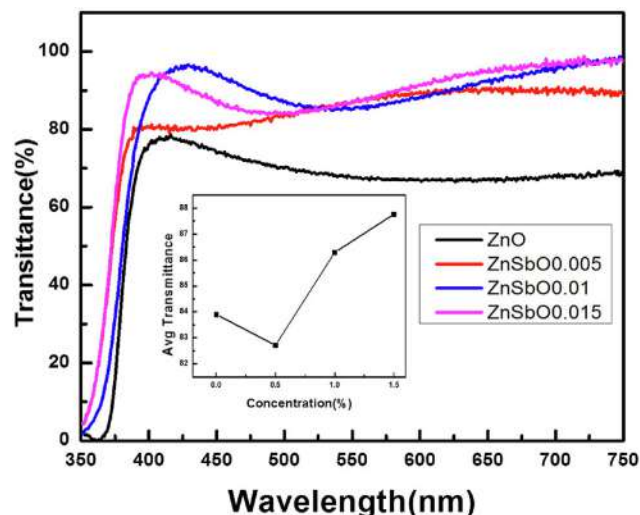


Fig. 4. Transmittance spectra of ZnO, 0.5%, 1% and 1.5% ZnSbO thin films. Inset: Plot of Average Transmittance vs Antimony concentration.

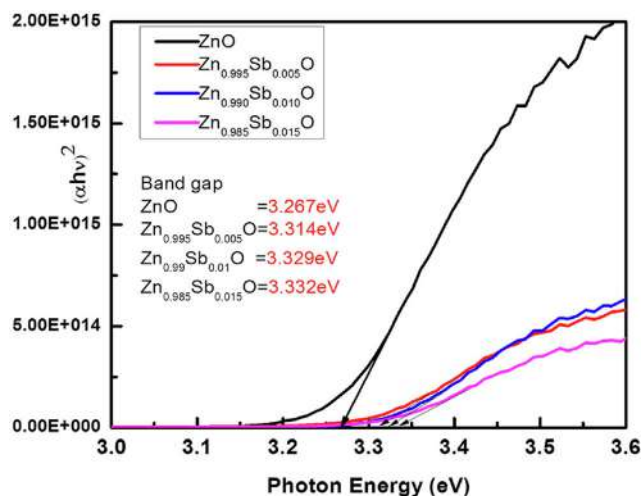


Fig. 5. Band gap estimation of 0%, 0.5%, 1%, 1.5% ZnSbO thin films.

Table 2

Transmittance data of 0%, 0.5%, 1% and 1.5% ZnSbO thin films.

Antimony concentration (%)	Average Transmittance (%)	Band Gap (eV)	FOM
0	85.28465	3.267	1.9138E-10
0.5	91.57675	3.314	5.41E-11
1	91.4281	3.329	8.9785E-11
1.5	92.53568	3.332	5.9473E-11

Fig. 5 showed plot of photon energy versus absorption coefficient for ZnO films with various Sb doping concentration. The extrapolation of the linear region of the curves gives the band gap values. The band gap values of the films were noted in the Table 2. The Sb^{3+} ions affect the localized regions in band gap with the formation of active levels leading to a decrease in optical band gap [25,26]. From 0.5 % to 1.5 % Sb doping, the band gap values show an increase. The corresponding transmittance data is summarized in Table 2.

4. Conclusion

Antimony doped films with different concentration were successfully deposited by spin coating technique. Films were studied and observation shows dramatically decrease in grain size with hexagonal structure measured by XRD pattern. Grain size decreases from 33.3 nm to 12.595 nm. by antimony doping. Grain size reduced due to the lattice distortion caused by difference between dopant antimony atom and replaced element. FESEM and EDAX confirm incorporation of Sb in ZnO. Transmittance of ZnSbO films shows more than 80 % average values of transmittance. More than 80 % transmittance is indicated good optical properties of the deposited films. Figure of merit values shows the good quality of deposited films. Band gap is increased from 3.267 eV to 3.332 eV in ZnSbO films. These results can be explored for use of ZnSbO films in optoelectronics device.

CRedit authorship contribution statement

Leena.M. Mahajan: Writing – original draft, Data curation, Writing – original draft, Visualization, Writing – review & editing.

Data availability

No data was used for the research described in the article.

Declaration of Competing Interest

The authors declare that they have no known competing financial interests or personal relationships that could have appeared to influence the work reported in this paper.

References

- [1] M. Kazeoka, H. Hiramatsu, W.-S. Seo, K. Koumoto, Improvement in thermoelectric properties of $(\text{ZnO})_5\text{In}_2\text{O}_3$ through partial substitution of yttrium for indium, *J. Mater. Res.* 13 (3) (1998) 523–526.
- [2] X. Wu, T.J. Coutts, W.P. Mulligan, Properties of transparent conducting oxides formed from CdO and ZnO alloyed with SnO_2 and In_2O_3 , *J. Vacuum Sci. Technol. A: Vacuum, Surf., Films* 15 (3) (1997) 1057–1062.
- [3] G.B. Palmer, K.R. Poepplmeier, T.O. Mason, Conductivity and transparency of ZnO/ SnO_2 -cosubstituted In_2O_3 , *Chem. Mater.* 9 (12) (1997) 3121–3126.
- [4] R. Wang, A.W. Sleight, D. Cleary, High conductivity in gallium-doped zinc oxide powders, *Chem. Mater.* 8 (2) (1996) 433–439.
- [5] W. Tang, D.C. Cameron, Aluminum-doped zinc oxide transparent conductors deposited by the sol-gel process, *Thin Solid Films* 238 (1) (1994) 83–87.
- [6] Ohtomo, A., M. Kawasaki, T. Koida, K. Masubuchi, H. Koinuma, Y. Sakurai, Yasuda Yoshida, T. Yasuda, and Y. Segawa. "Mg_xZn_{1-x}O as an II–VI widegap semiconductor alloy." *Applied physics letters* 72, no. 19 (1998): 2466–2468
- [7] V. Srikant, D.R. Clarke, Anomalous behavior of the optical band gap of nanocrystalline zinc oxide thin films, *J. Mater. Res.* 12 (6) (1997) 1425–1428.
- [8] K. Djembo-Taty, L. Plaindoux, J. Kossanyi, J.C. Ronfard-Haret, Conduction électrique dans les électrodes polycristallines de ZnO semiconducteur. Importance des joints de grains, *J. Chim. Phys. Phys.-Chim. Biol.* 95 (3) (1998) 595–616.
- [9] Y. Shimizu, F.-C. Lin, Y. Takao, M. Egashira, Zinc oxide varistor gas sensors: II, effect of chromium (III) oxide and yttrium oxide additives on the hydrogen-sensing properties, *J. Am. Ceram. Soc.* 81 (6) (1998) 1633–1643.
- [10] S. Bernik, P. Zupančič, D. Kolar, Influence of $\text{Bi}_2\text{O}_3/\text{TiO}_2$, Sb_2O_3 and Cr_2O_3 doping on low-voltage varistor ceramics, *J. Eur. Ceram. Soc.* 19 (6–7) (1999) 709–713.
- [11] G. Agarwal, R.F. Speyer, Effect of rate controlled sintering on microstructure and electrical properties of ZnO doped with bismuth and antimony oxides, *J. Mater. Res.* 12 (9) (1997) 2447–2454.
- [12] G. Wang, H. Wang, Y. Ling, Y. Tang, X. Yang, R.C. Fitzmorris, C. Wang, J.Z. Zhang, Y. Li, Hydrogen-treated TiO_2 nanowire arrays for photoelectrochemical water splitting, *Nano Lett.* 11 (7) (2011) 3026–3033.
- [13] C.X. Shan, Z. Liu, S.K. Hark, Temperature dependent photoluminescence study on phosphorus doped ZnO nanowires, *Appl. Phys. Lett.* 92 (7) (2008) 073103.
- [14] Q. Zhang, S. Yodyingyong, J. Xi, D. Myers, G. Cao, Oxide nanowires for solar cell applications, *Nanoscale* 4 (5) (2012) 1436–1445.
- [15] A. Gulino, I. Fragala, Deposition and characterization of transparent thin films of zinc oxide doped with Bi and Sb, *Chem. Mater.* 14 (1) (2002) 116–121.
- [16] J.-W. Kang, Y.-S. Choi, M. Choe, N.-Y. Kim, T. Lee, B.-J. Kim, C.W. Tu, S.-J. Park, Electrical and structural properties of antimony-doped p-type ZnO nanorods with self-corrugated surfaces, *Nanotechnology* 23 (49) (2012) 495712.
- [17] C.-L. Hsu, K.-C. Chen, T.-J. Hsueh, UV photodetector of a homojunction based on p-type Sb-doped ZnO nanoparticles and n-type ZnO nanowires, *IEEE Trans. Electron Devices* 61 (5) (2014) 1347–1353.
- [18] S. Limpijumngong, S.B. Zhang, S.-H. Wei, C.H. Park, Doping by large-size-mismatched impurities: the microscopic origin of arsenic- or antimony-doped p-type zinc oxide, *Phys. Rev. Lett.* 92 (15) (2004).
- [19] J.K. Liang, H.L. Su, P.Y. Chuang, C.L. Kuo, S.Y. Huang, T.S. Chan, Y.C. Wu, J.C.A. Huang, Origin of p-type conductivity of Sb-doped ZnO nanorods and the local structure around Sb ions, *Appl. Phys. Lett.* 106 (21) (2015) 212101.
- [20] Waghchaure, Ravindra Haribhau, Vishnu Ashok Adole, Babu Sonu Jagdale, and Prashant Bhimrao Koli. "Fe³⁺ modified zinc oxide nanomaterial as an efficient, multifaceted material for photocatalytic degradation of MB dye and ethanol gas sensor as part of environmental rectification." *Inorganic Chemistry Communications* 140 (2022): 109450

- [21] R.S. Shinde, S.D. Khairnar, M.R. Patil, V.A. Adole, P.B. Koli, V.V. Deshmane, D.K. Halwar, R.A. Shinde, T.B. Pawar, B.S. Jagdale, A.V. Patil, Synthesis and characterization of ZnO/CuO nanocomposites as an effective photocatalyst and gas sensor for environmental remediation, *J. Inorg. Organomet. Polym Mater.* 32 (3) (2022) 1045–1066.
- [22] R.S. Shinde, R.A. More, V.A. Adole, P.B. Koli, T.B. Pawar, B.S. Jagdale, B.S. Desale, Y.P. Sarnikar, Design, fabrication, antitubercular, antibacterial, antifungal and antioxidant study of silver doped ZnO and CuO nano candidates: a comparative pharmacological study, *Curr. Res. Green Sustain. Chem.* 4 (2021) 100138.
- [23] Shinde, Sachin Girdhar, Maheshkumar Prakash Patil, Gun-Do Kim, and Vinod Shankar Shrivastava. "Multi-doped ZnO photocatalyst for solar induced degradation of indigo carmine dye and as an antimicrobial agent." *Journal of Inorganic and Organometallic Polymers and Materials* 30, no. 4 (2020): 1141-1152
- [24] G. Kim, J. Bang, Y. Kim, S.K. Rout, S.I. Woo, Structural, electrical and optical properties of boron doped ZnO thin films using LSMCD method at room temperature, *Appl. Phys. A* 97 (4) (2009) 821–828.
- [25] S. Guo, Z. Du, S. Dai, Analysis of Raman modes in Mn-doped ZnO nanocrystals: Analysis of Raman modes in Mn-doped ZnO nanocrystals, *Phys. Stat. Sol. (b)* 246 (10) (2009) 2329–2332.
- [26] T.K. Pathak, V. Kumar, L.P. Purohit, High quality nitrogen-doped zinc oxide thin films grown on ITO by sol-gel method, *Phys. E: Low-dimensional Syst. Nanostruct.* 74 (2015) 551–555.



Removal of nitrate from aqueous solution by using orange peel and wheat straw

Sarkale Prajkta Shahaji, Chougale Sanjivani Tanaji, Jadhav Aasawari Suhas*

Department of Environmental Science, Shivaji University, Kolhapur, India

ARTICLE INFO

Article history:
Available online 1 November 2022

Keywords:
Nitrate
Wheat straw
Orange peel
Adsorbent
Adsorption isotherm

ABSTRACT

Increasing nitrate contamination in water bodies causing various human health and environmental challenges. Nitrate enters the human body through the drinking water and causes number of health issues such as methaemoglobinemia, gastric cancer, hormonal imbalance disorder, birth malformations, hypertension etc. when present in high concentration in drinking water. Hence there is strong need for economic and ecofriendly technology to treat the excess nitrate from water.

There are chemical and physical methods are available for removal of nitrate but as compare to such methods biological methods are considered to be an effective solution due to its low cost, easy availability and high efficiency. The present study aims to examine the efficiency of orange peel and wheat straw an adsorbent for removal of nitrate from aqueous solution. The batch method was used to study the adsorption. The obtained results from the batch experiment have shown the ability of both the adsorbents in removing nitrate. The optimum bio-adsorption of nitrate over orange peel and wheat straw bio-adsorbent was obtained at contact time = 3 hr., Quantity of adsorbent = 3 g and initial concentration = 700 mg/l. Obtained results from batch experiment found that the orange peel is more efficient than wheat straw for nitrate removal. Adsorption isotherm was described by Langmuir isotherm model and model fitted well.

Therefore, the adsorbents are efficient and cost effective in the treatment of nitrate contaminated water.

© 2022 Elsevier Ltd. All rights reserved.

Selection and peer-review under responsibility of the scientific committee of the Integrative Nanotechnology Perspective for Multidisciplinary Applications - 2022.

1. Introduction

Water is an essential component for all life forms. It's available in various resources such as river, lake, spring, ground water etc., but due to the developmental activities there is scarcity of available water resources. Anthropogenic activities are responsible for contamination of water resources by pollutants. Water pollution represents risk to the human health and environment.

Nitrogen is essential to life on earth, but it is becoming a crucial environmental issue due to its increasing use in chemical fertilizers and the intensive development of industrial activity [1]. In recent years the quality of potable water has been negatively impacted by agricultural, commercial and industrial activities and has experienced rising nitrate (NO_3) levels [2].

Several nitrogenous compounds, including ammonia, nitrite and nitrate have been frequently present in drinking water and various types of agricultural, domestic and industrial wastewater [3]. Among these, nitrogen containing fertilizers are regarded as the crucial source of nitrate contamination in groundwater [4]. Synthetic fertilizer wastes contain enormous quantities of nitrates. This nitrate is also the end products of aerobic stabilization of organic nitrogen [5].

Further, nitrate in drinking water may also cause blue baby syndrome due to the conversion of hemoglobin to methemoglobin, which cannot carry oxygen [6]. High concentration also causes gastric & intestinal cancer [7]. Besides this gastric cancer, hypothyroidism, hormonal imbalance disorder, birth malformations and growing hypertension in the human beings is also attributed to the increased concentration of nitrate in the water [7].

Different organizations and countries have set standards for NO_3 in potable water to safeguard public health from the hazards

Abbreviations: G, Gram; ml, Millilitre; Hr, Hour; NO_3 , Nitrate.

* Corresponding author.

E-mail address: asj_env@unishivaji.ac.in (J. Aasawari Suhas).

associated with high concentration of nitrate [8]. The World Health Organization (who) standard has set the allowable maximum concentration of nitrate in drinking water 50 mg/l [9].

Nitrate removal from water is challenging task for researchers because of its high stability and solubility [10]. Therefore, the removal of nitrate from water is a very critical and essential topic and has attracted a considerable attention [11].

Various technologies, such as sorption, ion exchange, reverse osmosis, electro dialysis, chemical reaction and biological transformation have been developed to remove nutrients and pesticides from wastewater or prevent them from entering into water system [12]. However, this technology generally involves high investments or operational cost. In addition, there is insufficient removal of nutrients, e.g., total nitrogen (TN) and total phosphorous (TP) in the secondary effluent of conventional biological wastewater treatment processes [13].

Adsorption is the process that occurs when a gas or liquid solute accumulates on the surface of a solid or liquid (adsorbent), forming a molecular or atomic film [26]. Adsorption is very cheap and effective compared to other methods [30]. Adsorption has been a widely used technology for NO_3^- removal. The technique utilizes any of the following adsorbents: carbon based adsorbents, natural adsorbent, agricultural or industrial waste adsorbents. The corresponding nitrate adsorption mechanism could be identified as electrostatic attraction, anion exchange or pore adsorption [14]. Agricultural by products are usually composed of lignin and cellulose as major constituents and may also include other polar functional groups of lignin which includes alcohol, aldehydes, ketones, carboxylic, phenolic and other groups, these groups have ability to bind aquatic pollutant through different binding mechanisms [27]. The solid material used for the adsorption consists of a porous medium with a high internal surface area [28].

In the present work we have used orange peel and wheat straw as bio-adsorbent for nitrate removal from aqueous solution. Various parameters like contact time, adsorbent dose and initial concentration have been investigated.

2. Materials and methodology

Adsorbents:

1 Preparation of adsorbent by Orange peel powder (*Citrus reticulata*).

Peels of the orange fruit are collected from local area. Washed them with distilled water and dried in a hot oven at 100 °C for 24 h. After drying, peels were grinded with grinder. After grinding, the peel powder was stored in air tight container for further use.

2 Preparation of adsorbent by Wheat straw powder (*Triticum aestivum*).

Wheat straw collected from nearby farms and washed with distilled water, dried in a hot oven at 100 °C for 24 h. Oven dried wheat straw grinded with grinder to prepare fine powder. This prepared powder was kept in air tight container for further use.

Adsorbate:

The aqueous solution of varied concentrations of nitrate was prepared. A nitrate aqueous solution of 500 mg/l and 700 mg/l was prepared by dissolving 36.1 g of KNO_3 and 50.5 g of KNO_3 respectively in 100 ml of distilled water.

Batch mode adsorption experiment:

Experiment was carried out by using Batch method [29]. Effect of several parameters (Adsorbent dosage, agitation time and initial concentration) on adsorption of nitrate on pretreated orange peel powder and wheat straw powder as adsorbent was studied. In the batch adsorption method, 100 ml of nitrate solution of known concentration were agitated with dosage varying from 1 g to 3 g for both the adsorbents. A retention time of 1 to 4 h were provided. At

the end of experiment, sample was filtered through Whatman no. 42 filter paper.

Estimation of nitrate (NO_3^-)

By using brucine method

This method is based upon the reaction of nitrate ion with brucine sulphate in a concentrated sulphuric acid. After reaction it forms yellow colour which is measured photometrically. This method is applicable to the analysis of drinking, surface and ground water, domestic and industrial wastes.

Final concentration of nitrate was determined after each hour by spectrophotometer at 510 nm wavelength.

Nitrate removal efficiency was calculated by using following formula [15].

$$\text{Removal efficiency}(\%) = \frac{C_o - C_f}{C_o} \times 100$$

Where,

C_o = initial concentration of adsorbate.

C_f = final concentration of adsorbate.

Adsorption test

The adsorption capacity (q_e) determined using Eq. (1) [32].

$$q_e = \frac{(c_i - c_e)}{W} \times V$$

Where q_e represents the adsorption capacity (mg/g) and C_i and C_e respectively represents initial concentration and equilibrium concentration. Where, V stands for volume (L), W stands for the mass (g) of the adsorbent.

Adsorption isotherm were applied to represent (Langmuir) was applied to explain the equilibrium adsorption characteristics Eq. (2) [32] represents the Langmuir's isotherm.

$$q_e = \frac{q_{max} K_L C_e}{1 + K_L C_e}$$

The Langmuir's isotherm was transformed into its linear form, as represented in Eq. (3) [32] to determine the adsorption of parameters.

$$\frac{1}{q_e} = \frac{1}{K_L q_{max}} \cdot \frac{1}{C_e} + \frac{1}{q_{max}}$$

Where, q_{max} represents the maximum adsorption capacity (mg/g) and K_L (L/mg) is the Langmuir's isotherm constant which shows the binding affinity between nitrate and adsorbents. The separation factor (R_L) was calculated using Eq. (4) [32].

$$R_L = \frac{1}{1 + C_i \times K_L}$$

There are four probabilities for R_L values. Where, R_L is the dimensionless Langmuir constant which indicate the adsorption possibility either favorable ($0 < R_L < 1$), unfavorable ($R_L > 1$), linear ($R_L = 1$) or irreversible adsorption ($R_L = 0$) [33].

3. Results and discussion

Effect of different experimental conditions

As adsorption is affected by chemical and physical variables, the influence of adsorbent dosage, agitation time and initial NO_3^- concentration are investigated in this study.

Effect of the adsorbent dosage:

The study was carried out to determine the effect of adsorbent dosage on the concentration of nitrate. One of the parameters that strongly affect the sorption capacity is the dosage of the adsorbent [16]. In general, increase in adsorbent dosage increased the percent removal of nitrate, which is due to the increase in adsorbent surface area of the adsorbents [3]. The increase in the number of active adsorption sites and the availability of the adsorption sites

increases the adsorption capacity [18]. Sorption of NO₃ increased as the sorbent amount increased [19].

Various amounts of the adsorbents ranging from 1 g to 3 g were taken in 100 ml of aqueous solution in a conical flask and tested for retention time of 1 hr. These samples were filtered and analyzed. As per the results, it is observed that removal efficiency increases with respect to dosage. In the present study, 3 g per 100 ml is found to be the optimum dose with decrease in the concentration of nitrate. In orange peel and wheat straw, it was found that higher doses lead to higher removal efficiency for nitrate.

It is evident from (Fig. 1) removal efficiency increases with the amount of adsorbent dosage.

Effect of the agitation time:

The agitation time is an important factor in adsorption process. Fig. 2 shows the effect of agitation time on removal capacity of nitrate ion from aqueous solution of nitrate by using orange peel and wheat straw. The effect of agitation time for adsorbent with nitrate solution in batch experiment was done under different time values i.e. 1 hr, 2 hr, 3 hr and 4 hr. The obtained results reveal that the nitrate removal efficiency was increased as the agitation time. It was seen that the efficiency of adsorbent for the removal of nitrate increased rapidly and then remained stable and achieved the adsorbent equilibrium time.

The effect of contact time was evaluated as an effective factor in efficient uptake [17]. It can be attributed to the fact that more time becomes available for the organic substances to stick with the adsorbent surface, as well as surface adsorption increases with time [21]. In some cases, the percent removal started to decrease which indicates that the adsorbent reach its optimum adsorption and desorption of the organic substances from the surface of adsorbent occurs [21]. The rate of adsorption declined as the active sites became saturated [6].

It is evident from (Fig. 2) that removal efficiency increased rapidly with agitation time and then remained stable after achieving adsorbent equilibrium time.

Effect of the initial concentration

The efficiency of nitrate removal was affected by the initial nitrate ion concentration. To determine the performance of adsorbent for the adsorption of nitrate it was necessary to introduce different initial concentrations. The influence of initial concentration

of solution on the adsorption of nitrate was done with the two initial concentrations 500 mg/l and 700 mg/l are presented in Fig. 3. The result clearly shows that adsorption capacity enhanced with increase in the initial concentration of nitrate.

The nitrate removal efficiency of *Citrus limetta* (Mosambi) peel increased with increase in initial nitrate concentration [7]. The relation of available number of nitrate ion in solution to the available binding sites of adsorbent can be used to report for high nitrate adsorption capacity in high initial concentration [11]. With increase in the initial concentration of NO₃⁻ ions, the number of ions transported from the solution to the bulk of the adsorbent increases and facilitates the interaction between NO₃⁻ ions and active sites of the bio-adsorbent [17].

Adsorption on orange peel (*Citrus reticulata*)

Orange peel is the material used as bio-adsorbent for removing nitrate from aqueous solution. Orange peel is an economic and easily available bio-adsorbent.

The main components of Orange peel are cellulose, pectin, hemicelluloses and lignin which contain functional group as possible binding sites [16]. The fruit peel waste (FPW) produced by the industry is an abundantly available material with practically zero cost which has been extensively studied as an important adsorbent for the removal of different pollutants from waste waters [22]. Orange peels which control the following parameter in the industrial waste water such as pH, COD, TSS (Total suspended solids), TDS (Total dissolved solids), chloride, Sulphate and total nitrogen, nitrate and nitrite, total phosphorous [23].

Table 1 shows the removal efficiency of orange peel for the NO₃ at different adsorbent dosage (1 g to 3 g), agitation time (1 hr to 4 hr) and initial concentrations (500 mg/l and 700 mg/l). Efficiency of orange peel increased with adsorbent dosage, agitation time and at high initial concentration removal efficiency is found more as compared to low initial concentration. As per the observations, the removal efficiency of orange peel for the NO₃ removal was about 64 % to 81 %.

Adsorption on wheat straw (*Triticum aestivum*)

Wheat straw is the material used as bio-adsorbent for removing nitrate from aqueous solution. It is low cost and easily available material.

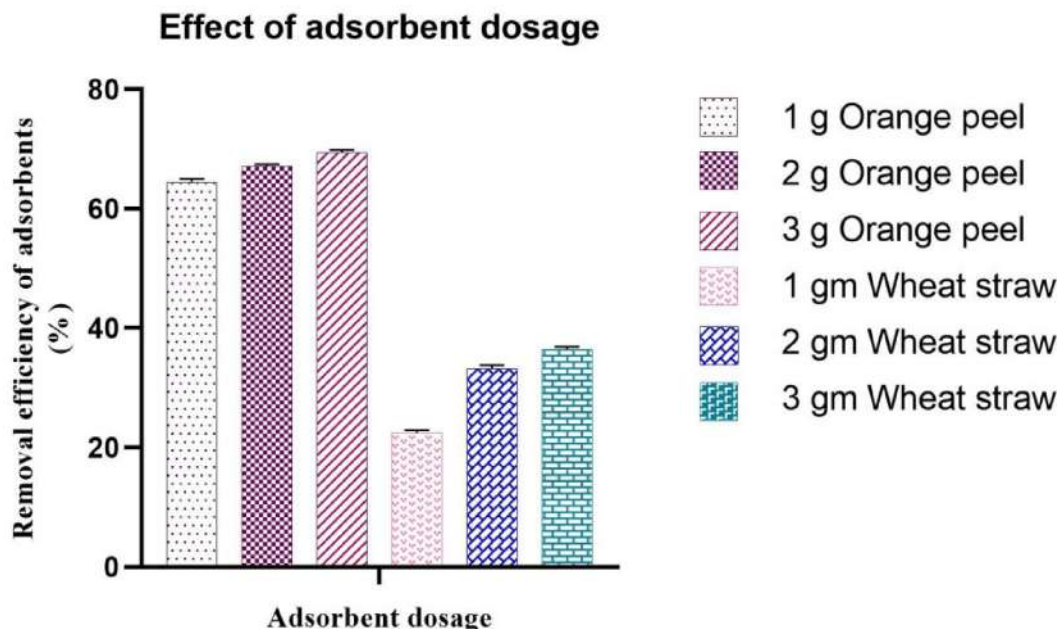


Fig. 1. Effect of adsorbent dosage on nitrate removal efficiency.

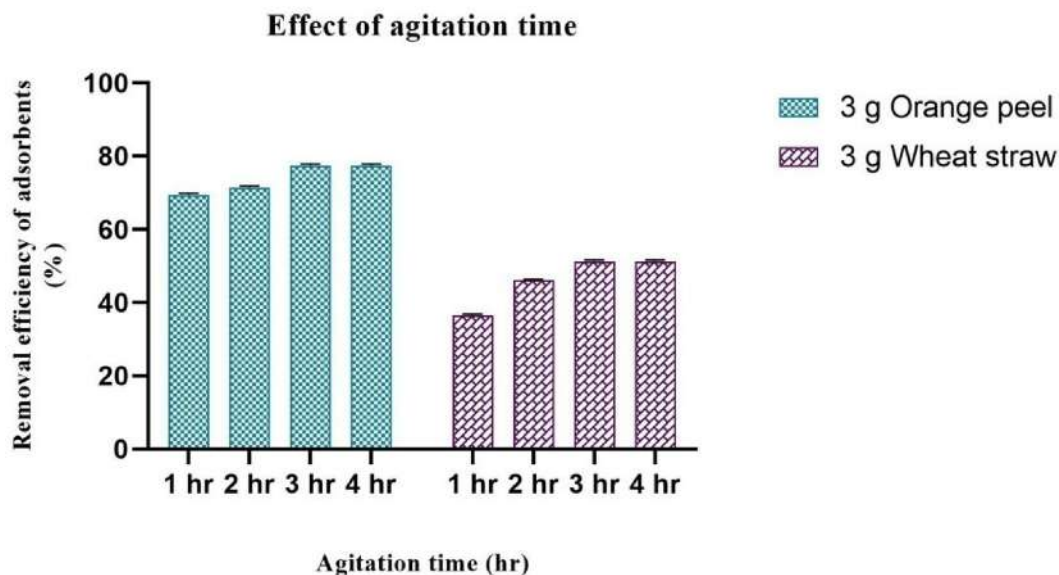


Fig. 2. Effect of agitation time on nitrate removal efficiency.

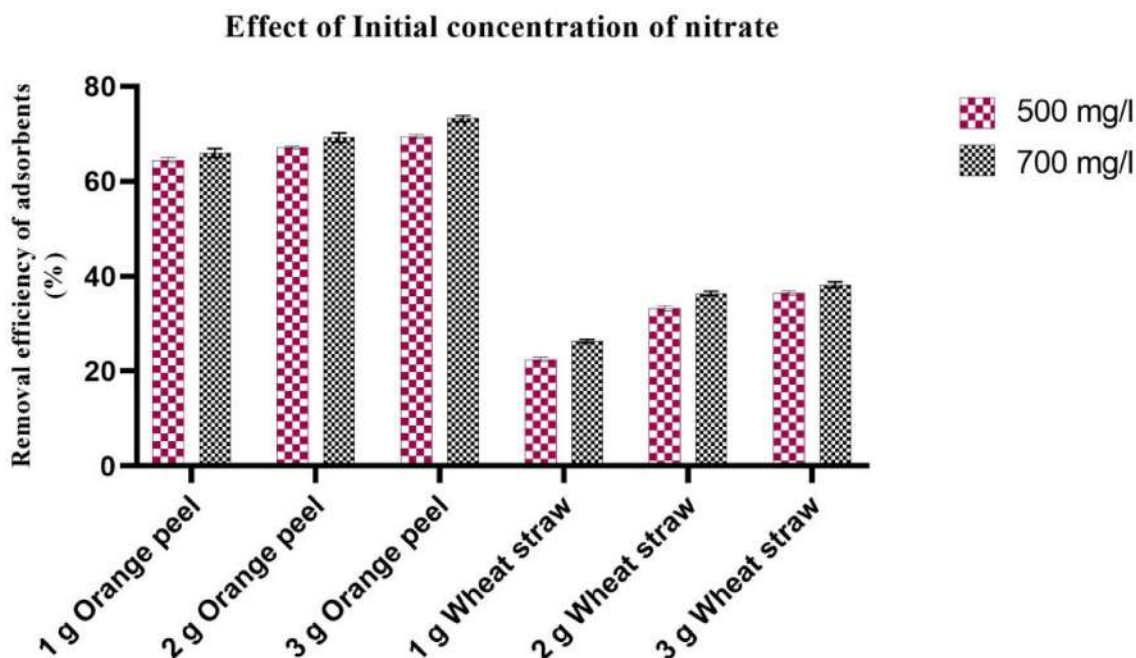


Fig. 3. Effect of initial concentration of nitrate on removal efficiency.

Table 1

Efficiency of orange peel powder for the removal of nitrate, based on its quantity, agitation time and initial concentration of aqueous solution of nitrate.

Sr. No.	Agitation time (hr)	Initial concentration of adsorbate (mg/l)	Removal efficiency (%) for various adsorbent dosage		
			1 g	2 g	3 g
1	1	500	64.5 ± 0.5	67.13 ± 0.321	69.43 ± 0.404
2	2	500	68.13 ± 0.416	69.96 ± 0.950	71.46 ± 0.450
3	3	500	73.23 ± 0.493	75.63 ± 0.550	77.43 ± 0.404
4	4	500	73.23 ± 0.493	75.63 ± 0.550	77.43 ± 0.404
5	1	700	65.96 ± 0.950	69.23 ± 0.585	73.2 ± 0.624
6	2	700	71.36 ± 0.404	73.3 ± 0.264	77.3 ± 0.360
7	3	700	75.43 ± 0.450	78.36 ± 0.404	81.3 ± 0.360
8	4	700	75.43 ± 0.450	78.36 ± 0.404	81.3 ± 0.360

Table 2
Efficiency of wheat straw powder for the removal of nitrate based on its quantity, agitation time and initial concentration of aqueous solution of nitrate.

Sr. No.	Agitation time (hr)	Initial concentration of adsorbate (mg/l)	Removal efficiency (%) for various adsorbent dosage		
			1 g	2 g	3 g
1	1	500	22.46 ± 0.450	33.23 ± 0.585	36.46 ± 0.450
2	2	500	38.36 ± 0.472	43 ± 0.8	46.13 ± 0.251
3	3	500	42.6 ± 0.6	48.23 ± 0.493	51.33 ± 0.416
4	4	500	42.6 ± 0.6	48.23 ± 0.493	51.33 ± 0.416
5	1	700	26.33 ± 0.351	36.36 ± 0.472	38.23 ± 0.585
6	2	700	39.3 ± 0.264	45.36 ± 0.472	46.4 ± 0.4
7	3	700	44.26 ± 0.305	51.33 ± 0.351	55.3 ± 0.3
8	4	700	44.26 ± 0.305	51.33 ± 0.351	55.3 ± 0.3

Table 3
Results of Langmuir isotherm for adsorption of nitrate.

Adsorbent	qmax (mg/g)	K _L	R _L	R ²
Orange Peel	55.80357143	0.0077647	0.20320353	0.77
Wheat Straw	94.25070688	0.00211639	0.48586293	0.71

The straw body is generally composed of macromolecules such as cellulose, hemicelluloses, lignin and protein which consist of C, H, O, N and S. These macromolecules contain functional groups such as hydroxyl, carboxyl and amino groups. These functional groups have strong coordination ability [24]. Wheat straw (WS) is one of the best-known fiber crops, whose industrial potential is now being intensively reconsidered [25].

Table 2 shows the removal efficiency of wheat straw for the NO₃ at different adsorbent dosage (1 g to 3 g), agitation time (1 hr to 4 hr) and initial concentrations (500 mg/l and 700 mg/l). Efficiency of wheat straw increased with adsorbent dosage, agitation time and at high initial concentration removal efficiency is found more as compared to low initial concentration. As per the observations, the removal efficiency of wheat straw for the NO₃ removal was about 22 % to 53 %.

Langmuir isotherm

The adsorption capacity of nitrate was investigated using Langmuir isotherm model. The experimental data of the isotherm model is summarized in Table 3.

Adsorption isotherm models are commonly used to describe the adsorption mechanism. In this study, Langmuir isotherms were used to analyze the experimental data. A linear plot confirms the applicability of Langmuir isotherm [5]. An adsorption isotherm provides useful information about adsorption capacity, binding affinity as well as the surface properties of the bioadsorbent which help understand the binding mechanism of adsorbate [32]. Adsorption isotherms are useful for understanding the mechanism of the adsorption. Langmuir model assumes that adsorption takes place at specific homogeneous sites on the surface of the adsorbent and also, when a site is occupied by an adsorbate molecule, no further adsorption can take place at this site [31].

Graph and results of Langmuir isotherm were drawn by using OriginPro2021b.

The plot of both the graphs is linear therefore it confirms the applicability of Langmuir isotherm from Fig. 4 and Fig. 5 [5]. There are four probabilities for R_L values. Where, R_L is the dimensionless Langmuir constant which indicate the adsorption possibility either favorable (0 < R_L < 1), unfavorable (R_L > 1), linear (R_L = 1) or irreversible adsorption (R_L = 0) [33]. The value of separation factor (R_L) in Langmuir isotherm model represents the suitability of adsorption. R_L value for nitrate adsorption on Orange peel is ~ 0.21 and for wheat straw is ~ 0.49 which are greater than zero and smaller than one which is favorable for adsorption. So, it is clearly observed from results obtained by applying the Langmuir isotherm shows the favorable adsorption of nitrate on orange peel powder and wheat straw powder.

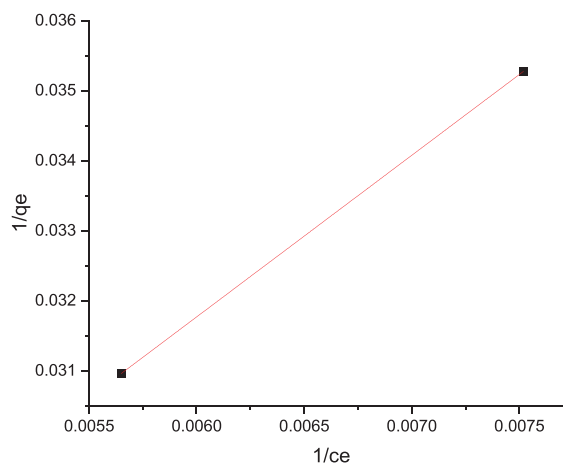


Fig. 4. Langmuir isotherm for Orange peel powder. (For interpretation of the references to colour in this figure legend, the reader is referred to the web version of this article.)

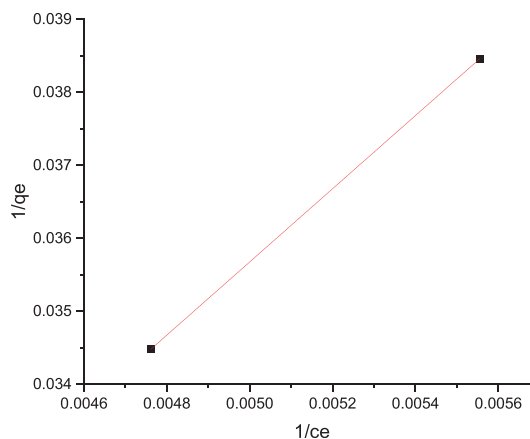


Fig. 5. Langmuir isotherm for wheat straw powder.

4. Conclusion

In this study Orange peel and Wheat straw was used successfully for the adsorption of nitrate from their aqueous solution.

The obtained results revealed that the adsorption of nitrate ions is time dependent, dosage dependent and initial concentration dependent. Nitrate removal efficiency increases with the quantity from 1 g to 3 g and 3 g is optimum quantity for removal of nitrate. Nitrate removal efficiency increased with agitation time rapidly and then remained stable after achieving equilibrium time. Removal efficiency is more in high initial concentration as compared to low initial concentration. The Langmuir adsorption isotherm illustrated the favorable adsorption of nitrate on orange peel and wheat straw powder. Various physical and chemical methods are used for removal of nitrate but those method requires high cost, man power and skilled person etc. but use of bio-adsorbent for nitrate removal is simple, low cost and environment friendly. Orange peels and wheat straw are inexpensive natural waste and readily available, thus this study provides a cost effective means for removal of nitrate ions from contaminated water.

CRedit authorship contribution statement

Sarkale Prajkta Shahaji: Conceptualization, Methodology, Software, Data curation, Writing – original draft. **Chougale Sanjivani Tanaji:** Writing – review & editing. **Jadhav Aasawari Suhas:** Visualization, Investigation, Supervision, Validation.

Data availability

Data will be made available on request.

Declaration of Competing Interest

The authors declare that they have no known competing financial interests or personal relationships that could have appeared to influence the work reported in this paper.

References

- [1] H.Y. Cheng, A.A. Xu, A.M. Kumar, D.D. Kong, J.S. Chen, Y.F. Wang, P. Xu, Aerobic denitrification performance and nitrate removal pathway analysis of novel fungus *Fasariumsolani* RADF-77, *Bioresour. Technol.* (2019).
- [2] J. Makover, D. Hasson, Y. Huang, R. Semiat, H. Shemer, electrochemical removal of nitrate from a Dannan dialysis waste stream, *Water Sci. Technol.* 80 (4) (2019) 727–736.
- [3] N. Öztürk, T.E. Bektaş, Nitrate removal from aqueous solution by adsorption onto various materials, *J. Hazard. Mater.* 112 (1–2) (2004) 155–162.
- [4] M.A. Akber, M.A. Islam, M. Dutta, S.M. Billah, M. Islam, Nitrate contamination of water in dug wells and associated health risks of rural communities in southwest Bangladesh, *Environ. Monit. Assess.* (2020) 192–1163.
- [5] M. Vasanthi, C. Thamaraiselvi, Removal of the nitrate from aqueous solutions using powdered peel of citrus reticulate fruits, *Nat. Environ. Pollut. Technol.* 6 (4) (2007) 737–740.
- [6] M.S. Afjeh, G.B. Marandi, M. Zohuriaan-Mehr, Nitrate removal from aqueous solutions by adsorption onto hydrogel-rice husk biochar composite, *Water Environ.* (2020) 934–947.
- [7] S. Yadav, D. Rahi, Assessment of removal of nitrate by water using Mosambi peel powder as adsorbent, *Int. J. Sci. Res. Develop.* 7 (11) (2010) 67–69.
- [8] D. Mujumdar, Gupta Mavindu, Nitrate pollution of groundwater and associated human health disorders, *Indian J. Environ. Health* 42 (1) (2000) 28–39.
- [9] World Health Organization, Guideline for drinking water quality, 4th edition, 2011.
- [10] A. Bhatnagar, M. Ji, Y. Choi, W. Jung, S. Lee, S. Kim, J. Kang, Removal of nitrate from water by adsorption onto zinc chloride treated activated carbon, *Sep. Sci. Technol.* 43 (4) (2008) 886–907.
- [11] F. Yazdi, M. Anbia, S. Salehi, Characterization of functionalized chitosan-clinoptilolitenanocomposite for nitrate removal from aqueous media, *Int. J. Biol. Micromol.* 130 (2019) 545–555.
- [12] D. Tong, J. Zhuang, J. Lee, J. Buchanan, X. Chen, Concurrent transport and removal of nitrate, Phosphate and pesticides in low-cost metal and carbon-based materials, *Chemosphere* (2019) 84–91.
- [13] Y. Yang, T. Chen, X. Zhang, C. Qing, J. Wang, Z. Yeu, Z. Yang, Simultaneous removal of nitrate and phosphate from wastewater by siderite based autotrophic denitrification 199 (2018) 130–137.
- [14] J. Li, S. Dong, Y. Wang, X. Dou, H. Hao, Nitrate removal from aqueous solutions by magnetic cationic hydrogel: Effect of electrostatic adsorption and mechanism, *J. Environ. Sci.* (2020) 1–12.
- [15] I.J. Syama, A.K. Thalla, D.S. Manu, Performance of laterite soil grains as adsorbent in the removal of chromium, *Curr. World Environ.* 10 (2015) 270–280.
- [16] T.J. Jisha, C.H. Lubna, V. Habeeba, Removal of Cr (VI) using orange peel as an adsorbent, *IJARIE* 3 (4) (2017) 276–283.
- [17] M. Shojaipour, M. Ghaemy, S.M. Amininasab, Removal of NO₃⁻ ion from water using bioadsorbent based on gum tragacanth carbohydrate biopolymer, *Carbohydr. Polym.* (2020).
- [18] A. Battas, A.E. Gaidoumi, A. Ksakas, A. Kherbeche, Adsorption study for the removal of nitrate from water using local clay, *Sci. World J.* (2019) 1–10.
- [19] A.N. Zainab, Sorption of nitrate salt from wastewater without and with modification orange peel, *Iraqi J. Chem. Petrol. Eng.* 17 (3) (2016) 109–116.
- [21] S. Feroz, T. Khusaibi, J. Dumarán, G. Devi, N.R. Lakkimsetty, Treatment of dairy wastewater using orange and banana peels, *J. Chem. Pharm. Res.* 7 (2015) 1385–1391.
- [22] K. Jusufi, B. Korça, A. Berisha, J. Halili, T. Selimi, M. Sadiku, N. Troni, F. Ferataj, J. Hasanaj, V. Mehmeti, A. Halili, Potential application of orange peels as bio-adsorbents in the removal of organic molecules from wastewater, *RAD Conf. Proc.* 1 (2016) 176–178.
- [23] S. Adarsh, M.P. Manasa, N.M. Sheshaprakash, Chandanbalu, Dairy wastewater treatment using orange peels as an adsorbents, *Int. Res. J. Eng. Technol.* 7 (2020) 105–114.
- [24] Y. Chen, Q. Chen, H. Zhao, J. Dang, R. Jin, W. Zhao, Y. Li, Wheat straws and corn straws as adsorbents for the removal of Cr(VI) and Cr(III) from aqueous solution: Kinetics, Isotherm and Mechanism, *ACS Omega* (2020) 6003–6009.
- [25] J. Liu, Y. Su, Q. Li, Q. Yeu, B. Gao, Preparation of wheat straw based superabsorbent resins and their applications as adsorbents for ammonium and phosphate removal, *Bioresour. Technol.* 143 (2013) 32–39.
- [26] N.B. Singh, G. Nagpal, S. Agrawal, Rachna, Water purification by using Adsorbents: A Review, *Environ. Technol. Innovat.* 11 (2018) 187–240.
- [27] A. Bhatnagar, M. Sillanpää, A. Witek-Krowiak, Agricultural waste peels as versatile biomass for water purification – A review, *Chem. Eng. J.* 270 (2015) 244–271.
- [28] R. Yousef, H. Qiblawey, M.H. El-Naas, Adsorption as a Process for Produced Water Treatment: A Review, *Processes* 8 (12) (2020) 1657.
- [29] E. Disli, Batch and Column Experiments to Support Heavy Metals (Cu, Zn and Mn) Transport Modeling in Alluvial Sediments Between The Mogan Lake And The EymirLake, Golbasi, Ankara, *Groundwater Monitor. Remediation* 30 (3) (2010) 125–139.
- [30] K.S. Geetha, S.L. Belagali, Removal Of Heavy Metals And Dyes Using Low Cost Adsorbent From Aqueous Medium- A Review, *ISOR J. Environ. Sci. Toxicol. Food Technol.* 4 (2013) 56–68.
- [31] H.B. Senturk, D. Ozdes, A. Gundogdu, C. Duran, M. Soylak, Removal of phenol from aqueous solutions by adsorption onto organo-modified Tirebolu bentonite: equilibrium, kinetic and thermodynamic study, *J. Hazard. Mater.* 172 (2009) 353–362.
- [32] A. Ayub, Z.A. Raza, M.I. Majeed, M.R. Tariq, A. Irfan, Development of sustainable magnetic chitosan biosorbent beads for kinetic remediation of arsenic contaminated water, *Int. J. Biol. Macromol.* 163 (2020) 603–617.
- [33] T. Meftah, M. Zerafat, Nitrate Removal from Drinking Water using Organo-Silane Modified Natural Nano-Zeolite, *Int. J. Nanosci. Nanotechnol.* 12 (4) (2016) 223–232.



IoT based dielectric constant measurement system for solid or semi-liquid materials using Arduino WeMos D1R1

Somnath A. Wankhede^{a,*}, Vijay S. Kale^b, A.D. Shaligram^c, Arun Patil^d, Dharma K Halwar^e

^a Dept. of Electronic Science, MVP Samaj's K. K. Wagh College, Pimpalgaon (B), Dist. Nashik, Maharashtra 422 209, India

^b Dept. of Electronic Science, MVP Samaj's KTHM College, Nashik, Maharashtra 422003, India

^c Dept of Electronic Science, SPPU, Pune, Maharashtra 411 007, India

^d Dept of Physics, Arts, Science and Commerce College, Manmad, Maharashtra 423 104, India

^e Dept. of Electronic Science, MSG College, Malegaon, Maharashtra 422 401, India

ARTICLE INFO

Article history:

Available online 15 October 2022

Keywords:

Measurement

WeMos

IoT

Capacitance

Arduino

Dielectric Constant

ABSTRACT

The measurement-system mainly consists of sensing-element, signal conditioning circuit and signal-processing unit. The sensing-element of a measuring system is directly affected by materials carrying quantity to be measured. This system supports solid or semi-liquid material. This paper signifies the designed system for dielectric constant measurement using Arduino with Wi-Fi and capacitive sensing element which sends/shows information continuously on android app or cloud to build IoT based system.

With the help of Polarization, Dielectric properties, Cole-Cole diagram, Microwave Measurement Methods and Arduino with IC-555, many techniques with limitations and complications are available to calculate dielectric constant. But this advanced system consists only Arduino without any other bulky circuit. In this system, measurement of dielectric constant depends on parameters of capacitive sensing element and property time constant of capacitor. Capacitor with larger capacitance takes more time to charge as well as discharge. The charging and discharging voltage of the capacitor is applied to Arduino (WeMos D1-R1) with signal conditioning. Here, from capacitance, dielectric constant of material is calculated and verified with standard values. WeMos D1-R1 Arduino has Wi-Fi facility to transmit data continuously on cloud. Designed system gives the capacitance, dielectric constant of substance, and displays it on android app and cloud or website with accuracy about approximately 99.46%.

Copyright © 2022. Elsevier Ltd. All rights reserved.

Selection and peer-review under responsibility of the scientific committee of the Integrative Nanotechnology Perspective for Multidisciplinary Applications - 2022.

1. Introduction

The elements are insulators or dielectric materials, conductors, and semiconductors. Insulators or dielectrics play vital role in our day-to-day life appliances as well as all electrical and electronic equipments. The applications of dielectric constant measurement system are in quality testing of various fruits and vegetables [1]. Also useful in transformer manufacturing, for dielectric properties measurements of paper, pressboard and transformer oil, with effect of the ageing and moisture [2,3].

Electronic circuits having high frequency applications uses dielectric-material and the working principle of all high-frequency circuits depends on the dielectric properties of the material. In designing of high frequency circuits, it is necessary to have proper acquaintance of the properties of the dielectric materials particularly the dielectric constant (real-part of complex permittivity) and loss tangent at the working conditions [4]. Dielectric property is also a key parameter of plant and fruits mainly due to the large amount of water content and the structure of the biomaterials. Dielectric materials are electrically insulating materials which will be polarized under an electric field, such a phenomenon is called as dielectric polarization. The dielectric properties of material give considerable data about the dissipation and storage of magnetic and electric fields in materials [5]. The permittivity expresses the polarizability of the material. The permittivity is always in the form of complex number and its real part

Abbreviations: IoT, Internet of Things; RF, Radio Frequency; TDR, Time domain spectroscopy.

* Corresponding author.

E-mail address: sa.wankhede@gmail.com (S.A. Wankhede).

is generally known as dielectric constant. Though the perfect dielectric material has electrical conductivity zero, every insulator is not a dielectric-material [6].

2. Dielectric property measurement techniques

Ninety-three years ago, polar dielectrics and modelling studies were used to determine grain moisture content and permittivity measurement techniques were based on dc electrical resistance [7]. A non-linear rise in the resistance of grains, as the temperature decreased provides useful readings [8]. The ac measurement techniques used to measure the variations in capacitance and suitable sample holding capacitors were industrialized [9]. Based on the dielectric properties, grain moisture measurement data turn out to be the most projecting agricultural applications. Novel instruments with their calibration led to the advance of a standard oven technique that more contributed to several applications of RF dielectric heating and added the pursuit for more quantitative values. In past 25 years, techniques of the permittivity measurement have been extended and used to various bio-resource, food and agricultural problems.

The dielectric properties of the food or agricultural materials in the microwave region can be resolute by numerous methods using different micro-wave measuring sensors [10]. The use of specific method be subject to the expected frequency range and the type of the material to be tested. Selection of the equipment for measurement and sample holder design depends upon the dielectric materials to be examined, available equipment, resources for the studies and the extent of the research [11]. For measuring the dielectric-properties of homogeneous food materials, the cavity perturbation technique is often used because of its simplicity, easy data reduction, accuracy, and high temperature capability [12]. The transmission line technique is inconvenient because the sample to be available in annular geometry or a slab. Only the coaxial line technique is practical because of the requirement of larger size of the waveguide [13]. A microwave resonator completely filled or partly with a material can be used in the measurement of the permittivity. The resonator or perturbation technique is generally standardized with materials having known dielectric properties, typically with organic solvents like ethanol, methanol, etc. The frequency range for measurement is from 50 MHz to 100 GHz. If the transmission line is enclosed (waveguide), it is possible to measure the permittivity of a material without the resonator by keeping it inside the waveguide directly. The method is applicable to all solid and liquid materials, but not for the gases because of lower permittivity of gas [14]. TDR (Time domain spectroscopy) or reflectometry methods were developed in the 1980 s and applied in studies related to dielectric properties of the food materials. Basically, to compute dielectric properties, the reflection characteristic of the material is utilized. This measurement method is rapid and gives high accuracy, within very small percent error [15]. Free space transmission technique is grouped under nondestructive and contactless measuring methods. It does not require particular sample preparation. So, it is mostly suitable for inhomogeneous dielectric and for material at the high temperature. Moreover, it may be simply implemented in industrial applications for control and continuous monitoring. e.g., density measurement and moisture content determination [16]. In microstrip transmission line method, microstrip has been used as microwave component, it shows numerous properties which overcome some limitations, hence makes it suitable for dielectric permittivity measurement. The effective permittivity of a microstrip transmission line highly depends on the permittivity of region above line. This is used in designing of the microwave circuits and to smaller amount examination of dielectric permittivity [17]. The Colloid Dielectric Probe is implemented

in permittivity evaluation of the colloidal liquid material in pharmaceutical, chemical, biochemical, and food industries. It works from 200 kHz – 20 MHz with the precision LCR meter [11].

3. Methodology

The IoT based dielectric constant measurement system is designed using Arduino WeMos D1R1. Here, non-polar capacitor is built by using two parallel copper plates with dimensions $0.05 \text{ m} \times 0.015 \text{ m}$ as shown in Fig. 1, with gap of 0.10 mm and air as a dielectric material between them. On LCR meter, it gives capacitance 64.1pF with small variations as shown in Fig. 2.

The parallel plate capacitor is interfaced with Arduino WeMos D1R1 at pins D13 and A0 as shown in Fig. 3.



Fig. 1. Photograph of parallel plates of designed capacitor.



Fig. 2. Photograph of designed capacitor with air as dielectric medium for capacitance measurement using LCR meter.

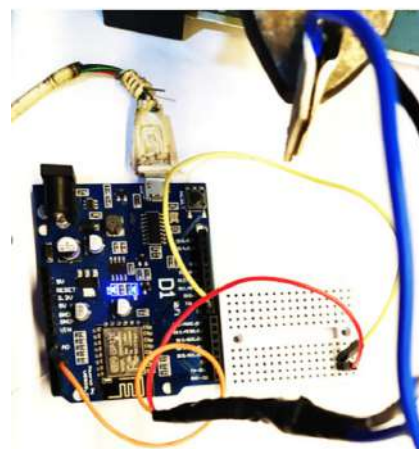


Fig. 3. Photograph of dielectric constant measurement system using Arduino WeMos D1R1 for parallel plate capacitor with air as dielectric medium.

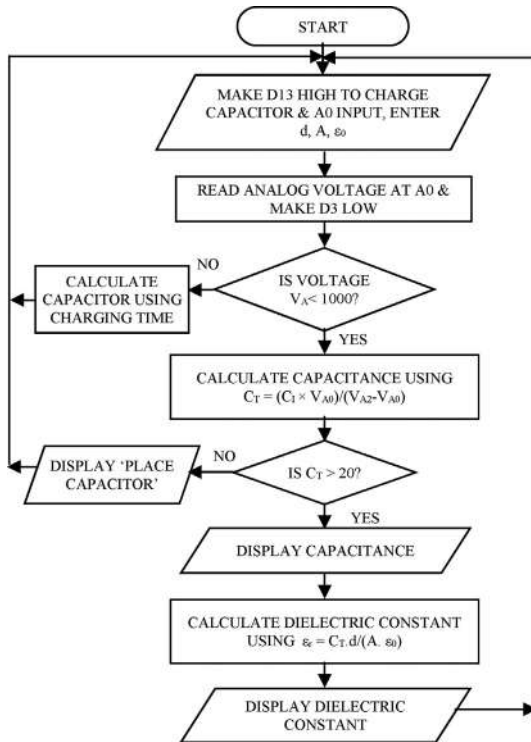


Fig. 4. Flowchart for capacitance measurement using WeMos D1R1 for nonpolar capacitors with the range 20 pF–1000 nF.

This system is useful for the capacitance measurement from 20pF to 1000nF. Arduino C program is written to measure capacitance and dielectric constant with logic shown in Fig. 4.

The unknown capacitor is connected between D13 and A0. Here, pin D13 is used as the charging pin and pin A0 used as the discharging pin. Initially, the unknown capacitor is charged by setting D13 as HIGH and measure the voltage at A0 from the following formula.

$$V_{A0} = (V_{A2} \times C_T)/(C_T + C_1)$$

where

- V_{A0} = voltage at pin A₀,
- V_{A2} = voltage at pin A₂,
- C_T = capacitor under test and.
- C_1 = internal capacitor.

But voltage at A₀ is measured with the help of analog read function. Hence, using that value in the above equation, the unknown capacitance is obtained.

$$C_T = (C_1 \times V_{A0})/(V_{A2} - V_{A0}) \text{ [18].}$$

Substituting distance between parallel plates (d), area of rectangular plates (A) and $\epsilon_0 = 8.84 \times 10^{-12}$ in standard equation $\epsilon_r = C_T \cdot d/(A \cdot \epsilon_0)$ [19], dielectric constant of the material placed between two copper plates is calculated. Figs. 5 and 6 shows readings of



Fig. 5. Screenshot of designed Android app showing readings of dielectric constant measurement system.

Dielectric constant measurement system on designed Android app and webpage respectively.

Specifications of LCR Meter:

- Brand Name: Aplab.
- Type of Product: Digital LCR Q - Meter.
- Model No: Aplab 4910.
- Measurement Frequency: User selectable 100 Hz or 1KHz.
- Display: 3½ Digit.
- Operating Temp. Range: 0° to 40 °C.
- Measurement Ranges.
 - Inductance Range: 0.1µH to 9999H.
 - Capacitance Range: 0.1pF to 9999µF.
 - Resistance Range (Ohm): 0.001 to 100 M.
 - Quality Factor: 0.1 to 99.
- Resolution.
 - Inductance: 0.1µH.
 - Capacitance: 0.1pF.
 - Resistance: 0.001 O.
 - Quality Factor: 0.01.
- Accuracy: ±0.25%.

Features of WeMos D1R1:

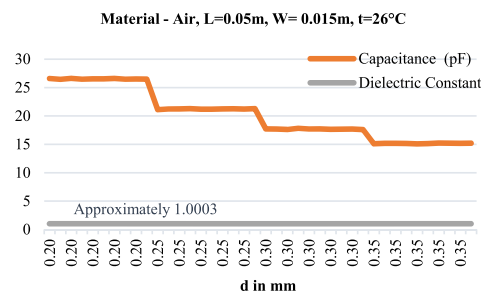
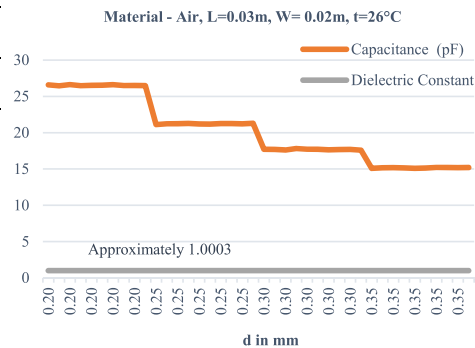
- 11 × I/O × pin.
- 1 × ADC × pin (input range 0–3.3 V).
- Support OTA wireless upload.
- Integrated 5 V 1A switching power supply (maximum voltage 24 V).
- Based on ESP-8266EX.
- Arduino compatible, using IDE Arduino to program.
- CPU 80 MHz [20].

Following tables and graphs show measured capacitance and dielectric constants of air, mica, glass and talcum powder at different temperatures with accuracy about approximately 99.46%.

Accuracy is calculated by using formula: Accuracy = $(1 - (\text{Observed value} - \text{Actual value})/\text{Actual value}) \times 100$.

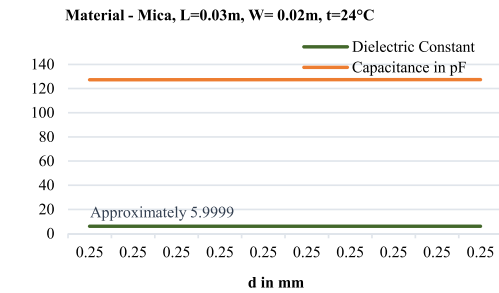
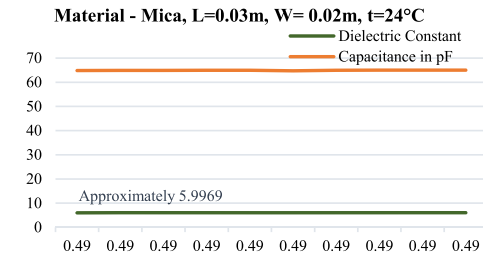
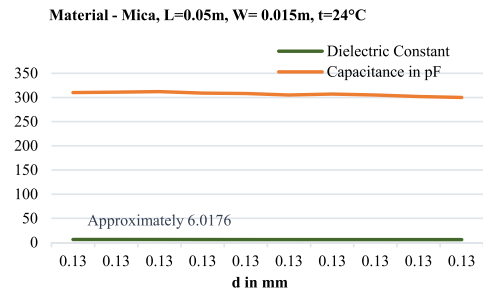
Dielectric Medium - Air $\epsilon_0 = 8.84 \times 10^{-12}$ Temperature = 26°C

Sr. No.	Dimension of C				Capacitance by Arduino in pF	Dielectric Constant $\epsilon_r = C.d/(A. \epsilon_0)$
	L in m	W in m	Area (A) in m ²	d in m		
1	0.03	0.02	0.0006	0.00020	26.59	1.0026
2	0.03	0.02	0.0006	0.00020	26.46	0.9977
3	0.03	0.02	0.0006	0.00020	26.62	1.0038
4	0.03	0.02	0.0006	0.00020	26.48	0.9985
5	0.03	0.02	0.0006	0.00020	26.52	1.0000
6	0.03	0.02	0.0006	0.00020	26.53	1.0004
7	0.03	0.02	0.0006	0.00020	26.61	1.0034
8	0.03	0.02	0.0006	0.00020	26.49	0.9989
9	0.03	0.02	0.0006	0.00020	26.50	0.9992
10	0.03	0.02	0.0006	0.00020	26.47	0.9981
11	0.03	0.02	0.0006	0.00025	21.11	0.9950
12	0.03	0.02	0.0006	0.00025	21.23	1.0007
13	0.03	0.02	0.0006	0.00025	21.22	1.0002
14	0.03	0.02	0.0006	0.00025	21.27	1.0025
15	0.03	0.02	0.0006	0.00025	21.19	0.9988
16	0.03	0.02	0.0006	0.00025	21.18	0.9983
17	0.03	0.02	0.0006	0.00025	21.24	1.0011
18	0.03	0.02	0.0006	0.00025	21.25	1.0016
19	0.03	0.02	0.0006	0.00025	21.21	0.9997
20	0.03	0.02	0.0006	0.00025	21.29	1.0035
21	0.03	0.02	0.0006	0.00030	17.70	1.0011
22	0.03	0.02	0.0006	0.00030	17.68	1.0000
23	0.03	0.02	0.0006	0.00030	17.62	0.9966
24	0.03	0.02	0.0006	0.00030	17.82	1.0079
25	0.03	0.02	0.0006	0.00030	17.72	1.0023
26	0.03	0.02	0.0006	0.00030	17.71	1.0017
27	0.03	0.02	0.0006	0.00030	17.64	0.9977
28	0.03	0.02	0.0006	0.00030	17.66	0.9989
29	0.03	0.02	0.0006	0.00030	17.69	1.0006
30	0.03	0.02	0.0006	0.00030	17.59	0.9949
31	0.03	0.02	0.0006	0.00035	15.09	0.9958
32	0.03	0.02	0.0006	0.00035	15.16	1.0004
33	0.03	0.02	0.0006	0.00035	15.17	1.0010
34	0.03	0.02	0.0006	0.00035	15.14	0.9991
35	0.03	0.02	0.0006	0.00035	15.08	0.9951
36	0.03	0.02	0.0006	0.00035	15.12	0.9977
37	0.03	0.02	0.0006	0.00035	15.21	1.0037
38	0.03	0.02	0.0006	0.00035	15.20	1.0030
39	0.03	0.02	0.0006	0.00035	15.18	1.0017
40	0.03	0.02	0.0006	0.00035	15.19	1.0024
Average						1.0003
1	0.05	0.015	0.00075	0.00010	66.30	1.0000
2	0.05	0.015	0.00075	0.00010	66.29	0.9998
3	0.05	0.015	0.00075	0.00010	66.32	1.0003
4	0.05	0.015	0.00075	0.00015	44.19	0.9998
5	0.05	0.015	0.00075	0.00015	44.21	1.0002
6	0.05	0.015	0.00075	0.00020	33.14	0.9997
7	0.05	0.015	0.00075	0.00020	33.18	1.0009
8	0.05	0.015	0.00075	0.00025	26.51	0.9996
9	0.05	0.015	0.00075	0.00025	26.53	1.0004
10	0.05	0.015	0.00075	0.00025	26.54	1.0008
Average						1.0002
Accuracy						99.82



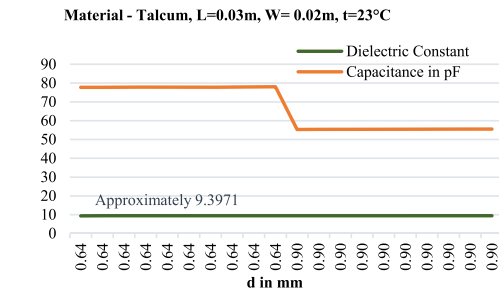
Dielectric Medium - Mica $\epsilon_0 = 8.84 \times 10^{-12}$ **Temperature = 24°C**

Sr. No.	Dimension of C				Capacitance by Arduino in pF	Dielectric Constant $\kappa = C.d/(A. \epsilon_0)$
	L in m	W in m	Area (A) in m ²	d in m		
1	0.05	0.015	0.00075	0.00013	310.00	6.0784
2	0.05	0.015	0.00075	0.00013	311.00	6.0980
3	0.05	0.015	0.00075	0.00013	312.00	6.1176
4	0.05	0.015	0.00075	0.00013	309.00	6.0588
5	0.05	0.015	0.00075	0.00013	308.00	6.0392
6	0.05	0.015	0.00075	0.00013	305.00	5.9804
7	0.05	0.015	0.00075	0.00013	307.00	6.0196
8	0.05	0.015	0.00075	0.00013	305.00	5.9804
9	0.05	0.015	0.00075	0.00013	302.00	5.9216
10	0.05	0.015	0.00075	0.00013	300.00	5.8824
11	0.03	0.02	0.0006	0.00049	64.84	5.9901
12	0.03	0.02	0.0006	0.00049	64.87	5.9929
13	0.03	0.02	0.0006	0.00049	64.91	5.9966
14	0.03	0.02	0.0006	0.00049	64.94	5.9994
15	0.03	0.02	0.0006	0.00049	64.95	6.0003
16	0.03	0.02	0.0006	0.00049	64.70	5.9769
17	0.03	0.02	0.0006	0.00049	64.96	6.0012
18	0.03	0.02	0.0006	0.00049	64.99	6.0040
19	0.03	0.02	0.0006	0.00049	64.98	6.0031
20	0.03	0.02	0.0006	0.00049	65.00	6.0049
21	0.03	0.02	0.0006	0.00025	127.21	5.9959
22	0.03	0.02	0.0006	0.00025	127.23	5.9969
23	0.03	0.02	0.0006	0.00025	127.27	5.9988
24	0.03	0.02	0.0006	0.00025	127.28	5.9992
25	0.03	0.02	0.0006	0.00025	127.29	5.9997
26	0.03	0.02	0.0006	0.00025	127.30	6.0002
27	0.03	0.02	0.0006	0.00025	127.31	6.0007
28	0.03	0.02	0.0006	0.00025	127.33	6.0016
29	0.03	0.02	0.0006	0.00025	127.35	6.0025
30	0.03	0.02	0.0006	0.00025	127.37	6.0035
Average						6.0048
Accuracy						99.60



Dielectric Medium - Talcum $\epsilon_0 = 8.84 \times 10^{-12}$ **Temperature = 23°C**

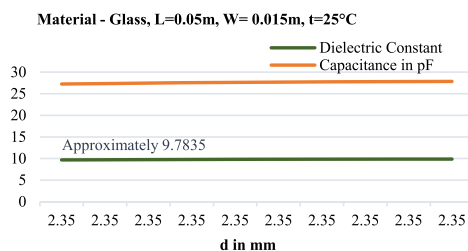
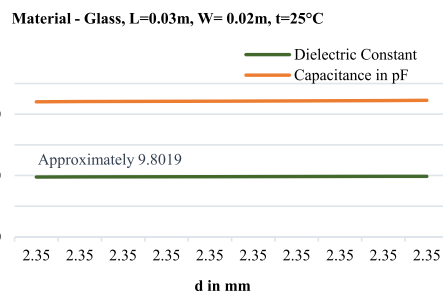
Sr. No.	Dimension of C				Capacitance by Arduino in pF	Dielectric Constant $\kappa = C.d/(A. \epsilon_0)$
	L in m	W in m	Area (A) in m ²	d in m		
1	0.03	0.02	0.0006	0.00064	77.72	9.3780
2	0.03	0.02	0.0006	0.00064	77.74	9.3804
3	0.03	0.02	0.0006	0.00064	77.81	9.3888
4	0.03	0.02	0.0006	0.00064	77.89	9.3985
5	0.03	0.02	0.0006	0.00064	77.70	9.3756
6	0.03	0.02	0.0006	0.00064	77.78	9.3852
7	0.03	0.02	0.0006	0.00064	77.82	9.3900
8	0.03	0.02	0.0006	0.00064	77.86	9.3949
9	0.03	0.02	0.0006	0.00064	77.92	9.4021
10	0.03	0.02	0.0006	0.00064	77.98	9.4094
11	0.03	0.02	0.0006	0.00090	55.32	9.3869
12	0.03	0.02	0.0006	0.00090	55.35	9.3920
13	0.03	0.02	0.0006	0.00090	55.37	9.3954
14	0.03	0.02	0.0006	0.00090	55.39	9.3988



15	0.03	0.02	0.0006	0.00090	55.40	9.4005
16	0.03	0.02	0.0006	0.00090	55.41	9.4021
17	0.03	0.02	0.0006	0.00090	55.44	9.4072
18	0.03	0.02	0.0006	0.00090	55.48	9.4140
19	0.03	0.02	0.0006	0.00090	55.51	9.4191
20	0.03	0.02	0.0006	0.00090	55.53	9.4225
Average						9.3971
Accuracy						98.96

Dielectric Medium - Glass $\epsilon_0 = 8.84 \times 10^{-12}$ Temperature = 25°C

Sr. No.	Dimension of C				Capacitance by Arduino in pF	Dielectric Constant $\kappa = C.d/(A.\epsilon_0)$
	L in m	W in m	Area (A) in m ²	d in m		
1	0.03	0.02	0.0006	0.00235	22.00	9.7474
2	0.03	0.02	0.0006	0.00235	22.05	9.7695
3	0.03	0.02	0.0006	0.00235	22.07	9.7784
4	0.03	0.02	0.0006	0.00235	22.08	9.7828
5	0.03	0.02	0.0006	0.00235	22.09	9.7872
6	0.03	0.02	0.0006	0.00235	22.14	10.1904
7	0.03	0.02	0.0006	0.00235	22.16	10.1993
8	0.03	0.02	0.0006	0.00235	22.18	10.2037
9	0.03	0.02	0.0006	0.00235	22.21	10.2126
10	0.03	0.02	0.0006	0.00235	22.25	10.2259
1	0.05	0.015	0.00075	0.00235	27.23	9.6517
2	0.05	0.015	0.00075	0.00235	27.32	9.6836
3	0.05	0.015	0.00075	0.00235	27.45	9.7296
4	0.05	0.015	0.00075	0.00235	27.54	9.7615
5	0.05	0.015	0.00075	0.00235	27.63	9.7934
6	0.05	0.015	0.00075	0.00235	27.68	9.8112
7	0.05	0.015	0.00075	0.00235	27.74	9.8324
8	0.05	0.015	0.00075	0.00235	27.78	9.8466
9	0.05	0.015	0.00075	0.00235	27.82	9.8608
10	0.05	0.015	0.00075	0.00235	27.83	9.8643
Average						9.7927
Accuracy						99.82



Dielectric Constant Measurement using WeMos D1R1
Mr. S. A. Wankhede
Research Centre: MGV's LVH College, Panchavati, Nashik

Date	Time	Material	Capacitance	Dielectric Constant	Temperature
21-10-2021	13:58:21	Air	77.72	9.3780	23°C
21-10-2021	13:55:25	Air	77.74	9.3804	23°C
21-10-2021	13:55:28	Air	77.81	9.3888	23°C
21-10-2021	13:55:33	Air	77.89	9.3985	23°C
21-10-2021	13:55:34	Air	77.70	9.3756	23°C
21-10-2021	13:55:39	Air	77.78	9.3852	23°C

© Copyright 2019

Fig. 6. Screenshot of designed webpage showing readings of dielectric constant measurement system.

4. Conclusion

The IoT based dielectric and capacitance measurement system using Arduino WeMos D1R1 is designed and developed for non-polar capacitor. The non-polar capacitance measurement range 20 pF to 1000 nF is tested. Accuracy of capacitance varies depending on the value of capacitance. Designed capacitor provides approximately 99% accuracy for the range 20 pF to 600 pF. Major application of this system will be in various industries where not only capacitance and dielectric property measurement is required but also that storage is possible and available anywhere, anytime as it is IoT based. For different size and shape of material, modification in program and capacitor like area of plates and distance between plates is required. Dielectric constant of material placed between two plates can be easily measured. This increases application of this system in quality testing of various fruits and vegetables. Also useful in transformer manufacturing, for dielectric properties measurements of paper, pressboard and transformer oil, with effect of the ageing and moisture.

CRedit authorship contribution statement

Somnath A. Wankhede: Methodology, Software, Data curation, Writing – original draft, Visualization, Investigation. **Vijay S. Kale:** Conceptualization. **A.D. Shaligram:** Supervision. **Arun Patil:** Validation. **Dharma K Halwar:** Writing – review & editing.

Data availability

The data that has been used is confidential.

Declaration of Competing Interest

The authors declare that they have no known competing financial interests or personal relationships that could have appeared to influence the work reported in this paper.

References

- [1] Dalia El Khaled, Nuria Novas, Jose A. Gazquez, Rosa M. Garcia and Francisco Manzano-Agugliar, Fruit and Vegetable Quality Assessment via Dielectric Sensing, *Sensors* 15 (2015) 15363–15397; doi: [10.3390/s150715363](https://doi.org/10.3390/s150715363).
- [2] Martin Anglhuber, Michael Krüger, Dielectric analysis of high voltage power transformers, OMICRON electronics, Klaus, Austria.
- [3] C.F. Ten, M.A.R.M. Fernando, Z.D. Wang, Dielectric properties measurements of transformer oil, paper and pressboard with the effect of moisture and ageing, in: 2007 Annual Report - Conference on Electrical Insulation and Dielectric Phenomena, Canada, ISSN: 0084-9162.
- [4] G.W. Parker, Electric field outside a parallel plate capacitor, *Am. J. Phys.* 70 (2002) 502–507.
- [5] G.T. Carlson, B.L. Illman, The circular disk parallel plate capacitor, *Am. J. Phys.* 62 (1994) 1099–1105.
- [6] Raham Brodie, Mohan V. Jacob, Peter Farrell, Microwave and Radio-Frequency Technologies in Agriculture, An Introduction for Agriculturalists and Engineers, Publisher: De Gruyter Open Poland, ISBN: 9783110455397, Published: February 22, 2016.
- [7] P. Debye, Polar Molecules. The Chemical Catalog Company, New York, 1929, pp. 172.
- [8] S.O. Nelson, Dielectric properties of agricultural products - Measurements and applications, *IEEE Trans. Electr. Insulat.* 26 (5) (1991) 845–869.
- [9] S.O. Nelson, Measurement of microwave dielectric properties of particulate materials, *J. Food Eng.* 21 (3) (1994) 365–384.
- [10] A. Kraszewski, Microwave Aquametry – Electromagnetic Interaction with Water Containing Materials, IEEE Press, Piscataway, NJ, 1996.
- [11] M.S. Venkatesh, G.S.V. Raghavan, An overview of dielectric properties measuring techniques, *Can. Biosyst. Eng.* 47 (2005).
- [12] A.C. Metaxas, R. Meredith, Industrial Microwave Heating (IEEE Power Engineering Series), Peter Peregrinus, Piscataway, NJ, 1983.
- [13] L.E. Stetson, S.O. Nelson, A method for determining dielectric properties of grain and seed in the 200- to 500-MHz range, *Trans. ASAE* 13 (4) (1970) 491–495.
- [14] S.E. Engelder, C.R. Buffer, Measuring dielectric properties of food products at microwave frequencies, *Microwave World* 12 (2) (1991) 6–15.
- [15] M.N. Afsar, J.R. Birch, R.N. Clarke, G.W. Chantry, The measurement of the properties of materials, *IEEE Trans. Instrum. Meas.* 74 (1) (1986) 183–199.
- [16] A.W. Kraszewski, Microwave aquametry - A review, *J. Microwave Power* 15 (4) (1980) 209–220.
- [17] R.B. Keam, W.S. Holmes, Uncertainty analysis of measurement of complex permittivity using microstrip transmission line, in: Proceedings SBMO/IEEE MTT-S, IMOC'95, 137–142. IEEE, Piscataway, NJ, 1995.
- [18] Anusha, Arduino Capacitance Meter, ELECTRONICS HUB, <https://www.electronicshub.org/arduino-capacitance-meter>.
- [19] T.T. Grove, M.F. Masters, R.E. Miers, Determining dielectric constants using a parallel plate capacitor, American Association of Physics Teachers, *Am. J. Phys.* 73(1), January 2005, <http://aapt.org/ajp>.
- [20] <https://protosupplies.com/product/esp8266-di-wifi-with-uno-footprint/>.



Synthesis of Benzimidazole and Benzothiazole Derivatives using Reusable Waste Stem of *Trigonella Foenum-graecum* Assisted Zinc Sulphide Nanoparticles: A Green and Efficient Solid Acid Catalyst

Arun K. Valvi^a, Hemangi J. Gavit^a, Shubhada S. Nayak^b, Vitthal S. Shivankar^c, Gurumeet C. Wadhawa^{b,*}

^a Annasaheb Awate Arts, Commerce and Hutatma Babu Genu Science College, Manchar, Pune, Maharashtra, India

^b Rayat Shikshan Sanstha's Karmaveer Bhaurao Patil College, Vashi, Navi Mumbai, India

^c Rayat Shikshan Sanstha's Chhatrapati Shivaji College, Satara, Maharashtra, India

ARTICLE INFO

Article history:

Available online 21 October 2022

Keywords:

Benzimidazole
Benzothiazole
Condensation reaction
Nanoparticles
Plant extract

ABSTRACT

In this study, the simple and rapid methods for the preparation of benzimidazole and benzothiazole by the condensation of *o*-phenylenediamine with the aromatic aldehyde in presence of the zinc sulphide nanoparticles derived from the waste stem of the *Trigonella foenum-graecum*. The catalyst was prepared by using the waste stem of the *Trigonella foenum-graecum*. Most of the reaction carried under the mild condition with very high excellent yield. The method is used for the aromatic, unsaturated and heteroaromatic aldehyde. The main advantage of this method is that it takes very short reaction time, solvent free reaction condition, reusable catalyst, milder reaction, easy workup and waste stem of the plant was used. © 2022 Elsevier Ltd. All rights reserved.

Selection and peer-review under responsibility of the scientific committee of the Integrative Nanotechnology Perspective for Multidisciplinary Applications - 2022. All rights reserved.

1. Introduction

Naturally occurring nucleotides, i.e., adenine base of the DNA, as well as a component of vitamin B12 have extensively been used in drug synthesis and medicinal chemistry containing the benzimidazole or 1H-1,3-benzothiazole-based heterocyclic compounds (shown in fig.) [1–6]. Due to the presence of aromatic ring and nitrogen present in the ring of Benzimidazoles, it can show the large number of the biological activity such as antiviral activities [7–8], anticancer [9–11], antidiabetics [12,13], level modulators [14], antimicrobial [15–17], anti-inflammatory [18–20], and antioxidant [21].

There are various methods for the synthesis of benzimidazole derivatives. The most common traditional methods are coupling of the nitriles, amides, esters, chlorides, carboxylic acids with the *o*-phenylenediamine [22–23]. There are several methods in which thermal, microwave or the sonication method was used, most of time the benzimidazoles synthesized using the condensation of orthophenyl diamine with 2-nitroamines [24], aldehydes [25], car-

boxylic acids [26], carbonitriles, [27], arylamino oximes [28], cyclization of *o*-bromoaryl derivatives [29] and orthoesters [30].

The second route involves condensation reactions between *o*-phenylenediamine and aldehyde or alcohols via a dehydrogenated coupling, followed by oxidative cyclode hydrogenation [24,25], but in many of these methods, a stoichiometric number of oxidizing agents is a prerequisite [26–29].

Other important method which involves the direct regioselective C-2 arylation of imidazole with aryl halides using Pd(II)/Cu(I) catalytic amount at the high temperature, or pressure with low yield. There are several green catalyst like the inorganic salts zeolites [31–33], micelles [34], heterogeneous ionic liquid gel [35], metal oxides [36–40] *p*-toluenesulfonic acid/graphite and *N,N*-dimethyl aniline/graphite [41], benzimidazoles using various catalysts such as rose bengal [42], NH₄Cl [43] ytterbium perfluorooctane sulfonates (Yb(OPf)₃) [44] and base or metal catalysts [45] produces benzimidazoles. Generally, the condensation of *o*-phenylenediamines with aldehydes in the presence of acid [20], the dehydration of *N*-acylated, *o*-phenylenediamines using acetic acid [46], *p*-TSA [47] or amberlyst-15 Other methods include condensation of *o*-phenylenediamines with carboxylic acids, nitriles and *ortho*-esters under dehydrating conditions [48].

* Corresponding author.

E-mail addresses: arunvalvi99@gmail.com (A.K. Valvi), wadhava.gurumeet@gmail.com (G.C. Wadhawa).

Benzothiazole derivatives are known for different biological properties, including antitubercular, antimalarial, anticonvulsant, antihelmintic, analgesic, antidiabetic, antimicrobial, antibacterial, antifungal, herbicidal, antiproliferative and anti-inflammatory activities [49–52]. These compounds have shown antitumor activity against a range of human breast, ovarian, and colon cancers [53,54]. They are also useful for the *in-vivo* diagnosis of Alzheimer's disease [55,56].

Conventionally, 2-substituted benzothiazoles are synthesized by condensation of 2-aminothiophenol with aldehyde derivatives in different conditions. Various catalysts such as ZnO-beta zeolite [56], solid silica supported ferric chloride ($\text{SiO}_2\text{-FeCl}_3$) [57], glucose oxidase (GOX)/chloroperoxidase (CPO) [58], perchloric acid-doped polyaniline ($\text{HClO}_4/\text{PANI}$) [59], $\text{Sc}(\text{OTf})_3$ [60], YCl_3 and mixed metal oxide nano crystals of $\text{Al}_2\text{O}_3\text{-Fe}_2\text{O}_3$, $\text{Al}_2\text{O}_3\text{-V}_2\text{O}_5$ and $\text{Al}_2\text{O}_3\text{-CuO}$ were used in the synthesis of benzothiazoles. However, there is still room for improvement in the present methods to overcome the limitations and disadvantages of using organic solvents, long reaction times, lower yields and tedious work-up procedures. In this paper, we have reported the development of an environmental friendly protocol for the synthesis of 1,3-benzothiazole derivatives.

Nowadays, ZnS is an important member of this family as it has been extensively investigated [26]. ZnS nanoparticles have attracted a tremendous amount of attention because of their remarkable properties such as low cost, easy synthesis, high stability, small size etc [27]. Because of the importance of benzimidazoles and the catalytic ability of ZnS nanoparticles in the organic reactions, we wish to report a facile and efficient method for the synthesis of benzimidazole derivatives in the presence of catalytic amounts of ZnS nanoparticles in ethanol as solvent at 70°C.

2. Experimental

Chemicals are used of the S.D.Fine chemicals and Loba Chemicals products were characterized by their physical constant via the comparison with the authentic samples. Samples are purified by using column chromatography and progress of the reaction was monitored by using thin layer chromatography. Thin layer chromatography was performed using the aluminium plates with silica coating.

2.1. Synthesis of ZnS nanoparticles

ZnS nanoparticles were prepared by chemical method [5]. The reactants used for synthesis of ZnS nanoparticles were sodium sulphide ($\text{Na}_2\text{S}\cdot 7\text{H}_2\text{O}$) and Zinc sulphate ($\text{ZnSO}_4\cdot 5\text{H}_2\text{O}$). Using stoichiometric ratio in grams, 1 M solution of each reactant was prepared in distilled water. Freshly prepared aqueous solutions of these chemicals were used for the synthesis of nanoparticles at room temperature. The ZnS nanoparticles were prepared in the following sequence: First the extract prepared from waste stem of the *Trigonella foenum-graecum* (0.25 g) was added to the Zinc sulphate solution. The solution containing sodium sulphide was then added drop wise in solution of zinc sulphate and extract under continuous stirring until the white precipitates were formed. Stirring was done for 20 min to complete the reaction.

These precipitates were washed several times with distilled water to remove the impurities of sodium. After washing, the precipitates were centrifuged and dried at 100°C for 24 h. After drying, nanoparticles were grinded to achieve fine powder for characterization.

2.2. General procedure for the synthesis of benzimidazole derivatives

o-phenylenediamine (1 mmol) was added to a mixture of plant assisted nanoparticles (30 mg) and aldehyde (1 mmol) and the

resulting mixture was sonication on the probe sonicate. After completion of the reaction, as monitored by TLC (EtOAc: hexane 5:5), ethyl acetate (20 mL) was added and the catalyst was separated by filtration. The solvent was then removed under reduced pressure and the resulting solid product was recrystallized from ethanol, producing the pure product in good to high yields.

2.3. General procedure for the synthesis of benzothiazole derivatives

o-phenylenediamine (1 mmol) was added to a mixture of Plant assisted nanoparticles (30 mg) and aldehyde (1 mmol) and the resulting mixture was sonication on the probe sonicate. After completion of the reaction, as monitored by TLC (EtOAc: hexane 8:2), ethyl acetate (20 mL) was added and the catalyst was separated by filtration. The solvent was then removed under reduced pressure and the resulting solid product was recrystallized from ethanol, producing the pure product in good to high yields.

2.4. UV-visible spectrum for ZnS nanoparticles

The UV-Visible spectrum of the prepared ZnS nanoparticles is shown in the Fig. 1. It shows a strong absorption peak around 265–270 nm which is large blue shifted from the bulk absorption. From the absorption peak the optical energy band gap of ZnS nanostructure has been calculated using the formula, $E_{gn} = h\nu_{gn} = hc/\lambda_{gn}$ where h is plank's constant and E_g is energy band gap of the semiconducting nanoparticles in the optical spectra.

2.5. XRD study

X-ray diffraction patterns of the synthesized ZnS colloidal powders have been depicted in Fig. 2. The XRD traces shows that the prepared zinc sulphate is crystalline having zinc blende type structure. The cubic zinc blende structure was confirmed from the agreement of 2θ values with standard data. Fig. 2, showed three diffraction peaks at 2θ values of 28.96, 48 and 56.52. The peaks were identified to originate from (111), (220) and (311) planes of the cubic zinc-blende phase of ZnS, respectively.

The particle size calculated using Debye Scherer formula was 2.8 nm. The Debye Scherer formula is $D = 0.9 \lambda / (\beta \cos \theta)$ (2) where D is the mean grain size, λ is the X-ray wavelength, θ is the diffraction angle and β is full width at half maximum.

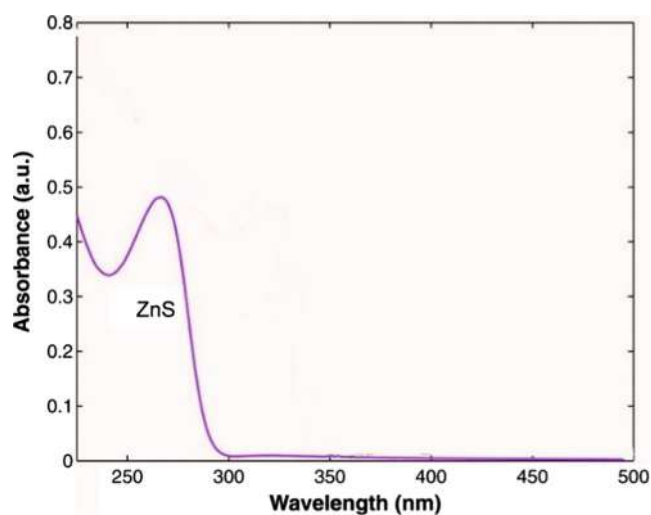


Fig. 1. UV spectrum of prepared ZnS nanoparticles.

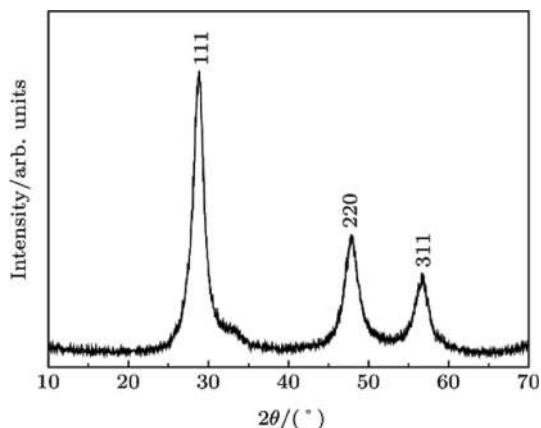


Fig. 2. X-ray diffraction patterns of the synthesized ZnS colloidal powders.

2.6. FTIR

The FTIR spectrum of ZnS nanoparticles at room temperature is shown in Fig. 3. This spectrum shows the IR absorption due to the various vibration modes. The characteristic major peaks of ZnS can be observed at about 1060, 1236, 1404, 788, 592, which are in good agreement with the reported results. The observed peaks at 1538 cm^{-1} – 1659 cm^{-1} are assigned to the C=O stretching modes, and also the broad absorption peaks in a range of 3434 cm^{-1} – 3965 cm^{-1} correspond to O–H stretching modes arising from the absorption of water on the surface of nanoparticles via –COOH group.

2.7. SEM

The SEM microstructural analysis shows that the synthesized ZnS contains mainly the grains of ZnS particles (crystallite) with regular shape (Fig. 4). One can see that nearly spherical nanoparticles have an almost homogenous size distribution with a mean size of 80–90 nm. In the absence of EDTA, a bulk ZnS sample is formed (not shown here). In the synthesis process, the usage of EDTA causes the stabilization of the small particles and the inhibition of this agglomeration. Due to the existence of –COOH group in EDTA molecules which absorbed on the particle surface, EDTA-

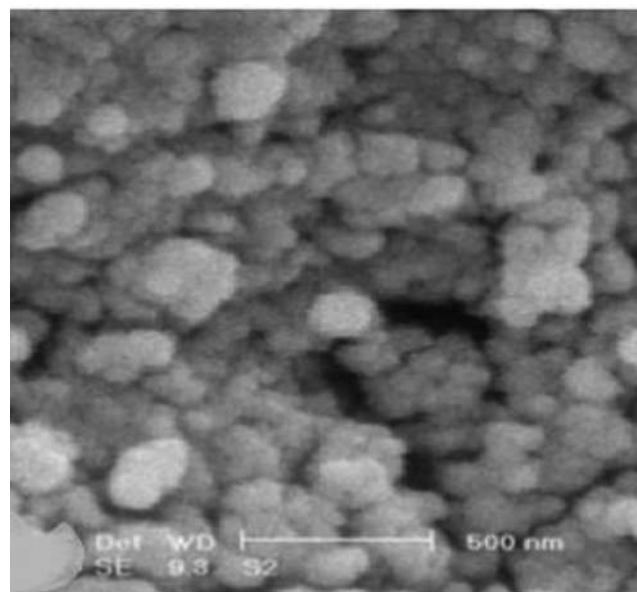


Fig. 4. The SEM image of ZnS nanoparticles.

capped ZnS sample is formed. The maximum particle size does not exceed 70 nm.

In order to establish the better catalytic activity of nano-ZnS, the reaction in the presence of other catalysts in ethanol at 70°C was investigated. The results showed that the nano-ZnS, as compared to other catalysts, gave the better yield of the desired product.

To determine the optimum quantity of nano-ZnS, the reaction of benzaldehyde and *o*-phenylenediamine was carried out in ethanol at 70°C using different quantities of nano-ZnS. The results showed that 0.03 g for benzimidazole and for benzothiazole 0.09 of the catalyst gave the excellent yield of the product. (See Tables 1–6).

3. Results and discussion

On the basis of the research information obtained on the applicability of plant assisted nanoparticles in the promotion of different types of organic reactions, we expected that this reagent

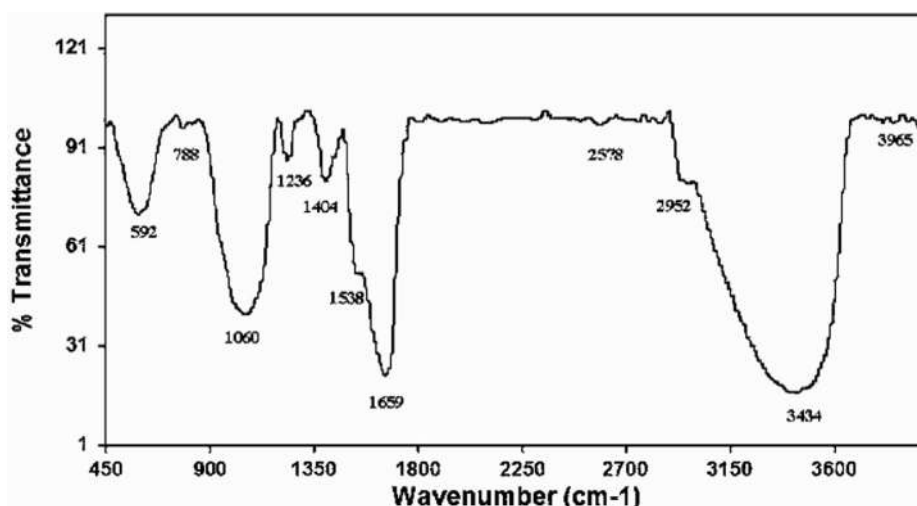


Fig. 3. The FTIR spectrum of ZnS nanoparticles.

Table 1
Evaluation of the activity of different catalysts for the synthesis of 2-phenyl-1H-benzimidazole.

Entry	Catalyst	Time (min)	Yield (%) (Benzimidazole)	Yield (%) (Benzothiazole)
1	–	60	25	35
2	Zinc Oxide	60	70	45
3	Alum	60	65	67
4	Hydrochloric Acid	60	65	55
5	Para-toluene Sulphonic Acid	60	67	54
6	NH ₄ Cl	60	87	86
7	Nano ZnS	60	97	96

Table 2
Optimization amount of nano-ZnS for the synthesis of 2-phenyl-1H-benzimidazole.

Entry	Catalyst (g)	Time (min)	Yield (%) (Benzimidazole)	Yield (%) (Benzothiazole)
1	–	60	40	43
2	0.01	60	56	67
3	0.03	60	98	56
4	0.09	60	78	97
5	0.20	60	67	78

Table 3
Optimization of the reaction temperature in the synthesis of 2-phenyl-1H-benzimidazole using nano-ZnS.

Entry	Temperature (°C)	Time (min)	Yield (%) (Benzimidazole)	Yield (%) (Benzothiazole)
1	70	60	97	95
2	60	60	70	80
3	40	60	78	70
4	25	60	67	45

Table 4
Reaction between *o*-phenylenediamine and different aldehydes catalyzed by nano-ZnS (0.03 g) in EtOH at 70 °C.

Entry	Ar	Time (min)	Yield (%) (Benzimidazole)	Yield (%) (Benzothiazole)
1	2-NO ₂ C ₆ H ₄	60	95	92
2	3-NO ₂ C ₆ H ₄	60	95	94
3	4-NO ₂ C ₆ H ₄	60	96	91
4	4-NHCH ₃ C ₆ H ₄	60	91	89
5	2-OH-3CH ₃ OC ₆ H ₄	60	85	81
6	4-ClC ₆ H ₄	60	87	86
7	4-OHC ₆ H ₄	60	98	95
8	3,4(CH ₃ O) ₂ C ₆ H ₃	60	89	92

Table 5
Catalyst Reusable for Benzimidazole.

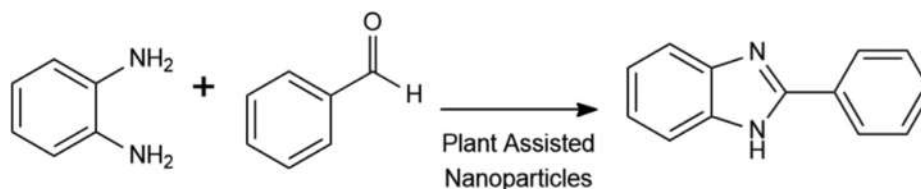
Entry	Catalyst (g)	Time (min)	Catalyst Cycle	Yield (%) (Benzimidazole)
1	0.03	60	1	96
2	0.03	60	2	82
3	0.03	60	3	78
4	0.03	60	4	56
5	0.03	60	5	40

Table 6
Catalyst Reusable Benzothiazole.

Entry	Catalyst (g)	Time (min)	Catalyst Cycle	Yield (%) (Benzothiazole)
1	0.03	60	1	94
2	0.03	60	2	78
3	0.03	60	3	67
4	0.03	60	4	56
5	0.03	60	5	45

could also be efficiently used in promoting the synthesis of benzimidazole and benzothiazole; these compounds function as acidic catalysts and speed up the reaction. Initially, optimize reaction conditions were studied by investigating the effect of various reac-

tant molar ratios and solvents. and also, solvent-free conditions, on the reaction of substituted benzaldehyde (10 mmol) and *o*-phenylenediamine (10 mmol) in terms of time and the product yield. The obtained results showed that the reaction using 30 mg



Scheme 1. Organic transformation using plant assisted nanoparticles.

of the catalyst at room temperature under a solvent-free condition in sonication produced the highest yield during a very short time.

Any further increase of the temperature or the catalyst amount did not improve the reaction time and yield. After optimizing the reaction conditions and in order to show the general applicability of this method, the preparation of benzimidazoles derivatives with a variety of simple, readily available substrates under the optimal conditions was investigated. Several aldehydes having electron donating and electron withdrawing groups underwent the conversion to form a series of aryl benzimidazoles in good to excellent yields. As can be seen, o-phenylenediamines with electron-withdrawing groups gave the desired products in higher yields within longer times in excellent yields.

After the successful synthesis of benzimidazoles, the preparation of benzothiazole derivatives, as the other useful heterocyclic compounds, in the presence of plant assisted nanoparticles, was nominated for further study.

Our investigations clarified that by using this method, the best results can be obtained when the reaction proceeded using lower amounts of the catalyst (90 mg) under solvent-free conditions at ambient temperatures. It is important to note that this reaction was not completed in different types of solvents even after a long time under reflux conditions. The selected conditions are shown in Scheme 1. To assess the efficiency of plant assisted nanoparticles in the preparation of benzothiazole derivatives, various aromatic aldehydes were subjected to the optimal conditions. It was observed that under the selected conditions, all the substrates containing electron-withdrawing groups, as well as electron-donating groups, were easily reacted in short reaction times with good to excellent isolated yields.

To check the reusability of the catalyst, the reaction of o-phenylenediamine with benzaldehyde or aromatic aldehyde under the optimized reaction condition was studied again. When the reaction was completed, ethyl acetate was added and the catalyst was separated by filtration. The recovered catalyst was washed with dichloromethane, dried and reused for the same reaction. The recovered catalyst was reused five times with a slight decrease in reusability in comparison to fresh catalyst. In order to show the efficiency of the present method, our result obtained from the reaction between o-phenylenediamine and benzaldehyde in the presence of plant assisted nanoparticles was compared with some of the other results reported in the literature for the same reaction. This method avoids the disadvantages of other procedures such as long reaction times, excess reagents and organic solvents.

4. Conclusion

We have used plant assisted nanoparticles as a highly catalyst for the simple and efficient synthesis of benzimidazole and benzothiazole and their derivatives. The procedure has several advantages, such as ease of preparation and handling of the catalyst, being a simple experimental procedure, having high reaction rates, producing excellent yields and the use of inexpensive and reusable catalyst. Furthermore, this process avoids problems associated with the use of organic solvents and liquid acids, which makes it

a useful and attractive strategy in view of these economic and environmental advantages.

Data availability

Data will be made available on request.

Declaration of Competing Interest

The authors declare that they have no known competing financial interests or personal relationships that could have appeared to influence the work reported in this paper.

Acknowledgments

We are thankful to Rayat Shikshan Sanstha, Satara for providing research facilities.

References

- [1] M. Boiani, M. Gonzalez, Imidazole and benzimidazole derivatives as chemotherapeutic agents, *Mini-Rev. Med. Chem.* 5 (2005) 409–424.
- [2] B. Narasimhan, D. Sharma, P. Kumar, Benzimidazole: A medicinally important heterocyclic moiety, *Med. Chem. Res.* 21 (2012) 269–283.
- [3] Y. Bansal, O. Silakari, The therapeutic journey of benzimidazoles: a review, *Bioorg. Med. Chem.* 20 (2012) 6208–6236.
- [4] K. Shah, S. Chhabra, S.K. Shrivastava, P. Mishra, Benzimidazole: a promising pharmacophore, *Med. Chem. Res.* 22 (2013) 5077–5104.
- [5] G. Yadav, S. Ganguly, Structure activity relationship (SAR) study of benzimidazole scaffold for different biological activities: a mini-review, *Eur. J. Med. Chem.* 97 (2015) 419–443.
- [6] M. Gaba, C. Mohan, Development of drugs based on imidazole and benzimidazole bioactive heterocycles: recent advances and future directions, *Med. Chem. Res.* 25 (2016) 173–210.
- [7] Starcevic, K.; Kralj, M.; Ester, K.; Sabol, I.; Grce, M.; Pavelić, K.; Karminski-Zamola, G. Synthesis, antiviral and antitumor activity of 2-substituted-5-amidino-benzimidazoles. *Bioorg. Med. Chem.* 2007, 15, 4419–4426.
- [8] A. Gellis, H. Kovacic, N. Boufatah, P. Vanelle, Synthesis and cytotoxicity evaluation of some benzimidazole-4,7-diones as bioreductive anticancer agents, *Eur. J. Med. Chem.* 43 (2008) 1858–1864.
- [9] Purushottamachar, P.; Ramalingam, S.; Njar, V.C. Development of benzimidazole compounds for cancer therapy. In *Chemistry and Applications of Benzimidazole and Its Derivatives*; Marinescu, M., Ed.; IntechOpen: Rijeka, Croatia, 2019; ISBN 978-1-78984-552-5.
- [10] Hranjec, M.; Starcević, K.; Pavelić, S.K.; Lucin, P.; Pavelić, K.; Karminski Zamola, G. Synthesis, spectroscopic characterization and antiproliferative evaluation in vitro of novel Schi₁ bases related to benzimidazoles. *Eur. J. Med. Chem.* 2011, 46, 2274–2279.
- [11] N. Shrivastava, M.J. Naim, M.J. Alam, F. Nawaz, S. Ahmed, O. Alam, Benzimidazole sca_{old} as anticancer agent: Synthetic approaches and structure-activity relationship: Benzimidazole Sca_{old} as Anticancer Agent, *Arch. Pharm. Chem. Life Sci.* 350 (2017) e201700040.
- [12] R.V. Shingalapur, K.M. Hosamani, R.S. Keri, M.H. Hugar, Derivatives of benzimidazole pharmacophore: synthesis, anticonvulsant, antidiabetic and DNA cleavage studies, *Eur. J. Med. Chem.* 45 (2010) 1753–1759.
- [13] M. Ishikawa, K. Nonoshita, Y. Ogino, Y. Nagae, D. Tsukahara, H. Hosaka, H. Maruki, S. Ohyama, R. Yoshimoto, K. Sasaki, et al., Discovery of novel 2-(pyridine-2-yl)-1H-benzimidazole derivatives as potent glucokinase activators, *Bioorg. Med. Chem. Lett.* 19 (2009) 4450–4454.
- [14] D.A. Powell, Y. Ramtohol, M.-E. Lebrun, R. Oballa, S. Bhat, J.-P. Falgueyret, S. Guiral, Z. Huang, K. Skorey, P. Tawa, et al., 2-Aryl benzimidazoles: Human SCD1-specific stearyl coenzyme-A desaturase inhibitors, *Bioorg. Med. Chem. Lett.* 20 (2010) 6366–6369.
- [15] Kazimierzczuk, Z.; Upcroft, J.A.; Upcroft, P.; Górska, A.; Starósciak, B.; Laudy, A. Synthesis, antiprotozoal and antibacterial activity of nitro- and halogeno-substituted benzimidazole derivatives. *Acta Biochim. Pol.* 2002, 49, 185–195.

- [16] K.F. Ansari, C. Lal, Synthesis and evaluation of some new benzimidazole derivatives as potential antimicrobial agents, *Eur. J. Med. Chem.* 44 (2009) 2294–2299.
- [17] K.F. Ansari, C. Lal, Synthesis, physicochemical properties and antimicrobial activity of some new benzimidazole derivatives, *Eur. J. Med. Chem.* 44 (2009) 4028–4033.
- [18] L.K. Labanauskas, A.B. Brukštus, P.G. Gaidelis, V.A. Buchinskaitė, Ė.B. Udrenaitė, V.K. Daukšas, Synthesis and antiinflammatory activity of some new 1-acyl derivatives of 2-methylthio-5,6-diethoxybenzimidazole, *Pharm. Chem. J.* 34 (2000) 353–355.
- [19] G. Tsukamoto, K. Yoshino, T. Kohno, H. Ohtaka, H. Kagaya, K. Ito, 2-Substituted azole derivatives. 1. synthesis and antiinflammatory activity of some 2-(substituted-pyridinyl)benzimidazoles, *J. Med. Chem.* 23 (1980) 734–738.
- [20] K. Ito, H. Kagaya, T. Fukuda, K. Yoshino, T. Nose, Pharmacological studies of a new non-steroidal antiinflammatory drug: 2-(5-ethylpyridin-2-yl)benzimidazole (KB-1043), *Arzneimittelforschung* 32 (1982) 49–55.
- [21] B. Can-Eke, M. Orhan Puskullu, E. Buyukbingol, M. Iscan, A study on the antioxidant capacities of some benzimidazoles in rat tissues, *Chem. Biol. Interact.* 113 (1998) 65–77.
- [22] J.B. Wright, The chemistry of the benzimidazoles, *Chem. Rev.* 48 (1951) 397–541.
- [23] P.N. Preston, Synthesis, reactions, and spectroscopic properties of benzimidazoles, *Chem. Rev.* 74 (1974) 279–314.
- [24] S.I. Alaqeel, Synthetic approaches to benzimidazoles from o-phenylenediamine: a literature review, *J. Saudi Chem. Soc.* 21 (2017) 229–237.
- [25] E.J. Hanan, B.K. Chan, A.A. Estrada, D.G. Shore, J.P. Lyssikatos, *Synlett* 18 (2010) 2759.
- [26] D. Yang, D. Fokas, J. Li, L. Yu, C.M. Baldino, *Synthesis* 1 (2005) 47.
- [27] W. Cui, R.B. Kargbo, Z. Sajjadi-Hashemi, F. Ahmed, J.F. Gauuan, *Synlett* 23 (2012) 247.
- [28] J. Sluiter, J. Christoffers, *Synlett* 1 (2009) 63.
- [29] B.C. Wray, J.P. Stambuli, *Org. Lett.* 12 (2010) 4576.
- [30] P. Saha, T. Ramana, N. Purkait, M.A. Ali, R. Paul, T. Punniyamurthy, *J. Org. Chem.* 74 (2009) 8719.
- [31] A. Hegedüs, Z. Hell, A. Potor, Zeolite-catalyzed environmentally friendly synthesis of benzimidazole derivatives, *Synth. Commun.* 36 (2006) 3625–3630.
- [32] A. Mobinikhaledi, N. Forughifar, M. Zendehtdel, M. Jabbarpour, Conversion of aldehydes to benzimidazoles using NaY zeolite, *Synth. React. Inorg. Met. Org. Nano-Met. Chem.* 38 (2008) 390–393.
- [33] A. Mobinikhaledi, M. Zendehtdel, F. Goudarzi, G.R. Bardajee, Nano-Ni(II)/Y Zeolite catalyzed synthesis of 2-aryl- and 2-alkyl benzimidazoles under solvent-free conditions, *Synth. React. Inorg. Met. Org. Nano-Met. Chem.* 46 (2016) 1526–1531.
- [34] K. Bahrami, M.M. Khodaei, A. Nejati, Synthesis of 1,2-disubstituted benzimidazoles, 2-substituted benzimidazoles and 2-substituted benzothiazoles in SDS micelles, *Green Chem.* 12 (2010) 1237–1241.
- [35] a) T.T. Nguyen, X.-T.-T. Nguyen, T.-L.-H. Nguyen, P.H. Tran, Synthesis of benzoxazoles, benzimidazoles, and benzothiazoles using a Brønsted acidic ionic liquid gel as an efficient heterogeneous catalyst under solvent-free condition, *ACS Omega* 4 (2019) 368–373; b) M. Adharvana Chari, D. Shobha, T. Sasaki, Room temperature synthesis of benzimidazole derivatives using reusable cobalt hydroxide (II) and cobalt oxide (II) as efficient solid catalysts, *Tetrahedron Lett.* 52 (2011) 5575–5580.
- [36] B. Das, B.S. Kanth, K.R. Reddy, A.S. Kumar, Sulfonic acid functionalized silica as an efficient heterogeneous recyclable catalyst for one-pot synthesis of 2-substituted benzimidazoles, *J. Heterocycl. Chem.* 45 (2008) 1499–1502.
- [37] K. Bahrami, M. Bakhtiaran, Mesoporous titania-alumina mixed oxide: A heterogeneous nanocatalyst for the synthesis of 2-substituted benzimidazoles, benzothiazoles and benzoxazoles, *ChemistrySelect* 3 (2018) 10875–10880.
- [38] B. Chen, C. Zhang, L. Niu, X. Shi, H. Zhang, X. Lan, G. Bai, Biomass-derived N-doped carbon materials with silica-supported ultrasmall ZnO nanoparticles: robust catalysts for the Green synthesis of benzimidazoles, *Chem. Eur. J.* 24 (2018) 3481–3487.
- [39] P. Bandyopadhyay, M. Sathe, S. Ponmariappan, A. Sharma, P. Sharma, A.K. Srivastava, M.P. Kaushik, Exploration of in vitro time point quantitative evaluation of newly synthesized benzimidazole and benzothiazole derivatives as potential antibacterial agents, *Bioorg. Med. Chem. Lett.* 21 (2011) 7306–7309.
- [40] R. Fazaeli, H. Aliyan, A Heterogeneous catalyst for efficient and green synthesis of 2-arylbenzothiazoles and 2-arylbenzimidazoles, *Appl. Catal. A Gen.* 353 (2009) 74–79 [CrossRef].
- [41] K. Jeshma, B. Nagaraju, A. Kamal, K.S. Ajay, *ACS Comb. Sci.* 18 (2016) 644.
- [42] H. Sharghi, O. Asemani, S.M.H. Tabaei, *Chem. Susc.* 45 (2008) 1293.
- [43] D. Kathirvelan, P. Yuvaraj, K. Babu, A.S. Nagarajan, B.S.R. Reddy, *J. Indian. Chem.* 52 (2013) 1152.
- [44] M.S. Kedar, N.S. Dighe, S.H.R. Pattan, D.S. Musmade, T. Dipak, M. Bhosale, G.V. M. Der, *Pharma Chem.* 2 (2010) 249.
- [45] a) H. Baars, A. Beyer, S.V. Kohlhepp, C. Bolm, *Org. Lett.* 16 (2014) 536; b) J. Sluiter, J. Christoffers, *Synlett* (2009) 63; c) P. Saha, T. Ramana, N. Purkait, M.A. Ali, R. Paul, T. Punniyamurthy, *J. Org. Chem.* 74 (2009) 8719.
- [46] a) Zhang Z.H., Yin L., Wang Y.M. *Catal. Commun.*, 2007, 8:1126; b) Kommi D.N., Kumar D., Bansal R., Chebolu R., Chakraborti A.K. *Green Chem.*, 2012, 14:3329; c) Bressi J.C., Jong R.D., Wu Y., Jennings A.J., Brown J.W., Connell O.S., Tari L.W., Skene R.J., Vu P., Naver M., Cao X., Gangloff A.R. *Bioorg. Med. Chem. Lett.*, 2010, 20:3138.
- [47] a) D. Mahesh, P. Sadhu, T. Punniyamurthy, *J. Org. Chem.* 80 (2015) 1644; b) A.J. Blacker, M.M. Farah, M.I. Hall, S.P. Marsden, O. Saidi, J.M.J. Williams, *Org. Lett.* 11 (2009) 2039.
- [48] a) Dudd L.M., Venardou E., Garcia-Verdugo E., Licence P., Blake A.J., Wilson C., Poliakov M. *Green Chem.*, 2003, 5:187; b) Rambabu D., Murthi P.R.K., Dulla B., Rao B.M.V., Pal M. *Synth. Commun.*, 43:3083.
- [49] Z. Wang, X.H. Shi, J. Wang, T. Zhou, Y.Z. Xu, T.T. Huang, Y.F. Li, Y.L. Zhao, L. Yang, S.Y. Yang, L.T. Yu, Y.Q. Wei, *Bioorg. Med. Chem. Lett.* 21 (2011) 1097.
- [50] M. D. Altıntop, Z. A. Kaplancıklı, G. I. T. Zitouni, A. O. zdemir, F. Demirci, G. k. Is, can, G. Revial, *Synth. Commun.*, 41, 2234 (2011).
- [51] P. Datta, D. Sardar, A.P. Mukhopadhyay, E.L. Torres, C.J. Pastor, C. Sinha, *J. Organomet. Chem.* 696 (2011) 488.
- [52] Y. Q. Yuan, S. R. Guo, *Synth. Commun.*, 41, 2169 (2011).
- [53] a) T. H. Al-Tel, R. A. Al-Qawasmeh, R. Zaarour, *Eur. J. Med. Chem.*, 46, 1874 (2011), b) B. H. Yousefi, A. Manook, A. Drzezga, B. V. Reutern, M. Schwaiger, H. J. Wester, G. Henriksen, *J. Med. Chem.*, 54, 949 (2011).
- [54] T.I.A. Gerber, K.C. Potgieter, P. Mayer, *Inorg. Chem. Commun.* 14 (2011) 1115.
- [55] S.S. Katkar, P.H. Mohite, L.S. Gadekar, K.N. Vidhate, M.K. Lande, *Chin. Chem. Lett.* 21 (2010) 421.
- [56] M.H. Mosslemin, A. Fazlinia, Phosphorus, Sulfur Silicon Relat. Elem. 185 (2010) 2165.
- [57] A. Kumar, S. Sharma, R.A. Maurya, *Tetrahedron Lett.* 51 (2010) 6224.
- [58] M. Abdollahi-Alibeik, S. Poorirani, Phosphorus, Sulfur Silicon Relat. Elem. 184 (2009) 3182.
- [59] T. Itoh, K. Nagata, H. Ishikawa, A. Ohsawa, *Heterocycles* 62 (2004) 197.
- [60] L.-J. Zhang, J. Xia, Y.-Q. Zhou, H. Wang, S.-W. Wang, *Synth. Commun.* 42 (2012) 328.



Synthesis and biological screening of novel series of 2-(4-hydroxy-3-methoxy-5-nitro-phenyl)-[1,3,4]oxadiazole by conventional and non conventional techniques

Ranjana Jadhav^{a,*}, Sunayna Pawar^a, Chandrakant Khilare^a, Arun Nikumbh^b

^a P.G. & Research, Department of Chemistry, S. M. Joshi College, Hadapsar, Pune 411028, Maharashtra, India

^b Department of Chemistry, Annasaheb Aawate College Manchar, Pune, Maharashtra, India

ARTICLE INFO

Article history:

Available online 25 October 2022

Keywords:

Acid
Hydrazide
[1,3,4] oxadiazole
Biological activities

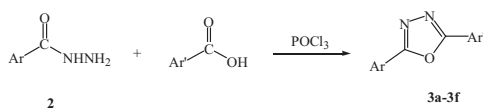
ABSTRACT

Novel acid hydrazide **1** when reacted with a series of different carboxylic acids in presence of phosphorous oxychloride to give novel series of 2-(4-hydroxy-3-methoxy-5-nitro-phenyl)-[1,3,4]oxadiazole **3a-3f**. Use of conventional and non-conventional techniques is adapted to study the duration time of reaction. These oxadiazole compounds are studied by using spectral analysis like ¹H NMR, FT-IR and mass spectroscopy. Further they are screened for antibacterial and anti-fungal biological activities.

Copyright © 2022. Elsevier Ltd. All rights reserved.

Selection and peer-review under responsibility of the scientific committee of the Integrative Nanotechnology Perspective for Multidisciplinary Applications - 2022.

Scheme:



1. Introduction

Oxadiazoles are five - membered heterocycles, contains two carbon, one oxygen, and two nitrogen atoms, which attracted a lot of interest in different scientific disciplines: from medicine [1,2] and agro chemistry [3] to materials science [4,5].

Depending on nitrogen atoms position, oxadiazoles exist in four different isomeric forms 1,2,3-, 1,2,4-, 1,2,5-, and 1,3,4-oxadiazoles Fig. 1.

Among the four isomers, 1,2,4- and 1,3,4-oxadiazoles frequently occur in a large series of drug-like molecules [6], including antiviral [2,7], antihypertensive [8], anti-diabetic [9], anti-inflammatory, analgesic [10] and anticancer compounds [11–15].

This is one of the popular classes of heterocyclic compounds in medicinal chemistry which is confirmed by the presence of several

drugs based on the oxadiazole moiety. The reasons for their success lie in an efficient and simple synthesis, remarkable stability, high versatility, structural diversity, and a key feature for in vivo applications. Oxadiazoles easily interact with bio-targets establishing π -stacking interactions or forming strong hydrogen bonds.

During the last decades, the design of new oxadiazole-based scaffolds increasing attention in medicinal chemistry, most of these compounds to the preclinical stage or, even, to commercialization. Among these, the most commercially available drugs are Oxolamine, a cough suppressant [16,17], Butalamine, a vasodilator, Proxazole, a drug for functional gastrointestinal disorders, Fasiplon, an anxiolytic drug [18], Ataluren, indicated for the treatment of muscular dystrophy [19] and Raltegravir, an antiretroviral drug used to treat HIV [20], which has been recently proposed as repurposing drug against SARS COV-2 [21] and the antiviral Pleconaril selected for the SARS COV-2 spike protein [22]. Introducing oxadiazole moiety with known drug enhanced there activity [23] Fig. 2.

Microwave-assisted synthesis is a branch of green chemistry. Microwave-assisted synthesis has gained much attention in recent years. Microwave irradiation-assisted chemical transformations are pollution free, eco-friendly and offer high yields together with simplicity in processing and handling [24–28].

Nowadays, microwave-assisted organic synthesis is gaining widespread acceptance in drug discovery laboratories. Temperature increases uniform throughout the sample, leading to fewer

* Corresponding author.

E-mail address: jadhavranjana2211@yahoo.co.in (R. Jadhav).

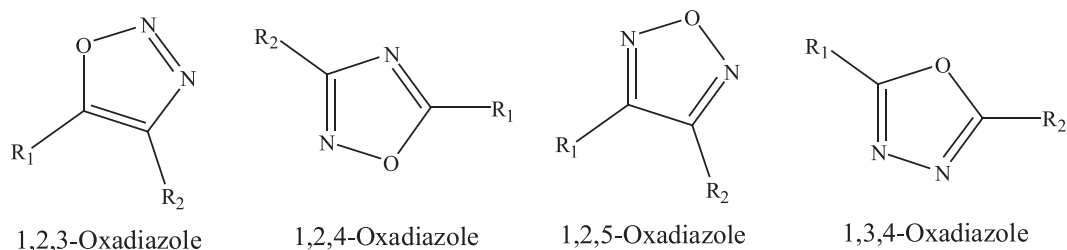


Fig. 1. Isomers of oxadiazoles.

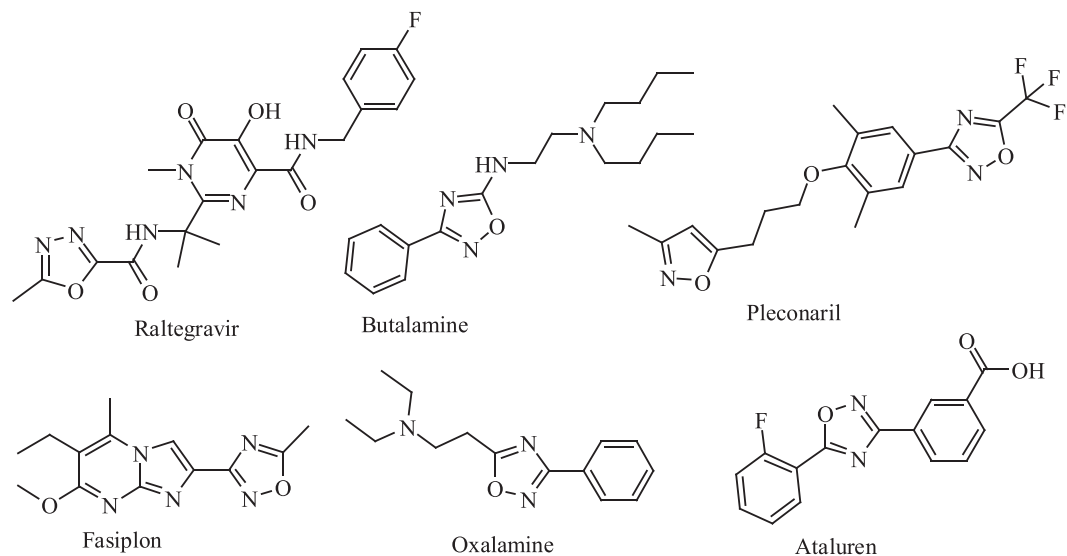


Fig. 2. Structures of some of the most famous drugs having oxadiazole moiety.

by-products and/or product decomposition. The use of microwave energy instead of conventional heating often results in good yields in a short time as compared with reaction by classical synthetic methods [29,30].

The synthesis of oxadiazoles was prompted us by the strong biological activity associated with them and therefore we synthesized novel oxadiazole molecules and characterized them by NMR, IR, Mass spectral analysis and screened them for antimicrobial activity.

2. Material and methods

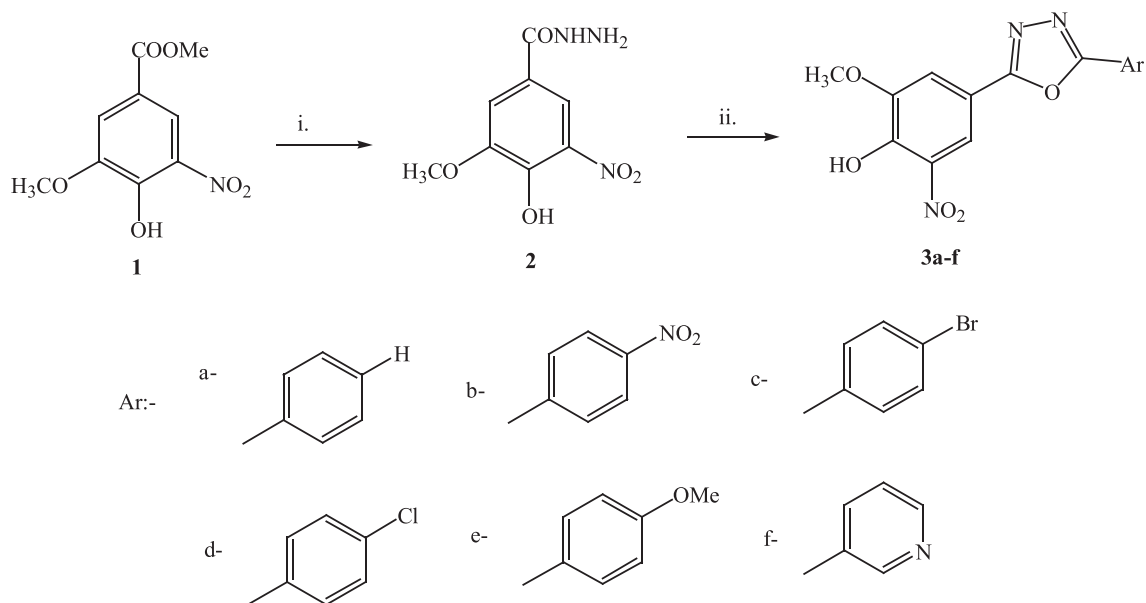
2.1. General experimental procedures

Reagents and chemicals used in this study were purchased from Sigma Aldrich. All organic solvents were distilled and

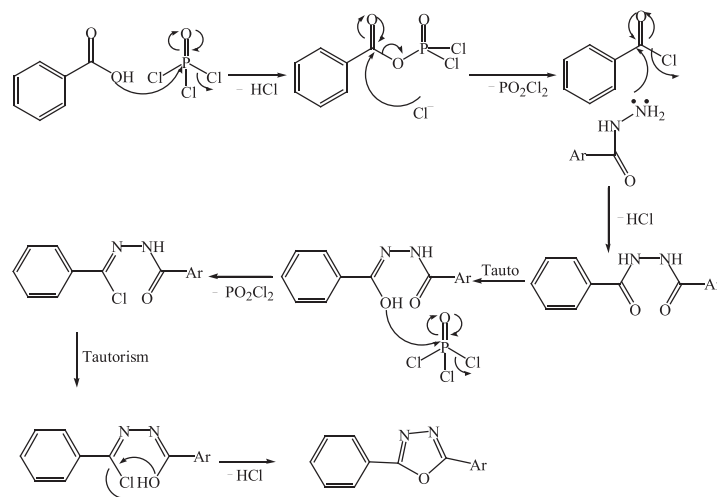
dried according to standard procedures. IR spectra were recorded on a Jasco Spectrum FT-IR spectrometer. Thin layer chromatography (TLC) was performed using Merck Kieselgel 60 F₂₅₄ plates.

¹H and ¹³C NMR spectra were recorded at 298 K with 5–10 mg samples dissolved in 0.5 ml of DMSO in 5 mm NMR tubes using a Bruker Avance^{III}300 MHz NMR spectrophotometer (9.4 T; Bruker, Germany) (300 MHz for ¹H, 75 for ¹³C NMR). Coupling constants (*J*) are stated in Hz, and chemical shifts (δ) are recorded in ppm. The ¹H and ¹³C NMR chemical shifts of the deuterated solvent were 2.50 and 39.52 respectively, referenced to the internal standard, TMS.

- i) 5-nitro methyl vanillate, hydrazine hydrate, EtOH, 100° C, reflux, 24 hr;
- ii) acid, POCl₃, 110° C, reflux, 24 - 48 hr.



Scheme 1. . Synthetic scheme for the synthesis of hydrazide (1) and oxadiazoles (3a-3f):



Proposed mechanism for Oxadiazole

General procedure for the synthesis of the hydrazide as a starting material.

4-hydroxy-3-methoxy-5-nitrohydrazide2.

5-nitro methyl vanillate (1.0 g, 0.0238 mol) was reacted with hydrazine hydrate (15.0 ml, 0.0952 mol) in ethanol, reaction mixture reflux at 100° C for 24 hr. The reaction was monitored by TLC using EtOAc: *n*-hexane (20:80, *R_f* = 0.6). After reaction completion it was cooled to room temperature, the product gets precipitated in reaction mixture. Obtained crude product after filtration was purified by re-crystallization using water to afford hydrazide(4-hydroxy-3-methoxy-5-nitrohydrazide)2 as a brown crystalline solid (80.6 % yield) with a melting point of 126 °C.

¹H NMR (300 MHz, DMSO): δ14.15 (1H, s, OH), 9.81 (1H, s, NH), 8.05 (1H, d, *J* = 1.5 Hz), 7.71 (1H, d, *J* = 1.5 Hz), 4.49 (1H, s, NH₂), 3.83 (3H, s, CH₃). ¹³C NMR (75 MHz, DMSO): δ167.2, 152.4, 141.4, 138.1, 128.7, 120.8, 120.8, 114.8, 56.1.

General procedure for the synthesis of oxadiazoles, 3a – 3f.

Conventional method:

The oxadiazoles were prepared according to our previously developed method [31] as outlined in Scheme 1.

A mixture of hydrazides (1) (100 mg, 0.5 mmol), the substituted acid (0.054 mg, 0.5 mmol) and phosphorus oxychloride (2.5 ml) were added at room temperature. The reaction mixture was refluxed for 24 – 48 hr at 110° C and monitored by TLC using EtOAc:hexane (10:90, *R_f* = 0.4). The reaction mixture was cooled

by drop-wise addition of ice-water (10 ml). Further reaction mixture neutralized by aqueous sodium hydroxide solution to obtain a precipitate of crude oxadiazole product. This crude oxadiazole product was purified by re-crystallization using ethanol. Pure oxadiazole compounds **3a–3f** obtained as brown solids and were characterized by ^1H and ^{13}C NMR, IR and Mass. NMR data for **3a–3f** are reported below.

Microwave method:

A mixture of hydrazides (**2**) (100 mg, 0.5 mmol), the substituted acid (0.054 mg, 0.5 mmol) and phosphorus oxychloride (2.5 ml) were added at room temperature. The reaction mixture was irradiated in microwave synthesizer at 350 W for time as shown in Table 1-1 for different analogs. The reaction mixture was cooled by drop-wise addition of ice-water (10 ml). Further reaction mixture neutralized by aqueous sodium hydroxide solution to obtain a precipitate of crude oxadiazole product. This crude oxadiazole product was purified by re-crystallization using ethanol. Pure oxadiazole compounds **3a–3f** obtained as brown solids.

2-(4-Hydroxy-3-methoxy-5-nitro-phenyl)-5-phenyl-[1,3,4]oxadiazole (3a) yellow solid; mp 114–115 °C; $R_f = 0.5$ (EtOAc:hexane, 10:90); IR λ^{max} 3431, 1640, 1571, 1343, 1290, 1084 cm^{-1} ; ^1H NMR (300 MHz, DMSO): δ 14.15 (1H, s, OH), 8.11 (1H, d, $J = 1.5$ Hz), 7.98 (2H, m), 7.84 (1H, d, $J = 1.5$ Hz), 7.62 (3H, m), 3.83 (3H, s, CH_3). ^{13}C NMR (75 MHz, DMSO): δ 164.5, 152.8, 138.5, 138.0, 133.7, 129.2, 128.7, 127.5, 120.6, 118.8, 116.5, 56.1; MS (m/z) ($m + 1$) = 314.07 ($\text{C}_{15}\text{H}_{11}\text{N}_3\text{O}_5$).

2-(4-Hydroxy-3-methoxy-5-nitro-phenyl)-5-(4-nitro-phenyl)-[1,3,4]oxadiazole (3b) yellow solid; mp 128 °C; $R_f = 0.6$ (EtOAc:hexane, 10:90); IR λ^{max} 3430, 1649, 1571, 1343, 1286, 1064, cm^{-1} ; ^1H NMR (300 MHz, DMSO): δ 14.18 (1H, s, OH), 8.41 (2H, dd, $J = 7.5, 1.5$ Hz), 8.23 (2H, dd, $J = 7.5, 1.5$ Hz), 8.22 (1H, d, $J = 1.5$ Hz), 7.92 (1H, d, $J = 1.5$ Hz), 3.80 (3H, s, CH_3). ^{13}C NMR (75 MHz, DMSO): δ 164.6, 152.8, 147.9, 138.5, 138.0, 132.2, 130.9, 128.8, 120.6, 118.8, 116.5, 55.1; MS (m/z) ($m + 1$) = 368.05 ($\text{C}_{15}\text{H}_{10}\text{N}_4\text{O}_7$).

2-(4-Bromo-phenyl)-5-(4-Hydroxy-3-methoxy-5-nitro-phenyl)-[1,3,4]oxadiazole (3c) orange solid; mp 136 °C; $R_f = 0.6$ (EtOAc:hexane, 10:90); IR λ^{max} 3331, 1630, 1570, 1344, 1279, 1064, cm^{-1} ; ^1H NMR (300 MHz, DMSO): δ 14.20 (1H, s, OH), 8.02 (1H, d, $J = 1.5$ Hz), 7.66 (2H, d, $J = 7.5, 1.5$ Hz), 7.83 (1H, d, $J = 1.5$ Hz), 7.62 (2H, d, $J = 7.5, 1.5$ Hz), 3.83 (3H, s, CH_3). ^{13}C NMR (75 MHz, DMSO): δ 164.7, 152.8, 138.5, 138.0, 132.1, 129.7, 125.1, 123.1, 120.6, 118.8, 116.5, 56.2; MS (m/z) ($m + 1$) = 392.98 ($\text{C}_{15}\text{H}_{10}\text{BrN}_3\text{O}_5$).

2-(4-Hydroxy-3-methoxy-5-nitro-phenyl)-5-(4-chloro-phenyl)-[1,3,4]oxadiazole (3d) yellow solid; mp 162 °C; $R_f = 0.6$ (EtOAc:hexane, 10:90); IR λ^{max} 3341, 1634, 1569, 1343, 1277, 1084, cm^{-1} ; ^1H NMR (300 MHz, DMSO): δ 14.22 (1H, s, OH), 8.01 (1H, d, $J = 1.5$ Hz), 7.71 (2H, d, $J = 7.5, 1.5$ Hz), 7.81 (1H, d, $J = 1.5$ Hz), 7.53 (2H, d, $J = 7.5, 1.5$ Hz), 3.83 (3H, s, CH_3). ^{13}C NMR (75 MHz, DMSO): δ 164.8, 152.8, 138.5, 138.0, 132.1, 129.7, 125.1, 123.1, 120.6, 118.8, 116.5, 56.2; MS (m/z) ($m + 1$) = 348.03 ($\text{C}_{15}\text{H}_{10}\text{ClN}_3\text{O}_5$).

2-(4-Hydroxy-3-methoxy-5-nitro-phenyl)-5-(4-methoxy-phenyl)-[1,3,4]oxadiazole (3e) brown solid; mp 141 °C; $R_f = 0.7$ (EtOAc:hexane, 10:90); IR λ^{max} 3430, 1664, 1561, 1340, 1290, 1084, cm^{-1} ; ^1H NMR (300 MHz, DMSO): δ 14.23 (1H, s, OH), 8.17 (1H, d, $J = 1.5$ Hz), 8.02 (2H, d, $J = 7.5, 1.5$ Hz), 7.89 (1H, d, $J = 1.5$ Hz), 7.03 (2H, d, $J = 7.5, 1.5$ Hz), 3.81 (3H, s, CH_3), 3.83 (3H, s, CH_3). ^{13}C NMR (75 MHz, DMSO): δ 164.8, 160.6, 152.8, 138.5, 138.0, 129.0, 120.6, 118.8, 116.5, 115.9, 114.8, 56.1, 55.8; MS (m/z) ($m + 1$) = 344.08 ($\text{C}_{16}\text{H}_{13}\text{N}_3\text{O}_6$).

3-[5-(4-Hydroxy-3-methoxy-5-nitro-phenyl)-[1,3,4]oxadiazole-2-yl]-pyridine (3f) yellow solid; mp 186 °C; $R_f = 0.4$ (EtOAc:hexane, 10:90); IR λ^{max} 3450, 1668, 1571, 1344, 1286, 1084, cm^{-1} ; ^1H NMR (300 MHz, DMSO): δ 14.28 (1H, s, OH), 9.24 (1H, dd, $J = 1.5, 0.4$ Hz), 8.70 (1H, m), 8.34 (1H, d, $J = 1.5$ Hz), 7.57 (1H, t, $J = 7.5, 7.5$ Hz), 7.98 (1H, d, $J = 1.5$ Hz), 8.42 (1H, m), 3.83 (3H, s, CH_3). ^{13}C NMR (75 MHz, DMSO): δ 165.1, 152.8, 152.7, 147.9, 138.5, 138.0, 134.0, 124.4, 124.0, 120.6, 118.8, 116.5, 55.7; MS (m/z) ($m + 1$) = 315.07 ($\text{C}_{14}\text{H}_{10}\text{N}_4\text{O}_5$).

3. Biological activity

3.1. Antimicrobial assay

Antifungal/antibacterial agents: Stock solutions of compounds were prepared in DMSO and diluted before assays. Amphotericin-B and neomycin purchased from Sigma Aldrich were used as reference drugs for the antifungal and antibacterial assays, respectively. The final concentration of the synthesized compounds ranged from 0.0012 to 200 $\mu\text{g mL}^{-1}$, amphotericin-B ranged from 0.0015 to 100 $\mu\text{g mL}^{-1}$ and neomycin from 0.0076 to 500 $\mu\text{g mL}^{-1}$. All drug dilutions were carried out in 96-well flat bottom microtitre plates.

Antifungal susceptibility test: Evaluation of the susceptibility of *Candida albicans* and non-*Candida albicans* species were performed using the broth micro dilution method according to M27-A2 for yeast guidelines. Yeast strains were grown aerobically overnight at 35 °C on Sabouraud dextrose agar plates. Yeasts were harvested and suspended in 1 % sterile saline and the turbidity of the supernatants measured using a spectrophotometer at 625 nm with an absorbance of 0.08–0.1 equivalents to a 0.5 McFarland standard following the NCCLS M27-A2 guidelines. The working suspension was diluted to 1:20 in a mixture containing RPMI 1640 medium and 0.165 M morpholinepropanesulfonic acid buffered to pH 7.0. The working suspension was further diluted with the medium (1:50) to obtain the final test inoculums ($1-5 \times 10^3$ CFU mL^{-1}). The microtitre plates containing different concentrations of test compounds were allowed to thaw and equilibrate to room temperature under aseptic conditions. Aliquots of working inoculum suspensions were dispensed into each well and the plates incubated in an aerobic environment at 35 °C for 24 h. After incubation, 20 μL of 3-(4,5-dimethylthiazol-2-yl)-5-(3-carboxymethoxyphenyl)-2-(4-sulfophenyl)-2H-tetrazolium salt (MTS, Promega Corporation, Madison, USA) was added to each well, incubated at 37 °C for 4 h and the absorbance recorded at 490 nm on a 96-well plate reader

Table 1-1

Yield and reaction time of conventional and non-conventional method.

Comp.	Acid used	Conventional Method		Non-Conventional Method	
		Yield (%)	Time (Hr)	Yield (%)	Time (Min)
3a	Benzoic acid	72	24	88	15
3b	4-NO ₂ Benzoic acid	40	18	75	25
3c	4-Br Benzoic acid	57	16	87	16
3d	4-Cl Benzoic acid	71	24	92	18
3e	4-OMe Benzoic acid	65	20	89	22
3f	Nicotinic acid	70	24	90	20

(Biotek, Powerwave XS2). All analyses were performed in triplicate and the data was found to be reproducible. The minimum inhibitory concentration (MIC) is the lowest concentration at which growth of the fungi was inhibited.

Antibacterial susceptibility test: Bacterial susceptibility tests were carried out using the micro broth dilution method. Overnight cultures after 16–18 h of incubation at 37 °C were adjusted to the turbidity of a 0.5 McFarland standard. Inoculation was adjusted to an absorbance of 0.08–0.10 to yield a stock suspension of $0.4\text{--}5 \times 10^8$ CFU mL⁻¹, which was diluted one hundred fold to obtain a working suspension of 10^6 CFU mL⁻¹ at 625 nm. Microtitre plates were placed in a laminar flow unit to equilibrate to room temperature under aseptic conditions. Aliquots of 100 µL of bacterial inoculate were added to the microtiter plates containing different concentrations of test compounds. Plates were incubated aerobically for 16–18 h at 37 °C. Following incubation, 40 µL of freshly prepared iodinitrotetrazolium chloride [2-(4-iodophenyl)-3-(4-nitrophenyl)-5-phenyl-2H tetrazolium chloride] (INT) solution ($200 \mu\text{g mL}^{-1}$) was added to each well and the plate further incubated for 45 min at 37 °C in the dark. If the colorless INT is reduced to red after incubation, persistent growth of bacteria is indicated. No color change signifies the absence of bacterial growth. Neomycin was used as a control drug in this study. All analyses were made in triplicate and the data was found to be reproducible. The minimum inhibitory concentration (MIC) is the lowest concentration at which growth of the bacteria was inhibited.

4. Results and discussion

The oxadiazole compounds (**3a–3f**) were synthesized from the reaction of 5-nitro methyl vanillate with hydrazide followed by cyclization with different carboxylic acids in presence of phosphorous oxychloride. The mechanism of this reaction involves first formation of acid chloride of corresponding acid then reaction with hydrazide (**2**) as shown in **mechanism**.

Both conventional & non-conventional procedures were applied from which microwave irradiation method given the completion of reaction within less time period followed by good yield (**Table 1-1**).

The structures of the produced (**3a–3f**) compounds were confirmed by NMR and FT-IR.

FT-IR spectra of the prepared compounds showed characteristic absorption bands at

(1612–1671) cm⁻¹, (3315–3457) cm⁻¹, (1250–1290) cm⁻¹ and (1052–1084) cm⁻¹ due to (C=N), (O–H), (C–O–C) and (N–N) group.

The ¹H NMR spectra of compounds showed the following characteristics chemical shifts (DMSO as a solvent) were appeared, doublet signal at $\delta(7.84\text{--}8.11, \text{ and } 8.11\text{--}8.40)$ ppm, respectively, that maybe attributed to the deshielding effect of protons as com-

pare to hydrazide compound (**2**). In addition, deshielding signal of OH group observed.

In ¹³C NMR sharp peak observed at 164.5 ppm that could be attributed to the quaternary carbon in Oxadiazoles ring carbon. Also, signals at $\delta(120.0 \text{ and } 120.6)$ ppm, respectively that could be assigned to benzene ring carbon.

4.1. Antibacterial activity

The compounds were evaluated for their *in vitro* antibacterial activity against *Staphylococcus aureus*, *Enterococcus faecalis*, *Escherichia coli*, *Klebsiella pneumoniae* and *Pseudomonas aeruginosa*. **Table 1-2** summarizes the MIC results obtained for the active compounds against the five different bacterial species. Four compounds showed a broad spectrum of activity, having antimicrobial activity against all the bacterial strains used in the assay. These were the unsubstituted oxadiazole **3a**, with MICs between 32.2 and 32.2 µM, the nitro - substituted oxadiazole **3b** (MIC between 18.7 and 64.4 µM), the 4- Br (**3c**), 4-OCH₃ oxadiazole(**3e**) (MICs between 123.0 and 117.8 µM) and the 4-Cl oxadiazole**3d** (MICs between 30.7 and 118.2 µM). The best activity was shown by **3f** for all strain it showing activity (MICs 29.6).

In general, the oxadiazole had better activity than its hydrazide precursor**2**, indicating that the 5 membered oxadiazole nucleus contributed to better activity than the hydrazide moiety**2**. Whereas compound **2** do not have any activity for gram positive strain as shown in **Table 1-2**.

The activity of the 4-Cl derivative **3d** was not as good as the unsubstituted derivatives, being 2-fold less active than **3a** and **4a** in some of the bacterial strains *S. aureus* but in *P. aeruginosa* its reverse way. The 4-OCH₃ derivative **3e** shows activity against only *E. coli*. Compared to the neomycin control, **3a** and **3b** had a 2-fold decrease in activity with regard to *S. aureus* and **3b** was 2-fold better than neomycin against *E. faecalis*.

The 4-Broxadiazole **3c** showed activity against the Gram negative strains *E. coli* only.

The para NO₂oxadiazole **3b** showed excellent activity against *S. aureus*, *E. faecalis* 32.2, 18.7 µM, as compare to gram negative bacteria *K. pneumoniae*, *P. aeruginosa* but *E.coli* show same activity.

3f did not show any activity against *E. faecalis* and very high MIC values against the Gram negative strains. However, this could be an excellent agent as an antibiotic against *S. aureus*.

4.2. Antifungal activity

The same set of compounds were evaluated for their *invitro* antifungal activity against four *Candida* species comprising *C. albicans* ATCC 90028, *C. albicans* ATCC 10231, *C. krusei* ATCC 6258, and *C. parapsilosis* ATCC 22019. The results are reported in **Table 1-3**.

Table 1-2
MIC (µM) of test compounds on Gram positive and Gram negative bacterial strains.

Compound	Gram positive		Gram negative		
	<i>S. aureus</i>	<i>E. faecalis</i>	<i>E. coli</i>	<i>K. pneumoniae</i>	<i>P. aeruginosa</i>
2	–	–	83.2	166.5	166.5
3a	32.2	32.2	32.2	128.7	128.7
3b	32.2	18.7	32.2	64.4	64.4
3c	–	–	123.0	–	–
3d	61.5	–	30.7	118.2	30.7
3e	–	–	117.8	–	–
3f	48.6	–	29.6	29.6	29.6
Neomycin	16.3	32.5	8.1	16.3	8.1

“–” indicates no activity.

Table 1-3
Minimum Inhibitory Concentration (MIC, μM) of test compounds on *Candida* species.

Compound	<i>C. albicans</i> ATCC 90,028	<i>C. albicans</i> ATCC 10,231	<i>C. krusei</i> ATCC 6258	<i>C. parapsilosis</i> ATCC 22,019
2	332.9	392.9	232.9	352.9
3a	128.7	64.4	32.2	32.2
3b	64.4	64.4	64.4	64.4
3c	30.8	61.5	246.0	246.0
3d	30.8	61.5	61.5	61.5
3e	117.8	117.8	117.8	117.8
3f	59.7	59.7	119.5	239.0
Amp-B	1.3	1.3	5.4	1.3

Amp- B indicates Amphotericin-B.

In general, the oxadiazole had better activity than its hydrazide precursor **2**, indicating that the 5 membered oxadiazole nucleus contributed to better activity than the hydrazide moiety **2**. Whereas compound **2** have activity greater than 230 for all strain as shown in Table 1-3.

Compounds **3f** showed good activity against both strain of *C. albicans* having MIC values of 59.7. Of these, only **3a** had an MIC of 128.7 against *C. albicans* ATCC 9002 other having good activity MIC 32.2–64.4. In addition, **3b** (4-nitro), showed good activity against all four fungal strain (MIC 64.4). 4-Br (**3c**) showing good activity against both *C. albicans* species (30.8, 61.5 μM), but very low activity Inc. *krusei* and *C. parapsilosis*. These results indicate that the halogen groups (Br, Cl) on the Oxadiazoles skeleton is a good scaffold for anti-fungal activity and that this activity can be increased by fluorogroups being substituted on the phenyl ring or by substituting the phenyl ring with a heterocyclic ring. However, these compounds were not as active as the standard drug amphotericin-B (Amp-B).

5. Conclusion

A series of novel oxadiazoles were synthesized and characterized by NMR and FT-IR spectroscopy. The hydrazide was converted to the oxadiazoles with the moderate to good yields. In microwave method reaction time reduced from hrs to min. Some interesting observations were made. The 4-nitro substitute (**3b**) and unsubstituted (**3a**) oxadiazoles having better activity for gram positive bacterial and pyridine ring **3f** active against gram negative strain. These compounds were also having good activities in antifungal assays. However, oxadiazoles could be good lead compounds for antimicrobial agents.

CRedit authorship contribution statement

Ranjana Jadhav: Supervision. **Sunayna Pawar:** . **Chandrakant Khilare:** . **Arun Nikumbh:** .

Data availability

Data will be made available on request.

Declaration of Competing Interest

The authors declare the following financial interests/personal relationships which may be considered as potential competing interests: Dr. Ranjana Khanduji Jadhav reports administrative support was provided by S. M. Joshi College Hadapsar.

References

[1] J. Jampilek, *Heterocycles in Medicinal Chemistry*, *Molecules* 24 (2019) 3839.

- [2] J. Berger, M. Li, S. Berger, M. Meilak, J. Rientjes, P.D. Currie, Effect of Ataluren on dystrophin mutations, *J. Cell Mol. Med.* 24 (2020) 6680–6689.
- [3] F. Caputo, S. Corbetta, O. Piccolo, D. Vigo, Seeking for Selectivity and Efficiency: New Approaches in the Synthesis of Raltegravir, *Org. Process Res. Dev.* 24 (2020) 1149–1156.
- [4] A. Khallaf, P. Wang, H. Liu, S. Zhuo, H. Zhu, 1,2,4-Oxadiazole ring-containing pyridylpyrazole-4- carboxamides: Synthesis and evaluation as novel insecticides of the anthranilic diamide family, *J. Heterocycl. Chem.* 57 (2020) 1981–1992.
- [5] L.L. Fershtat, N.N. Makhova, 1,2,5-Oxadiazole-Based High-Energy-Density Materials: Synthesis and Performance, *ChemPlusChem* 85 (1) (2020) 13–42.
- [6] J. Boström, A. Hogner, A. Llinàs, E. Wellner, A.T. Plowright, Oxadiazoles in Medicinal Chemistry, *J. Med. Chem.* 55 (2012) 1817–1830.
- [7] K. Biernacki, M. Daško, O. Ciupak, K. Kubiński, J. Rachon, S. Demkowicz, Novel 1,2,4-Oxadiazole Derivatives in Drug Discovery, *Pharmaceuticals* 13 (6) (2020) 111.
- [8] M. Tassinari, A. Lena, E. Butovskaya, V. Pirota, M. Nadai, M. Freccero, F. Doria, S. N. Richter, A Fragment-Based Approach for the Development of G-Quadruplex Ligands: Role of the Amidoxime Moiety, *Molecules* 2018 (1874) 23.
- [9] W. Zhu, X. Bao, H. Ren, P. Liao, Y. Yan, L. Wang, Z. Chen, Design, synthesis, and pharmacological evaluation of 5-oxo-1,2,4-oxadiazole derivatives as AT1 antagonists with antihypertension activities, *Clin. Exp. Hypertens.* 38 (2016) 435–442.
- [10] M.T. Ibrahim, A. Uzairu, G.A. Shallangwa, A. Ibrahim, In-silico studies of some oxadiazoles derivatives as anti-diabetic compounds, *J. King Saud Univ.-Sci.* 32 (2020) 423–432.
- [11] G. Chawla, B. Naaz, A.A. Siddiqui, Exploring 1,3,4-Oxadiazole Scaffold for Anti-inflammatory and Analgesic Activities: A Review of Literature From 2005–2016, *Mini Rev. Med. Chem.* 18 (2018) 216–233.
- [12] S. Bajaj, V. Asati, J. Singh, Roy pp., 1,3,4-Oxadiazoles: An emerging scaffold to target growth factors, enzymes and kinases as anticancer agents, *Eur. J. Med. Chem.* 97 (2015) 124–141.
- [13] M.H. Baig, M. Adil, R. Khan, S. Dhadi, K. Ahmad, G. Rabbani, T. Bashir, M.A. Imran, F.M. Husain, E.J. Lee, et al., Enzyme targeting strategies for prevention and treatment of cancer: Implications for cancer therapy, *Semin. Cancer Biol.* 56 (2019) 1–11.
- [14] T. Eitsuka, K. Nakagawa, S. Kato, J. Ito, Y. Otoki, S. Takasu, N. Shimizu, T. Takahashi, T. Miyazawa, Modulation of Telomerase Activity in Cancer Cells by Dietary Compounds: A Review, *Int. J. Mol. Sci.* 19 (2018) 478.
- [15] Q.-Z. Zheng, X.M. Zhang, Y. Xu, K. Cheng, Q.C. Jiao, H.L. Zhu, Synthesis, biological evaluation, and molecular docking studies of 2-chloropyridine derivatives possessing 1,3,4-oxadiazole moiety as potential antitumor agents, *Bioorganic Med. Chem.* 18 (2010) 7836–7841.
- [16] J. Boström, A. Hogner, S. Schmitt, Do Structurally Similar Ligands Bind in a Similar Fashion, *J. Med. Chem.* 49 (2006) 6716–6725.
- [17] E. Landfeldt, S. Sejersen, M. Tulinius, A mini-review and implementation model for using ataluren to treat nonsense mutation Duchenne muscular dystrophy, *Acta Paediatr.* 108 (2019) 224–230.
- [18] M.W. Konstan, D.R. VanDevanter, S.M. Rowe, M. Wilschanski, E. Kerem, I. Sermet-Gaudelus, E. DiMango, P. Melotti, J. McIntosh, K. De Boeck, Efficacy and safety of ataluren in patients with nonsense-mutation cystic fibrosis not receiving chronic inhaled aminoglycosides: The international, randomized, double-blind, placebo-controlled Ataluren Confirmatory Trial in Cystic Fibrosis (ACT CF), *J. Cyst. Fibros.* 19 (2020) 595–601.
- [19] B.B. Ceyhan, S. Karakurt, Effect of oxolamine on cough sensitivity in COPD patients, *Respir. Med.* 96 (2002) 61–63.
- [20] W.R. Tully, C.R. Gardner, R.J. Gillespie, R. Westwood, 2-(Oxadiazolyl)- and 2-(thiazolyl)imidazo [1,2-a]pyrimidines as agonists and inverse agonists at benzodiazepine receptors, *J. Med. Chem.* 34 (1991) 2060–2067.
- [21] D.M. Cecchini, M.G. Martinez, L.M. Morganti, C.G. Rodriguez, Antiretroviral Therapy Containing Raltegravir to Prevent Mother-to-Child Transmission of HIV in Infected Pregnant Women, *Infect. Dis. Rep.* 9 (2017) 7017.
- [22] J.M. Toombs, K. Van den Abbeele, J. Democratis, R. Merricks, A.K.J. Mandal, C.G. Missouri, COVID-19 in three people living with HIV in the United Kingdom, *J. Med. Virol.* 1–3 (2020).
- [23] M.D. Lloyd, High-Throughput Screening for the Discovery of Enzyme Inhibitors, *J. Med. Chem.* 63 (2020) 10742–10772.

- [24] K. Mahajan, N. Fahmi, R.V. Singh, Synthesis, characterization and antimicrobial studies of Sb(III) complexes of substituted thioimines, *Indian J Chem.* 46A (2007) 1221–1225.
- [25] K. Mahajan, M. Swami, R.V. Singh, Microwave synthesis, spectral studies, antimicrobial approach, and coordination behavior of antimony (III) and bismuth (III) compounds with benzothiazoline, *Russ. J. Coord. Chem.* 35 (2009) 179–185.
- [26] K. Mohanan, S. Kumari, G. Rijulal, Microwave assisted synthesis, spectroscopic, thermal, and antifungal studies of some lanthanide (III) complexes with a heterocyclic bishydrazone, *J. Rare Earths* 26 (2008) 16–21.
- [27] R. Garg, M.K. Saini, N. Fahmi, R.V. Singh, Spectroscopic and biochemical studies of some manganese (II), Oxovanadium (V) and Dioxomolybdenum (VI) complexes S/O and N donor agents synthesized under microwave conditions, *Trans Met Chem.* 31 (2006) 362–367.
- [28] K. Sharma, R. Singh, N. Fahmi, R.V. Singh, Microwave assisted synthesis, characterization and biological evaluation of palladium and platinum complexes with azomethines, *Spectrochim Acta A Mol Biomol Spectrosc.* 75A (2010) 422–427.
- [29] F. Mavandadi, A. Pilotti, The impact of microwave-assisted organic synthesis in drug discovery, *Drug Discov Today.* 11 (2006) 165–174.
- [30] A. Vasudevan, Microwave-assisted organic synthesis an enabling technology with disruptive potential. *Drug Discov, World.* (2008) 83–90.
- [31] A. Benassi, D. Filippo, V. Pirota, Groundbreaking Anticancer Activity of Highly Diversified Oxadiazole Scaffolds, *Int. J. Mol. Sci.* 21 (2020) 8692.



Applications of plant-based nanomedicines for wound healing – An emerging paradigm for effective therapy

Priya Lokare^{a,*}, E. Keshamma^b, Anil Kumar^c, Yasser Ali Abdullah Alsowadi^d,
Mohammad Mobarak Hossain^e, Laxmi Kirana Pallathadka^f

^a Loknete Ramdas Patil Dhumal Arts, Science & Commerce College, Rahuri, India

^b Department of Biochemistry, Maharani Cluster University, Palace Road, Bangalore 560 001, India

^c Department of Botany, DDU Gorakhpur University, Gorakhpur 273009, India

^d IBB University, Yemen

^e Textile Engineering (Fabric Manufacturing), Bangladesh University of Textiles, Dhaka, Bangladesh

^f Manipur International University, Imphal, Manipur, India

ARTICLE INFO

Article history:

Available online 22 October 2022

Keywords:

Wound-healing

Plant-based nanomaterials

Infection control

Nanomedicines

Herbal nanostructures

ABSTRACT

Wound healing is well-organized but a cascade of complex biochemical and cellular process to revive the normal morphology and functioning of skin. There are several plant-derived active biocomponents which are known to have their applications in wound healing due their negligible side effects. Present wound healing therapies, techniques and products are not that efficient to recover the wounds without affecting skin morphology and function. The approach/technique is considered to be the ideal if it cures/heals the wound without affecting the normal functioning of the skin, without scar formation, inhibit bacterial infection, speeds up the healing mechanism and keep the wound moisturized. Nanotechnological-based approaches are developed to increase the efficacy of the drug as well as herbal/plant-based organic products through direct delivery to the target, enhanced bioavailability and biocompatibility, controlled release of drug and enhanced solubility. The following literature review is about the different plant-based nanomaterials, their role in wound healing and delivery of herbal drugs to site of infection. For this purpose, profound research has been done to discover how and why natural product-based nanomaterials are being used to cure wound. This review will tell you the mechanism of action of plant-based nanomaterials to heal the wound and the elimination of challenges which are usually faced during the wound healing process such as bacterial infection, biofilm formation that leads towards chronic wound. As compared to the classical therapies of wound healing, nanotechnological based methods keep the wound moisturized. Various plant-based nano-formulations show remarkable activity in wound healing and management and are considered to be the future of pharmaceuticals.

Copyright © 2022. Elsevier Ltd. All rights reserved.

Selection and peer-review under responsibility of the scientific committee of the Integrative Nanotechnology Perspective for Multidisciplinary Applications - 2022.

1. Introduction

Present wound healing therapies, techniques and products are not that efficient to recover the wounds without affecting skin morphology and function and this makes this area of research so intensified and prompted. The technique or healing system should be considered efficient if it heals the wounds fast [1], stops scar formation [2], inhibits infections, fastens up healing mechanisms [3], and keeps the wound moisturized [4]. Nanotechnology has started

a new area of research through the treatment of wounds by nanomaterials which owe unique antimicrobial properties [5]. There are two sort of strategies for the use of nanomaterials that have been employed: organic and inorganic nanomaterials. Plant based nanomaterials fall under the category of organic nature in which NPs with antimicrobial properties is inserted into biopolymers from natural resources. [Table 1.](#)

Conventional approaches to treat wounds are by using antiseptics and antibacterial. There are several ways scientists have developed to produce organic and inorganic nanoparticles. For the latter one, there are physical and chemical methods of synthesis which

* Corresponding author.

Table 1
Plant-based nanomaterials, their applications in wound-healing and main findings.

Organic Nanomaterials	Applications	Main findings	Ref.
Polymeric Nanoparticles	Encapsulated Enoxaparin in polymeric nanoparticles SDF-1-NPs response to ROS	Wound healing improvement; Good skin penetration	[21]
		No toxicity in vitro; Wound vascularization; Targeting of SDF-1a to the wound site; Full-thickness wounds healing	[43,50]
Dendrimers	Gelatin-dendrimer conjugates dressing Vascular endothelial growth factor (VEGF) based gene therapy and cationic dendrimer E-selectin coating of Stem cell surface	Excellent wound healing; Angiogenesis	[17], Smith-Freshwater, 2009)
		Increased angiogenesis, Increased collagen deposition and speedy proliferation	[30,7,8]
Nano-emulsions	Nanoemulsion of licorice and Lavender essential oil Levofloxacin nanoemulsion gel	No toxicity; biocompatibility Wound closure; Increase peroxidase activity; epithelialization	[28,25,26]
		Wound contraction; Collagen production; Better wound healing effect than silver sulfadiazine formulation	[44,51]
	Curcumin nanoemulsion	Healing effects like fusidic acid; Edema healing; shows anti-inflammatory activity; Nontoxic;	[2,39]
Liposomes	Nanoliposomes loaded with Daptomycin Quercetin and curcumin nanovesicles	Antibacterial action and against biofilms Inhibit the activity of ROS; Inhibit edema formation; fibroblast proliferation	[35], Li et al., 2013) [11,39]
Cyclodextrins	b-cyclodextrin-eugenol hydrogel Hyperforin/HP-b-cyclodextrin	antimicrobial; angiogenesis; anti-inflammatory	[33,53]
		Increased keratinocytes proliferation; wound healing effect; increased aqueous solubility	[45,49]
Lipid nanoparticles	Lipid nanoparticles loaded with Morphine rhEGF (recombinant human EGF)-loaded lipid nanoparticles	High drug loading capacity; sustainable release of drug; re-epithelialization	[29], Caldón, 2013)
		new connective tissues and blood vessels; enhanced wound closure	[19,22]
	Tumor necrosis factor α silencing	Chronic inflammation reduction; increased closure of diabetic wounds	[27]

are laborious and expensive [6]. Inexpensive, ecofriendly and much greener way of NPs synthesis is by using plants [9].

Nanomedicine is the use of nanotechnology for medical objectives. Treatment, prevention, diagnosis, and monitoring of disease are executed by the help of nanomaterials that are given because of their certain properties that will help against the disease [11]. Use of different therapeutic nano-based approaches when combine together give synergistic effects [12]. Wound care has always been an expensive entity and has proven a burden on healthcare system. In 2014 survey, wound care cost around \$2.8 billion annually worldwide and is estimated to rise up to \$3.5 billion at the end of 2021. Global market of wound care products is expected to cross \$15 billion by 2022 with 300 million chronic wound patients [13]. Scientists are putting efforts to give market more sustainable approaches of wound care that are expected to be more efficient and less expensive.

The purpose of this review is to elaborate plant-based nanomaterial approaches of wound care and management as well as encouraging researchers to expand their research to make these viable and sustainable nano-based products.

2. Wound healing challenges

For certain, nanotechnology is helping us in wound healing. There are some challenges that are being faced during wound healing; the objective is to eliminate them somehow by using nanotechnology. Before going towards how nanomaterials are used to cure wounds, it is very important to understand what is going on inside wound and the phases of wound healing. It will help us to solve the mystery that how nanomaterials are being helpful for wound healing.

There are three stages of wound healing process: 1) Hemostasis 2) Inflammation, 3) Proliferation and 4) Remodeling. Inflammation does not be there too long but less than a week, proliferation takes

the next two weeks and then remodeling which is the longest stage and lasts up to two years. Due to real time control of anti-inflammatory and pro-inflammatory cytokines (IL-1 and TNF- α), these phases are overlapped in vivo.

Blood clots formation is the first homeostatic response in wound healing that initiates the inflammatory phase. Following, leukocytes are recruited on the site of infection with the help of chemoattractants released by the injured cells. Leukocytes wipe out the infectious agents and they also initiate the proliferative stage by releasing cytokines which, in turn, stimulate cell growth and division [14]. The covering of wound by granulation indicates the proliferative phase transition. In this third stage of wound healing, fibroblasts play an active role in the production of collagen as well as extracellular matrix and the development of new blood vessels [15]. While the normal functioning and appearance of the tissue are revived during the fourth phase of wound healing, remodeling [16].

Wound healing stages can take more time than the normal one because of some factors that can be damaging for the healing process. These factors include contamination of the wound, necrosis, entrapment of any foreign material within the wound and specific comorbidity such as diabetes mellitus. All these factors halt the normal wound healing process and unsatisfactory results arise [17]. Wound healing process is often impeded by the colonization of infection bacteria at the site of wound. Even the beneficial bacteria from the skin microbiota which stop infectious bacteria to colonize the wound can be a problem in case they form biofilms by reaching their threshold. The colonization of pathogens directly lead towards insufficient healing [18]. Initial stages of wound healings are affected by the presence of *Staphylococcus aureus*, methicillin resistant *Staphylococcus aureus* whereas chronic and deep skin wounds are infected by *Pseudomonas aeruginosa* and *E. coli* [19].

Synergistic activities of multiple type of microbes at the site of infection lead towards the onset of chronic wound [20]. For exam-

ple, to inhibit aerobic bacteria that require more oxygen for cell division, this leads towards having hypoxic environment. As a result, anaerobic bacteria for which hypoxic environment is suitable grow and produce short chain fatty acids that block the activity of macrophages to engulf the pathogens. In addition, microorganisms make each other sustainable by exchanging nutrients, this makes them grow together simultaneously in chronic wounds [20,21].

Bacteria produce extracellular polymers which acts as a shield against the host defense and help them to form biofilms which is a closed environment for bacteria to grow and reproduce [23,24,27]. Biofilms inhibit epithelial cells to grow by producing chronic inflammation. Moreover, biofilms also protect and support colonized bacteria against antimicrobial therapies [28]. There some organic nanomaterials shown in Fig. 1 and their efficiency at different stages of wound healing.

3. Current wound therapies

3.1. Dressings

Cotton and wool dressings are one of the most traditional approach to protect wound against bacterial infection and entrapment of dust particles. Dressings act as barrier between the wound and external environment. Now a days, these classical dressings have been replaced with more advanced ones which not only protect the wound but also provides active compounds that will provide aid in healing as well as keep the wound moisturized. These dressings are hydrogels, films, hydrofiber mats etc. [29,48,30].

3.2. Honey

Angiogenesis, re-epithelialization, and granulation tissue formation are observed to be promoted by honey. Honey does not let bacteria to form biofilm because its acidic nature stimulates macrophages to eat them. In addition, oxidative cascade, which is damaging for pathogens, is initiated by the peroxidases present

in honey(Li et al., 2013). To make this traditional medicinal product more efficient, scientists proposed the idea of using nanomaterials for targeted delivery and controlled release of drug [23].

3.3. Hydrogels

Hydrogel is a three-dimensional polymeric network formed by the cross interaction of various hydrophilic groups which can entrap liquids e.g., wound exudates [6]. Hydrogel dressings keep the wound moist and eliminate the risk of dressing-dependent infection because it can absorb wound exudates [32].

3.4. Silver products

Silver products have antimicrobial properties and are used in burn dressings. Silver ions cause cell lysis by reacting with thiol group of peptidoglycan [33]. Moreover, silver products (e.g., silver sulphadiazine) inhibit biofilm formation. However silver products cause tissue toxicity [20].

3.5. Vac

Vacuum-assisted closure is a wound healing therapy through application of pressure suction which clear off the edema as well micromechanical forces are applied to the cells to stretch them, so they express transcription factors and stimulate cell proliferation and blood vessels formation [34].

3.6. Organic nanomaterials/ plant-based nanomedicines for wound healing

As described earlier that wound healing is a complex four staged process; hemostasis inflammation, proliferation and remodeling of the wounded tissue. And we have already studied different stage requires variable time to complete. It is very difficult to contemplate that what is required by the damaged tissue to be regenerated fully. The use of each material (plant-based

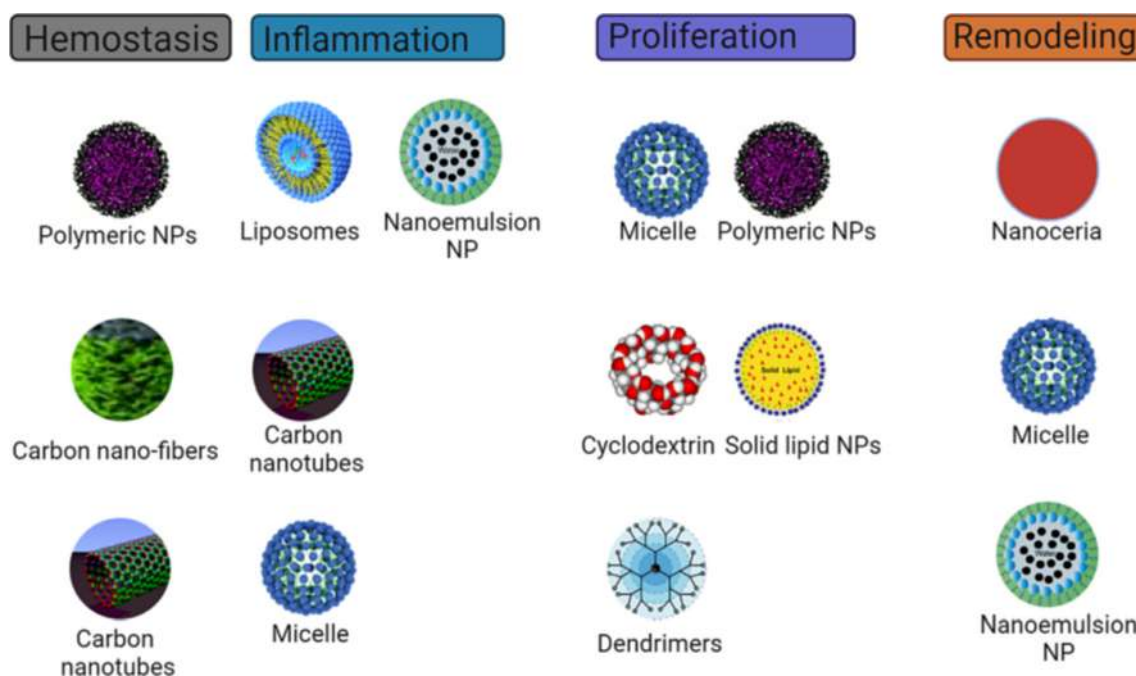


Fig. 1. Nanoparticles' efficiency at different stages of wound healing: 1) Hemostasis, 2) Inflammation, 3) Proliferation and 4) Remodeling.

nanomaterials/nanomedicine) strongly depends not only upon which stage of wound-healing is there but also upon deepness of the wound, duration of therapeutic effect and dose. There are some organic nanomaterials shown below in Fig. 2 with their main properties highlighted. Fig. 3.

Researchers have tried to develop suitable environment for wound to be healed at faster rates and this is provided by nanotechnological based products which have antimicrobial activity against the colonized pathogens in the wound as well as these product gives moisturized environment to the wound. Various types of natural products combinations with nanomaterials have been formulated; each is described below. For an example, biopolymers when given to the wound, incredible deposition of collagen has been seen. Along with keeping the wound moisturize, collagen is considered as an excellent healing-scaffold, and it provides mechanical support. On the other hand, soon after the cut in the skin, primary blood clot is formed by the fibrin. Likewise, keratin and silk fibroin are being used in wound healing in combine with nanomaterials for mechanical support.

Self-healing mechanisms are promoted using potential nano-material based bioproducts. But there are different types of tissues in wound, so it is important to know the cellular mechanism to personalize different nano-based products for each type wound healing. Polymeric nanofibers scaffolds can mimic the extracellular matrix properties and they stimulate the production of fibroblasts in the wound. In the following section, organic, plant-based nanomaterials along with their applications are explained.

3.7. Micelles

Inner core of micelles, which is hydrophobic, is surrounded by shell of hydrophilic nature. Polymeric micelles being non-toxic and biocompatible has properties such as high load efficiency

and release of drug in a controlled way which makes it an efficient delivery system for agents of both hydrophilic and hydrophobic nature [5].

In another example, when silver sulfadiazine has been encapsulated in chitosan oleate micelles, this combination not only made the drug concentrated by increasing surface-volume ratio, but it also provides protection to the cells against cytotoxicity of the drug. Study has demonstrated that enhanced antimicrobial activity has been shown by silver sulfadiazine micelles on *Staphylococcus aureus* and *Escherichia coli* strains [16].

Pluronic F127, P123 and Tween 80 are Cur-loaded polymeric micelles and in a recent study, done on diabetic rats, anti-diabetic wound-healing effects has been shown by this formulation. Higher amounts of Cur have been shown to reduce blood glucose level as well as lipid profile in rats which depicts that this formulation has anti-diabetic as well as wound healing effect [3]. Another micelle matrix-based surfactant product, PluroGel®, which keeps the wound moisturized and controls fluid loss [5].

3.8. Polymeric NPs

Drug is encapsulated in biodegradable polymers or copolymers. Polymeric NPs are composed of natural as well as synthetic polymers such as chitosan, PLGA [poly (lactic-co-glycolic acid)], alginates, albumin and many other. Plant-based Polymeric NPs are used for the encapsulation of drugs and their antimicrobial activities along with certain other properties such as release of drug in a controlled way, non-toxic to human cells, and biocompatibility with target tissue [5].

Polymeric NPs has applications in wound healing and examples are there. Cherreddy et al. showed that when mice were given LL37 (host defence peptide) in combine with lacted encapsulated in PLGA NPs, considerable results were observed in the form of higher

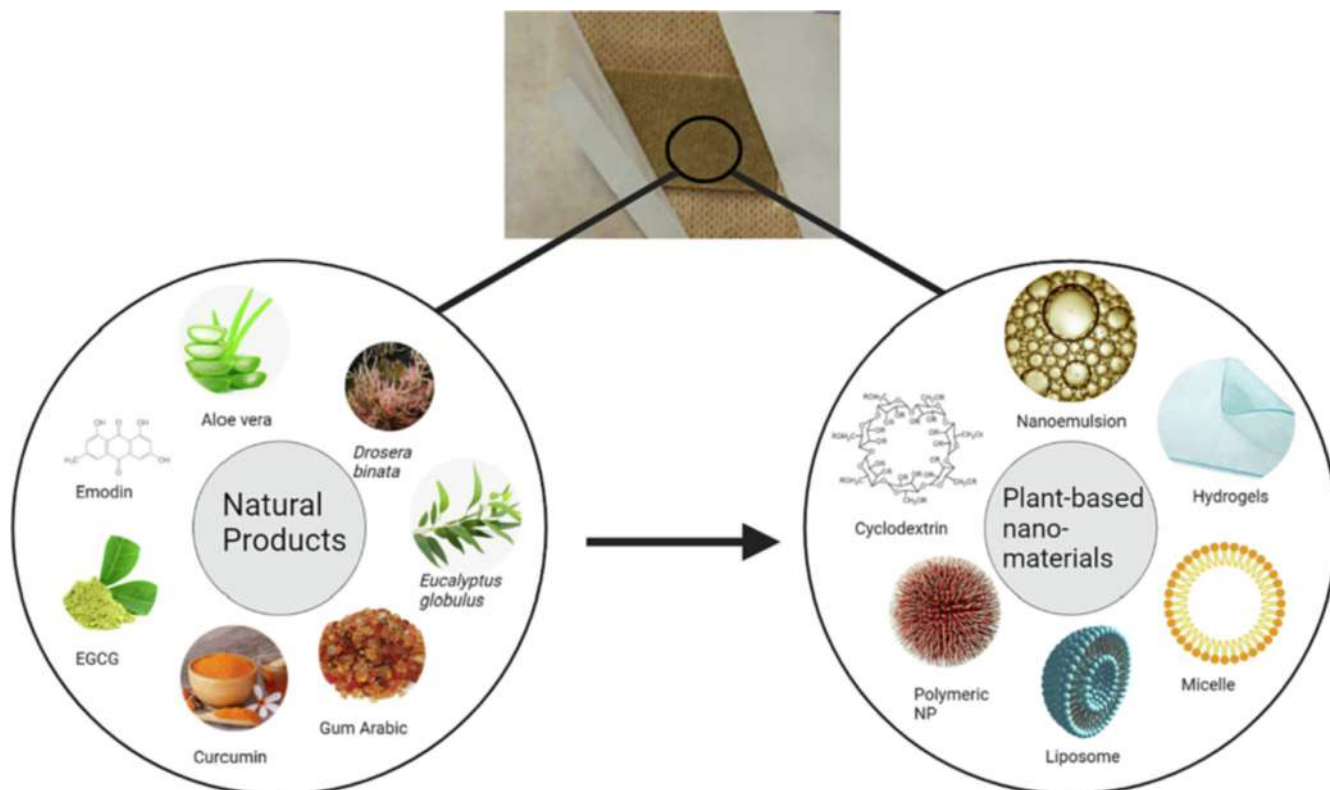


Fig. 2. Nano-formulations created from natural products.

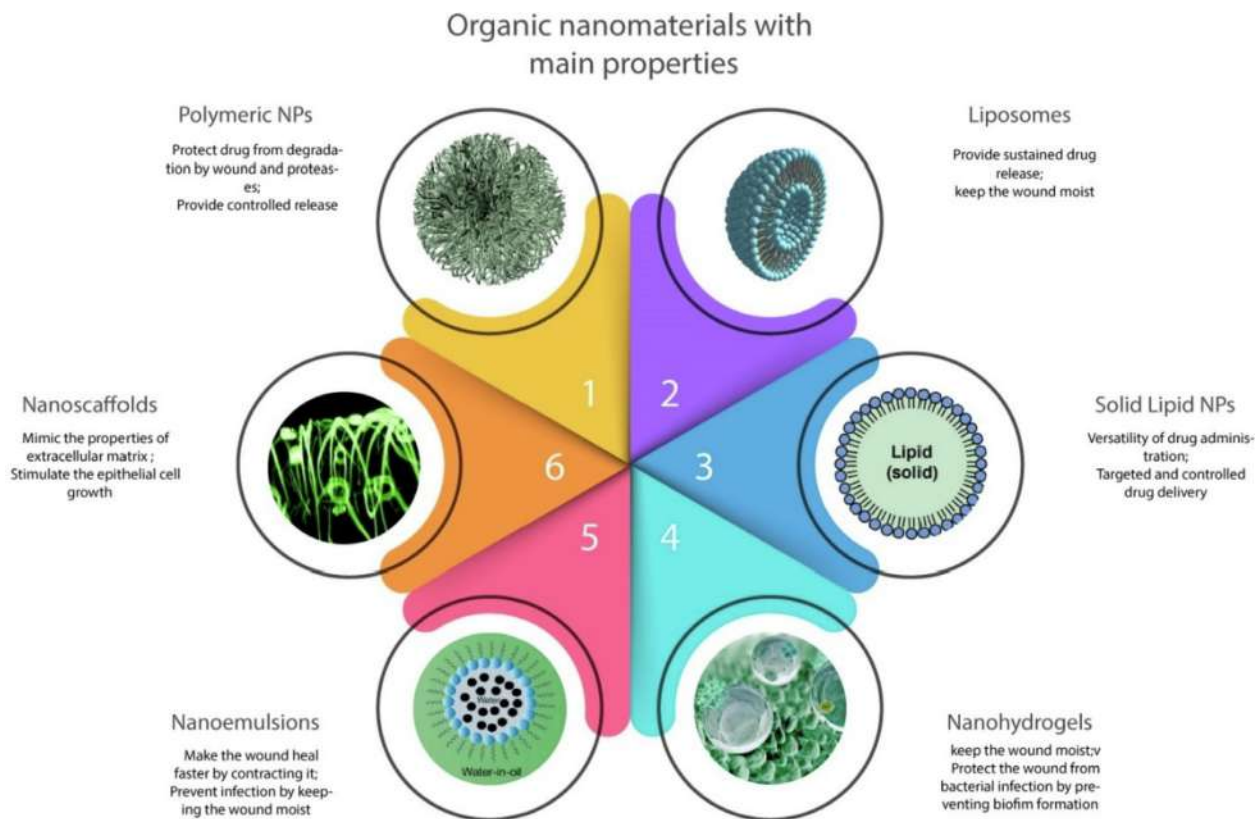


Fig. 3. Nanotechnology-based systems for wound treatment with main properties highlighted.

granulation tissue formation (IL-6 upregulation), re-epithelialization and increased collagen content and blood vessels formation. Moreover, it was also observed that inflammatory response had been modulated by TNF α down-regulation [14].

In another model (murine burn), Amphotericin B was encapsulated in silane-hydrogel NPs [46]. Significant results were observed in the form of higher killing efficiency of candida spp., 72–91 % reduction in candida spp. had been observed as compared to the control group where no Amphotericin B was given. Furthermore, Amphotericin B also inhibited fungal biofilm formation making the wound-healing faster [36].

3.9. Dendrimers

Branched monomers are used to synthesize dendrimers [1]. The effect of VEGF (Vascular Endothelial Growth Factor) encoding plasmid in combination with Arginine, (Arg-grafted cationic dendrimer) was observed on diabetic mice wounds [30]. This makes the wound heal rapidly by collagen deposition and faster proliferation rate. The proliferation rate of both keratinocytes and fibroblasts was observed much higher relatively by injecting mice with Gelatin scaffolds along with poly (amidoamine) (PAMAM) [37].

In addition, angiogenesis (development of new blood vessels) had also been shown to increased due to increase in the expression of H1F1a (the angiogenesis stimulator) by gelatin-PAMAM blend [38].

3.10. Nano emulsions

Nano emulsion system contains such NPs in which core is made up of water or oil and is used as a delivery system for water-poor soluble drugs. Nanoemulsions have their application in cosmetics

industry [5]. What makes the nanoemulsions an efficient drug delivery system are; prevents enzymatic degradation, higher drug carrying capacity, biocompatibility, solubility of drug and the release of drug in a controlled way [5].

75–82 % scratch area was produced during the first 36 h of wound-healig when phenytoin-loaded alkyl nanoemulsion were given as compared to when pure phenytoin without nanoemulsion formulation was injected. Keratinocytes proliferation was significantly enhance by the controlled release of phenytoin [38].

In another study, eucalyptus essential oil (EEO) nanoemulsion showed significantly higher results in the form of abundant deposition of collagen and significant wound wound contraction from day 12 to 24 of wound healing process [4].

3.11. Liposomes

Liposome consists of an external phospholipid bilayer which surrounds the internal aqueous portion; wholly formed a nano vesical. Liposomes provide so many benefits such as non-toxic, biocompatible, biodegradable and can be loaded with both hydrophilic and lipophilic agents which make liposome an efficient system for drug delivery. The common issue with using liposome is its poor stability and the leakage of loaded drug [40]. A study conducted by Mao et al. in 2017 showed that when wounded mice is injected with bFGF (basic Fibroblast Growth Factor)-loaded liposomes. bFGF speeds up the wound closure by re-epithelialization, collagen deposition and angiogenesis [40].

Cur-loaded liposome efficiency was compared with the pure drug by Choudhary et al. in 2019. It was observed that liposomes loaded with Cur showed improved rate of wound closure on 14th day after wound-cut [15].

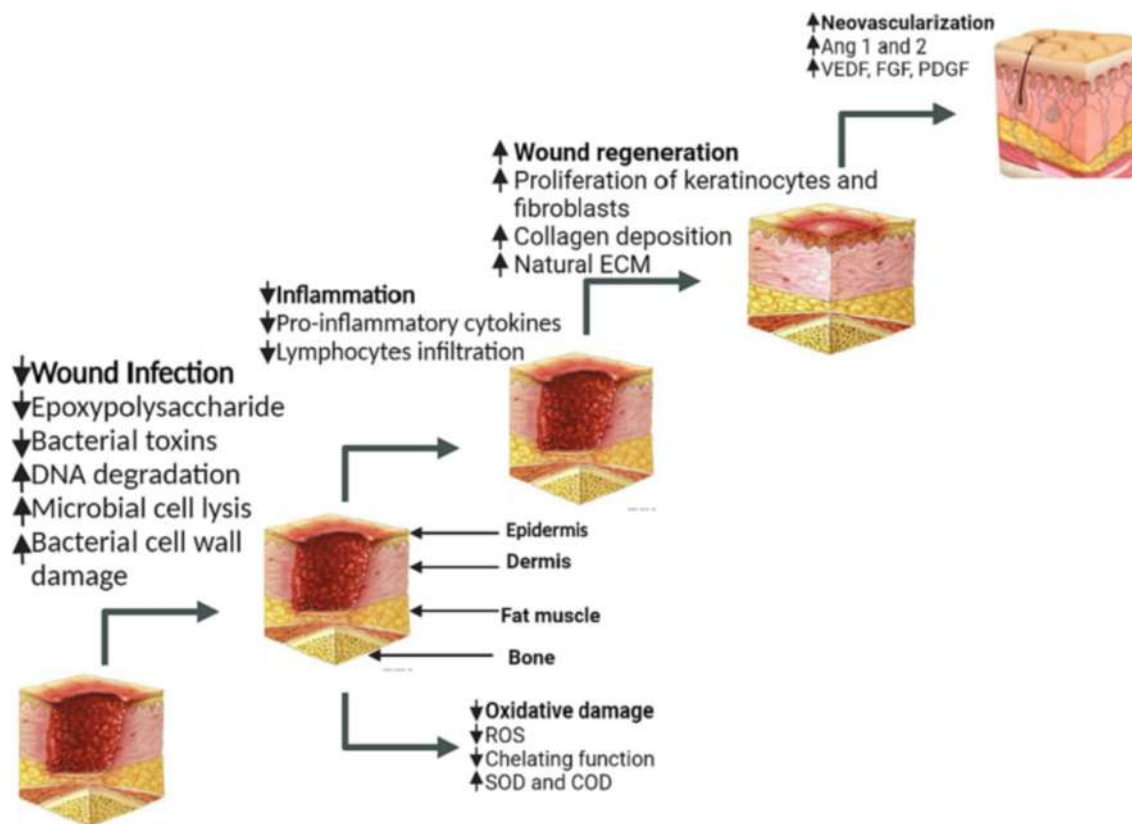


Fig. 4. Role of several nano-formulations at different stages of wound healing. Abbreviations: SOD; Superoxide Dismutase, PDGF; Platelets Derived Growth Factor, VEGF; Vascular Endothelial Growth Factor, FGF; Fibroblast Growth Factor, ECM; Extracellular.

Recently, the efficacy of Retinoic Acid (TRA) and EGF (Epidermal Growth Factor) containing liposomal ointment was tested. The synergistic effect of EGF and retinoic acid promoted cell proliferation and wound closure by collagen production. Furthermore, it was suggested that the synergistic effect of TRA and EGF produced by the increased expression of EGF receptor and HB-EGF (Heparin Binding-Epithelial Growth Factor) [41].

3.12. Cyclodextrins

Cyclodextrins (CDs) are produced by the enzymatic breakdown of starch which produces cyclic oligosaccharides such as glucopyranose. CDs are of lipophilic nature at the center and hydrophilic at outer surface. CDs make the water-poor soluble drug stable and increase the aqueous solubility so that drugs can easily be soluble [12].

Re-epithelialization improvement and enhanced activity of neo-vascularization and inflammatory response modulation has been seen with application of hydroxypropyl-beta-cyclodextrin along with insulin [9].

CD-modified sacran (mega-molecular polysaccharide) hydrogel, due to its moisturizing ability, has been shown to bring improvements in wound healing process such as faster closure as compared to the gel without CD-modification [52]. It was described that sacran improved skin barrier function and by the production of cytokines (IL-5 and TNF- α), it also influenced anti-inflammatory activity [42]. In Fig. 4, it is being shown that how several nano-formulations are playing their role at different stage of wound healing.

4. Conclusion and future perspective

Since the last decades, there has been many remarkable studies by the researchers on nanotechnology-based techniques for wound healing. There is a lot of work and research has been done on inorganic nanomaterials by the scientists to determine how efficiently these can be used as delivery vehicle and their pros and cons are studied. But recently, there has been a trend of studying the organic nature of plant-based nanomaterials such as lipid and polymer-based NPs. They play a significant role in wound healing in several ways by stimulating cell proliferation through different growth factors which are carried by these polymer or lipid-based NPs, by collagen deposition, or by inhibiting pathogenic activities (biofilm formation). These plant-based/organic nanomaterials can be used as an efficient drug delivery system with many advantages such as controlled drug release, non-toxicity, stability, bioavailability, biocompatibility of the drug with target cells as well several other benefits in terms of wound healing such faster angiogenesis and vascularization.

The composition and the properties of nanomaterial are the factors that decide which kind of nanomaterial will be suitable for use at different stages of wound healing. These newly designed nanotechnology-based approaches of wound healing work on principle of synergy. Despite all these advanced nano-based remarkable pieces work, there is something that still needs our attention is to know the molecular mechanisms behind the wound healing process and how these nanomaterials are influencing different stages of this process. Moreover, reoccurrence of resistant bacteria which cause skin discoloration and safety of the nanomaterial should be assessed.

Declaration of Competing Interest

The authors declare that they have no known competing financial interests or personal relationships that could have appeared to influence the work reported in this paper.

References

- [1] E. Abbasi, S.F. Aval, A. Akbarzadeh, M. Milani, H.T. Nasrabadi, S.W. Joo, Y. Hanifehpour, K. Nejati-Koshki, R.J.N.R.L. Pashaei-Asl, Dendrimers: synthesis, applications, and properties 9 (2014) 1–10.
- [2] N. Ahmad, R. Ahmad, A. Al-Qudaihi, S.E. Alaseel, I.Z. Fita, M.S. Khalid, F.H. Pottou, Preparation of a novel curcumin nanoemulsion by ultrasonication and its comparative effects in wound healing and the treatment of inflammation 9 (35) (2019) 20192–20206.
- [3] M.U. Akbar, K.M. Zia, M.S.H. Akash, A. Nazir, M. Zuber, M.J.I.J.O.B.M. Ibrahim, In-vivo anti-diabetic and wound healing potential of chitosan/alginate/maltodextrin/pluronic-based mixed polymeric micelles, Curcumin therapeutic potential. 120 (2018) 2418–2430.
- [4] P. Alam, F. Shakeel, M.K. Anwer, A.I. Foudah, M.H. Alqarni, Wound Healing Study of Eucalyptus Essential Oil Containing Nanoemulsion in Rat Model, *J. Oleo Sci.* 67 (8) (2018) 957–968.
- [5] T. Alberti, D.S. Coelho, A. Voytina, H. Pitz, M. de Pra, L. Mazzarino, S. Kuhnen, R. M. Ribeiro-do-Valle, M. Maraschin, B. Veleirinho, Nanotechnology: A promising tool towards wounds healing 23 (24) (2017).
- [6] M.G. Arafa, R.F. El-Kased, M.M.J.S.R. Elmazar, Thermoresponsive gels containing gold nanoparticles as smart antibacterial and wound healing agents 8 (2018) 1–16.
- [7] P. Bao, A. Kodra, M. Tomic-Canic, M.S. Golinko, H.P. Ehrlich, H.J.J.O.S.R. Brem, The role of vascular endothelial growth factor in wound healing 153 (2009) 347–358.
- [8] D.O. Bates, R.O.P. Jones, The role of vascular endothelial growth factor in wound healing 2 (2) (2003) 107–120.
- [9] J.C.F. Besson, L. Hernandez, J.M. de Campos, K.A. Morikawa, C.A. Bersani-Amado, G.J.I. Matioli, Insulin complexed with cyclodextrins stimulates epithelialization and neovascularization of skin wound healing in rats 48 (2017) 2417–2425.
- [10] I. Castangia, A. Năcher, C. Caddeo, D. Valenti, A.M. Fadda, O. Diez-Sales, A. Ruiz-Sauri, M.J.A.B. Manconi, Fabrication of quercetin and curcumin bionanovesicles for the prevention and rapid regeneration of full-thickness skin defects on mice 10 (2014) 1292–1300.
- [11] R. Challa, A. Ahuja, J. Ali, R.K. Khar, Cyclodextrins in drug delivery: an updated review 6 (2) (2005) E329–E357.
- [12] L. Cheng, Z. Cai, T. Ye, X. Yu, Z. Chen, Y. Yan, J. Qi, L. Wang, Z. Liu, W.J.A.F.M. Cui, Injectable Polypeptide-Protein Hydrogels for Promoting Infected Wound Healing 30 (2020) 2001196.
- [13] K.K. Cherreddy, C.-H. Her, M. Comune, C. Moia, A. Lopes, P.E. Porporato, J. Vanacker, M.C. Lam, L. Steintraesser, P.J.J.O.C.R. Sonveaux, PLGA nanoparticles loaded with host defense peptide LL37 promote wound healing 194 (2014) 138–147.
- [14] V. Choudhary, H. Shivakumar, H.J.J.O.D.D.S. Ojha, Technology, Curcumin-loaded liposomes for wound healing: Preparation, optimization, in-vivo skin permeation and bioevaluation 49 (2019) 683–691.
- [15] E. Dellera, M.C. Bonferoni, G. Sandri, S. Rossi, F. Ferrari, C. Del Fante, C. Perotti, P. Grisoli, C. Caramella, BIOPHARMACEUTICS, Development of chitosan oleate ionic micelles loaded with silver sulfadiazine to be associated with platelet lysate for application in wound healing 88 (3) (2014) 643–650.
- [16] A.A. Dongargaonkar, G.L. Bowlin, H.J.B. Yang, Electrospun blends of gelatin and gelatin-dendrimer conjugates as a wound-dressing and drug-delivery platform 14 (2013) 4038–4045.
- [17] J.S. Freed, J.J.M.M. Ko, An innovative advance in non-invasive wound closure: a new paradigm 183 (2018) 472–480.
- [18] G. Gainza, M. Pastor, J.J. Aguirre, S. Villullas, J.L. Pedraz, R.M. Hernandez, M. Igartua, A novel strategy for the treatment of chronic wounds based on the topical administration of rhEGF-loaded lipid nanoparticles: In vitro bioactivity and in vivo effectiveness in healing-impaired db/db mice 185 (2014) 51–61.
- [19] S. Hamdan, I. Pastar, S. Drakulich, E. Dikici, M. Tomic-Canic, S. Deo, S. Daunert, Nanotechnology-driven therapeutic interventions in wound healing: potential uses and applications 3 (3) (2017) 163–175.
- [20] S. Huber, P. Marcato, R. Barbosa, N. Duran, J. Annichino-Bizzacchi, In vivo toxicity of enoxaparin encapsulated in mucoadhesive nanoparticles: topical application in a wound healing model, *J. Phys.: Conf. Ser.* (2013), 012031.
- [21] H.-J. Hwang, S. Han, S. Jeon, J. Seo, D. Oh, S.-W. Cho, Y.W. Choi, S. Lee, Recombinant human epidermal growth factor (rhEGF)-loaded solid lipid nanoparticles: fabrication and their skin accumulation properties for topical rhEGF delivery 35 (8) (2014) 2290–2294.
- [22] B. Jamil, R. Abbasi, S. Abbasi, M. Imran, S.U. Khan, A. Ihsan, S. Javed, H. Bokhari, M. Imran, Encapsulation of cardamom essential oil in chitosan nanocomposites: In-vitro efficacy on antibiotic-resistant bacterial pathogens and cytotoxicity studies 7 (2016).
- [23] A. Kalashnikova, S. Das, S. Seal, Nanomaterials for wound healing: scope and advancement 10 (16) (2015) 2593–2612.
- [24] Z. Karimi Taheri, M.H. Aarabi, A. Nazari Alam, M. Nejati, M. Shayestehpour, H.R. Gilasi, A. Salehi, M.E.J.J.O.A.U.O.M.S. Shahaboddin, Evaluation of Anti-Proliferative Effects of Nanoemulsion Containing Licorice Extract and Lavender Essential Oil Against Cancer Cells and Its Antimicrobial Properties: An in Vitro Study 23 (2020) 9.
- [25] Z. Karimi Taheri, M.H. Aarabi, A. Nazari Alam, M. Nejati, M. Shayestehpour, H.R. Gilasi, A. Salehi, M.E.J.J.O.A.U.O.M.S. Shahaboddin, Evaluating the Anti-proliferative Effects of Nanoemulsion Containing Licorice Extract and Lavender Essential Oil on, *Cancer* 24 (2021) 84–97.
- [26] L.N. Kasiewicz, K.A.J.B. Whitehead, T. Medicine, Lipid nanoparticles silence tumor necrosis factor α to improve wound healing in diabetic mice. 4 (2019) 75–82.
- [27] M. Kazemi, M. Mohammadifar, E. Aghadavoud, Z. Vakili, M.H. Aarabi, S.A. Talaei, Deep skin wound healing potential of lavender essential oil and licorice extract in a nanoemulsion form: Biochemical, histopathological and gene expression evidences 29 (2) (2020) 116–124.
- [28] S. Küchler, N.B. Wolf, S. Heilmann, G. Weindl, J. Helfmann, M.M. Yahya, C. Stein, M. Schäfer-Korting, 3D-wound healing model: influence of morphine and solid lipid nanoparticles 148 (1) (2020) 24–30.
- [29] M.J. Kwon, S. An, S. Choi, K. Nam, H.S. Jung, C.S. Yoon, J.H. Ko, H.J. Jun, T.K. Kim, S.J. Jung, J.H. Park, Y. Lee, J.-S. Park, Effective healing of diabetic skin wounds by using nonviral gene therapy based on minicircle vascular endothelial growth factor DNA and a cationic dendrimer 14 (4) (2012) 272–278.
- [30] J. Li, J. Chen, R.J.C.I.D. Kirsner, Pathophysiology of acute wound healing. 25 (2007) 9–18.
- [31] M. Li, F. Li, T. Wang, L. Zhao, Y.J.J.O.B.A. Shi, Fabrication of carboxymethylcellulose hydrogel containing β -cyclodextrin-eugenol inclusion complexes for promoting diabetic wound healing 34 (2020) 851–863.
- [32] Z.-J. Liu, P. Daftarian, L. Kovalski, B. Wang, R. Tian, D.M. Castilla, E. Dikici, V.L. Perez, S. Deo, S.J.P.O. Daunert, Directing and potentiating stem cell-mediated angiogenesis and tissue repair by cell surface e-selectin coating 11 (2016) e0154053.
- [33] K.-J. Lu, W. Wang, X.-L. Xu, F.-Y. Jin, J. Qi, X.-J. Wang, X.-Q. Kang, M.-L. Zhu, Q.-L. Huang, C.-H. Yu, J. You, Y.-Z. Du, A dual deformable liposomal ointment functionalized with retinoic acid and epidermal growth factor for enhanced burn wound healing therapy 7 (6) (2019) 2372–2382.
- [34] M. Madalina Mihai, A. Maria Holban, C. Giurcaneanu, L. Gabriela Popa, R. Mihaela Oanea, V. Lazar, M. Carmen Chifriuc, M. Popa, M.J.C.T.I.M.C. Ioan Popa, Microbial biofilms: impact on the pathogenesis of periodontitis, cystic fibrosis, chronic wounds and medical device-related infections 15 (2015) 1552–1576.
- [35] S. Maji, T. Agarwal, T.K.J.C. Maiti, S.B. Biointerfaces, PAMAM (generation 4) incorporated gelatin 3D matrix as an improved dermal substitute for skin tissue engineering 155 (2017) 128–134.
- [36] M. Malone, K. Johani, S.O. Jensen, I.B. Gosbell, H.G. Dickson, H. Hu, K.J.E. Vickery, Next generation DNA sequencing of tissues from infected diabetic foot ulcers 21 (2017) 142–149.
- [37] M.L. Manca, I. Castangia, C. Caddeo, D. Pando, E. Escribano, D. Valenti, S. Lampis, M. Zaru, A.M. Fadda, M.J.C. Manconi, S.B. Biointerfaces, Improvement of quercetin protective effect against oxidative stress skin damages by incorporation in nanovesicles 123 (2014) 566–574.
- [38] K.-L. Mao, Z.-L. Fan, J.-D. Yuan, P.-P. Chen, J.-J. Yang, J. Xu, D.-L. ZhuGe, B.-H. Jin, Q.-Y. Zhu, B.-X. Shen, Y. Sohawon, Y.-Z. Zhao, H.-L. Xu, Skin-penetrating polymeric nanoparticles incorporated in silk fibroin hydrogel for topical delivery of curcumin to improve its therapeutic effect on psoriasis mouse model 160 (2017) 704–714.
- [39] M.M. Mihai, A.M. Holban, C. Giurcaneanu, L.G. Popa, M. Buzeta, M. Filipov, V. Lazăr, M.C. Chifriuc, M.I.J.R.J.M.E. Popa, Identification and phenotypic characterization of the most frequent bacterial etiologies in chronic skin ulcers. 55 (2014) 1401–1408.
- [40] M.M. Mihai, M. Preda, I. Lungu, M.C. Gestal, M.I. Popa, A.M.J.I.J.O.M.S. Holban, Nanocoatings for chronic wound repair—modulation of microbial colonization and biofilm formation 19 (2018) 1179.
- [41] M.-C. Miller, J.J.B. Nanchahal, Advances in the modulation of cutaneous wound healing and scarring 19 (2005) 363–381.
- [42] I. Negut, V. Grumezescu, A.M.J.M. Grumezescu, Treatment strategies for infected wounds 23 (2018) 2392.
- [43] S.K. Nethi, S. Das, C.R. Patra, S. Mukherjee, Recent advances in inorganic nanomaterials for wound-healing applications 7 (7) (2019) 2652–2674.
- [44] D.A. Sanchez, D. Schairer, C. Tuckman-Vernon, J. Chouake, A. Kutner, J. Makdisi, J.M. Friedman, J.D. Nosanchuk, A.J. Friedman, Amphotericin B releasing nanoparticle topical treatment of *Candida* spp. in the setting of a burn wound, *Nanomed. Nanotechnol. Biol. Med.* 10 (1) (2014) 269–277.
- [45] P.T. Sudheesh Kumar, V.-K. Lakshmanan, T.V. Anilkumar, C. Ramya, P. Reshmi, A.G. Unnikrishnan, S.V. Nair, R. Jayakumar, Flexible and microporous chitosan hydrogel/nano ZnO composite bandages for wound dressing: in vitro and in vivo evaluation 4 (5) (2012) 2618–2629.
- [46] H. Takada, J. Yonekawa, M. Matsumoto, K. Furuya, M. Sokabe, Hyperforin/HP- β -Cyclodextrin Enhances Mechanosensitive Ca²⁺ Signaling in HaCaT Keratinocytes and in Atopic Skin Ex Vivo Which Accelerates Wound Healing, *BioMed Res. Int.* 2017 (2017) 1–9.
- [47] T. Tang, H. Jiang, Y. Yu, F. He, S.-Z. Ji, Y.-Y. Liu, Z.-S. Wang, S.-C. Xiao, C. Tang, G.-Y.-J.-I.-J.-O.-N. Wang, A new method of wound treatment: targeted therapy of skin wounds with reactive oxygen species-responsive nanoparticles containing SDF-1 α 10 (2015) 6571.

- [51] A. Valizadeh, M. Shirzad, M.R. Pourmand, M. Farahmandfar, H. Sereshti, A.J.D. D. Amani, T. Research, Levofloxacin nanoemulsion gel has a powerful healing effect on infected wound in streptozotocin-induced diabetic rats 11 (2021) 292–304.
- [52] N. Wathoni, K. Motoyama, T. Higashi, M. Okajima, T. Kaneko, H.J.I.J.O.B.M. Arima, Enhancing effect of γ -cyclodextrin on wound dressing properties of sacran hydrogel film 94 (2017) 181–186.
- [53] N. Wathoni, D.P. Sari, I. Suharyani, K. Motoyama, A.F.A. Mohammed, A. Cahyanto, M. Abdassah, M.J.P. Muchtaridi, Enhancement of α -Mangostin wound healing ability by complexation with 2-hydroxypropyl- β -cyclodextrin in hydrogel formulation 13 (2020) 290.

Further reading

- [10] N.B. Caldon, Effect of Solid Lipid Nanoparticle-Encapsulated Antimicrobial Peptide on Keratinocyte Migration and Wound Healing, Uniformed Services University of The Health Sciences Bethesda United States, 2013.
- [31] C. Li, X. Zhang, X. Huang, X. Wang, G. Liao, Z.J.I.J.O.N. Chen, Preparation and characterization of flexible nanoliposomes loaded with daptomycin, a novel antibiotic, for topical skin therapy 8 (2013) 1285.
- [47] A.P. Smith-Freshwater, Preparation and Characterization of an Electrospun Gelatin/dendrimer Hybrid Nanofiber Dressing, 2009.



Study of solvation and pollution approach of atrazine and chlorothalonil pesticides in binary liquid mixtures

Kalyan R. Langore^{a,*}, Arun B. Nikumbh^b

^a Department of Chemistry, E. S. Divekar College, Varvand-412215, M.S, India

^b P. G. Department of Chemistry, Annasaheb Awate Arts, Commerce and Hutatma Babu Genu College, Manchar-410503, M.S., India

ARTICLE INFO

Article history:

Available online 26 October 2022

Keywords:

Viscosity
Relative viscosity
Solvation number
Atrazine Chlorothalonil

ABSTRACT

Thermodynamic properties of liquid mixtures are communally used to examine the deviation from ideality. The thermodynamic properties, which depend on temperature, composition and pressure, describe interaction between the component molecules. The solubility is a property of solute and solvent that effect on extent of adsorption–desorption of pesticides. Hence solution chemistry utilized for investigation of environmental fate of agrochemicals and pollutants in the environment. Some pesticides can leach through the soil and enter into the groundwater. In India about 60 % of the population depends upon ground water for drinking purpose and almost 95 % of the households in rural areas use ground water as their primary source of drinking water. Drinking water supplies might be contaminated by pesticides. The excess use of pesticides leads to environmental contamination and the pesticide residues are found in food, water and air. This paper addresses a study of solvation behavior of Atrazine and Chlorothalonil pesticides in binary mixture of DMF and DMSO. The measured densities (ρ) and viscosities (η) at 298.15 to 313.15 K using a bicapillary pycnometer and Ubbelohde viscometer were utilize to study salvation and pollution approach of pesticides. The obtained parameters were interpreted in terms of solute–solute and solute–solvent interactions. The proposed method for study of solvation behavior of pesticides by viscometer is simple, robust and requires less computational time. Each pesticide and solvent molecules are nanoparticles. Recommendation from this research work could help to change physiochemical behavior of pesticides used in agriculture field to becomes more eco-friendly for the sustainable development in environment.

Copyright © 2022. Elsevier Ltd. All rights reserved.

Selection and peer-review under responsibility of the scientific committee of the Integrative Nanotechnology Perspective for Multidisciplinary Applications - 2022.

1. Introduction

The solution chemistry plays important role in pharmaceuticals, agro based industries, and engineering. The density and viscosity data of pesticides in binary liquid mixtures are interpreted as solute–solute and solute–solvent interactions. The solubility is a property of solute and solvent that affect on extent of adsorption–desorption of pesticides [1–4]. So solution chemistry utilized for investigation of environmental fate of agrochemicals and pollutants in the environment. The solute–solvent interactions of pesticides have complex mechanism. Solute-solvent interactions at

different temperatures applied to study mode of action of pesticides [5,6]. (See Table 1–8).

Atrazine is most regularly utilized herbicides of the triazine class. Atrazine is utilized to control pre and post-development broadleaf weeds in yields, for example, sugarcane, corn, pineapples, sorghum, and macadamia nuts [7,8]. It is also utilized for fairways and private gardens. Chlorothalonil is non-systemic foliar fungicide used very widely on peanuts and potatoes, as well as in many other applications [9,10].

Pesticides were used to control many different kinds of pests, including termites, mosquitoes, and roundworms. They also have residential and indoor applications for pest control, especially for cockroaches and termites [11–15]. Pesticides being complex in their structure are stable and non-degradable in the environment. The use of pesticides is rapidly increases in agricultural for storage of grains, public health and controlled diseases. Pesticides used in

* Corresponding author.

E-mail addresses: kalyanlangore1973@gmail.com (K.R. Langore), aob.nikumbh@gmail.com (A.B. Nikumbh).

Table 1
Viscosity and relative viscosity of Chlorothalonil in DMF at various temperatures.

Molar Conc. of Chlorothalonil in DMF (mol.dm^{-3})	Temperatures (K)			
	298.15	303.15	308.15	313.15
Viscosity (η), (mPa.s)				
0.0150	0.8240	0.7827	0.7352	0.7052
0.0231	0.8330	0.7906	0.7442	0.7162
0.0329	0.8432	0.8013	0.7556	0.7285
0.0445	0.8552	0.8128	0.7665	0.7420
0.0577	0.8668	0.8232	0.7798	0.7571
0.0727	0.8795	0.8378	0.7933	0.7751
0.0894	0.8958	0.8539	0.8102	0.7966
0.1079	0.9141	0.8733	0.8313	0.8189
0.1281	0.9332	0.8925	0.8492	0.8419
0.1500	0.9535	0.9101	0.8704	0.8681
Relative Viscosity, (η_r)				
0.0150	1.0250	1.0262	1.0268	1.0331
0.0231	1.0363	1.0366	1.0394	1.0493
0.0329	1.0489	1.0506	1.0552	1.0673
0.0445	1.0639	1.0657	1.0705	1.0870
0.0577	1.0784	1.0793	1.0891	1.1092
0.0727	1.0942	1.0985	1.1079	1.1355
0.0894	1.1144	1.1195	1.1316	1.1669
0.1079	1.1372	1.1449	1.1611	1.1997
0.1281	1.1610	1.1701	1.1860	1.2334
0.1500	1.1862	1.1933	1.2156	1.2717

Table 2
Viscosity and relative viscosity of Chlorothalonil in 50 % DMSO at various temperatures.

Molar Conc. of Chlorothalonil in 50 % DMSO (mol.dm^{-3})	Temperatures (K)			
	298.15	303.15	308.15	313.15
Viscosity (η), (mPa.s)				
0.0150	1.2550	1.1551	1.0735	1.0332
0.0231	1.2723	1.1713	1.0873	1.0494
0.0329	1.2929	1.1902	1.1047	1.0691
0.0445	1.3171	1.2103	1.1266	1.0925
0.0577	1.3429	1.2331	1.1497	1.1193
0.0727	1.3738	1.2622	1.1794	1.1447
0.0894	1.4038	1.2945	1.2087	1.1751
0.1079	1.4429	1.3324	1.2458	1.2129
0.1281	1.4824	1.3679	1.2799	1.2482
0.1500	1.5241	1.4088	1.3189	1.2959
Relative Viscosity, (η_r)				
0.0150	1.0313	1.0319	1.0340	1.0368
0.0231	1.0455	1.0463	1.0472	1.0531
0.0329	1.0624	1.0633	1.0640	1.0729
0.0445	1.0823	1.0812	1.0850	1.0963
0.0577	1.1036	1.1016	1.1073	1.1232
0.0727	1.1289	1.1276	1.1359	1.1487
0.0894	1.1536	1.1564	1.1642	1.1792
0.1079	1.1857	1.1902	1.1999	1.2172
0.1281	1.2181	1.2220	1.2327	1.2526
0.1500	1.2524	1.2585	1.2702	1.3005

agriculture in different way like wet power, spray, dust and smoke. The pesticides leading to accumulations in all segment of environment included lithosphere, hydrosphere, atmosphere and biosphere. The contamination of surface and ground water by pesticides were reported by many researchers [16–18]. The contaminations of soil profile by pesticides and their residues [19–20]. The pesticides introduce in food chain of living organism. Further some studies on contamination of pesticides in aerated drinks. Therefore, many researchers were reported on uses of pesticides, pathway of their distribution in environment, toxic effect of pesticides, and their factsheet. In view of this the author decided to work on solvation behavior of pesticides. This use of pesticides in agriculture and gardening were contributed to environmental pollution. As the pesticides residues are in the food chain, its sub-chronic exposure is practically unavoidable for human population. In a number of recent studies, pesticide exposure was claimed to

induce insulin resistance. This sub-chronic exposure to these leads to development of diabetes. The quantity of pesticides absorption-desorption depends on biological and physicochemical factors. Physicochemical factors include solubility, salt complexation, diffusion rate, toxicity and viscosity.

The aim of the present study is to understand solvation behavior of some pesticides in binary liquid mixtures of DMF and DMSO at different temperatures.

2. Materials and method

The chemicals DMSO and DMF employed were of analytical grade and were purchased from E. Merck, Germany (99.5 %), were used as such without further purification. Pesticides Imidacloprid, Chlorothalonil, Atrazine and Chlorpyrifos were purchased from local mark.

Table 3
Viscosity and relative viscosity of Chlorothalonil in DMSO at various temperatures.

Molar Conc. of Chlorothalonil in DMSO (mol.dm ⁻³)	Temperatures (K)			
	298.15	303.15	308.15	313.15
Viscosity (η), (mPa.s)				
0.0150	2.0693	1.8703	1.6833	1.5795
0.0231	2.1024	1.9024	1.7142	1.6132
0.0329	2.1415	1.9396	1.7513	1.6541
0.0445	2.1897	1.9847	1.7958	1.6970
0.0577	2.2443	2.0369	1.8437	1.7533
0.0727	2.3017	2.0936	1.8986	1.8103
0.0894	2.3621	2.1593	1.9579	1.8737
0.1079	2.4364	2.2281	2.0253	1.9495
0.1281	2.5202	2.3030	2.1044	2.0216
0.1500	2.6056	2.3823	2.1827	2.1042
Relative Viscosity, (η_r)				
0.0150	1.0395	1.0407	1.0423	1.0455
0.0231	1.0561	1.0586	1.0614	1.0678
0.0329	1.0757	1.0792	1.0844	1.0949
0.0445	1.1000	1.1044	1.1119	1.1233
0.0577	1.1274	1.1334	1.1416	1.1606
0.0727	1.1562	1.1649	1.1756	1.1982
0.0894	1.1866	1.2015	1.2123	1.2402
0.1079	1.2239	1.2398	1.2540	1.2904
0.1281	1.2660	1.2815	1.3030	1.3381
0.1500	1.3089	1.3256	1.3515	1.3928

Table 4
Viscosity and relative viscosity of Atrazine in DMF at various temperatures.

Molar Conc. of Atrazine in DMF (mol.dm ⁻³)	Temperatures (K)			
	298.15	303.15	308.15	313.15
Viscosity (η), (mPa.s)				
0.0150	0.8076	0.7658	0.7182	0.6845
0.0231	0.8110	0.7687	0.7213	0.6875
0.0329	0.8151	0.7734	0.7258	0.6915
0.0445	0.8199	0.7792	0.7305	0.6960
0.0577	0.8268	0.7851	0.7368	0.7011
0.0727	0.8335	0.7923	0.7432	0.7079
0.0894	0.8419	0.8003	0.7503	0.7146
0.1079	0.8512	0.8082	0.7594	0.7239
0.1281	0.8623	0.8184	0.7693	0.7339
0.1500	0.8744	0.8302	0.7803	0.7441
Relative Viscosity, (η_r)				
0.0150	1.0047	1.0040	1.0031	1.0028
0.0231	1.0089	1.0078	1.0073	1.0072
0.0329	1.0140	1.0140	1.0137	1.0131
0.0445	1.0200	1.0217	1.0203	1.0196
0.0577	1.0286	1.0294	1.0291	1.0271
0.0727	1.0369	1.0388	1.0380	1.0371
0.0894	1.0473	1.0492	1.0478	1.0468
0.1079	1.0589	1.0597	1.0606	1.0605
0.1281	1.0727	1.0730	1.0744	1.0752
0.1500	1.0878	1.0884	1.0898	1.0900

2.1. Viscosity measurements

The viscosity measurements were made using a suspended level Ubbelohde viscometer. The viscometer was clamped vertically in the bath, and 20 cm³ of the solution was added from a burette. The viscometer was calibrated with triple distilled water using the viscosity and density values reported by Marsh. Viscosity values were determined using the relation.

$$\eta_1/\eta_2 = \rho_1 t_1/\rho_2 t_2 \quad (1)$$

3. Results and discussion

The evaluated viscosities and relative viscosities of Chlorothalonil pesticide in pure DMF, 50 %, and 100 % DMSO are reported in

table no. 1 to 3. It is observed that for table no. 1 the viscosities of Chlorothalonil pesticide in pure DMF increases with increase in molar concentration at all temperatures under consideration. While it decreases with increase in temperature. The similar trend in viscosities is observed in table no. 2 and 3 with the molar concentrations and temperatures. The relative viscosities (η_r) increases with increase in molar concentration of Chlorothalonil pesticide in pure DMF. ' η_r ' shows increasing trend with increase in temperature. The similar trends in relative viscosities are observed for table no. 2 and 3 in all compositions of binary liquid mixtures of DMF and DMSO. Viscosity and relative viscosity is the measure of molecular interaction.

The observation of table no. 1 to 3 shows the smallest value of viscosity of Chlorothalonil is 0.7052 (mPa.s) for 0.0150 M in pure DMF at 313.15 K and higher 2.6056 (mPa.s) for 0.1500 M in pure

Table 5
Viscosity and relative viscosity of Atrazine in 50 % DMSO at various temperatures.

Molar Conc. of Atrazine in 50 % DMSO (mol.dm^{-3})	Temperatures (K)			
	298.15	303.15	308.15	313.15
Viscosity (η), (mPa.s)				
0.0150	1.2208	1.1232	1.0416	1.0001
0.0231	1.2262	1.1283	1.0462	1.0042
0.0329	1.2327	1.1350	1.0537	1.0109
0.0445	1.2422	1.1433	1.0625	1.0193
0.0577	1.2518	1.1534	1.0707	1.0286
0.0727	1.2634	1.1641	1.0815	1.0385
0.0894	1.2756	1.1764	1.0937	1.0504
0.1079	1.2907	1.1893	1.1068	1.0635
0.1281	1.3063	1.2048	1.1210	1.0786
0.1500	1.3242	1.2217	1.1358	1.0951
Relative Viscosity, (η_r)				
0.0150	1.0032	1.0034	1.0032	1.0036
0.0231	1.0076	1.0079	1.0077	1.0077
0.0329	1.0129	1.0140	1.0149	1.0145
0.0445	1.0208	1.0213	1.0233	1.0229
0.0577	1.0287	1.0304	1.0313	1.0322
0.0727	1.0382	1.0400	1.0416	1.0421
0.0894	1.0482	1.0509	1.0534	1.0541
0.1079	1.0606	1.0625	1.0660	1.0672
0.1281	1.0735	1.0763	1.0796	1.0824
0.1500	1.0881	1.0913	1.0940	1.0989

Table 6
Viscosity and relative viscosity of Atrazine in DMSO at various temperatures.

Molar Conc. of Atrazine in DMSO (mol.dm^{-3})	Temperatures (K)			
	298.15	303.15	308.15	313.15
Viscosity (η), (mPa.s)				
0.0150	1.9982	1.8032	1.6205	1.5164
0.0231	2.0075	1.8114	1.6283	1.5243
0.0329	2.0183	1.8221	1.6394	1.5343
0.0445	2.0326	1.8353	1.6524	1.5451
0.0577	2.0492	1.8520	1.6678	1.5592
0.0727	2.0698	1.8703	1.6843	1.5751
0.0894	2.0910	1.8892	1.7042	1.5965
0.1079	2.1163	1.9146	1.7255	1.6194
0.1281	2.1474	1.9403	1.7495	1.6432
0.1500	2.1785	1.9672	1.7786	1.6694
Relative Viscosity, (η_r)				
0.0150	1.0038	1.0034	1.0034	1.0037
0.0231	1.0085	1.0079	1.0082	1.0090
0.0329	1.0139	1.0139	1.0151	1.0156
0.0445	1.0211	1.0212	1.0232	1.0227
0.0577	1.0294	1.0305	1.0327	1.0321
0.0727	1.0397	1.0407	1.0429	1.0426
0.0894	1.0504	1.0512	1.0552	1.0568
0.1079	1.0631	1.0654	1.0684	1.0719
0.1281	1.0787	1.0796	1.0833	1.0876
0.1500	1.0944	1.0946	1.1013	1.1050

Table 7
' β ' values for Pesticides Chlorothalonil and Atrazine in 50% of DMSO in binary liquid mixture DMF and DMSO at various temperatures.

Temp.	DMF	50 % DMSO	DMSO
Chlorothalonil			
298.15	1.1829	1.6357	1.9883
303.15	1.2473	1.6803	2.1180
308.15	1.3945	1.7660	2.2853
313.15	1.7624	1.9246	2.5743
Atrazine			
298.15	0.6134	0.6304	0.6713
303.15	0.6224	0.6523	0.6815
308.15	0.6393	0.6777	0.7215
313.15	0.6468	0.7086	0.7546

Table 8
Solvation numbers (n_s) for pesticides Chlorothalonil and Atrazine in 50% of DMSO in binary liquid mixture DMF and DMSO at various temperatures.

Temp.	DMF	50 % DMSO	DMSO
Chlorothalonil			
298.15	1.8921	4.5477	6.3839
303.15	0.4642	2.8955	5.2493
308.15	0.1578	2.1511	4.9340
313.15	0.0295	0.7854	4.5484
Atrazine			
298.15	1.3541	1.7079	1.9937
303.15	0.9695	1.2811	1.5506
308.15	0.6397	0.9407	1.2598
313.15	0.1966	0.5915	0.8984

DMSO at 298.15 K. The small value of viscosity indicates lower molecular interactions while higher for high molecular interactions. The molecular interactions are of solvent–solvent and solute–solvent type. The higher value of relative viscosity is 1.3928 for 0.1500 M in pure DMSO at 313.15 K and smaller value is 1.0250 for 0.0150 M in pure DMF at 298.15 K. Smaller magnitude of relative viscosity indicates presence of weak solute–solute interactions higher magnitude indicates strong solute–solute interactions. The solute–solvent, solute–solvent and solvent–solvent interactions varying between minimum to maximum values from pure DMF to pure DMSO.

The observed viscosities and relative viscosities of Atrazine pesticide in pure DMF, 50 %, and 100 % DMSO are reported in table no. 4 to 6. It is observed that for table no. 4 the viscosities of Atrazine pesticide in pure DMF increases with increase in molar concentration at all temperatures under consideration. While it decreases with increase in temperature. The similar trend in viscosities is observed in table no. 5 and 6 with the molar concentrations and temperatures.

The relative viscosities (η_r) increases with increase in molar concentration of Atrazine pesticide in pure DMF. The relative viscosities are positive and greater than one indicate that solute–solvent interaction persist at all temperatures.

Viscosity and relative viscosity is the measure of molecular interaction. Table no. 4 to 6 shows the smallest value of viscosity of Atrazine is 0.6845 (mPa.s) for 0.0150 M in pure DMF at 313.15 K and higher 2.1785 (mPa.s) for 0.1500 M in pure DMSO at 298.15 K. The small value of viscosity indicates lower molecular interactions while higher for high molecular interactions. The molecular interactions are of solvent–solvent and solute–solvent type. The higher value of relative viscosity is 1.1050 for 0.1500 M in pure DMSO at 313.15 K and smaller value is 1.0028 for 0.0150 M in pure DMF at 313.15 K. Smaller magnitude of relative viscosity indicates presence of weak solute–solute interactions higher magnitude indicates strong solute–solute interactions.

The ' β ' values were obtained as slopes of linear plots of η_r versus C for Chlorothalonil and Atrazine pesticides at all compositions and temperatures are listed in Table 7. All the ' β ' values are positive.

The solvation numbers (n_s) represent the number of solvent molecules that remain gather around the ion at the time of its movement in the solution. The solvation number is more importance because all solute undergo constant thermal motion. The solvation numbers determine the effective size of the solute. The extent of solvation directly proportional to the size of solute and the solvation is results of dispersion interaction between solute and solvent.

The number of solvent molecules (n_s) to the solute in the primary sphere of solvation may be evaluated by using combine equation of Einstein with the Jone- Dole equation.

$$B = \frac{2.5}{1000} + (V_i + n_s V_s) \quad (5.1)$$

Where V_i are molar volume of the solute and it is evaluated using crystallographic radius, r_c , of the solute, ($=4/3 \pi N r_c^3 = 2.52 r_c^3$, r in \AA), v_s is the molar volume of solvent. Viscosity of a solution depends on many factors such as viscosity of solvent, type of solute, the amount of solute and temperature. The simple equations related with viscosity of solution are based on few assumptions. The first is assuming the shape of the solute particles in the solution as spheres. The second is assumption the particle size of solute is much bigger than that of the solvent. Taken the ratio of viscosity of the solution to that of the pure solvent (η/η_0) is related to the volume fraction (Φ) occupied by the solute particle. The relation of these assumptions is explain by equation show below,

$$\frac{\eta}{\eta_0} = 1 + (2.5 \times \phi) \quad (5.2)$$

The above equation can be written as.

$$\frac{\eta}{\eta_0} = 1 + (6.3 \times 10^{21} \times C \times r^3) \quad (5.3)$$

Whereas r is radius of particle in cm, C is the concentration.

The radius can be also determined by slope of straight line graph of relative viscosity against concentration, C for pesticides in binary liquid mixture DMF + DMSO.

$$\text{slope} = (6.3 \times 10^{21}) r^3 \quad (5.4)$$

The solvation of solute may be deciding form the value of ionic (B/Φ_0^0). The values of (B/Φ_0^0) were explained that the whether a solute shows unsolvated or solvated. If the value of (B/Φ_0^0) lies between the range 0 to 2.5 points, then the species remained unsolvated and the value become larger than 2.5 point then species are solvated.

The values of solvation number (n_s) are evaluated with help of equation no. 5.1, and are tabulated in table no. 8. The degree of interactions was evaluated in terms of solvation number (n_s). The solvation number is a measure of the solvent–solute interactions. The solvation numbers of both pesticides are positive. The solvation numbers of all pesticides decreases with increases in temperature implying removal of solvent molecules form secondary layer of solvation at higher temperatures. This might be due to weakening of solute–solvent interaction at higher temperatures. On an average the solvation numbers increase form pure DMF to pure DMSO. It indicates that DMSO preferentially solvates pesticides as compared to DMF.

The present study shows that the varying molecular interactions are observed for selected binary liquid mixture and at all temperatures. Each model suggests the existence of molecular interactions. The present study is not only useful to enrich the transport properties of pesticides but also useful to predict novel pesticide structure for its better activity as pesticides.

Declaration of Competing Interest

The authors declare that they have no known competing financial interests or personal relationships that could have appeared to influence the work reported in this paper.

References

- [1] R. Zarrougui, M. Dhahbi, D. Lemordant, Effect of temperature and composition on the transport and thermodynamic properties of binary mixtures of ionic liquid N-Butyl-N-methylpyrrolidiniumbis (Trifluoromethane sulfonyl) imide and propylene carbonate, *J. Sol. Chem.* 39 (7) (2010) 921–942, <https://doi.org/10.1007/s10953-010-9562-5>.
- [2] A. Heintz, J.K. Lehmann, C. Wertz, Thermodynamic properties of mixtures containing ionic liquids. 3. Liquid-liquid equilibria of binary mixtures of 1-ethyl-3-methylimidazolium Bis(trifluoromethylsulfonyl) imide with propan-1-ol, butan-1-ol, and pentan-1-ol, *J. Chem. Eng. Data* 48 (3) (2003) 472–474, <https://doi.org/10.1021/je0201931>.
- [3] S. Oswal, H. Desai, Studies of viscosity and excess molar volume of binary mixtures, *Fluid Phase Equilib.* 149 (1–2) (1998) 359–376, [https://doi.org/10.1016/s0378-3812\(98\)00318-5](https://doi.org/10.1016/s0378-3812(98)00318-5).
- [4] S.L. Oswal, H.S. Desai, Studies of viscosity and excess molar volume of binary mixtures, *Fluid Phase Equilib.* 186 (1–2) (2001) 81–102, [https://doi.org/10.1016/s0378-3812\(01\)00504-0](https://doi.org/10.1016/s0378-3812(01)00504-0).
- [5] Pal, A., and Kumar, A., Excess molar volumes and kinematic viscosities for binary mixtures of Dipropylene Glycol Monobutyl Ether and Dipropylene Glycoltert-Butyl Ether with 2-Pyrrolidinone, N-Methyl-2-pyrrolidinone, N, N-Dimethylformamide, and N, N-Dimethylacetamide at 298.15 K. *Journal of Chemical & Engineering Data*, 2005, 50(3), 856–862. doi:10.1021/je049657g.
- [6] H. Kidd, D.R. James (Eds.), *The Agrochemicals Handbook, Third Edition.*, Royal Society of Chemistry Information Services, Cambridge, UK, 1991, as updated.
- [7] Weed Science Society of America. *Herbicide Handbook*, Seventh Edition. Champaign, IL, 1994. 8–16

- [8] P.P. Parsons, Mammalian toxic kinetics and toxicity of Chlorothalonil, Hayes' Handbook Pesticide Toxicol. (2010) 1951–1966, <https://doi.org/10.1016/b978-0-12-374367-1.00091-4>.
- [9] A.M. Mozzachio, J.A. Rusiecki, J.A. Hoppin, R. Mahajan, R. Patel, L. Beane-Freeman, M.C. Alavanja, Chlorothalonil exposure and cancer incidence among pesticide applicator participants in the agricultural health study, Environ. Res. 108 (3) (2008) 400–403, <https://doi.org/10.1016/j.envres.2008.07.018>.
- [10] P.K. Mutiyar, A.K. Mittal, Status of organochlorine pesticides in Ganga river basin: anthropogenic or glacial?, Drinking Water Eng Sci. 6 (2) (2013) 69–80, <https://doi.org/10.5194/dwes-6-69-2013>.
- [11] C.P. Kaushik, H.R. Sharma, A. Kaushik, Organochlorine pesticide residues in drinking water in the rural areas of Haryana, India, Environ. Monit. Assess. 184 (1) (2011) 103–112, <https://doi.org/10.1007/s10661-011-1950-9>.
- [12] U. Ali, J.H. Syed, R.N. Malik, Organochlorine pesticides (OCPs) in South Asian region: a review, Sci. Total Environ. 476 (2014) 705–717.
- [13] B.S. Bhadouria, V.B. Mathur, R. Kaul, Monitoring of organochlorine pesticides in and around Keoladeo National Park, Bharatpur, Rajasthan, India, Environ. Monit. Assess. 184 (9) (2011) 5295–5300, <https://doi.org/10.1007/s10661-011-2340-z>.
- [14] M.W. Aktar, M. Paramasivam, D. Sengupta, S. Purkait, M. Ganguly, S. Banerjee, Impact assessment of pesticide residues in fish of Ganga river around Kolkata in West Bengal, Environ. Monit. Assess. 157 (2009) 97–104.
- [15] X. Wang, X. Piao, J. Chen, J. Hu, F. Xu, S. Tao, Organochlorine pesticides in soil profiles from Tianjin, China, Chemosphere 64 (9) (2006) 1514–1520, <https://doi.org/10.1016/j.chemosphere.2005.12.052>.
- [16] T. Harner, J.L. Wideman, L.M.M. Jantunen, T.F. Bidleman, W.J. Parkhurst, Residues of organochlorine pesticides in Alabama soils, Environ. Pollut. 106 (3) (1999) 323–332, [https://doi.org/10.1016/s0269-7491\(99\)00110-4](https://doi.org/10.1016/s0269-7491(99)00110-4).
- [17] Y.F. Jiang, X.T. Wang, Y. Jia, F. Wang, M.H. Wu, G.Y. Sheng, J.-M. Fu, Occurrence, distribution and possible sources of organochlorine pesticides in agricultural soil of Shanghai, China, J. Hazard. Mater. 170 (2–3) (2009) 989–997, <https://doi.org/10.1016/j.jhazmat.2009.05.082>.
- [18] N. Kannan, T.B.H. Reusch, D.E. Schulz-Bull, G. Petrick, J.C. Duinker, Chlorobiphenyls: model compounds for metabolism in food chain organisms and their potential use as ecotoxicological stress indicators by application of the metabolic slope concept, Environ. Sci. Technol. 29 (7) (1995) 1851–1859, <https://doi.org/10.1021/es00007a024>.
- [19] M.R. Zavon, Chlorinated hydrocarbon insecticides in human body fat in the United States, J. Am. Med. Assoc. 193 (10) (1965) 837–839, <https://doi.org/10.1001/jama.1965.03090100083035>.
- [20] S. Suchail, D. Guez, L.P. Belzunces, Discrepancy between acute and chronic toxicity induced by Imidacloprid and its metabolites in Apismellifera, Environ. Toxicol. Chem. 20 (11) (2001) 2482–2486, <https://doi.org/10.1002/etc.5620201113>.



Silica supported phosphotungstic acid catalyzed one pot efficient synthesis of pyrazolopyranopyrimidine derivatives”

Mantosh B. Swami ^{a,*}, Ashok R. Karad ^b, Shreeram D. Ganapure ^c, Arvind H. Jadhav ^{d,*}, Sudhakar G. Patil ^e

^a Department of Chemistry, Mahatma Basweshwar College, Latur, India

^b Department of Chemistry, Mahatma Gandhi Mahavidyalaya Ahmedpur, Dist. Latur, India

^c Department of Chemistry, Annasaheb Awate Arts, Commerce and Hutatma Babu Genu Science College, Manchar, India

^d Centre for Nano and Material Sciences, Jain University, Bangalore, India

^e Department of Chemistry, Maharashtra Udaygiri College, Udgir, India

ARTICLE INFO

Article history:

Available online 6 December 2022

Keywords:

Silica supported phosphotungstic acid
Barbituric acid
3-methyl-5-pyrazolone
Pyrazolopyranopyrimidines derivatives
MCR

ABSTRACT

A simple highly efficient method for synthesis of pyrazolopyranopyrimidine derivative has been developed. We have prepared heterogeneous silica supported phosphotungstic acid catalyst and characterized completely by different spectroscopic and analytical techniques. After successful characterization of catalyst, it was employed in the synthesis of pyrazolopyranopyrimidine derivatives from barbituric acid, 3-methyl-5-pyrazolone and substituted aryl aldehydes under optimized reaction conditions. Results showed that, silica supported phosphotungstic acid catalyst much more effective and selective catalyst for the synthesis of pyrazolopyranopyrimidine derivatives under greener conditions. Key advantage of this method was easy work up, recyclability of catalyst up to five cycles, highly efficient synthesis of eleven derivatives of pyrazolopyranopyrimidines with 96–88 % isolated yield with maximum purity.

Copyright © 2022. Elsevier Ltd. All rights reserved.

Selection and peer-review under responsibility of the scientific committee of the Integrative Nanotechnology Perspective for Multidisciplinary Applications - 2022.

1. Introduction

Multi-component reactions involve more than two reactants that combine in the proper way to form a single product that contains the essential part of the reactants [1]. A multicomponent reaction is a powerful tool in synthetic organic chemistry and drug design processes, because of its molecular diversity, allowing the rapid and automated generation of organic compounds [2]. Knoevenagel reaction is the most important route for the construction of the C—C bond in modern organic chemistry [1–3]. Knoevenagel product usually undergoes Michael-type addition reactions [4]. Several multi-component strategies involving Knoevenagel condensation and Michael addition followed by intramolecular cyclization have been reported for the synthesis of new fused heterocycles [4–6]. Heterocyclic compounds containing pyrimidine, pyrazole and pyran together has found to possess various pharmacological activities [7]. The pyrimidine nucleus is the core unit of many pharmacological agents which exhibits a broad spectrum of biological

properties [7,8]. Furthermore, Pyrazole is another important structural motif that plays a vital role in many pharmaceutical and agro-chemical industries [9,10]. The pyran skeleton is the most important structural unit in bioactive compounds, a number of natural products, photochromic and luminescence materials [11,12]. The more prominent effect is observed when two or more heterocyclic units are present in a single molecule. The pyranopyrazole moiety signifies a fascinating template in the pharmaceutical field and shows a wide range of biological activities such as antidepressant, [13] insecticidal [14], hypotensive [15], and anticancer. [16] In contrast, the pyranopyrimidine scaffold as a key member of the pyrimidine family has gained considerable attention due to its wide range of antitumors [17] and prominent antimicrobial & antitubercular activities. [18] Significant biological activity of pyranopyrimidine is due to their occurrence in the structures of various natural products [19]. Fused heterocycle consisting of both Pyranopyrazole & Pyranopyrimidine moieties fascinates probing possible cumulative biological properties. Recently, considerable attention has been given to design strategies leading to structurally diverse and complex molecules.

Heteropolyacid plays an important role in the catalytic system which possesses both Bronsted acidity and redox potentiality

* Corresponding authors.

E-mail addresses: mantoshswami123@gmail.com (M.B. Swami), jadhav.ah@gmail.com, j.arvind@jainuniversity.ac.in (A.H. Jadhav).

[20–22]. Different HPAs (Heteropoly acids) are used for catalyzing numerous photochemical, organic [23–26], electrochemical [27], and petrochemical [28] reactions. Although all the interesting features of HPAs such as their non-corrosive and nontoxic nature, are sensitive to light and electricity, they suffer from some drawbacks like low surface area and high water solubility and conventional organic solvents. Recently, heterogeneous catalysis attracted the researcher's attention due to its basic characteristic of easy separation. Supported Heteropolyacid have more important applications due to it have high specific area with more acidic sites on the surface compared to Heteropolyacid [29]. So, it is necessary to find out appropriate support to increase specific areas of phosphotungstic acid. Silica- supported phosphotungstic acid was utilized in different reactions like α -pinene polymerization [30], β -pinene polymerization [31] and many others.

The most common method for synthesis of pyrazolopyranopyrimidinedione derivatives is condensation reaction between pyrazoline, aromatic aldehyde and barbituric acid in presence of various catalyst such as, Meglumine [32], SBA-Pr-SO₃H as a Nanoporous acid catalyst [33], Nano Fe₂O₃ supported organocatalyst [34]. Reported literature suffers from a few limitations such as long reaction time, low yield, the requirement of excess and toxic reagent and tedious work-up procedure therefore, there is need to develop highly efficient catalytic system in the synthesis of Pyrazolopyranopyrimidinedione.

In continuation of our research work on the development of constructive methodologies, we reported highly efficient environment pleasant, silica supported phosphotungstic acid as catalyst for synthesis of Pyrazolopyranopyrimidines derivatives. In addition detail, the synthesis and characterization of synthesized catalyst were obtained and structural confirmation has been done. In addition, optimization of reaction conditions was studied in detail and the same has been discussed. Recyclability of catalyst and number of substituted derivatives were prepared in good to efficient yield.

2. Materials and methods

2.1. Materials

All the chemicals including Phosphotungstic acid (99.0 %), aryl aldehydes (99.0 %), Pyrazoline (99.0 %) fumed silica & barbituric acid (99.0 %) were purchased from Sigma Aldrich and used directly without further purification.

2.2. Catalyst preparation

Fumed silica was treated with 1 M hydrochloric acid. A mixture of 10.0 g of silica (mesh size 0.2–0.3 μ m) & 40 ml of 1 M hydrochloric acid was added in a 100 ml round-bottomed flask with a stirrer bar and stirring continued for 5 h at room temperature, the pre-treated silica was collected by filtration, washed with distilled water until the pH was more than 6.0; then dry in an oven at 100 °C for 5 h. Then impregnation of phosphotungstic acid was done. Phosphotungstic acid 1.2 g, pretreated silica 2.0 g, and 20 ml of distilled water were put into a 100 ml flask, the resulting mixture was refluxed by stirring in an oil bath for 5 h at 100 °C, then evaporated to dryness at 90 °C, and further dry in an oven at 100 °C for 5 h.

2.3. Catalyst characterization methods

FT-IR spectra of catalyst were recorded by using a Varian 2000 IR spectrometer by employing the KBr pellet technique. X-ray diffraction patterns of pure silica and catalyst were obtained by using a powder XRD patterns were noted on a Rigaku Miniflex

(Rigaku Corporation, Japan) X-ray diffractometer using Ni filtered Cu K α radiation ($\lambda = 1.5406 \text{ \AA}$) with a 20 min⁻¹ scan speed and a scan range of 5–80° at 30 kV and 15 mA. Energy Dispersive X-ray spectrometry (EDX) of prepared material gave information for elemental study which was determined using SEM instrument combined with an INCA instrument for energy dispersive X-ray spectroscopy-scanning electron microscopy (EDX-SEM), with scanning electron electrode at 20 kV.

2.4. General reaction procedure for synthesis of pyrazolopyranopyrimidines derivative by using Si-PTA catalyst

A mixture of Barbituric acid (1 mmol), aryl aldehyde (1 mmol), 3-methyl-1-phenyl-5-pyrazolone (1 mmol) & 10 wt% Si-PTA catalyst were added in 50 ml RBF containing 5 ml EtOH /H₂O and the mixture were heated under reflux for the appropriate time. The progress of the reaction was monitored with help of TLC. After completion of the reaction, the mixture was cooled and the precipitate was filtered, dried and dissolved it in hot ethanol in order to separate the catalyst from product. Finally, pure product was obtained by recrystallization from hot ethanol.

2.5. Spectral data of representative compounds (4-b to 4-h)

2.5.1. 3-methyl-4-(4-nitrophenyl)-1-phenyl-6,8-dihydropyrazolo [4',3':5,6]pyrano[2,3-d]pyrimidine-5,7-(1H,4H)-dione(4-b)

M.P: 230–232 °C; IR (KBr, in cm⁻¹): 3284, 3116, 1666, 1597, 1566, 1460 and 1274; ¹H NMR (DMSO, in δ ppm): 10.16 (s,1H), 9.16 (s,1H), 8.07–8.12 (d,2H), 7.61–7.65(d,2H), 7.12–7.37(m, 5H), 4.85 (s,1H), 2.20 (s,3H); ¹³C NMR (DMSO, in δ ppm): 162.00, 153.90, 150.70, 147.70, 142.90, 140.70, 137.16, 133.89, 131.40, 129.20, 128.82, 126.20, 120. 53, 118.21, 104.89, 81.10, 40.31, 30.28, 11.77; MS (*m/z*): 417 (M⁺, 100 %),

2.5.2. 4-(4-Hydroxyphenyl)-3-methyl-1-phenyl-6,8-dihydropyrazolo [4',3':5,6]pyrano[2,3-d] pyrimidine-5,7-(1H,4H)-dione(4-c)

M.P: 254–256 °C; IR (KBr, in cm⁻¹): 3278, 3120, 2989, 1693, 1589, 1249; ¹H NMR (DMSO, in δ ppm): 11.21 (s, 1H), 9.13 (s, 1H), 7.65–7.75 (d, 2H), 7.50 (d, 2H), 7.35–7.45(t, 1H), 6.90 (d, 2H), 6.62–6.65 (d, 2H), 5.30 (s,1H), 4.75 (s,1H), 1.95 (s,3H), ¹³C NMR (DMSO, in δ ppm): 163.02, 154.00, 151.71, 148.40, 137.41, 135.30, 130.40, 128.70, 122.36, 118.22, 112.18, 81.20, 32.20, 13.06, MS (*m/z*): 388 (M⁺,100 %).

2.5.3. 4-(3,4-Dimethoxyphenyl)-3-methyl-1-phenyl-6,8-dihydropyrazolo[4',3':5,6] pyrano- [2,3-d] pyrimidine-5,7-(1H,4H)-dione(4-e)

M.P: 270–272 °C; IR (KBr, in cm⁻¹): 3213, 3080, 1678, 1595, 1274; ¹H NMR (DMSO, in δ ppm): 10.37 (s,1H), 8.85 (s,1H), 7.80 (d,2H), 7.64 (d,2H), 7.45 (t,1H), 6.95–7.02 (s,1H), 6.78 (d,1H), 6.63 (d,1H), 4.85 (s,1H), 3.89 (s,3H), 3.86 (s,3H), 2.32 (s,3H); ¹³C NMR (DMSO, in δ ppm): 164.52, 162.80, 161.22, 155.90, 154.15, 150.72, 148.7, 148.32, 132.20, 125.84, 117.30, 115.70, 111.62, 56.30, 56.00, 55.92, 10.53; MS (*m/z*): 432 (M⁺,100 %).

2.5.4. 4-(2,4-Dichlorophenyl)-3-methyl-1-phenyl-6,8-dihydropyrazolo[4',3':5,6]pyrano[2,3-d] pyrimidine-5,7-(1H,4H)-dione(4-g)

M.P: 234–235 °C; IR (KBr, in cm⁻¹): 3223, 3143, 3076,1739, 1695, 1541, 1390, 804; ¹H NMR (DMSO, in δ ppm): 9.76–10.0 (s,1H), 8.91 (s,1H), 7.89–7.92 (d,2H), 7.67–7.70 (d,2H), 7.55 (t,1H), 7.12–7.29 (m,3H), 5.03(s,1H), 2.16 (s,3H); ¹³C NMR (DMSO, in δ ppm): 162.10, 155.92, 150.23, 147.72, 142.90, 139.10, 137.16, 135.32, 132.80, 130.89, 129.60, 127.82, 126.20, 122.53, 118.21, 82.04, 32.15, 12.22; MS (*m/z*): 440 (M⁺,100 %).

2.5.5. 4-(4-Chlorophenyl)-3-methyl-1-phenyl-6,8-dihydropyrazolo [4',3':5,6]pyrano[2,3-d]pyrimidine-5,7-(1H,4H)-dione(4-h)

M.P: 225 °C; IR (KBr, in cm^{-1}): 3215, 3054, 1686, 1623, 1588, 1488, 1369, 836, 870; ^1H NMR (DMSO, in δ ppm): 10.19 (s, 2H), 7.27 (d, 2H), 7.06 (d, 2H), 7.35–7.45(t,1H), 7.50 (d,2H), 7.65–7.75 (d,2H), 5.41(s, 1H), 2.23 (s, 3H); ^{13}C NMR (DMSO, in δ ppm):160.35, 150.57, 141.58, 134.64, 129.92, 128.59, 128.06, 127.71, 127.27,89.45, 30.16, 9.96; MS (m/z):406 (M^+ , 100 %),

3. Results and discussion

3.1. Catalyst characterization

3.1.1. FT-IR analysis of prepared materials

The characteristic bands for keggin structure of HPW (phosphotungstic acid) are exhibited at 1080, 985, 890 and 839 cm^{-1} . All the characteristic bands of keggin structure are observed at the same wave number in prepared catalyst which indicates the preservation of the basic keggin structure in the silica-supported phosphotungstic acid catalyst. Fig. 1, shows the band at 1080 and 890 cm^{-1} are more intense in Si-PTA compared to pure silica; it confirms the presence of the undegraded anion of the catalyst. A strong peak at close to 3400 indicates the presence of silica impregnated with phosphotungstic acid (see).

3.2. XRD analysis of catalysts

The XRD pattern of pure silica and silica-supported phosphotungstic acid is shown in Fig. 2. Silica displays a broad band centered at $2\theta = \sim 25^\circ$. When phosphotungstic acid was impregnated with silica, the characteristic peaks assigned to PTA are comparable to those for the Si-PTA, which implies retention of their crystalline character. As seen in Fig. 2, reduction in the peak of Si-PTA was exhibited at 25° compared to silica which indicates the surface of silica was accumulated by particles of phosphotungstic acid in the impregnation method. Obtained intense peaks indicate that there is no significant change in the structure of phosphotungstic acid and silica structures during preparation of catalyst, confirmed by XRD.

3.3. FE-SEM and Elemental analysis (EDX) of Si-PTA

The surface structures of Si-PTA catalyst were studied using SEM analysis. In the morphology study of pure Si, no agglomeration of particles occurred, while Si-PTA showed the agglomeration

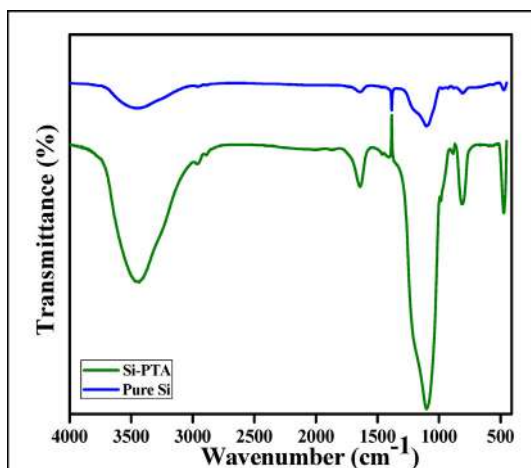


Fig. 1. FT-IR analysis of pure Si and prepared Si-PTA catalyst.

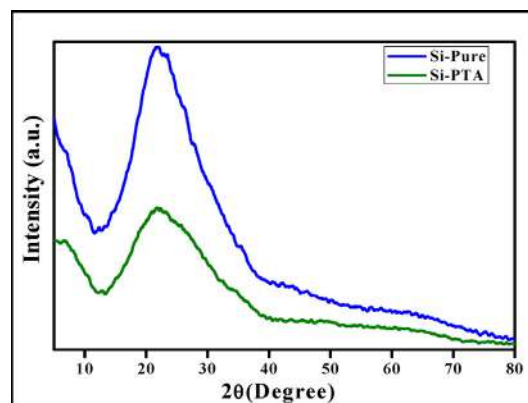


Fig. 2. XRD analysis of pure Si and prepared Si-PTA catalyst.

of particles, it reveals that uniform distribution of phosphotungstic acid on silica in prepared material and slight agglomeration occurred. Moreover, the Elemental analysis was studied by energy dispersive X-ray spectroscopy. EDS mapping of pure silica showed the presence and uniform distribution of silicon and oxygen throughout the structure. Further, the presence of Si, W, P and O elements in the catalyst was observed by EDX mapping and a uniform distribution was also observed (the second image of Fig. 3).

3.4. Catalyst activity

To find out suitable reaction conditions for the synthesis of the Pyrazolopyranopyrimidines, several experiments were conducted and develop multicomponent condensation reaction of Barbituric acid, 3-methyl-5-pyrazolone and Benzaldehyde in presence of Si-PTA. In order to find the optimum conditions for this reaction, initially, the effect of solvent, temperature, amount of catalyst, and reaction time was tested. As per the results summarized in Table 1, the catalyst effect on reaction rate and yield was investigated, and find out the reaction cannot proceed without a catalyst in presence of different solvents at room temperature for up to several hours (Table 1, entries from 1 to 6). As shown in Table 1, good to efficient yield was obtained when the reaction was conducted at reflux temperature in ethanol: water (1:1) solvent system (Table 1, entry 7) in a short reaction time. However, the same reaction continues for a longer time in ethanol: water (1:1) under reflux temperature obtains a low yield (Table 1, entries 8–10). One more experiment was carried out in presence of the catalyst under solvent-free conditions the reaction proceeded with a lower yield of product (Table 1, entry 13). Obtained results in Table 1 shows that the reaction proceeded highly efficiently with a high yield in a polar solvent and become sluggish and low yield in nonpolar solvent. In the final, we conclude that reflux temperature in ethanol: water (1:1) solvent system with 10 wt% of catalyst is highly effective for this reaction and same has been considered for further study.

Si-PTA is a selective heterogeneous catalyst in the synthesis of Pyrazolopyranopyrimidines in ethanol: water under reflux conditions. The next examination was a screening of the effect of catalytic amount on the conversion of reactants. The results of catalytic screening as shown in Table 1 (Entry 7–9), it was showed 10 wt% of catalyst is sufficient for complete conversion with maximum yield (Entry 7). With the decrease in the amount of catalyst up to 5 wt%, the yield was also decreased and more time was required for the completion of the reaction (Entry 9). However, an increase in the amount of catalyst up to 20 wt% does not affect the yield as well rate of reaction (Table 1, Entry 8) and hence 10 wt % of Si-PTA was selected for further investigation to compare the

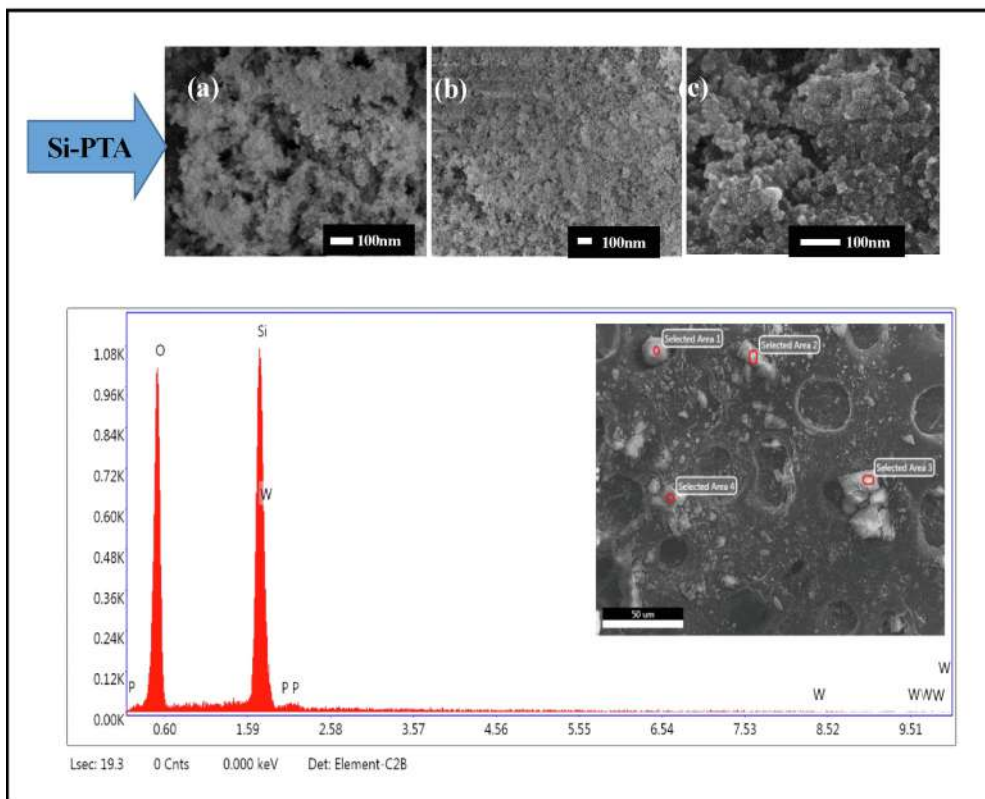
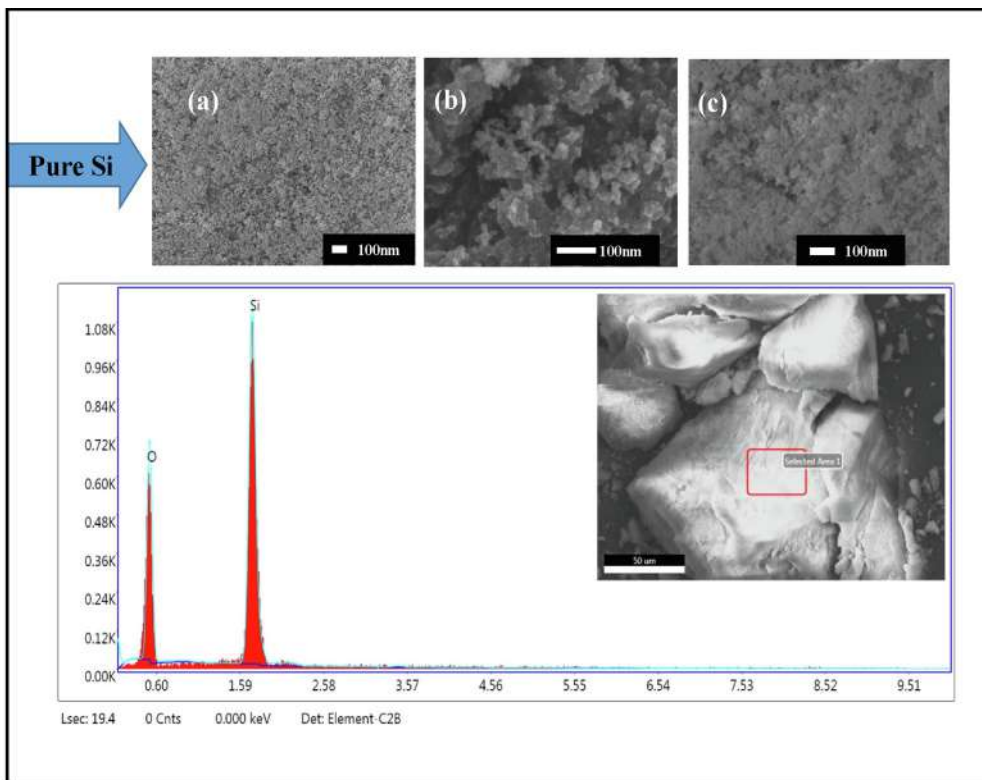
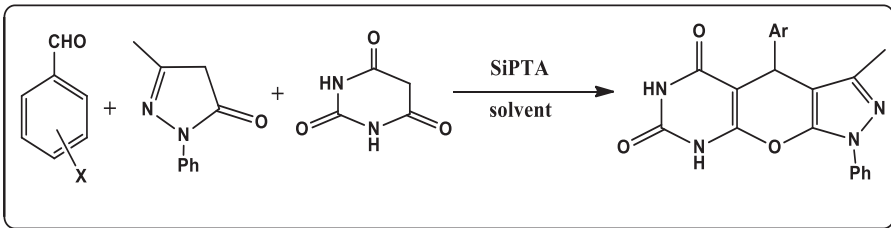


Fig. 3. FE-SEM and Elemental analysis (EDX) of pure Si and Si-PTA.

Table 1
Optimization of reaction conditions for the synthesis of Pyrazolopyranopyrimidines^a.



Entry	Solvent	Cat.(wt%)	Temp.(°C)	Time(hr)	Yield (%) ^b
1	Toulene	10	Reflux	04	50
2	DCM	10	Reflux	04	58
3	CH ₃ CN	10	Reflux	04	65
4	MeOH	10	Reflux	01	75
5	EtOH	10	Reflux	01	80
6	H ₂ O	10	Reflux	01	78
7	EtOH: H ₂ O	10	Reflux	01	96
8	EtOH: H ₂ O	20	Reflux	01	96
9	EtOH: H ₂ O	05	Reflux	02	80
10	EtOH: H ₂ O	–	Reflux	04	50
11	EtOH: H ₂ O	10	RT	04	60
12	EtOH: H ₂ O	10	60 °C	24	82
13	–	10	RT	24	45

Reaction conditions:(a) Barbituric acid (1 mmol), aryl aldehyde (1 mmol), 3-methyl-1-phenyl-5-pyrazolone (1 mmol); In presence of Catalyst; Reaction completion was monitored by TLC.(b) Isolated yield.

effectiveness of various catalysts in the synthesis of pyrazolopyranopyrimidines.

As evidently shown in Table 2, the yield obtained using different reported catalyst were found comparatively low. The comparison of the catalytic activity of Si-PTA and oleic acid clearly shows, SI-PTA can catalyze the reaction with a higher yield of desired product within a short reaction time. OMWCNTs, DABCO, & [BNPs-Caff] HSO₄ catalysts exhibit high and comparable catalytic activities but slightly lower than that of Si-PTA (Table 2, entry 1, 2, 3, 5 respectively) with lots of weaknesses in the reaction.

With results in hand, we were encouraged to examine the scope and generality of this method using a variety of substituted aryl aldehydes. Thus various aromatic and heteroaromatic aldehydes were reacted with 3-methyl-5-pyrazolone and barbituric acid; the obtained experimental results are tabulated in Table 3 (entries 1–10). As seen in Table 3, it is evident that, most of the reactions were performed with a good to high yield of pyrazolopyranopyrimidines. Aromatic aldehydes bearing electron withdrawing and electron donating group reacts under optimized conditions, and the

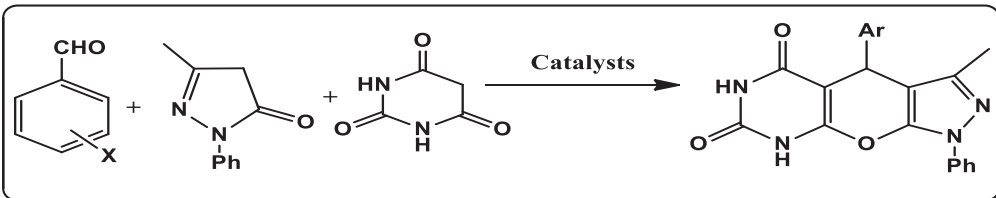
corresponding products are obtained in good to high yield. In general comparison, aromatic aldehyde containing electron withdrawing group as well as heteroaromatic aldehydes reacts to produce a high yield (Table 3, entry 2, 10, 11), while aromatic aldehydes containing electron donating group react to provide a comparatively low yield (Table 3, entry 3, 6).

3.5. Proposed reaction mechanism

3.5.1. Plausible SiPTA catalyzed reaction mechanism for synthesis of pyrazolopyranopyrimidines

We believe that, at first, the catalyst interacts with the oxygen atom of the carbonyl group of Barbituric acid and forced it to convert into enol form. In the next step, the catalyst protonates oxygen of the carbonyl group of aromatic aldehyde and makes carbon electrophilic which fascinates nucleophilic attack results in C–C bond formation followed by dehydration. Further, 3-methyl-5-pyrazolone (IV-f) undergoes tautomerization to form compound (IV-e), it is the most prominent candidate for cyclization. Finally

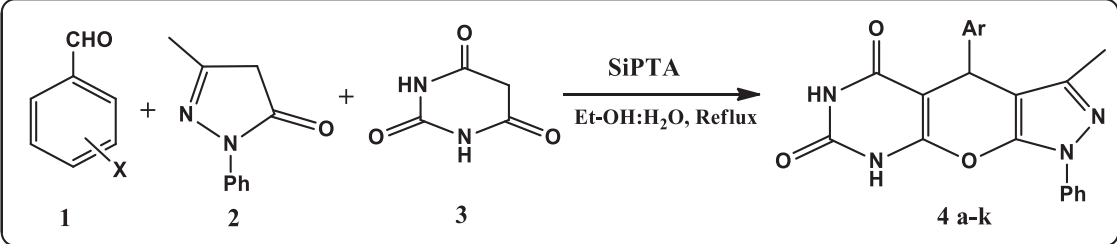
Table 2
Comparisons of various catalysts with Si-PTA in the synthesis of Pyrazolopyranopyrimidines^a.



Entry	Catalyst	Time(min) ^e	Yield (%) ^f
1	OMWCNT's	70	94
2	DABCO	45	84
3	[BNPsCaff]HSO ₄	50	85
4	Oleic acid	120	78
5	Si-PTA	60	96 [present work]

Reaction conditions: (a) Synthesis of pyrazolopyranopyrimidine from Barbituric acid, 3-methyl-5-pyrazolone and aryl aldehydes under optimized reaction condition, (b) catalyst amount 10 wt%. (c) Solvent: EtOH:H₂O (1:1). (d) Reflux temperature, (e) reaction time is monitored by TLC.(f) Isolated yield.

Table 3
Synthesis substituted Pyrazolopyranopyrimidines derivatives using Si-PTA under optimized reaction conditions.



Entry	Aldehyde	Product code	Time (hr)	Yield (%) ^b
1.	Benzaldehyde	4-a	01	96
2.	p-nitrobenzaldehyde	4-b	01	96
3.	4-hydroxybenzaldehyde	4-c	01	90
4.	4-hydroxy-3-methoxy benzaldehyde	4-d	01	92
5.	3,4-Dimethoxy benzaldehyde	4-e	01	94
6.	4-Methyl benzaldehyde	4-f	01	88
7.	2,4-Dichlorobenzaldehyde	4-g	01	91
8.	4-Chlorobenzaldehyde	4-h	01	89
9.	2-Hydroxybenzaldehyde	4-i	01	90
10.	3-Bromobenzaldehyde	4-j	01	94
11.	4-Fluorobenzaldehyde	4-k	01	92

(a) All reactions were conducted using 1 mmol reactant (1,2&3) and 10 wt% catalyst in EtOH:H₂O(1:1) at reflux temperature. (b) Isolated yield.

nucleophilic addition of compound (IV-e) on compound (IV-d) followed by cyclization and then dehydration to gave 3-methyl-4-(p henyl)-1-phenyl-6,8-dihydropyrazolo [3-6]pyrano[2,3-d] pyrimidine-5,7(1*H*,4*H*)-dione. In this reaction, Si-PTA plays an important role in cyclization as well as dehydration due to which we achieved our target with efficiency, after completion of the reaction catalyst can be removed easily and utilized in many more reactions. However, further catalyst characterization and in-depth correlation for the catalyzed mechanism are under study.

3.6. Recyclability test of Si-PTA

The advanced, highly efficient, and recyclable heterogeneous catalyst for the synthesis of pyrazolopyranopyrimidines derivatives is the ultimate objective of our research. It is essential to know the stability of heterogeneous catalysts at given reaction conditions. In order to know the reusability of the catalyst, we separated the Si-PTA catalyst from reaction mixture by simple filtration and washed it two to three times using water and ethanol to remove all types of impurities and reused it for further successive five cycles. Recyclability test reveals that, no significant loss in the yield of pyrazolopyranopyrimidines. Moreover, complete conversion of the reactant with a comparable yield of product was maintained during the recycling test of Si-PTA. Further study and comparison of fresh and recycled catalysts is going on and some other applications are in process.

4. Conclusions

We have prepared a heterogeneous Si-PTA catalyst and characterized it completely by different spectroscopic and analytical techniques. After the successful characterization of the catalyst, it was utilized in the synthesis of pyrazolopyranopyrimidines derivatives from barbituric acid, 3-methyl-5-pyrazolone and substituted aryl aldehydes under optimized reaction conditions. The catalyst showed 96–88 % isolated yield of product with maximum purity. Finally, the catalyst was recycled by simple filtration and reused up to five cycles without loss of catalytic efficiency during the experimental procedure. Silica-supported phosphotungstic acid

exhibits key advantages such as simplicity, recyclability, and efficiency.

Data availability

Data will be made available on request.

Declaration of Competing Interest

The authors declare that they have no known competing financial interests or personal relationships that could have appeared to influence the work reported in this paper.

Acknowledgement

The authors are grateful to the Principals of Mahatma Basweshwar College, Latur and Maharashtra Udaygiri College, Udgir. We are thankful to Vishnu chemicals limited, Hyderabad. The Director, CSIR-IICT, Hyderabad for providing spectra, and Director, Centre for Nano and Material Sciences, Jain University, Bangalore for their continuous support.

References

- [1] Y. Ogiwara, K. Takahashi, T. Kitazawa, N. Sakai, Indium (III)-catalyzed Knoevenagel condensation of aldehydes and activated methylenes using acetic anhydride as a promoter, *J. Org. Chem.* 80 (6) (2015) 3101–3110.
- [2] G. Jones, The Knoevenagel condensation, *Org. React.* 15 (1967) 204–599.
- [3] N. Mase, T. Horibe, Organocatalytic Knoevenagel condensation by means of carbamic acid ammonium salt, *Org. Lett.* 15 (2013) 1854–1857.
- [4] H. Shaterian, M. Arman, F. Rigi, Domino Knoevenagel condensation, Michael addition, and cyclization using ionic liquid, 2-hydroxyethyl ammonium formate as recoverable catalyst, *J. Mol. Liq.* 158 (2011) 145–150.
- [5] O.H. Qareaghaj, S. Mashkouri, M.R. Naimi-Jamal, G. Kaupp, Ball milling for quantitative and for specific Knoevenagel condensation+Michael addition cascade in the synthesis of various-2-amino-4-aryl-3-cyano-4*H*-chromenes without heating, *RSC Adv.* 4 (2014) 48191–48201.
- [6] J. Quiroga, C. Cisneros, B. Insuasty, R. Abonia, M. Noguera, A. Sánchez, A regioselective three-component one-step cyclocondensation to 6-cyano-5,8-dihydropyrido[2,3-*d*]pyrimidin-4(3*H*)-ones using microwaves under solvent-free conditions, *Tetrahedron Lett.* 42 (33) (2001) 5625–5627.
- [7] P.J. Chen, A. Yang, Y.F. Gu, X.S. Zhang, K.P. Shao, D.Q. Xue, P. He, T.F. Jiang, Q.R. Zhang, H.M. Liu, Synthesis of in vitro antimicrobial and cytotoxic activities of novel pyrimidine benzimidazole combination, *Bioorg. Med. Chem. Lett.* 24 (2014) 2741–2743.

- [8] A.M. El-Agrody Fouda, A.A. Al-Dies, Studies on synthesis, in vitro antitumor activity of 4-H-benzochromenes, 7H-benzochromene [2,3-d] pyrimidines derivative and structure activity relationship of 2,3-positions and fused rings at 2,3-positions, *Med. Chem. Res.* 23 (2014) 3187–3199.
- [9] S. Mert, R. Kasimogullari, T. Ica, F. Colak, A. Altun, S. Ok, Synthesis structure activity relationship, and in vitro antibacterial and antifungal activity evaluation of pyrazole carboxylic acid and dicarboxylic acid derivatives, *Eur. J. Med. Chem.* 78 (2014) 86–96.
- [10] J.V. Faria, P.F. Vegi, A.G.C. Miguita, M.S. dos Santos, N. Boechat, A.M.R. Bernardino, Recently reported biological activities of pyrazole compounds, *Bioorg. Med. Chem.* 25 (21) (2017) 5891–5903.
- [11] H.S. Chung, Y. Kim, S.J. Oh, H. Kim, S.I. Choi, Y. Zhang, J.H. Jeong, H. Bae, A synthetic compound 4-acetyl-3-methyl-6-(3,4,5-trimethoxyphenyl) pyrano [3,4-c]pyran-1,8-dione, ameliorates ovalbumin-induced asthma, *Bioorg. Med. Chem.* 21 (2013) 6359–6365.
- [12] S. Karpov, Y. Kayukov, A. Grigorev, V. Tafeenko, et al., Synthesis and solid state luminescence of highly substituted 6-amino-2-H pyran-2-one derivative, *Tetrahedron. Lett.* 61 (2020).
- [13] Y.R. Prasad, A.L. Rao, L. Prasoona, K. Murali, P.R. Kumar, Synthesis and antidepressant activity of some 1,2,3-triphenyl -2-pyrazoline and 3-(2'-hydroxynaphthalene-1"-yl)-1,5-diphenyl-2-pyrazoline, *Bioorg. Med. Chem. Lett.* 15 (2005) 5030–5034.
- [14] Z.H. Ismail, G.M. Aly, M.S. El-Degwi, H.I. Herba, M.M. Ghorab, Synthesis and insecticidal activity of some pyranopyrazole, pyrazolopyranopyrimidines and pyrazolopyranopyridines, *J. Egypt Bio.* 13 (2003) 73–82.
- [15] V.K. Ahluwalia, A. Dahiya, V. Garg, Reaction of 5-amino-4-formyl-3-methyl (or phenyl)-1-phenyl-1H-pyrazoles with active methylene compounds: Synthesis of fused heterocyclic rings, *Indian J. Chem.* 36B (1997) 88–90.
- [16] J.L. Wang, D. Liu, Z.J. Zheng, S. Shan, X. Han, S.M. Srinivasula, C.M. Croce, E.S. Alnemri, Z. Huang, Structure based discovery of an organic compound that bind Bc 1–2 protein and induces apoptosis of tumor cells, *Proc. Natl. Acad. Sci. U.S.A.* 97 (2009) 7124–7129.
- [17] E.M. Grivsky, S. Lee, C.W. Sigel, D.S. Duch, C.A. Nicol, Synthesis and antitumor activity of 2,4-diamino-6-(25-dimethoxybenzyl)-5-methylpyrido[2,3-d] pyridine, *J. Med. Chem.* 23 (1980) 327–329.
- [18] N.R. Kamdar, D.D. Haweliwala, P.T. Mistry, S.K. Patel, Design synthesis and invitro evulsion of antitubercular and antimicrobial activity of some novel pyranopyrimidines, *Eur. J. Med. Chem.* 45 (2010) 5056–5063.
- [19] H.M. Aly, M.M. Kamal, Efficient one pot preparation of novel fused chromeno [2,3-d] pyrimidine and pyrano [2,3-d] pyrimidine derivatives, *Eur. J. Med. Chem.* 47 (2012) 18–23.
- [20] Y. Ren, B. Liu, Z. Zhang, J. Lin, Silver exchanged heteropolyacid catalyst: An efficient heterogeneous catalyst for synthesis of 5-ethoxymethylfurfural from 5-hydroxymethylfurfural and fructose, *J. Ind. Eng. Chem.* 21 (2015) 1127–1131.
- [21] B. Yang, J.J. Pignatello, D. Qu, B. Xing, Reoxidation of photoreduced polyoxotungstate by different oxidant in presence of a model pollutant. Kinetic and reaction mechanism, *J. Phys. Chem. A* 119 (2015) 1055–1065.
- [22] S. Sadjadi, M.M. Heravi, Recent advances in applications POMs and their hybrid in catalysis, *Curr. Org. Chem.* 20 (2016) 1404–1444.
- [23] S.H. Teo, M. Goto, Y.H. Taufiq-Yap, Biodiesel production from *Jatropha curcas* L. oil with Ca and La mixed oxide catalyst in near supercritical methanol conditions, *J. Supercrit. Fluids* 104 (2015) 243–250.
- [24] A. Escobar, A. Sathicq, L. Pizzio, M. Blanco, G. Romanelli, Biomass valorization derivatives: Clean esterification of 2-furoic acid using tungstophosphoric acid/zirconia composite as recyclable catalyst, *Process Saf. Environ. Prot.* 98 (2015) 176–186.
- [25] H. Eshghi, A. Javid, A. Khojastehnezhad, F. Moeinpour, F.F. Bamoharram, M. Bakavoli, M. Mirzaei, Preyssler heteropolyacid supported on silica coated NiFe₂O₄ nanoparticle for the catalytic synthesis of bis (dihydropyrimidinones) benzene and 3,4-dihydropyrimidine-2-1H-ones, *Chin. J. Catal.* 36 (2015) 299–307.
- [26] M.S. Tiwari, G.D. Yadav, Kinetics of Friedel craft benzoylation of veratrole benzoic anhydride using Cs_{2.5}H_{0.5}PW₁₂O₄₀/K-10 solid acid catalyst, *Chem. Eng. J.* 266 (2015) 64–73.
- [27] L. Hong, Y. Gui, J. Lu, J. Hu, J. Yuan, L. Niu, High performance of polyoxometalate/ Pt, Pd nanoparticle/carbon nanotube electrocatalyst for methanol electrooxidation, *Int. J. Hydrogen Energy* 38 (2013) 11074–11079.
- [28] Y. Zhu, M. Zhu, L. Kang, F. Yu, B. Dai, Phosphotungstic acid supported on mesoporous graphitic carbon nitride as catalyst for oxidative desulfurization of fuel, *Ind. Eng. Chem. Res.* 54 (2015) 2040–2047.
- [29] V. Kozhevnikov, Friedel craft acylation and related reaction catalyzed by heteropolyacid, *Appl. Catal. A: General.* 256 (2003) 3–18.
- [30] S. Cao, W. Zeng, S. Wang, T. Zhang, Z. Liu, X. Xie, Silica supported phosphotungstic acid as green heterogeneous catalyst for α -pinene polymerization, *Adv. Res. Materials* 781–784 (2013) 448–451.
- [31] Z. Liu, S. Cao, S. Wang, W. Zeng, T. Zhang, Silica supported phosphotungstic acid as novel heterogeneous catalyst for β -pinene polymerization, *Reac. Kinet. Mech. Cat.* 111 (2014) 577–590.
- [32] X.-T. Li, A.-D. Zhao, L.-P. Mo, Z.-H. Zhang, Z.-H. Zhang, Meglumine catalyzed expeditious four component domino protocol for synthesis of pyrazolopyranopyrimidines in aqueous medium, *RSC Adv.* 4 (93) (2014) 51580–51588.
- [33] G.M. Ziarani, F. Aleali, N. Lashgiri, A. Badiei, A. Abolhasani, Efficient synthesis and antimicrobial evaluation of pyrazolopyranopyrimidines in the presence of SBA-Pr-SO₃H as a nanoporous acid catalyst, *Iran. J. Pharm. Res.* 17 (2018) 525–534.
- [34] M. Pirhayati, A. Kakanejadifard, H. Veisi, A new nano Fe₃O₄-supported organocatalyst based on 3, 4-dihydropyridine: an efficient heterogeneous nanocatalyst for one pot synthesis of pyrazolopyridines and pyranopyrimidines, *Appl. Organometal. Chem.* 30 (2016) 1004–1008.



Formulation of healthy cookies incorporated with orange peel powder and *Moringa oleifera* leaf powder

Nikita Vilas Teke, Karuna Wasudeo Patil, Hemangi Jayram Gavit *

Rayat Shikshan Sanstha's Annasaheb Awate College, Manchar, Pune 410503, India

ARTICLE INFO

Article history:

Available online 9 December 2022

Keywords:

Moringa leaf powder
Orange peel powder
Wheat flour
Cookies
Waste utilization
Phytochemicals

ABSTRACT

Studies were conducted for the incorporation of OPP (Orange peel powder) and MLP (Moringa leaves powder) in cookies. The OPP and MLP were analyzed and used in whole WF 100gm (0.5 gm, 1 gm, 1.5 gm, 2 gm, 2.5 gm, 3 gm, 3.5 gm, 4 gm) and MLP (0.5 gm, 1 gm, 1.5 gm 2 gm, 2.5 gm, 3 gm, 3.5 gm, 4 gm) proportion respectively. Based on sensory evaluation, 3% of OPP and 1% of MLP were selected for the preparation of healthy cookies. In the present work, OPP and MLP were prepared by using the tray dryer method. Jaggery and whole wheat flour were used instead of sugar and maida. The final formulation of the cookie mixture containing wheat flour (WF), OPP, and MLP was in the 96:3:1 ratio and resulted in the highest sensory score. The cookies were analyzed for various nutrients and phytochemical compounds. The utilization of waste orange peel and Moringa leaves was the most significant aspect of this study.

Copyright © 2022. Elsevier Ltd. All rights reserved.

Selection and peer-review under responsibility of the scientific committee of the Integrative Nanotechnology Perspective for Multidisciplinary Applications - 2022.

1. Introduction

Health-promoting foods including cookies have recently been in focus and of great interest to consumers, dieticians, experts, and producers. Cookies were classified as one of the most highly distributed bakery products in the market worldwide, because it is ready to eat, cheap, nutritionally rich, available in different tastes and have a longer shelf life [1].

The nutritional composition of Moringa of the South African ecotype has also been reported that including the profiling of chemical composition, fatty acids, amino acids, and vitamins. Amino acids, fatty acids, minerals, and vitamins are essential in animal feed. These nutrients are used for osmotic adjustment; activate enzymes, hormones, and other organic molecules that enhance growth, function and maintenance of life process [2].

Studies have also revealed that the leaves have immense nutritional value to combat malnutrition, especially among infants and nursing mothers. In addition, nutrition plays a crucial role in both humans and livestock as short-term alternative to chemoprophylaxis. In animals, nutrition plays a major role in animal's ability to overcome the detrimental effects of parasitism and diseases [3].

It is important to emphasize that orange peel, a byproduct of citrus manufacturing that is typically discarded, is actually valued as a functional food. Citrus peels may therefore boost health in addition to the usual nutrients they contain and help ward off disorders linked to food, such as osteoporosis, metabolic syndrome, type II diabetes, coronary heart disease, obesity, and hypertension [4].

The nutritional benefits of Moringa vary widely and are influenced by things like genetic makeup, environmental conditions, and production practices [5]. As a potential inhibitor of some microorganisms, such as bacteria (*Escherichia coli*, *Staphylococcus aureus*, *Vibrio parahaemolyticus*, *Enterococcus faecalis*, *Pseudomonas aeruginosa*, *Salmonella enteritidis*, and *Aeromonas caviae*) and fungi (*Trichophyton rubrum*, *Trichophyton mentagrophytes*, *Epidermophyton floccosum* and *Microsporium canis*), moringa leaf extracts were also able to act as a biocidal agent [6].

In addition to energy, proteins, minerals (zinc, copper, and iron), and vitamins (A and E) are all necessary for an animal to develop immunity (for the production of antibodies and cells) [7]. These nutrients also help organs and tissues communicate with one another to fight infections. Due to its several uses, moringa oleifera is regarded as a plant of versatility. Its leaves are an excellent source of calcium, iron, and vitamins A, B, and C [8].

* Corresponding author.

E-mail address: nikitateke03@gmail.com (N.V. Teke).

The majority of the world's population enjoys eating baked items made only with wheat flour. In nations like Nigeria, these goods have continually been consumed [9]. A well-fed animal is more resistant to disease than one that is already weak from starvation, even when exposed to infection. An animal's immune system responds to pathogen exposure by mounting an attack to ward off infection. This includes raising antibodies to fight the infection, as well as using white blood cells to attack pathogens [10]. In Africa, nursing mothers have been shown to produce much more milk when they add Moringa leaves to their diet. Severely malnourished children were reported to have made significant weight gains when caregivers add the leaves to their diet to increase their nutritional content [11].

Citrus by-products, if utilized fully, could be major sources of phenolic compounds. The peels, in particular, are an abundant source of natural flavonoids and contain a higher amount of phenolics compared to the edible portions [12].

The healing of abdominal tumors, hysteria, scurvy, paralytic attacks, helminthic bladder, prostate issues, ulcers, skin infections, inflammation, cardiovascular, and liver illnesses are just a few of the health issues and diseases that moringa is helpful for. Moringa, also protects body from arsenic-induced oxidative stress and in the depletion of arsenic concentration. Moringa is considered as a hypocholesterolemic agent, regulation of thyroid hormone status, anti-diabetic agent, antipyretic, antiepileptic gastric ulcers, antitumor agent, and hypotensive agent [13–15]. It is considered as one of the World's most useful trees, as almost every part of the Moringa tree can be used for food, medication and industrial purposes [16].

The wastes of fruits and vegetables are inexpensive, abundantly available, and are a good source of dietary fiber [17]. The orange peel is thought to contain some essential nutrients and has certain qualities that help the gastrointestinal tract operate properly. It is also great for diabetics and heart patients. Besides the nutritional aspect, it is having an affordable aspect as well. A segment membrane of citrus fruits appears to be able to prevent prostate and other cancers by acting as a mediator in cell communication, a factor known to reduce the likelihood of abnormal cell growth. Sour fruits such as lemon appear to have the greatest effect [18]. Moringa leaves are more potent in nutritional value. Its vitamin C content is seven times more than that of oranges, it has thirteen times more vitamin than spinach, and is on a lead on its own when it comes to the amino acid, 2,000 times more than green tea and 242 times more than apples. The leaves are sources of sulfur-containing amino acid such as methionine and cystine which are often in short supply in most legumes [19].

Bakery products have become more popular in India since earlier times. Among the different bakery products cookies constitutes the most popular group. Cookies were created fairly early. Because of their extremely low moisture content, they can be preserved for a long period. Cookies are chemically leavened bakery items with a high fat and sugar content [20].

Wheat as a major source of raw material for the production of these baked products such as cookies also lacks some nutrients. *Moringa oleifera* is an important food commodity that has had enormous attention as the 'natural nutrition of the tropics. The leaves, seeds, and flowers of *Moringa oleifera* all have great nutritional and therapeutic value [21].

The seeds are eaten like peas or roasted like nuts when still green; the dry seeds are apparently not used for human consumption, perhaps because the bitter coating becomes hardened while the flowers are eaten when cooked and taste like mushrooms [22]. The leaves are outstanding as a source of vitamins A, B group and (C when raw) and are among the best sources of minerals. They are also excellent sources of protein, but poor sources of car-

bohydrate and fat. Moringa leaves are one of the best plant foods available in nature.

The leaves of Moringa was considered as a very nutritional material as it contains vitamin A, vitamin C, iron, calcium and potassium in concentrations as much as in carrot, orange, spinach and banana. It is also a good protein source based on a comparison between its amino acid profiles and FAO/WHO/UNO reference protein for children. Its content of protein are more than that found in egg and soybean and contains a wide range of amino acids including zeatin, glutamic, arginine, and aspartic acid. Also, it contains carotenoid pigments, flavonoids, minerals, sterols and some phenolic compounds. Moringa leaves was proved to possess a high antioxidant activity values which played a potential rule in cancer chemoprevention, protein oxidation reduction and lipid peroxidation inhibition [23].

Since ancient times, 70 percent of the total production of oranges is used for the manufacture of derivative products, but 30 percent of processed fruits are converted into citrus peels waste, so these wastes contain many nutrients. Fruit peels serve as a barrier, shielding the edible components of the fruit from external elements as well as microorganisms and enzymes. They may or may not be considered fruits depending on their thickness and flavor. People frequently discard the peels of fruits after eating them, although the peels contain many of the fruit's nutritional benefits. They help protect our bodies from many diseases and increase disease resistance. Apart from this, various types of dishes, cosmetics, and medicines are also prepared by using these nutritious peels properly [24].

According to the World Health Organization (2003) report, "Dietary nutrition and prevention of chronic disease", it prevents heart disease due to folate present in citrus fruits, which is essential to lower levels of the heart. Potassium helps lower blood pressure, prevents stroke and kidney disease, and vitamins, carotenoids, and flavonoids are found in citrus fruits, all of them as protective cardiovascular effects.

2. Methodology

Refined wheat flour, jaggery, hydrogenated vegetable oil, baking powder, baking soda, salt, and milk were obtained from the local market of Manchar. Essence was obtained from the natural orange peel powder, moringa leaves powder to prepare at a college level by using the tray dryer method. All chemicals and reagents used were of analytical grade.

2.1. Preparation of orange peel powder

First, The orange fruits were washed under running water, disinfected and rinsed. The orange peels were manually removed using stainless steel knives and weighed to determine the yield. Material preparation and physicochemical analyses were performed at the laboratory. After the peels were weighed, they were cut into small pieces then dried in a tray dryer at 40 °C for 24 h and ground, then sieved through a 50 mesh sieve to obtain a powder. The peel powder was again weighed to calculate the yield, then orange peel powder was vacuum packed and stored at room temp for future analysis.

2.2. Preparation of Moringa leaves powder

First, the fresh moringa leaves were separated from the stalks of the ties, it was then removed from the leaf petal by hand. The leaves were placed on a tray dryer 45 °C for 24 h. After drying, dried moringa leaves were ground in the grinder to reduce the particle size. The ground material is then allowed to pass through a sieve

size 50 mesh, the larger particle on the sieve was again taken for grinding and passed through the sieve to obtain a fine powder. The moringa leaves powder was vacuum-packed and stored at room temperature for future analysis.

2.3. Preparation of cookies

Cookies were prepared by using the standardized recipe and method given by (Table 1):

According to the recipe, blends were made by combining milk, wheat flour, moringa leaf powder, and orange peel powder in various dry-weight ratios. These mixtures were standardized to produce products with acceptable physical characteristics and greater nutritional value. The dry ingredients i.e. wheat flour, MLP(moringa leaves powder), OOP(orange peel powder), baking powder, baking soda, salt, and flavour (cardamom and nutmeg powder) were mixed. A homogenous paste of fat and jaggery was prepared by hand to obtain a uniformly mixed dough. The prepared dough was rolled in a uniform shape and cut into round shape cookies with the help of a cutter. These cookies were baked at 160 °C top and 150 °C bottom for 25 min. Preparation of cookies was carried out using wheat flour samples replaced separately with (0.5, 1, 1.5, 2, 2.5, 3, 3.5, 4) OOP and MLP (0.5, 1, 1.5, 2, 2.5, 3, 3.5, 4) The method of cookies is a flow sheet in Fig. 1.

2.3.1. Optimization of Moringa powder in final cookies

Moringa powder optimization in the final cookies is shown in Table 2. Wheat flour, fat, baking powder, baking soda, salt, milk, and jaggery were all used in constant amount as mentioned in the Table 2. While the amount of Moringa leaf powder was changed in respective sample, to achieve an acceptable level of quality for optimization. The range of the MLP was 0.5gm to 4.0gm. Further, the sensory assessment of the product was carried out using 9 point Hedonic scale depending on which the suitable sample was selected. Sample T2 was chosen based on the sensory assessment.

2.3.2. Optimization of orange peel powder in final cookies

Orange peel powder optimization in the finished cookies is shown in Table 3. Wheat flour, fat, baking powder, baking soda, salt, milk, jaggery, and moringa powder were all kept constant in the final cookies while orange peel powder was changed to achieve an acceptable level of quality. The range of the OPP was 0.5gm to 4.0gm. Further, the sensory assessment of the product was carried out using 9 point Hedonic scale depending on which the suitable sample was selected. Sample T6 was chosen based on the sensory assessment.

Table 1
Ingredients used for preparation of cookies.

Sr. no	Ingredient Quantity
1	Wheat flour
2	Jaggery
3	Fat
4	Salt
5	Baking powder
6	Baking soda
7	Milk

2.4. Analysis of orange peel powder and Moringa leaves powder cookies

2.4.1. Physical analysis

Orange peel powder and moringa leaves powder cookies were analyzed for weight, Diameter, thickness, spread ratio, by following the respective procedures (AACC, 2000) [25].

Diameter (D): Six cookies were placed horizontally (edge to edge) and rotated at 90°angle for reading. Measured by vernier caliper.

Thickness (T): biscuits thickness was measured with a vernier caliper in triplicate. Means were recorded. Six cookies were measured one-by-one.

Spread ratio (SF): It was calculated according to the following equation.

$$SF = D/T$$

2.4.2. Chemical analysis

Moisture: Estimation of moisture content by hot air oven method at 105 °C for 4 hrs (AOAC, 1995) [26].

Ash: By using muffle furnace method up to constant weigh. Ignite in a muffle furnace at 550+/- 250c for 4 hrs. [27].

Fat: Extracting the sample in a Soxhlet apparatus for 6-8h using petroleum ether. The solvent is evaporated and the residue is weighed [27].

2.4.3. Sensory analysis

Sensory evaluation: Evaluate the products for acceptability based on its flavour, texture, appearance, amount of bitterness and overall acceptability using nine-point hedonic scale.

(1 = dislike extremely to 9 = like extremely; Meilgaard et al., 1999).

Shelf life analysis: The Orange peel powder and moringa leaves powder cookies samples were packed in LDPE packaging material under ambient temperature for 45 days has evaluated.

3. Result and discussion

3.1. Optimization

The optimization of control cookies was carried out by varying proportion of different components such as flour, jaggery, salt, milk and fat. In the 1st trial Wheat flour content was varied to get an acceptable quality of cookies. The preparation of control cookies the amount of wheat flour was varied as 90 %, 95 % and 100 %. sample 100 % was finalized due to its good characteristics (Fig. 2).

In 2nd trial the control cookies were prepared by using wheat flour, jaggery, baking powder, baking soda milk. In this case of fat were optimized i.e. 50, 70, and 90 gm respectively. Depending upon sensory evaluation cookies having good taste, texture and overall acceptability 70 gm were finalized.

In 3rd trial the control cookies were prepared by using wheat flour, fat, baking powder, baking soda milk. In this case of jaggery were optimized i.e. 25, 50, 75 gm respectively. Depending upon sensory evaluation cookies having good taste, texture and overall acceptability 50 gm were finalized.

In 4th trial, the control cookies were prepared by using wheat flour, fat, baking powder, baking soda, and jaggery. In this case of milk was optimized. i.e. 30, 45, 60 ml respectively. Depending upon sensory evaluation cookies having good taste, texture, and overall acceptability 45 ml were finalized.

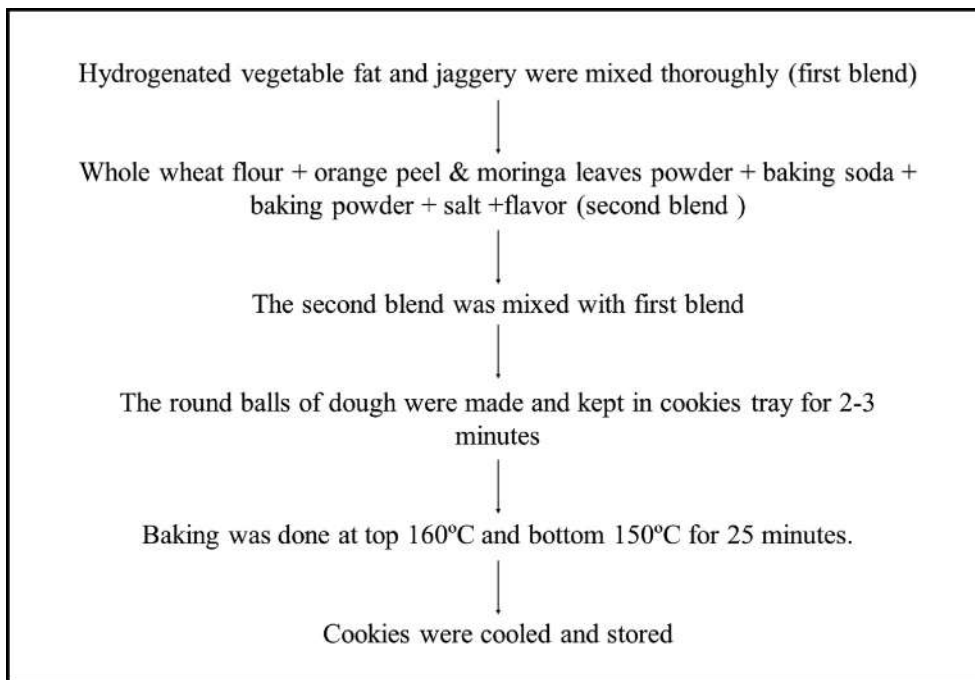


Fig. 1. Flow sheet for preparation of cookies.

Table 2
Optimization process of Moringa powder.

Sample code	Wheat flour (gm)	Fat (gm)	Baking powder (gm)	Baking soda (gm)	Salt (gm)	Milk (ml)	Jaggery (gm)	Moringa powder (gm)
T1	100	70	2	2	0.5	45	50	0.5
T2	100	70	2	2	0.5	45	50	1
T3	100	70	2	2	0.5	45	50	1.5
T4	100	70	2	2	0.5	45	50	2
T5	100	70	2	2	0.5	45	50	2.5
T6	100	70	2	2	0.5	45	50	3
T7	100	70	2	2	0.5	45	50	3.5
T8	100	70	2	2	0.5	45	50	4

Table 3
Optimization of orange peel powder.

Sample code	Wheat flour (gm)	Fat (gm)	Baking powder (gm)	Baking soda (gm)	Salt (gm)	Milk (ml)	Jaggery (gm)	Moringa powder (gm)	Orange peel powder (gm)
T1	100	70	2	2	0.5	45	50	1	0.5
T2	100	70	2	2	0.5	45	50	1	1
T3	100	70	2	2	0.5	45	50	1	1.5
T4	100	70	2	2	0.5	45	50	1	2
T5	100	70	2	2	0.5	45	50	1	2.5
T6	100	70	2	2	0.5	45	50	1	3
T7	100	70	2	2	0.5	45	50	1	3.5
T8	100	70	2	2	0.5	45	50	1	4

In 5th trial, all ingredients were kept constant only varied salt content based on taste parameters i.e. 0.3, 0.5, 0.7gm respectively. Depending upon sensory evaluation cookies having good taste, texture, and overall acceptability of 0.5 gm were finalized.

In the 6th trial, whole wheat flour 100gm with *Moringa oleifera* leaves powder 0.5gm, 1gm, 1.5gm, 2gm, 2.5gm, 3gm, 3.5 gm, 4gm based on taste parameters. Depending upon sensory evaluation cookies having good taste, texture, and overall acceptability of 1 gm were finalized.

In 7th trial whole wheat flour 100gm with orange peel powder 0.5gm, 1gm, 1.5gm, 2gm, 2.5gm, 3gm, 3.5 gm, 4gm based on taste

parameter. Depending upon sensory evaluation cookies having good taste, texture, and overall acceptability 3 gm were finalized.

In 8th trial, all ingredients were kept constant only varied time and temperature. i.e. top and bottom temp (180–160 for 15 min, 160–160 for 18 min, 160–150 °C for 25 min).

After the trails, the final cookies were prepared using ingredients as per mentioned in Table 4. These cookies were used for sensory evaluation.

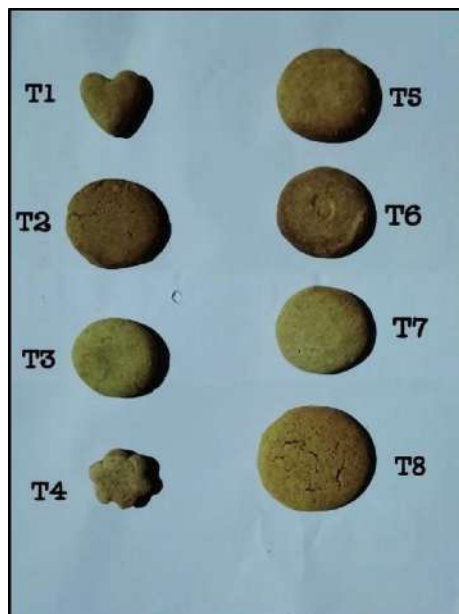


Fig. 2. Image of cookies trial (trial 1 to 8).

Table 4
Standardized recipe for cookies.

Sr. no	Ingredient	Quantity
1	Wheat flour	100 gm
2	Jaggery	50 gm
3	Fat	70 gm
4	Salt	0.5 gm
5	Baking powder	2.0 gm
6	Baking soda	2.0 gm
7	Milk	45 ml

3.2. Sensory evaluation of cookies

The effect of MLP fortification on sensory characteristics (color, taste, flavour, texture and overall acceptability) of wheat flour cookies is shown in Table 5 and Table 6. The color, taste, flavour and texture of control sample and cookies fortified with 1 % MLP and 3 % OPP extract were significantly superior to MLP and OPP cookies. Cookies fortified with 1 % MLP and 3 % OPP extract had the highest scores of flavour, texture and overall acceptability being (8.5, 8.3, 8.4) and (8.3, 8.5, 8.5) respectively. Cookies fortified with above 1 % MLP and 3 % were not acceptable. The results of

Table 5
Sensory evaluation of moringa leaves powder in cookies.

Sample Ccode	Sensory attributes				
	Color and appearance	Texture	Flavour	Taste	Overall acceptability
Control	8.5	8.5	8.5	8.5	8.5
MLP (0.5)	8.0	8.0	8.5	8.0	8.0
MLP (1.0)	8.5	8.3	8.3	8.4	8.3
MLP (1.5)	8.0	8.5	8.0	8.3	8.3
MLP (2.0)	8.0	8.5	8.5	7.0	7.0
MLP (2.5)	7.5	8.5	7.5	7.5	7.5
MLP (3.0)	7.5	8.5	6.0	6.5	6.5
MLP (3.5)	6.5	8.5	5.5	6.0	6.0
MLP (4.0)	6.5	8.5	5.0	5.5	5.5
Mean	7.66	8.42	7.31	7.3	7.28

MLP =Moringa leaves powder.

sensory evaluation indicated that 1 % MLP and 3 % OPP extract can be successfully used in wheat flour cookies.

3.3. Physical parameters of cookies

Various physical parameters such as thickness, diameter, weight and spread ratio were studied before and after baking and are shown in Table 7. The cookies observed are shown in Fig. 3 and Fig. 4.

3.4. Shelf life of orange peel powder and moringa leaves powder cookies

Shelf life of orange peel powder and moringa leaves powder cookies was carried out from 0 days to 45 days packed in LDPE pouches at ambient temperature (Fig. 5).

4. Conclusion

The present investigation focused on utilization of orange peel powder and moringa leaves powder for formulation of healthy cookies. The development and consumption of such products can also aid in improving the nutritional status of developing children. Orange peel powder and moringa leave powder are waste products derived from orange and moringa oleifera and possess good nutritional value, functional properties, dietary fiber, antioxidant, and antimicrobial properties. The MLP and OPP were optimized and the best sample was selected on the basis of sensory evaluation using nine-point Hedonic scale. Different optimization techniques were tested, and among those formulations, the product made with moringa powder was chosen for a 1 % sample based on sensory analysis, and the product made with orange peel powder for a 3 % sample.

Seven trials were conducted to formulate the ingredients in final cookies which included wheat flour, fat, jaggery, milk, salt, MLP and OPP. In the last eight trial, time and temperature were optimized. The final cookies were prepared according to the optimized ingredients and parameters. Further, the final product was subjected to the sensory evaluation. The cookies were evaluated depending on the color, texture and taste.

The results of Moringa’s nutrient characterization provide strong evidence that the plant’s leaves are nutrient-rich. Orange peel is thought to include several essential nutrients and possesses particular qualities that help the gastrointestinal tract work properly and is great for diabetics and heart patients. This study suggest that the moringa leaves and orange peels can be incorporated in the diet through the bakery products and be used as a nutritional supplement. The products can further be analyzed for its nutritional components.

Table 6
Sensory evaluation of orange peel powder in cookies.

Sample code	Sensory attributes				
	Color & appearance	Texture	Flavour	Taste	Overall acceptability
Control	8.5	8.5	8.5	8.5	8.5
OPP (0.5)	8.0	8.5	8.0	8.3	8.3
OPP (1.0)	8.5	8.5	8.4	8.3	8.0
OPP (1.5)	8.0	8.5	8.0	8.3	8.3
OPP (2)	8.3	8.5	8.0	8.0	8.0
OPP(2.5)	8.0	8.5	8.3	8.3	8.3
OPP(3)	8.3	8.5	8.4	8.5	8.5
OPP (3.5)	8.0	8.5	7.5	7.5	7.5
OPP (4)	8.0	8.5	7.0	7.0	7.0
Mean	8.17	8.5	8.01	8.07	8.04

OPP = Orange peel powder.

Table 7
Testing of physical parameters.

Sr.No	Timing	Thickness(T)	Diameter(D)	Weight (mg)	Spread ratio
1	Before baking	1.0	4.9	20.34	4.9
2	After baking	1.4	6.5	20.34	4.5



Fig. 3. Prepared cookies before baking.



Fig. 4. Prepared cookies after baking.



Fig. 5. Packaging of cookies.

CRedit authorship contribution statement

Teke Nikita Vilas: Data curation, Investigation. **Patil Karuna Wasudeo:** Data curation, Investigation. **Gavit Hemangi Jayram:** Visualization, Investigation.

Data availability

Data will be made available on request.

Declaration of Competing Interest

The authors declare that they have no known competing financial interests or personal relationships that could have appeared to influence the work reported in this paper.

References

- [1] C.M. Ajila, K. Leelavathi, U.J.S. Prasada Rao, Improvement of dietary fiber content and antioxidant properties in soft dough biscuits with the incorporation of mango peel powder, *J. Cereal Sci.* 48 (2) (2008) 319–326.
- [2] T.S. Anjorin, P. Ikokoh, S. Okolo, Mineral composition of *Moringa oleifera* leaves, pods and seeds from two regions in Abuja, Nigeria. *Int. J. Agric Biol.* 12 (2010) 431–434.
- [3] F. Anwar, S. Latif, M. Ashraf, A.H. Gilani, *Moringa oleifera*: a food plant with multiple medicinal uses, *Phytotherapy Res.* 21 (1) (2007) 17–25.
- [4] G. Block, B. Patterson, A. Subar, Fruit, vegetables and cancer prevention: A review of the epidemiological evidence, *Nutri. Cancer* 18 (1992) 1–29.
- [5] E.A. Brisibe, U.E. Umoren, F. Brisibe, P.M. Magalhaes, J.F.S. Ferreira, D. Luthria, X. Wu, R.L. Prior, Nutritional characterization and antioxidant capacity of different tissues of *Artemisia annua* L, *Food Chem.* 115 (2009) 1240–1246.
- [6] P.H. Chuang, C.W. Lee, J.Y. Chou, M. Murugan, B.J. Shieh, H.M. Chen, Anti fungal activity of crude extracts and essential oil of *Moringa oleifera* Lam, *Bioresource Techno.* 98 (1) (2007) 232–236.
- [7] R.L. Coop, P.H. Holmes, *Nutrition and Parasite Interaction*, *Int. J. Parasitol.* 26 (8–9) (1996) 951–962.
- [8] M.U. Dahot, *Vitamin Contents of the Flowers and Seeds of Moringa oleifera*, *Pakistan J. Biochem.* 21 (1988) 21–24.
- [9] M.O. Edema, L.O. Sanni, A.L. Sanni, Evaluation of maize –soybean flour blends for soy-maize bread production in Nigeria, *Afr. J. Biotechnol.* 4 (2005) 911–918.
- [10] FAO, *Improved animal health for poverty reduction and sustainable livelihoods*, *FAO Animal Prod. Health Papers.* 153 (2002).
- [11] L.J. Fuglie, *The Miracle Tree: the multiple attributes of Moringa*. Church world service, west African regional office, Dakar, Senegal, 2001, pp 103–36.
- [12] S.O. Gorinstein, Y.S. Martín-Belloso Park, Trakhtenberg, Comparison of some biochemical characteristics of different citrus fruits, *Food Chem* 74 (2001) 309–315.
- [13] A.P. Guevara, C. Vargas, H. Sakurai, Y. Fujiwara, K. Hashimoto, T. Maoka, M. Kozuka, Y. Ito, H. Tokuda, H. Nishino, An antitumor promoter from *Moringa*

- oleifera* Lam, Mutation Res./Genetic Toxicol. Environ. Mutagenesis 440 (2) (1999) 181–188.
- [14] R. Gupta, G.M. Kannan, M. Sharma, S. Flora, Therapeutic effects of *Moringa oleifera* Lam. on arsenic-induced toxicity in rats, Environ. Toxicol. Pharmacol. 20 (3) (2005) 456–464.
- [15] A.A. Hamza, A meliorative effects of *Moringa oleifera* Lam. seed extract, Food Chem. Toxicol. 48 (1) (2010) 345–355.
- [16] M.M. Khalafalla, E. Abdellatef, H.M. Dafalla, A.A. Nassrallah, K.M. Aboul-Enein, D.A. Lightfoot, F.E. El-Deeb, H.A. El-Shemy, Active principle from *Moringa oleifera* Lam Leaves effective against two leukemias and a hepatocarcinoma, Afr. J. Biotechnol. 9 (49) (2010) 8467–8471.
- [17] B. Knudsen, A. Serena, Chemical and physicochemical characterization of co-products from vegetable food and agro industries, Anim. Feed Sci. Technol 139 (2007) 109–124.
- [18] Y. Liu, H. Ahmad, Y. Luo, D.T. Gardina, R.S. Guasekera, W.L. Mc Keehan, B.S. Patil, Citrus pectin: Characterization and inhibitory effect on fibroblast growth factor-receptor interaction, J. Agric. Food Chem. 49 (6) (2001) 3051–3057.
- [19] F.W. Martin, R.M. Ruberte, L.S. Meitzner, Edible leaves of the tropics. 3rd ed. Educational concerns for hunger organization, Inc., N.ft. Meyers, Fl. 1998, 194pp.
- [20] N. Navy, Bakery products in the middle east especially in the Arab countries obtained in Egypt, J. Food Sci. Technol 22 (8) (1980) 342–347.
- [21] A.T.E. Olushola, The Miracle tree", *Moringa oleifera* (Drumstick), in : Achieve Vibrant Health with Nature, Keep Hope Alive Series 1, Unijos Consultancy Limited press, Jos, Nigeria, 2006, pp. 120–136.
- [22] L.L. Price, The *Moringa* tree. www.echonet.org. Accessed on 14/11/2010. Samphal metz; 2000, (1998) hand book of bakery and confectionary.
- [23] S. Sreelatha, A. Jeyachitra, P.R. Padma, Antiproliferation and induction of apoptosis by *Moringa oleifera* Lam. leaf extract on human cancer cells, Food Chem. Toxicol. 49 (6) (2011) 1270–1275.
- [24] M.K.E. Youssef, Foods that fight cancer, in: Proceedings of the sixth Conference of Woman and Scientific Research & Development in Upper Egypt. 17–19 April 2007, Assiut University, 2007, pp. 213–228.
- [25] American Association of Cereal Chemists AACC, Approved methods of The AACC. 10th Ed. The Association: St. Paul, MN, 2000.
- [26] AOAC, Official methods of analysis, 16th ed., Association of Official Analytical Chemists, Washington, DC, 1995, pp. 27–29.
- [27] S. Rangana, Hand Book of Analysis and Quality Control for the Fruit and Vegetable Products, Tata McGraw Hills Limited, New Delhi, 1986.



Isolation of biofilm formers from aquaculture and study, the effect of antibiofilm activity of chitosan mediated silver nanoparticle

G. Ganga

Department of Microbiology, Sree Ayyappa College Eramallikara Chengannur, Kerala India 689109

ARTICLE INFO

Article history:

Available online 16 December 2022

Keywords:

Chitosan Silver Nano biofilm
Screening of biofilm formers
Antibiofilm properties

ABSTRACT

Bacterial biofilms are the root cause of biofouling and are due to the agglomeration of microbes and microorganisms on a surface that is surrounded or held together by extracellular polymeric substances. Bacteria produce extracellular polymeric substances (EPS), lipopeptides, and other extracellular matrix proteins, which enable them to adhere on to help them attach to surfaces and bind to one another. These extracellular substances can adhere to metals and varied surfaces, possibly producing toxic compounds such as. sulfhydryl groups, In Aquaculture fam and Ponds such Biofilm forms are of greatest threat by paving the way to settle down for broad diversity of epibiotic organisms. They together can contribute economic impact of Aquaculture and farms and ponds.

Chitin, the second most abundant polymer on earth, is a commercially valuable product. The deacetylated form of chitin, chitosan possesses more attractive and useful properties. In this study, the raw material used was the waste of the Spp of shrimp, *Penaeus indicus*. Chitosan-Ag Nano complex was synthesized and used for its antibiofilm-forming properties. Microbes capable to form biofilm isolated from contaminated sites were isolated and characterized for their identity using microtiter plate assay, tube culture assay, and slide culture assay biofilm formers were observed from two different environments such as paddy fields and ponds. Antibiofilm-forming properties of chitosan nanoparticles were assessed using microtiter plate assay.

© 2022 Elsevier Ltd. All rights reserved.

Selection and peer-review under responsibility of the scientific committee of the Integrative Nanotechnology Perspective for Multidisciplinary Applications - 2022.

1. Introduction

Biofilms are communities of microorganisms that are colonies in a polluted environment by bacterial adherence. These biofilms are a collection of one or more types of microorganisms including fungi, bacteria, and protists [1,2]. Biofilm-forming microbes are mostly involved in biofouling activities and are highly resistant to usual antimicrobial treatments. These biofilms are formed by extracellular proteins and exopolysaccharides, extracellular DNA (eDNA) which is embedded with a wide range of bacteria with Highly resistant bacterial communities. Antibiotic-resistant bacteria have been found to depend on ionic interactions of eDNA with Pel, a protein that maintains cell-to-cell contacts inside biofilms [3]. Understanding the microbial communities and their putative role in fouling is a prerequisite for taking effective measures for its protection and management, Targeting and disrupting this biofilm are one of the major challenges to biofouling forming sites and cleaning such contaminated sites.

Antimicrobial management methods like ultrasound irradiation, sonication, chemical, mode of degradation, etc, Biofouling is becoming a worldwide problem and antifouling paints/chemical agents are being extensively used to mitigate biofouling-related problems in aquaculture fields. Biocidal chemical toxic coating as an antifouling agent is being widely used in Aquaculture. To an extent, a small number of such coatings are released into water bodies and can cause the bioaugmentation of toxic materials. Environmental toxic materials are reported from fish and other aquatic animals such as farms [4]. So prevention of biofouling using eco-friendly methods is suggesting control options for aquafarms [3,4].

Nanotechnology is an emerging field with high potential in the field of antimicrobial and antibiofilm research. Chitosan has been used as nanoparticle material owing to its versatile biodegradability, biocompatibility, and natural origin. Chitosan is a biodegradable and biocompatible natural polymer that may be utilized as an adhesive, as well as an antibacterial and antifungal agent because There are several reports available on the extraction of cheaply available resources for fungal cell walls and crab shells [5,6].

E-mail address: drangaimb@gmail.com

Chitosan-based nanoparticles have an antimicrobial effect on gram-positive bacteria (*Listeria monocytogenes*, *Bacillus megaterium*, *B. cereus*, *Staphylococcus aureus*, *Lactobacillus plantarum*, *L. brevis*, and *L. bulgaris*) Chitosan nanoparticle antimicrobial activity against gram negative organism such as (*E. coli*, *Pseudomonas fluorescens*, *Salmonella typhimurium*, Tamara, (2018)[7] found that the antibacterial activity of chitosan is related to its molecular weight, degree of acetylation, chitosan concentration, and inoculum size [8]. According to certain research, coating nanoparticles formed from other materials with chitosan reduces their influence on the body and increases bioavailability.[9].

Progress in Green and eco-friendly method of Nanoparticle synthesis is a promising area of research to act against biofilm formers. Owing to their unique properties, Nanoparticles have great potential in application in the removal of biofilms which could be a possible threat to the environment. The study's major objectives are to isolate putative biofilm formers from two contaminated sites with biofouling activity sites and apply Chitosan mediated Silver nanoparticles against these biofilm formers and understand their efficacy. In addition to that to improve the cost-effective method of chitosan from the shells of shrimp, *Penaeus indicus*.

2. Materials and methods

2.1. Sample collection

The samples were collected from Aquaculture fields and freshwater ponds having biofouling activities of Alappuzha All the samples were collected in sterile containers aseptically collected (Fig. 1). Triplicates of samples were collected from each location, pooled together, and selected for the study.(See Fig 2.)

2.2. Isolation of biofilm-forming microbes

Serial dilution of the biofilm containing samples up to 10^{-6} dilutions was prepared, reducing the concentration of bacteria at each successive dilution. Each of the serially diluted samples was plated in a nutrient Agar medium and incubated overnight for the growth of bacterial colonies.

2.3. Tube culture assay

A qualitative tube culture experiment was performed to detect biofilm-producing bacteria. In test tubes, a loopful of test organisms were inoculated in 10 mL of trypticase soy broth with 1 % glucose and incubated at 37 °C for 48 h, after which the tubes were decanted, washed with phosphate buffer saline (pH 7.3), and air-dried. The dried tubes were stained with crystal violet (0.1 %) as an indicator dye. Tubes were washed with deionized water and were dried.. Triplicate of each sample was kept and un-inoculated tubes were kept as control. Outcomes of the result were measured in comparison with *Pseudomonas* MTCC biofilm producer as control and control uninoculated sample as it was as the negative control [10]. The development of biofilm was observed by observing visible film lined in the tube's wall and bottom. Based on the amount of biofilm developed, it was graded as 1-weak/none, 2-moderate, and 3-high/strong [10].

2.4. Slide culture test for biofilm formers

Biofilm formation has focused on bacterial attachment and accumulation on abiotic surfaces and was done based on the experimental procedures described by Walker *et al.*,(2012) [11]. Static biofilm formed was later observed through the Cristal Violet staining method. The *Pseudomonas* sample was kept as Positive control and the uninoculated broth was kept as a negative control.

2.5. Identification of biofilm forming bacteria

Biofilm formers were identified through morphological analysis, Biochemical characterization, and Molecular Characterization Using 16S rRNA sequencing methods. Database similarity search using NCBI BLAST. Obtained sequences were used for database similarity search to find sequence matches using the nucleotide BLAST program in NCBI GenBank.



Fig. 1. Site for BF1 SITE 1 and BF2 Site 2 Selected for Biofilm screening study.

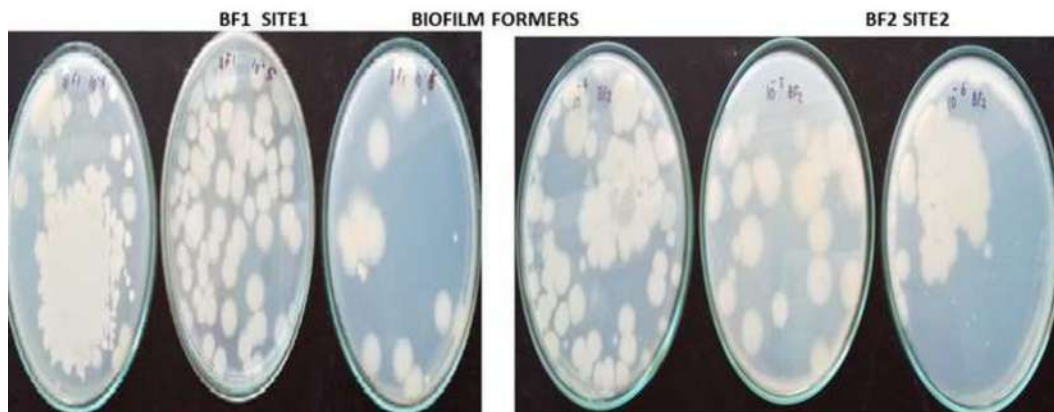


Fig. 2. Showed isolates from two sites BF1 and BF2.

2.6. Synthesis of chitin

Chitosan Nanoparticle are synthesized from raw materials such as the wastes of the Spp of shrimp, *Penaeus indicus*. from Kadavunthira Cochin For the synthesis of Nanoparticles Chitosan was extracted by deproteinization, demineralization, decolorization, and deacetylation processes. Antibiofilm-forming properties of chitosan nanoparticles were studied.

Prawn waste shells were collected and washed thoroughly and chitosan was prepared from them by chemical processes like demineralization, deproteinization, and decolorization For demineralization washed Prawn shells powder(1Kg) was treated with 1 M HCl in a 1:15 weight/volume ratio. The obtained solid materials were washed till they reached neutral pH. Deproteinization was later done with (200gm) NaOH solution in a 1:10 weight/volume ratio. The mixture was heated at 60 °C for 3.5 h in a reaction round bottom flask. Chitin obtained was subjected to Decolorization (DC) Chitin (30 g) was then decolorized by 2 % sodium hypochlorite solution (600 mL) in a 1:20 ratio of chitin and the mixture was continuously stirred and finally washed and dried.

2.6.1. Deacetylation of Chitin into chitosan

Sodium Hydroxide (50 %) in a 1:10 weight/volume ratio at a temperature of 100 °C with a substantial degradation in presence of oxygen [12]. The residues were separated and washed and purified with water. Degree of Acetylation was carried out by Acid-base titration.

2.6.2. Acid-base titration

0.4 g of Prawn Chitosan was dissolved in 40 mL of 0.1 M HCl and the mixture was constantly stirred for 20 min at room temperature. Later it was titrated against 0.1 M NaOH solution in the presence of methyl orange indicator. The percentage of moisture content was measured by gravimetric method [12] and the percent of free NH_2 groups in chitosan was calculated as follows [10].

$$\text{NH}_2 \text{ Content} = \frac{C1V1 - C2V2 \times 0.016}{G \times 100 - W} \times 100$$

$$\text{NH}_2 \% = \frac{\text{NH}_2 \%}{9.94} \times 100$$

The chitosan powder was stored at room temperature for further studies. Identity was Confirmed using UV-Visible spectra and FTIR.

2.7. Average molecular weight determination

The synthesized Chitosan was subjected to average molecular weight determination using viscometric measurement by a vis-

cometer. Late the intrinsic viscosity of the chitosan sample was determined from the Huggins equation [13]. From the data obtained from Intrinsic viscosity the Molecular weight of the sample was prepared using From the intrinsic viscosity, the molecular weight was determined by employing the Mark- Houwink equation [13,14].

2.8. Biosynthesis of silver nanoparticles from chitosan

Silver Nitrate (AgNO_3) was purchased from Merk, India. For the synthesis of Silver Nano Particle 0.2 gm of Chitosan powder was thoroughly dissolved in 1 % of glacial acetic acid with a constant stirring for 30 min. The resultant mixture was filtered and to the clear solution add 0.1 M of AgNO_3 and 1 M NaOH and stirred overnight in dark for 90 of Change in color from Yellow to Dark yellow was observed for the formation of Ag NPs.

2.8.1. Evaluation of biofilm inhibition activity of silver nanoparticles

The biofilm inhibition activity was studied using the microtiter plate assay, Trypticase soy broth (TSB) was mixed with 1 % glucose and was distributed in each well of flat-bottomed microtiter plate To each well Chito-AgNP Nano was added through serial dilution in order to get a range of 50 μL , 75 μL and 100 μL of 1 mg/ml stock silver nano solution were added. The micro-plates were incubated at 37 °C after being prepared with nanoparticles and infected with 10^5 cfu/ml bacteria. After the wells had been incubated, the contents were taken out, the wells were cleaned with a saline solution 0.9 %, and the plates were dried at room temperature. After then, 99 % methanol was used to fix the microorganisms that had adhered to the microtiter well. methanol was taken out after fixing, and the plates were then allowed to dry again 0.05 %. Crystal violet dye was later added. The wells were rewashed with autoclaved distilled water after the excess dye was removed. At 570 nm, the optical density (OD) was measured using a microplate reader. The lowest dose at which biofilm formation was 90 % prevented was known as the minimum biofilm inhibitory concentration (MBIC) [15]. The tests were performed in duplicate.

3. Results of the study

3.1. Isolation and characterization of biofilm formers

Biofilm formers were isolated from two different Biofouling Aquaculture sites Fig. 1 showed isolates from two sites. Cultural characteristic of various biofilm formers was observed and the results are given in Table 1 A total of 14 isolates with specific cul-

Table 1
Culture characteristics of biofilm-forming isolates obtained from BF1 Site 1 and BF2 Site 2.

Sl. No	Bacterial colony	BF1 Site Morphology	Bacterial colony	BF2 Site Morphology
1.	BF1-C1	Large, off-white, regular margin, dry.	BF2-C1	White, medium, rough
2	BF1-C2	Small, off-white, creamy, opaque	BF2-C2	White, rough, medium, transparent
3	BF1-C3	Dry, small, opaque	BF2-C3	Transparent, small, white
4	BF1-C4	White, small, opaque, round, creamy	BF2-C4	White, medium, rough
5	BF1-C5	Transparent, large, irregular	BF2-C5	White, rough, medium
6	BF1-C6	Round, opaque	BF2-C6	White, rough, medium
7	BF1-C7	Medium, large, off-white, opaque	BF2-C7	Off white, small
8	BF1-C8	White, irregular, dry	BF2-C8	White, rough, medium -
9	BF1-C9	White, small, opaque, round, creamy	BF2-C9	Transparent, large, irregular
10	BF1-C10	Cream opaque	BF2-C10	Round, opaque
11	BF1-C11	White, rough, medium	BF2-C11	Yellow round
12	BF1-C12	Transparent, large, irregular	BF2-C12	Yellow round
13	BF1-C13	White, irregular, dry	BF2-C13	Transparent, small, white
14	BF1-C14	Cream opaque	BF2-C14	Cream opaque

tural characteristics were isolated separately each from two different sites was maintained and were tested for their characteristic biofilm formation by Tube Assay and Slide culture Assay. The number of bacterial colonies was 45×10^6 and 30×10^6 BF1 site 1 and BF2 site 1.

3.2. Screening of biofilm-forming bacteria

For the screening of biofilm-forming bacteria tube cultures and slides, cultures were performed and results are given.

3.2.1. Tube culture assay

From BF1 Site1 only Two samples were highly positive for Biofilm formation and from the BF2 site One sample was showing high biofilm formation and the rest of the samples were either moderate or low biofilm formers when compared with the control. The results of the Tube culture are given in Table 2 and Fig. 3.

3.2.2. Slide culture assay

The presence of biofilm was observed after 48 h of incubation at 37 °C. Slide culture Assay also in accordance with Tube culture Assay were (Table 2).

Table 2

Indicating classification of biofilm formers BF1 Site 1 from site 1 based on staining intensity. Table 2 Tube culture and Slide culture comparison indicating classification biofilm formers BF1 Site 1 and BF2 Site 2 from site 1 based on staining intensity NC (Negative control) PC (Positive control).

Bacterial isolate BF SITE 1	Staining intensity Tube culture	Staining intensity Slide culture	Bacterial isolate BF2 SITE 2	Staining intensity Tube culture	Staining intensity Slide culture
BF1C1	NC	NC	BF2C1	PC	PC
BF1C2	PC	PC	BF2C2	+	+
BF1C3	+++	+++	BF2C3	+++	+++
BF1C4	++	++	BF2C4	++	++
BF1C5	+++	+++	BF2C5	++	++
BF1C6	++	+	BF2C6	++	++
BF1C7	++	+	BF2C7	++	++
BF1C8	++	++	BF2C8	+	+
BF1C9	++	+	BF2C9	+	+
BF1C10	++	+	BF2C10	+	+
BF1C11	++	++	BF2C11	++	++
BF1C12	+	+	BF2C12	+	+
BF1C13	+	+	BF2C13	++	++
BF1C14	++	++	BF2C14	+	+
BF1C15	++	++	BF2C15	-	-
BF1C16	++	++	BF2C16	control	control

3.3. Identification and characterization

Characterization of those three isolates which showed maximum Biofilm production was characterized by staining and Biochemical methods. All three isolates showed similar biochemical characteristics and gram stain reactions. Fig. 4 From the results, all three samples were gram-positive and rod-shaped bacteria, catalase positive, oxidase positive, indole test negative, methyl red negative, Voges Proskauer test negative, citrate negative, and TSI test is glucose, lactose, fructose fermenting and mannitol test is no fermenting and non-motile. On the basis of gram staining and biochemical tests, the organism was identified as bacillus sp. All three samples showing biofilm production were identified as bacillus [16]. Fig. 6 shows the molecular characterization of Biofilm formers using an I6SrNA Universal primer with an amplicon size of 1500 bp indicating the amplification of 16srRNA. Sequencing and BLAST analysis showed a 93 % homology with Bacillus species (See Fig. 7.)

3.4. Chitosan silver nanoparticle

Chitosan was prepared and from the prepared synthesized from wastes of the Spp of prawns and a deacetylation reaction was carried out. By Acid-base titration procedure degree of deacetylation was carried out and the result is in Fig. 5 It was observed that the degree of deacetylation of chitosan linearly increased with

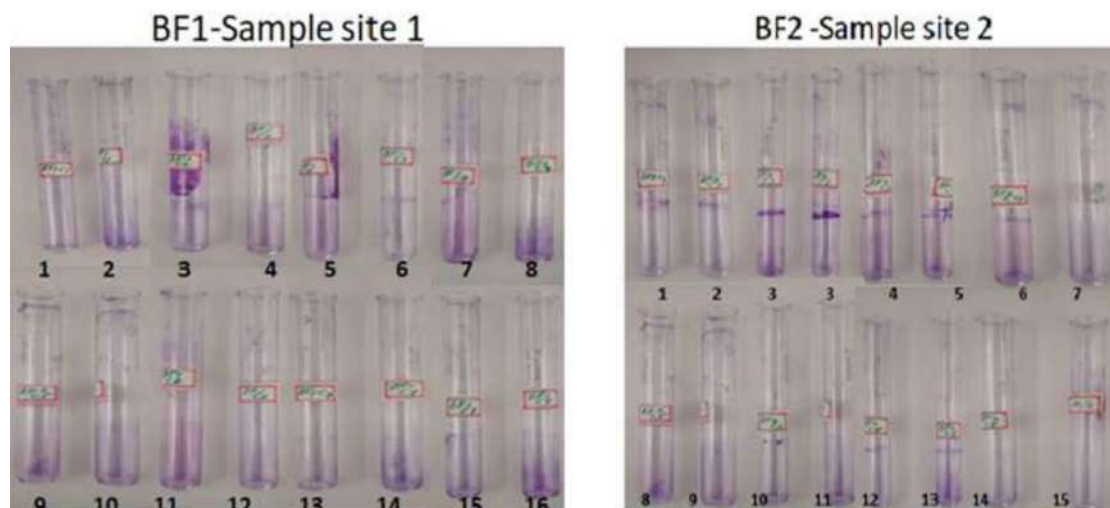


Fig. 3. Tube culture assay for the detection of Biofilm formers from sample sites BF1 and BF2.

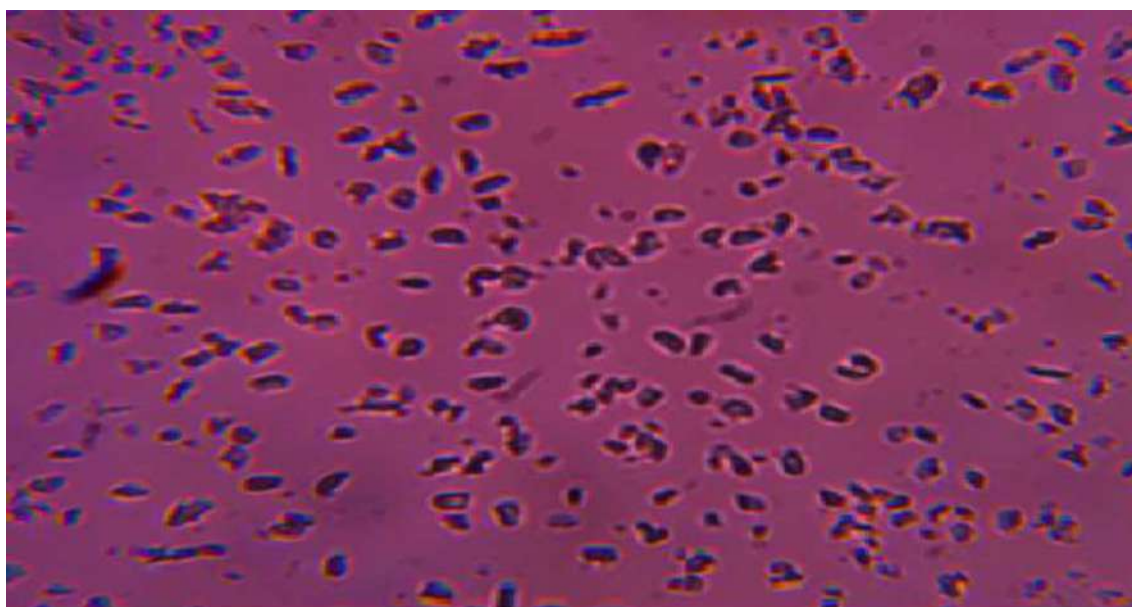


Fig. 4. Slide culture of biofilm formers and identification.

the increase of reaction time and was 63.7 % and was compared with that of standard. Based on the viscosity molecular weight determination method the molecular weight of Chitosan was 3.25×10^3 (g/mole) which was in comparison with reference standards previously reported.

Chitosan silver nanoparticle was synthesized from wastes of the Spp of shrimp, *Penaeus indicus* s exoskeleton, and was Chitosan was extracted by deproteinization, demineralization, decolorization, and deacetylation processes later it was analyzed for its identity using UV spectrophotometer, FTIR and SEM analysis (unpublished data). The prepared sample was kept at 4°C and used for the present study, UV visible spectrometer reading of chitosan was 320 nm and the Silver nanoparticle was 435 nm.

3.4.1. Antibiofilm activity of chitosan silver nanoparticles

Silver nanoparticles synthesized from chitosan were used against Biofilm formers selected from two different sites. Microtiter plate assay was used to assess the anti-biofilm activity of differ-

ent concentrations of silver. nanoparticles were added to the bacterial culture. Except for Control, all the wells showed a considerable reduction in biofilm formation, estimated using staining and estimating the intensity of colour. It was observed that biofilm formation was inhibited by Chitosan Silver Nanoparticles. The results of antibiofilm activity are given in Fig. 6 and Table 3 Different concentration of silver nanoparticles was added to bacterial culture In the study Biofilm formation can be screened using tube assay and microtitre assay. Three isolates BF1C5, BF2C2, and BF1C3 selected as the potent biofilm formers.

4. Discussion

In an aquaculture system biofouling is a significant problem where the specific culture species or infrastructures required for its growth are directly or indirectly affected. This can leads to significant production impact and economical loss.

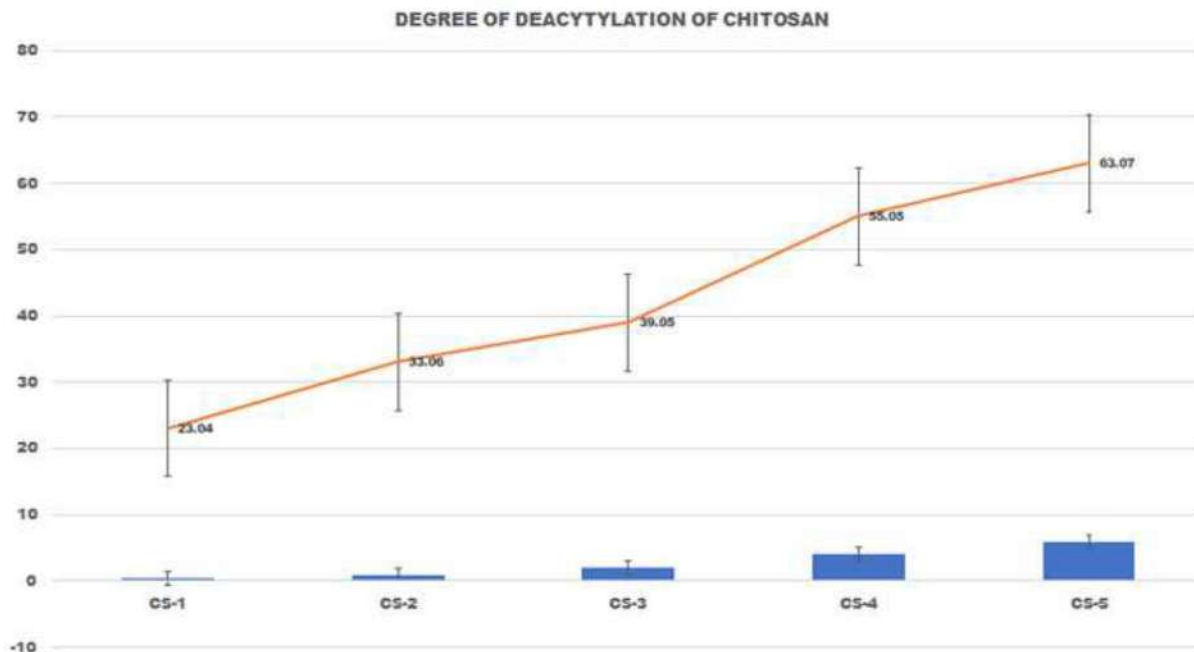


Fig. 5. 16S RNA PCR Analysis for the maximum biofilm producer.

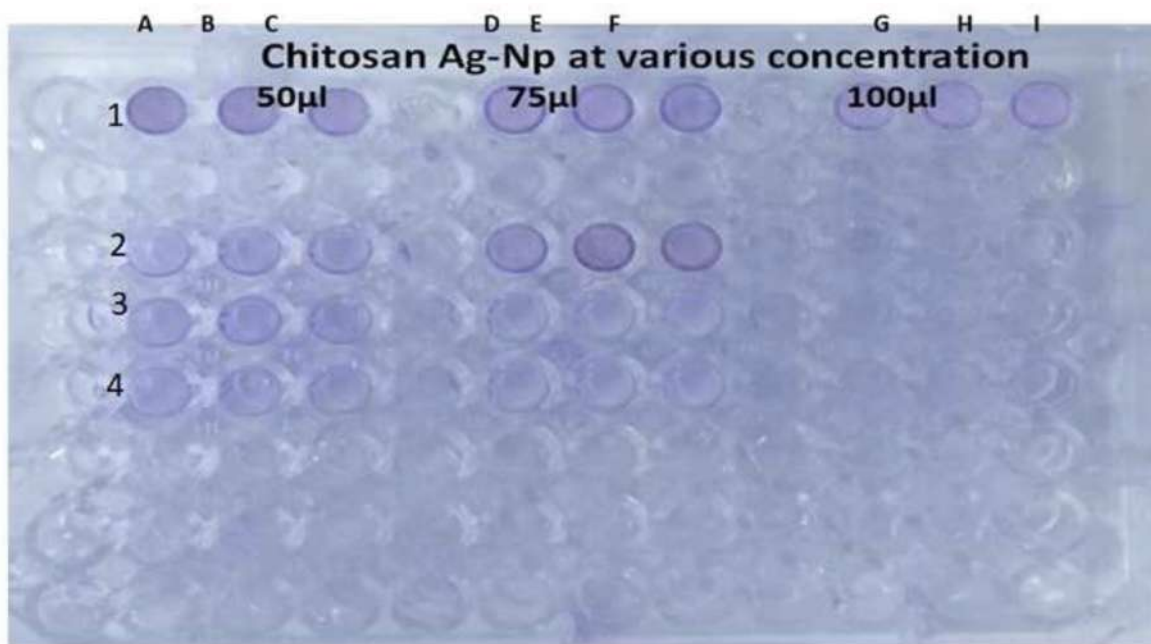


Fig. 6. Degree of deacetylation of Chitosan, In Graph CS1–CS6 shows an increase in deacetylation of chitosan with an increase in time.

In this study, two pilot fields are being selected to understand the effect of biofilm formers at two bio-fouled aquaculture sites in Alappuzha districts where surface water is heavily contaminated with algal blooms, microflora and debris of organic and inorganic matter with low Dissolved oxygen(DO) and COD (Chemical Oxidation Demand) BOD (Biological Oxidation Demand) was alarmingly high (Unpublished data). Based on Water quality parameters (Unpublished data) tested BF1 site was having more Biofouling activities than BF2 site is having low biofouling activities. BF1 had high BOD and COD low DO is due to the presence of biofouling activity at site 1 may be due to the putrefaction of organic com-

pounds and organic feed and insecticides that were used at this site. Heavy growth of algae weeds was observed in this site that could contribute to the formation of biofilm-forming microbes Biofilm formation and specific organism involved in it is thought to be the major root cause of all biofouling activities. Hedrik *et al.*, in 2017 [17] also reported the role of biofilm formers in biofouling activities. In this study 13, morphologically distinct. Bacteria was isolated and screened for biofilm activity. The most potent three bacteria showing antibiofilm assay were selected and characterized. The biochemical characteristics were performed for the isolates, all three isolates were catalase-negative and sugar

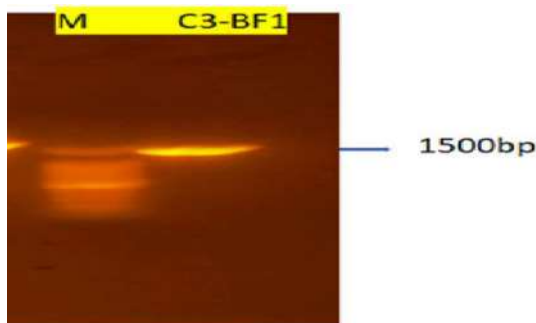


Fig. 7. Microtitre pale assay of Inhibitory activity of Silver Nanoparticle against biofilm bacteria from three different sites BF1 and BF2 (Chitosan AgNp at various Concentration A-C50 μL,D-F-75 μL, G-H-100 μL).

fermentation indicated only acid production. DNA isolation and sequencing and NCBI BLAST analysis helped to identify them accu-

Table 3

Anti-biofilm activity of silver nanoparticles of three important biofilm-forming bacteria from BF1 SITE1 and BF2 SITE2 Table 3 anti-biofilm activity of silver nanoparticles of three important biofilm forming bacteria from BF1 and BF2 (A-C50μL,D-F-75 μL,G-H-100 μL) (Chitosan AgNp at various Concentration) absorbance was measured at 550 nm A1,B1 C1 D1 E1 G1,H1,-I1 is the control sample.A2,B2,C2.D2. E2 F2,G2 H2.-I2 (Pseudomonas without AgNp) Sample BF1C3,(A3,B3,C3.D3.E3.F3.G3. H3.I3)SampleBF1C4(A4,B4,C4.D4.E4.F4.G4.H4.I4,A4-I4) SampleBF2C3- (A4,B4,C4.D4. E4.F4.G4.H4.I4,A4-I4).

Wells	50 μL-AgNP	75 μL AgNP	100 μL AgNP
A1	1.86	1.9	1.9
A2	1.5	1.6	1.35
A3	1.6	1.7	1.2
A4	0.9	0.9	0.5
B1	1.86	1.88	1.2
B2	1.5	1.6	1.2
B3	1.6	1.5	1.4
B4	0.8	0.5	0.3
C1	1.86	1.88	1.1
C2	1.5	1.5	1.35
C3	1.6	1.6	1.6
C4	0.9	0.8	0.8
D1	1.9	1.88	1.88
D2	1.5	1.5	1.5
D3	0.55	1.6	1.6
D4	0.4	0.8	0.8
E1	1.9	1.79	1.88
E2	1.5	1.45	1.0
E3	0.6	1.56	1.1
E4	0.35	0.8	0.8
F1	1.9	1.80	1.00
F2	1.4	1.1	1.0
F3	0.65	1.0	0.9
F4	0.35	0.7	0.66
G1	1.9	1.75	1.00
G2	1.3	1.25	1.0
G3	0.6	1.0	0.6
G4	0.44	0.8	0.4
H1	1.9	1.82	0.67
H2	1.34	1.45	0.9
H3	0.55	1.2	0.9
H4	0.4	0.5	0.66
I1	1.9	1.86	0.66
I2	1.0	1.45	0.6
I3	0.5	1.56	0.4
I4	0.3	0.8	0.3

rately as bacillus spp. Qin et al., 2022 [18] reported Bacillus species is found to be the predominant flora present in all 13 isolates each from two various sites. Quin et al (2022) [18] reported the ability of *Bacillus substillis* to perform cell differentiation to form Biofilm.

As described by Christensen et al (1985),[10] tube assay was found to be a cost-effective and simple methodology for the qualitative identification and observation of biofilm detection. Microtiter assay. Was found to be an effective methodology for the detection of antibiofilm formers at various concentrations it was observed that 100 μL of chitosan showed maximum inhibition of the biofilm O'Toole, (2011) [19] reported that a 96-well plate is well suited for qualitative and quantitative spectrophotometric assay for biofilm formers. The synthesis of nanoparticles from chitosan biowaste sources has been paid great attention. because of their biocompatibility, biodegradability, and hydrophilic properties, which endow them with opportunities for various applications. [20,21]. The polymeric feature of chitosan interacts with negatively charged molecules and polymers [22]. Due to the interaction that takes place between the active amino groups in chitosan and nanoparticle synthesized from metals, chitosan is chosen as a protecting agent in the synthesis of metal nanoparticles. There are many reports available on antibiofilm research however chitosan mediated nanoparticles and silver Nanoparticles were not much explored. In this research, the anti-biofilm activities of chitosan silver nanoparticles (AgNPs) against biofilm formers from different environmental conditions were evaluated. In this study, an attempt was made to study the anti-biofilm effect of chitosan AgNPs derived from natural resources. Al-Naamani, et al., (2016) [23] reported Chitosan is a natural polymer that is formed from the partial deacetylation of crustacean waste. In his study, he reported. The nanocomposite of Chitosan with Zinc oxide can be used as a coating agent for antifouling activity.

In the present study, chitosan was prepared, silver nanoparticles were synthesized, and the results observed were corroborated with earlier reports [24]. The characteristic properties of chitosan prepared in this study are comparable with the reference given by Hedrik et al., [17] in which the molecular weight of commercial chitosan was mentioned as 3.5×10^5 (g/mole). Hence, it was confirmed that the molecular weight of commercial chitosan was observed higher than the sample synthesized in this study. The deacetylation was also comparable with the report on chitosan produced from crabs' skeletons as the source material. Hedrik et al., in 2017 [17,25,26] UV spectrophotometric analysis of chitosan Silver nano obtained from Chitosan was 430 nm it was in accordance with the earlier report of Kalaivani et al.,(2018) [27].

According to Banerjee et al. (2011) [28], biofouling activity can be reduced by reducing biofilm formers, which can be seen in any environment. In their study, they explained how biofilm formers contribute to the biofouling effect in polluted environments The antibiofilm activity of the biosynthesized Chitosan based silver nanoparticles shows a reduction in the biofilm formation when individually tested against the putative biofilm formers from a contaminated site. The study opens the gateway for a new treatment regime against biofilm In this study AgNPs chitosan was used for anti-biofilm activity and the results showed that. AgNPs successfully prevented biofilm development and killed bacteria in existing biofilms, suggesting that AgNPs chitosan could be utilized to prevent and cure biofilm-related infections. The findings of the study corroborate with the findings of Franci et al., (2015) [8], in that study AgNp was effectively used as an antibiofilm and fouling agent.

The chitosan-based silver nanoparticle is proven to be a better antimicrobial agent by Many workers. Saberpour et al., 2020 [29] also reported the effect of silver nanoparticles as one of the most potent anti-bacterials and antibiofilm candidates which can able to resolve many problems associated with biofilm effects [30].

However, there have been few publications on silver nanoparticles' anti-biofilm activity, and the actual mechanism behind their action is yet unknown. Hence, this paper discusses some of the most cutting-edge biofilm treatment techniques.

5. Conclusion

Chitosan AgNp is found to be effective against all tested biofilm-forming bacteria as well as selected biofouling-forming bacteria under study. This study can be further extended to understand the mechanism behind the action against other EPS-forming microbes.

Data availability

No data was used for the research described in the article.

Declaration of Competing Interest

The authors declare that they have no known competing financial interests or personal relationships that could have appeared to influence the work reported in this paper.

Acknowledgement

The author is thankful to all the staff of Nexgene lab Cochin for their constant support for the completion of the work.

References

- [1] Dang, H., and Lovell, C. R. Microbial Surface Colonization and Biofilm Development in Marine Environments. *Microbiology and molecular biology reviews* : MMBR, (2015) 80(1) 91–138. <https://doi.org/10.1128/MMBR.00037-15>.
- [2] Muhammad Musa Hassan, Idris Aisha Lawan, Fan Xiao, Guo Yachong, Yu Yiyang, Jin Xu, Qiu Junzhi, Guan Xiong, Huang Tianpei Beyond Risk: Bacterial Biofilms and Their Regulating Approaches Frontiers in Microbiology (2020) 119:28 DOI=10.3389/fmicb.2020.00928 ISSN=1664-302X
- [3] L.K. Jennings, K.M. Storek, H.E. Ledvina, et al., Pel is a cationic exopolysaccharide that cross-links extracellular DNA in the *Pseudomonas aeruginosa* biofilm matrix, *Proc. Nat. Acad. Sci.* 112 (36) (2015) 11353–11358. <https://doi.org/10.1073/pnas.1503058112>.
- [4] Archana S , B. Sundaramoorthy B and Faizullah M.M Review on Impact of Biofouling in Aquafarm Infrastructures Int.J.Curr.Microbiol.App.Sci (2019) 8 (1): 2942–2953 2942 Review Article <https://doi.org/10.20546/ijcmas.2019.807.365>.
- [5] T.K. Varun, S. Senani, N. Jayapal, J. Chikkerur, S. Roy, V.B. Tekulapally, M. Gautam, N. Kumar, Extraction of chitosan and its oligomers from shrimp shell waste, their characterization and antimicrobial effect, *Vet. World* 10 (2) (2017) 170–175. <https://doi.org/10.14202/vetworld.2017.170-175>, Epub 2017 12 PMID: 28344399.
- [6] A. Pellis, G.M. Guebitz, G.S. Nyanhongo, Chitosan: sources, processing and modification techniques, *Gels* 8 (2022) 393, <https://doi.org/10.3390/gels8070393>.
- [7] Tamara, F. R., Lin, C., Mi, F. L., & Ho, Y. C. 2018. Antibacterial Effects of Chitosan/Cationic Peptide Nanoparticles. *Nanomaterials (Basel, Switzerland)* (2018)8(2), 88. <https://doi.org/10.3390/nano8020088>.
- [8] Franci G, Falanga A, Galdiero S, Palomba L, Rai M, Morelli G, Galdiero M, Silver nanoparticles as potential antibacterial agents. *Molecules.* (2015) 18:20 (5):8856–74. doi: 10.3390/molecules20058856. PMID: 25993417
- [9] Yanat M., and Schroën K, Preparation Methods and applications of chitosan nanoparticles; with an outlook toward reinforcement of biodegradable packaging, *Reactive and Functional Polymers,* (2021)161,1048–49, ISSN 1381-5148.
- [10] Christensen G.D, Simpson W.A, Yonger J.J, Baddor LM, Barrett F.F, Melton D.M, Beachey E.H. Adherence of coagulase-negative staphylococci to plastic tissue culture plates: a quantitative model for the adherence of staphylococci to medical devices. *J Clin Microbiol.* (1985) ;22: 6 996–1006. doi: 10.1128/jcm.22.6.996-1006.1985
- [11] J.N. Walker, A.R. Horswill, A coverslip-based technique for evaluating *Staphylococcus aureus* biofilm formation on human plasma. *Front. Cell Infect. Microbiol.* 27 (2) (2012) 39, <https://doi.org/10.3389/fcimb.2012.00039>, PMID: 22919630; PMCID: PMC3417647.
- [12] Sekwon, K. 2010. Chitin, Chitosan, Oligosaccharides and Their Derivatives: Biological Activities and Applications (1st ed.).P 37–45 in G. H. Jo, R. D. Park and W. J. Jung, editors. *Enzymatic production of chitin from crustacean shell waste.* CRC Press, New York.
- [13] R. Lapasin, S. Pricl, *Rheology of industrial polysaccharides: theory and applications* ISBN-13: (1995) 978–1461359159.
- [14] D. Elieh-Ali-Komi, M.R. Hamblin, ChitiMarylandn and chitosan: production and application of versatile biomedical nanomaterials, *Int. J. Adv. Res.* 4 (3) (2016) 411–427, PMID: 27819009.
- [15] Adukwu E.C , Allen S.C.H , Phillips C.A, The anti-biofilm activity of lemongrass (*Cymbopogon flexuosus*) and grapefruit (*Citrus paradisi*) essential oils against five strains of *Staphylococcus aureus* *J Appl Microbiol* (2012) 113:5 doi: 10.1111/j.1365-2672.2012.05418.x.
- [16] Collee J G, Mackie TJ, and McCartney J. E, Mackie & McCartney practical medical microbiology. 14th ed. Churchill Livingstone 1996 <https://openlibrary.org>
- [17] Hendrik J. de Vries, Eva Kleibusch, Gerben D.A. Hermes, Paula van den Brink, Caroline M. Plugge „Biofouling control: the impact of biofilm dispersal and membrane flushing, *Water Research,*(2021)198: 117–163, <https://doi.org/10.1016/j.watres.2021.117163>.
- [18] Y. Qin, L.L. Angelini, Y. Chai, *Bacillus subtilis* cell differentiation, biofilm formation and environmental prevalence, *Microorganisms* 10 (2022) 1108, <https://doi.org/10.3390/microorganisms10061108>.
- [19] G.A. O'Toole, Microtiter dish biofilm formation assay, *J Vis Exp.* 47 (2011) 2437, <https://doi.org/10.3791/2437>. PMID: 21307833; PMCID: PMC3182663.
- [20] D. Zhao, S. Yu, B. Sun, S. Gao, S. Guo, K. Zhao, Biomedical applications of chitosan and its derivative nanoparticles, *Polymers* 10 (2018) 4, <https://doi.org/10.3390/polym10040462>.
- [21] Sedigh V ,Shahnaz R, Golozar, M. Saeed K , Mohammad M .K Mahdi.K . Effects of Some Parameters on Particle Size Distribution of Chitosan Nanoparticles Prepared by Ionic Gelation Method. *Journal of Cluster Science.* (2013) 24. 10.1007/s10876-013-0583-2
- [22] Khanmohammadi M, Elmizadeh H, Ghasemi K. Investigation of Size and Morphology of Chitosan Nanoparticles Used in Drug Delivery System Employing Chemometric Technique. *Iran J Pharm Res.* (2015) 14(3):665-75. PMID: 26330855; PMCID: PMC4518095.
- [23] L. Al-Naamani, S. Dobretsov, J. Dutta, J.G. Burgess, Chitosan-zinc oxide nanocomposite coatings for the prevention of marine biofouling, *Chemosphere* 168 (2017) 408–417, <https://doi.org/10.1016/j.chemosphere.2016.10.033>, Epub 2016 Oct 28 PMID: 27810541.
- [24] Pokhrel S, Lach R, Grellmann W, Wutzler A, Lebek W, Godehardt R, Yadav P.N . Adhikari R, Synthesis of Chitosan from Prawn Shells and Characterization of its Structural and Antimicrobial Properties Nepal Journal of Science and Technology (Nepal J Sci Tech) (2016), 17(1): 5–9
- [25] H. Tajik, M. Moradi, S.M.R. Rohani, A.M. Erfani, F.S.S. Jalali, Preparation of chitosan from brine shrimp (*Artemia urmiana*) cyst shells and effects of different chemical processing sequences on the physicochemical and functional properties of the product, *Molecules* 13 (2018) 1263–1274.
- [26] Vijayan T, Venkatesan S, Kasi G , Chinnasamy B, Marimuthu G Mothana, R Siddiqui R, S.N Jamal K Giovanni.B Single Step Fabrication of Chitosan Nanocrystals Using Penaeus semisulcatus: Potential as New Insecticides, Antimicrobials and Plant Growth Promoters. *J. Clust. Sci.* (2018) 29:2 DOI:10.1007/s10876-018-1342-1
- [27] M. Kalaivani, T. Maruthupandy, A.H. Muneeswaran, M. Beevi, C.M.R. Anand, A. K. Kumaraguru, Synthesis of chitosan mediated silver nanoparticles (Ag NPs) for potential antimicrobial applications, *Front. Lab. Med.* 2 (1) (2018) 30–35, <https://doi.org/10.1016/j.flm.2018.04.002>.
- [28] I. Banerjee, R.C. Pangule, R.S. Kane, Antifouling coatings: recent developments in the design of surfaces that prevent fouling by proteins, bacteria, and marine organisms, *Adv. Mater.* 23 (2011) 690–718, <https://doi.org/10.1002/adma.201001215>. [PubMed].
- [29] Saberpour, Masoumeh Peerayeh, Shahin, Evaluation of the Antimicrobial and Antibiofilm Effect of Chitosan Nanoparticles as Carrier for Supernatant of Mesenchymal Stem Cells on Multidrug-Resistant *Vibrio cholerae* Infection-and-drug-resistance-journal (2020) 13: 22151–2260 <https://doi.org/10.2147/IDR.S244990>
- [30] dos Santos, E.M.P., Martins, C.C.B., de Oliveira Santos, J.V. et al. Silver nanoparticles–chitosan composites activity against resistant bacteria: tolerance and biofilm inhibition. *J Nanopart Res* (2021) 23, 196 (2021). <https://doi.org/10.1007/s11051-021-05314-1>.



Development of value-added cookies supplemented with giloy and tulsi powder

Disha Sunil Gawade, Karuna Wasudeo Patil, Gavit Hemangi Jayram *

Rayat Shikshan Sansths's Annsaheb Awate College Manchar, Pune 410503, India

ARTICLE INFO

Article history:

Available online 26 December 2022

Keywords:

Giloy Powder
Tulsi powder
Wheat Flour
Cookies
Phytochemical

ABSTRACT

Medical plants are widely used in various industries like agriculture, cosmetics, pharmaceuticals, and food. In some pandemic situations, every-one focused on developing immunity. The best way to increase the nutritional value of a person's daily diet is through a variety of ayurvedic practices. In this research conducted, herbal biscuits were developed. Cookies are eaten worldwide so it is the largest confectionary product and it is suitable for all age groups. In the present work, cookies are especially replaced with jaggery, wheat flour, and milk. Giloy stem powder was optimized by replacing whole wheat flour 100gm with (0.5gm, 1gm, 1.5gm, 2gm, 2.5gm, 3gm, 3.5gm, 4gm) and Tulsi leaves powder ((0.5gm, 1gm, 1.5gm, 2gm, 2.5gm, 3gm, 3.5gm, 4gm). Then final 1.5gm of giloy stem powder and 3gm of tulsi leaves powder were finalized based on sensory score. Both herbal powders which is an effective anti-aging herb. It also nourishes the skin. It is an anti-bacterial, antiviral and anti-fungal property that protects from a variety of infections. The use of this herbal powder focuses on developing organic products for human consumption and medicament.

© 2022 Elsevier Ltd. All rights reserved.

Selection and peer-review under responsibility of the scientific committee of the Integrative Nanotechnology Perspective for Multidisciplinary Applications - 2022. All rights reserved.

1. Introduction

Cookies are a popular form of bakery snack consumed all over the world for taste as well as nutrition. With long shelf life they also have high sugar and fat content thereby providing healthy nutrients. [1]. Due to fat rich content, they are highly susceptible to rancidity or oxidation. Hence, the quality of food deteriorates leading to unpleasant flavor, negative impact on health, and economic devaluation [2].

Creating novel meals by incorporating functional ingredients into a carrier food, like cookies, gives food producers better marketing prospects [3]. The majority of these investigations concentrate on organic substances having a range of physiological functions. It is intriguing to employ these herbs as food supplements due to their rising consumption. These herbs can provide a potent biochemicals including antioxidants, antimutagens, anticarcinogens and so on. [4,5].

Tinospora cordifolia Miers (Wild.) belonging to family Menispermaceae, is called by various local names in India such as giloy,

guduchi, or amrita. Ayurveda and conventional medicine highly regard this species for its wonderful therapeutic efficacy. [6]. India is home to this big deciduous climbing shrub whose extract is used as a treatment for a variety of illnesses, such as diabetes and hepatitis. This ancient herb giloy is rich in various phytochemicals such as ascorbic acid, lycopene alkaloids, terpenoids, lignans, carotene, etc. [7].

According to reports, giloy have phytochemicals having potent cytotoxic and immune-modulating properties. They work by stimulating immune cells exhibiting i-tumor effects. They increase the phagocytic activity of macrophages and boosts the generation of nitric oxide. According to Ayurveda, eating giloy with jaggery is more effective and cures the majority of ailments thereby lengthening a person's life. [8].

Additionally, the stem of giloy is used to treat a number of viral disorders as well as fever, jaundice, emaciation, skin conditions, diabetes, and anaemia. The proximate analyses of stem of giloy are carried out using standard methods, while mineral elements were analyzed using Atomic Absorption Spectrophotometer, equipped with air acetylene flame [9]. Numerous fascinating results have been published following thorough phytochemical,

* Corresponding author.

E-mail addresses: dishagawade2010@gmail.com (D.S. Gawade), gavit.hemangi@gmail.com (G. Hemangi Jayram).

pharmacological, and clinical examinations into the substance [10].

The scented perennial plant *Ocimum sanctum* L. also known as tulsi, belongs to the Lamiaceae family. The medicinal relevance of these plants is due to their bioactive phytochemical components, which have specific physiological effects on the human body [11]. *Ocimum sanctum* has been used and is known as the “Queen of Herbs” since the beginning of Bangladesh’s ancient civilization. It has been employed in ayurvedic and traditional medicine since ancient times. Tulsi is grown for its aromatic leaves. Due to its numerous therapeutic characteristics, it has also significantly influenced contemporary study. The plant’s various parts have been proven to have antibacterial, anti-inflammatory, analgesic, antipyretic, antiulcer, antidiabetic, and anticancer properties. [12]. When coupled with vitamin C, tulsi has helpful antiviral and antibacterial properties. Tulsi leaves and jaggery are a great combo for treating viral infections of the digestive system as well as the common cold and flu. It is known to improve cardiovascular health, promote immunity, and speed up the healing process after infections [13].

Apart from many significant components present in plants, dietary fiber cannot be digested by human digestive enzymes present in the small intestine [14]. It is mostly a complex carbohydrate, is a crucial component of a balanced diet because it aids in the effective passage of food and waste through the digestive system. These are of two types, viz., soluble and insoluble dietary fibre. [15]. If the soluble dietary fibre is present in food, it dissolves in water and makes the passage of food slowly. It also aids in maintaining a healthy cholesterol level, normalizes blood sugar levels in diabetics, and may help reduce blood pressure. Gums and Pectins are examples of soluble fibers, and they are also found in herbs like Tulsi. [16].

Jaggery is frequently used in Indian families and boosts immunity. Minerals like zinc and selenium, which are known to have antioxidant properties, are found in jaggery [17].

Children in rural areas of developing countries like India are especially at risk since the food that is easily accessible to them does not support their ability to develop physically or to resist disease. According to research conducted by the Nutrition Monitoring Bureau and The National Institute of Nutrition in 12 Indian states, the rural population’s diets are inadequate and low in the majority of nutrients, including calories, vitamins, and other nutrients, particularly protein. [18].

2. Materials and methods

2.1. Materials

Refined wheat flour, jaggery, fat, baking powder, baking soda, and milk, were obtained from the local market of Manchar. Flavor powder was obtained from naturally giloy stem powder and tulsi leaves powder to prepared at the college level by using the tray dryer method. All chemicals and reagents used were of analytical grade.

2.2. Preparation of giloy stems powder

Giloy stems creeping over neem were collected and washed thoroughly. After the stem were washed under running water, disinfected for the rinsed. Giloy stem covering were removed manually or by using stainless steel knives and weighed to determine the yield. Material preparation and physico-chemical properties analyses were performed at the laboratory. After the weighed the giloy stem, was cut into small slices and then dried in a tray dryer

at 40 °C – 60 °C for 8 h and ground. The crushed material was sieved through a 50 mesh to obtain a powder. The giloy stem powder was again weighed to calculate the yield, then giloy stem powder was vacuum packed and stored at 4 °C for future analysis.

2.3. Preparation of tulsi leaves powder

Tulsi was collected near the farm of Manchar. It was washed under the running tap water and disinfected. Tulsi was weighed to determine the yield. Material preparation and Physico-chemical properties analyses were performed at the laboratory. After tulsi leaves were removed manually and then dried in a tray dryer at 40 °C – 65 °C for 24 h and grind. The crushed material was sieved through a 50 mesh to obtain a powder. The tulsi leaves powder was again weighed to calculate the yield, then tulsi leaves powder was vacuum packed and stored at 4 °C for future analysis.

2.4. Development of herbal cookies by supplementing giloy stem powder and tulsi leaves powder.

Herbal cookies were formulated using giloy stem powder and tulsi leaves powder. Giloy stem and tulsi leaves were collected from the college campus. They were further processed and used as ingredients for development of herbal cookies. Giloy stem powder, tulsi leaves powder, wheat flour, milk, baking soda, baking powder and salt was used as raw material for development of herbal cookies. See Fig. 1

3. Result and discussion

3.1. Optimization and development of herbal cookies

In the case of final cookies wheat flour, fat, baking powder, baking soda, salt, and milk, were kept constant while giloy stem powder was optimized by replacing whole wheat flour 100gm with (0.5gm, 1gm, 1.5gm, 2gm, 2.5gm, 3gm, 3.5gm, 4gm) Then final 1.5gm of giloy stem powder (trial 3) was finalized based on the sensory score. (Table 1).

Tulsi leaves powder was optimized by replacing whole wheat flour 100gm with ((0.5gm, 1gm, 1.5gm, 2gm, 2.5gm, 3gm, 3.5gm, and 4gm). The final 3 gm of tulsi stem powder (trial 6) was finalized based on the sensory score (Table 2). So sensory evaluation was done with the 1.5 % incorporation of giloy stem powder or 3 % of tulsi leaves. The powder was used development of herbal cookies. The prepared cookies were baked at 160 °C at the top and 150 °C at the bottom for 25 min in the baking oven. The baked cookies are cooled at room temperature and packed in LDPE and HDPE pouches for another analysis. Cookies were prepared with whole wheat flour to serve as a control.

3.2. Quality characteristics of cookies:

3.2.1. Physical analysis of cookies

The physical properties of Before and After cookies were analyzed for their weight using a balance (ELB3000, Shimadzu, Japan), and the Thickness(T) of the cookies (distance between top to the bottom surface of cookies) and Width(W) (distance across the cookies) were determined using Vernier caliper.

Giloy stem powder and tulsi leave powder in the herbal cookies were analyzed for weight, Diameter, thickness, and spread ratio, by following the respective procedures (AACC, 2000). [19].

Spread ratio – The spread ratio of baked cookies was determined by the ratio of width and ratio of thickness.

$$SF = W/T$$

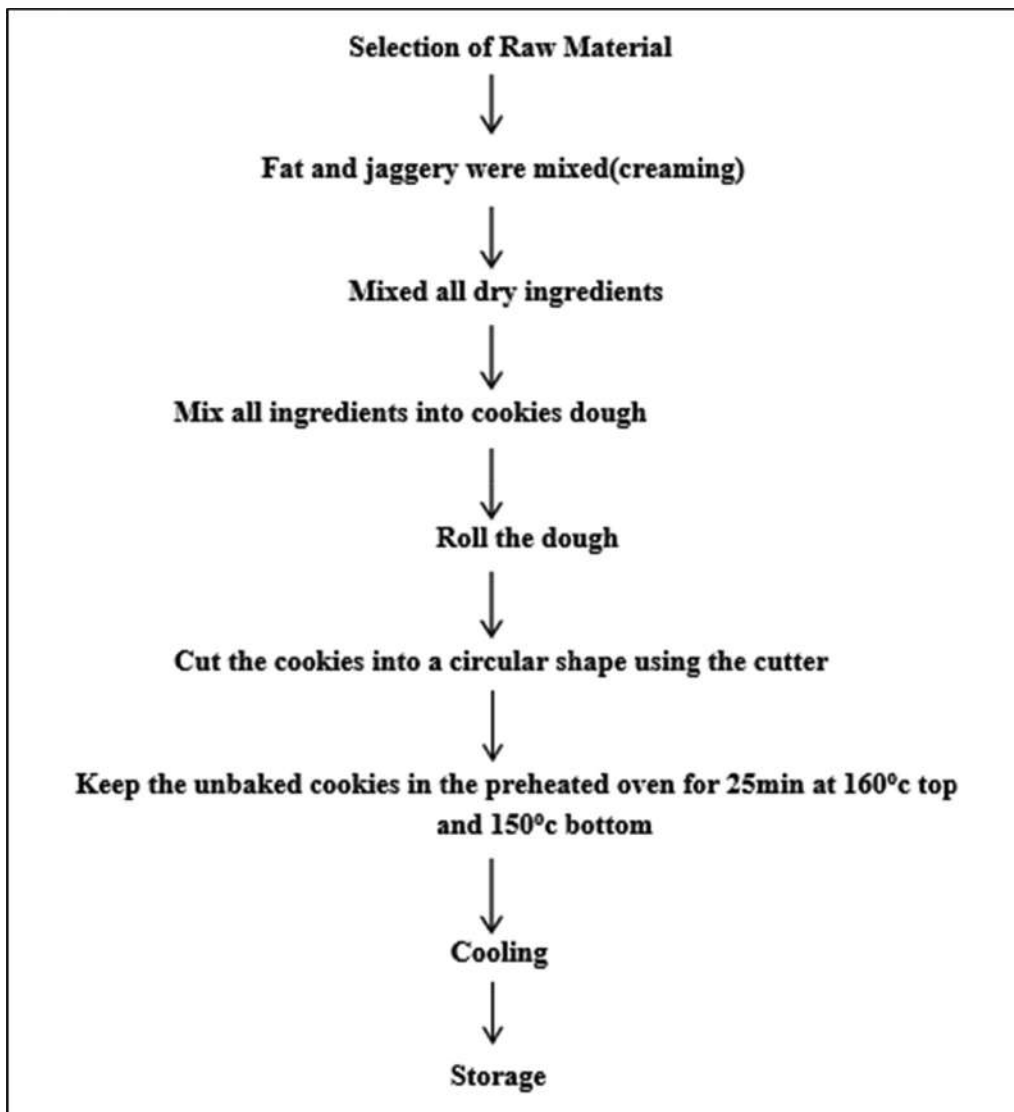


Fig. 1. Flowchart of preparation of cookies.

Table 1
Optimization of cookies based on Giloy stem powder.

Materials	T1	T2	T3	T4	T5	T6	T7	T8
Wheat flour	100	100	100	100	100	100	100	100
Fat	70	70	70	70	70	70	70	70
Baking soda	2	2	2	2	2	2	2	2
Baking powder	2	2	2	2	2	2	2	2
Milk	43	43	43	43	43	43	43	43
Salt	0.5	0.5	0.5	0.5	0.5	0.5	0.5	0.5
Giloy powder	0.5	1	1.5	2	2.5	3	3.5	4
Tulsi powder	3	3	3	3	3	3	3	3

Table 2
Optimization of cookies based on tulsi leaves powder.

Materials	T1	T2	T3	T4	T5	T6	T7	T8
Wheat flour	100	100	100	100	100	100	100	100
Fat	70	70	70	70	70	70	70	70
Baking soda	2	2	2	2	2	2	2	2
Baking powder	2	2	2	2	2	2	2	2
Milk	43	43	43	43	43	43	43	43
Salt	0.5	0.5	0.5	0.5	0.5	0.5	0.5	0.5
Giloy powder	1.5	1.5	1.5	1.5	1.5	1.5	1.5	1.5
Tulsi powder	0.5	1	1.5	2	2.5	3	3.5	4

Results of the physical analysis of before and after cookies are shown in (Table 3) (Figs. 2,3). The product parameters like weight, thickness, width, spread ratio, and spread factor in the case of cookies have a direct relation to product uniformity, quality, and consumer acceptance [20]. The quality of cookies is widely determined by the spread factor. As shown in (Table 3). The highest spread ratio before cookies is (5.2) and the lowest spread ratio after cookies is (4.3).

3.3. Sensory evaluation of cookies:

Sensory evaluation of cookies added with giloy stem powder was done and the results were noted. (Table 4). The sample prepared by using 100 g whole wheat flour, 45 ml milk, 0.5 g salt, 2 g baking powder, 2 g baking soda, 50 g jaggery, and 70 g fat was used control sample. Baking this formulation at 160°C top and 150°C bottom for 25 min was used as a control procedure. The whole wheat flour was replaced with giloy stem powder at a level (0.5gm, 1gm, 1.5gm, 2gm, 2.5gm, 3gm, 3.5gm, and 4gm) of from the results of a sensory analysis it was observed that flavor, color, and the taste was affected significantly by addition 1.5gm of giloy stem powder selected.

Sensory evaluation of cookies added with tulsi powder was done and the results were noted. (Table 5). The sample prepared by using 100 g whole wheat flour, 45 ml milk, 0.5 g salt, 2 g baking powder, 2 g baking soda, 50 g jaggery, and 70 g fat was used control sample. Baking this formulation at 160°C top and 150°C bottom for 25 min was used as a control procedure. The whole wheat flour was replaced with tulsi stem powder at a level (0.5gm, 1gm, 1.5gm, 2gm, 2.5gm, 3gm, 3.5gm, and 4gm) of from the results of a sensory analysis it was observed that flavor, color, and taste were affected significantly by the addition of 3gm of Tulsi leaves powder selected.

3.4. Proximate composition of herbal Cookies:-

The proximate composition of refined wheat flour, giloy stem powder, and tulsi leaves powder was estimated using standard AACC methods [21]. Moisture: Estimation of moisture content is determined by using the hot air oven method at 105°C for 4 hrs. (AOAC, 1995). [21].

Ash: By using the muffle furnace method up to constant weight. Ignite in a muffle furnace at 550+/- 250c for 4 hrs. [22].

Fat: Extracting the sample in a Soxhlet apparatus for 6-8h using petroleum ether. The solvent is evaporated and the residue is weighed [22].

3.5. Shelf life study of prepared cookies:

The prepared cookies were packed in PP and LDPE bags at room temperature for the shelf life study (Fig. 4). The moisture content of cookies was analyzed at a regular interval of 15 days along with sensory analysis. Results summarized in the Sensory evaluation showed that prepared cookies were of good quality throughout the storage period. The sensory quality mainly in terms of taste

Table 3 Physical analysis of before and after cookies.

Parameter	Before cookies	After cookies
Weight	14.80	15.82
Thickness	5.2	6.1
Width	1.0	1.4
Spread ratio	5.2	4.3



Fig. 2. Cookies before baking.



Fig. 3. Cookies after baking.

Table 4 Sensory evaluation of giloy stem powder.

Attribute	Sensory Score								
	GP 0	GP 1	GP 2	GP 3	GP 4	GP 5	GP 6	GP 7	GP 8
Color	7	7	7.5	8.5	8	7.5	7	7.2	6.5
Texture	7.5	7.5	8	8	8	8	8	8	8
Taste	8	7.5	7.7	8.3	7.5	7	7.2	6.5	6
Flavor	7.5	7.5	8	8.5	8	7.5	7	6.5	6
Overall	7.5	7.3	7.8	8.3	7.8	7.5	7.3	7	6.6
Acceptability									

Table 5 Sensory evaluation of Tulsi leaves powder.

Attribute	Sensory Score								
	TL 0	TL 1	TL 2	TL 3	TL 4	TL 5	TL 6	TL 7	TL 8
Color	7	7	7.5	8	8	7.5	8.5	7.2	6.5
Texture	7.5	7.5	8	8	8	8	8	8	8
Taste	8	7.5	7.7	7.6	7.5	7	8.7	6.5	6
Flavor	7.5	7.5	8	7	8	7.5	8.5	6.5	6
Overall	7.5	7.3	7.8	8.2	7.8	7.5	8.5	7	6.6
Acceptability									

was decreased to some extent but the product was acceptable. There was a gradual increase in the moisture content during the storage period.



Fig. 4. Value added cookies supplemented with giloy powder and tulsi powder.

4. Conclusion

The use of giloy stem powder and tulsi leaves powder is partially replaced by whole wheat flour in the preparation of herbal cookies. They are supplemented with nutritional properties such as anti-cancer, anti-inflammatory, antioxidant, and anti-microbial properties and the richness of dietary fibers.

The found sensory evaluation, textural and color properties that the overall acceptability of 1.5 % giloy stem powder and 3 % of tulsi leaves powder based on herbal cookies. The herbal cookies are suitable for the best nutritional value as well as sensory score.

Ayurveda has several advantages in India. It helps the body digest food more easily while also preventing some illnesses and infections. In a pandemic emergency, every-one concentrates on building their body's energy and immune system in order to make herbal cookies that are both good for testing and beneficial to our health. Every generation consumes cookies on a daily basis, which is a terrific way for some medicinal components to originate from our bodies or our food.

Although the sensory evaluation of the prepared value-added cookies supplemented with giloy and tulsi powder have good acceptability rate, it is also important to analyze the composition of final product.

CRedit authorship contribution statement

Gawade Disha Sunil: Data curation, Investigation. **Patil Karuna Wasudeo:** Conceptualization, Methodology, Supervision. **Gavit Hemangi Jayram:** Visualization, Investigation.

Data availability

Data will be made available on request.

Declaration of Competing Interest

The authors declare that they have no known competing financial interests or personal relationships that could have appeared to influence the work reported in this paper.

References

- [1] L.C. Okpala, E.C. Okoli, Development of cookies made with cocoyam, fermented sorghum, and germinated pigeon pea flour blends using response surface methodology, *J. Food Sci. Technol.* 51 (10) (2012) 2671–3267.
- [2] J. Ullah, M. Humayun, T. Ahmad, M. Ayub, M. Zarafullah, Effect of light, natural and synthetic antioxidants on stability of edible oil and fats, *Asian Journal Plant Science.* 2 (17–24) (2003) 1192–1194.
- [3] R. Krutulyte, K.G. Grunert, J. Scolderer, L. Lähteenmääki, K.S. Hagemann, P. Elgaard, B. Neilsen, J.P. Graverholt, Perceived Fit of Different Combinations of Carriers and Functional Ingredients and Its Effect on Purchase Intention, *Food Qual. Prefer.* 22 (2011) 11–16.
- [4] C.J. Dillard, J.B. German, *Phytochemicals: Nutraceuticals and Human Health*, *J. Sci. Food Agric.* 80 (2000) 1744–1756.
- [5] V.J. Sharma, P.M. Patel, Evaluation of Antibacterial Activity of Methanolic Extract of Plant *Rivea Ornata*, *International Research Journal of Pharmacy* 4 (2013) 233–234.
- [6] L.N. Sankhala, R.K. Saini, B.S. Saini, A review on chemical and biological properties of *Tinospora Cordifolia*, *Int J Med AromatPlants* 2 (2012) 340–344.
- [7] P. Srivastava, Study of medicinal properties of herb *Tinospora cordifolia* (Giloy) in preventing various diseases/abnormalities by increasing immunity naturally in human bodies, *Int. J. Eng. Res. and Gen. Sci.* 8 (4) (2020) 10–14.
- [8] S. Saha, S. Ghosh, *Tinospora Cordifolia: One plant, many roles*, *Anc. Sci. Life* 31 (4) (2012) 151–159, <https://doi.org/10.4103/0257-7941.107344>.
- [9] A.K. Sharma, M. Tafazul, Y. Badkhane, D.K. Raghuvanshi, A review on *Adhatodavasica* Nees- An important and high demanded medicinal plant, *Indo American Journal of Pharmaceutical Research* 2 (2014) 2231–6876.
- [10] A.K. Nadkarni, *Indian Materia Medica*, 3 edn., M/s Popular Prakashan Pvt Ltd, Bombay, 2005, p. 1(II).
- [11] C.A. Akinmoladun, E.O. Ibukun, E.M. Obuotor, E.O. Farombi, Phytochemical constituent and antioxidant activity of extract from leaves *Ocimum gratissimum*, *Science Research Essay* 2 (2007) 163–166.
- [12] R. Maheshwari, B. Rani, R.K. Yadav, M. Prasad, "Usage of Holy Basil for Various Aspects" (2012). *Bull. Env. Phar. and Life Sci.* 1: 63 – 65.
- [13] R.K. Upadhyay, *Tulsi: A holy plant with high medicinal and therapeutic value*, *Int. J. Green Pharma.* 11 (1) (2017) S1–S12.
- [14] *Dietary Fiber*. The University of California, Berkeley Bancroft Way Berkeley, CA 9472.
- [15] D.J.A. Jenkins, T.M.S. Wolever, A.R. Leeds, et al., *Dietary fiber, Fiber Analogues, and Glucose Tolerance: Importance of Viscosity*. 1 (1978) 1392–1394p.
- [16] S. Holt, R.C. Heading, D.C. Carter, et al., Effect of gel fiber on gastric emptying and absorption of glucose and paracetamol, *Lancet* 1 (1979) 636–639p.
- [17] A.K. Shrivastava, P. Singh, *Jaggery (Gur): The Ancient Indian Open-pan Non-centrifugal Sugar*. In: Mohan N, Singh P (eds) *Sugar and Sugar Derivatives: Changing Consumer Preferences*. Springer, Singapore, 2020, pp 283–307 https://doi.org/10.1007/978-981-15-6663-9_19.
- [18] K. Vijayaraghavan, H.D. Rao, *Diet and nutrition situations in rural India*, *IndJMed Res* 108 (1998) 243–253.
- [19] AACC, *Approved Methods of the American Association of Cereal Chemists*, America Association of Cereal Chemists. Inc., St. Paul, Minnesota, 2000.
- [20] A. Chauhan, D. Saxena, S. Singh, Total dietary fiber and antioxidant activity of gluten-free cookies made from raw and germinated amaranth (*Amaranthus spp.*) flour, *LWT Food Sci. Technol* 63 (2) (2015) 939–945.
- [21] AOAC, *Official methods of analysis*, 16th ed., Association of Official Analytical Chemists, Washington, DC, 1995, pp. 27–29.
- [22] S. Rangana, *Hand Book of Analysis and Quality Control for the Fruit and Vegetable Products*, Tata McGraw Hills Limited New Delhi, 1986.



Structural, morphological and anti - bacterial activities of pure SnO₂ nanoparticles prepared by chemical precipitation method

S. Abirami^a, G. Viruthagiri^{b,*}, K. Ashokkumar^c

^a Department of Physics, R&D centre, Bharathiar University, Coimbatore, Tamilnadu, India

^b Department of Physics, Annamalai University, Annamalaiagar, Chidambaram 608 002, Tamilnadu, India

^c Department of Physics, V.R.S college of Engineering and Technology, Arasur 607107, Villupuram, Tamilnadu, India

ARTICLE INFO

Article history:

Available online 19 December 2022

Keywords:

Tin oxide

Antibacterial activity

SnO₂ nanoparticles

XRD

SEM-EDX

ABSTRACT

The tin oxide (SnO₂) nanopowders were synthesized by a simple chemical method (precipitation). The sample was studied for XRD, FESEM, and EDX analyses. The XRD results of synthesized SnO₂ nanoparticles exhibited a tetragonal structure with an average crystallite size of 18.79 nm. The FE-SEM exhibited the microstructure of the prepared nanoparticles. The FESEM images reveal that the shape of the prepared product was spherical. The impact of SnO₂ NPs on food and water poisoning growth was investigated with the help of antibacterial activities. This paper deals with the properties and applications of tin oxide nanostructures. Antibacterial activity was carried out against three bacterial strains: *Bacillus subtilis*, *Escherichia Coli*, and *Pseudomonas aeruginosa*.

Copyright © 2022. Elsevier Ltd. All rights reserved.

Selection and peer-review under responsibility of the scientific committee of the Integrative Nanotechnology Perspective for Multidisciplinary Applications - 2022.

1. Introduction

Researchers are attracted to nanostructured materials due to their size-dependent physical, chemical, and energy properties which are ideal candidates for novel applications [1]. Particle sizes and shapes are mainly important in nanomaterial applications [2]. As a result, these materials are considered the most promising and suitable for use in data storage, sensing devices, electronics, and biomedical applications that change their electrical, optical, and magnetic properties [3]. Many researchers have reported that in the medical field, SnO₂ applications are used as a material with antibacterial capabilities [4]. SnO₂ as a stable material, is broadly used in various biological, electrochemical, photocatalytic, and antibacterial applications [5–7]. In addition, SnO₂ nanoparticles have excellent anti-bacterial activity and can be widely used in nanomedicine. The application of anti-bacterial activity is much wider and more effective globally. Hence, SnO₂ has received much recognition in the paramedical and biomedical fields [8]. The development of nanomaterials as antibacterial agents is the most difficult due to their stability and eco-friendly nature when compared to other organic antibacterial agents [5,9–11]. Bacterial cell membrane integrity is altered due to these

interactions, and toxic free radicals are released, causing oxidative stress [12–14]. The antibacterial efficiency of metal oxide NPs is influenced by particle size, light, and the composition of the aqueous medium used in the assay, among other factors. The pure SnO₂ nanoparticles revealed outstanding antibacterial activity of the product.

2. Experimental techniques

2.1. Preparation of pure SnO₂ nanoparticles

All chemicals were procured from (AR) grade (99 % purity). For pure SnO₂, 0.5 M SnCl₂·2H₂O was dissolved in 50 ml of deionized water and then stirred vigorously using a magnetic stirrer. Then, 1 M of oxalic acid (C₂H₂O₄·2H₂O) was dissolved in 50 ml of deionized water. The above solution was heated at 60 °C then continuously stirred for 4 h. The precipitate sample was formed in a pale white color. After the precipitate product was washed subsequently with deionized water and then filtered. The purified sample was dried at 100 °C for 1 h and annealed at 400 °C in for 3 h.

2.2. Characterization techniques

The successfully synthesized nanoparticles were characterized by XRD (SHIMADZU-6000) and SEM, (JSM-6360LA) to study the

* Corresponding author.

E-mail address: gvgiri2002@gmail.com (G. Viruthagiri).

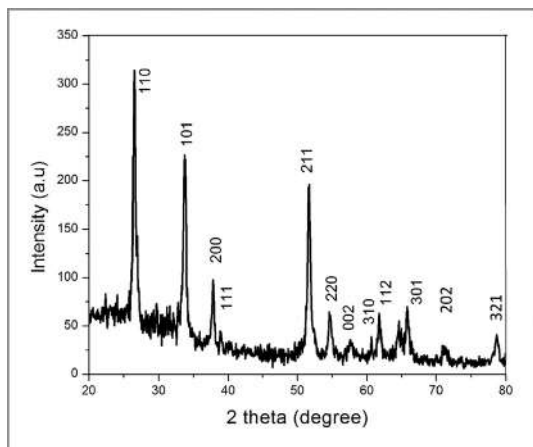


Fig. 1. XRD patterns of as synthesized SnO₂ nanoparticles.

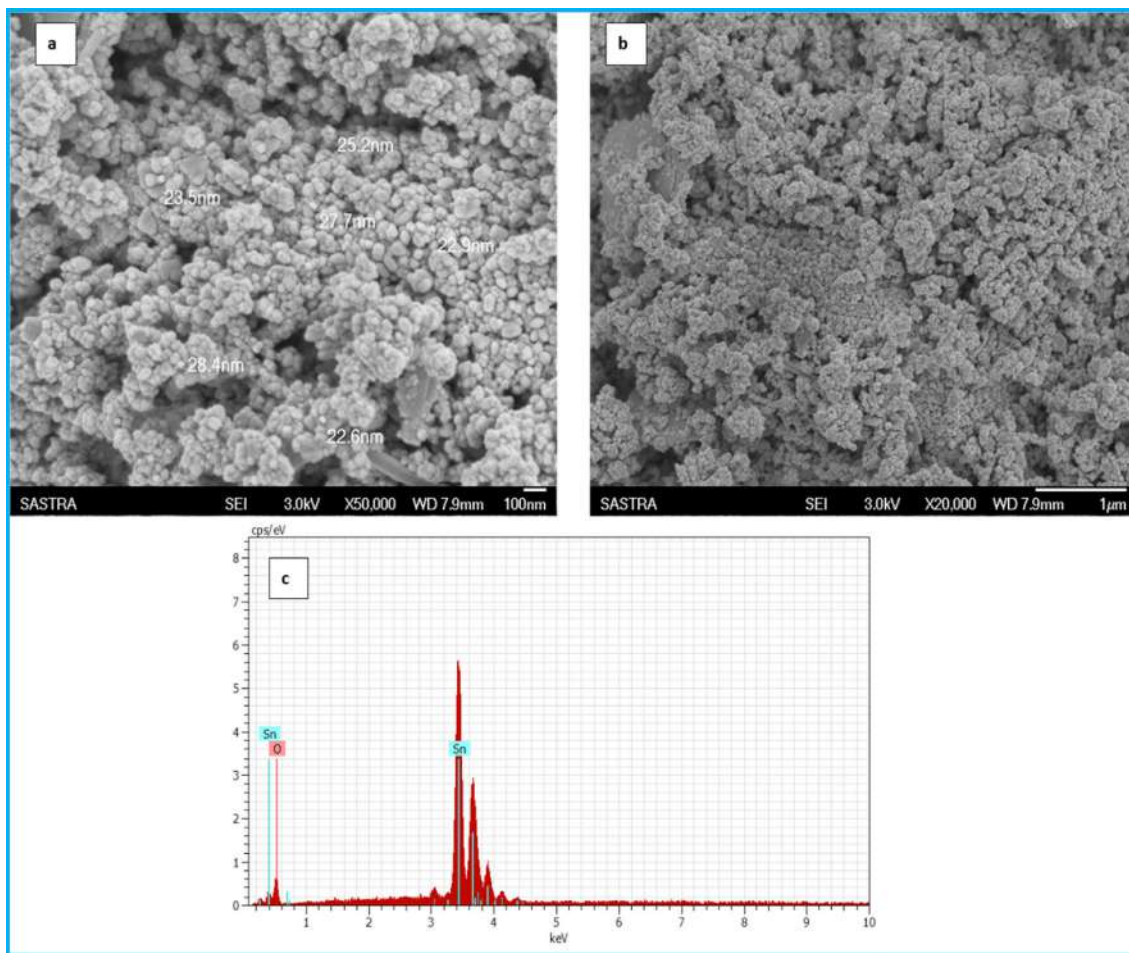
crystal nature and morphology of the product. The elemental composition of the prepared sample was analyzed by using EDAX. Further, the antibacterial activity of the synthesized SnO₂ nanoparticles was tested using the Kirby-Bauer disc diffusion method against *Bacillus subtilis*, *Escherichia coli*, and *Pseudomonas aeruginosa*. These cultures were procured from the Medical Microbiology Department (RMMCH), Annamalai University, Tamilnadu.

3. Results and discussion

3.1. Structure and morphology analysis

The X-ray diffraction technique was employed to study structural parameter values of the as-prepared SnO₂ nanoparticles at 400 °C for 3 hr. The XRD pattern is shown in Fig. 1.

All the diffraction patterns confirmed the tetragonal rutile crystalline phases of tin oxide nanoparticles with predominant peaks, corresponding to the indices (110), (101), (200), and (211) in



Spectrum: sample 5216

El	AN	Series	unn. C	norm. C	Atom. C	Error (1 Sigma)
[wt.%]	[wt.%]	[at.%]		[wt.%]		
O	8	K-series	12.89	14.00	54.70	3.48
Sn	50	L-series	79.20	86.00	45.30	2.45
Total:			92.09	100.00	100.00	

Fig. 2. FESEM images of bare SnO₂ (a, b) with different magnification and c) EDAX spectrum of SnO₂ nanoparticles.

these directions of preferential growth. The obtained XRD pattern is in excellent agreement with (JCPDS 41–1445) (space group $P4_2m$). There are no impurity phases observed in the as-prepared sample (SnO_2). The diffraction peaks intensity becomes sharper and narrower as synthesized SnO_2 product. The particle size effect and lattice strain are two possible mechanisms for presenting the narrowing peaks. The average crystallite size of the product was calculated by the Debye - Scherrer equation [15].

$$D = \frac{k\lambda}{\beta \cos \theta} \quad (1)$$

Where k is the shape factor, λ is the wavelength of Cu- α radiation ($\lambda = 1.5406 \text{ \AA}$), θ is the diffraction Bragg's angle, β is the full width at half maximum.

The obtained average crystal size of the SnO_2 nanoparticles was found to be 18.79 nm. The lattice parameters 'a' and 'c' for the tetragonal structure ($a = b \neq c$, $\alpha = \beta = \gamma = 90^\circ$) calculated from the following formula [16]

$$\frac{1}{d^2} = \frac{h^2 + k^2}{a^2} + \frac{l^2}{c^2} \quad (2)$$

Where h , k , and l are the miller indices of the peaks from the values of 'a' and 'c', the unit cell volume (V) can be determined. The calculated lattice parameters of the tin oxide nanoparticles are $a = b = 4.7573 \text{ \AA}$, $c = 3.1928 \text{ \AA}$, and volume is 72.2617 \AA^3 are in good agreement with the literature values.

Fig. 2 shows FE-SEM photographs of pure SnO_2 nanoparticles. The surface morphological result outcome is shown in Fig. 2 (a-b). Fig. 2 (a-b) shows that the spherical-shaped SnO_2 nanoparticles have a nearly uniform size with a slightly aggregated state [17–19]. The size distribution of the particles in the FE-SEM images, we find a mean particle size of approximately 23 nm is in very good agreement with our XRD data discussed above. The corresponding EDAX spectrum Fig. 2 (c) shows the direct information regarding the peaks of tin (Sn) and oxygen (O). The EDX spectrum confirms the existence of the tin and oxygen elements. The oxygen component (atomic percentage) in the developed sample is almost double that of tin, confirming the chemical composition to be SnO_2 . As such, the EDX studies confirm the successful distribution of the dopant metals in the SnO_2 nanoparticles. Important to note are the Cu $K\alpha$ and $L\alpha$ peaks at 8.04 and 0.93 eV, respectively, from the sample slides. The EDX-mapping reveals that the Cu is mostly detected from the areas on the wafer with sparse distribution of the nanoparticles (Not shown in fig i.e, additional peak), consistent with these peaks arising from the Cu-covered Si wafer. The Si peaks in the spectra probably arise from wafer particulates or the tweezers used to handle the samples.

3.2. Antibacterial activity

The antibacterial activity of SnO_2 NPs was tested on *P. aeruginosa*, *E. Coli*, and *B. Subtilis*. The presence or absence of bacterial growth around the disc can therefore be used to determine the bacterial susceptibility to the test nonmaterial. The degree of antibacterial efficacy of the test compound can then be indirectly



Fig. 3. Antibacterial activity of SnO_2 NPs against *Bacillus subtilis*, *Escherichia coli* and *Pseudomonas aeruginosa*.

determined by calibrating the diameters of the inhibition zone (ZOI) around the disc.

Table 1 displays the measured zone of inhibition values that were found to be positive results against all the tested pathogens when compared to ciprofloxacin (control). The bacterial strains were tested against various concentrations of 50, 100, and 200 mg. The zone of inhibition varied from 8 to 12 mm against all the pathogens. The lowest inhibition zone was achieved at 50 mg, whereas the highest inhibition zone was achieved at 200 mg of SnO_2 nanoparticles. When concentrations were increased, the inhibition zone also increased. It can be seen clearly in Fig. 3. The synthesized SnO_2 nanoparticles were effective in a dose-dependent manner. The presence of inhibitory growth clearly demonstrated that the biocidal action of SnO_2 NPs involves membrane disturbance with a high rate of surface oxygen species production, which ultimately leads to pathogenic agent death [20]. Metal oxide nanoparticles have a high surface area responsible for their increased chemical and biological activity. Compared to bacteria, which are more active than vitamins and antibiotics in our daily food. Doctors may recommend a higher dose for the body, which is a chemically synthesized medicine that kills bacteria and may cause side effects or other health issues. The synthesized nanoparticles do not have any side effects on human pathogens or good medicine. The excellent antibacterial activity results were revealed by the disc diffusion method—zone of inhibition [21,22]. Thus, SnO_2 NPs may be utilized as possible antibacterial agents by increasing resistance to traditional bactericides in treating bacterial diseases. Table.1 shows antibacterial results for the different bacteria used against SnO_2 NPs.

4. Conclusion

The successfully synthesized SnO_2 nanoparticles by chemical precipitation method. The results of XRD confirmed that the bare- SnO_2 nanoparticles were crystalline in nature with a tetragonal structure. FESEM studies confirmed the spherical-like morphology of synthesized SnO_2 nanoparticles. In the present study, good results for antibacterial activities were exhibited by the prepared SnO_2 nanoparticles for use and found potential applications in the medical field.

Table 1

The effect of synthesized SnO_2 NPs against the growth of different bacterial pathogens tested.

Sl. No.	Pathogens	Different Concentrations			Control
		50 μg	100 μg	200 μg	
		Zone of inhibition in diameter (mm)			
1.	<i>P. aeruginosa</i>	8	11	12	22
2.	<i>E. Coli</i>	8	11	12	19
3.	<i>B. Subtilis</i>	8	11	12	14

CRedit authorship contribution statement

S. Abirami: Conceptualization, Formal analysis, Writing – original draft. **G. Viruthagiri:** Supervision, Validation, Visualization, Writing – review & editing. **K. Ashokkumar:** Investigation, Visualization.

Data availability

The data that has been used is confidential.

Declaration of Competing Interest

The authors declare that they have no known competing financial interests or personal relationships that could have appeared to influence the work reported in this paper.

References

- [1] S. Patnaik, D.P. Sahoo, K. Parida, *Renew. Sustain. Energy Rev.* **82** (2018) 1297–1312.
- [2] M. Tadic, D. Trpkov, L. Kopanja, S. Vojnovic, M. Panjan, *J. Alloy. Compd.* **792** (2019) 599–609.
- [3] Tibayan Jr, Eduardo B and Muffikhun, Muhammad Akhsin and Kumar, Vipin and Fisher, Christine and Al Rey, C Villagrancia and Santos, Gil Nonato C, *Ain Shams Engineering Journal*.11 (2020) 767–776
- [4] S. Dong, L. Cui, Y. Tian, L. Xia, Y. Wu, J. Yu, D.M. Bagley, J. Sun, M. Fan, *J. Hazard. Mater.* **399** (2020).
- [5] S. Matussin, M.H. Harunsani, A.L. Tan, M.M. Khan, *ACS Sustain. Chem. Eng.* **8** (2020) 3040–3054.
- [6] H.M. Lwin, W. Zhan, S. Song, F. Jia, J. Zhou, *Chem. Phys. Lett.* **736** (2019).
- [7] Thangavel, K and Roshini, T and Balaprakash, V and Gowrisankar, P and Sudha, S and Mohan. Mahitha, *Materials Today: Proceedings*,33 (2020)2160–2166
- [8] E. Fortunati, A. Mazzaglia, G.M. Balestra, *J. Sci. Food Agric.* **99** (2019) 986–1000.
- [9] P. Gnanamozihi, V. Renganathan, S.-M. Chen, V. Pandiyan, M.A. Arockiaraj, N.S. Alharbi, S. Kadaikunnan, J.M. Khaled, K.F. Alanzi, *Ceram. Int.* **46** (2020) 18322–18330.
- [10] Y. Zhong, H. Xiao, F. Seidi, Y. Jin, *Biomacromolecules* **21** (2020) 2983–3006.
- [11] J.C. Ontong, S. Paosen, S. Shankar, S.P. Voravuthikunchai, *J. Microbiol. Methods* **165** (2019).
- [12] Xin, Qi and Shah, Hameed and Nawaz, Asmat and Xie, Wenjing and Akram, Muhammad Zain and Batool, Aisha and Tian, Liangqiu and Jan, Saad Ullah and Boddula, Rajender and Guo, Beidou and others, *Advanced Materials*.31(2019) 1804838.
- [13] R.K. Kankala, W.-Z. Lin, C.-H. Lee, *Nanomaterials* **10** (2020) 597.
- [14] K. Li, J. Qian, P. Wang, C. Wang, X. Fan, B. Lu, X. Tian, W. Jin, X. He, W. Guo, *Environ. Sci. Technol.* **53** (2019) 4542–4555.
- [15] Kumar, Shalendra and Sharma, Mayuri and Aljawfi, RezaqNaji and Chae, KH and Kumar, Rajesh and Dalela, Sourabh and Alshoaibi, Adil and Ahmed, Faheem and Alvi, PA, *Journal of Electron Spectroscopy and Related Phenomena*.240 (2020)146934.
- [16] Blessi, S and Manikandan, Ayyar and Anand, S and Sonia, MML and Vinoseel, V Maria and Paulraj, P and Slimani, Y and Almessiere, MA and Iqbal, M and Guner, S and others, *Materials Chemistry and Physics*.273(2021)125122.
- [17] Blessi, S and Manikandan, Ayyar and Anand, S and Sonia, MML and Vinoseel, V Maria and Paulraj, P and Slimani, Y and Almessiere, MA and Iqbal, M and Guner, S and others, *Materials Chemistry and Physics*.273(2021) 125122.
- [18] Subbarao, P Srinivasa and Aparna, Y and Chitturi, Kanchana Latha, *Materials Today: Proceedings*.26(2020)1676–1680.
- [19] R.A. Nachiar, S. Muthukumar, *Opt. Laser Technol.* **112** (2019) 458–466.
- [20] R. Pandiyan, S. Mahalingam, Y.-H. Ahn, *J. Photochem. Photobiol. B Biol.* **191** (2019) 18–25.
- [21] S.K. Evstropiev, A.V. Karavaeva, M.A. Petrova, N.V. Nikonorov, V.N. Vasilyev, L.L. Lesnykh, K.V. Dukelskii, *Mater. Today Commun.* **21** (2019).
- [22] Khan, Shakeel Ahmad and Kanwal, Sadia and Rizwan, Komal and Shahid, Sammia, *Microbial pathogenesis*.125(2018)366–384.

Call for Papers

- Insightful papers with theme of conference at the focal point are invited.
- The abstract should include **title of the paper, Authors name, affiliation and correspondence address with email id.**
- Abstract (limited to 300 words, in MS word format, Times New Roman, Font Size 12 & 1.5 line spacing) should be send to E-Mail awateannasaheb@gmail.com **by December 31, 2021.**
- Selected authors will be communicated to submit soft copy of full paper in A4 size in MS word format, Times New Roman, Font Size 12 with 1.5 line spacing and send to E-Mail: awateannasaheb@gmail.com **by January 05, 2022.**
- The selected reviewed papers will be published in an international journal/ UGC Care listed journal with ISSN number.
- Paper will be accepted only when it has not been published, copyrighted, presented or accepted elsewhere.

Important Dates

Conference Dates : **January 16-18, 2022**

Commencement of abstract submission : **December 01,2021**

Last date of abstract submission: **December 31,2021.**

Last date of paper submission: **January 05,2022**

Oral/Poster submission date: **January 05,2022**

Acceptance Notification: **January 10,2022**

Overseas Key Note Speakers

Dr. Seeram Ramakrishna, National University of Singapore

Prof. Ganpati Ramanath, Rensselaer Polytechnic Institute, Troy, NY

Prof. Animesh Jha, University of Leeds, UK

Dr. Matjaz Valant, University of Nova Gorica, Slovenia

Dr. Katia Vutova, Bulgarian Academy of Science, Bulgaria

Dr. Toshihiro Moriga, Tokushima University, Japan

Dr. Taesung Kim, Sungkyunkwan University, South Korea

Dr. Nanasaheb Thorat, Marie Curie Fellow, Oxford University, UK

Dr. Anna Axelsson, London South Bank University, London

Dr. Ashok Joshi, University Utah, USA

Dr. Jin Ook Baeg,

Korea Research Institute of Chemical Technology, South Korea

Dr. Haiwon Lee, Professor, Hanyang University, South Korea

Prof. Venkatesan Renugopalakrishnan, Scientist,

Harvard/Northeastern University, Boston, US.

Advisory Committee

Dr. Ashok Joshi, University Utah, USA

Dr. Seeram Ramakrishna, National University of Singapore

Dr. Shivajirao Kadam, Chancellor, Bharati Vidyapeeth, Pune

Prof. Dr. Nitin Karmalkar, Vice Chancellor, SPPU, Pune

Dr. S. F. Patil, Former Vice Chancellor, NMU, Jalgaon

Dr. R. S. Mali, Former Vice Chancellor, NMU, Jalgaon

Dr. G. D. Yadav, Former Vice Chancellor, ICT, Mumbai

Prof. Animesh Jha, University of Leeds, UK

Dr. D. P. Amalnekhar, Hanyang University, South Korea

Dr. B. B. Kale, C-MET, India

Prof. Dr. Manohar Chaskar, Dean, Sci. & Tech.SPPU, Pune

Dr. Goutam Mukhopadhyay, MAKA University, Kolkata

Dr. Chinnakonda Gopinath, Chief Scientist, NCL.Pune

Dr. Angshuman Nag, IISER, Pune

Dr. P. S. Patil Pro Vice Chancellor, Shivaji University

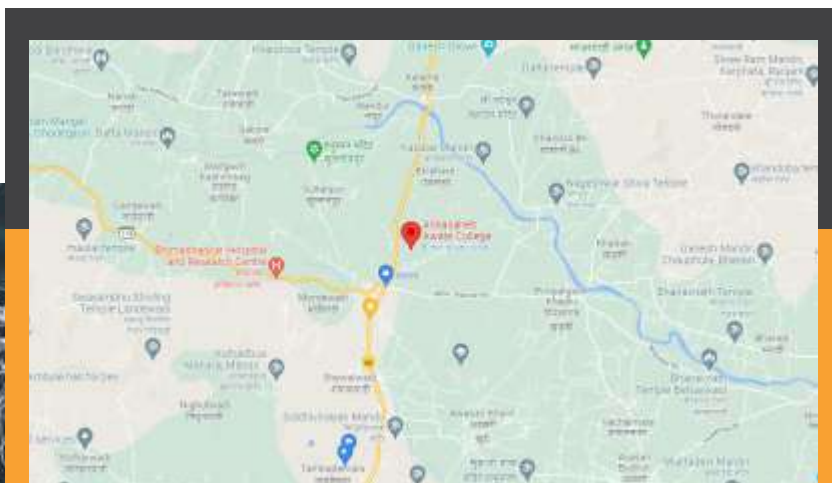
Dr. A. M. Deshmukh, President, Microbiologist Society of India

Dr. Bapurao Shigate, Asst.Prof. Dr.BAMU, Aurangabad

AAC, Manchar, Pune



QR Code Scan



Organizing Committee

Chief Patron

Padmavibhushan Hon'ble Shri Sharadraoji Pawar
President, Rayat Shikshan Sanstha, Satara

Patron(s)

Hon. Shri. Diliprao Walse Patil
Minister of Home Affairs, Government of Maharashtra

Hon. Dr. Anil A. Patil
Chairman, Rayat Shikshan Sanstha, Satara

Hon. Prin. Dr. Vitthal Shivankar
Secretary, Rayat Shikshan Sanstha, Satara

Hon. Prin. Dr. Pratibha Gaikwad
Jt. Secretary, Rayat Shikshan Sanstha, Satara

Chairman

Hon. Prin. Dr. K. G. Kanade
Annasaheb Awate College, Manchar

Convener

Prof. (Dr.) A. B. Nikumbh
Co-ordinator

Prof. (Dr.) S. N. Bolbhat
Organizing Secretary

Dr. A. A. Kale
Treasurer

Mr. V. B. Fasale
Technical Co-ordinator

Ms. A. M. Dange

Co-convener

Dr. R. S. Nimbalkar
Co-coordinator

Dr. S. T. Shinde
Co-organizing Secretary

Ms. H. J. Gavit
Co-treasurer

Ms. S. C. Mahakal
Technical Co-coordinator

Mr. U. D. Patil

Local Organizing Committee

Mr. R.S. Naik
Mr. S.A. Belage
Mr. V.S. Kumavat
Mr. V.P. Maske
Mr. H.S. Shirke
Ms. M.B. Kharde
Ms. P.P. Indore
Mr. M.D. Rokade
Mr. D.V. Doke
Mrs. R.S. Pawar

Dr. S.B. Misal
Dr. S.T. Shinde
Dr. A.K. Valvi
Mr. A.K. Bhor
Ms. M.R. Ekshinge
Mr. V.B. Hinge
Mr. P.D. Naik
Mr. S.B. Bhalke
Mr. S.N. Suse
Ms. P.B. Khillari

For Accomodation

Accommodation can be arranged on request,
charges will be born by the participant.

Contact : Mr. S.T. Pokale : 9850652907

College Website: aacmanchar.edu.in

For more details please visit:

<https://www.aacmanchar.edu.in/conf/>

